

Controlling Molecular Properties with Light

Author:

Kennedy, Aaron

Publication Date:

2020

DOI:

<https://doi.org/10.26190/unsworks/21920>

License:

<https://creativecommons.org/licenses/by-nc-nd/3.0/au/>

Link to license to see what you are allowed to do with this resource.

Downloaded from <http://hdl.handle.net/1959.4/68200> in <https://unsworks.unsw.edu.au> on 2024-05-01

CONTROL OF MOLECULAR PROPERTIES
WITH LIGHT



Aaron David William Kennedy

A thesis presented in fulfilment of the requirements for the degree of

Doctor of Philosophy

School of Chemistry

Faculty of Science

March 2020

ORIGINALITY STATEMENT

‘I hereby declare that this submission is my own work and to the best of my knowledge it contains no materials previously published or written by another person, or substantial proportions of material which have been accepted for the award of any other degree or diploma at UNSW or any other educational institution, except where due acknowledgement is made in the thesis. Any contribution made to the research by others, with whom I have worked at UNSW or elsewhere, is explicitly acknowledged in the thesis. I also declare that the intellectual content of this thesis is the product of my own work, except to the extent that assistance from others in the project's design and conception or in style, presentation and linguistic expression is acknowledged.’

Signed

Date

Aaron David William Kennedy

Sydney

COPYRIGHT STATEMENT

'I hereby grant the University of New South Wales or its agents a non-exclusive licence to archive and to make available (including to members of the public) my thesis or dissertation in whole or part in the University libraries in all forms of media, now or here after known. I acknowledge that I retain all intellectual property rights which subsist in my thesis or dissertation, such as copyright and patent rights, subject to applicable law. I also retain the right to use all or part of my thesis or dissertation in future works (such as articles or books).'

'For any substantial portions of copyright material used in this thesis, written permission for use has been obtained, or the copyright material is removed from the final public version of the thesis.'

Signed

Date

AUTHENTICITY STATEMENT

'I certify that the Library deposit digital copy is a direct equivalent of the final officially approved version of my thesis.'

Signed

Date



Inclusion of Publications Statement

UNSW is supportive of candidates publishing their research results during their candidature as detailed in the UNSW Thesis Examination Procedure.

Publications can be used in their thesis in lieu of a Chapter if:

- The candidate contributed greater than 50% of the content in the publication and is the “primary author”, ie. the candidate was responsible primarily for the planning, execution and preparation of the work for publication
- The candidate has approval to include the publication in their thesis in lieu of a Chapter from their supervisor and Postgraduate Coordinator.
- The publication is not subject to any obligations or contractual agreements with a third party that would constrain its inclusion in the thesis

Please indicate whether this thesis contains published material or not:

- This thesis contains no publications, either published or submitted for publication
- Some of the work described in this thesis has been published and it has been documented in the relevant Chapters with acknowledgement
- This thesis has publications (either published or submitted for publication) incorporated into it in lieu of a chapter and the details are presented below

CANDIDATE’S DECLARATION

I declare that:

- I have complied with the UNSW Thesis Examination Procedure
- where I have used a publication in lieu of a Chapter, the listed publication(s) below meet(s) the requirements to be included in the thesis.

Candidate’s Name	Signature	Date (dd/mm/yy)

LIST OF INCLUDED PUBLICATIONS

Diastereoselective control of tetraphenylethene reactivity by metal template self-assembly

A. D. W. Kennedy, N. de Haas, H. Iranmanesh, E. T. Luis, C. Shen, P. Wang, J. R. Price, W. A. Donald, J. Andréasson, F. Huang, and J. E. Beves, *Chem. - Eur. J.*, **2019**, *25*, 5708-5718.

Visible light photoswitching by azobenzazoles

A. D. W. Kennedy, I. Sandler, J. Andréasson, J. Ho, and J. E. Beves, *Chem. - Eur. J.*, **2020**, *5*, 1103-1110.

ABSTRACT

The work in this thesis explores photoactive units and self-assembly, both individually and at the intersection of these fields. The various approaches are unified by the interaction between molecules and light irradiation, with a special focus on visible-light photoswitching.

Chapter 2 explores the incorporation of the photoactive unit tetraphenylethene (TPE) into larger self-assembled architectures using iron pyridyl-imine templation. A $[\text{Fe}_2\text{L}_3]^{4+}$ triple helicate assembly was thoroughly characterised and derivatised through amide formation. Unsymmetrical TPE derivatives were isolated and their emission and self-assembly properties were studied.

Chapter 3 discusses the problems of accurately determining photostationary state (PSS) composition. Methodologies are discussed, with specific reference to known and assumed quantities. Examples are presented where the PSS composition can be estimated and these methodologies are also used in Chapters 4 and 5. A guide to the measurements required in more difficult cases is presented.

Chapter 4 reports on new visible light photoswitches, based on azobenzazoles. Their photoswitching properties are thoroughly studied, and the effect of protonation on the switching properties is explored. Photoswitching is possible using yellow light, and high-level *ab initio* calculations validate the proposed protonation of the ring nitrogen.

Chapter 5 describes the derivatisation of *o*-fluoroazobenzenes, with specific reference to incorporation into larger structures. A macrocyclic architecture is described, based on imine condensation reactions. The combination of a pyridyl functionalised ligand with palladium(II) gives a mixture of self-assembled species, which were individually characterised. Visible light irradiation leads to reversible configurational change, and out-of-equilibrium behaviour.

LIST OF ABBREVIATIONS AND ACRONYMS

Abbreviation	Full name
AIE	Aggregation Induced Emission
COSY	Correlation Spectroscopy
DASA	Donor-Acceptor Stenhouse Adducts
DCC	Dynamic Covalent Chemistry
DCM	Dichloromethane
DIBAL-H	Diisobutyl-Aluminium Hydride
DLS	Dynamic Light Scattering
DMAP	4-dimethylaminopyridine
DMF	<i>N,N</i> -dimethylformamide
DMSO	Dimethylsulfoxide
DOSY	Diffusion-Ordered Spectroscopy
Dppf	1,1'-bis(diphenylphosphino)ferrocene
DTE	Dithienylethene
EDTA	Ethylenediaminetetraacetic acid
EtOAc	Ethyl acetate
HMBC	Heteronuclear Multiple Bond Correlation
HPLC	High-Performance Liquid Chromatography
HSQC	Heteronuclear Single Quantum Coherence
HR-ESI-MS	High-Resolution Electrospray Ionisation Mass Spectrometry
LED	Light Emitting Diode
LR-ESI-MS	Low-Resolution Electrospray Ionisation Mass Spectrometry
MeCN	Acetonitrile
MeOH	Methanol
MLCT	Metal-ligand charge transfer
MOF	Metal Organic Framework
NMR	Nuclear Magnetic Resonance
NOESY	Nuclear Overhauser Effect Spectroscopy
NTf	bis(trifluoromethane)sulfonimide

Abbreviation	Full name
PSD	Photostationary Distribution
PSS	Photostationary State
ROESY	Rotating frame Overhauser Effect Spectroscopy
RT	Room Temperature
STAB	Sodium triacetoxyborohydride
$t_{1/2}$	Half-life
TEA	Triethylamine
TFA	Trifluoroacetic acid
THF	Tetrahydrofuran
TPE	1,1,2,2-tetraphenylethene
tren	tris(2-aminoethyl)amine
TsOH	<i>p</i> -toluenesulfonic acid
UPLC	Ultra-Performance Liquid Chromatography
UV-Vis	Ultraviolet-Visible

ACKNOWLEDGEMENTS

I owe thanks to many people for this thesis and to everyone who has helped me over the past couple years: Thank You.

Obviously, several people need specific thanks and most of all is my supervisor Jon. Thank you for your boundless enthusiasm, your infectious laughter and brilliant insights. You have shaped me into the independent chemist I am today, and I will always be grateful for that. Thank you for the challenging and exciting projects I've had the opportunity to work on.

To past and present members of the Beves group, thank you for making the Bever Dam a place that I want to work in. Ena, thank you for being a great friend, occasional gig buddy, a sounding board for ideas and an inspiration to do the best work I can. Tom, thank you for fruitful discussions, many fun facts and advice about NMR and photoswitching. Neil, a lot of the photoswitching work would not have been possible without you. Thank you also for the camping trips, houseparties, and submission rum. Hasti, you will always be a better crystallographer than I am, thank you for teaching me some of what you know. Laura and Lucy, we haven't known each other for long, but I'm confident we're leaving the Beves group in good hands! Good luck, and hopefully our paths cross again. Varsha and Ray, thank you for all the support, and hopefully parts of this thesis are useful to you! Shen, Pi and Nick, thank you for your important contributions to this work. To all the past members of the Beves group, even if your time was short thank you for providing variety and enjoyment to this small, close-knit group.

A lot of this work relied on important collaborations and I would like to specifically thank a couple people. Jason Price, thank you for your seemingly endless crystallography knowledge, and as a part of my supervisory team. Alex Donald, your mass spectrometry experience was vital to several parts of this work, thank you for taking the time to help me. Junming Ho and Isolde Sandler, thank you for performing computations which helped enlighten the photoswitching work. Joakim Andreasson, thank you for plentiful advice on photoswitching and the work in Chapter 3 is in good part inspired by discussion with you.

This work involved many hours collecting NMR spectra and the help provided by the NMR facility staff was invaluable. Don Thomas, Doug Lawes and Adelle Amoore, thank you very much. Similarly, thank you to Mohan Bhadbhade for crystallography advice, and allowing me to collect a lot of (bad!) data.

To all past and present members of both Lab 333 and the level 2 office, you have made that space an enjoyable place to work. Apologies if the music wasn't to your tastes at time! To all of those I spent time with outside of the lab, especially on a Friday evening, thank you for many enjoyable stories, especially James, Dan, Jack and Lyss.

My friends outside of chemistry have helped keep me sane(ish), and I've made several wonderful friends in Sydney. Thank you to all the Rock Touchers for trips away, fried chicken and many hours touching rocks. Special thanks go to Ash, Oce, Brenda and Jared, although you're scattered across the globe now. Dungeons and Dragons has been another amazing stress reliever, so thank you Matt for introducing me to it (and being an excellent friend). To my current groups, and anyone who has joined us: +1 inspiration.

Much like any good drama I've saved the best for last. Nat, thank you for believing in me, as much as anyone ever has. I'll never forget the coffees, cocktails, climbs and gigs we shared. Caitlin, you are my oldest friend and Australia has been a big place without you. Thank you for coming to visit and always supporting me.

Tess and Cam, I think we have talked every day for the last year. We've shared triumphs and failures, and I don't tell you enough how much you two mean to me. We will always be friends, no matter where we are living.

To my family in New Zealand: Mum, Dad, Lochlan, Regan and Briana. This thesis is dedicated to you. I can always rely on you, no matter how far away I am. I can never thank you enough for all the support and I know you're proud of me

CONTENTS

1 Introduction	1
1.1 Light.....	3
1.2 Photoswitchable molecules.....	3
1.3 Azobenzenes and azoheteroarenes	4
1.4 Visible light photoswitches	6
1.5 <i>o</i> -Fluoroazobenzenes	7
1.6 Tetraphenylethene	8
1.7 Light responsive supramolecular assemblies	9
1.7.1 <i>Photoswitchable guests</i>	10
1.7.2 <i>Photoswitchable hosts</i>	11
1.8 Metal template self-assembly	12
1.9 Control of function and form.....	14
1.9.1 <i>Post-assembly modification</i>	15
1.10 Stimuli-responsive metal ligand self-assemblies.....	16
1.10.1 <i>Guest responsive architectures</i>	16
1.10.2 <i>Competing ligands</i>	17
1.10.3 <i>Guest release</i>	18
1.11 Light responsive metal ligand self-assemblies	19
1.12 Aims and outlines of this thesis.....	22
1.13 References	23
2 Metal template helicates of tetraphenylethene	31
2.1 Summary.....	32
2.2 Tetraphenylethene in metallocsupramolecular self-assembly.....	32
2.3 Synthesis and identification of the $[\text{Fe}_2\text{L}_3]^{4+}$ species	33
2.4 Characterisation of $[\text{Fe}_2(2.2)_3]^{4+}$ by NMR.....	38
2.5 X-Ray crystallography of $[\text{Fe}_2(2.2)_3](\text{PF}_6)_4$	41
2.6 Reactivity of $[\text{Fe}_2(2.2)_3]^{4+}$	42
2.7 Diffusion ^1H NMR of self-assembled species.....	46
2.8 X-Ray crystallography of $[\text{Fe}_2(2.5)_3](\text{PF}_6)_4$	47
2.9 Electronic properties of iron(II) helicates.....	48
2.10 Isolation of selectively functionalised TPE molecules.....	49
2.11 Electronic properties of organic components 2.1, 2.8, 2.9 and 2.10	52
2.11.1 <i>UV-Visible absorption and emission properties</i>	52
2.11.2 <i>DLS measurement of self-assembly behaviour</i>	53

2.12 Conclusions	56
2.13 Experimental.....	56
2.13.1 Synthesis of 1,1,2,2-tetrakis(4-nitrophenyl)ethene	56
2.13.2 Synthesis of 4,4',4'',4'''-(ethene-1,1,2,2-tetrayl)tetraaniline (2.1)....	57
2.13.3 Synthesis of N,N',N'',N'''-(ethene-1,1,2,2-tetrayltetrakis(benzene-4,1-diyl))tetrakis(1-(pyridin-2-yl)methanimine) (2.3)	57
2.13.4 Synthesis of $[Fe(2.7)_3](PF_6)_2$	58
2.13.5 Synthesis of $[Fe_2(2.2)_3](PF_6)_4$ helicate	59
2.13.6 Synthesis of $[Fe_2(2.4)_3](PF_6)_4$ helicate	60
2.13.7 Syntheses of $[Fe_2(2.5)_3](PF_6)_4$ helicate	61
2.13.8 Synthesis of $[Fe_2(2.6)_3](PF_6)_4$ helicate	62
2.13.9 X-Ray crystallography	64
2.13.10 $2[Fe_2(2.2)_3](PF_6)_8 \cdot H_2O$	65
2.13.11 $[Fe_2(2.5)_3](PF_6)_4$	66
2.14 References.....	67
3 Calculating photostationary state ratios with UV-vis spectroscopy	71
3.1 Summary.....	72
3.2 Quantifying photoswitching	72
3.3 Thermally bistable systems	73
3.4 Examples where the spectrum of one species is known.....	74
3.5 Examples where relative concentrations are known.....	76
3.6 Calculation of spectra where no relative concentrations are known	78
3.7 Conclusion	80
3.8 References.....	80
4 Visible light photoswitching by azobenzazoles	83
4.1 Summary.....	84
4.2 Symmetric azoheteroarene pH switch	84
4.3 Synthesis and characterisation.....	85
4.3.1 Symmetric azobenzazoles	85
4.3.2 Attempted syntheses of azo(bisimidazole).....	87
4.4 Absorption and photoswitching properties.....	90
4.4.1 UV-Vis absorption.....	90
4.5 Photoswitching properties	91
4.5.1 The effect of different LED sources.....	95
4.6 Thermal half-life measurements	96
4.7 Unsymmetrical azobenzimidazole.....	97
4.8 <i>In situ</i> 1H NMR photoswitching	100

4.9	Modulation of photoswitching by acid addition.....	101
4.10	Computed geometries and proton affinities.....	106
4.10.1	<i>Computed geometries</i>	106
4.11	Conclusion.....	108
4.12	Experimental.....	109
4.12.1	<i>Synthesis of 1,2-bis(1-methyl-benzo[d]imidazol-2-yl)diazene (4.1)</i>	109
4.12.2	<i>Synthesis of 1,2-bis(benzo[d]oxazol-2-yl)diazene (4.2)</i>	109
4.12.3	<i>Synthesis of 1,2-bis(benzo[d]thiazol-2-yl)diazene (4.3)</i>	110
4.12.4	<i>Synthesis of 1,2-bis(1-methyl-1H-imidazol-2-yl)diazene (4.4)</i>	110
4.12.5	<i>Synthesis of 1-methyl-2-(phenyldiazenyl)-1H-benzo[d]imidazole (4.6)</i>	111
4.12.6	<i>General information for photoswitching</i>	112
4.13	X-ray crystallography	113
4.13.1	<i>Structure of E-4.1</i>	116
4.13.2	<i>Structure of E-4.2</i>	117
4.13.3	<i>Structure of E-4.3</i>	118
4.13.4	<i>Structure of E-4.4</i>	119
4.13.5	<i>Structure of E-4.5</i>	120
4.13.6	<i>Structure of [E-4.6D]Cl·H₂O</i>	121
4.14	References	122
5	Photoswitchable self-assembled structures	125
5.1	Summary.....	126
5.2	Strategies for derivatising <i>o</i> -fluoroazobenzenes.....	126
5.3	Synthesis of aldehyde appended <i>o</i> -fluoroazobenzene	126
5.4	Photoswitching of dialdehyde functionalised <i>o</i> -fluoroazobenzene	128
5.4.1	<i>Absorption spectra and visible-light photoswitching</i>	128
5.5	Reaction with aliphatic diamines.....	130
5.6	Limited reactivity of 5.2 in imine formation	132
5.7	Palladium catalysed couplings of <i>o</i> -fluoroazobenzenes	134
5.8	Suzuki coupling of <i>o</i> -fluoroazobenzenes	136
5.9	Synthesis of pyridyl substituted <i>o</i> -fluoroazobenzenes.	137
5.10	An aside: the green impurity	138
5.11	Characterisation of pyridyl ligand 5.9	139
5.12	Synthesis of self-assembled structures with palladium	141
5.13	High resolution ESI-MS of the Pd(II) assemblies	144
5.14	Elucidation of structure	145

5.15 Kinetics of formation.....	148
5.16 Variable temperature measurements.....	150
5.17 Perturbing equilibrium with light irradiation.....	152
5.18 Conclusion.....	158
5.19 Experimental.....	158
5.19.1 Synthesis of 4-amino-3,5-difluorobenzaldehyde (5.1)	158
5.19.2 Synthesis of 4,4'-(diazene-1,2-diyl)bis(3,5-difluorobenzaldehyde) (5.2).....	159
5.19.3 Synthesis of 1,2-bis(4-bromo-2,6-difluorophenyl)diazene (5.3)	159
5.19.4 Synthesis of 1,2-bis(2,6-difluoro-4-((trimethylsilyl)ethynyl)phenyl)diazene (5.4).....	160
5.19.5 Synthesis of 1,2-bis(2,6-difluoro-4-(4,4,5,5-tetramethyl-1,3,2-dioxaborolan-2-yl)phenyl)diazene (5.5)	161
5.19.6 Synthesis of 1,2-bis(3,5-difluoro-[1,1'-biphenyl]-4-yl)diazene (5.6)	161
5.19.7 Synthesis of 1,2-bis(3,5-difluoro-4'-methyl-[1,1'-biphenyl]-4-yl)diazene (5.7).....	162
5.19.8 Synthesis of 1,2-bis(2,6-difluoro-4-(pyridin-3-yl)phenyl)diazene (5.9)	162
5.19.9 Synthesis of $[Pd_3(5.9)_6](BF_4)_6$ and $[Pd_4(5.9)_8](BF_4)_8$	163
5.20 X-Ray crystallography.....	164
5.20.1 Structure of 5.4.....	166
5.20.2 Structure of 5.8.....	167
5.20.3 Structure of 5.10.....	168
5.21 References.....	169
6 Conclusions and future outlook	173
6.1 References.....	176
7 Appendix - Chapter 2	177
8 Appendix - Chapter 4	240
9 Appendix - Chapter 5	316

1 INTRODUCTION



*“And AC said: “LET THERE BE LIGHT!”,
and there was...”*

-Isaac Asimov, The Last Question

1.1 Light

In many respects irradiation with light is the ideal stimuli to control molecular behaviour. It is easily generated, can be applied externally to the reaction vessel, is generally non-destructive and provides good temporal and spatial control. Due to these appealing features, a variety of methodologies to control molecular properties with light have been developed.

One such example is photocatalysis, where light promotes unusual reactivity *via* the generation of an excited state.¹ In recent years photoredox catalysis, involving an excited state with substantially different redox properties, has seen a renaissance in organic synthetic chemistry, with the development of new catalysts and methodologies.² Another class of photoactive species are photocaged molecules, where light triggers an irreversible chemical transformation to “uncage” a functional molecule.³ This has been widely exploited in chemical biology for example, to probe structure with a high degree of temporal control.⁴ However, to generate reversible control over function, systems must be developed where both states can be accessed. The most common way to achieve this is through molecular photoswitches.

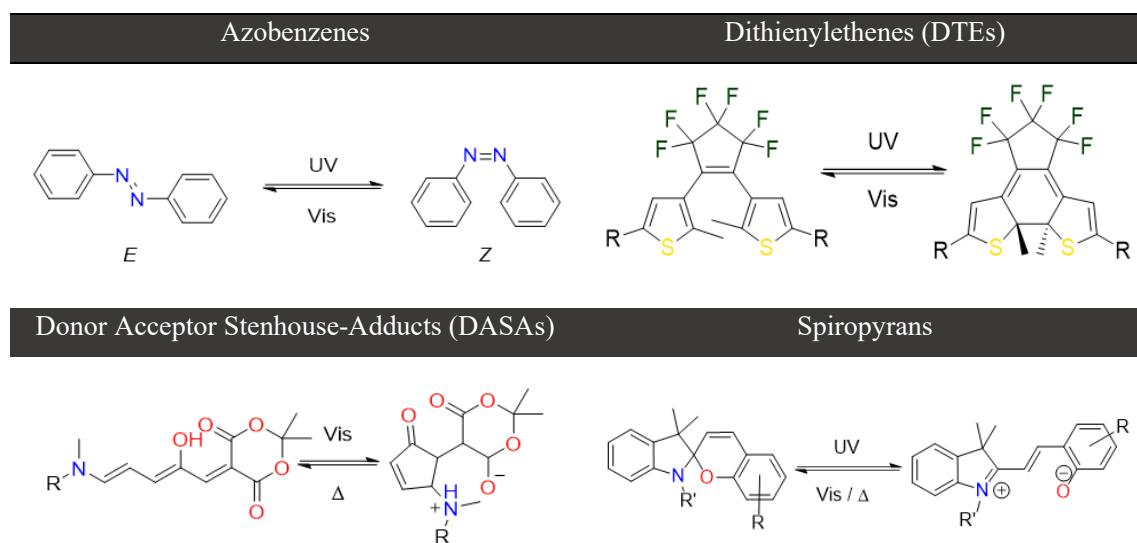
1.2 Photoswitchable molecules

A molecular photoswitch can broadly be defined as a molecule which undergoes a reversible change upon light irradiation. The classic examples of such changes are isomerisation about a double bond (in the case of stilbenes, azobenzenes and related derivatives) or ring closing/opening (in the case of dithienylethenes, spiropyrans and Donor-Acceptor Stenhouse Adducts (DASAs)). These structural changes are often accompanied by a change in properties such as polarity, absorbance, pK_a or luminescence, allowing spatial and temporal control of these properties.⁵ Photoswitches have been widely exploited, including for use in biological conjugates,⁶ stimuli-responsive polymers,⁷ nanoparticles,⁸ and materials.⁹ The change in structure can also be exploited as components of molecular machines,¹⁰ where light is used to generate systems out-of-equilibrium that can be harnessed to perform macroscopic work.¹¹

Some of the major classes of photoswitches are shown in Table 1.1, along with their structural changes upon irradiation. Despite the large structural diversity, there are several key parameters which are used to quantify the photoswitching behaviour and to

subdivide the switch type. These include the wavelength of maximum light absorption; the relative thermal stability of the two states; the ability to selectively generate a single isomer upon irradiation; the significance of the structural change upon irradiation; and the resistance to fatigue over multiple switching cycles. Rational design can allow these properties to be manipulated, often by synthetic modifications which affect the electronic structure.

Table 1.1 Representative structures of common photoswitches. Note that substantial structure variation exists, especially for the DTE and DASA photoswitches, however the key geometric change is highlighted.^a



^a For instructive reviews see: azobenzenes,¹² diarylethenes,¹³ DASAs¹⁴ and spiropyrans.¹⁵

1.3 Azobenzenes and azoheteroarenes

Azobenzene is the quintessential example of a photoswitch, undergoing a reversible *E* to *Z* isomerisation upon exposure to light irradiation.^{12, 16} Azobenzene and related derivatives hold a privileged position amongst photochromic molecules due to the pronounced structural changes associated with the isomerisation process. They show good conversion from the thermally stable *E* isomer to the metastable *Z* isomer upon irradiation and excellent photostability. While commonly used, the parent unsubstituted azobenzene does have some drawbacks. Isomerisation from the *E* to *Z* isomer is induced by UV light, which can lead to degradation of other molecules in the system and is not compatible with biological applications. The thermal half-life ($t_{1/2}$) of the *Z*-isomer is long (≈ 2 days at 298 K),¹² but extended half-lives are desirable for some applications. In an

attempt to tune these properties several variations have been made to the azobenzene core structure.

One class of related compounds are the azoheteroarenes, which have one or both of the phenyl rings of azobenzene replaced by a heteroaromatic ring.¹⁷ Although they remain much less widely studied than azobenzene derivatives, these compounds allow tuning of their thermal switching rates, the degree of isomerisation under irradiation, and the absorption maxima.¹⁸ They have been employed in the context of photopharmacology^{6a} as the majority of small-molecule drugs contain aromatic heterocycles.¹⁹ Azoheteroarenes also allow light modulation of molecular properties such as magnetism,²⁰ luminescence,²¹ and pK_a .²²

Arylazopyrazoles,^{7e, 23} a class of azoheteroarenes, undergo light-driven bidirectional switching between the *E* and *Z* isomers and display some of the longest thermal half-lives for the *Z*→*E* isomerisation of azo derivative photoswitches ($t_{1/2} \approx 1000$ d).^{23a} This extended half-life was rationalised by considering the T-shaped conformation adopted by the *Z*-isomers of the compounds, which is stabilised by non-covalent C-H... π interactions (Figure 1.1a). If the *Z* isomer adopts a more twisted conformation the thermal half-life is reduced (Figure 1.1b), but the selective photoswitching is enhanced due to an increase in the intensity of the $n-\pi^*$ band for the *Z* isomer.^{23b} Balancing these considerations allowed the design of a phenylazopyrazole (Figure 1.1) which possesses excellent switching properties ($\geq 97\%$ of either isomer can be generated) and a half-life of 74 days at 298 K.

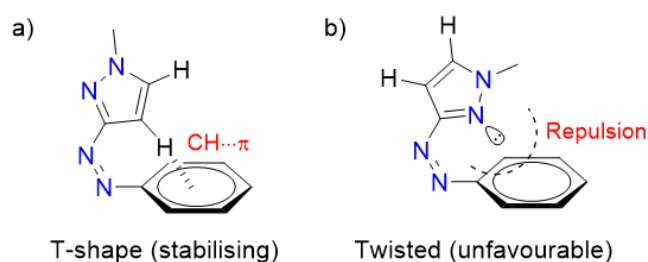


Figure 1.1 Possible conformations of the *Z*-isomer of an azopyrazole photoswitch. Formation of the T-shaped isomer (a) leads to longer thermal half-lives.

To exploit more members of this class of compounds for applications such as photopharmacology or incorporation into larger structures it is important to determine their structure function relationships. The compounds have shown a good ability to be

tuned for purpose based on rational design, but the complete design principles are yet to be fully elucidated.

1.4 Visible light photoswitches

There are strong motivations for developing visible light responsive²⁴ azobenzene-type photochromic molecules, including for biological applications.²⁵ Historically it has been difficult to combine visible light photoswitching and thermal bistability for azobenzene derivatives as the strategies employed to red shift the absorbance spectra typically increase the rate of thermal reversion of the metastable isomer.²⁶ Azo compounds possessing an electron donating and an electron withdrawing group on either side of the azo group, so called “push-pull” systems, can shift the absorption into the visible.²⁷ However, these push-pull systems often possess very short (μs to ms) thermal half-lives due to resonance or tautomerisation lowering the barrier for rotation around the azo double bond (Figure 1.2).^{12, 28}

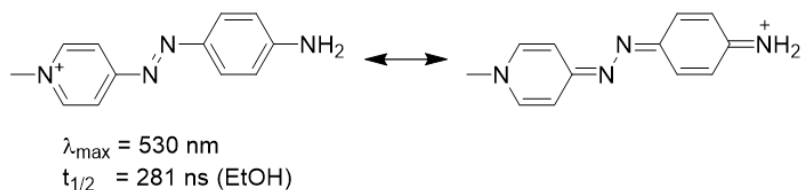
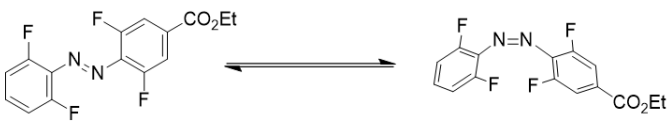
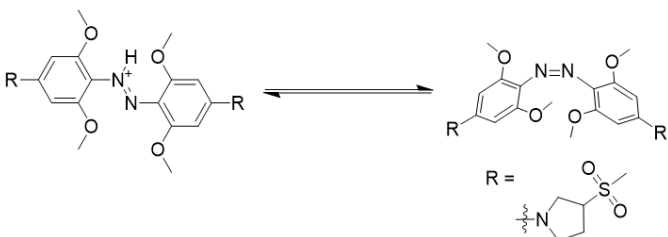
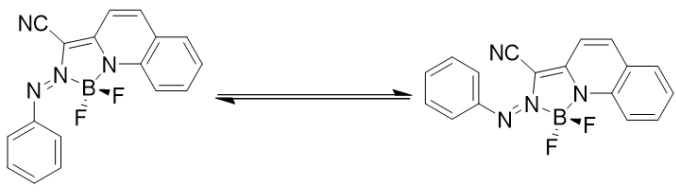


Figure 1.2 Example of resonance destabilisation of the azo double-bond for a “push-pull” system, leading to a very short thermal half-life of the *Z*-isomer.^{27a}

Protonation of azobenzenes at the azo-bridge can also result in a red shift of the absorption.^{25b, 29} Azonium ions typically have thermal half-lives for the *Z*→*E* isomerisation on the order of μs to ms , again due to a decrease in the azo double bond character.^{12, 30} This short half-life limits the accessible population of the *Z* isomer in acidic solutions.^{25d} This problem was solved by the *ortho*-ether azobenzenes developed by the Woolley group (Table 1.2) where the *E* and *Z* isomers have sufficiently different $\text{p}K_{\text{a}}$ values that at physiological pH the *E* isomer is protonated while the thermally unstable *Z* is not protonated. This allows visible light photoswitching of the protonated *E* isomer, while still allowing a substantial portion of *Z* isomer to be generated.

Table 1.2 Selected visible light azobenzene photoswitches compared to the parent azobenzene. In all cases the more thermally stable isomer is shown on the left. Switching wavelength denotes the λ_{max} of light irradiation leading to the relevant isomerisation.

Azobenzene ¹²		Switching wavelengths / nm (PSS distribution / E:Z)		
		<i>E</i> to <i>Z</i> : 313 (20:80)	<i>Z</i> to <i>E</i> : 436 (80:20)	$t_{1/2}$ = 2d at 298 K
ortho-fluoroazobenzenes ^{24b}				
		<i>E</i> to <i>Z</i> : > 500 (5:95)	<i>Z</i> to <i>E</i> : 410 (95:5)	$t_{1/2}$ = 30 h at 333 K
ortho-methoxyazobenzenes ^{29a}				
		<i>E</i> to <i>Z</i> : 720 (n.r.)	<i>Z</i> to <i>E</i> : n.r.	$t_{1/2}$ = 0.7 s at 298 K
Heterodiazocines ³¹				
		<i>E</i> to <i>Z</i> : 660 (> 99% <i>Z</i>)	<i>Z</i> to <i>E</i> : 405 (70:30)	$t_{1/2}$ = 3.5 d at 300 K
BF ₂ -azobenzene ³²				
		<i>E</i> to <i>Z</i> : 570 (97:3)	<i>Z</i> to <i>E</i> : 450 (80:20)	$t_{1/2}$ = 12.5 h at 294 K

1.5 *o*-Fluoroazobenzenes

One of the most successful examples of generating bidirectional visible light photoswitches was developed by Hecht and co-workers by incorporating fluorine atoms *ortho*- to the azobenzene core (Figure 1.3).^{24a, 24b} This separates the $n\text{-}\pi^*$ bands for the *E* and *Z* isomers, allowing selective irradiation of only one isomer and leading to nearly quantitative photoconversion in either direction. The switches have exceptional bistability with a thermal half-life of up to 700 days in DMSO. These have subsequently been exploited for materials applications³³ and in Metal Organic Frameworks (MOFs).³⁴

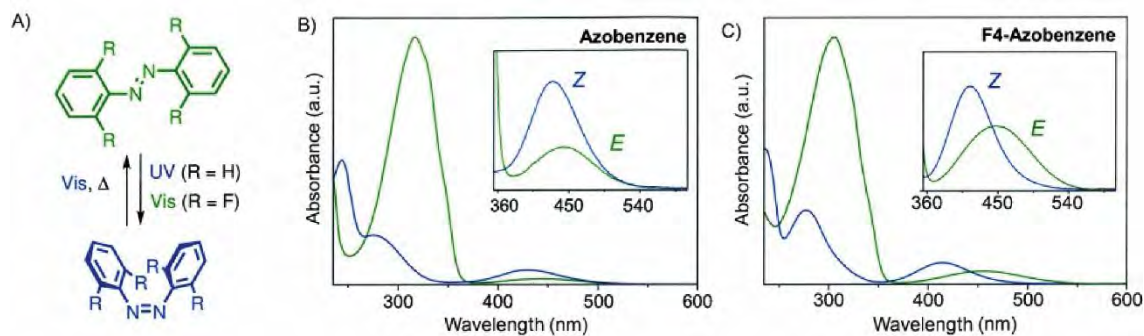


Figure 1.3 *o*-Fluoroazobenzenes as visible light photoswitches. A) Comparison of the irradiation wavelengths for azobenzene and *o*-fluoroazobenzene; B) UV-Vis spectra of azobenzene showing the overlap of the *E* and *Z* isomers and C) UV-vis spectra of *o*-azobenzene showing the band separation between isomers. Copyright 2014 Wiley. Adapted with permission from Knie, C.; Utecht, M.; Zhao, F.; Kulla, H.; Kovalenko, S.; Brouwer, A. M.; Saalfrank, P.; Hecht, S.; Bléger, D., ortho-Fluoroazobenzenes: Visible Light Switches with Very Long-Lived *Z* Isomers, *Chem.-Eur. J.* **2014**, *20* (50), 16492-16501.

A study^{24b} of the substituent effects in *o*-fluoroazobenzenes showed that electron-withdrawing substituents increase the $n-\pi^*$ absorbance band separation of the two isomers. This allows selective irradiation of only one isomer and excellent bidirectional photoconversion. Electron-withdrawing substituents lower the barrier to isomerisation resulting in a faster rate of thermal $Z \rightarrow E$ reversion. In all cases the half-lives are longer than unsubstituted azobenzene.

1.6 Tetraphenylethene

Another example of a photoactive unit is tetraphenylethene (TPE). TPE has been known since the 19th century,³⁵ however in the past two decades has seen a major increase in fundamental research and applications. This has primarily been driven by exploitation of the aggregation-induced emission (AIE)³⁶ effect whereby the emission intensity is strongly increased upon self-assembly between TPE units. The well-defined geometry of the TPE units lends itself to incorporation into larger self-assembled structures and allows incorporation of stimuli-responsive properties. For example, the TPE unit has been incorporated into metal-organic frameworks (MOFs),³⁷ covalent networks,³⁸ organic hydrogen-bonded networks,³⁹ halogen bonded networks,⁴⁰ stimuli responsive polymers,⁴¹ supramolecular polymers,⁴² and organic capsules.⁴³

1.7 Light responsive supramolecular assemblies

Incorporation of photoresponsive molecules into larger structures to generate responsive assemblies has been widely explored. These include polymers,⁴⁴ micelles,⁴⁵ nanoparticles,⁴⁶ MOFs⁴⁷ and discrete self-assembled systems, including coordination cages.⁴⁸ Both irreversible and reversible photoactivity have been exploited. Irreversible reactions are advantageous for polymeric applications due to the sharp change in structure associated with immolation of the main chain of the polymer.⁴⁹ Comparatively, reversible changes (such as *E-Z* isomerisation) have a smaller magnitude effect, however the ability to cycle between distinct states of assembly is advantageous.⁵⁰

One of the most commonly used reversible motifs is the modulation of host-guest binding between azobenzene and cyclodextrin. *E*-azobenzene is a good guest for α - and β -cyclodextrin, with a reported binding constant in water of $\approx 2500 \text{ M}^{-1}$. Upon photoswitching, the *Z*-azobenzene is a poor guest for the cyclodextrin, which can lead to dissociation of the self-assembly. This has been used to modulate polymeric materials,⁵¹ to control gel formation,⁵² for the preparation of artificial muscles,^{9a} and for controlled self-assembly.⁵³

Photoswitchable units have been used to introduce photoswitching behaviour into molecular machines, especially rotaxanes and pseudorotaxanes.⁵⁵ An early example of this was shown by Nakashima and co-workers, where the position of cyclodextrin moiety along an axle is controlled by the isomerisation of an azobenzene unit in the thread.⁵⁶ A more recent example by Credi and co-workers showed directional control of motion on a pseudorotaxane to push a system out of equilibrium (Figure 1.4).^{10c} Isomerisation of an azobenzene unit acted as a bulky stopper, leading to autonomous light-powered cycling between states.

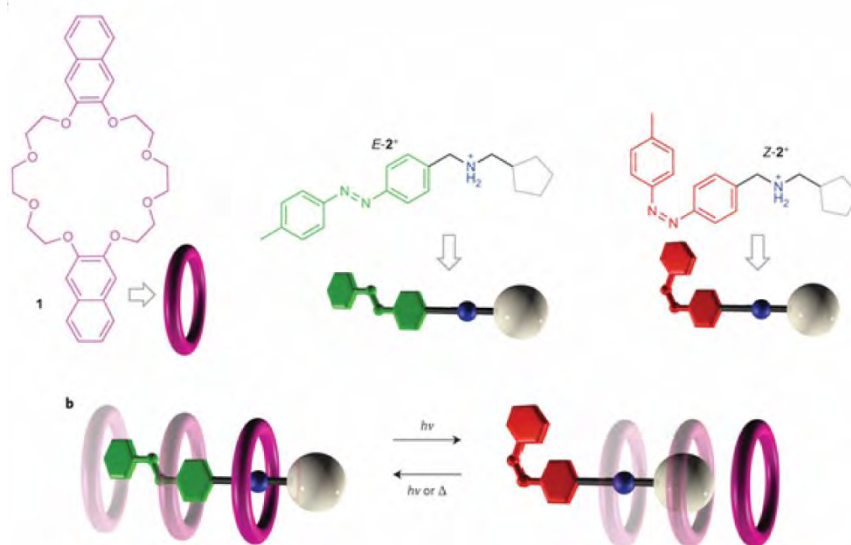


Figure 1.4 Unidirectional motion of a crown ether ring over an azobenzene based thread. Adapted with permission from Springer Nature. Ragazzon, G.; Baroncini, M.; Silvi, S.; Venturi, M.; Credi, A., *Nat. Nanotechnol.* **2014**, *10*, 70.^{55b}

To better allow discussion of the subtleties of photo-responsive self-assemblies, the light responsive behaviours can be divided into two examples: photoswitchable guests and photoswitchable hosts.

1.7.1 Photoswitchable guests

Photomodulation of guest binding strength *via* photoisomerisation of the guest is an appealing method of incorporating stimuli-response into a system.⁵⁴ This approach places less demand on the self-assembled species, because the geometric and electronic changes in the self-assembled structure are minor. An elegant example from Rebek and co-workers shows the exchange between linear guests in a self-assembled hydrogen-bonded cavity (Figure 1.5).^{54a} The *Z*-azobenzene generated upon irradiation is a poor guest for the dimeric host which allows binding of *n*-tridecane, which has much weaker binding than *E*-azobenzene. Upon heating the *E*-azobenzene is reformed, leading back to the initial host-guest complex.

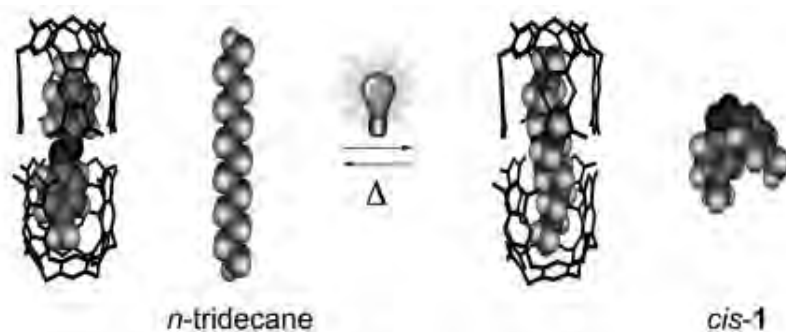


Figure 1.5 Light-induced guest exchange of *trans*-(4,4'-dimethylazobenzene) (*trans*-1) and *n*-tridecane in a self-assembled dimeric hydrogen-bonded capsule. Copyright 2010 Wiley. Adapted with permission from Dube, H.; Ajami, D.; Rebek Jr., J., *Angew. Chem. Int. Ed.* **2010**, *49* (18), 3192-3195.

1.7.2 Photoswitchable hosts

Incorporation of photoswitchable molecules into the structure of a known host system can allow irradiation to affect the binding of guest molecules.⁵⁷ The pioneering work in this field was shown by Shinkai and co-workers, with the development of a photoresponsive bis(crown ether) (Figure 1.6). Isomerisation from the *E* to *Z* isomer forms a defined cavity, which allows binding of large alkali-metal cations. Even in this work it was recognised that guest binding significantly affects the nature of the photoswitching unit. In this case, the effect was positive (greater *Z*-isomer content and longer $t_{1/2}$ value upon guest binding) but interplay of host and guest must be considered when designing such systems. More recent work by Ballester and co-workers has shown the ability to move host-guest systems out of equilibrium using light irradiation, based on the isomerisation of an azobenzene appended calix[4]arene.^{48e}

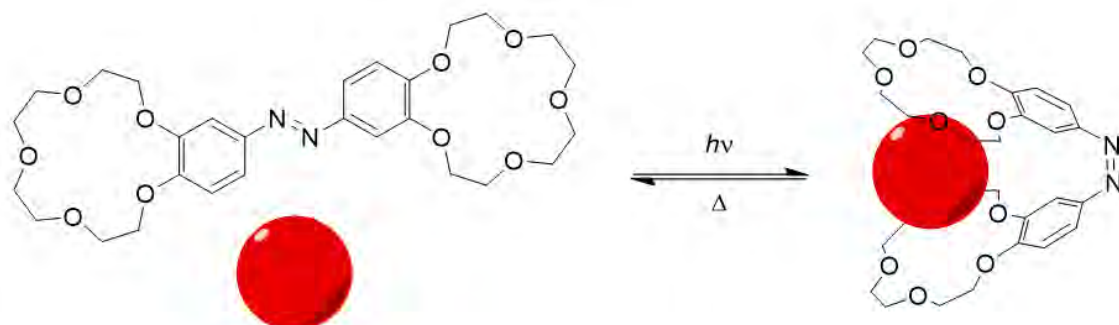


Figure 1.6 Control over alkali metal cation binding by isomerisation of an azobenzene crown-ether complex

The above selection of examples illustrates the diversity of structure and control of properties that can be developed through incorporation of photoswitching units into

larger architectures. In light of this, there are only relatively few examples in the literature of light-responsive metal-template self-assemblies, a major class of supramolecular structures.^{48a, 58}

1.8 Metal template self-assembly

The forming of predictable, directional and reversible interactions between molecular sub-components is the foundation of supramolecular chemistry. This allows the construction of complex, 3D structures which would otherwise be challenging or impossible to realise using conventional covalent chemistry. This methodology provides no means of “error-correcting” to form the thermodynamic minimum structure. The exception to this limitation is Dynamic Covalent Chemistry (DCC), which employs reversible covalent bond formation to access large and complex arrays. Of the varied non-covalent interactions employed, metal-template self-assembly remains one of the most powerful approaches for the construction of larger structures.⁵⁹ For a selection of metal ions, the geometry at the metal centre is (mostly) invariant. When combined with ligands of known geometry this allows designed construction of 3D architectures. To date, most structures have involved the use of labile transition metal centres bridged by organic linker ligands. The lability is required in order to allow for error-correction to generate the smallest, least-strained architecture.⁶⁰

There are many examples which show the power of metal-template assembly and the predictable structural variation that can be induced by subtle geometric changes in the ligand framework. However, there are equally as many examples of serendipitous and surprising assemblies, often resulting from the same subtle ligand variation. Pioneering constructions include the template synthesis of a catenane by Sauvage,⁶¹ formation of a molecular square by Fujita,⁶² assembly of a circular double helicate by Lehn⁶³ (Figure 1.7) and formation of a quadruple-stranded helicate by Steel.⁶⁴

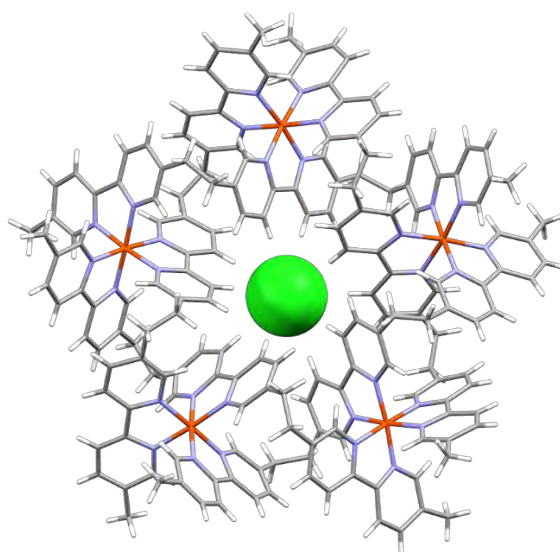


Figure 1.7 X-Ray structure of the circular double-helicate synthesised by combination of a tris-bipyridine strand and FeCl_2 . Helicate structure is shown as capped sticks, and the encapsulated chloride ion as a space filling model.⁶³

One major class of metal-templated structures are those possessing a well-defined 3D cavity, known as molecular cages. The development of a number of design strategies has allowed realisation of a wide family of geometries, including tetrahedra,⁶⁵ cubes,⁶⁶ and spheres⁶⁷, as well as less regular arrays.⁶⁸ Modular design of these structures allows relatively easy functionalisation, as well as the ability to regulate host-guest interactions. These cages can promote unusual reactions of small-molecule guests confined in their cavities. The internal environment is significantly different to that of the bulk solution due to the constrained orientation guest molecules must adopt, solvophobic effects and the relatively close contact with other substrates when multiple guests are bound. This can result in rate-enhancement of catalysis,^{65e, 69} enantio-/regioselectivity⁷⁰ or stabilisation of reactive molecules.^{65c} For example, Fujita and co-workers have shown an octahedral cage formed with palladium(II) can control the selectivity of a [2+2] photodimerization due to the formation of an inclusion complex.^{70b} In another example, Raymond and co-workers showed that acid-catalysed hydrolysis can take place in basic solution, due to encapsulation in a tetrahedral cage.^{69d} This selectivity would be difficult or impossible to achieve *via* other means, providing a unique approach to synthesising interesting structures.

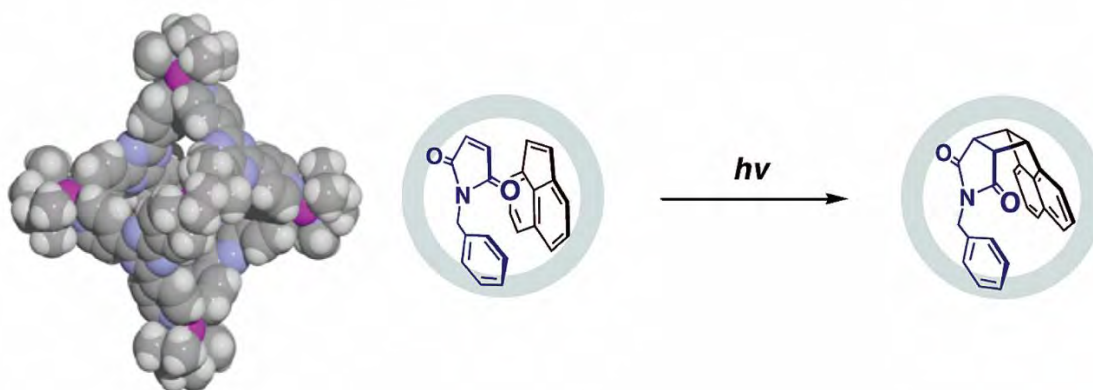


Figure 1.8 Control of molecular reactivity using a $[\text{Pd}_6\text{L}_4]^{12+}$ octahedral architecture. The restricted orientations possible in the cavity and the close contact leads to enhanced reaction rate and stereoselectivity. Adapted with permission from Yoshizawa, M.; Takeyama, Y.; Okano, T.; Fujita, M., *J. Am. Chem. Soc.* **2003**, *125* (11), 3243-3247. Copyright 2003 American Chemical Society.

1.9 Control of function and form

The early development of metal-template self-assembly led to increasingly complex architectures. However, the guiding principles of self-assembly are yet to be fully understood and serendipity continues to play a major role. For a given ligand and metal ion combination, can we predict the self-assembled structure formed? Or more elegantly, for a desired application can we tune the sub-components to give the desired 3D shape and properties? This ambitious goal is yet to be realised, but the many examples allow us to postulate design principles.⁷¹ The most successful example is the use of divergent pyridyl ligands by Fujita and co-workers.^{66c, 67c, 67e, 72} In their work they show that the bend angle of a short divergent dipyrindyl ligand determines the structure of the resulting polyhedral assembly formed upon combination with palladium(II). Use of a rigid ligand based on furan with a bend angle of 127° led to the exclusive formation of an $[\text{Pd}_{12}\text{L}_{24}]^{24+}$ sphere. Increasing the bend angle to 149° by incorporation of a thiophene unit led to the exclusive formation of a larger $[\text{Pd}_{24}\text{L}_{48}]^{48+}$ sphere. Inclusion of flexibility into the ligand framework generated a $[\text{Pd}_{30}\text{L}_{60}]^{60+}$ species (Figure 1.9).

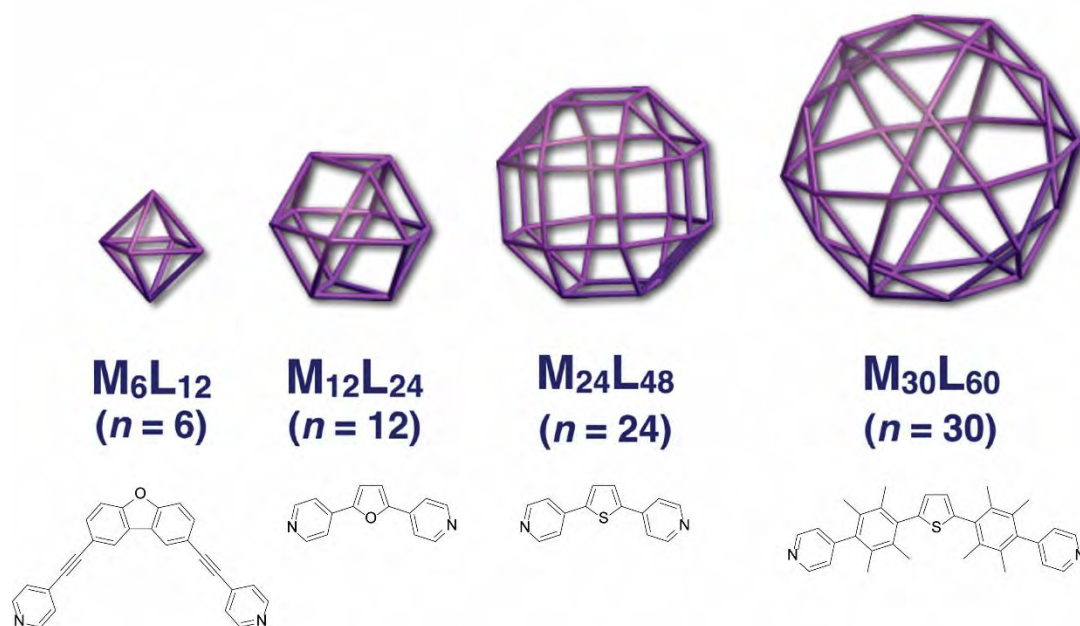


Figure 1.9 The family of edge capped polyhedra explored by Fujita and co-workers. Adapted from Fujita, D.; Ueda, Y.; Sato, S.; Yokoyama, H.; Mizuno, N.; Kumasaka, T.; Fujita, M., *Chem* (1), 91-101 with permission from Elsevier.

1.9.1 Post-assembly modification

An alternate methodology to control self-assembled structures is post-assembly modification.⁷³ This allows the incorporation of diverse functionality into the ligand backbone, which might not be compatible with the assembly process. Post-assembly modification can also trigger constitutional changes in the assembled structure, acting as an irreversible stimuli response. The challenge in this area has been identifying reactions compatible with the dynamic nature of metal-templated self-assemblies, as many useful organic reactions would serve to decompose the self-assembled structures. Both external⁷⁴ and internal⁷⁵ functionalisation of self-assembled species has been shown through a variety of methodologies. Control of the reaction outcome was displayed by Nitschke and co-workers, where irreversible reaction of an amine unit “locked-down” a $[Fe_2L_3]^{4+}$ helicate rather than the thermodynamically stable $[Fe_4L_6]^{8+}$ tetrahedral species (Figure 1.10).⁷⁶ Irreversible formation of an amide or azide trapped the $[Fe_2L_3]^{4+}$ kinetic product, allowing further structural diversity to be introduced at the periphery.

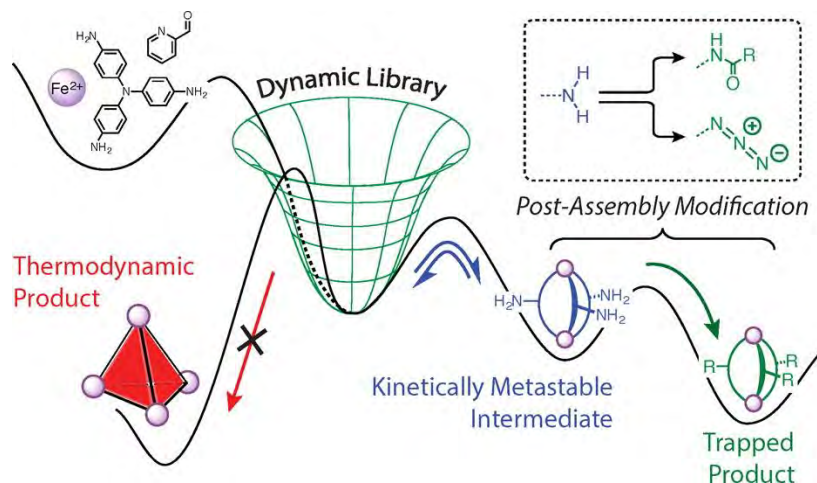


Figure 1.10 Kinetic reaction of metastable self-assembled intermediates allows access to otherwise unfavoured structures. Adapted with permission from Roberts, D. A.; Pilgrim, B. S.; Cooper, J. D.; Ronson, T. K.; Zarra, S.; Nitschke, J. R., *J. Am. Chem. Soc.* **2015**, *137* (32), 10068-10071.

1.10 Stimuli-responsive metal ligand self-assemblies

A substantial focus of metal-template self-assemblies has been on their guest binding properties, as models for complex biological phenomena, and their aesthetically pleasing nature. The next step in this evolution is to incorporate stimuli-responsive subunits into the self-assembled structure. In one sense, all self-assembled structures are responsive to stimuli as the methods used to construct such architectures are dynamic by their very nature. This means that perturbation of the system (heating, solvent, guest exchange, etc.) must affect the self-assembled species. These changes are often subtle; for example, changes in the conformation of the assembly upon binding a guest molecule. This responsive behaviour can be complex and difficult to predict. More appealing is the incorporation of stimuli responsive units into the framework of the self-assembled structure, as this can lead to more predictable responses based on the known behaviour of the free ligand. Numerous stimuli have been used to perturb supramolecular assemblies including light, guest molecules, pH change, coordinating anions, competing ligands and solvent change.⁷⁷

1.10.1 Guest responsive architectures

An early example of control of structure by a guest molecule was shown by Raymond and co-workers. Conversion between a M_2L_3 or M_4L_6 architecture is controlled by the presence of a NMe_4^+ guest (Figure 1.11).⁷⁸ The strong host-guest interaction shifts

the equilibrium, accompanied by subtle variation in the ligand framework to relieve strain. A closely related concept is templating the formation of a larger species around an anion, which has been exploited in many examples.⁷⁹ An elegant example was shown by Nitschke and co-workers,⁸⁰ where anion exchange led to the formation of new architectures. Specifically, introduction of triflate anions templated the formation of an M_4L_6 architecture, which was quantitatively converted to a $M_{10}L_{15}$ architecture upon addition of perchlorate anions. This control of structure by the application of chemical stimuli is suggestive of the complex responses seen in biology induced by relatively small changes.

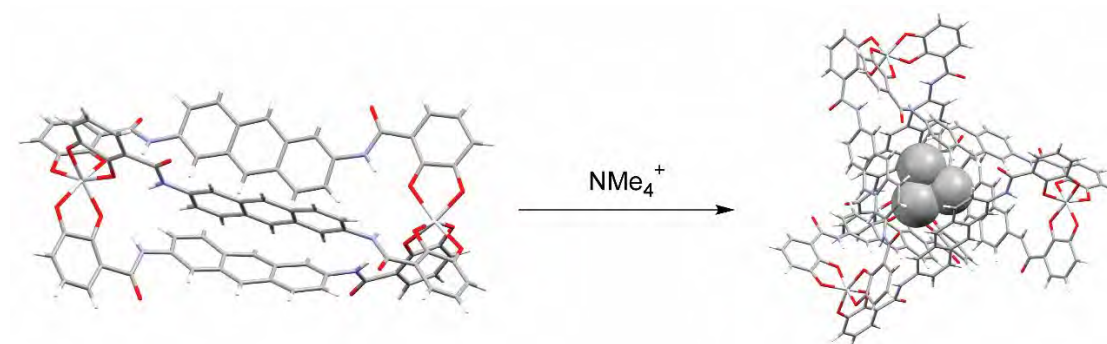


Figure 1.11 Configurational conversion between a M_2L_3 helicate and M_4L_6 tetrahedron induced by guest binding. X-Ray structures are shown as capped stick models excluding the encapsulated NMe_4^+ cation. Solvent and anion have been omitted for clarity.

1.10.2 Competing ligands

An example of the complexity that can be rapidly generated by using competing ligands as a stimuli response was explored by Hardie and co-workers (Figure 1.12).⁸¹ Combining pyridyl substituted cyclotrimeratrylene units with palladium(II) led to the formation of large $[Pd_6L_8]^{12+}$ cages. Addition of DMAP led to disassembly of the cage into the uncoordinated ligands and the mononuclear $[Pd(DMAP)_4]^{2+}$ complex. Subsequent addition of palladium(II) or *p*-toluenesulfonic acid led to reformation of heteroleptic cages. Further ligand addition reforms the initial homoleptic cages slowly. These stimuli responsive behaviours in well-defined structures inform models for less well-defined structures. In these cases, controlled disassembly could also be used to release or deliver an internally bound guest, changing the local environment.

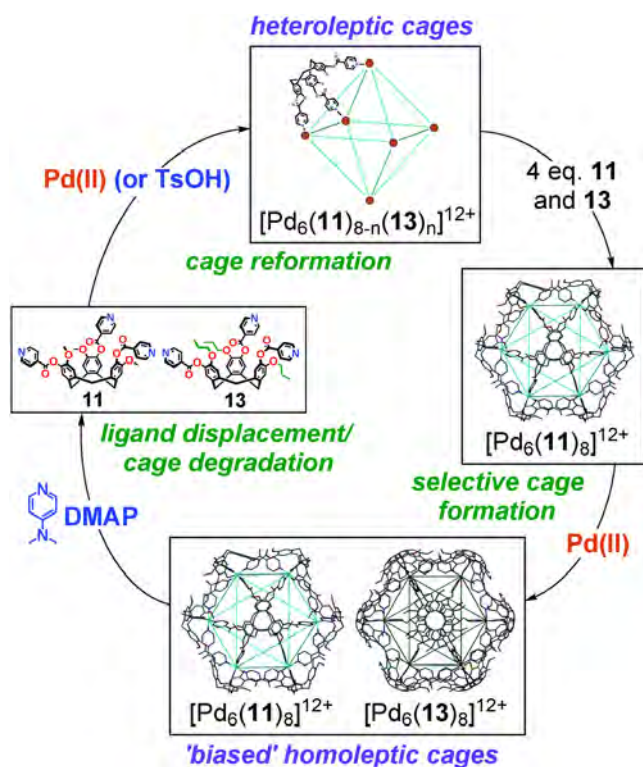


Figure 1.12 Sequential stimuli-response of a large cyclotrimeratrylene based metal-template assembly.⁸² Reproduced from Henkelis, J. J.; Hardie, M. J., *Chem. Commun.* **2015**, 51 (60), 11929-11943. Published by The Royal Society of Chemistry.

1.10.3 Guest release

The development of metal-template self-assemblies have often focused on their ability to bind guest molecules. It is important here to separate the thermodynamic and kinetics of guest binding. A guest may be strongly bound, reflected in a large binding constant, but have fast exchange kinetics or vice versa. This is especially important when discussing guest release mechanisms, as the application of stimuli will have different effects on fast or slow exchanging systems. A number of examples⁸³ show that the introduction of chemical stimuli or competing ligands alter the strength of the host-guest interaction, or cause the formation of a new assembly. Based on their expertise with $[\text{Pd}_2\text{L}_4]^{4+}$ cages, Crowley and co-workers explored the controlled release of cisplatin, triggered by the addition of chloride ions, a competitive ligand for palladium(II). Displacement of two of the dipyrindyl ligands by chloride leads to the formation of a $[\text{Pd}_2\text{L}_2]^{4+}$ metallocycle, and release of the guest molecule. Addition of silver(I) leads to the reformation of the $[\text{Pd}_2\text{L}_4]^{4+}$ architecture by sequestering the chloride ions.

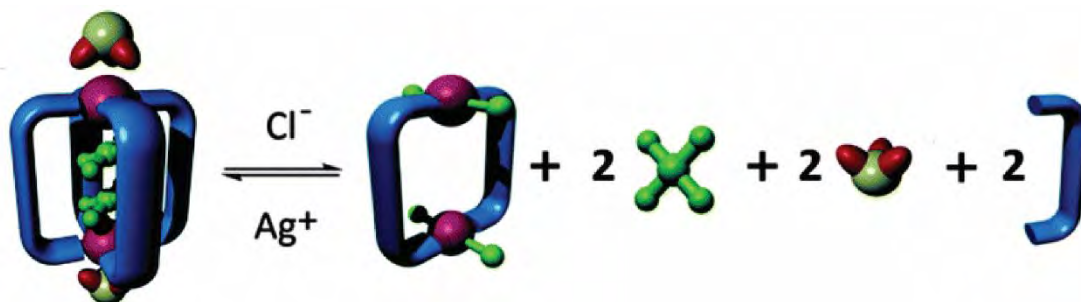


Figure 1.13 Disassembly of an $[\text{Pd}_2\text{L}_4]^{4+}$ architecture and guest release mediated by addition of chloride ions. Reproduced from Preston, D.; Fox-Charles, A.; Lo, W. K. C.; Crowley, J. D., *Chem. Commun.* **2015**, 51 (43), 9042-9045. Published by The Royal Society of Chemistry.

In examples where the stimulated response is ligand-centred, it is often unclear (and difficult to identify) if the structural change occurs on the assembled species. The lability of the metal-ligand bond (vital for supramolecular self-assembly) may allow the change to occur on the free ligand while not bound to the metal ion. This distinction is important in understanding the mechanism of guest release, for example, as “free” ligand switching will affect the kinetics of guest release differently to “on-cage” switching. For example, where the rate of ligand exchange is slow the overall rate of switching of the system is determined by this switching rate. If the system instead shows “on-cage” switching, the kinetics will be markedly different. The introduction of structural strain would generally seem to disfavour “on-cage” responsive behaviour, however some arguments have been made for this mechanism based on X-ray data of proposed intermediates.⁸⁴

1.11 Light responsive metal ligand self-assemblies

Light responsive assemblies can be divided into those where the photoswitching unit is a peripheral functionalisation and those where the photoswitch is integral to the structure of the assembly. An example of the former is the $[\text{Pd}_{12}\text{L}_{24}]^{24+}$ sphere explored by Fujita and co-workers with endohedral azobenzene units (Figure 1.14).^{48b} UV irradiation isomerises the azobenzene units, causing a change in hydrophobicity inside the cavity, leading to guest release.

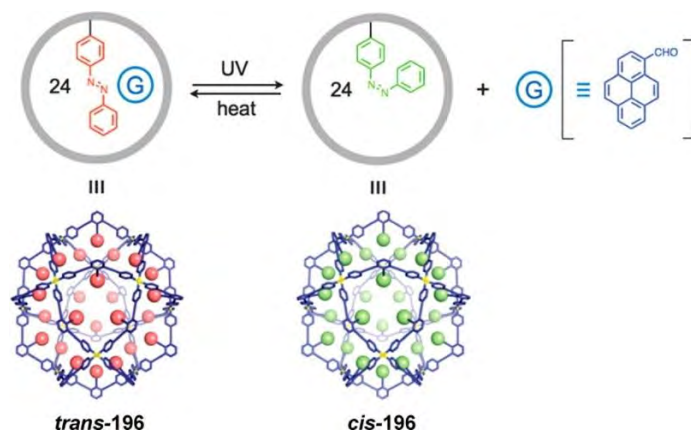


Figure 1.14 Modulation of the interior hydrophobicity of a metal-template self-assembly by azobenzene photoswitching. Copyright 2007 Wiley. Adapted with permission from Murase, T.; Sato, S.; Fujita, M., *Angew. Chem. Int. Ed.* **2007**, 46 (27), 5133-5136.

The second case is much rarer, owing to the additional restrictions placed on the photoswitching unit by self-assembly. In one landmark example, Lees and co-workers showed^{58b} three cases of reversible conversion between a tetranuclear and dinuclear macrocycle containing azobenzene or stilbene type ligands appended with pyridyl groups (Figure 1.15). In these cases, the geometry of the *Z*-isomer of the ligand favours the smaller macrocycle. The proposed mechanism of configurational change is dissociation of the ligand from the palladium ion and subsequent isomerisation in free solution.

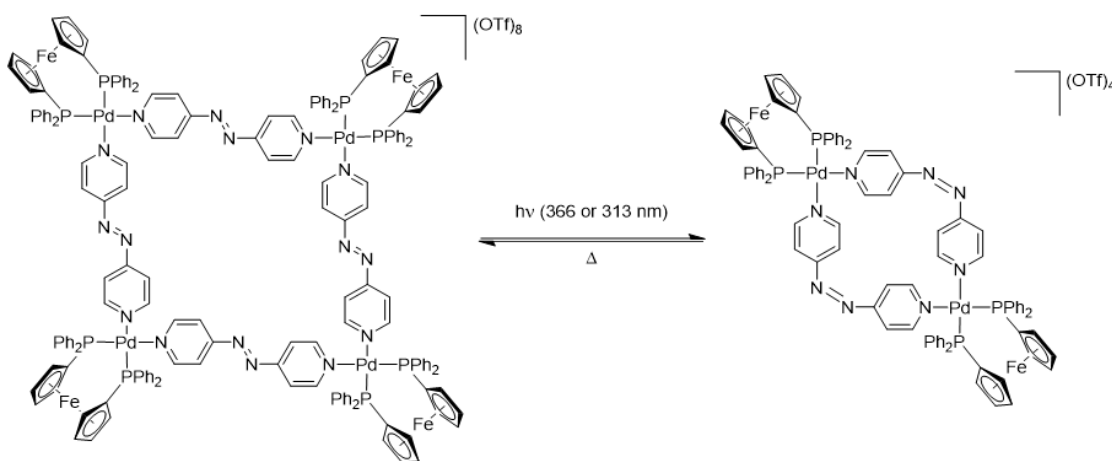


Figure 1.15 UV light controlled switching of configuration shown by Lees and co-workers

The most in-depth studies of switchable metal-template self-assemblies are those by Clever and co-workers. They have explored a variety of $[\text{Pd}_2\text{L}_4]^{4+}$ cage incorporating dithienylethene (DTE) photoswitching units.⁸⁴⁻⁸⁵ The ring-closing and opening is triggered by 365 nm and white light respectively, leading to two different cage structures depending on the ligand geometry. In both states the cages retain the $[\text{Pd}_2\text{L}_4]^{4+}$ architecture and were shown to have different affinities towards guest molecules,

allowing photo-controlled guest release.^{85a} A related example with a shorter linker led to the formation of a mixture of $[\text{Pd}_3\text{L}_6]^{6+}$ and $[\text{Pd}_4\text{L}_8]^{8+}$ architectures with the ring-open ligand (Figure 1.16).^{58a} Irradiation with 313 nm light promoted the ring-closing reaction, giving a more rigid divergent ligand. This led to very slow formation of a $[\text{Pd}_{24}\text{L}_{48}]^{48+}$ architecture, which was also observed to form when the ring-closed ligand was reacted with palladium(II).

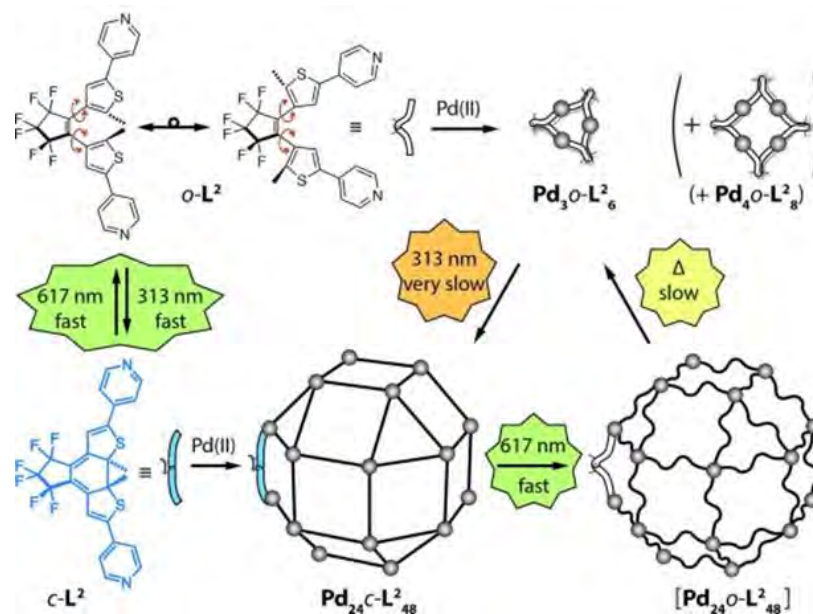


Figure 1.16 Light controlled conversion between a $[\text{Pd}_3\text{L}_6]^{6+}$ and $[\text{Pd}_{24}\text{L}_{48}]^{48+}$ assembly incorporating DTE units. Copyright 2016 Wiley. Adapted with permission from Han, M.; Luo, Y.; Damaschke, B.; Gómez, L.; Ribas, X.; Jose, A.; Peretzki, P.; Seibt, M.; Clever, G. H., *Angew. Chem. Int. Ed.* **2016**, 55 (1), 445-449.

1.12 Aims and outlines of this thesis

This thesis will outline methods to control structure and function with light, with an emphasis on bidirectional visible light photoswitching. The development of self-assembled structures incorporating photoactive units combines the benefits of directional and controllable self-assembly with responsive behaviours. This contributes to the ability to predict and rationally design self-assembled structures for a desired application.

Chapter 2 explores the incorporation of the photoactive unit tetraphenylethene (TPE) into larger self-assembled architectures using iron pyridyl-imine templation, to exploit this interesting functional unit for metal-template self-assembly. Generation of a $[\text{Fe}_2\text{L}_3]^{4+}$ helicate allowed access to unsymmetrical TPE derivatives, the photophysical properties of which were studied, including their self-assembly behaviour.

Chapter 3 summarises the problems with accurately determining photostationary state composition for photoswitches. This is a widely discussed problem in the literature, and no comprehensive methodologies have been developed. This chapter also outlines methodologies to calculate the ratio of isomers for some model systems.

Chapter 4 presents new azoheteroarene based visible light photoswitches, as a relatively underexplored class of photoswitches. The key photoswitching properties are discussed in depth, notably the ability to isomerise with visible light irradiation. The response to protonation is investigated, especially with regards to extending photoswitching well into the visible light spectrum.

Chapter 5 combines the knowledge from the previous chapters to incorporate photoswitches into larger self-assembled structures. *o*-Fluoroazobenzenes are derivatised for inclusion in larger structures, as the long thermal half-lives make them easier to study when incorporated into self-assembled systems. A visible light responsive system where irradiation leads to reversible and discrete configurational change is characterised and the details of the out-of-equilibrium behaviour are discussed.

This thesis is roughly ordered by increasing complexity. Initial investigation of self-assembled species does not look at stimuli-responsive behaviour, instead focusing on the unusual structure of the $[\text{Fe}_2\text{L}_3]^{4+}$ assembly. Similarly, the discussion of azoheteroarene photoswitches focuses on two stimuli, namely irradiation and protonation. This is limited to small organic molecules, with no incorporation into larger structures.

Building on this knowledge, I explored the intersection of these fields: incorporating photoswitchable molecules into self-assembled species. I then conclude with some avenues of future development.

1.13 References

1. Schultz, D. M.; Yoon, T. P., *Science* **2014**, *343* (6174), 1239176.
2. (a) Twilton, J.; Le, C.; Zhang, P.; Shaw, M. H.; Evans, R. W.; MacMillan, D. W. C., *Nat. Rev. Chem* **2017**, *1* (7), 0052; (b) Nicewicz, D. A.; MacMillan, D. W. C., *Science* **2008**, *322* (5898), 77-80; (c) König, B., *Eur. J. Org. Chem.* **2017**, *2017* (15), 1979-1981.
3. Rajasekharan Pillai, V. N., *Synthesis* **1980**, *1980* (01), 1-26.
4. (a) Mayer, G.; Heckel, A., *Angew. Chem. Int. Ed.* **2006**, *45* (30), 4900-4921; (b) Klán, P.; Šolomek, T.; Bochet, C. G.; Blanc, A.; Givens, R.; Rubina, M.; Popik, V.; Kostikov, A.; Wirz, J., *Chem. Rev.* **2013**, *113* (1), 119-191; (c) Yu, H.; Li, J.; Wu, D.; Qiu, Z.; Zhang, Y., *Chem. Soc. Rev.* **2010**, *39* (2), 464-473.
5. Feringa, B. L. B., Wesley R., *Molecular Switches*. 2 ed.; John Wiley & Sons: Weinheim, 2011; Vol. 1.
6. (a) Velema, W. A.; Szymanski, W.; Feringa, B. L., *J. Am. Chem. Soc.* **2014**, *136* (6), 2178-2191; (b) Broichhagen, J.; Frank, J. A.; Trauner, D., *Acc. Chem. Res.* **2015**, *48* (7), 1947-1960; (c) Pianowski, Z. L., *Chem.-Eur. J.* **2019**, *25* (20), 5128-5144.
7. (a) Natansohn, A.; Rochon, P., *Chem. Rev.* **2002**, *102* (11), 4139-4176; (b) Jochum, F. D.; Theato, P., *Chem. Soc. Rev.* **2013**, *42* (17), 7468-7483; (c) Kumar, K.; Knie, C.; Bléger, D.; Peletier, M. A.; Friedrich, H.; Hecht, S.; Broer, D. J.; Debije, M. G.; Schenning, A. P. H. J., *Nat. Commun.* **2016**, *7*, 11975; (d) Bushuyev, O. S.; Aizawa, M.; Shishido, A.; Barrett, C. J., *Macromol. Rapid Commun.* **2018**, *39* (1), 1700253; (e) Davidson-Rozenfeld, G.; Stricker, L.; Simke, J.; Fadeev, M.; Vázquez-González, M.; Ravoo, B. J.; Willner, I., *Polym. Chem.* **2019**, *10* (30), 4106-4115.
8. (a) Klajn, R.; Stoddart, J. F.; Grzybowski, B. A., *Chem. Soc. Rev.* **2010**, *39* (6), 2203-2237; (b) Kundu, P. K.; Samanta, D.; Leizrowice, R.; Margulis, B.; Zhao, H.; Börner, M.; Udayabhaskararao, T.; Manna, D.; Klajn, R., *Nat. Chem.* **2015**, *7*, 646.
9. (a) Takashima, Y.; Hatanaka, S.; Otsubo, M.; Nakahata, M.; Kakuta, T.; Hashidzume, A.; Yamaguchi, H.; Harada, A., *Nat. Commun.* **2012**, *3*, 1270; (b) Iamsaard, S.; Aßhoff, S. J.; Matt, B.; Kudernac, T.; Cornelissen, J. J. L. M.; Fletcher, S. P.; Katsonis, N., *Nat. Chem.* **2014**, *6*, 229; (c) Nie, H.; Self, J. L.; Kuenstler, A. S.; Hayward, R. C.; Read de Alaniz, J., *Adv. Optical Mater.* **2019**, *7* (16), 1900224.
10. (a) Harada, A., *Acc. Chem. Res.* **2001**, *34* (6), 456-464; (b) Browne, W. R.; Feringa, B. L., *Nat. Nanotechnol.* **2006**, *1* (1), 25-35; (c) Ragazzon, G.; Baroncini, M.; Silvi, S.; Venturi, M.; Credi, A., *Nat. Nanotechnol.* **2014**, *10*, 70; (d) Baroncini, M.; Silvi, S.; Venturi, M.; Credi, A., *Angew. Chem. Int. Ed.* **2012**, *51* (17), 4223-4226; (e) Erbas-Cakmak, S.; Leigh, D. A.; McTernan, C. T.; Nussbaumer, A. L., *Chem. Rev.* **2015**, *115* (18), 10081-10206.
11. Balzani, V.; Credi, A.; Venturi, M., *Chem. Soc. Rev.* **2009**, *38* (6), 1542-1550.
12. Bandara, H. M. D.; Burdette, S. C., *Chem. Soc. Rev.* **2012**, *41* (5), 1809-1825.

13. Irie, M., *Chem. Rev.* **2000**, *100* (5), 1685-1716.
14. Lerch, M. M.; Szymański, W.; Feringa, B. L., *Chem. Soc. Rev.* **2018**, *47* (6), 1910-1937.
15. (a) Berkovic, G.; Krongauz, V.; Weiss, V., *Chem. Rev.* **2000**, *100* (5), 1741-1754; (b) Minkin, V. I., *Chem. Rev.* **2004**, *104* (5), 2751-2776.
16. (a) Hartley, G. S., *Nature* **1937**, *140* (3537), 281-281; (b) Hartley, G. S., *Journal of the Chemical Society (Resumed)* **1938**, 10.1039/JR9380000633, 633-642; (c) Cembran, A.; Bernardi, F.; Garavelli, M.; Gagliardi, L.; Orlandi, G., *J. Am. Chem. Soc.* **2004**, *126* (10), 3234-3243; (d) Russew, M.-M.; Hecht, S., *Adv. Mater.* **2010**, *22* (31), 3348-3360.
17. (a) Coelho, P. J.; Carvalho, L. M.; Fonseca, A. M. C.; Raposo, M. M. M., *Tetrahedron Lett.* **2006**, *47* (22), 3711-3714; (b) Klapötke, T. M.; Piercey, D. G., *Inorg. Chem.* **2011**, *50* (7), 2732-2734; (c) Wendler, T.; Schütt, C.; Näther, C.; Herges, R., *J. Org. Chem.* **2012**, *77* (7), 3284-3287; (d) He, J.; Kimani, F. W.; Jewett, J. C., *J. Am. Chem. Soc.* **2015**, *137* (31), 9764-9767; (e) Garcia-Amoros, J.; Cuadrado, A.; Reig, M.; De Waele, V.; Poizat, O.; Velasco, D., *Chem.-Eur. J.* **2015**, *21* (41), 14292-14296; (f) Kolarski, D.; Szymanski, W.; Feringa, B. L., *Org. Lett.* **2017**, *19* (19), 5090-5093; (g) Travieso-Puente, R.; Budzak, S.; Chen, J.; Stacko, P.; Jastrzebski, J. T. B. H.; Jacquemin, D.; Otten, E., *J. Am. Chem. Soc.* **2017**, *139* (9), 3328-3331; (h) Bartova, K.; Cechova, L.; Prochazkova, E.; Socha, O.; Janeba, Z.; Dracinsky, M., *J. Org. Chem.* **2017**, *82* (19), 10350-10359; (i) Devi, S.; Saraswat, M.; Grewal, S.; Venkataramani, S., *J. Org. Chem.* **2018**, *83* (8), 4307-4322; (j) Stricker, L.; Boeckmann, M.; Kirse, T. M.; Doltsinis, N. L.; Ravoo, B. J., *Chem.-Eur. J.* **2018**, *24* (34), 8639-8647; (k) Harris, J. D.; Moran, M. J.; Aprahamian, I., *Proc. Natl Acad. Sci. U. S. A.* **2018**, *115* (38), 9414-9422; (l) Simeth, N. A.; Crespi, S.; Fagnoni, M.; König, B., *J. Am. Chem. Soc.* **2018**, *140* (8), 2940-2946; (m) Crespi, S.; Simeth, N. A.; Bellisario, A.; Fagnoni, M.; König, B., *J. Phys. Chem. A* **2019**, *123* (9), 1814-1823; (n) Kumar, P.; Srivastava, A.; Sah, C.; Devi, S.; Venkataramani, S., *Chem.-Eur. J.* **2019**, *25*, 11924-11932.
18. Crespi, S.; Simeth, N. A.; König, B., *Nat. Rev. Chem* **2019**, *3* (3), 133-146.
19. Vitaku, E.; Smith, D. T.; Njardarson, J. T., *J. Med. Chem.* **2014**, *57* (24), 10257-10274.
20. (a) Thies, S.; Sell, H.; Schütt, C.; Bornholdt, C.; Näther, C.; Tuczek, F.; Herges, R., *J. Am. Chem. Soc.* **2011**, *133* (40), 16243-16250; (b) Venkataramani, S.; Jana, U.; Dommaschk, M.; Soennichsen, F. D.; Tuczek, F.; Herges, R., *Science* **2011**, *331* (6016), 445-448; (c) Thies, S.; Sell, H.; Bornholdt, C.; Schuett, C.; Koehler, F.; Tuczek, F.; Herges, R., *Chem.-Eur. J.* **2012**, *18* (51), 16358-16368; (d) Dommaschk, M.; Peters, M.; Gutzeit, F.; Schuett, C.; Naether, C.; Soennichsen, F. D.; Tiwar, S.; Riedel, C.; Boretius, S.; Herges, R., *J. Am. Chem. Soc.* **2015**, *137* (24), 7552-7555; (e) Heitmann, G.; Schuett, C.; Herges, R., *Eur. J. Org. Chem.* **2016**, *22*, 3817-3823; (f) Schütt, C.; Heitmann, G.; Wendler, T.; Krahwinkel, B.; Herges, R., *J. Org. Chem.* **2016**, *81* (3), 1206-1215.
21. (a) Joe, O.; Koichi, N., *Bull. Chem. Soc. Jpn.* **2004**, *77* (8), 1537-1544; (b) Joe, O.; Koichi, N.; M., B. J., *Chem. Lett.* **2004**, *33* (3), 356-357.
22. Weston, C. E.; Richardson, R. D.; Fuchter, M. J., *Chem. Commun.* **2016**, *52* (24), 4521-4524.
23. (a) Weston, C. E.; Richardson, R. D.; Haycock, P. R.; White, A. J. P.; Fuchter, M. J., *J. Am. Chem. Soc.* **2014**, *136* (34), 11878-11881; (b) Calbo, J.; Weston, C. E.; White, A. J. P.; Rzepa, H. S.; Contreras-García, J.; Fuchter, M. J., *J. Am. Chem. Soc.* **2017**, *139* (3), 1261-1274; (c) Gibson, R. S. L.; Calbo, J.; Fuchter, M. J.,

- ChemPhotoChem* **2019**, *3* (6), 372-377; (d) Stricker, L.; Fritz, E.-C.; Peterlechner, M.; Doltsinis, N. L.; Ravoo, B. J., *J. Am. Chem. Soc.* **2016**, *138* (13), 4547-4554; (e) Wang, Y.-T.; Liu, X.-Y.; Cui, G.; Fang, W.-H.; Thiel, W., *Angew. Chem., Int. Ed.* **2016**, *55* (45), 14009-14013; (f) Zhang, Z.-Y.; He, Y.; Zhou, Y.; Yu, C.; Han, L.; Li, T., *Chem.-Eur. J.* **2019**, *25* (58), 13402-13410.
24. (a) Bléger, D.; Schwarz, J.; Brouwer, A. M.; Hecht, S., *J. Am. Chem. Soc.* **2012**, *134* (51), 20597-20600; (b) Knie, C.; Utecht, M.; Zhao, F.; Kulla, H.; Kovalenko, S.; Brouwer, A. M.; Saalfrank, P.; Hecht, S.; Bléger, D., *Chem.-Eur. J.* **2014**, *20* (50), 16492-16501; (c) Siewertsen, R.; Neumann, H.; Buchheim-Stehn, B.; Herges, R.; Naether, C.; Renth, F.; Temps, F., *J. Am. Chem. Soc.* **2009**, *131* (43), 15594-+; (d) Beharry, A. A.; Sadovski, O.; Woolley, G. A., *J. Am. Chem. Soc.* **2011**, *133* (49), 19684-19687; (e) Bléger, D.; Hecht, S., *Angew. Chem. Int. Ed.* **2015**, *54* (39), 11338-11349.
25. (a) Beharry, A. A.; Woolley, G. A., *Chem. Soc. Rev.* **2011**, *40* (8), 4422-4437; (b) Samanta, S.; Babalhavaeji, A.; Dong, M. X.; Woolley, G. A., *Angew. Chem. Int. Ed.* **2013**, *52* (52), 14127-30; (c) Samanta, S.; Beharry, A. A.; Sadovski, O.; McCormick, T. M.; Babalhavaeji, A.; Tropepe, V.; Woolley, G. A., *J. Am. Chem. Soc.* **2013**, *135* (26), 9777-9784; (d) Dong, M.; Babalhavaeji, A.; Samanta, S.; Beharry, A. A.; Woolley, G. A., *Acc. Chem. Res.* **2015**, *48* (10), 2662-2670; (e) Szymański, W.; Beierle, J. M.; Kistemaker, H. A. V.; Velema, W. A.; Feringa, B. L., *Chem. Rev.* **2013**, *113* (8), 6114-6178; (f) Ferreira, R.; Nilsson, J. R.; Solano, C.; Andreasson, J.; Grotli, M., *Sci. Rep.* **2015**, *5*.
26. (a) Sadovski, O.; Beharry, A. A.; Zhang, F.; Woolley, G. A., *Angew. Chem. Int. Ed.* **2009**, *48* (8), 1484-1486; (b) Lentès, P.; Stadler, E.; Röhricht, F.; Brahm, A.; Gröbner, J.; Sönnichsen, F. D.; Gescheidt, G.; Herges, R., *J. Am. Chem. Soc.* **2019**, *141* (34), 13592-13600.
27. (a) Garcia-Amorós, J.; Nonell, S.; Velasco, D., *Chem. Commun.* **2012**, *48* (28), 3421-3423; (b) Garcia-Amorós, J.; Castro, M. C. R.; Coelho, P.; Raposo, M. M. M.; Velasco, D., *Chem. Commun.* **2013**, *49* (97), 11427-11429; (c) Garcia-Amorós, J.; Bučinskas, A.; Reig, M.; Nonell, S.; Velasco, D., *J. Mater. Chem. C* **2014**, *2* (3), 474-480.
28. (a) Garcia-Amorós, J.; Nonell, S.; Velasco, D., *Chem. Commun.* **2011**, *47* (13), 4022-4024; (b) Garcia-Amorós, J.; Díaz-Lobo, M.; Nonell, S.; Velasco, D., *Angew. Chem. Int. Ed.* **2012**, *51* (51), 12820-12823; (c) García-Amorós, J.; Velasco, D., *Beilstein J. Org. Chem.* **2012**, *8*, 1003-1017; (d) Garcia-Amorós, J.; Maerz, B.; Reig, M.; Cuadrado, A.; Blancafort, L.; Samoylova, E.; Velasco, D., *Chem.-Eur. J.* **2019**, *25* (32), 7726-7732.
29. (a) Dong, M.; Babalhavaeji, A.; Collins, C. V.; Jarrah, K.; Sadovski, O.; Dai, Q.; Woolley, G. A., *J. Am. Chem. Soc.* **2017**, *139* (38), 13483-13486; (b) Dong, M.; Babalhavaeji, A.; Hansen, M. J.; Kálmán, L.; Woolley, G. A., *Chem. Commun.* **2015**, *51* (65), 12981-12984.
30. (a) Sanchez, A. M.; Barra, M.; de Rossi, R. H., *J. Org. Chem.* **1999**, *64* (5), 1604-1609; (b) Sokalski, W. A.; Góra, R. W.; Bartkowiak, W.; Kobylński, P.; Sworakowski, J.; Chyla, A.; Leszczyński, J., *J. Chem. Phys.* **2001**, *114* (13), 5504-5508.
31. Hammerich, M.; Schütt, C.; Stähler, C.; Lentès, P.; Röhricht, F.; Höppner, R.; Herges, R., *J. Am. Chem. Soc.* **2016**, *138* (40), 13111-13114.
32. Yang, Y.; Hughes, R. P.; Aprahamian, I., *J. Am. Chem. Soc.* **2012**, *134* (37), 15221-15224.

33. Hendrikx, M.; ter Schiphorst, J.; van Heeswijk, E. P. A.; Koçer, G.; Knie, C.; Bléger, D.; Hecht, S.; Jonkheijm, P.; Broer, D. J.; Schenning, A. P. H. J., *Small* **2018**, *14* (50), 1803274.
34. Castellanos, S.; Goulet-Hanssens, A.; Zhao, F.; Dikhtiarenko, A.; Pustovarenko, A.; Hecht, S.; Gascon, J.; Kapteijn, F.; Bléger, D., *Chem.- Eur. J.* **2016**, *22* (2), 746-752.
35. Bohr, A., *Chemisches Zentralblatt* **1872**, *43*, Book 1 (21), 276-325.
36. (a) Hong, Y.; Lam, J. W. Y.; Tang, B. Z., *Chem. Soc. Rev.* **2011**, *40* (11), 5361-5388; (b) Mei, J.; Hong, Y.; Lam, J. W. Y.; Qin, A.; Tang, Y.; Tang, B. Z., *Adv. Mater.* **2014**, *26* (31), 5429-5479; (c) He, Z.; Ke, C.; Tang, B. Z., *ACS Omega* **2018**, *3* (3), 3267-3277.
37. Zhang, M.; Feng, G.; Song, Z.; Zhou, Y.-P.; Chao, H.-Y.; Yuan, D.; Tan, T. T. Y.; Guo, Z.; Hu, Z.; Tang, B. Z.; Liu, B.; Zhao, D., *J. Am. Chem. Soc.* **2014**, *136* (20), 7241-7244.
38. (a) Ascherl, L.; Sick, T.; Margraf, J. T.; Lapidus, S. H.; Calik, M.; Hettstedt, C.; Karaghiosoff, K.; Döblinger, M.; Clark, T.; Chapman, K. W.; Auras, F.; Bein, T., *Nat. Chem.* **2016**, *8* (4), 310-316; (b) Pang, Z.-F.; Xu, S.-Q.; Zhou, T.-Y.; Liang, R.-R.; Zhan, T.-G.; Zhao, X., *J. Am. Chem. Soc.* **2016**, *138* (14), 4710-3; (c) Dalapati, S.; Jin, E.; Addicoat, M.; Heine, T.; Jiang, D., *J. Am. Chem. Soc.* **2016**, *138* (18), 5797-5800.
39. Lin, Y.; Jiang, X.; Kim, S. T.; Alahakoon, S. B.; Hou, X.; Zhang, Z.; Thompson, C. M.; Smaldone, R. A.; Ke, C., *J. Am. Chem. Soc.* **2017**, *139* (21), 7172-7175.
40. Pigge, F. C.; Kapadia, P. P.; Swenson, D. C., *CrystEngComm* **2013**, *15* (21), 4386-4391.
41. Song, N.; Chen, D.-X.; Qiu, Y.-C.; Yang, X.-Y.; Xu, B.; Tian, W.; Yang, Y.-W., *Chem. Commun.* **2014**, *50* (60), 8231-8234.
42. Bai, W.; Wang, Z.; Tong, J.; Mei, J.; Qin, A.; Sun, J. Z.; Tang, B. Z., *Chem. Commun.* **2015**, *51* (6), 1089-1091.
43. (a) Qu, H.; Wang, Y.; Li, Z.; Wang, X.; Fang, H.; Tian, Z.; Cao, X., *J. Am. Chem. Soc.* **2017**, *139* (50), 18142-18145; (b) Feng, H.-T.; Yuan, Y.-X.; Xiong, J.-B.; Zheng, Y.-S.; Tang, B. Z., *Chem. Soc. Rev.* **2018**, *47* (19), 7452-7476; (c) Qu, H.; Tang, X.; Wang, X.; Li, Z.; Huang, Z.; Zhang, H.; Tian, Z.; Cao, X., *Chem. Sci.* **2018**, *9* (47), 8814-8818.
44. (a) Yan, X.; Wang, F.; Zheng, B.; Huang, F., *Chem. Soc. Rev.* **2012**, *41* (18), 6042-6065; (b) Yu, Z.; Hecht, S., *Angew. Chem. Int. Ed.* **2011**, *50* (7), 1640-1643; (c) Liao, X.; Chen, G.; Liu, X.; Chen, W.; Chen, F.; Jiang, M., *Angew. Chem. Int. Ed.* **2010**, *49* (26), 4409-4413.
45. Gohy, J.-F.; Zhao, Y., *Chem. Soc. Rev.* **2013**, *42* (17), 7117-7129.
46. (a) Klajn, R.; Bishop, K. J. M.; Grzybowski, B. A., *Proc. Natl Acad. Sci. U. S. A.* **2007**, *104* (25), 10305-10309; (b) Angelos, S.; Yang, Y.-W.; Khashab, N. M.; Stoddart, J. F.; Zink, J. I., *J. Am. Chem. Soc.* **2009**, *131* (32), 11344-11346; (c) Evans, S. D.; Johnson, S. R.; Ringsdorf, H.; Williams, L. M.; Wolf, H., *Langmuir* **1998**, *14* (22), 6436-6440.
47. (a) Park, J.; Yuan, D. Q.; Pham, K. T.; Li, J. R.; Yakovenko, A.; Zhou, H. C., *J. Am. Chem. Soc.* **2012**, *134* (1), 99-102; (b) Wang, Z. B.; Heinke, L.; Jelic, J.; Cakici, M.; Dommaschk, M.; Maurer, R. J.; Oberhofer, H.; Grosjean, S.; Herges, R.; Brase, S.; Reuter, K.; Woll, C., *PCCP* **2015**, *17* (22), 14582-14587; (c) Brown, J. W.; Henderson, B. L.; Kiesz, M. D.; Whalley, A. C.; Morris, W.; Grunder, S.; Deng, H. X.; Furukawa, H.; Zink, J. I.; Stoddart, J. F.; Yaghi, O. M., *Chem. Sci.* **2013**, *4* (7), 2858-2864.

48. (a) Oldknow, S.; Martir, D. R.; Pritchard, V. E.; Blitz, M. A.; Fishwick, Colin W. G.; Zysman-Colman, E.; Hardie, M. J., *Chem. Sci.* **2018**, *9* (42), 8150-8159; (b) Murase, T.; Sato, S.; Fujita, M., *Angew. Chem. Int. Ed.* **2007**, *46* (27), 5133-5136; (c) Tang, H.-S.; Zhu, N.; Yam, V. W.-W., *Organometallics* **2007**, *26* (1), 22-25; (d) Sakano, T.; Ohashi, T.; Yamanaka, M.; Kobayashi, K., *Org. Biomol. Chem.* **2015**, *13* (30), 8359-8364; (e) Díaz-Moscoso, A.; Arroyave, F. A.; Ballester, P., *Chem. Commun.* **2016**, *52* (14), 3046-3049; (f) Arroyave, F. A.; Ballester, P., *J. Org. Chem.* **2015**, *80* (21), 10866-10873; (g) Osorio-Planes, L.; Espelt, M.; Pericàs, M. A.; Ballester, P., *Chem. Sci.* **2014**, *5* (11), 4260-4264.
49. (a) Jiang, J.; Tong, X.; Zhao, Y., *J. Am. Chem. Soc.* **2005**, *127* (23), 8290-8291; (b) Goodwin, A. P.; Mynar, J. L.; Ma, Y.; Fleming, G. R.; Fréchet, J. M. J., *J. Am. Chem. Soc.* **2005**, *127* (28), 9952-9953.
50. Hubbard, F. P.; Abbott, N. L., *Langmuir* **2007**, *23* (9), 4819-4829.
51. Harada, A.; Takashima, Y.; Nakahata, M., *Acc. Chem. Res.* **2014**, *47* (7), 2128-2140.
52. Zhao, Y. L.; Stoddart, J. F., *Langmuir* **2009**, *25* (15), 8442-8446.
53. Wang, Y.; Ma, N.; Wang, Z.; Zhang, X., *Angew. Chem. Int. Ed.* **2007**, *46* (16), 2823-2826.
54. (a) Dube, H.; Ajami, D.; Rebek Jr., J., *Angew. Chem. Int. Ed.* **2010**, *49* (18), 3192-3195; (b) Dube, H.; Rebek Jr., J., *Angew. Chem. Int. Ed.* **2012**, *51* (13), 3207-3210; (c) Qu, D.-H.; Wang, Q.-C.; Zhang, Q.-W.; Ma, X.; Tian, H., *Chem. Rev.* **2015**, *115* (15), 7543-7588.
55. (a) Kathan, M.; Hecht, S., *Chem. Soc. Rev.* **2017**, *46* (18), 5536-5550; (b) Ragazzon, G.; Baroncini, M.; Silvi, S.; Venturi, M.; Credi, A., *Nat. Nanotechnol.* **2015**, *10* (1), 70-75.
56. Murakami, H.; Kawabuchi, A.; Kotoo, K.; Kunitake, M.; Nakashima, N., *J. Am. Chem. Soc.* **1997**, *119* (32), 7605-7606.
57. (a) Liu, M.; Yan, X.; Hu, M.; Chen, X.; Zhang, M.; Zheng, B.; Hu, X.; Shao, S.; Huang, F., *Org. Lett.* **2010**, *12* (11), 2558-2561; (b) Ryan, S. T. J.; del Barrio, J.; Suardiaz, R.; Ryan, D. F.; Rosta, E.; Scherman, O. A., *Angew. Chem. Int. Ed.* **2016**, *55* (52), 16096-16100.
58. (a) Han, M.; Luo, Y.; Damaschke, B.; Gómez, L.; Ribas, X.; Jose, A.; Peretzki, P.; Seibt, M.; Clever, G. H., *Angew. Chem. Int. Ed.* **2016**, *55* (1), 445-449; (b) Sun, S.-S.; Anspach, J. A.; Lees, A. J., *Inorg. Chem.* **2002**, *41* (7), 1862-1869; (c) Yan, X.; Xu, J.-F.; Cook, T. R.; Huang, F.; Yang, Q.-Z.; Tung, C.-H.; Stang, P. J., *Proc. Natl Acad. Sci. U. S. A.* **2014**, *111* (24), 8717-8722.
59. Dalgarno, S. J.; Power, N. P.; Atwood, J. L., *Coord. Chem. Rev.* **2008**, *252* (8), 825-841.
60. Steed, J. W., *Supramolecular chemistry*. 2nd ed. ed.; Chichester, UK : Wiley: Chichester, UK, 2009.
61. Dietrich-Buchecker, C. O.; Sauvage, J. P.; Kintzinger, J. P., *Tetrahedron Lett.* **1983**, *24* (46), 5095-5098.
62. Fujita, M.; Yazaki, J.; Ogura, K., *J. Am. Chem. Soc.* **1990**, *112* (14), 5645-5647.
63. Hasenknopf, B.; Lehn, J.-M.; Kneisel, B. O.; Baum, G.; Fenske, D., *Angew. Chem., Int. Ed. Engl.* **1996**, *35* (16), 1838-1840.
64. McMorran, D. A.; Steel, P. J., *Angew. Chem. Int. Ed.* **1998**, *37* (23), 3295-3297.
65. (a) Caulder, D. L.; Brückner, C.; Powers, R. E.; König, S.; Parac, T. N.; Leary, J. A.; Raymond, K. N., *J. Am. Chem. Soc.* **2001**, *123* (37), 8923-8938; (b) Fleming, J. S.; Mann, K. L. V.; Carraz, C.-A.; Psillakis, E.; Jeffery, J. C.; McCleverty, J. A.; Ward, M. D., *Angew. Chem. Int. Ed.* **1998**, *37* (9), 1279-1281; (c) Mal, P.;

- Breiner, B.; Rissanen, K.; Nitschke, J. R., *Science* **2009**, *324* (5935), 1697-1699; (d) Neelakandan, P. P.; Jimenez, A.; Nitschke, J. R., *Chem. Sci.* **2014**, *5* (3), 908-915; (e) Kaphan, D. M.; Levin, M. D.; Bergman, R. G.; Raymond, K. N.; Toste, F. D., *Science* **2015**, *350* (6265), 1235-1238; (f) Caulder, D. L.; Powers, R. E.; Parac, T. N.; Raymond, K. N., *Angew. Chem., Int. Ed.* **1998**, *37* (13-14), 1840-1843.
66. (a) Cullen, W.; Misuraca, M. C.; Hunter, C. A.; Williams, N. H.; Ward, M. D., *Nat. Chem.* **2016**, *8* (3), 231-236; (b) Turega, S.; Whitehead, M.; Hall, B. R.; Haddow, M. F.; Hunter, C. A.; Ward, M. D., *Chem. Commun.* **2012**, *48* (22), 2752-2754; (c) Suzuki, K.; Tominaga, M.; Kawano, M.; Fujita, M., *Chem. Commun.* **2009**, (13), 1638-1640.
67. (a) Fujita, M.; Oguro, D.; Miyazawa, M.; Oka, H.; Yamaguchi, K.; Ogura, K., *Nature* **1995**, *378* (6556), 469-471; (b) Tominaga, M.; Suzuki, K.; Murase, T.; Fujita, M., *J. Am. Chem. Soc.* **2005**, *127* (34), 11950-11951; (c) Sun, Q.-F.; Iwasa, J.; Ogawa, D.; Ishido, Y.; Sato, S.; Ozeki, T.; Sei, Y.; Yamaguchi, K.; Fujita, M., *Science* **2010**, *328* (5982), 1144-1147; (d) Sun, Q.-F.; Murase, T.; Sato, S.; Fujita, M., *Angew. Chem. Int. Ed.* **2011**, *50* (44), 10318-10321; (e) Harris, K.; Fujita, D.; Fujita, M., *Chem. Commun.* **2013**, *49* (60), 6703-6712.
68. (a) Paul, R. L.; Bell, Z. R.; Jeffery, J. C.; McCleverty, J. A.; Ward, M. D., *Proc. Natl Acad. Sci. U. S. A.* **2002**, *99* (8), 4883-4888; (b) Clever, G. H.; Tashiro, S.; Shionoya, M., *Angew. Chem. Int. Ed.* **2009**, *48* (38), 7010-7012; (c) Han, M.; Engelhard, D. M.; Clever, G. H., *Chem. Soc. Rev.* **2014**, *43* (6), 1848-1860; (d) Lewis, J. E. M.; Gavey, E. L.; Cameron, S. A.; Crowley, J. D., *Chem. Sci.* **2012**, *3* (3), 778-784; (e) Preston, D.; Barnsley, J. E.; Gordon, K. C.; Crowley, J. D., *J. Am. Chem. Soc.* **2016**, *138* (33), 10578-10585; (f) Yang, J.; Bhadbhade, M.; Donald, W. A.; Iranmanesh, H.; Moore, E. G.; Yan, H.; Beves, J. E., *Chem. Commun.* **2015**, *51* (21), 4465-4468.
69. (a) Fiedler, D.; Bergman, R. G.; Raymond, K. N., *Angew. Chem. Int. Ed.* **2004**, *43* (48), 6748-6751; (b) Leung, D. H.; Bergman, R. G.; Raymond, K. N., *J. Am. Chem. Soc.* **2007**, *129* (10), 2746-2747; (c) Pluth, M. D.; Bergman, R. G.; Raymond, K. N., *Angew. Chem. Int. Ed.* **2007**, *46* (45), 8587-8589; (d) Pluth, M. D.; Bergman, R. G.; Raymond, K. N., *Science* **2007**, *316* (5821), 85-88; (e) Pluth, M. D.; Bergman, R. G.; Raymond, K. N., *J. Am. Chem. Soc.* **2008**, *130* (34), 11423-11429; (f) Brown, C. J.; Bergman, R. G.; Raymond, K. N., *J. Am. Chem. Soc.* **2009**, *131* (48), 17530-17531; (g) Brown, C. J.; Miller, G. M.; Johnson, M. W.; Bergman, R. G.; Raymond, K. N., *J. Am. Chem. Soc.* **2011**, *133* (31), 11964-11966; (h) Wang, Z. J.; Brown, C. J.; Bergman, R. G.; Raymond, K. N.; Toste, F. D., *J. Am. Chem. Soc.* **2011**, *133* (19), 7358-7360; (i) Wang, Z. J.; Clary, K. N.; Bergman, R. G.; Raymond, K. N.; Toste, F. D., *Nat. Chem.* **2013**, *5* (2), 100-103; (j) Brown, C. J.; Toste, F. D.; Bergman, R. G.; Raymond, K. N., *Chem. Rev.* **2015**, *115* (9), 3012-3035.
70. (a) Yoshizawa, M.; Takeyama, Y.; Kusakawa, T.; Fujita, M., *Angew. Chem., Int. Ed.* **2002**, *41* (8), 1347-1349; (b) Yoshizawa, M.; Takeyama, Y.; Okano, T.; Fujita, M., *J. Am. Chem. Soc.* **2003**, *125* (11), 3243-3247; (c) Murase, T.; Horiuchi, S.; Fujita, M., *J. Am. Chem. Soc.* **2010**, *132* (9), 2866-2867.
71. Smulders, M. M. J.; Riddell, I. A.; Browne, C.; Nitschke, J. R., *Chem. Soc. Rev.* **2013**, *42* (4), 1728-1754.
72. (a) Fujita, D.; Ueda, Y.; Sato, S.; Yokoyama, H.; Mizuno, N.; Kumasaka, T.; Fujita, M., *Chem* **1** (1), 91-101; (b) Takeda, N.; Umemoto, K.; Yamaguchi, K.; Fujita, M., *Nature* **1999**, *398* (6730), 794-796.

73. Roberts, D. A.; Pilgrim, B. S.; Nitschke, J. R., *Chem. Soc. Rev.* **2018**, *47* (2), 626-644.
74. (a) Pilgrim, B. S.; Roberts, D. A.; Lohr, T. G.; Ronson, T. K.; Nitschke, J. R., *Nat. Chem.* **2017**, *9*, 1276; (b) Roberts, D. A.; Pilgrim, B. S.; Sirvinskaite, G.; Ronson, T. K.; Nitschke, J. R., *J. Am. Chem. Soc.* **2018**, *140* (30), 9616-9623; (c) Roberts, D. A.; Pilgrim, B. S.; Cooper, J. D.; Ronson, T. K.; Zarra, S.; Nitschke, J. R., *J. Am. Chem. Soc.* **2015**, *137* (32), 10068-10071.
75. (a) Young, M. C.; Johnson, A. M.; Hooley, R. J., *Chem. Commun.* **2014**, *50* (11), 1378-1380; (b) Holloway, L. R.; McGarraugh, H. H.; Young, M. C.; Sontising, W.; Beran, G. J. O.; Hooley, R. J., *Chem. Sci.* **2016**, *7* (7), 4423-4427; (c) Holloway, L. R.; Bogie, P. M.; Lyon, Y.; Julian, R. R.; Hooley, R. J., *Inorg. Chem.* **2017**, *56* (18), 11435-11442; (d) Bogie, P. M.; Holloway, L. R.; Lyon, Y.; Onishi, N. C.; Beran, G. J. O.; Julian, R. R.; Hooley, R. J., *Inorg. Chem.* **2018**, *57* (7), 4155-4163; (e) Brega, V.; Zeller, M.; He, Y.; Peter Lu, H.; Klosterman, J. K., *Chem. Commun.* **2015**, *51* (24), 5077-5080; (f) Frank, M.; Hey, J.; Balcioglu, I.; Chen, Y.-S.; Stalke, D.; Suenobu, T.; Fukuzumi, S.; Frauendorf, H.; Clever, G. H., *Angew. Chem. Int. Ed.* **2013**, *52* (38), 10102-10106.
76. Roberts, D. A.; Castilla, A. M.; Ronson, T. K.; Nitschke, J. R., *J. Am. Chem. Soc.* **2014**, *136* (23), 8201-8204.
77. (a) Wang, W.; Wang, Y.-X.; Yang, H.-B., *Chem. Soc. Rev.* **2016**, *45* (9), 2656-2693; (b) McConnell, A. J.; Wood, C. S.; Neelakandan, P. P.; Nitschke, J. R., *Chem. Rev.* **2015**, *115* (15), 7729-7793; (c) Goswami, A.; Saha, S.; Biswas, P. K.; Schmittel, M., *Chem. Rev.* **2020**, *120* (1), 125-199.
78. Scherer, M.; Caulder, D. L.; Johnson, D. W.; Raymond, K. N., *Angew. Chem. Int. Ed.* **1999**, *38* (11), 1587-1592.
79. Vilar, R., *Eur. J. Inorg. Chem.* **2008**, *2008* (3), 357-367.
80. Riddell, I. A.; Smulders, M. M. J.; Clegg, J. K.; Hristova, Y. R.; Breiner, B.; Thoburn, J. D.; Nitschke, J. R., *Nat. Chem.* **2012**, *4* (9), 751-756.
81. Henkelis, J. J.; Fisher, J.; Warriner, S. L.; Hardie, M. J., *Chem.-Eur. J.* **2014**, *20* (14), 4117-4125.
82. Henkelis, J. J.; Hardie, M. J., *Chem. Commun.* **2015**, *51* (60), 11929-11943.
83. (a) Preston, D.; Fox-Charles, A.; Lo, W. K. C.; Crowley, J. D., *Chem. Commun.* **2015**, *51* (43), 9042-9045; (b) Gan, Q.; Ronson, T. K.; Vosburg, D. A.; Thoburn, J. D.; Nitschke, J. R., *J. Am. Chem. Soc.* **2015**, *137* (5), 1770-1773; (c) Mal, P.; Schultz, D.; Beyeh, K.; Rissanen, K.; Nitschke, J. R., *Angew. Chem. Int. Ed.* **2008**, *47* (43), 8297-8301; (d) Zhang, D. W.; Ronson, T. K.; Guryel, S.; Thoburn, J. D.; Wales, D. J.; Nitschke, J. R., *J. Am. Chem. Soc.* **2019**, *141* (37), 14534-14538; (e) Jansze, S. M.; Cecot, G.; Severin, K., *Chem. Sci.* **2018**, *9* (18), 4253-4257; (f) Kim, T. Y.; Vasdev, R. A. S.; Preston, D.; Crowley, J. D., *Chem.-Eur. J.* **2018**, *24* (56), 14878-14890.
84. Li, R. J.; Han, M. X.; Tessarolo, J.; Holstein, J. J.; Lubben, J.; Dittrich, B.; Volkmann, C.; Finze, M.; Jenne, C.; Clever, G. H., *ChemPhotoChem* **2019**, *3* (6), 378-383.
85. (a) Han, M.; Michel, R.; He, B.; Chen, Y.-S.; Stalke, D.; John, M.; Clever, G. H., *Angew. Chem. Int. Ed.* **2013**, *52* (4), 1319-1323; (b) Li, R.-J.; Holstein, J. J.; Hiller, W. G.; Andréasson, J.; Clever, G. H., *J. Am. Chem. Soc.* **2019**, *141* (5), 2097-2103.

2 METAL TEMPLATE HELICATES OF TETRAPHENYLETHENE

This chapter is based on the following publication: A. D. W. Kennedy, N. de Haas, H. Iranmanesh, E. T. Luis, C. Shen, P. Wang, J. R. Price, W. A. Donald, J. Andréasson, F. Huang, and J. E. Beves, Diastereoselective control of tetraphenylethene reactivity by metal template self-assembly, *Chem. - Eur. J.*, **2019**, *25*, 5708-5718.

Contributions: Nicholas de Haas, Chao Shen and Dr Pi Wang all contributed to synthesis and characterisation for $[\text{Fe}_2(\mathbf{2.2})_3]^{4+}$, **2.3** and $[\text{Fe}(\mathbf{2.7})_3]^{2+}$. Dr Hasti Iranmanesh collected and initially refined the crystallographic data for $[\text{Fe}_2(\mathbf{2.2})_3](\text{PF}_6)_4$. Dr Jason Price advised on refinement of crystallographic data. Dr Ena Luis and Associate Professor Alex Donald collected mass spectrometry data. Professor Joakim Andréasson provided insight into electronic spectra and experimental design.

2.1 Summary

This chapter discusses the incorporation of tetraphenylethene (TPE) into larger self-assembled architectures. The reaction of amine functionalised TPE molecules with 2-pyridylcarboxaldehyde and iron(II) salts led to the formation of larger structures, which were unstable with respect to hydrolysis. The $[\text{Fe}_2\text{L}_3]^{4+}$ helicate generated after the hydrolysis was used to access unsymmetric TPE derivatives, which were then isolated as pure organic species. The photophysical properties of these molecules were studied, as well as their self-assembly behaviours in mixed solvent systems.

2.2 Tetraphenylethene in metallosupramolecular self-assembly

The well-defined geometry of the TPE unit is appealing for self-assembly into metallosupramolecular structures and a handful of examples having been reported using palladium(II),⁸⁶ platinum(II),⁸⁷ ruthenium(II),⁸⁸ silver(I)⁸⁹ or lanthanide⁹⁰ ions. Cube-like structures formed with iron(II) trifluoromethanesulfonate have been characterised in the solid state,⁹¹ (Figure 2.1) although solution state behaviour remains unclear, and a recent report of an analogous structure was reported using zinc(II) ions.⁹²

Considering the interesting properties of TPE and the promising results outlined above, we aimed to use the TPE unit to form imine chelate groups suitable for binding first row transition metal ions. Metal template self-assembled triple-stranded helicate⁹³ structures of the type M_2L_3 are well established in the literature, including through the use of one-pot syntheses of diimine chelate units from 2-pyridinecarboxaldehyde and

suitable diamine units.^{93c} Nitschke and co-workers have used a similar self-assembly approach to prepare an impressive collection of more elaborate functional assemblies,^{74a, 74b, 76, 83c, 94} including cubic M_8L_6 molecular cages from a C_4 -symmetric tetraaniline-functionalised porphyrin unit,^{94a, 95} and related structures.⁹⁶ Inspired by these reports, here we investigate the C_2 -symmetric 4,4',4'',4'''-(ethene-1,1,2,2-tetrayl)tetraaniline (**2.1**) as a component for metal-template self-assembly with iron(II) salts.

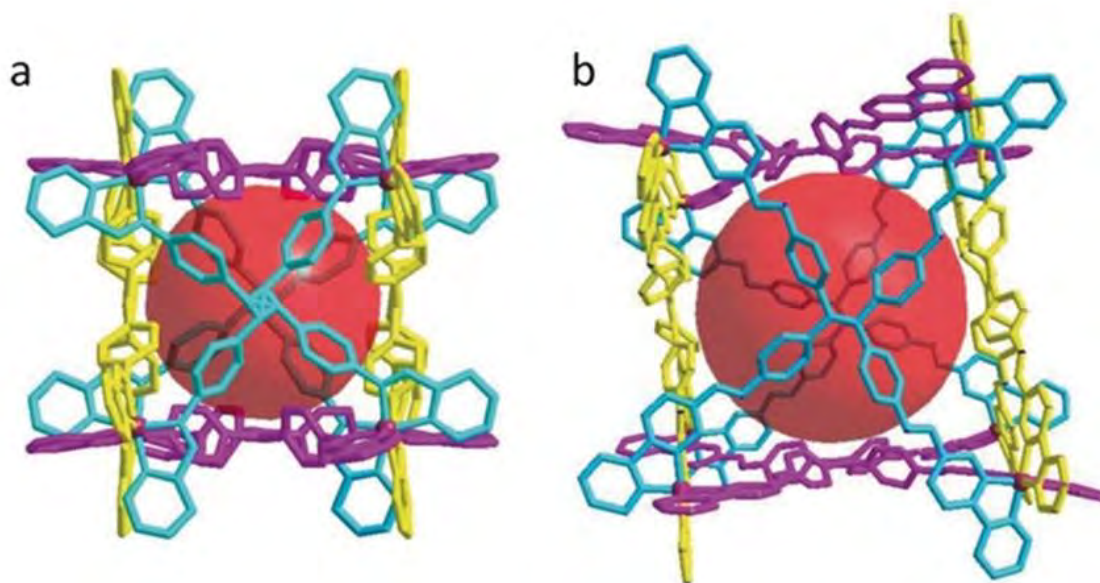
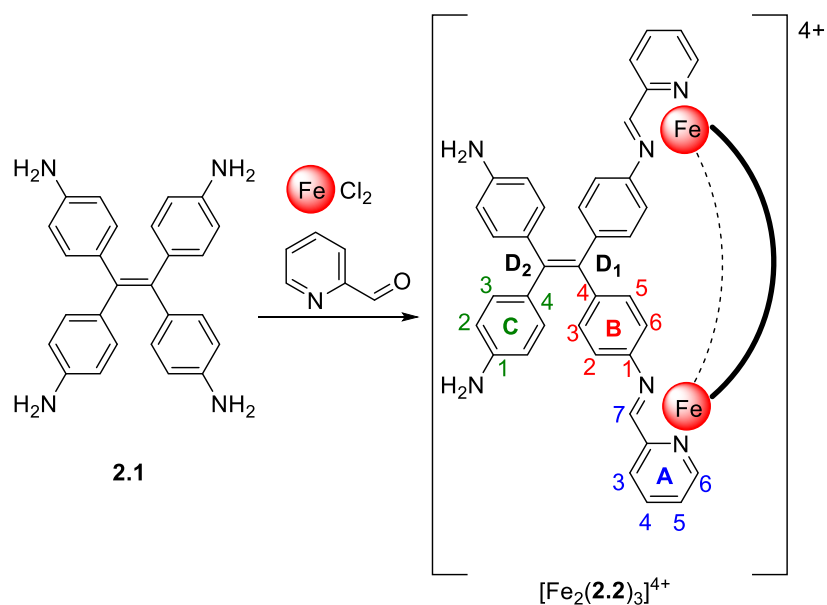


Figure 2.1 Stick representations of the crystal structures of $[Fe_8L_6]^{16+}$ TPE cages showing the coordination geometries of the iron ions and the internal cavity space (red ball). Solvent molecules, anions and hydrogen atom have been omitted for clarity. Copyright 2016 Wiley. Adapted from Yang, L.; Jing, X.; He, C.; Chang, Z.; Duan, C., *Chem.-Eur. J.* **2016**, *22* (50), 18107-18114.

2.3 Synthesis and identification of the $[Fe_2L_3]^{4+}$ species

Tetraaniline **2.1** was prepared in 76% yield following a literature procedure⁹⁷ by the reduction of 1,1,2,2-tetrakis(4-nitrophenyl)ethene⁹⁸ using Pd/C and hydrazine (See section 2.13.2). The reaction of tetraaniline **2.1** with iron(II) chloride and 2-pyridinecarboxaldehyde in ethanol or DMF, followed by anion exchange with aqueous potassium hexafluorophosphate gave a purple-red solid. This was identified as a single species by 1H NMR spectroscopy in CD_3CN (Scheme 2.1).



Scheme 2.1 Synthesis of triple-stranded helicate $[\text{Fe}_2(\mathbf{2.2})_3]^{4+}$ from tetraaniline **2.1**, 2-pyridinecarboxaldehyde and iron(II) chloride and the numbering scheme adopted.

Electrospray ionisation mass spectrometry (ESI-MS, Figure 2.2 and 7.12) identified the major species as the $[\text{Fe}_2(\mathbf{2.2})_3]^{4+}$ triple-stranded helicate shown in Scheme 2.1. The same product was obtained in up to 83% isolated yield and was not dependent on the stoichiometry of the reagents (see Section 7.5).

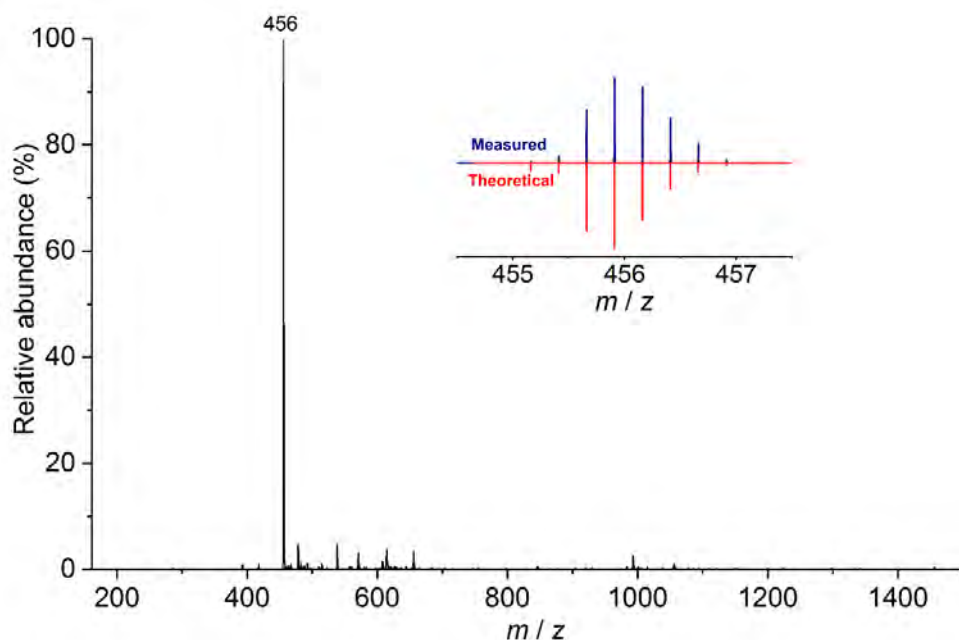


Figure 2.2 ESI-MS of $[\text{Fe}_2(\mathbf{2.2})_3]^{4+}$ in acetonitrile with an inset of the measured 4+ peak (blue) and theoretical values (red).

To account for stoichiometry differences, tetraimine **2.3** was formed by condensation of **2.1** and 2-pyridinecarboxaldehyde. The connectivity was confirmed by single crystal X-ray diffraction (Figure 2.3). Combination of tetraimine **2.3** with iron(II) chloride in DMF or ethanol gave, after workup, the same result as the self-assembly directly from tetraaniline **2.1**: exclusive isolation of the triple-stranded helicate product. This indicates that the formation of the helicate is not due to simple differences in stoichiometry, or due to slow formation of the tetraimine. It is also known that iron pyridyl-imine helicites can rearrange in solution to give larger species such as tetrahedra, however the helicate structure is stable in acetonitrile solution with no change in the ^1H NMR spectrum after prolonged heating (Figure 2.4). To further explore the factors controlling these assemblies, we considered the use of different anions and solvents.

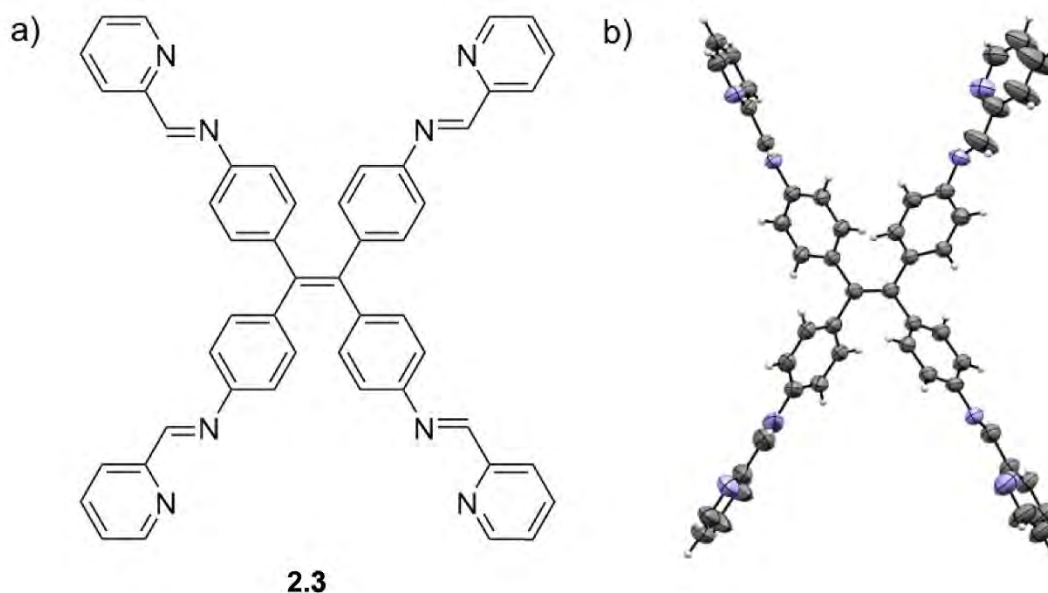


Figure 2.3 a) Structure of tetraimine ligand **2.3**. b) An ORTEP representation of the asymmetric unit of the X-ray crystal structure of **2.3** Thermal ellipsoids are drawn at 50% probability.

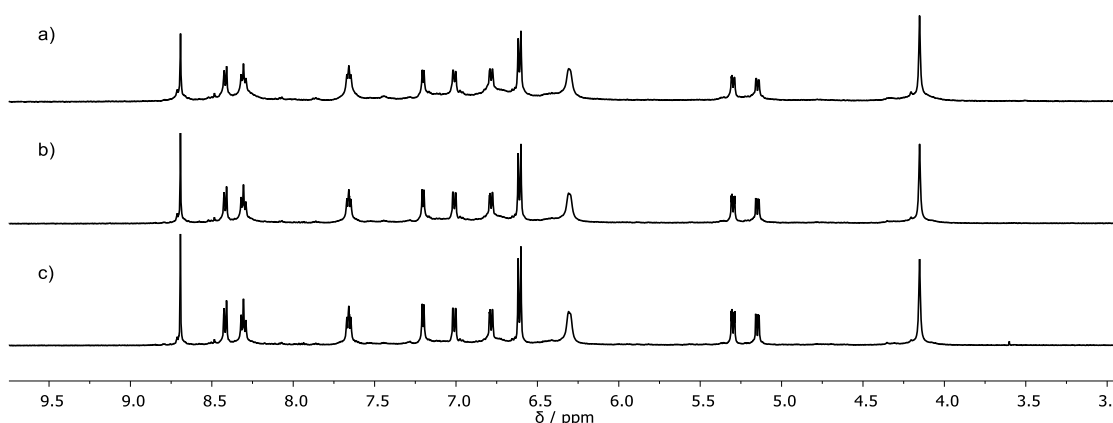


Figure 2.4 ^1H NMR (CD_3CN , 500 MHz, 298 K) spectra of $[\text{Fe}_2(\mathbf{2.2})_3]^{4+}$ a) initial spectra; b) after 2 h at 323 K and c) after 4 days at 323 K.

The use of $\text{Fe}(\text{BF}_4)_2 \cdot 6\text{H}_2\text{O}$ as the iron(II) source in DMF (see Sections 7.9.1-7.9.3) or acetonitrile (see sections 7.9.4-7.9.6) resulted in the formation of new products controlled by the reaction stoichiometry, with different ratios of tetraaniline **2.1**, 2-pyridinecarboxaldehyde and the iron salt giving mixtures of species which are difficult to assign by ^1H NMR spectroscopy. However, after aqueous workup the major species in all instances remained the $[\text{Fe}_2(\mathbf{2.2})_3]^{4+}$ triple-stranded helicate. Where iron(II) bistriflimide is used with tetraimine **2.3** in acetonitrile (Figure 2.5 and Section 7.10), the ^1H NMR spectrum features significantly broader signals, consistent with the formation of a complex mixture potentially containing unsymmetrical species (i.e. partial imine formation around the helicate) as well as larger assemblies.

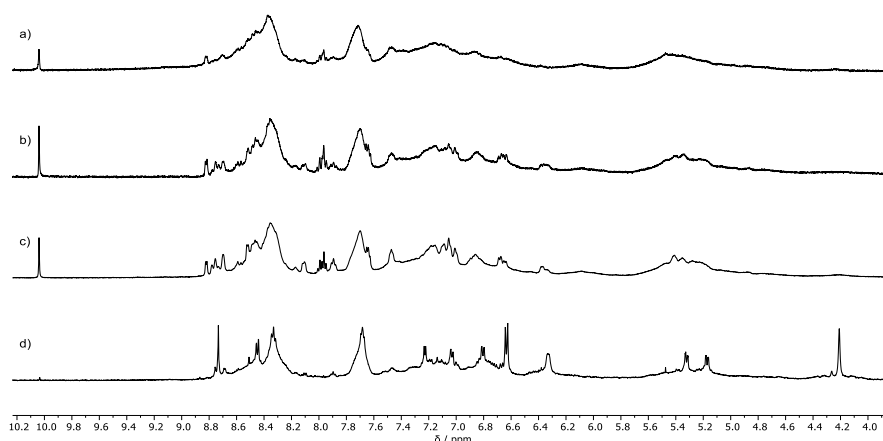
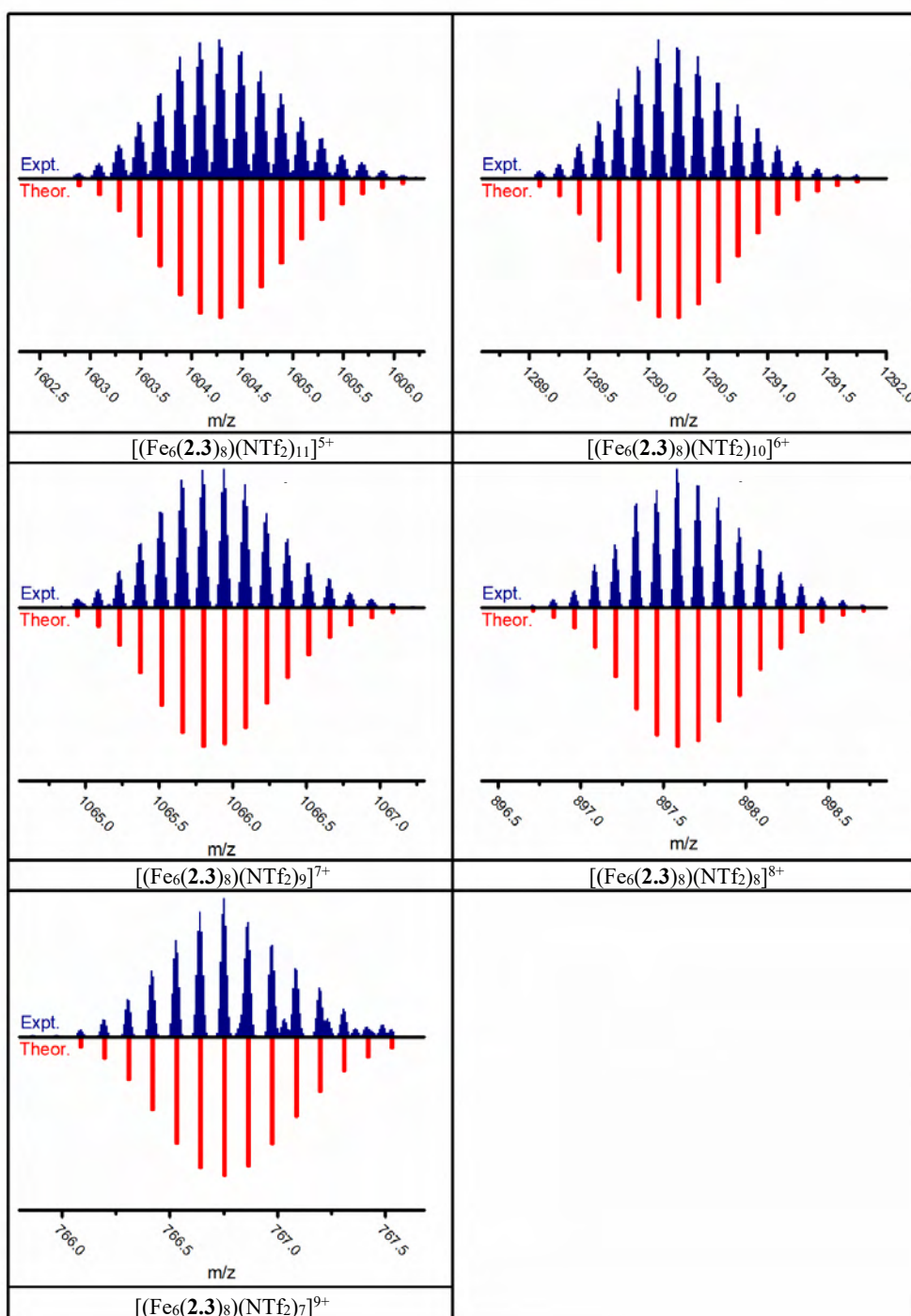


Figure 2.5 ^1H NMR spectrum (CD_3CN , 298K) of $\text{Fe}(\text{NTf}_2)_2 \cdot 4\text{H}_2\text{O}$ and tetraimine **2.3** after a) 24 h heating at 323K (400 MHz); b) 48 h (400 MHz); c) 7 days (500 MHz) and d) after aqueous workup as previously discussed (500 MHz). The major signals in d) are consistent with the $[\text{Fe}_2(\mathbf{2.2})_3]^{4+}$ species.

ESI-MS of this sample was consistent with the formation of a $[\text{Fe}_8(\mathbf{2.3})_6]^{16+}$ cube analogous to previous reports (Table 2.1).⁹¹ However, when this sample was subjected to aqueous work-up conditions, the major product is the $[\text{Fe}_2(\mathbf{2.2})_3]^{4+}$ helicate, indicating the aqueous work-up alters the equilibrium distribution of structures, leading to isolation of the triple-stranded helix.

Table 2.1 Zoom scans of select ESI-MS peaks (blue) for the $[\text{Fe}_6(\mathbf{2.3})_8]^{12+}$ cube, with simulated isotope patterns (red).



2.4 Characterisation of $[\text{Fe}_2(\mathbf{2.2})_3]^{4+}$ by NMR

The ^1H NMR spectrum of the self-assembled product (Figure 2.6c) showed the tetraaniline core was non-symmetrical, with signals for the phenyl rings being split into two groups. The typical shifts of the pyridyl ring on coordination are observed, with a significant upfield shift of the H^{A6} proton ($\Delta\delta = -1.6$ ppm, see Scheme 2.1 for labelling) due to shielding by an adjacent pyridine ring.⁹⁹ The phenyl ring closest to the metal centre (labelled ‘B’, Scheme 2.1) was found to exhibit slow rotation on the NMR timescale, to give four separate ^1H NMR signals, similar to that observed for literature examples of related self-assembled systems.^{94a} The ring furthest from the metal centre (labelled ‘C’) showed unrestricted rotation to give two ^1H NMR signals only. The aromatic ^1H NMR signals of $\text{H}^{\text{B2/B6}}$ are shifted upfield by over 1 ppm unit (from 6.36 ppm to 5.30 and 5.15 ppm respectively), consistent with shielding by adjacent phenyl rings. The ^1H NMR signals corresponding to the non-coordinated ring (H^{C2} , H^{C3}) are essentially unchanged between the free amine and the helicate, indicating this environment located on the periphery of the helicate is not significantly influenced by the helical core.

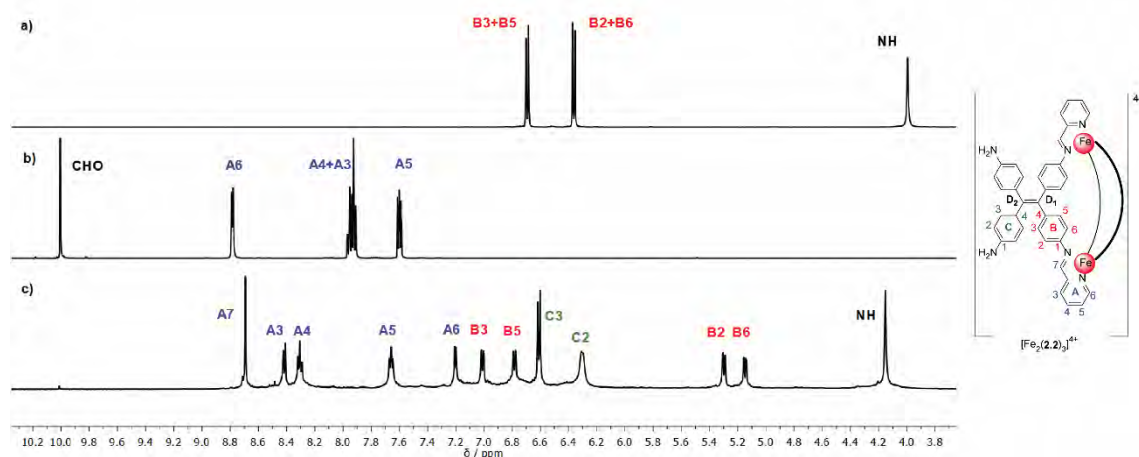


Figure 2.6 ^1H NMR (500 MHz, CD_3CN , 298 K) spectra of a) tetraaniline **2.1**, b) 2-pyridinecarboxaldehyde, c) $[\text{Fe}_2(\mathbf{2.2})_3]^{4+}$.

Variable temperature ^1H NMR spectra of $[\text{Fe}_2(\mathbf{2.2})_3](\text{PF}_6)_4$ in CD_3CN (Figure 7.14) showed a sharpening of the signals of the C ring upon heating, a result of the increased rate of exchange of the amine protons at higher temperature. However, the ^1H NMR signals of the ‘B’ ring broadened on heating, consistent with the proposed restricted rotation.

Two-dimensional NMR spectroscopy was used to unambiguously establish the structure of the $[\text{Fe}_2(\mathbf{2.2})_3]^{4+}$ helicate in solution (Figures 7.6-7.10). A ^1H - ^1H NOESY spectrum was used to identify interactions between rings (key NOE interactions shown in Figure 2.7 which allowed assignment of the ^1H signals of the B and C rings. Multinuclear ^1H - ^{13}C HSQC (Figure 7.7) and HMBC (Figure 2.8) spectra allowed identification of all quaternary carbons, and importantly confirmed the presence of two different quaternary alkene environments, with appropriate HMBC coupling to the protons on rings B and C (*i.e.*, $\text{H}^{\text{B}3}$ - $\text{C}^{\text{D}1}$; $\text{H}^{\text{B}5}$ - $\text{C}^{\text{D}1}$; $\text{H}^{\text{C}3}$ - $\text{C}^{\text{D}2}$). This allows assignment of the orientation of the ethylene bond and shows exclusive formation of the 1,1-isomer of the helicate in solution with no evidence for formation of the 1,2-isomer (Figure 2.9).

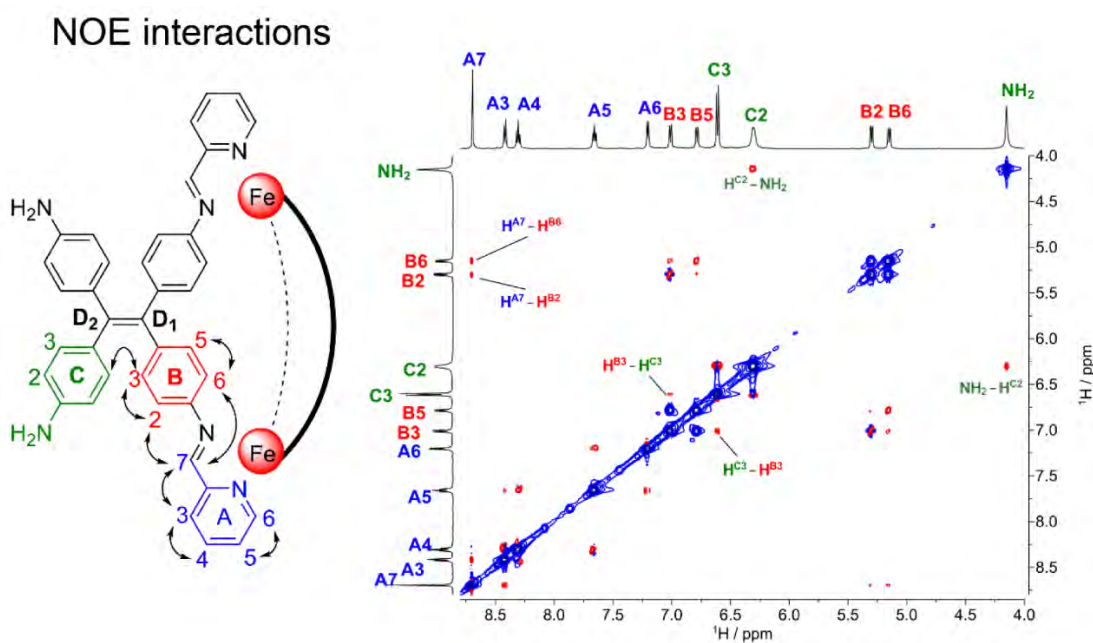


Figure 2.7 ^1H - ^1H NOESY (500 MHz, CD_3CN , 298 K) interactions observed for $[\text{Fe}_2(\mathbf{2.2})_3]^{4+}$ showing the interaction between $\text{H}^{\text{B}3}$ and $\text{H}^{\text{C}3}$, and $\text{H}^{\text{C}2}$ and the amine protons.

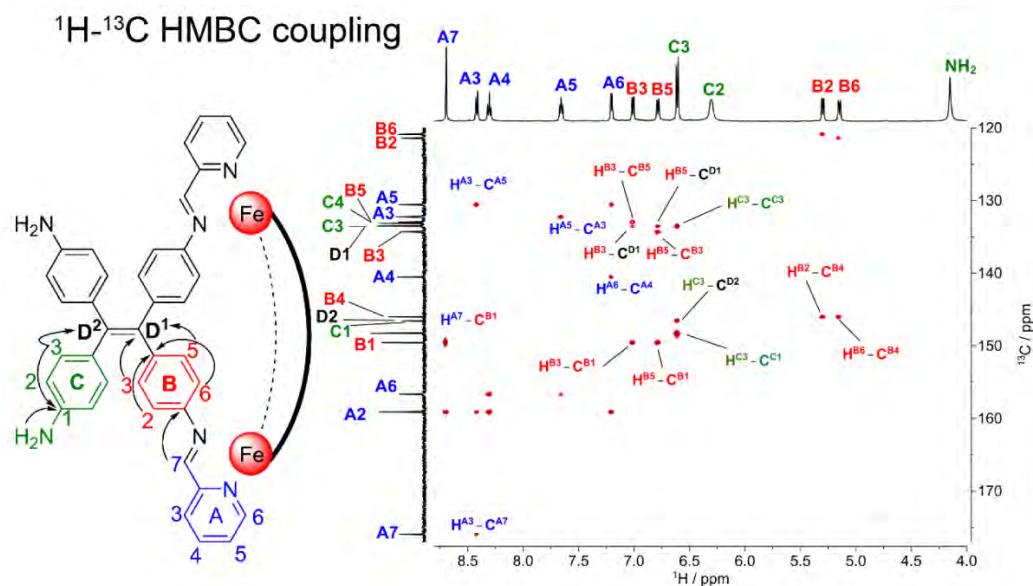


Figure 2.8 Observed ¹H-¹³C HMBC (600 MHz, CD₃CN, 298 K) couplings of [Fe₂(**2.2**)₃]⁴⁺.

The observed formation and stability of exclusively the 1,1-isomer of the helicate indicates the 1,2-isomer—a conformation that must be present in the [Fe₈(**2.3**)₆]¹⁶⁺ cube or any helicate formed with a mixture of 1,1- and 1,2-isomers—must be significantly less thermodynamically stable. An unfavourable distortion within the TPE unit as it coordinates to the iron(II) centre to produce the 1,2-isomer is the likely origin of the instability of these structures. Such unfavourable distortion does not appear to be required for the formation of the 1,1-isomer, allowing the observed stereoselective formation of the 1,1-helicate structure.

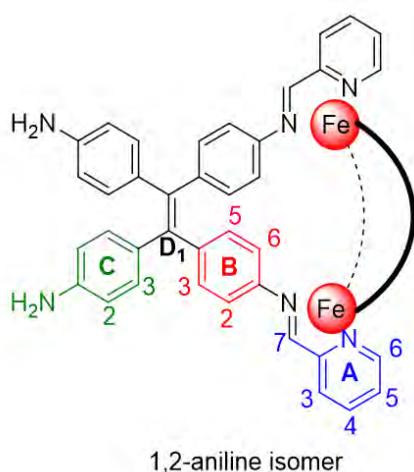


Figure 2.9 The structure of (non-observed) 1,2-isomer of [Fe₂(**2.2**)₃]⁴⁺.

2.5 X-Ray crystallography of $[\text{Fe}_2(\mathbf{2.2})_3](\text{PF}_6)_4$

Single crystals of $2[\text{Fe}_2(\mathbf{2.2})_3](\text{PF}_6)_8 \cdot \text{H}_2\text{O}$ were grown by slow evaporation of a DMF/MeOH solution of the complex. The asymmetric unit has two crystallographically independent but structurally similar¹⁰⁰ complexes and one is shown in Figure 2.10. The complex is the same 1,1-isomer as identified in solution by NMR spectroscopy. The two iron(II) centres are 11.4 Å apart and have the same stereochemistry with coordination geometries around the metal ions that are unremarkable. The overall crystal structure is racemic due to the presence of an inversion centre, allowing generation of the opposite enantiomer, for both crystallographically independent helicates. The $\text{N}_{\text{imine}} \cdots \text{N}_{\text{imine}}$ distances within one ligand range from 9.56(1) to 9.75(1) Å, which is consistent with expected values (e.g. separations of amine groups in the structure of tetrakis(4-dimethylaminophenyl)ethene are 9.578(9) and 9.636(8) Å, CSDCODE: GORFUO¹⁰¹). This is consistent with the ligand undergoing minimal strain to accommodate the metal centres. The central alkene bond lengths range from 1.34(2) to 1.38(1) Å, as expected for the formal double bond of unsubstituted TPE¹⁰² ($\text{C}=\text{C}$ 1.35 Å, CSDCODE: TPHETY¹⁰³). There are no significant differences between the $\text{C}_{\text{alkene}}-\text{C}_{\text{Ar}}$ bond lengths on the imine side of the TPE compared with the amine side (i.e. $\text{C}^{\text{D1}}-\text{C}^{\text{B4}}$ vs $\text{C}^{\text{D2}}-\text{C}^{\text{C4}}$, labelling in Scheme 1) with bond lengths ranging from 1.44(2) to 1.56(1) Å and from 1.45(2) to 1.52(2) Å respectively. These bond lengths are in the range expected for typical neutral TPE derivatives (e.g. the equivalent bond lengths for TPE = 1.49 Å, CSDCODE: TPHETY¹⁰³), indicating the introduction of positively charged metal centres adjacent to the TPE unit have minimal structural effects on the TPE unit.

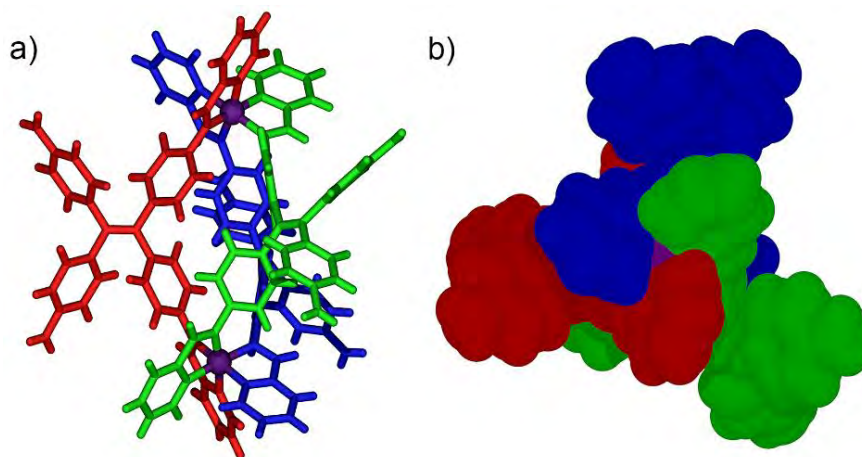
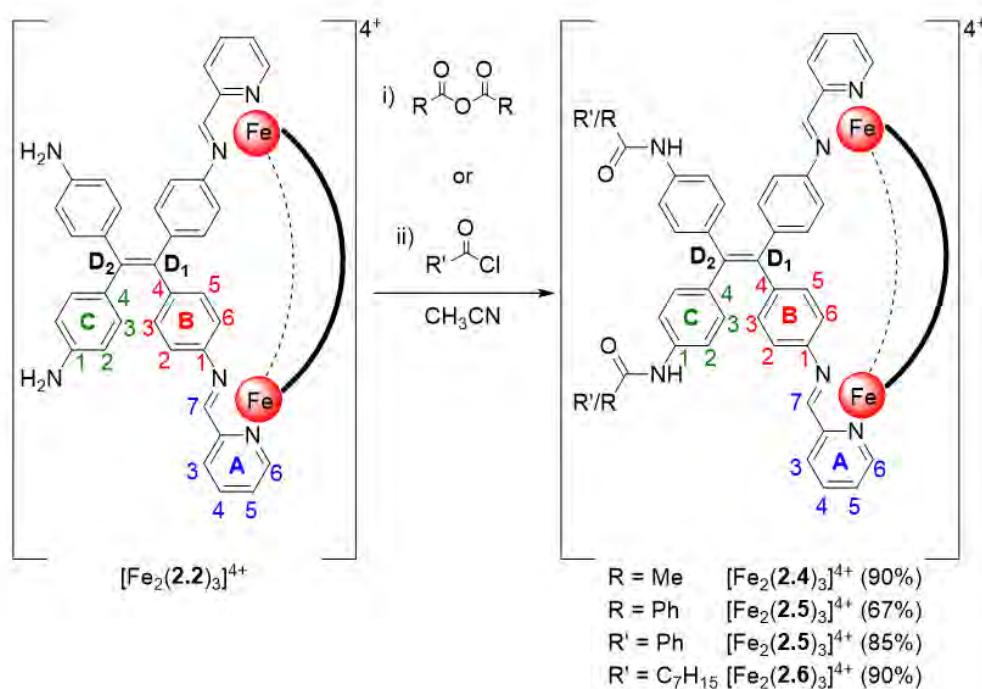


Figure 2.10 Single crystal X-ray structure of $2[\text{Fe}_2(\mathbf{2.2})_3](\text{PF}_6)_8 \cdot \text{H}_2\text{O}$. Anions and solvent have been omitted for clarity. a) Stick representation of one of the two cationic units in the structure, with the three independent ligands shown in red, blue, and green. b) CPK representation of the same cationic unit, viewed approximately down the crystallographic c axis.

2.6 Reactivity of $[\text{Fe}_2(\mathbf{2.2})_3]^{4+}$

Without the metal ion to template¹⁰⁴ the formation of the helicate, discrimination of reactivity between the different possible amine sites of **2.1** would be difficult. We looked to perform post-assembly modification^{73, 74b, 75a-d, 76, 105} upon the helicate to selectively functionalise the TPE core. Previous studies have shown that pendant amines of self-assembled structures can be modified using acylation and azidation.⁷⁶ The reaction of $[\text{Fe}_2(\mathbf{2.2})_3](\text{PF}_6)_4$ with acetic anhydride or benzoic anhydride in acetonitrile at 70 °C for 18 h gave the acylated helicates $[\text{Fe}_2(\mathbf{2.4})_3](\text{PF}_6)_4$ and $[\text{Fe}_2(\mathbf{2.5})_3](\text{PF}_6)_4$ in good yield (90 and 67% respectively), see Scheme 2.2. The success of these reactions also reflects the stability of the triple-stranded helicate product as despite extended heating in acetonitrile and the presence of multiple equivalents of acid (formed as a by-product of the amide formation), minimal cage degradation was observed. Although previous reports suggest similar self-assembled systems are not stable to chloride anions,⁷⁶ acylation can also be performed using acid chloride reagents. Reaction of $[\text{Fe}_2(\mathbf{2.2})_3](\text{PF}_6)_4$ with benzoyl chloride or octanoyl chloride in acetonitrile at room temperature for 2 h gave the acylated cages $[\text{Fe}_2(\mathbf{2.5})_3](\text{PF}_6)_4$ and $[\text{Fe}_2(\mathbf{2.6})_3](\text{PF}_6)_4$ in 85% and 90% yields respectively.



Scheme 2.2 Functionalisation of helicate $[\text{Fe}_2(\mathbf{2.2})_3](\text{PF}_6)_4$ by reaction with anhydrides or acyl chlorides.

The ^1H NMR spectra of the derivatised helicates are shown in Figure 2.11d-f, with additional spectra contained in Section 7.6. In all cases the ^1H NMR signal corresponding to the amine proton (4.15 ppm) is replaced by a new downfield signal ($[\text{Fe}_2(\mathbf{2.4})_3]^{4+}$ and $[\text{Fe}_2(\mathbf{2.6})_3]^{4+}$: 8.24 ppm; $[\text{Fe}_2(\mathbf{2.5})_3]^{4+}$: 8.69 ppm) consistent with the formation of an amide bond. The ^1H NMR signals corresponding to the non-coordinated ring ($\text{H}^{\text{C}2}$, $\text{H}^{\text{C}3}$) are both shifted downfield ($\Delta\delta \text{H}^{\text{C}3} \approx 0.3$ ppm; $\Delta\delta \text{H}^{\text{C}2} \approx 1.0$ ppm) and are sharper as the amide nitrogen undergoes slow proton exchange compared with the exchange rate of the free amine. The protons on the rings A and B do not shift significantly upon forming the amide, indicating the helical structure is retained upon functionalisation. Two-dimensional NMR techniques allowed unambiguous assignment of the derivatised helicates, analogous to that described for the parent helicate. The ^1H NMR signal of the amide proton is identified from the ^1H - ^{13}C HSQC spectrum, where no coupling is observed to a ^{13}C NMR signal.

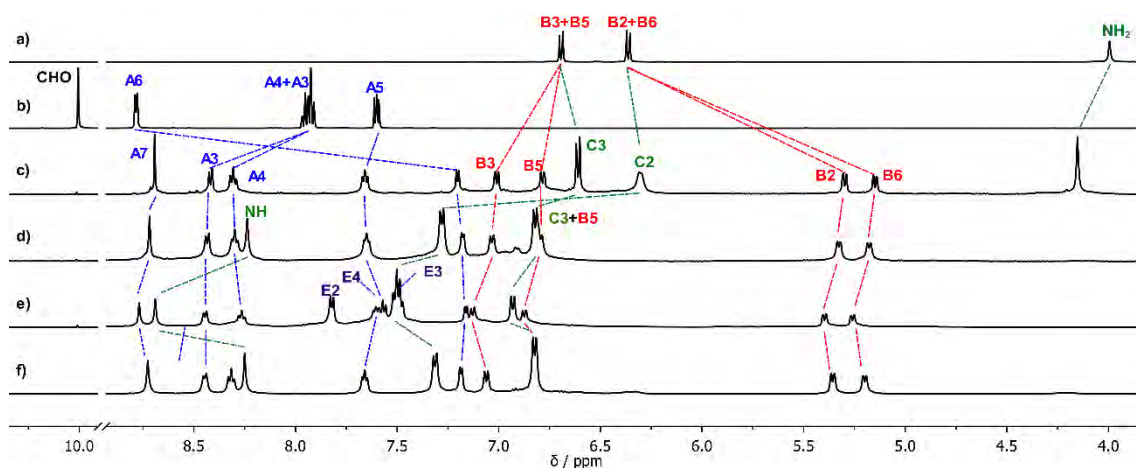


Figure 2.11 ^1H NMR (500 MHz, CD_3CN , 298 K) spectra of a) tetraaniline 1, b) 2-pyridinecarboxaldehyde, c) $[\text{Fe}_2(\mathbf{2.2})_3]^{4+}$, d) $[\text{Fe}_2(\mathbf{2.4})_3]^{4+}$, e) $[\text{Fe}_2(\mathbf{2.5})_3]^{4+}$ and f) $[\text{Fe}_2(\mathbf{2.6})_3]^{4+}$. See Scheme 1 for numbering scheme adopted.

In the ^1H - ^{13}C HMBC spectrum of $[\text{Fe}_2(\mathbf{2.5})_3]^{4+}$ (Figure 2.12 and Figure 2.13) connectivity can be traced from proton C2 on the aromatic ring, through the amide linkage and to proton E2 on the benzylic ring, confirming the formation of the benzylic amide. We see no evidence of lower symmetry structures (*i.e.* those with free amine groups) although this may be because such structures would have significantly reduced intensity in the ^1H NMR spectrum due to loss of symmetry.

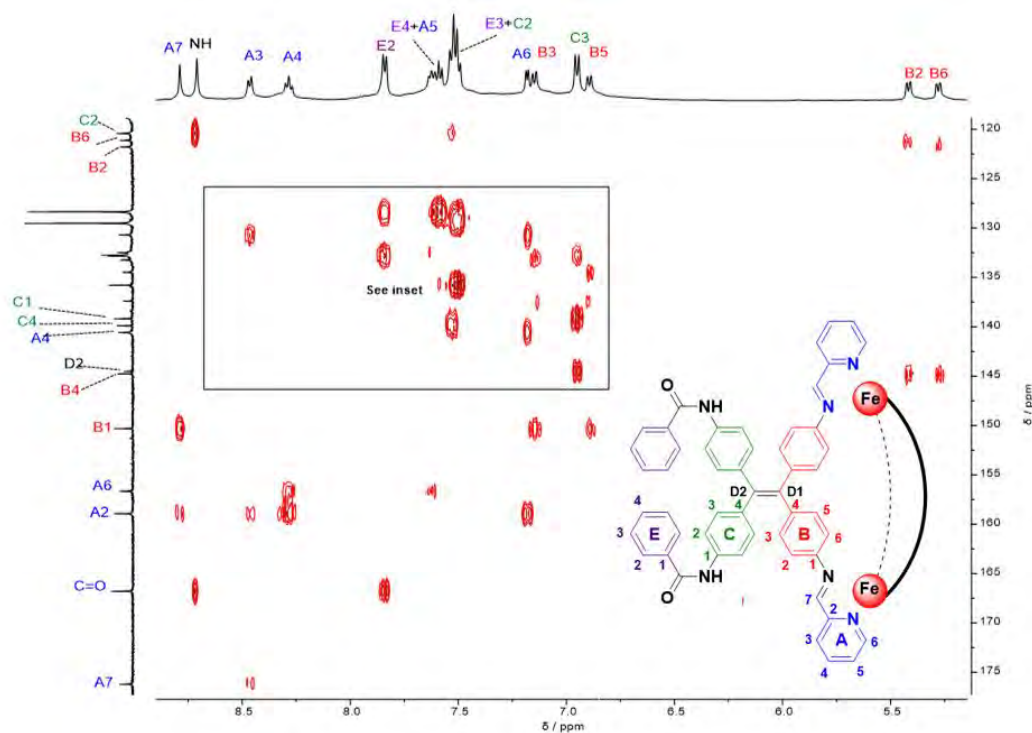


Figure 2.12 ^1H - ^{13}C HMBC spectrum (500 MHz, CD_3CN , 298 K) of $[\text{Fe}_2(\mathbf{2.5})_3]^{4+}$.

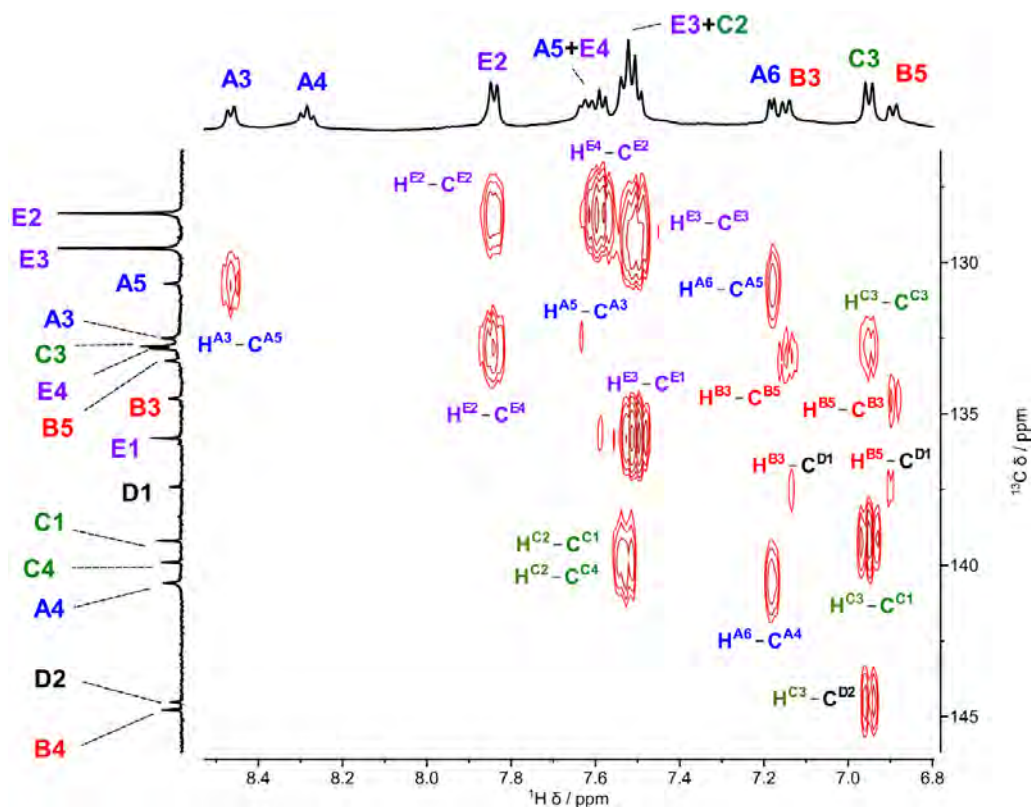


Figure 2.13 Partial ^1H - ^{13}C HMBC spectrum (500 MHz, CD_3CN , 298 K) of $[\text{Fe}_2(\mathbf{2.5})_3]^{4+}$ with relevant $^1\text{H} - ^{13}\text{C}$ couplings highlighted.

High resolution ESI-MS of helicates $[\text{Fe}_2(\mathbf{2.4})_3]^{4+}$, $[\text{Fe}_2(\mathbf{2.5})_3]^{4+}$, and $[\text{Fe}_2(\mathbf{2.6})_3]^{4+}$ showed a series of peaks with the formula $\text{M}^{n+} = [(\text{Fe}_2(\mathbf{L})_3) + (\text{PF}_6^-)_{4-n}]^{n+}$ where $n = 1-4$, which match the predicted isotope patterns and confirm the helicate structure is retained (See Figure 2.14 for a representative example and Figures 7.22–23, Figures 7.31–32 and Figures 7.36–37 for full isotope peak patterns). Unexpectedly, when samples of $[\text{Fe}_2(\mathbf{2.4})_3]^{4+}$ and $[\text{Fe}_2(\mathbf{2.5})_3]^{4+}$ were analysed under identical conditions to $[\text{Fe}_2(\mathbf{2.2})_3]^{4+}$ a number of additional ESI-MS peaks were observed consistent with $[\text{Fe}_4(\mathbf{L})_6]^{8+}$ and $[\text{Fe}_2(\mathbf{L})_4]^{4+}$ stoichiometries, potentially a tetrahedron and an intermediate between this and the helicate.

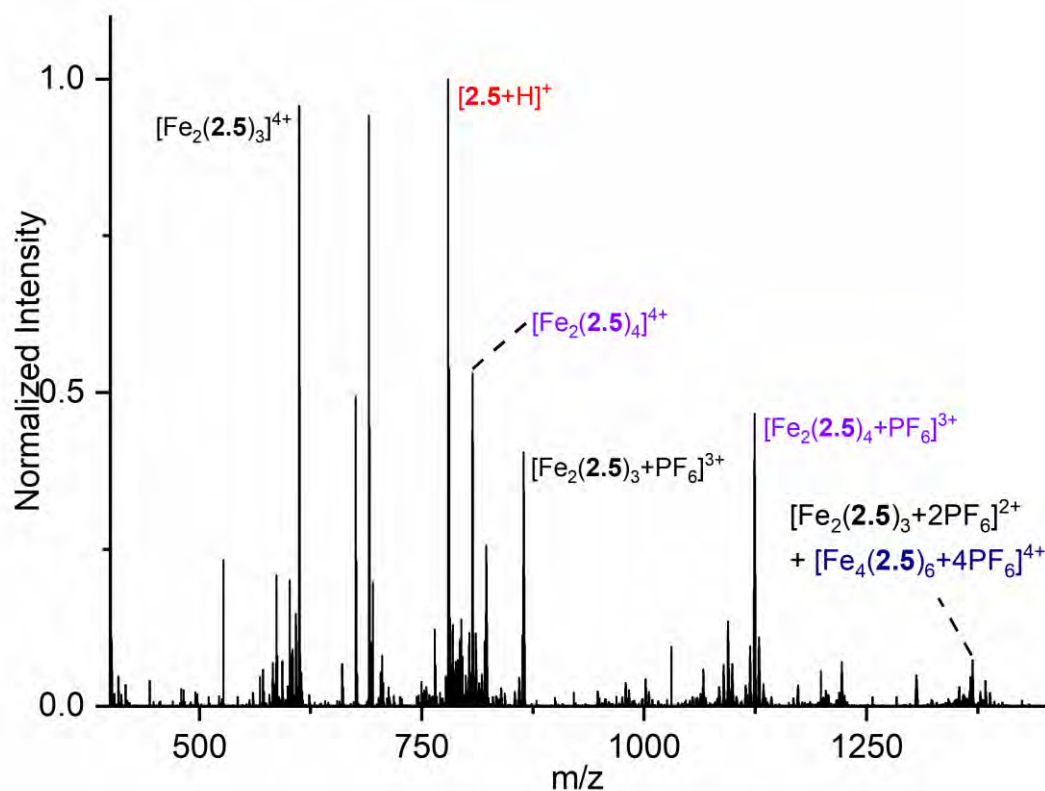


Figure 2.14 HR ESI-MS of $[\text{Fe}_2(\mathbf{2.5})_3]^{4+}$ helicite.

2.7 Diffusion ^1H NMR of self-assembled species

Diffusion NMR¹⁰⁶ is commonly used to probe the hydrodynamic radii of self-assembled systems to provide information about relative sizes of species in solution.^{58a, 107} Table 2.2 shows the diffusion coefficients and the calculated hydrodynamic radii for each of the self-assembled structures analysed here. Although the helicites possess significant shape anisotropy, the longest radius in the solid-state structure of $[\text{Fe}_2(\mathbf{2.2})_3]^{4+}$ (half the distance between the pendant nitrogen atoms = 9.8 Å) is in good agreement with the measured hydrodynamic radius (10.3 Å). The derivatised helicites all have larger hydrodynamic radii than the parent $[\text{Fe}_2(\mathbf{2.2})_3]^{4+}$ helicite with the largest calculated radii for the benzoyl derivatised $[\text{Fe}_2(\mathbf{2.5})_3]^{4+}$. No evidence for larger species was detected in the diffusion experiments. This indicates that if these species are present, as suggested by ESI-MS, then their abundance is insufficient to identify by ^1H NMR spectroscopy. Diffusion measurements were also performed on the $[\text{Fe}_8(\mathbf{2.3})_6]^{16+}$ cube assembly which was formed *in situ*, which has a diffusion coefficient corresponding to a hydrodynamic radius of 15.6 Å, in good agreement with the previous reported X-ray structure (half the longest axis = 13.2 Å).⁹¹

Table 2.2 Diffusion coefficients for selected compounds as calculated by NMR ^a

Complex	Diffusion coefficient / $10^{-10} \text{ m}^2 \text{ s}^{-1}$ ^b	Hydrodynamic radius / Å
[Fe ₂ (2.2) ₃](PF ₆) ₄	6.2 ± 0.2	10.3 ± 0.3
[Fe ₂ (2.4) ₃](PF ₆) ₄	5.6 ± 0.2	11.5 ± 0.5
[Fe ₂ (2.5) ₃](PF ₆) ₄	4.8 ± 0.1	13.4 ± 0.3
[Fe ₂ (2.6) ₃](PF ₆) ₄	5.4 ± 0.2	11.9 ± 0.5
[Fe ₈ (2.3) ₆](NTf) ₁₆	4.1 ± 0.1	15.6 ± 0.4

^a CD₃CN, 298 K, 500 MHz, all collected with $\delta = 2$ ms and $\Delta = 100$ ms. Average diffusion values were determined by fitting multiple ¹H NMR signals for each structure. Hydrodynamic radii were calculated using the Stokes-Einstein equation. ^b Errors are estimated as 3% for the diffusion coefficient as data fitting for any data set gives errors below 1%, which are not reasonable.

2.8 X-Ray crystallography of [Fe₂(**2.5**)₃](PF₆)₄

Single crystals of [Fe₂(**2.5**)₃](PF₆)₄ were grown by vapour diffusion of methyl *tert*-butyl ether into an acetonitrile solution of the complex. The crystals only diffracted to low angle; however, the data is sufficient to confirm connectivity. The asymmetric unit contains one iron centre, two PF₆⁻ anions, one complete ligand unit and half of another ligand unit. One of the PF₆ anions was substantially disordered and was restrained using the RIGU command in Olex2. The derivatised helicate structure is shown in Figure 2.15 below, showing the complete substitution around the periphery. As expected, the orientation of the TPE unit is retained upon benzoyl functionalisation. The distance between iron centres is 11.5 Å, comparable to [Fe₂(**2.2**)₃](PF₆)₄ and the longest axis distance is 28.1 Å, in agreement with the diffusion data.

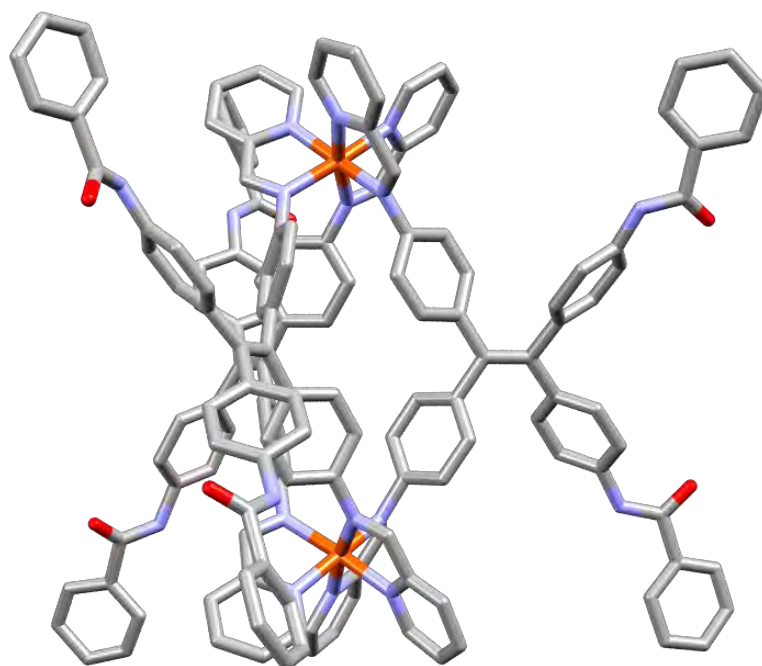


Figure 2.15 Stick representation of the single crystal X-ray structure of $[\text{Fe}_2(\mathbf{2.5})_3](\text{PF}_6)_4$. PF_6^- anions have been omitted for clarity

2.9 Electronic properties of iron(II) helicates

The UV-Vis spectra of helicates $[\text{Fe}_2(\mathbf{L})_3](\text{PF}_6)_4$, where $\mathbf{L} = \mathbf{2.2}, \mathbf{2.4-6}$ were each recorded in acetonitrile (Figure 2.16), and compared with the parent TPE **2.1**. Tetraaniline **2.1** has two strong absorptions centred at 276 and 348 nm, corresponding to the $\pi-\pi^*$ and $n-\pi^*$ transitions respectively. The $\pi-\pi^*$ transition is at approximately the same energy in $[\text{Fe}_2(\mathbf{2.2})_3](\text{PF}_6)_4$ as in the free ligand **2.1**, although two overlapping bands are observed, and the increase in absorptivity is proportional to the number of TPE units in the helicate. The lower energy $n-\pi^*$ transition is red-shifted from **2.1** to $[\text{Fe}_2(\mathbf{2.2})_3]^{4+}$ and is significantly broadened, overlapping with the metal centred and associated charge transfer transition(s). The lowest energy metal-to-ligand charge transfer absorption of the helicate is centred at 575 nm and is essentially identical to that of the mononuclear model complex $[\text{Fe}(\mathbf{2.7})_3](\text{PF}_6)_2$ (**2.7** = 1-(pyridin-2-yl)-*N*-(*p*-tolyl)methanimine, see Section 2.13.4), suggesting that the responsible chromophore is largely localised on the pyridyl-imine unit with little involvement of the TPE unit. This is also consistent with the solid-state X-ray data where no significant difference in the TPE bond lengths is observed upon coordination of the pendant chelate groups to the iron(II) centres.

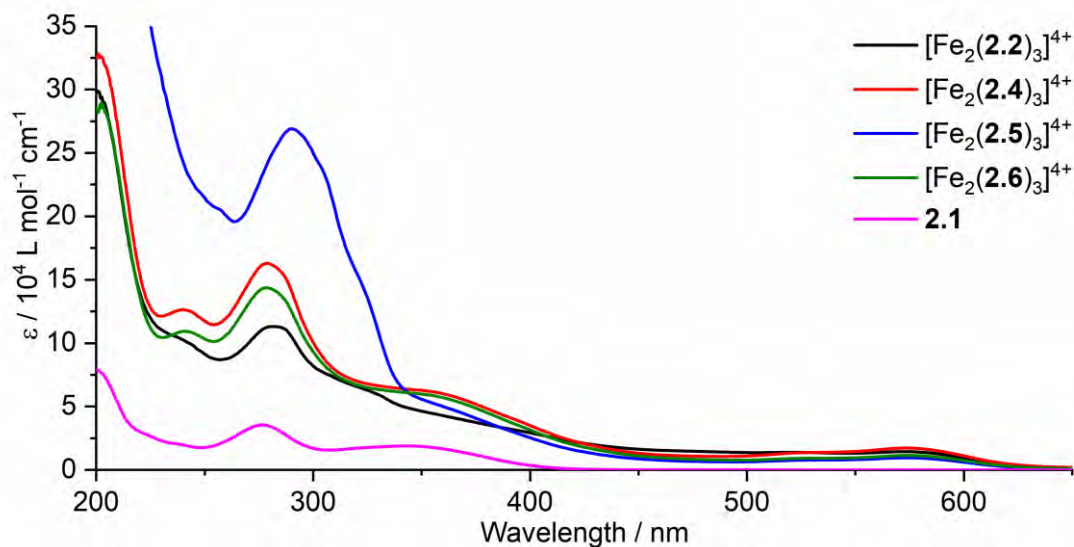
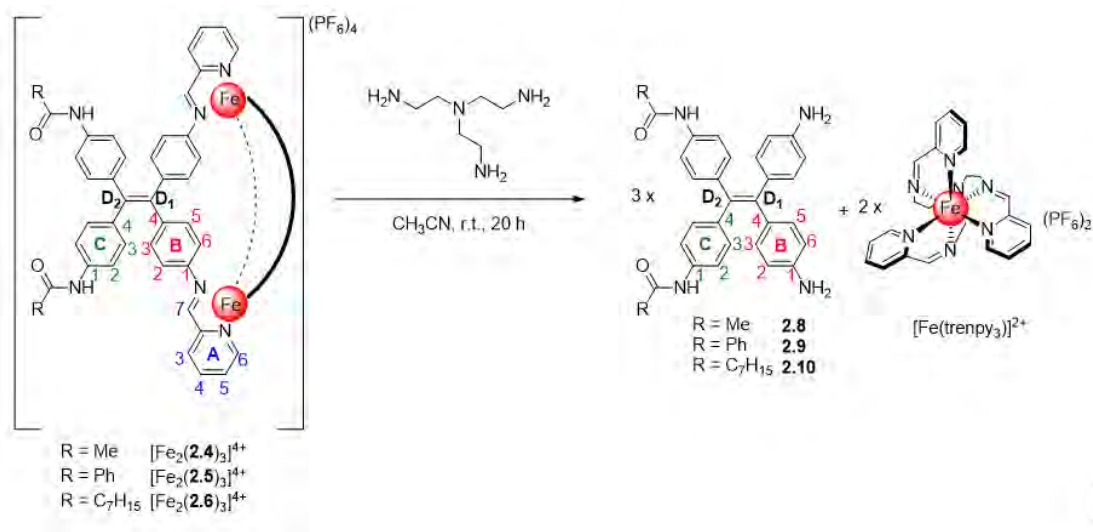


Figure 2.16 UV-Visible absorption spectra (acetonitrile) of tetraaniline **2.1**, and the helicates $[\text{Fe}_2(\text{L})_3]^{4+}$ ($\text{L} = \mathbf{2.2}, \mathbf{2.4-6}$).

The emission spectrum of dilute $[\text{Fe}_2(\mathbf{2.2})_3]^{4+}$ in acetonitrile was collected ($0.8 \mu\text{M}$, $\lambda_{\text{ex}} = 280 \text{ nm}$), and the complex was found to be non-emissive. This is consistent with quenching of the TPE emission by the iron(II) centre and the observation that the TPE units are non-planar with a considerable degree of freedom under these conditions. Aggregation-induced-emission (AIE) is typically responsible for significant enhancement in TPE emission by preventing vibrational relaxation,^{36a, 36b} a phenomenon not likely for a dilute solution of helicate $[\text{Fe}_2(\mathbf{2.2})_3]^{4+}$.

2.10 Isolation of selectively functionalised TPE molecules

We initially attempted to isolate the free organic components using ethylenediaminetetraacetic acid (EDTA) to sequester the iron(II) ions, and hydrolysis of the imine bonds to generate the free amine. This approach invariably gave complex mixtures of products which were difficult to isolate. However, Nitschke and co-workers have used imine exchange to great effect to manipulate metal-template assemblies,^{83c, 94b-d} which proved extremely effective. Reaction of helicates $[\text{Fe}_2(\mathbf{2.4})_3](\text{PF}_6)_4$, $[\text{Fe}_2(\mathbf{2.5})_3](\text{PF}_6)_4$ or $[\text{Fe}_2(\mathbf{2.6})_3](\text{PF}_6)_4$ with an excess of the competitive tridentate tris(2-aminoethyl)amine (tren) resulted in the quantitative formation of monomeric complex $[\text{Fe}(\text{trenpy}_3)]^{2+}$, as found for related systems,¹⁰⁸ and the release of the organic compound **2.8**, **2.9** or **2.10** respectively (Scheme 2.3).



Scheme 2.3 Isolation of functionalised TPE units by imine exchange.

Isolation of the organic units was achieved by extraction of the reaction mixture with diethyl ether, followed by column chromatography giving organic units **2.8**, **2.9** and **2.10** in 50, 53 and 86% yields respectively. The resulting units were characterised by NMR (Figure 2.17 and Section 7.12) and ESI-MS. Upon release from the helicate the signals corresponding to protons $\text{H}^{\text{B}2}$ and $\text{H}^{\text{B}6}$ move significantly downfield ($\Delta\delta \approx 1.1$ ppm) and coalesce as the phenyl ring is no longer undergoing restricted rotation. The signals corresponding to protons $\text{H}^{\text{B}3}$ and $\text{H}^{\text{B}5}$ move slightly upfield ($\Delta\delta -0.4$ and -0.1 ppm respectively) and coalesce. The protons on rings C (and E in the case of **2.9**) are mostly unaffected, consistent with their distance from the helical structure.

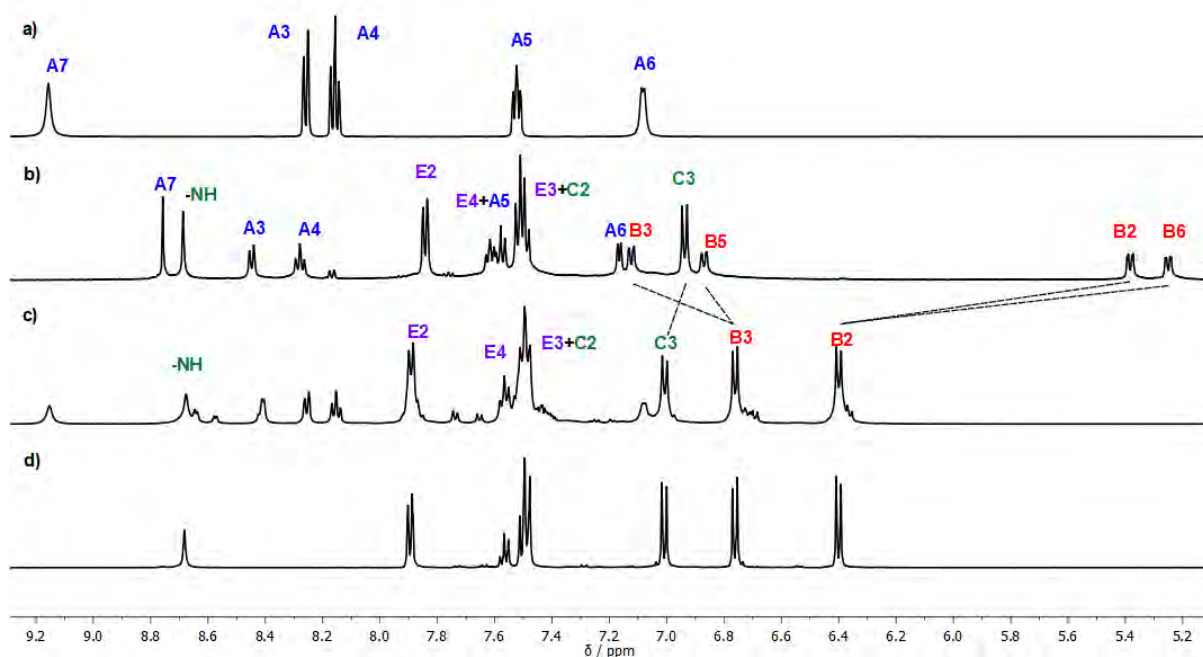
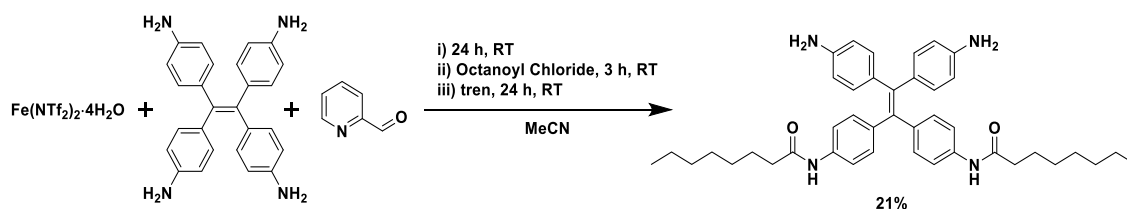


Figure 2.17 ^1H NMR spectra (CD_3CN , 500 MHz, 298 K) showing isolation of functionalised TPE units by imine exchange. a) $[\text{Fe}(\text{trenpy}_3)]^{2+}$, b) $[\text{Fe}_2(\mathbf{2.5})_3]^{4+}$, c) combination of tren and $[\text{Fe}_2(\mathbf{2.5})_3]^{4+}$ and d) isolated **2.9**.

The entire synthesis of the functionalised ligands can also be completed in one pot without isolation of the helicate species and an example is shown in Scheme 2.4. Combination of **2.1**, 2-pyridinecarboxaldehyde and $\text{Fe}(\text{NTf}_2)_2 \cdot 4\text{H}_2\text{O}$ in acetonitrile led to *in situ* formation of the $[\text{Fe}_2(\mathbf{2.2})_3]^{4+}$ helicate which was reacted directly with octanoyl chloride. After complete conversion to the $[\text{Fe}_2(\mathbf{2.6})_3]^{4+}$ species, tren was added to facilitate the imine exchange and the organic component **2.10** was isolated in a non-optimised yield of 21% (see Section 7.13). The spectral data for this compound was identical to that reported above, proving the versatility of this method for generating unsymmetrical functional TPE units.



Scheme 2.4 One-pot synthesis and isolation of functionalised TPE unit **2.10** by imine exchange.

2.11 Electronic properties of organic components **2.1**, **2.8**, **2.9** and **2.10**

2.11.1 UV-Visible absorption and emission properties

The UV-visible absorption spectra of tetraaniline **2.1** and the functionalised TPE units **2.8–10** were recorded in THF (Figure 2.18). The absorption spectra of **2.1** and **2.8–10** in THF are essentially identical, indicating the peripheral functionalisation does not significantly change the electronic properties of the central chromophore.

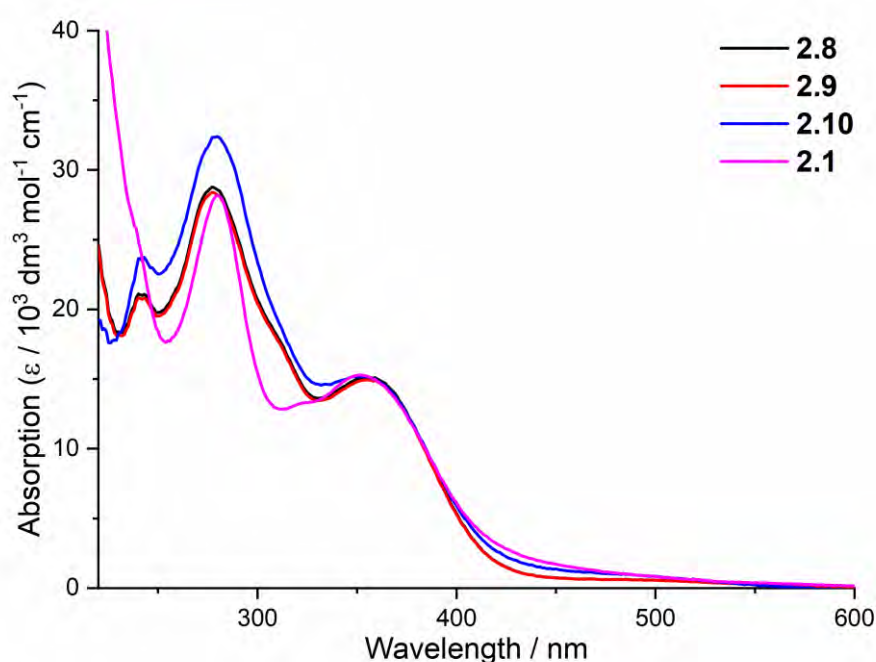


Figure 2.18 UV-Visible absorbance spectra (THF) of tetraaniline **2.1**, and the functional TPE molecules **2.8–10**.

The absorption and emission behaviour were studied using solutions of **2.1**, **2.8–10** in THF with increasing water content (see Section 7.14). All compounds showed an increase in the emission intensity on water addition, consistent with emission in the aggregated state. The parent tetraaniline **2.1** displays complex behaviour consistent with multiple emissive species, presumably different protonation states. Compound **2.8** is emissive in pure THF with the emission intensity increasing with water content up to 30% water, followed by a decrease in intensity at higher water contents, similar to other TPE derivatives.

Compounds **2.9** and **2.10** show similar emission profiles at low water content, but significant differences were found at higher water content (Figure 2.19). An enhancement of emission intensity was found for **2.9** and **2.10** up to 85% and 30% water content respectively with the emission of **2.9** being red-shifted and approximately four times higher than that of **2.10**. The red-shift of the emission maxima is as expected as the solvent polarity increases.¹⁰⁹ At higher water content ($\approx 90\%$), the emission intensity of **2.10** is reduced, likely due to the formation of larger non-emissive aggregates.

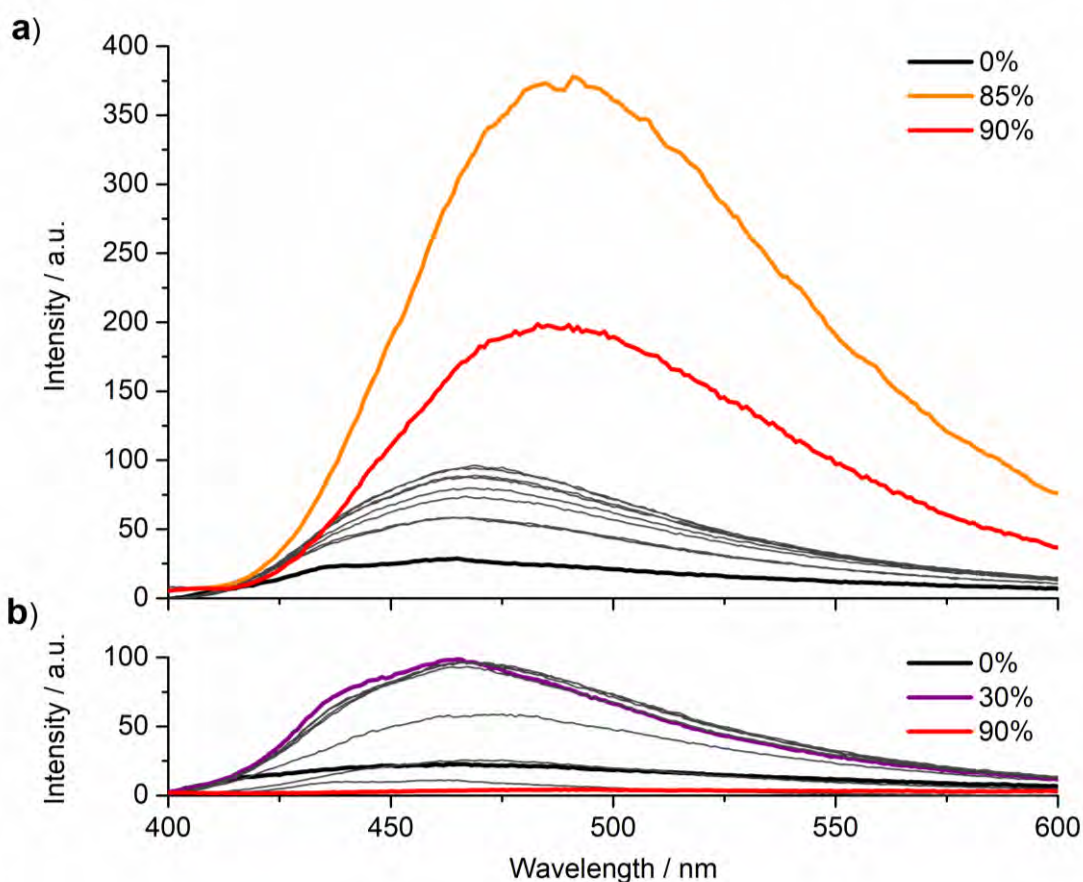


Figure 2.19 Emission data for a) **2.9** and b) **2.10** in THF/water mixtures.

2.11.2 DLS measurement of self-assembly behaviour

Dynamic Light Scattering (DLS) was used to estimate the size distribution of the aggregates formed in solution (Figure 2.20). Compound **2.8** showed different sized aggregates at varying water content. At 30% water content, which corresponded to the water content of maximum emission, only small aggregates are formed ($d \approx 5$ nm). At 80–90% water content much larger aggregates ($d \approx 80$ –200 nm) are formed, which

correspond to a red-shifted and weaker emission. Intermolecular hydrogen-bonding by compound **2.8** may limit the π - π stacking interactions that result in increased emission.

Compound **2.9** displays typical TPE emission: as water content is increased the absorption undergoes minimal changes, while the emission intensity increases to reach a maximum at 85% water content, with a maximum emission at 490 nm. DLS data did not indicate the formation of larger structures, with small aggregates ($d \approx 5$ nm) at low water content, and higher water content leading to polydisperse aggregates too large to be measured using DLS. The pendant benzoyl groups may drive self-assembly behaviour towards 2D sheets, allowing favourable π - π interactions between adjacent units without requiring the flattening of the TPE units. This is consistent with the behaviour of the tetrakis(4-benzoyloxyphenyl)ethene derivative, which is suggested to form 2D hydrogen-bonded networks.¹¹⁰

Compound **2.10** showed more interesting self-assembly behaviour. Below 30% water content small aggregates ($d \approx 4$ nm) dominate, and these are the conditions which correspond to maximum emission intensity. However, at higher water content (e.g. 90%) larger structures are assembled with an average diameter of 250 nm and low polydispersity (PDI = 0.10). These large species are significantly less emissive than the smaller aggregates, indicating that the assembly disrupts the efficient packing of the TPE cores to result in a decrease in the emission intensity. Intermolecular hydrophobic interactions between the octyl chains presumably drive the self-assembly of these large structures.

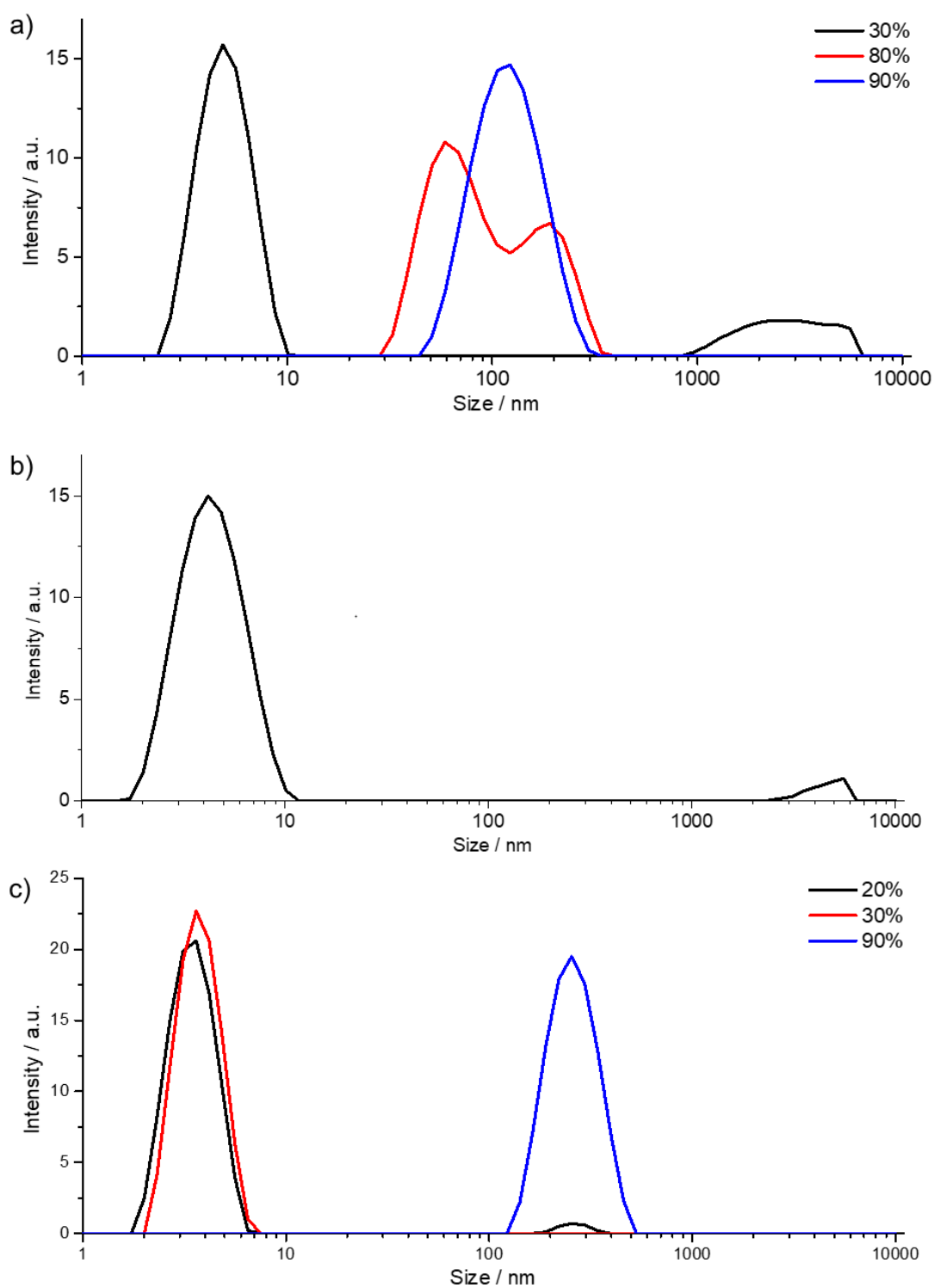


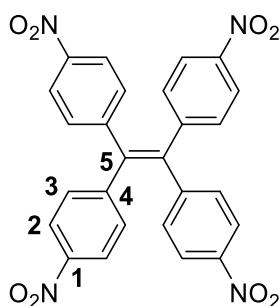
Figure 2.20 DLS measurements of compounds **2.8-10**. a) Compound **2.8** with different percentages of water in THF; b) compound **2.9** in water/THF (70:30) and c) compound **2.10** with different percentages of water in THF.

2.12 Conclusions

The amine functionalised TPE derivative **2.1** is suitable for forming imines for metal ion complexation and subsequent self-assembly into larger structures. Reaction with iron(II) ions and 2-pyridinecarboxaldehyde, followed by an aqueous workup procedure, gives a diastereoselective $[\text{Fe}_2\text{L}_3]^{4+}$ helicate with pendant amines suitable for functionalisation. This metal template synthesis demonstrates the ability to control functionalisation of organic components by selective metal ion coordination controlled by the geometry and separation of the binding sites and may allow their selective inclusion into larger molecules and assemblies. Finally, the “supramolecular protecting group” strategy allowed the synthesis of functionalised TPE derivatives with amphiphilic character that can be self-assembled into large emissive assemblies in solution.

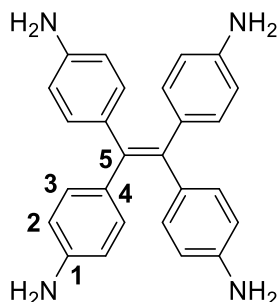
2.13 Experimental

2.13.1 Synthesis of 1,1,2,2-tetrakis(4-nitrophenyl)ethene



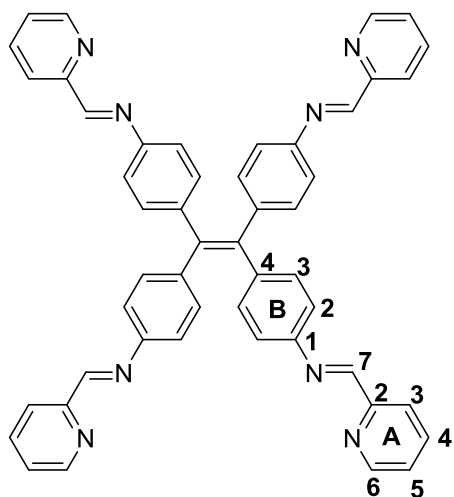
Synthesised following a modified literature procedure.⁹⁸ 1,1,2,2-Tetraphenylethene (2.00 g, 6.02 mmol) was added in portions to 70% HNO_3 (50 mL) and stirred at 50 °C for 24 hours. An orange solid was precipitated with excess water and recrystallised from a 1,4-dioxane/water mixture (4:1) to afford 1,1,2,2-tetrakis(4-nitrophenyl)ethene as yellow crystals (2.18 g, 4.25 mmol, 71 %). ^1H NMR (400 MHz, CDCl_3) δ 8.07 (dt, $J = 8.8$ Hz, 2.1 Hz, 8H, H^2), 7.19 (dt, $J = 8.8$, 2.1 Hz, 8H, H^3). ^{13}C NMR (101 MHz, CD_3CN) δ 148.7 (C^1), 148.2 (C^5), 142.4 (C^4), 133.0 (C^3), 124.5 (C^2). The ^1H NMR data matches that previously reported.⁹⁷

2.13.2 Synthesis of 4,4',4'',4'''-(ethene-1,1,2,2-tetrayl)tetraaniline (2.1)



Synthesised following a literature procedure.⁹⁷ Hydrazine monohydrate (6.4 mL, 132 mmol, 90 eq.) was added to a stirring solution of 1,1,2,2-tetrakis(4-nitrophenyl)ethene (745 mg, 1.45 mmol) and 10% Pd/C (75 mg, cat.) in ethanol (150 mL). The reaction was heated at reflux for 24 hours and filtered through Celite. Evaporation of the filtrate afforded 4,4',4'',4'''-(ethene-1,1,2,2-tetrayl)tetraaniline as an orange solid (432 mg, 1.10 mmol, 76 %). ¹H NMR (400 MHz, CD₃CN) δ 6.69 (dt, *J* = 8.7, 2.1 Hz, 8H, H²), 6.36 (dt, *J* = 8.7, 2.1 Hz, 8H, H³), 4.00 (s, 8H, H^{NH}). ¹³C NMR (101 MHz, CD₃CN) δ 146.7 (C¹), 138.8 (C⁵), 135.4 (C⁴), 133.0 (C³), 114.5 (C²). ESI-MS *m/z* 393.42 [2.1+H]⁺ requires 393.21; 785.92 [2(2.1)+H]⁺ requires 785.41.

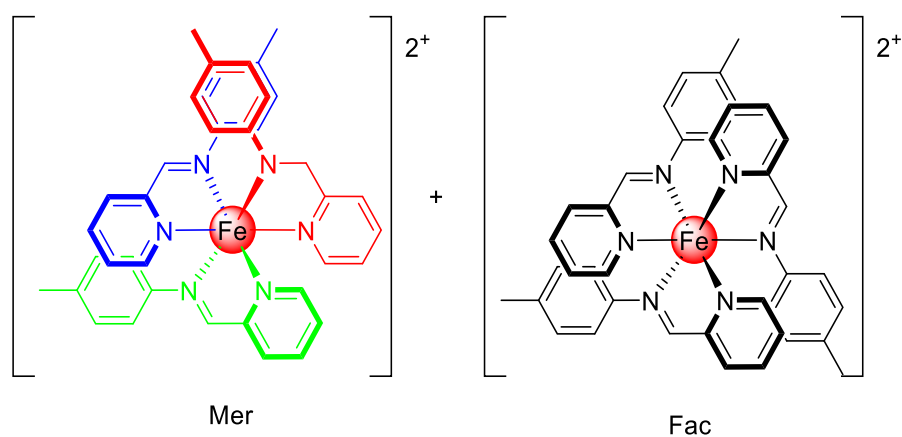
2.13.3 Synthesis of N,N',N'',N'''-(ethene-1,1,2,2-tetrayl)tetrakis(benzene-4,1-diyl)tetrakis(1-(pyridin-2-yl)methanimine) (2.3)



2-Pyridinecarboxaldehyde (19.6 μL, 22 mg, 0.21 mmol) was added to a solution of 1,1,2,2-tetrakis(4-aminophenyl)ethene (20 mg, 51 μmol) in methanol (20 mL) and heated at reflux for 2 hours. The resulting precipitate was collected via filtration and washed with methanol (2 × 15 mL) to give a yellow solid (36 mg, 48 μmol, 94%). ¹H

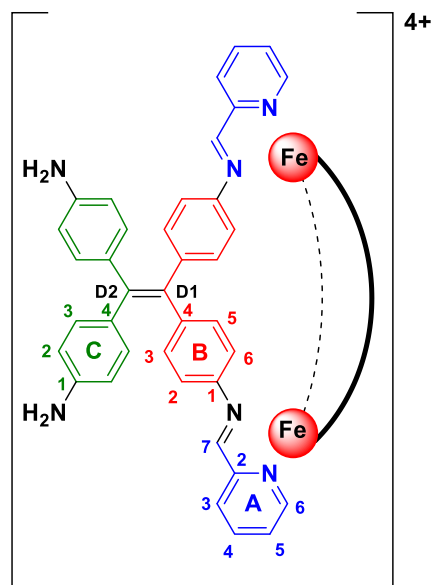
NMR (500 MHz, CDCl₃) δ 8.69 (dt, $J = 4.6, 1.4$ Hz, 4H, H^{A6}), 8.60 (s, 4H, H^{NH}), 8.18 (dt, $J = 8.0, 1.1$ Hz, 4H, H^{A3}), 7.80 (td, $J = 7.8, 1.8$ Hz, 4H, H^{A4}), 7.35 (ddd, $J = 7.5, 4.8, 1.3$ Hz, 4H, H^{A5}), 7.19 – 7.08 (m, 16H, H^{B2+B3}). ¹³C NMR (101 MHz, CDCl₃) δ 160.3 (C^{A7}), 154.8 (H^{A2}), 149.8 (H^{A6}), 149.3 (C^{B1}), 142.5 (C^{B4}), 140.5 (C^{C=C}), 136.8 (C^{A4}), 132.6 (C^{B3}), 125.2 (C^{A5}), 121.96 (C^{A3}), 120.99 (C^{B2}).

2.13.4 Synthesis of [Fe(2.7)₃](PF₆)₂



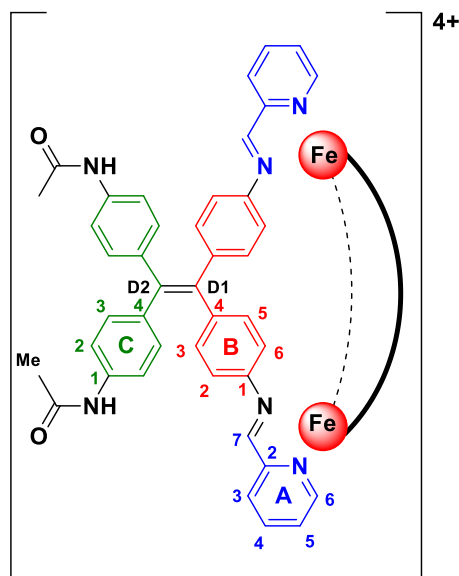
p-Toluidine (50 mg, 0.47 mmol) and Fe(BF₄)₂·6H₂O (57 mg, 0.17 mmol) was added to a solution of 2-pyridinecarboxaldehyde (45 μ L, 51 mg, 0.47 mmol) in methanol (30 mL) and stirred at room temperature for 2 hours. Excess saturated aqueous KPF₆ was added and the resulting purple solid was collected on Celite, washed with water (3 \times 30 mL), DCM (2 \times 30 mL) and diethyl ether (1 \times 30 mL). The solid was dissolved in acetonitrile and solvent was removed to afford the title compound as a purple solid (110 mg, 0.12 mmol, 70%) ¹H NMR (500 MHz, CD₃CN) δ 9.26 (s, 1H), 9.06 (s, 1H), 8.76 (d, $J = 3.4$ Hz, 2H), 8.54 – 8.47 (m, 2H), 8.42 (dt, $J = 7.6, 1.1$ Hz, 1H), 8.37 – 8.29 (m, 2H), 8.24 (td, $J = 7.8, 1.3$ Hz, 1H), 8.00 (td, $J = 7.7, 1.3$ Hz, 1H), 7.97 – 7.91 (m, 1H), 7.93 – 7.83 (m, 2H), 7.74 – 7.64 (m, 2H), 7.61 (d, $J = 5.5$ Hz, 1H), 7.53 (dd, $J = 7.7, 5.6$ Hz, 2H), 7.35 (d, $J = 5.5$ Hz, 1H), 7.15 (d, $J = 8.0$ Hz, 2H), 7.01 (d, $J = 8.0$ Hz, 1H), 6.96 (d, $J = 7.9$ Hz, 2H), 6.78 (d, $J = 8.0$ Hz, 2H), 6.62 (d, $J = 8.3$ Hz, 2H), 6.53 (d, $J = 8.2$ Hz, 2H), 6.05 (d, $J = 8.3$ Hz, 2H), 5.31 (d, $J = 8.3$ Hz, 1H), 2.32 (s, 2H), 2.28 (s, 3H), 2.24 (s, 3H), 2.14 (s, 4H). UV-vis: 1.6×10^{-5} mol dm⁻³, MeCN, λ_{max} /nm ($\epsilon / 10^3$ dm³ mol⁻¹ cm⁻¹) 238 (33), 284 (24), 327 (26), 527 (5), 575 (6). ESI-MS m/z 322.08 [Fe(2.7)₃]²⁺ requires 322.12, 788.67 [(Fe(2.7)₃) + PF₆]⁺ requires 789.20.

2.13.5 Synthesis of [Fe₂(**2.2**)₃](PF₆)₄ helicate



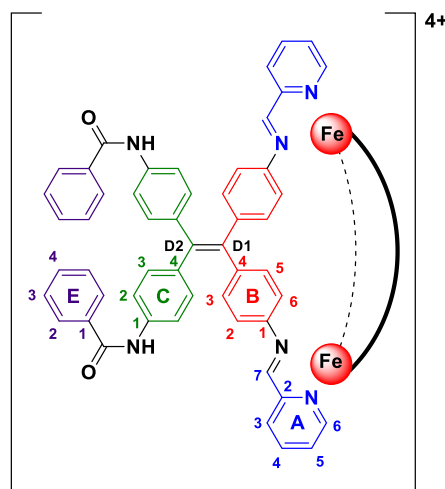
1,1,2,2-Tetrakis(4-aminophenyl)ethene (200 mg, 0.51 mmol) was added to a solution of 2-pyridinecarboxaldehyde (97 μ L, 110 mg, 1.0 mmol) in ethanol (100 mL) and the solution was stirred at room temperature for five minutes. FeCl₂·4H₂O (68 mg, 0.34 mmol) was then added, resulting in the formation of a dark red solution which was stirred for 24 hours. Excess saturated aqueous KPF₆ was added (150 mL) and the resulting purple-red precipitate was collected on Celite, washed with water (3 x 50 mL), DCM (2 x 50 mL) and diethyl ether (2 x 50 mL). The solid was dissolved in acetonitrile and solvent was removed under reduced pressure to afford the title compound as a dark purple-red solid (341 mg, 0.14 mmol, 83 %). ¹H NMR (500 MHz, CD₃CN) δ 8.69 (s, 2H, H^{A7}), 8.42 (d, J = 7.4 Hz, 6H, H^{A3}), 8.31 (dd, J = 7.8, 1.1 Hz, 6H, H^{A4}), 7.66 (td, J = 6.7, 1.3 Hz, 6H, H^{A5}), 7.20 (d, J = 5.4 Hz, 6H, H^{A6}), 7.01 (dd, J = 8.3, 1.7 Hz, 6H, H^{B3}), 6.79 (dd, J = 8.2, 1.7 Hz, 6H, H^{B5}), 6.61 (d, J = 8.7 Hz, 12H, H^{C3}), 6.30 (d, J = 5.3 Hz, 12H, H^{C2}), 5.30 (dd, J = 8.3, 2.3 Hz, 6H, H^{B2}), 5.15 (dd, J = 8.2, 2.3 Hz, 6H, H^{B6}), 4.15 (s, 12H, H^{NH}). ¹³C {¹H} NMR (101 MHz, CD₃CN) δ 175.9 (C^{A7}), 159.1 (C^{A2}), 156.7 (C^{A6}), 149.5 (C^{B1}), 148.3 (C^{C1}), 146.6 (C^{D2}), 146.0 (C^{B4}), 140.5 (C^{A4}), 134.3 (C^{B3}), 133.5 (C^{D1}), 133.5 (C^{C3}), 133.1 (C^{C4}), 133.0 (C^{B5}), 132.2 (C^{A3}), 130.6 (C^{A5}), 121.4 (C^{B2}), 120.9 (C^{B6}), 114.5 (C^{C2}). UV-vis: 8.3×10^{-6} mol dm⁻³, MeCN, λ_{max} /nm (ϵ / 10³ dm³ mol⁻¹ cm⁻¹) 282 (113), 574 (14). ESI-MS m/z 455.9079 [Fe₂(**2.2**)₃]⁴⁺ requires 455.9097; 571.2610 [**2.2** + H]⁺ requires 571.2610; 656.1994 [(Fe₂(**2.2**)₃) + PF₆]³⁺ requires 656.2010; 1056.7800 [(Fe₂(**2.2**)₃) + (PF₆)₂]³⁺ requires 1056.7835.

2.13.6 Synthesis of $[\text{Fe}_2(\mathbf{2.4})_3](\text{PF}_6)_4$ helicate



Acetic anhydride (21 μL , 22 mg, 220 μmol) was added to a solution of $[\text{Fe}_2(\mathbf{2.4})_3](\text{PF}_6)_4$ (79 mg, 33 μmol) in dry CH_3CN (4 mL). The mixture was heated at 70 $^\circ\text{C}$ for 18 h, then cooled and poured into excess aqueous KPF_6 solution (20 mL) leading to the formation of a dark burgundy precipitate. The precipitate was collected on Celite and washed with H_2O (2×10 mL) and DCM (2×10 mL), then dissolved in CH_3CN (20 mL) and the solvent removed under reduced pressure to give the title compound as a purple solid (78 mg, 90%) ^1H NMR (500 MHz, CD_3CN) δ 8.75 (s, 6H, $\text{H}^{\text{A}7}$), 8.46 (d, $J = 7.7$ Hz, 6H, $\text{H}^{\text{A}3}$), 8.33 (t, $J = 7.7$ Hz, 6H, $\text{H}^{\text{A}4}$), 8.27 (s, 6H, -NH), 7.68 (s, 6H, $\text{H}^{\text{A}5}$), 7.31 (d, $J = 8.2$ Hz, 12H, $\text{H}^{\text{C}2}$), 7.21 (d, $J = 5.4$ Hz, 6H, $\text{H}^{\text{A}6}$), 7.06 (d, $J = 8.1$ Hz, 6H, $\text{H}^{\text{B}3}$), 6.85 (m, 18H, $\text{H}^{\text{C}3+\text{B}5}$), 5.36 (d, $J = 7.5$ Hz, 6H, $\text{H}^{\text{B}2}$), 5.20 (d, $J = 7.5$ Hz, 6H, $\text{H}^{\text{B}6}$), 2.01 (s, 18H, $\text{H}^{\text{C}6}$). $^{13}\text{C}\{^1\text{H}\}$ NMR (151 MHz, CD_3CN) δ 176.2 ($\text{C}^{\text{A}7}$), 169.6 ($\text{C}^{\text{C}=\text{O}}$), 159.0 ($\text{C}^{\text{A}2}$), 156.7 ($\text{C}^{\text{A}6}$), 150.2 ($\text{C}^{\text{B}1}$), 144.8 ($\text{C}^{\text{B}4}$), 144.6 ($\text{C}^{\text{D}2}$), 140.6 ($\text{C}^{\text{A}4}$), 139.4 ($\text{C}^{\text{C}1}$), 139.3 ($\text{C}^{\text{C}4}$), 137.0 ($\text{C}^{\text{D}1}$), 134.4 ($\text{C}^{\text{B}3}$), 133.1 ($\text{C}^{\text{B}5}$), 132.7 ($\text{C}^{\text{C}3}$), 132.5 ($\text{C}^{\text{A}3}$), 130.7 ($\text{C}^{\text{A}5}$), 121.7 ($\text{C}^{\text{B}2}$), 121.0 ($\text{C}^{\text{B}6}$), 119.3 ($\text{C}^{\text{C}2}$), 24.4 (C^{Me}). UV-Vis: 7.8×10^{-6} mol dm^{-3} , MeCN, λ_{max} /nm ($\epsilon / 10^3$ dm^3 mol $^{-1}$ cm $^{-1}$) 279 (163), 361 (60), 574 (18). ESI-MS m/z 518.9232 $[\text{Fe}_2(\mathbf{2.4})_3]^{4+}$ requires 518.9255; 655.2811 $[\mathbf{2.4} + \text{H}]^+$ requires 655.2821; 682.4916 $[\text{Fe}_2(\mathbf{2.4})_4]^{4+}$ requires 682.4941; 740.2191 $[(\text{Fe}_2(\mathbf{2.4})_3) + \text{PF}_6]^{3+}$ requires 740.2221; 917.2562 $[(\text{Fe}_4(\mathbf{2.4})_6) + 3\text{PF}_6]^{5+}$ requires 917.2594; 958.3106 $[(\text{Fe}_2(\mathbf{2.4})_4) + \text{PF}_6]^{3+}$ requires 958.3136; 1182.8118 $[(\text{Fe}_2(\mathbf{2.4})_3) + 2(\text{PF}_6)]^{2+}$ and $[(\text{Fe}_4(\mathbf{2.4})_6) + 4\text{PF}_6]^{4+}$ require 1182.8153; 1625.4045 $[(\text{Fe}_4(\mathbf{2.4})_6) + 5\text{PF}_6]^{3+}$ requires 1625.4084.

2.13.7 Syntheses of $[\text{Fe}_2(\mathbf{2.5})_3](\text{PF}_6)_4$ helicate



a) Benzoic anhydride (50 mg, 220 μmol) was added to a solution of $[\text{Fe}_2(\mathbf{2.2})_3](\text{PF}_6)_4$ (80 mg, 33 μmol) in dry CH_3CN (5 mL). The solution was heated at 70 $^\circ\text{C}$ for 18 h, then cooled and poured into excess aqueous KPF_6 solution (15 mL) leading to the formation of a dark burgundy precipitate. The precipitate was collected on Celite and washed with H_2O (2×10 mL), DCM (2×5 mL), then dissolved in CH_3CN and the solvent removed under reduced pressure to give the title compound as a purple solid (67 mg, 67%).

b) Benzoyl chloride (35 μL , 42 mg, 300 μmol) was added to a solution of $[\text{Fe}_2(\mathbf{2.2})_3](\text{PF}_6)_4$ (120 mg, 50 μmol) in dry CH_3CN (10 mL). The solution was stirred at room temperature for 1.5 h, then poured into excess aqueous KPF_6 solution (60 mL) leading to the formation of a dark burgundy precipitate. The precipitate was collected on Celite and washed with H_2O (2×40 mL), DCM (2×40 mL) then dissolved in CH_3CN (20 mL) and the solvent removed under reduced pressure to give the title compound as a purple solid (78 mg, 85%). ^1H NMR (500 MHz, CD_3CN) δ 8.79 (s, 6H, $\text{H}^{\text{A}7}$), 8.71 (s, 6H, -NH), 8.47 (d, $J = 7.3$ Hz, 6H, $\text{H}^{\text{A}3}$), 8.28 (t, $J = 7.6$ Hz, 6H, $\text{H}^{\text{A}4}$), 7.84 (d, $J = 7.4$ Hz, 12H, $\text{H}^{\text{E}2}$), 7.66-7.56 (m, 18H, $\text{H}^{\text{D}4+\text{A}5}$), 7.56-7.47 (m, 24H, $\text{H}^{\text{D}3+\text{C}2}$), 7.18 (d, $J = 5.4$ Hz, 6H, $\text{H}^{\text{A}6}$), 7.15 (d, $J = 8.2$ Hz, 6H, $\text{H}^{\text{B}3}$), 6.95 (d, $J = 8.3$ Hz, 12H, $\text{H}^{\text{C}3}$), 6.89 (d, $J = 8.4$ Hz, 6H, $\text{H}^{\text{B}5}$), 5.42 (d, $J = 8.3$ Hz, 6H, $\text{H}^{\text{B}2}$), 5.28 (d, $J = 6.6$ Hz, 6H, $\text{H}^{\text{B}6}$). $^{13}\text{C}\{^1\text{H}\}$ NMR (151 MHz, CD_3CN) δ 176.2 ($\text{C}^{\text{A}7}$), 166.8 ($\text{C}^{\text{C}=\text{O}}$), 158.8 ($\text{C}^{\text{A}2}$), 156.7 ($\text{C}^{\text{A}6}$), 150.3 ($\text{C}^{\text{B}1}$), 144.8 ($\text{C}^{\text{B}4}$), 144.5 ($\text{C}^{\text{D}2}$), 140.6 ($\text{C}^{\text{A}4}$), 139.9 ($\text{C}^{\text{C}1}$), 139.2 ($\text{C}^{\text{C}4}$), 137.4 ($\text{C}^{\text{D}1}$), 135.8 ($\text{C}^{\text{E}1}$), 134.5 ($\text{C}^{\text{B}3}$), 133.3 ($\text{C}^{\text{B}5}$), 132.8 ($\text{C}^{\text{E}4} + \text{C}^{\text{C}3}$), 132.5 ($\text{C}^{\text{A}3}$), 130.7 ($\text{C}^{\text{A}5}$), 129.5 ($\text{C}^{\text{E}3}$), 128.4 ($\text{C}^{\text{E}2}$), 121.8 ($\text{C}^{\text{B}2}$), 121.1 ($\text{C}^{\text{B}6}$), 120.4 ($\text{C}^{\text{C}2}$). UV-Vis: 5.3×10^{-6} mol dm^{-3} , MeCN, λ_{max}

(C^{E2}), 32.4 (C^{E4-7}), 29.9 (C^{E4-7}), 29.7 (C^{E4-7}), 26.2 (C^{E3}), 14.4 (C^{Me}). UV-Vis: 1.0×10^{-6} mol dm⁻³, MeCN, λ_{\max} /nm ($\epsilon / 10^3$ dm³ mol⁻¹ cm⁻¹) 279 (144), 360 (57), 574 (11). ESI-MS 645.0653 [Fe₂(**2.6**)₃]⁴⁺ requires 645.0664; 866.4204 [Fe₂(**2.6**)₃ + F]³⁺ requires 866.4213; 908.4090 [(Fe₂(**2.6**)₃) + PF₆]³⁺ requires 908.4099; 1119.2848 [(Fe₄(**2.6**)₆) + 3PF₆]⁵⁺ requires 1119.2847; 1435.5980 [(Fe₂(**2.6**)₃) + 2PF₆]²⁺ and [(Fe₄(**2.6**)₆) + 4PF₆]⁴⁺ requires 1435.0970 and 1435.3470 *m/z* respectively.

2.13.9 X-Ray crystallography

	[Fe ₂ (2.2) ₃](PF ₆) ₄ ·H ₂ O	[Fe ₂ (2.5) ₃](PF ₆) ₄
Empirical formula	C ₂₂₈ H ₁₈₂ F ₄₈ Fe ₄ N ₃₆ OP ₈	C ₇₈ H ₅₄ F ₁₂ FeN ₉ O ₃ P ₂
Formula weight	4825.24	1511.09
Temperature/K	100.0	100
Crystal system	triclinic	monoclinic
Space group	P-1	C2/c
a/Å	19.445(4)	32.650(7)
b/Å	20.664(4)	15.547(3)
c/Å	33.774(7)	30.727(6)
α/°	75.14(3)	90
β/°	87.00(3)	92.57(3)
γ/°	64.24(3)	90
Volume/Å ³	11786(5)	15582(5)
Z	2	8
ρ _{calc} /cm ³	1.360	1.288
μ/mm ⁻¹	0.393	0.315
F(000)	4932.0	6184.0
Crystal size/mm ³	0.03 × 0.02 × 0.01	0.2 × 0.1 × 0.1
Radiation	Synchrotron (λ = 0.71073)	Synchrotron (λ = 0.71073)
2θ range for data collection/°	1.25 to 41.488	2.902 to 52.746
Index ranges	-19 ≤ h ≤ 19, -20 ≤ k ≤ 20, -33 ≤ l ≤ 33	-40 ≤ h ≤ 40, -19 ≤ k ≤ 19, -38 ≤ l ≤ 38
Reflections collected	84580	110183
Independent reflections	23222 [R _{int} = 0.0486, R _{sigma} = 0.0489]	15371 [R _{int} = 0.1701, R _{sigma} = 0.0808]
Data/restraints/parameters	23222/993/2756	15371/114/935
Goodness-of-fit on F ²	1.512	1.532
Final R indexes [I ≥ 2σ (I)]	R ₁ = 0.1266, wR ₂ = 0.3579	R ₁ = 0.1919, wR ₂ = 0.4555
Final R indexes [all data]	R ₁ = 0.1593, wR ₂ = 0.3913	R ₁ = 0.2997, wR ₂ = 0.5134

2.13.10 $2[\text{Fe}_2(\mathbf{2.2})_3](\text{PF}_6)_8 \cdot \text{H}_2\text{O}$

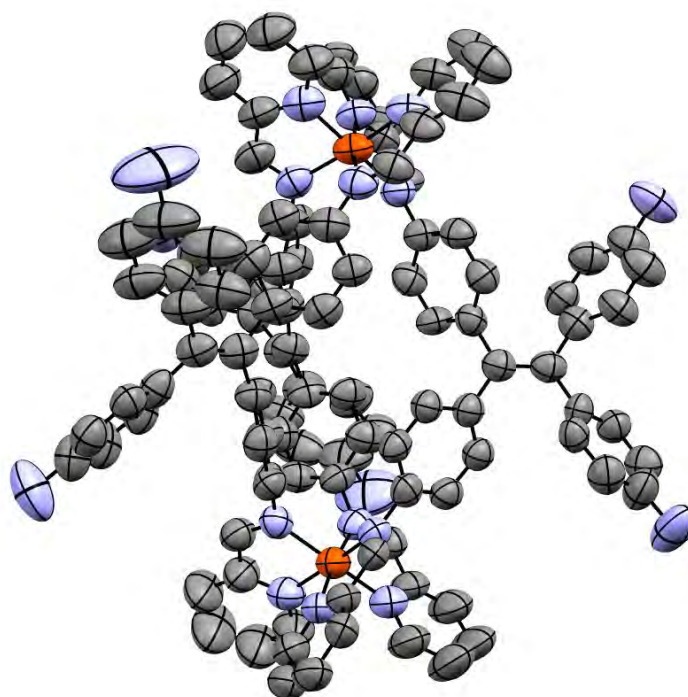


Figure 2.21 An ORTEP representation of one of the complex cations in the asymmetric unit of the X-ray crystal structure of $[\text{Fe}_2(\mathbf{2.5})_3](\text{PF}_6)_4$. Thermal ellipsoids are drawn at 50% probability.

Brown plate like crystals of $2[\text{Fe}_2(\mathbf{2.2})_3](\text{PF}_6)_8 \cdot \text{H}_2\text{O}$ were grown by slow evaporation of a DMF/methanol solution of the complex. The crystal with dimensions of $0.03 \times 0.02 \times 0.01$ mm was coated in immersion oil type NVH and transferred to the goniometer, where it was cooled with a nitrogen cold stream (100 K) provided by an Oxford Instruments Cryojet 5. Diffraction measurements were carried out using Si<111> monochromated synchrotron X-ray radiation ($\lambda = 0.71023$ Å) (MX2 Beamline at Australian Synchrotron). Data collection was carried out using Blu-Ice suite of software and unit cell refinement, data reduction and processing was carried out with XDS.¹¹¹ Absorption correction was carried out with SADABS.¹¹² The structure was solved using dual space methods with SHELXT.¹¹³ The full-matrix least-square refinements were carried out using SHELXL-2015¹¹³ through Olex2¹¹⁴ suite of software. The crystal only diffracted to low resolution. One molecule of solvent water could be identified from the difference map and was included in the least-squares refinement. The structure has large solvent accessible voids in the crystal lattice. To address this, solvent mask was used in Olex2 (similar to the SQUEEZE procedure in PLATON). As a result of this solvent mask the R1 was improved 4.67% (from 17.33% to 12.66% and represented two major voids (140 electrons each, possibly two disordered DMF solvent molecules). The PF_6^- anions

in the unit cell were disordered and were restrained to have similar ADPs (using RIGU) and similar bond lengths (using SADI). There are 3 partial occupancy PF_6^- anions in the unit cell, with a combined occupancy of 2. Two of these were modelled isotropically due to poor data quality.

2.13.11 $[\text{Fe}_2(2.5)_3](\text{PF}_6)_4$

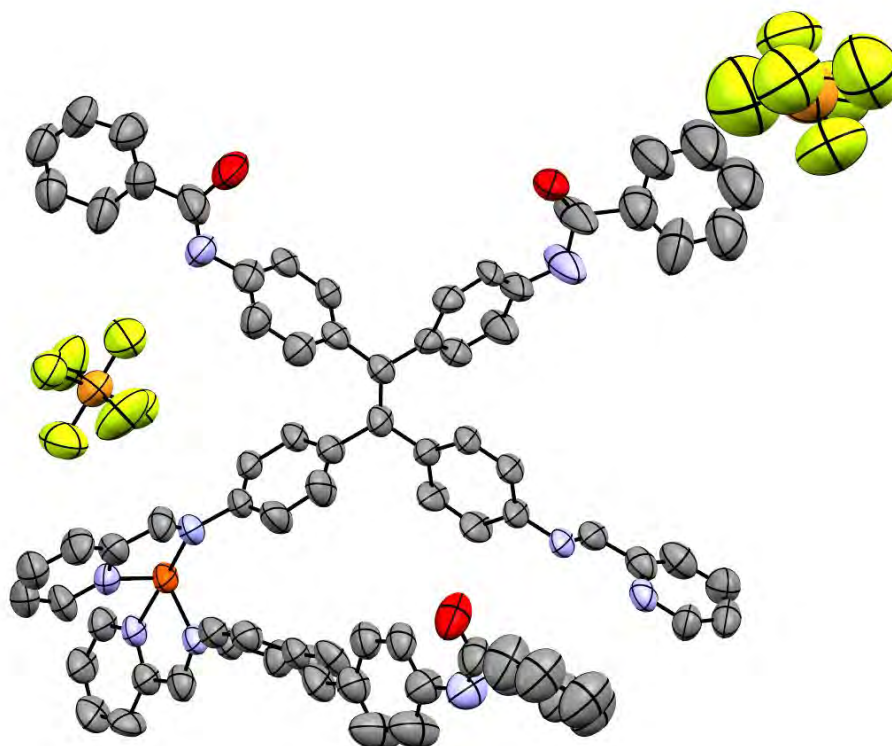


Figure 2.22 An ORTEP representation of the asymmetric unit of the X-ray crystal structure of $[\text{Fe}_2(2.5)_3](\text{PF}_6)_4$. Thermal ellipsoids are drawn at 50% probability.

Brown plate like crystals of $2[\text{Fe}_2(2.2)_3](\text{PF}_6)_8 \cdot \text{H}_2\text{O}$ were grown by slow evaporation of a DMF/methanol solution of the complex. The crystal with dimensions of $0.03 \times 0.02 \times 0.01$ mm was coated in immersion oil type NVH and transferred to the goniometer, where it was cooled with a nitrogen cold stream (100 K) provided by an Oxford Instruments Cryojet 5. Diffraction measurements were carried out using Si<111> monochromated synchrotron X-ray radiation ($\lambda = 0.71023$ Å) (MX2 Beamline at Australian Synchrotron). Data collection was carried out using Blu-Ice suite of software and unit cell refinement, data reduction and processing was carried out with XDS.¹¹¹ Absorption correction was carried out with SADABS.¹¹² The structure was solved using dual space methods with SHELXT.¹¹³ The full-matrix least-square refinements were carried out using SHELXL-2015¹¹³ through Olex2¹¹⁴ suite of software. The crystal only

diffracted to low resolution. One molecule of solvent water could be identified from the difference map and was included in the least-squares refinement. The structure has large solvent accessible voids in the crystal lattice. To address this, solvent mask was used in Olex2 (similar to the SQUEEZE procedure in PLATON). As a result of this solvent mask the R1 was improved 4.67% (from 17.33% to 12.66% and represented two major voids (140 electrons each, possibly two disordered DMF solvent molecules). The PF₆⁻ anions in the unit cell were disordered and were restrained to have similar ADPs (using RIGU) and similar bond lengths (using SADI). There are 3 partial occupancy PF₆⁻ anions in the unit cell, with a combined occupancy of 2. Two of these were modelled isotropically due to poor data quality.

2.14 References

36. (a) Hong, Y.; Lam, J. W. Y.; Tang, B. Z., *Chem. Soc. Rev.* **2011**, *40* (11), 5361-5388; (b) Mei, J.; Hong, Y.; Lam, J. W. Y.; Qin, A.; Tang, Y.; Tang, B. Z., *Adv. Mater.* **2014**, *26* (31), 5429-5479; (c) He, Z.; Ke, C.; Tang, B. Z., *ACS Omega* **2018**, *3* (3), 3267-3277.
58. (a) Han, M.; Luo, Y.; Damaschke, B.; Gómez, L.; Ribas, X.; Jose, A.; Peretzki, P.; Seibt, M.; Clever, G. H., *Angew. Chem. Int. Ed.* **2016**, *55* (1), 445-449; (b) Sun, S.-S.; Anspach, J. A.; Lees, A. J., *Inorg. Chem.* **2002**, *41* (7), 1862-1869; (c) Yan, X.; Xu, J.-F.; Cook, T. R.; Huang, F.; Yang, Q.-Z.; Tung, C.-H.; Stang, P. J., *Proc. Natl Acad. Sci. U. S. A.* **2014**, *111* (24), 8717-8722.
73. Roberts, D. A.; Pilgrim, B. S.; Nitschke, J. R., *Chem. Soc. Rev.* **2018**, *47* (2), 626-644.
74. (a) Pilgrim, B. S.; Roberts, D. A.; Lohr, T. G.; Ronson, T. K.; Nitschke, J. R., *Nat. Chem.* **2017**, *9*, 1276; (b) Roberts, D. A.; Pilgrim, B. S.; Sirvinskaite, G.; Ronson, T. K.; Nitschke, J. R., *J. Am. Chem. Soc.* **2018**, *140* (30), 9616-9623; (c) Roberts, D. A.; Pilgrim, B. S.; Cooper, J. D.; Ronson, T. K.; Zarra, S.; Nitschke, J. R., *J. Am. Chem. Soc.* **2015**, *137* (32), 10068-10071.
75. (a) Young, M. C.; Johnson, A. M.; Hooley, R. J., *Chem. Commun.* **2014**, *50* (11), 1378-1380; (b) Holloway, L. R.; McGarraugh, H. H.; Young, M. C.; Sontising, W.; Beran, G. J. O.; Hooley, R. J., *Chem. Sci.* **2016**, *7* (7), 4423-4427; (c) Holloway, L. R.; Bogie, P. M.; Lyon, Y.; Julian, R. R.; Hooley, R. J., *Inorg. Chem.* **2017**, *56* (18), 11435-11442; (d) Bogie, P. M.; Holloway, L. R.; Lyon, Y.; Onishi, N. C.; Beran, G. J. O.; Julian, R. R.; Hooley, R. J., *Inorg. Chem.* **2018**, *57* (7), 4155-4163; (e) Brega, V.; Zeller, M.; He, Y.; Peter Lu, H.; Klosterman, J. K., *Chem. Commun.* **2015**, *51* (24), 5077-5080; (f) Frank, M.; Hey, J.; Balcioglu, I.; Chen, Y.-S.; Stalke, D.; Suenobu, T.; Fukuzumi, S.; Frauendorf, H.; Clever, G. H., *Angew. Chem. Int. Ed.* **2013**, *52* (38), 10102-10106.
76. Roberts, D. A.; Castilla, A. M.; Ronson, T. K.; Nitschke, J. R., *J. Am. Chem. Soc.* **2014**, *136* (23), 8201-8204.
83. (a) Preston, D.; Fox-Charles, A.; Lo, W. K. C.; Crowley, J. D., *Chem. Commun.* **2015**, *51* (43), 9042-9045; (b) Gan, Q.; Ronson, T. K.; Vosburg, D. A.; Thoburn, J. D.; Nitschke, J. R., *J. Am. Chem. Soc.* **2015**, *137* (5), 1770-1773; (c) Mal, P.; Schultz, D.; Beyeh, K.; Rissanen, K.; Nitschke, J. R., *Angew. Chem. Int. Ed.* **2008**,

- 47 (43), 8297-8301; (d) Zhang, D. W.; Ronson, T. K.; Guryel, S.; Thoburn, J. D.; Wales, D. J.; Nitschke, J. R., *J. Am. Chem. Soc.* **2019**, *141* (37), 14534-14538; (e) Jansze, S. M.; Cecot, G.; Severin, K., *Chem. Sci.* **2018**, *9* (18), 4253-4257; (f) Kim, T. Y.; Vasdev, R. A. S.; Preston, D.; Crowley, J. D., *Chem.- Eur. J.* **2018**, *24* (56), 14878-14890.
86. Paramita, D.; Atul, K.; Prodip, H.; Sarathi, M. P., *Chem.- Eur. J.* **2017**, *23* (51), 12565-12574.
87. (a) Yan, X.; Cook, T. R.; Wang, P.; Huang, F.; Stang, P. J., *Nat. Chem.* **2015**, *7* (4), 342-348; (b) Yan, X.; Wang, H.; Hauke, C. E.; Cook, T. R.; Wang, M.; Saha, M. L.; Zhou, Z.; Zhang, M.; Li, X.; Huang, F.; Stang, P. J., *J. Am. Chem. Soc.* **2015**, *137* (48), 15276-15286; (c) Yan, X.; Wang, M.; Cook, T. R.; Zhang, M.; Saha, M. L.; Zhou, Z.; Li, X.; Huang, F.; Stang, P. J., *J. Am. Chem. Soc.* **2016**, *138* (13), 4580-4588; (d) Zhang, M.; Saha, M. L.; Wang, M.; Zhou, Z.; Song, B.; Lu, C.; Yan, X.; Li, X.; Huang, F.; Yin, S.; Stang, P. J., *J. Am. Chem. Soc.* **2017**, *139* (14), 5067-5074.
88. Kilbas, B.; Mirtschin, S.; Scopelliti, R.; Severin, K., *Chem. Sci.* **2012**, *3* (3), 701-704.
89. Feng, J.; Yao, L.; Zhang, J.; Mu, Y.; Chi, Z.; Su, C.-Y., *Dalton Trans.* **2016**, *45* (4), 1668-1673.
90. Zhu, Y.-X.; Wei, Z.-W.; Pan, M.; Wang, H.-P.; Zhang, J.-Y.; Su, C.-Y., *Dalton Trans.* **2016**, *45* (3), 943-950.
91. Yang, L.; Jing, X.; He, C.; Chang, Z.; Duan, C., *Chem.- Eur. J.* **2016**, *22* (50), 18107-18114.
92. Jiao, J.; Li, Z.; Qiao, Z.; Li, X.; Liu, Y.; Dong, J.; Jiang, J.; Cui, Y., *Nat. Commun.* **2018**, *9* (1), 4423.
93. (a) Carrano, C. J.; Raymond, K. N., *J. Am. Chem. Soc.* **1978**, *100* (17), 5371-5374; (b) Kramer, R.; Lehn, J. M.; Marquis-Rigault, A., *Proc. Natl Acad. Sci. U. S. A.* **1993**, *90* (12), 5394-5398; (c) Hannon, M. J.; Painting, C. L.; Jackson, A.; Hamblin, J.; Errington, W., *Chem. Commun.* **1997**, *18*, 1807-1808; (d) Piguet, C.; Bernardinelli, G.; Hopfgartner, G., *Chem. Rev.* **1997**, *97* (6), 2005-2062; (e) Albrecht, M., *Chem. Rev.* **2001**, *101* (11), 3457-3498; (f) Hannon, M. J.; Childs, L. J., *Supramol. Chem.* **2004**, *16* (1), 7-22; (g) Archer, R. J.; Hawes, C. S.; Jameson, G. N. L.; McKee, V.; Moubaraki, B.; Chilton, N. F.; Murray, K. S.; Schmitt, W.; Kruger, P. E., *Dalton Trans.* **2011**, *40* (45), 12368-12373; (h) Kumar, S. V.; Lo, W. K. C.; Brooks, H. J. L.; Crowley, J. D., *Inorg. Chim. Acta* **2015**, *425*, 1-6; (i) Jana, B.; Cera, L.; Akhuli, B.; Naskar, S.; Schalley, C. A.; Ghosh, P., *Inorg. Chem.* **2017**, *56* (20), 12505-12513; (j) Chen, X.; Gerger, T. M.; Räuber, C.; Raabe, G.; Göb, C.; Oppel, I. M.; Albrecht, M., *Angew. Chem. Int. Ed.* **2018**, *57* (36), 11817-11820.
94. (a) Meng, W.; Breiner, B.; Rissanen, K.; Thoburn, J. D.; Clegg, J. K.; Nitschke, J. R., *Angew. Chem. Int. Ed.* **2011**, *50* (15), 3479-3483; (b) Bilbeisi, R. A.; Clegg, J. K.; Elgrishi, N.; Hatten, X. d.; Devillard, M.; Breiner, B.; Mal, P.; Nitschke, J. R., *J. Am. Chem. Soc.* **2012**, *134* (11), 5110-5119; (c) Ronson, T. K.; Zarra, S.; Black, S. P.; Nitschke, J. R., *Chem. Commun.* **2013**, *49* (25), 2476-2490; (d) Castilla, A. M.; Ramsay, W. J.; Nitschke, J. R., *Acc. Chem. Res.* **2014**, *47* (7), 2063-2073; (e) Ronson, T. K.; Meng, W.; Nitschke, J. R., *J. Am. Chem. Soc.* **2017**, *139* (28), 9698-9707; (f) Rizzuto, F. J.; Ramsay, W. J.; Nitschke, J. R., *J. Am. Chem. Soc.* **2018**, *140* (36), 11502-11509; (g) Fazio, E.; Haynes, C. J. E.; de la Torre, G.; Nitschke, J. R.; Torres, T., *Chem. Commun.* **2018**, *54* (21), 2651-2654.

95. Struch, N.; Bannwarth, C.; Ronson, T. K.; Lorenz, Y.; Mienert, B.; Wagner, N.; Engeser, M.; Bill, E.; Puttreddy, R.; Rissanen, K.; Beck, J.; Grimme, S.; Nitschke, J. R.; Lützen, A., *Angew. Chem. Int. Ed.* **2017**, *56* (18), 4930-4935.
96. (a) Ramsay, W. J.; Rizzuto, F. J.; Ronson, T. K.; Caprice, K.; Nitschke, J. R., *J. Am. Chem. Soc.* **2016**, *138* (23), 7264-7267; (b) Mosquera, J.; Szyszko, B.; Ho, S. K. Y.; Nitschke, J. R., *Nat. Commun.* **2017**, *8*, 14882; (c) Brenner, W.; Ronson, T. K.; Nitschke, J. R., *J. Am. Chem. Soc.* **2017**, *139* (1), 75-78.
97. Anuradha; La, D. D.; Al Kobaisi, M.; Bhosale, S. V., *Sci. Rep.* **2015**, *5*, 15652.
98. (a) Gorvin, J. H., *J. Chem. Soc.* **1959**, 678-682; (b) Donkers, R. L.; Workentin, M. S., *J. Am. Chem. Soc.* **2004**, *126* (6), 1688-1698.
99. Luis, E. T.; Ball, G. E.; Gilbert, A.; Iranmanesh, H.; Newdick, C. W.; Beves, J. E., *J. Coord. Chem.* **2016**, *69* (11-13), 1686-1694.
100. Kruger, P. E.; Mackie, P. R.; Nieuwenhuyzen, M., *Acta Crystallograph. Sect. C* **2000**, *56* (11), e532.
101. Hünig, S.; Kemmer, M.; Wenner, H.; Barbosa, F.; Gescheidt, G.; Perepichka, I. F.; Bäuerle, P.; Emge, A.; Peters, K., *Chem.-Eur. J.* **2000**, *6* (14), 2618-2632.
102. Bock, H.; Nather, C.; Havlas, Z., *J. Chem. Soc., Chem. Commun.* **1995**, *0* (11), 1111-1112.
103. Hoekstra, A.; Vos, A., *Acta Crystallograph. Sect. B* **1975**, *31* (6), 1716-1721.
104. Beves, J. E.; Blight, B. A.; Campbell, C. J.; Leigh, D. A.; McBurney, R. T., *Angew. Chem. Int. Ed.* **2011**, *50* (40), 9260-9327.
105. Wang, Z.; Cohen, S. M., *Chem. Soc. Rev.* **2009**, *38* (5), 1315-1329.
106. (a) Price, W. S., *Concepts Magn. Reson.* **1997**, *9* (5), 299-336; (b) Price, W. S., *Concepts Magn. Reson.* **1998**, *10* (4), 197-237.
107. (a) Beves, J. E.; Chapman, B. E.; Kuchel, P. W.; Lindoy, L. F.; McMurtrie, J.; McPartlin, M.; Thordarson, P.; Wei, G., *Dalton Trans.* **2006**, *5*, 744-750; (b) Beves, J. E.; Constable, E. C.; Housecroft, C. E.; Neuburger, M.; Schaffner, S.; Shardlow, E. J., *Dalton Trans.* **2007**, *1*, 1593-1602; (c) Wang, C.; Hao, X.-Q.; Wang, M.; Guo, C.; Xu, B.; Tan, E. N.; Zhang, Y.-Y.; Yu, Y.; Li, Z.-Y.; Yang, H.-B.; Song, M.-P.; Li, X., *Chem. Sci.* **2014**, *5* (3), 1221-1226; (d) Avram, L.; Cohen, Y., *Chem. Soc. Rev.* **2015**, *44*, 586; (e) Shen, C.; Kennedy, A. D. W.; Donald, W. A.; Torres, A. M.; Price, W. S.; Beves, J. E., *Inorg. Chim. Acta* **2017**, *458*, 122-128; (f) Bloch, W. M.; Holstein, J. J.; Hiller, W.; Clever, G. H., *Angew. Chem. Int. Ed.* **2017**, *56* (28), 8285-8289; (g) Turunen, L.; Warzok, U.; Schalley, C. A.; Rissanen, K., *Chem* **2017**, *3* (5), 861-869; (h) Jiang, Z.; Li, Y.; Wang, M.; Liu, D.; Yuan, J.; Chen, M.; Wang, J.; Newkome, G. R.; Sun, W.; Li, X.; Wang, P., *Angew. Chem. Int. Ed.* **2017**, *56* (38), 11450-11455; (i) Song, B.; Zhang, Z.; Wang, K.; Hsu, C.-H.; Bolarinwa, O.; Wang, J.; Li, Y.; Yin, G.-Q.; Rivera, E.; Yang, H.-B.; Liu, C.; Xu, B.; Li, X., *Angew. Chem. Int. Ed.* **2017**, *56* (19), 5258-5262; (j) Chen, Z.; Sahli, B. J.; MacLachlan, M. J., *Inorg. Chem.* **2017**, *56* (9), 5383-5391; (k) Luis, E. T.; Iranmanesh, H.; Arachchige, K. S. A.; Donald, W. A.; Quach, G.; Moore, E. G.; Beves, J. E., *Inorg. Chem.* **2018**, *57* (14), 8476-8486; (l) Findlay, J. A.; McAdam, C. J.; Sutton, J. J.; Preston, D.; Gordon, K. C.; Crowley, J. D., *Inorg. Chem.* **2018**, *57* (7), 3602-3614.
108. (a) Sarma, R. J.; Otto, S.; Nitschke, J. R., *Chem.-Eur. J.* **2007**, *13* (34), 9542-9546; (b) Schultz, D.; Nitschke, J. R., *Chem.-Eur. J.* **2007**, *13* (13), 3660-3665; (c) Mal, P.; Nitschke, J. R., *Chem. Commun.* **2010**, *46* (14), 2417-2419; (d) Castilla, A. M.; Ousaka, N.; Bilbeisi, R. A.; Valeri, E.; Ronson, T. K.; Nitschke, J. R., *J. Am. Chem. Soc.* **2013**, *135* (47), 17999-18006; (e) Mosquera, J.; Zarra, S.; Nitschke, J. R., *Angew. Chem. Int. Ed.* **2014**, *53* (6), 1556-1559.

109. Lakowicz, J. R., Effects of Solvents on Fluorescence Emission Spectra. In *Principles of Fluorescence Spectroscopy*, Springer US: Boston, MA, 1983, 10.1007/978-1-4615-7658-7_7pp 187-215.
110. Schreivogel, A.; Maurer, J.; Winter, R.; Baro, A.; Laschat, S., *Eur. J. Org. Chem.* **2006**, *2006* (15), 3395-3404.
111. Kabsch, W., *Acta Crystallograph. Sect. D* **2010**, *66* (2), 125-132.
112. Bruker *SADABS*, Bruker: 2001.
113. Sheldrick, G., *Acta Crystallograph. Sect. C* **2015**, *71* (1), 3-8.
114. Dolomanov, O. V.; Bourhis, L. J.; Gildea, R. J.; Howard, J. A. K.; Puschmann, H., *J. Appl. Crystallogr.* **2009**, *42* (2), 339-341.

3 CALCULATING PHOTOSTATIONARY STATE RATIOS WITH UV-VIS SPECTROSCOPY

3.1 Summary

This chapter presents strategies for calculating the ratio of isomers for a given photoswitch at a given photostationary state. Several strategies are discussed, with examples, along with their limitations and assumptions. A review of current methodologies is presented, and a discussion of the requirements to fully calculate the ratio of isomers solely using UV-vis spectroscopy.

3.2 Quantifying photoswitching

When designing new classes of switches, or incorporating photoswitches into larger structures, an important criteria is the ability to selectively generate one isomer upon light irradiation.¹⁸ This parameter is determined by the separation of the absorbance bands for the isomers, allowing selective irradiation of one species. This ratio can be quantified by calculation of the Photostationary Distribution of isomers (PSD) at the Photostationary State (PSS), and is important for maximising structural and functional change upon irradiation. However, determination of the PSD can prove difficult experimentally.

For a theoretical two-state system comprising a thermodynamically stable A and metastable B, the photostationary state composition at a given wavelength is determined by the relative photochemical (denoted Φ_{AB} and Φ_{BA}) and thermal rates (denoted k_{AB} and k_{BA}) at the irradiation wavelength. (Figure 3.1).

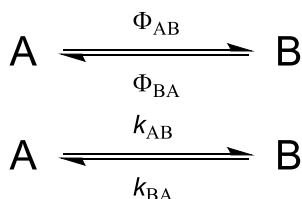


Figure 3.1 Relevant processes for a two-state system where photochemical and thermal processes are of comparable orders of magnitude.

For many photoswitches the forward rate of thermal switching, k_{AB} , is negligible at room temperature. In many cases the thermal back reaction rate, k_{BA} , is also negligible, which leads to effective “bistability”. The various scenarios will be discussed in this chapter increasing in complexity, along with the assumptions which allow approximate calculation of the A/B ratio for a given PSS. Finally, the limitations and requirements of

the current methods for determining the ratios solely using UV-vis spectroscopy will be discussed.

3.3 Thermally bistable systems

In the simplest case it is possible to disconnect the irradiation which generates the PSS from the measurement process, as the thermal half-life is sufficiently long that the system is essentially bistable in the dark. If the samples can be physically separated *via* chromatography, the quantification is straightforward by HPLC or alternate methods. Alternatively, *ex situ* irradiation combined with NMR spectroscopy allows direct quantification of the relative populations of the isomers by simple peak integration. This approach is commonly used for photoswitches with long thermal half-lives. For example, *o*-fluoroazobenzenes, which possess thermal half-lives greater than one year, can be quantified using UPLC integrations of the UV signal measured at the isosbestic point.^{24a} Measurement at the isosbestic point removes the effect of differences in the extinction coefficients of the two isomers, as they are identical at this wavelength. Another example is the hydrazone switches developed by Aprahamian and co-workers,¹¹⁵ as the half-lives are greater than a millennium, allowing trivial determination of the PSD using ¹H NMR spectroscopy.

It is not always desirable to have long thermal half-lives, for example in biological systems where high temporal control is important.^{25d} Upon moving to shorter thermal half-lives, the thermal reversion process (k_{BA}) becomes competitive with the photochemical process. This makes calculation of the PSD more difficult, as the irradiation process can no longer be separated from the measurement. In some cases, measurement at low temperature circumvents this problem, decreasing the thermal rate to where it is negligible compared with the photochemical rates. However, this is not always practical and limits the choice of solvents. When the thermal half-life is short the PSD is also dependant on light flux, with a higher flux leading to greater photoconversion. The problem of calculating the PSD for photoswitches can be subdivided into four categories, dependant on the known and assumed quantities, and these are outlined in the following sections.

3.4 Examples where the spectrum of one species is known

For species where the thermal half-life is relatively short, thermal equilibration in the dark allows the resulting UV-vis spectrum to be assigned to that of the stable isomer. The generated spectrum at the PSS is a linear combination of the known spectrum of the stable isomer and the unknown spectrum of the metastable isomer.

One method to estimate the spectrum of the pure metastable isomer is by knowing that absorbance by any non-emissive species cannot be negative at any wavelength. The maximum percentage of stable isomer remaining at the PSS is estimated by subtracting the highest percentage of the spectrum of the stable isomer from the PSS spectrum that ensures absorbance is positive at all wavelengths. This provides an upper bound of the stable isomer abundance at the PSS, which is often the parameter of most interest, as this reflects the degree of change in the system generated by light irradiation. For example, this methodology has been used to estimate the PSD for symmetric azoimidazoles where the $t_{1/2}$ value was calculated to be only 16 seconds.²²

A simulated example is shown in Figure 3.2 for a model azobenzene based system. The spectrum of the *E*-isomer is collected after allowing sufficient time for thermal relaxation (≥ 6 half-lives). Irradiation generates a PSS, comprised of a mixture of *E* and *Z* isomers. Subtracting 23% of the *E* isomer spectrum from the PSS spectrum is the maximum fraction that gave a positive absorbance at all wavelengths. Correcting for concentration (equation 3.1) gives the calculated *Z*-isomer spectrum.

$$A_Z = \frac{A_{PSS} - A_E \cdot f}{1 - f} \quad (3.1)$$

where f = maximal *E*-isomer percentage in PSS

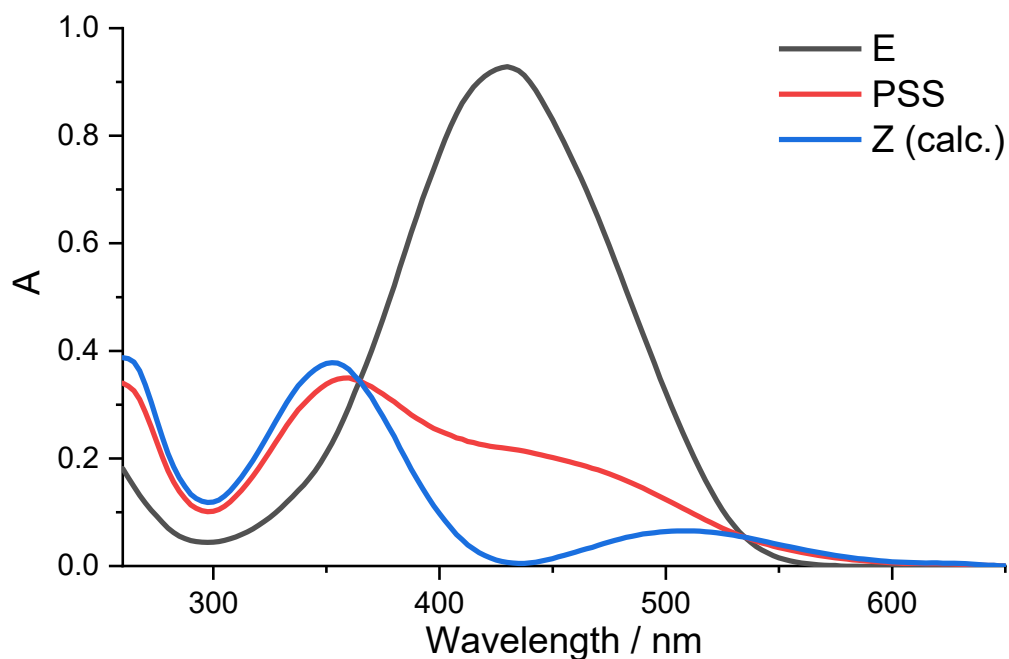


Figure 3.2 Calculating the spectrum of the metastable *Z* isomer (blue) from the known spectrum of the *E* isomer (grey) and a PSS spectrum (red). As the PSS is a linear combination of the spectrum of the *E* and *Z* isomers, the upper bound on the percentage of *E* isomer remaining can be calculated assuming the absorbance is positive at all points. In this case the upper bound on the amount of *E*-isomer remaining was 23%.

In certain cases, spectral features and chemical intuition can guide the estimation of the PSD. For example, the spectrum of the *E*-isomer of an azo-type switch (Figure 3.3) can show vibrational fine structure which is unlikely to be common to both isomers. Therefore, the percentage of *E* isomer remaining at the PSS can be estimated by subtracting a percentage of the spectrum of the authentic *E* isomer from the PSS until no fine structure remained in the spectrum. In both examples discussed here the estimations of PSD are sufficient for practical applications with errors generally $\leq 5\%$.

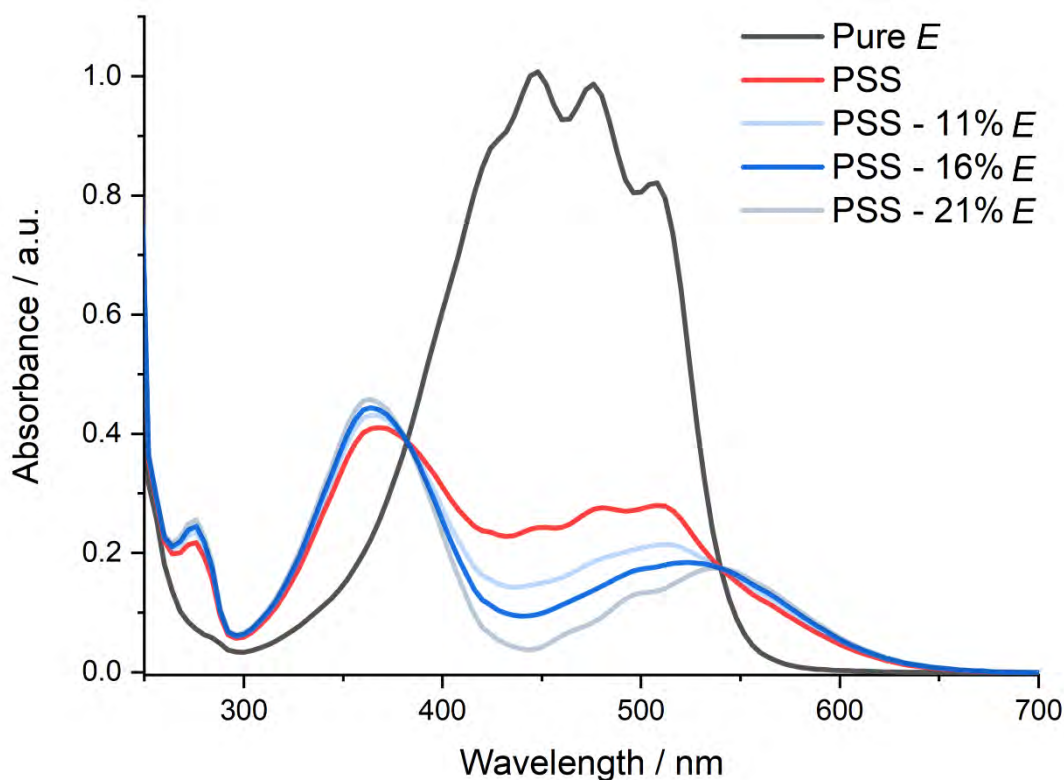


Figure 3.3 Example calculation of the *Z* isomer spectrum from the known spectra of the *E* isomer and the PSS. Subtraction of 16% of the *E*-isomer spectrum from the PSS was the minimum percentage which showed no vibrational fine structure, allowing estimation of the PSD as containing 84% of the *Z*-isomer.

3.5 Examples where relative concentrations are known

The above case assumed that after thermal equilibration only one species is present. There are examples where both k_{AB} and k_{BA} are non-negligible leading to a distribution of species after thermal equilibration. Alternatively, in species where the thermal half-life is very long, it can be impractical to thermally generate 100% of one isomer. These scenarios always generate mixtures of species, making the analysis more complex. However, as the PSS composition is dependent on irradiation wavelength it is possible to generate multiple PSS spectra using different irradiation wavelengths each of which are linear combinations of the spectra of the *E* and *Z* isomers. This can be coupled with an independent technique such as ^1H NMR or UPLC analysis to provide accurate determination of the relative compositions. The pure *E* and *Z* isomer spectra can then be calculated as below:

For two measured photostationary states each comprising only a mixture of *E* and *Z* isomers the absorbance ($A_{PSS,n}$) is:

$$A_{PSS,1} = \varepsilon_E[E]_1 + \varepsilon_Z[Z]_1 \quad (1)$$

$$A_{PSS,2} = \varepsilon_E[E]_2 + \varepsilon_Z[Z]_2 \quad (2)$$

Where $[X]_n$ is the concentration of X at a photostationary state n. If the relative concentrations of *E* and *Z* isomer at each photostationary state are known (for example measured with HPLC or ¹H NMR integration), then the above equation can be solved as a simultaneous equation in two variables.

$$\varepsilon_Z = \frac{A_{PSS,2} - \varepsilon_E[E]_2}{[Z]_2} \quad (3)$$

$$\varepsilon_E = \frac{[Z]_2 A_{PSS,1} - [Z]_1 A_{PSS,2}}{[E]_1 [Z]_2 - [E]_2 [Z]_1} \quad (4)$$

This allows calculation of ε_E at every wavelength from two photostationary states of known composition and subsequent calculation of ε_Z (by equation 3), which can be constructed to give the pure *E* and *Z* spectra. If absolute concentration is not known, scaled spectra can still be constructed by defining an arbitrary $[X]_0$ and representing $[X]_n$ as a fraction of this value. The estimation can also be cross-checked by verifying the position of the isosbestic points, which must be invariant to the *E/Z* isomer ratio.

A simulated example is shown in Figure 3.4, based on an azobenzene system. The spectra at different PSS comprise known percentages of *E* and *Z* isomer, for example using ¹H NMR integrations of a sample irradiated with the same light source. Generating two different PSS allows calculation of ε_E at every point, and subsequent calculation of ε_Z . The difference in concentrations required for UV-vis and NMR measurement may also affect the photostationary state obtained. Concentration effects on thermal half-lives are known,¹⁷¹ and the increased optical density increases the time to reach the PSS. However, as a true photostationary state is independent of photon flux, this methodology is valid for calculating the UV-vis spectra of the two isomers.

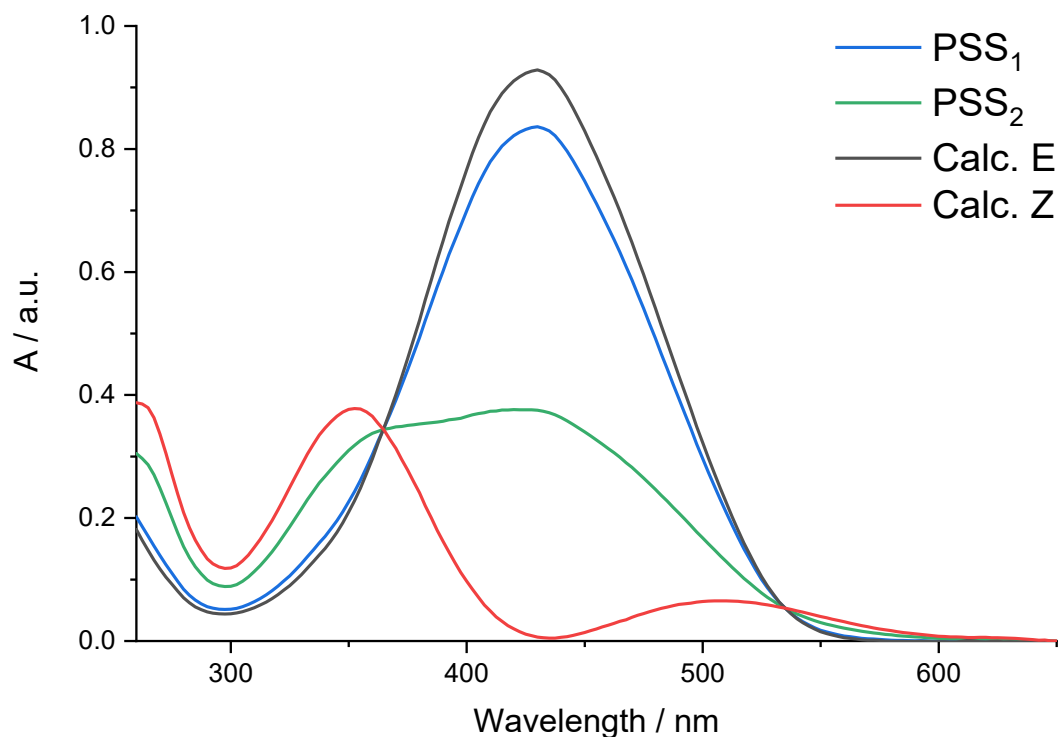


Figure 3.4 Simulated calculation of the spectra of the pure *E* and pure *Z* isomers when two photostationary states are known. PSS₁ comprises 90% *E* isomer and 10% *Z* isomer (determined by a complimentary technique such as ¹H NMR) and PSS₂ contains 40% *E* isomer and 60% *Z* isomer. Solving equation (4) allows calculation of ϵ_E at every wavelength, and determination of the spectrum of the *E* isomer.

3.6 Calculation of spectra where no relative concentrations are known

In the case where the spectrum of one species is known, the percentage of the stable isomer remaining at the PSS is given as an upper bound using the method presented in Section 3.4. However, the assumption that the absorbance of the metastable species is zero at this point is generally not reasonable. If the spectrum also lacks fine structure, this precludes the analysis shown in Figure 3.3. The ability to analytically calculate the PSS ratio is therefore required to accurately construct the spectra of both species. This has been the subject of debate and substantial research efforts in the field, however, it has not been widely applied due to several limitations.¹¹⁶ Methods do exist to solve the problem numerically, however these require several assumptions which may not be appropriate.

The data, and therefore experiments, required can be divided into those conducted without light irradiation and those under irradiation with two different light sources. The data required in the absence of light is such:

- Known light intensity of monochromatic light (e.g. from actinometry)
- Calculated k_{BA} from thermal equilibration after irradiation
- Known concentration at $t = 0$ of species A
- The extinction coefficient of A at the irradiation wavelength

The thermal rate can be easily calculated by fitting the absorbance data in the dark after light irradiation. This data is only limited by the temporal resolution of the instrument, i.e. if the thermal switching rate is very fast it may require specialised time-resolved instrumentation.

The data required from the irradiation experiments includes:

- Absorbance measured at the irradiation wavelength (not the isosbestic point) when PSS is reached
- The initial reaction velocity measured under irradiation at an isosbestic irradiation
- The initial reaction velocity measured under irradiation at a non-isosbestic point

Choice of irradiation wavelengths is important. One wavelength of irradiation should be chosen such that it is an isosbestic point for the isomerisation. This keeps the rate of photon absorption constant through the experiment, as the isosbestic point is defined such that $\epsilon_A = \epsilon_B$. This give a constant photokinetic factor,¹¹⁷ allowing the ratio of Φ_{AB} and Φ_{BA} to be determined.

Collection of this data requires careful experimental design and is dependent on both a collimated and monochromatic light source with known light intensity. This can be produced by monochromating a broadband light source; however, the light intensity is necessarily reduced which may affect the distribution where the thermal half-life is relatively short. The determination of light intensity is most easily achieved through chemical actinometry, for example using potassium ferrioxalate, but could also be measured directly using a power meter.¹¹⁸ The solution must also be homogenous, to ensure even irradiation.

For a real-life system, the precise calculation of half-life is less important than being able to rapidly screen a series of compounds to explore structure-function relationships. The approximate methods are more accessible and give good estimates of the PSD for most applications.

3.7 Conclusion

Current methodologies for calculating photostationary state distribution were discussed, including their limitations, and solutions to a subset of the problems were outlined. Although these techniques are commonly used, their presentation in the literature is opaque, presumably due to the diverse range of photoswitches investigated. In the case where the two species are relatively thermally stable calculation of a PSD is trivial. In the case where exclusively one species can be accessed thermally, the PSD can be estimated based on the requirement that absorbances is always be positive. Where a mixture of states exists, determination of the relative concentrations at distinct photostationary states allows the respective UV-vis spectra. Finally, for the analytically difficult case using exclusively UV-vis spectroscopy the required data to collect are presented, and the additional requirements that would be necessary for calculation of single isomer spectra. This remains an unsolved problem, but development of better methodologies is important to inform development of new photoswitches and work towards incorporating them into larger structures.

3.8 References

17. (a) Coelho, P. J.; Carvalho, L. M.; Fonseca, A. M. C.; Raposo, M. M. M., *Tetrahedron Lett.* **2006**, 47 (22), 3711-3714; (b) Klapötke, T. M.; Piercey, D. G., *Inorg. Chem.* **2011**, 50 (7), 2732-2734; (c) Wendler, T.; Schütt, C.; Näther, C.; Herges, R., *J. Org. Chem.* **2012**, 77 (7), 3284-3287; (d) He, J.; Kimani, F. W.; Jewett, J. C., *J. Am. Chem. Soc.* **2015**, 137 (31), 9764-9767; (e) Garcia-Amoros, J.; Cuadrado, A.; Reig, M.; De Waele, V.; Poizat, O.; Velasco, D., *Chem.-Eur. J.* **2015**, 21 (41), 14292-14296; (f) Kolarski, D.; Szymanski, W.; Feringa, B. L., *Org. Lett.* **2017**, 19 (19), 5090-5093; (g) Travieso-Puente, R.; Budzak, S.; Chen, J.; Stacko, P.; Jastrzebski, J. T. B. H.; Jacquemin, D.; Otten, E., *J. Am. Chem. Soc.* **2017**, 139 (9), 3328-3331; (h) Bartova, K.; Cechova, L.; Prochazkova, E.; Socha, O.; Janeba, Z.; Dracinsky, M., *J. Org. Chem.* **2017**, 82 (19), 10350-10359; (i) Devi, S.; Saraswat, M.; Grewal, S.; Venkataramani, S., *J. Org. Chem.* **2018**, 83 (8), 4307-4322; (j) Stricker, L.; Boeckmann, M.; Kirse, T. M.; Doltsinis, N. L.; Ravoo, B. J., *Chem.-Eur. J.* **2018**, 24 (34), 8639-8647; (k) Harris, J. D.; Moran, M. J.; Aprahamian, I., *Proc. Natl Acad. Sci. U. S. A.* **2018**, 115 (38), 9414-9422; (l) Simeth, N. A.; Crespi, S.; Fagnoni, M.; König, B., *J. Am. Chem. Soc.* **2018**,

- 140 (8), 2940-2946; (m) Crespi, S.; Simeth, N. A.; Bellisario, A.; Fagnoni, M.; König, B., *J. Phys. Chem. A* **2019**, *123* (9), 1814-1823; (n) Kumar, P.; Srivastava, A.; Sah, C.; Devi, S.; Venkataramani, S., *Chem.- Eur. J.* **2019**, *25*, 11924-11932.
18. Crespi, S.; Simeth, N. A.; König, B., *Nat. Rev. Chem* **2019**, *3* (3), 133-146.
22. Weston, C. E.; Richardson, R. D.; Fuchter, M. J., *Chem. Commun.* **2016**, *52* (24), 4521-4524.
24. (a) Bléger, D.; Schwarz, J.; Brouwer, A. M.; Hecht, S., *J. Am. Chem. Soc.* **2012**, *134* (51), 20597-20600; (b) Knie, C.; Utecht, M.; Zhao, F.; Kulla, H.; Kovalenko, S.; Brouwer, A. M.; Saalfrank, P.; Hecht, S.; Bléger, D., *Chem.- Eur. J.* **2014**, *20* (50), 16492-16501; (c) Siewertsen, R.; Neumann, H.; Buchheim-Stehn, B.; Herges, R.; Naether, C.; Renth, F.; Temps, F., *J. Am. Chem. Soc.* **2009**, *131* (43), 15594-+; (d) Beharry, A. A.; Sadovski, O.; Woolley, G. A., *J. Am. Chem. Soc.* **2011**, *133* (49), 19684-19687; (e) Bléger, D.; Hecht, S., *Angew. Chem. Int. Ed.* **2015**, *54* (39), 11338-11349.
25. (a) Beharry, A. A.; Woolley, G. A., *Chem. Soc. Rev.* **2011**, *40* (8), 4422-4437; (b) Samanta, S.; Babalhavaeji, A.; Dong, M. X.; Woolley, G. A., *Angew. Chem. Int. Ed.* **2013**, *52* (52), 14127-30; (c) Samanta, S.; Beharry, A. A.; Sadovski, O.; McCormick, T. M.; Babalhavaeji, A.; Tropepe, V.; Woolley, G. A., *J. Am. Chem. Soc.* **2013**, *135* (26), 9777-9784; (d) Dong, M.; Babalhavaeji, A.; Samanta, S.; Beharry, A. A.; Woolley, G. A., *Acc. Chem. Res.* **2015**, *48* (10), 2662-2670; (e) Szymański, W.; Beierle, J. M.; Kistemaker, H. A. V.; Velema, W. A.; Feringa, B. L., *Chem. Rev.* **2013**, *113* (8), 6114-6178; (f) Ferreira, R.; Nilsson, J. R.; Solano, C.; Andreasson, J.; Grotli, M., *Sci. Rep.* **2015**, *5*.
115. Qian, H.; Pramanik, S.; Aprahamian, I., *J. Am. Chem. Soc.* **2017**, *139* (27), 9140-9143.
116. (a) Fischer, E., *J. Phys. Chem.* **1967**, *71* (11), 3704-3706; (b) Pimienta, V.; Lavabre, D.; Levy, G.; Samat, A.; Guglielmetti, R.; Micheau, J. C., *J. Phys. Chem.* **1996**, *100* (11), 4485-4490; (c) K, S.; K, B., *Sci. Repts.* **2017**, *7* (1), 41145.
117. Maafi, M.; Brown, R. G., *Int. J. Chem. Kinet.* **2005**, *37* (3), 162-174.
118. Hatchard, C. G.; Parker, C. A., *Proc. R. Soc. A* **1956**, *235* (1203), 518-536.

4 VISIBLE LIGHT PHOTOSWITCHING BY AZOBENZAZOLES

This chapter is based on the following publication: A. D. W. Kennedy, I. Sandler, J. Andréasson, J. Ho, and J. E. Beves, Visible light photoswitching by azobenzazoles, *Chem. - Eur. J.*, **2020**, *5*, 1103-1110.

Contributions: Isolde Sandler and Dr Junming Ho performed the *ab initio* computations. Professor Joakim Andréasson advised on photoswitching measurements and experimental design.

4.1 Summary

This chapter discusses azo-based visible light photoswitches incorporating benzazole units. The molecules were synthesised by oxidative coupling, fully characterised by NMR and single crystal X-ray diffraction and their electronic properties measured. Irradiation with visible light generated a mixture of *E* and *Z* isomers, and both the *E/Z* distribution and thermal half-life of the *Z* isomer was measured in a variety of solvents. The effect of protonation was studied, leading to compound **4.1H⁺** which can be photoswitched using yellow light with a thermal half-life of around 5 minutes. These findings were supported with high-level *ab initio* calculations validating the proposed site of protonation.

4.2 Symmetric azoheteroarene pH switch

Azobis(2-imidazole) (Figure 4.1), is a symmetric azoheteroarene initially reported by Fuchter and co-workers,^{22, 119} which absorbs blue light and is protonated preferentially on the imidazole nitrogen leading to a red-shift in absorption and an *increase* in thermal half-life (from 16 to 352 s in H₂O). An intramolecular hydrogen bond stabilises the protonated *Z* isomer and leads to a significant difference in proton affinity between the two isomers (p*K*_a values in water: *E* 4.7; *Z* 6.0), which can be used to reversibly modulate the pH of a solution.²²

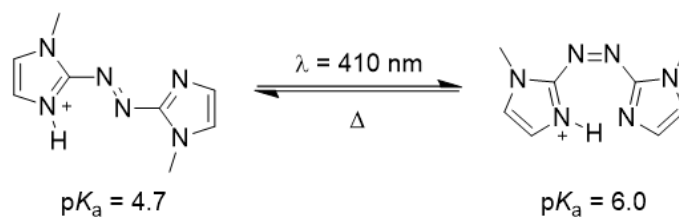


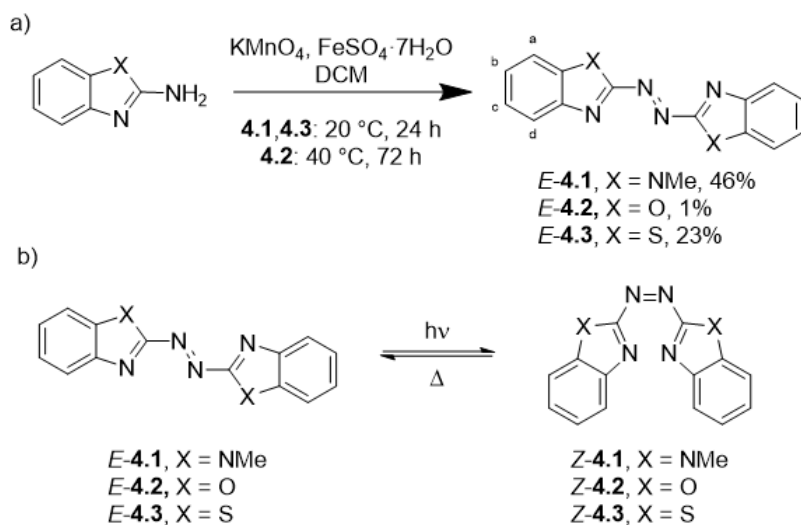
Figure 4.1 Reversible modulation of pK_a *via* light irradiation.

The majority of azoheteroarenes previously studied have shown switching using UV light, which has some disadvantages as discussed in section 1.4. An obvious strategy to shift the absorption of an azobenzene-type molecule into the visible is to extend the conjugation length of the system, for example by benzoannellation. Although the use of symmetric systems prevents the effective use of the symmetry forbidden $n-\pi^*$ transition,¹²⁰ it does avoid the potential problems of push-pull systems or relying on protonation to deliver visible light absorption. In this chapter the photoswitching properties of symmetric azobenzazole photoswitches are investigated.

4.3 Synthesis and characterisation

4.3.1 Symmetric azobenzazoles

Symmetric azobenzazoles **4.1**,¹²¹ **4.2** and **4.3**¹²² were synthesised in a single step by oxidative coupling of the commercially available amino compounds. The coupling used KMnO_4 supported on $\text{FeSO}_4 \cdot 7\text{H}_2\text{O}$ ¹²³ and gave **4.1–3** in low to moderate yields (Scheme 4.1). The *N*-methylated benzimidazole was used to form **4.1** as free amine groups *ortho* to the azo group are known to cause fast thermal relaxation through tautomerism.^{22, 124} The yield of **4.2** was particularly poor, which is tentatively attributed to hydrolysis



Scheme 4.1 a) Synthesis of symmetric azobenzazoles in this work. b) Photoswitching from the thermally stable *E* isomer to the unstable *Z* isomer.

No care was taken to exclude light from the preparation of these compounds, and ^1H NMR spectroscopy in CDCl_3 indicated the presence of a single symmetric isomer in solution (Figure 4.2), assigned to the *E* isomer in all cases.

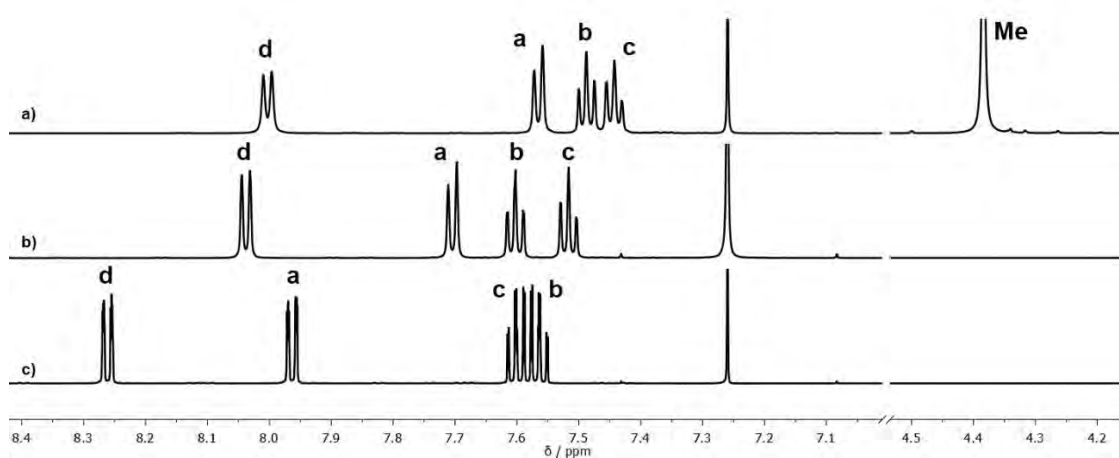


Figure 4.2 ^1H NMR spectra of **4.1-3** (600 MHz, CDCl_3 , 298 K), see Scheme 4.1 for atom labels.

Compounds **4.1-3** were characterised in detail using 1D and 2D NMR techniques, electrospray ionisation mass spectrometry (ESI-MS) and single crystal X-ray diffraction (see Sections 8.1-3).¹⁰⁰ Single crystals of compounds **4.1-3** were grown by slow solvent evaporation, allowing determination of their solid-state structures by X-ray diffraction (Figure 4.3). The crystal structures of **4.1-3** each have half a molecule in the asymmetric unit, with an inversion centre in the middle of the azo bond. The rings are therefore coplanar, and the molecules each adopt the *anti*-configuration about the azo bond. The $\text{N}=\text{N}$ bond lengths are slightly longer than average for azobenzene containing structures

ranging from 1.266(2) Å to 1.276(2) Å (From the CSD: average N=N distance = 1.254 Å, averaged from 2026 structures, CCDC accessed September 2019).

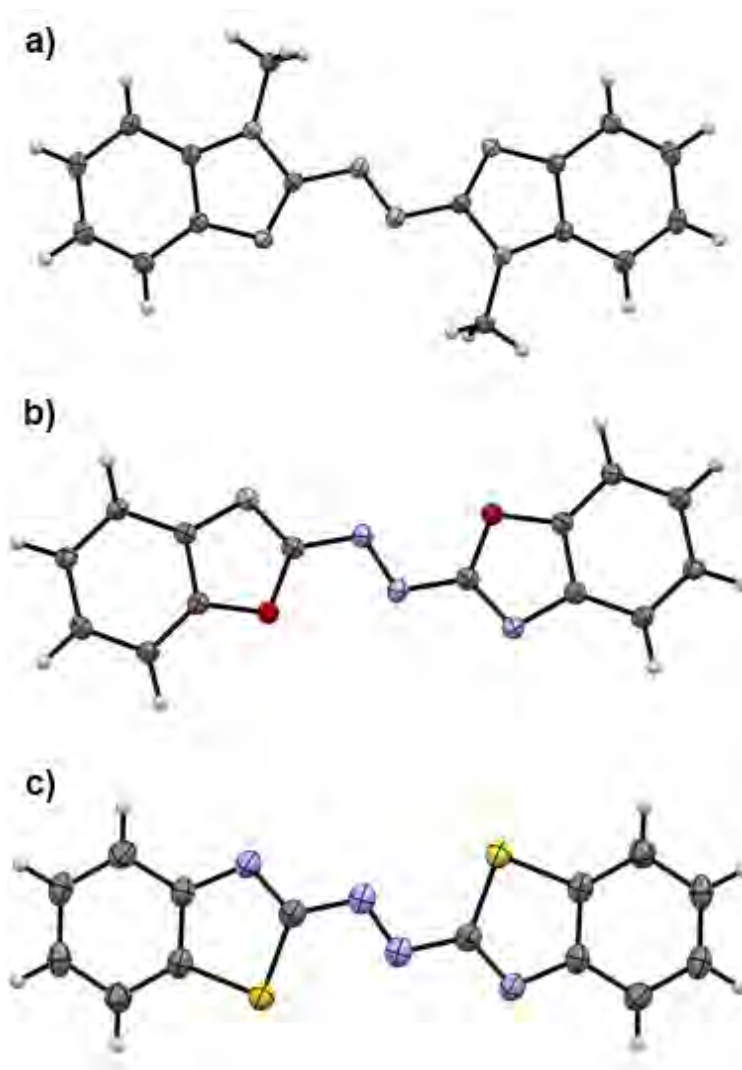
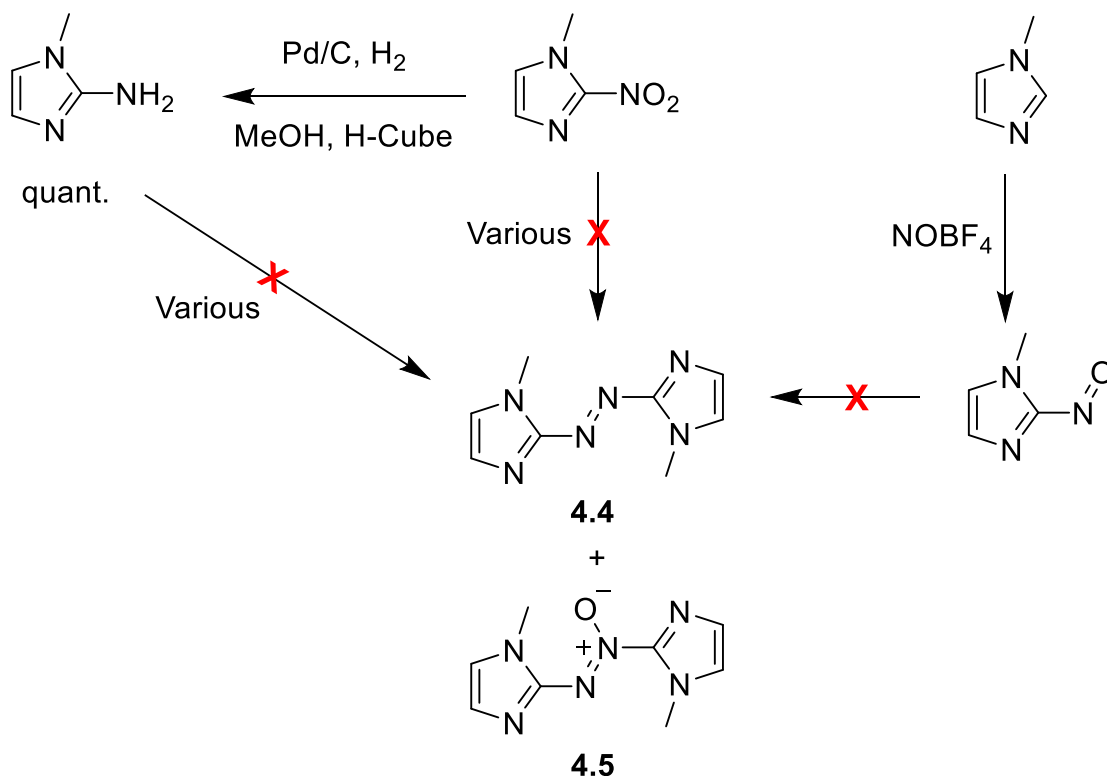


Figure 4.3 Single crystal X-ray structures of a) **4.1**, b) **4.2**, and c) **4.3**. Thermal ellipsoids are shown at the 50% probability level.

4.3.2 Attempted syntheses of azo(bisimidazole)

Various methods were attempted to synthesise compound **4.4**, previously reported by Fuchter and co-workers²² and Bieske and co-workers.¹¹⁹ These constitute three major routes: reductive coupling from 1-methyl-2-nitroimidazole (summarised in Table 4.1), oxidative coupling from 1-methyl-2-aminoimidazole and a modified Mills reaction, where 1-methyl-2-nitrosoimidazole is formed *in situ* and reacted with 1-methyl-2-aminoimidazole.



Scheme 4.2 Attempted synthesis of azobis(2-imidazole).

Table 4.1 Optimisation of the formation of **4.4** using reductive methodologies.

Conditions	Result
Zn, NH ₄ Cl, H ₂ O, 45 °C, 1h (lit.)	4.4 (49% yield)
Zn, NH ₄ Cl, H ₂ O, 45 °C, 1h (this work)	4.4 + 4.5 (17% as a mixture)
Zn, CaCl ₂ , H ₂ O, 45 min	Reduction of the azo bond
Zn, CaCl ₂ , H ₂ O, 25 min	4.4 (9%)
Zn, NaOH, H ₂ O/EtOH (1:2), 110 min	Starting material
NaBH ₄ , DMSO, 90 min	4.4 (17%)

The reductive coupling was unreliable and generally gave poor yields and was contaminated with a non-symmetric impurity, indicated by the presence of two non-equivalent methyl signals. This impurity was identified as the azoxy derivative (**4.5**) by ESI-MS. A single crystal structure of this azoxy species was also obtained (Figure 4.4), confirming the incomplete reduction. The crystal structure shows some disorder about the azo bond, attributed to the pedal motion commonly seen for azobenzene structures.¹²⁵ Interestingly, the molecule adopts the *syn*-conformation about the azo bond. This was not seen in any of the other azoheteroarene X-ray structures and is attributed to a favourable hydrogen-bonding interaction with the four water molecules also located in the unit cell.

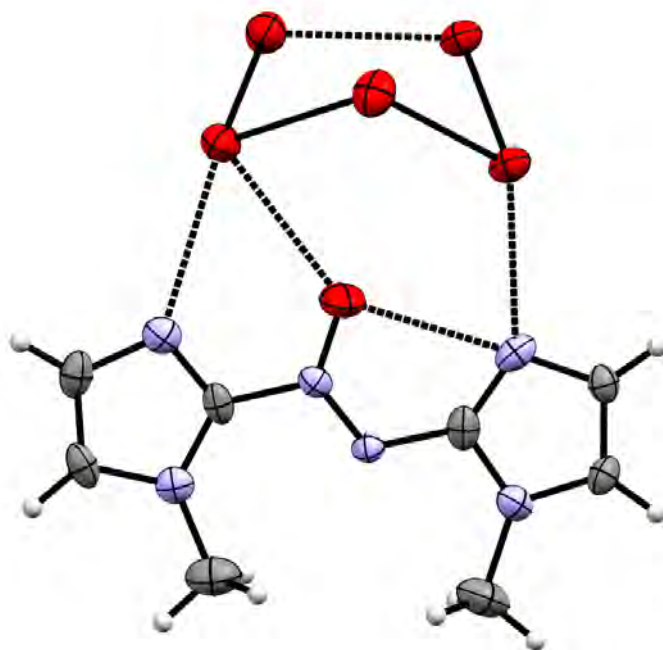


Figure 4.4 Single crystal X-ray structures of **4.5** showing the hydrogen bonding network formed between the water molecules and the azoxy unit. Thermal ellipsoids are shown at the 50% probability level and H-bonding interactions are shown as dashed lines (contact distance < sum of the Van de Waals radii). The azo bond disorder and water hydrogens have been omitted for clarity.

Several oxidative methods for producing azobenzenes from aromatic anilines are known, however they often have difficulties with over-oxidation or unwanted side-products.^{123b} 2-Amino-1-methylimidazole was readily formed by reduction of the corresponding nitro derivative using Pd/C and hydrogen gas. However, selective oxidation to the azo species using $\text{KMnO}_4/\text{FeSO}_4 \cdot 7\text{H}_2\text{O}$,^{123a} NCS/DBU¹²⁶ or Oxone¹²⁷ only lead to decomposition of the starting material. Finally, direct formation of the nitroso imidazole using NOBF_4 was investigated. Addition of NOBF_4 to 1-methylimidazole lead to formation of a green solution, consistent with nitroso formation. Subsequent addition of the amino-imidazole compound lead to the formation of a deep red solution, however the ^1H NMR on work up was not consistent with the azo(bisimidazole) product. The remainder of this chapter will therefore focus on the azobenzazole photoswitches.

4.4 Absorption and photoswitching properties

4.4.1 UV-Vis absorption

The UV-vis absorption properties of **4.1–3** were characterised in solution (Figure 4.5). The UV-vis absorption spectra after equilibration in the dark at room temperature were assigned to 100% *E* isomer, consistent with the single species observed by ^1H NMR spectroscopy. Compound **4.1** has a broad absorption band with a maximum at 439 nm (in acetonitrile, assigned as a $\pi\text{-}\pi^*$ transition), red-shifted by ≈ 40 nm relative to that of azobis(2-imidazole). Compounds **4.2** and **4.3** also absorb strongly in the visible with slightly narrower $\pi\text{-}\pi^*$ absorption bands at 430 and 421 nm respectively. The absorption spectra of **4.1–3** are relatively insensitive to solvent. The wavelength of maximum visible absorption, λ_{max} , varies by < 10 nm as the solvent is varied (methanol, acetonitrile, dichloromethane, chloroform, or toluene, see Figure 4.6).

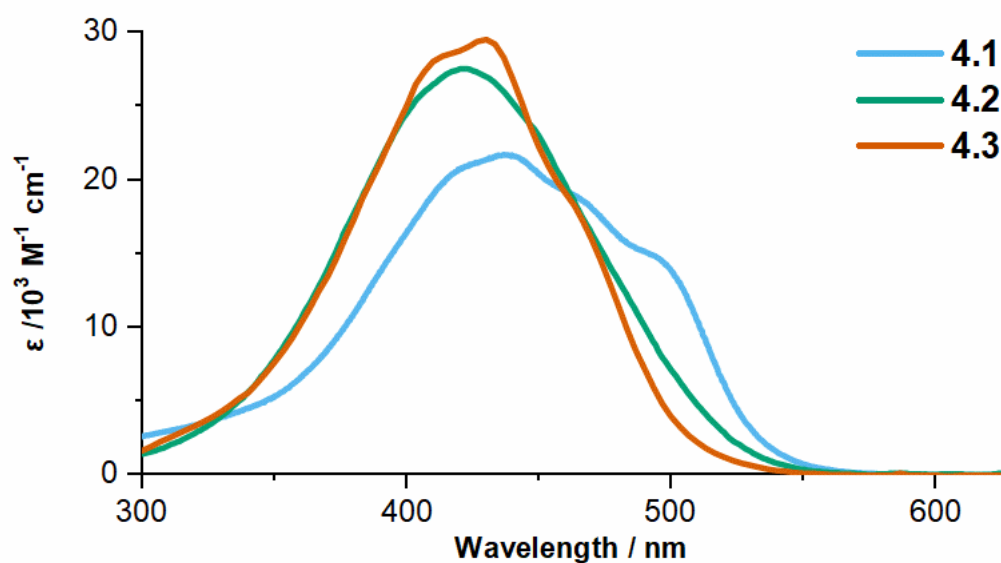


Figure 4.5 UV-Visible absorption spectra of **4.1–3** in acetonitrile at 298 K (pure *E* isomer in all cases).

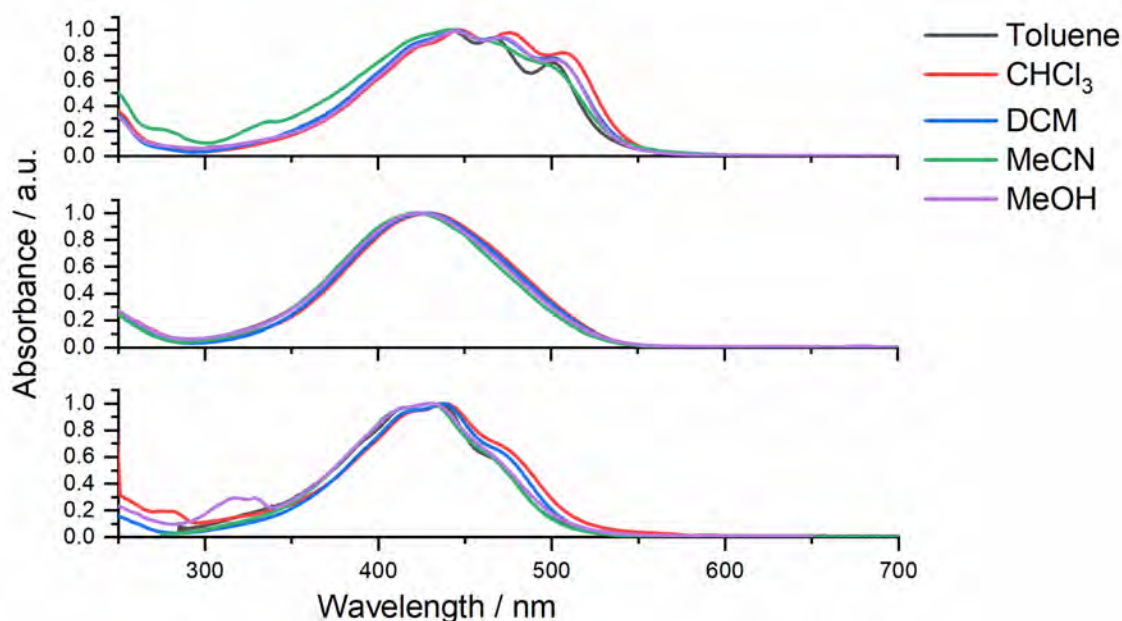


Figure 4.6 UV-Visible absorption spectra of **4.1–3** in a range of solvents at 298 K. a) **4.1**; b) **4.2** and c) **4.3**

4.5 Photoswitching properties

Irradiation with 448 nm light was used to enrich the samples in the *Z*-isomer. As the thermal half-life was relatively short, the distribution could not be quantified using NMR spectroscopy or HPLC. Therefore, the methodologies discussed in Chapter 3 were used to calculate the distribution of isomers at the 448 nm photostationary state. In all cases a PSS comprising ≥ 73 % of the *Z* isomer was generated (Table 4.2). Figure 4.7a shows the spectra recorded before and during irradiation at 448 nm. Like their absorption spectra, the PSD of **4.1–3** are largely independent of solvent. Absorption spectra and switching cycles of **4.1–3** in acetonitrile, methanol, chloroform, dichloromethane and toluene are shown in Sections 8.6-8.8 with corresponding data in Table 4.2 and Table 4.4. An important consideration for photoswitches is their resistance to degradation under irradiation. This was quantified by subjecting the compounds to 20 switching cycles comprising 10 seconds irradiation (448 nm) and 500 seconds in the dark. Each of **4.1–3** also has excellent fatigue resistance ($\geq 99\%$ recovery of absorbance/cycle) in all solvents tested.

The PSD of compound **4.1** in these solvents comprises between 87–84% of the *Z* isomer as the bands of the two isomers are similarly separated, and the relative quantum yields of switching comparable, in the solvents studied. Similarly, the PSD for compound

4.3 is 81–77% of the *Z* isomer in these solvents. Compound **4.2** has a slightly lower proportion of the *Z* isomer in the PSD (78–73%, except in methanol) due to the stronger relative absorption of the *Z* isomer at 448 nm. In methanol the PSD for **4.2** comprises only 45% of the *Z* isomer and some photo decomposition is also observed, hinting at more complicated behaviour (Figure 8.37).

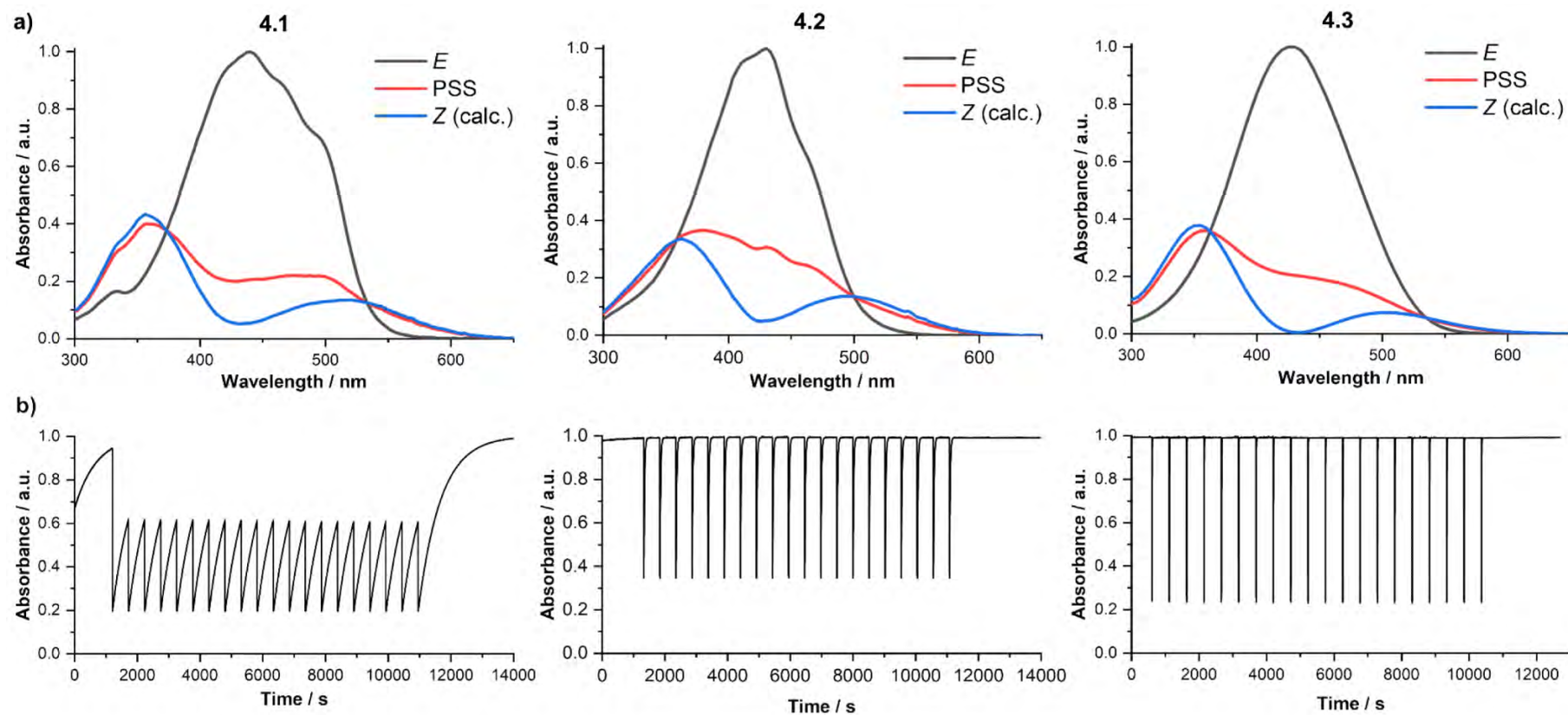


Figure 4.7 Photoswitching of **4.1-3** in acetonitrile. a) Comparison of the absorption spectra of the pure *E* isomer, the PSS (recorded under 448 nm irradiation) and calculated pure *Z* isomer. The *Z* isomer spectra were calculated using the assumption that the PSS spectrum is a linear combination of *E* and *Z* isomer spectra. b) 20 switching cycles of alternating irradiation (10 seconds, 448 nm LED, 1.3 W) and dark (500 seconds) at 298 K. Absorbance values were measured at the λ_{max} for each compound.

Table 4.2 Summary of measured and calculated photophysical and photoswitching properties for compounds **4.1-3** in several solvents.^a

Solvent	λ_{\max} / nm	$t_{1/2}$ / s	PSD (Z:E)	Recovery / cycle
4.1				
Toluene	442	100	87:13	quant.
CHCl ₃	447	114	84:16	99.9%
DCM	444	232	85:15	99.9%
MeCN	441	520	84:16	quant.
MeOH	445	147	86:14	99.9%
4.2				
Toluene	436	31	74:26	99.5
CHCl ₃	438	10	78:22	99.7
DCM	437	12	74:26	Quant.
MeCN	430	14	73:27	Quant.
MeOH	430	< 1	45:55	98.9
4.3				
Toluene	426	84	81:19	99.9%
CHCl ₃	430	32	77:23	quant.
DCM	428	39	79:21	99.9%
MeCN	421	0.4	80:20	quant.
MeOH	424	1	78:22	quant

^a Thermal lifetimes, PSD and recovery/cycle were determined by UV-vis spectroscopy as discussed in Chapter 3 and section 4.12.6.

4.5.1 The effect of different LED sources

Irradiation with a 448 nm light was used to isomerise compounds **4.1-3** from the *E* to *Z* isomer as this was found to maximise the proportion of the *Z* isomer formed. Several other wavelengths were investigated, and the corresponding PSS spectra are shown in Figure 4.8a for compound **4.1**. The PSD values were also calculated, using the method discussed in Chapter 3. Note that for the longest wavelengths no photoswitching was seen, as the *E* isomer of **4.1** does not absorb at these wavelengths (Figure 4.8b)

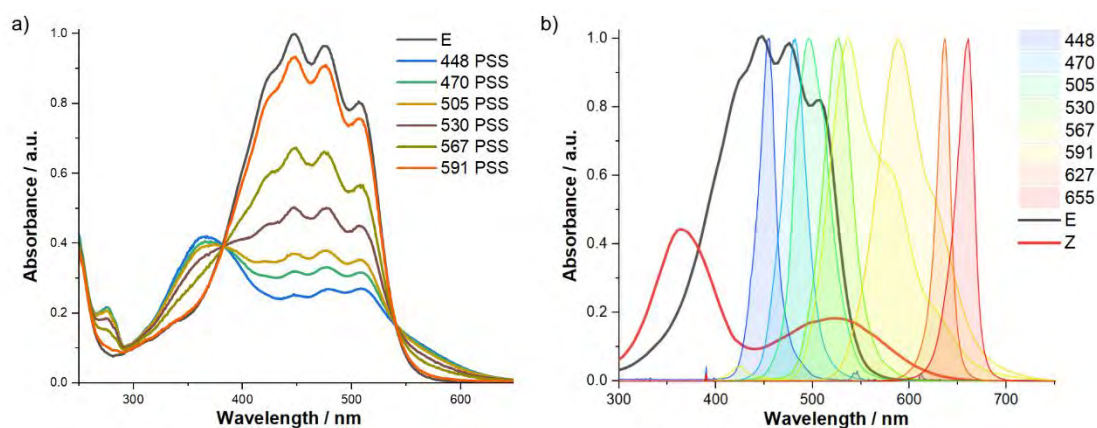


Figure 4.8 a) Effect of different LED light sources on the photoswitching of **4.1** (chloroform, 298 K). b) Overlap of the emission bands of the LED sources with the absorbance spectra of *E*-**4.1** (CHCl₃) and calculated absorbance spectra of *Z*-**4.1**.

Table 4.3 Calculated percent switching of **4.1** with irradiation from different LED sources ^a

Irradiation λ_{max}	PSD (<i>Z</i> : <i>E</i>)
448	84:16
470	79:21
505	74:26
530	57:43
567	36:64
591	> 90% <i>E</i> ^b
627	^c
655	^c

^a λ_{max} refers to the manufacturer's specified average value for dominant wavelength. ^b The extent of switching could not be fully quantified due to the low concentration of *Z* isomer. ^c No switching was observed.

4.6 Thermal half-life measurements

Examples of a single switching cycle for each of **4.1–3** in acetonitrile are shown in Figure 4.9 and key parameters are summarised in Table 4.4. The difference in the thermal half-lives ($t_{1/2}$) for the $Z \rightarrow E$ isomerisation is immediately apparent. Compound **4.1** has a half-life of 520 s in acetonitrile, which is among the longest known for visible light switchable azoheteroarenes.¹²⁸ Compounds **4.2** and **4.3** have shorter half-lives of 14 and 0.4 s respectively, showing that small differences in structure can drastically alter the photoswitching properties.

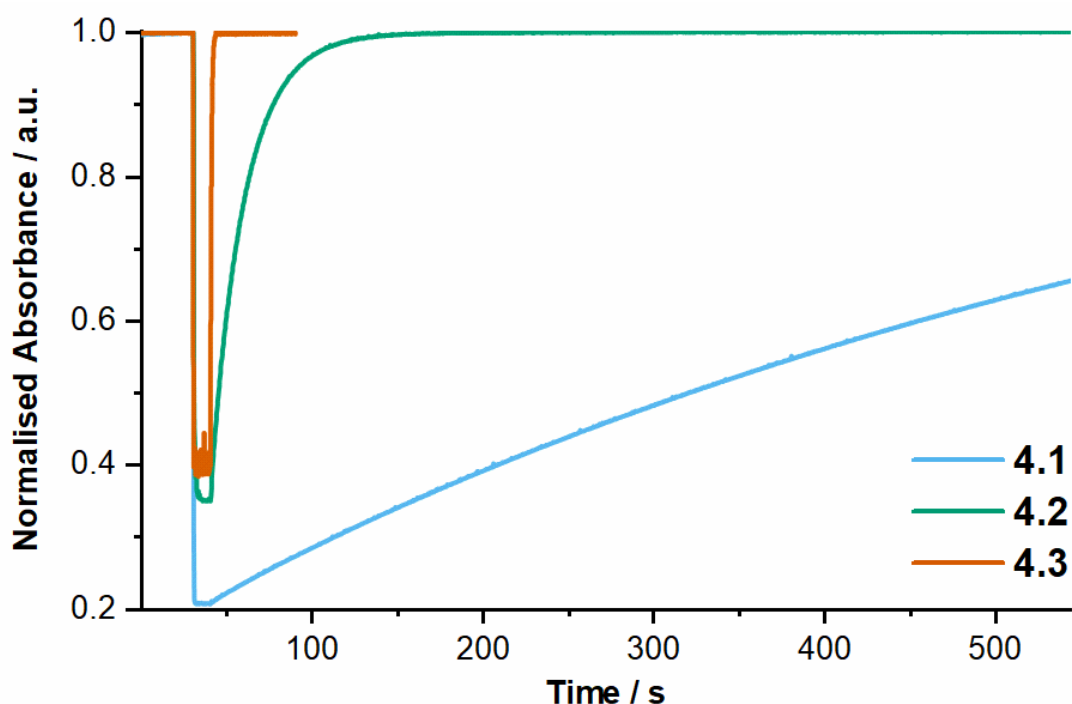


Figure 4.9 Normalised absorption of **4.1**, **4.2** and **4.3** each measured at λ_{max} in acetonitrile and irradiated with a 448 nm LED (1.3 W) for 10 s, followed by thermal equilibration in the dark. Further irradiation had no effect on the spectra, see Figures 8.26, 8.32 and 8.38.

Table 4.4 Key photoswitching properties of **4.1**, **4.2**, **4.3** and **4.4** in acetonitrile ^a

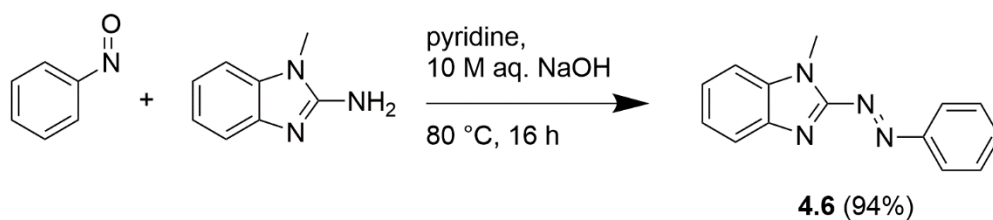
Compound	PSD (Z:E) ^b	$t_{1/2}$ / s ^c	Thermal Z to E barrier / kJ mol ⁻¹ ^d	% Recovery / cycle ^e
4.1	84:16	520	89	> 99.9
4.2	73:27	14	80	> 99.9
4.3	80:20 ^g	0.4	72	> 99.9
4.4 ²²	80:20 ^f	175 ^f	87	—

^[a] Measured in dry acetonitrile at 298 K by UV-vis spectroscopy. ^[b] Upon irradiation with 448 nm light. See Chapter 3 for discussion on calculation of PSD. ^[c] Thermal half-life of Z to E isomerisation, see section 4.12.6 for details. ^[d] Calculated from half-life. ^[e] Calculated after 20 switching cycles (10 s light irradiation). ^[f] Data from this work. Solution was irradiated at 448 nm for ease of comparison, however reported maximum switching (90:10) is with 408 nm irradiation.²² ^[g] Maximum E isomer remaining in the PSD. See Chapter 3, Section 3.4 for details.

The effect of solvent on the rate of thermal isomerisation was studied for **4.1–3**. The thermal half-life for the Z→E isomerisation of compound **4.1** ranges from 100 s in toluene to 520 s in acetonitrile, corresponding to a 4 kJ mol⁻¹ increase in the thermal barrier. Compound **4.2** shows much faster thermal isomerisation in all solvents ($t_{1/2} \leq 31$ s). Compound **4.3** shows the most pronounced solvent sensitivity: the difference between the thermal half-life in acetonitrile (0.4 s) and toluene (84 s) corresponds to an increase in thermal barrier of 13 kJ mol⁻¹. The observed thermal half-lives appear to roughly correlate with solvent polarity, *i.e.* more polar solvents result in shorter thermal half-lives.

4.7 Unsymmetrical azobenzimidazole

The compounds above are symmetrical about the azo bond, however significant investigation has been made into azo compounds comprising a heteroaromatic system and a (derivatised) phenyl group. Compound **4.6** was synthesised by a modified Mills coupling^{23a} of nitrosobenzene and 2-amino,1-methylbenzimidazole in excellent yield.



Scheme 4.3 Synthesis of unsymmetric azoheteroarene.

^1H NMR spectroscopy in CDCl_3 indicated the presence of only one isomer, assigned as *E*-**4.6**. Slow evaporation of a CDCl_3 solution of **4.6** gave dark orange crystals which were suitable for X-ray diffraction studies (Figure 4.10). Surprisingly, the crystal structure showed $[\text{4.6D}]\text{Cl}$, where the proton was localised on the benzimidazole ring. This is attributed to the known formation of DCl upon light exposure of CDCl_3 .¹²⁹ The rings are co-planar, and the $\text{N}=\text{N}$ bond length is 1.259 Å, comparable to the average in azobenzenes (From the CSD: average $\text{N}=\text{N}$ distance = 1.254 Å, averaged from 2026 structures, CCDC accessed September 2019.)

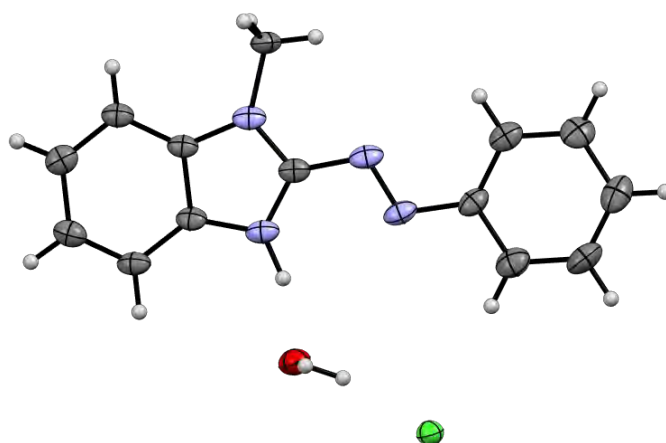


Figure 4.10 Single crystal X-ray structure of $[\text{4.6D}]\text{Cl}\cdot\text{H}_2\text{O}$. Thermal ellipsoids are shown at the 50% probability level.

UV-Vis spectroscopy in acetonitrile showed a relatively narrow absorbance band centred at 376 nm, red-shifted 20 nm relative to the non-benzoannulated compound phenylazo(2-methyl)imidazole (Figure 4.11).^{124a} The compound shows limited bidirectional photoisomerisation upon exposure to visible light ($E\rightarrow Z$: 448 nm, $Z\rightarrow E$: 530 nm). The compound possesses a much longer thermal half-life than the symmetric compounds, with a $t_{1/2}$ of 6.4 hours in acetonitrile (calculated $\Delta G^\ddagger = 99 \text{ kJ mol}^{-1}$). This has been rationalised in related compounds as stabilising $\text{C-H}\cdots\pi$ interactions in the *Z* isomer.^{23b} However as the visible light photoswitching was limited, future discussion will be limited to the symmetric azobenzazoles.

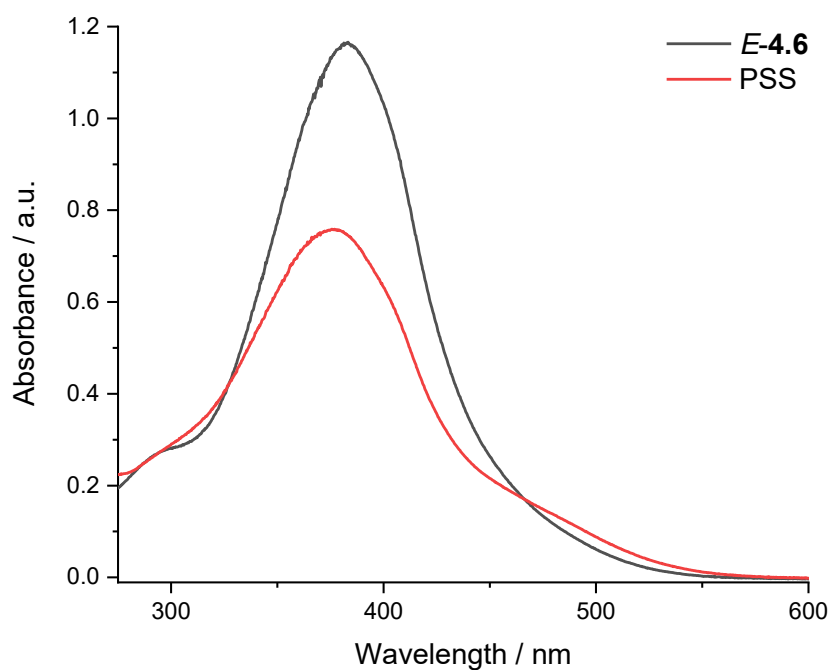


Figure 4.11 Photoswitching of 4.6 in acetonitrile.

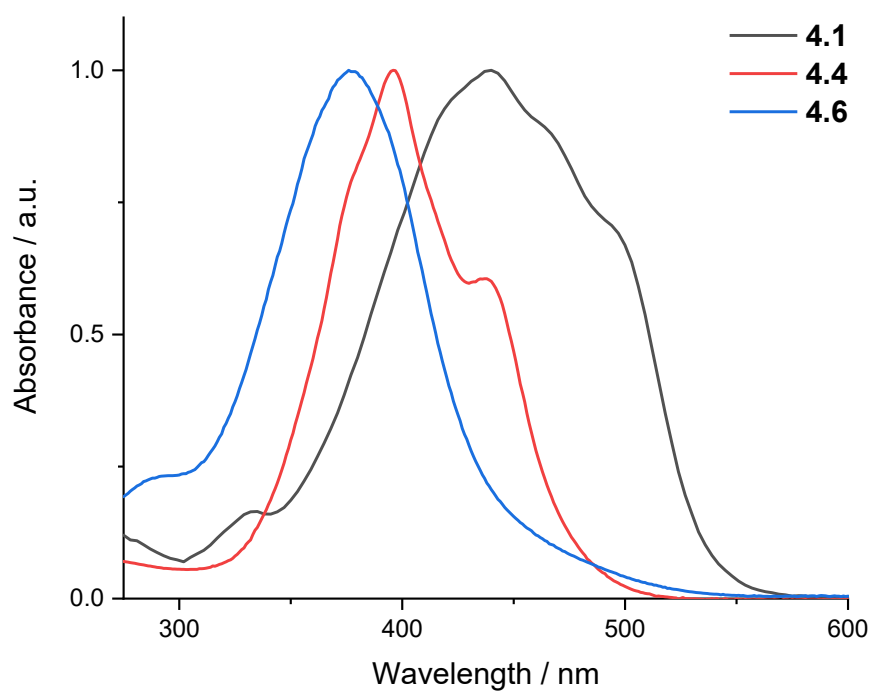


Figure 4.12 Normalised UV-visible absorption spectra of 4.1, 4.4 and 4.6 in acetonitrile at 298 K (pure *E* isomer in all cases).

4.8 *In situ* ^1H NMR photoswitching

We wanted to use *in situ* irradiation coupled with ^1H NMR spectroscopy¹³⁰ to confirm the PSD for **4.1-3** we calculated from UV-visible absorption data using the methodology discussed in Chapter 3. Due to the relatively short thermal half-lives, both intense light and low sample concentrations are required for accurate determination of the *E:Z* isomer ratio at room temperature. These conditions are easily achieved for UV-visible absorption studies but difficult at the concentrations required for ^1H NMR experiments. Therefore, ^1H NMR experiments were conducted at low temperature (243 K) in CDCl_3 to slow the thermal reversion. Light irradiation *in situ* was used to generate the *Z* isomer using the same light source as for UV-visible absorption experiments.¹³¹ The ^1H NMR spectra for **4.3** equilibrated in the dark, and at the PSS, are shown in Figure 4.13 and the related data for **4.1** and **4.2** are given in Section 8.9. Only two species were observed, allowing assignment of the ^1H NMR signals for the *Z* isomer.

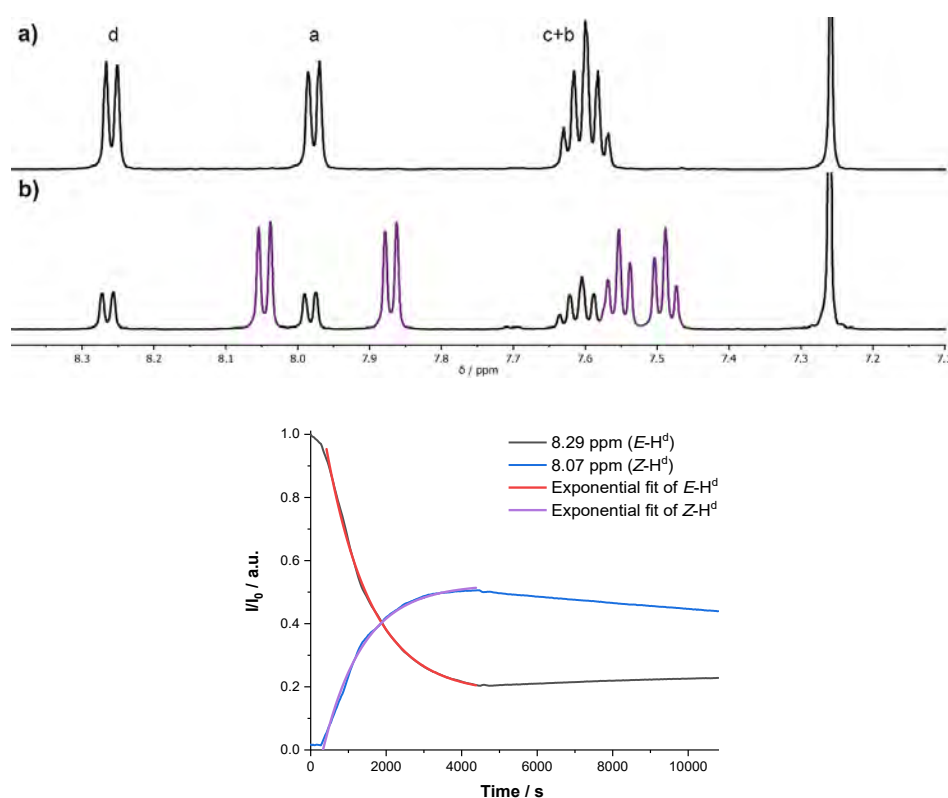


Figure 4.13 Top: Comparison of *E* and PSS ^1H NMR spectra of **4.3** (500 MHz, CDCl_3 , 243 K). a) Initial spectrum. b) After irradiation with 448 nm light for 70 minutes. Bottom: *In situ* photoswitching of **4.3** monitored by ^1H NMR (500 MHz, CDCl_3 , 243 K). The red and purple lines denote mono-exponential fits for the intensity of $E\text{-H}^d$ and $Z\text{-H}^d$ respectively while under constant irradiation.

Due to the long irradiation time required a degree of photodecomposition was observed, precluding the formation of a true steady state. The composition at the PSS was therefore extrapolated by fitting the forward switching curves to a monoexponential function (see Figure 4.13). The calculated *Z:E* isomer ratio (75:25) is very close to that found at room temperature by UV-visible absorption data (77:23). This data gives confidence in the PSD we have determined by UV-visible spectroscopy, as the distributions are essentially insensitive to solvent (Table 4.2). The calculated *Z*→*E* thermal isomerisation barrier was identical to that found from UV-vis spectroscopy at room temperature (80 kJ mol⁻¹, Table 4.5).

Table 4.5 Comparison of the photoswitching parameters of **4.3** as measured by ¹H NMR and UV-vis spectroscopies.

Method	PSD (<i>Z:E</i>)	<i>t</i> _{1/2} / s	Calculated <i>Z</i> → <i>E</i> barrier / kJ mol ⁻¹
¹ H NMR (CDCl ₃ , 243 K) ^a	75:25	16400	79.5
UV-Vis (CHCl ₃ , 298 K) ^b	77:23	32	79.5

^a Thermal lifetime was calculated for a single cycle using the equation discussed in 4.12.6. The proton signals for *E*-H^d and *Z*-H^d were fitted to a mono-exponential function, allowing calculation of the equilibrated PSD. ^b Thermal lifetime, PSD were calculated using UV-vis spectroscopy as discussed in 4.12.6 and Chapter 3.

4.9 Modulation of photoswitching by acid addition

The effects of acid on the properties of the photoswitches were studied by UV-vis and ¹H NMR spectroscopies (Sections 8.10 and 8.11). Compounds **4.2** and **4.3** only show minor changes in their ¹H NMR spectra (CDCl₃ or CD₃CN) on the addition of excess trifluoroacetic acid (TFA), see Figure 4.14, 8.55, 8.58, 8.68 and 8.75. However, the ¹H NMR signals for **4.1** are shifted significantly downfield on the addition of acid, consistent with protonation (See Figure 4.14, 8.52 and 8.65).

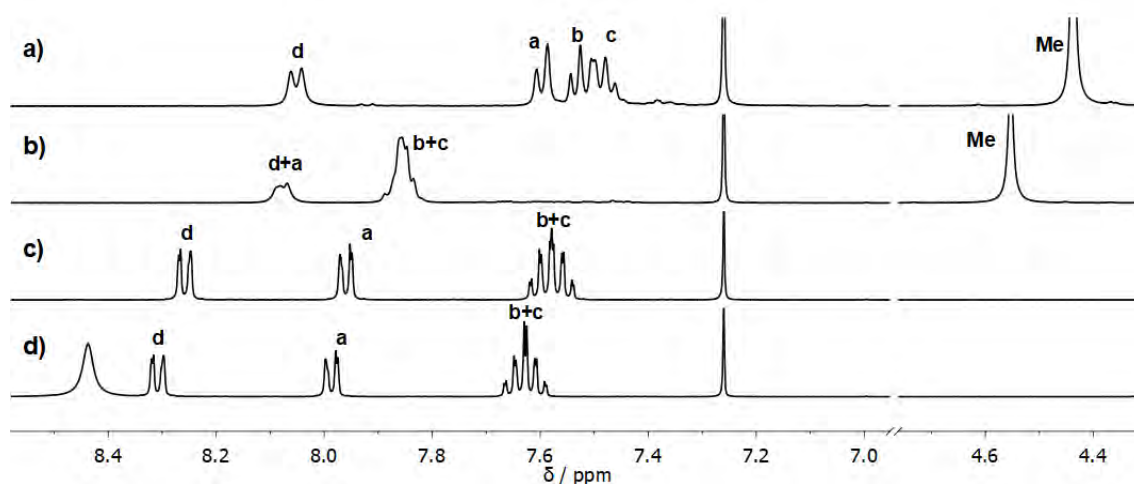


Figure 4.14 Partial ^1H NMR spectra (500 MHz, CDCl_3 , 298 K) showing the effect of adding TFA to **4.1** (17 mM) and **4.3** (23 mM). In both cases $[\text{TFA}] = 200$ mM. a) **4.1** in CDCl_3 ; b) **4.1** + TFA in CDCl_3 ; c) **4.3** in CDCl_3 and d) **4.3** + TFA in CDCl_3 . At all acid concentrations only one ^1H NMR signal is observed for the methyl groups of **4.1**, indicating acid does not appear to cause any isomerisation to the *Z* isomer. Labelling is as shown in Scheme 4.1.

Similar effects were observed by UV-vis absorption spectroscopy in acetonitrile.¹³² Additions of TFA (up to 15,000 equiv.) to acetonitrile solutions of **4.2** or **4.3** did not cause significant changes in their absorption spectra, consistent with the ^1H NMR data (Figures 8.66, 8.70 and 8.73). Compound **4.2** also showed no change in the thermal half-life on acid addition (Figure 8.72). It is clear that compound **4.2** is not protonated under these conditions.

In dry acetonitrile and in the absence of acid, compound **4.3** has the shortest half-life measured (0.4 s, Figure 4.15 and Table 4.6). This value was found to increase to 2 seconds in the presence of trace water. On addition of TFA (2.5 equiv.) the half-life *increases* ($t_{1/2} = 43$ s), corresponding to a 12 kJ mol^{-1} increase in the thermal *Z*→*E* barrier. Further addition of TFA (up to 250 equiv.) has no effect on the half-life, or on the PSS spectrum. This observed lack of spectral changes suggests that *E*-**4.3** is not substantially protonated under these conditions. Similarly, the insensitivity of the PSD spectrum to acid suggests that *Z*-**4.3** is not protonated. We therefore propose at low concentrations of acid there exists some protonated transition state that causes a substantial increase in the thermal isomerisation barrier. The identity of this species remains unclear, but potentially could be due to the mechanism of isomerisation changing from rotation to inversion, which is generally associated with slower kinetics.^{17m} A large excess of TFA decreases the thermal half-life (15,000 equiv. TFA, $t_{1/2} = 6$ s, Figure 4.15 and Table 4.6). At high

acid concentrations a small amount of $Z\text{-}4.3\text{H}^+$ is likely formed, with a significantly shorter half-life than $Z\text{-}4.3$, leading to the observed decrease in thermal half-life.

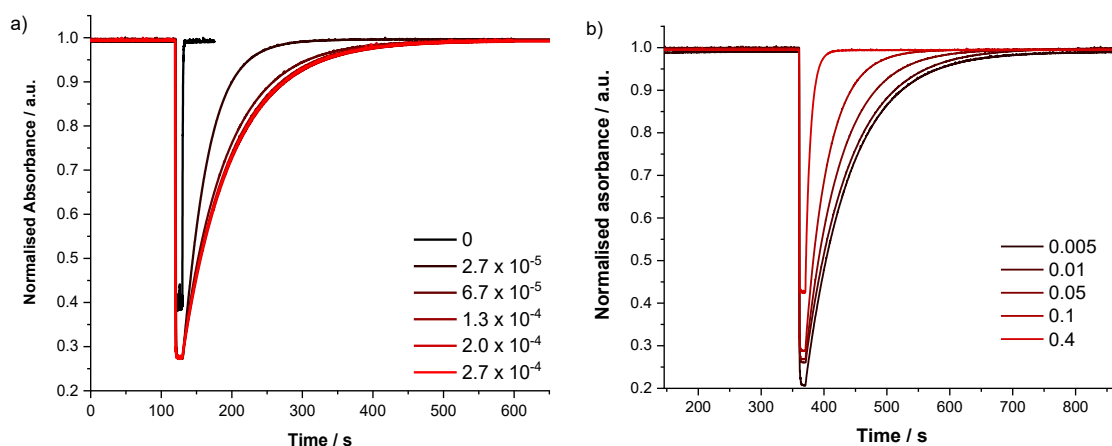


Figure 4.15 Change in the rate of Z to E thermal reversion of **4.3** (acetonitrile, $40 \mu\text{M}$, 298K) as TFA is added. The overall concentration of TFA (mol L^{-1}) is given on the right. a) TFA concentration range from 0 to 2.7×10^{-4} M. b) TFA concentration range from 0.005 to 0.4 M.

Table 4.6 Change in the photoswitching parameters of **4.3** as TFA is added in acetonitrile.

[TFA] / mol L^{-1}	$t_{1/2}$ / s^a	Change in absorbance at PSS (% of max, measured at $\lambda_{\text{max}, E}$)
0	0.4	60
2.7×10^{-5}	24	73
6.7×10^{-5}	43	73
1.3×10^{-4}	48	73
2.0×10^{-4}	49	73
2.7×10^{-4}	49	73
0.005	49	80
0.01	49	74
0.05	38	73
0.1	25	71
0.4	6	57

In contrast to the lack of absorption changes for **4.2** and **4.3**, an acetonitrile solution of **4.1** showed a significant red-shift in the absorption (Figure 4.16a, $\Delta\lambda_{\text{max}} = 62$ nm to $\lambda_{\text{max}} = 503$ nm) and an increase in absorbance upon excess TFA addition (≈ 50 equiv.), consistent with protonation under these conditions. A titration of TFA into an acetonitrile solution of **4.1** in the dark and monitored by UV-visible absorption was largely consistent with a single protonation event and suggests a $\text{p}K_{\text{a}}$ for $E\text{-}4.1\text{H}^+$ in acetonitrile around 11 (Figure 8.61; see Section 8.12 for details).

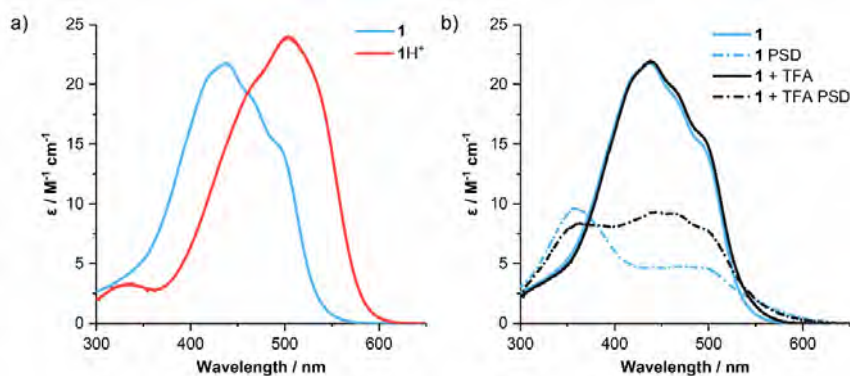


Figure 4.16 The response of **4.1** (50 μM in CH_3CN) to TFA addition. a) Comparison of UV-vis absorption of **4.1** and **4.1H⁺** in CH_3CN . **4.1H⁺** was generated by the addition of ≈ 50 equivalents of TFA (final $[\text{TFA}] = 2.5 \text{ mM}$) into a solution of **1** in CH_3CN . b) The effect of adding 2.5 equiv. of TFA to **4.1** in CH_3CN . **4.1 + TFA** refers to a solution of **4.1** in CH_3CN upon addition of 2.5 equivalents of TFA (final $[\text{TFA}] = 125 \mu\text{M}$). PSD were generated by irradiation with a 448 nm LED.

At high acid concentrations (≈ 50 equiv.) both the *Z* and *E* isomers of **4.1** are protonated (*E*-**4.1H⁺** and *Z*-**4.1H⁺**) and these species have overlapping absorption bands. However, the molecule can still be switched upon irradiation with 448 nm light. The thermal half-life of *Z*-**4.1H⁺** ($t_{1/2} = 281 \text{ s}$, Figure 4.17 and Table 8.7) remains relatively long compared to other examples of protonated azobenzenes^{30a} (typically μs , but some examples of minutes have been reported^{23c,25d}), or push-pull systems (typically ms to s^{12, 28c}).

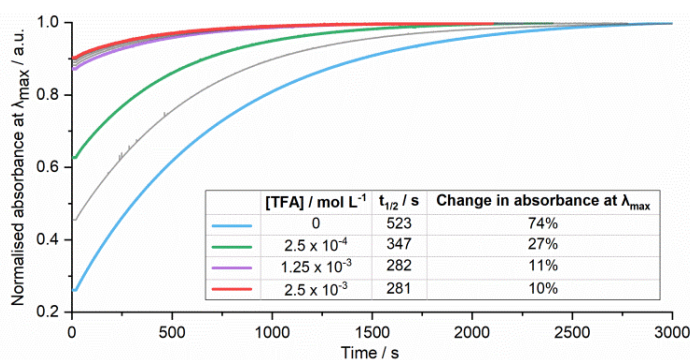


Figure 4.17 Change in the *Z*→*E* thermal half-life for **4.1** (CH_3CN , 50 μM , 298 K) as TFA is added. Data were collected in increments of $1.25 \times 10^{-4} \text{ M}$ in the range from 0 to $2.5 \times 10^{-4} \text{ M}$ and increments of $2.5 \times 10^{-4} \text{ M}$ from 2.5×10^{-4} to $2.5 \times 10^{-3} \text{ M}$. Selected data have been shown in the inset table. Solutions were irradiated with 448 nm light to reach a PSS and then monitored in the dark at the λ_{max} of the absorption band. Calculation of thermal half-life is as discussed in Section 4.12.6. Colours match the scheme used in Figure 4.16.

The absorption of $E\text{-4.1H}^+$ extends past 600 nm and a significant population of the $Z\text{-4.1H}^+$ isomer can be generated by irradiation at 591 nm in acetonitrile (Figure 4.18). The absolute change in absorbance is limited (up to 14%, Table 4.7) however it has been suggested for related compounds²² that both protonated isomers have similar absorption spectra. Therefore, the PSD could not be accurately determined.

Table 4.7 Change in absorbance for 4.1H^+ with irradiation from different LED sources^a

Irradiation λ_{max}	Change in absorbance at PSS (% of max, measured at $\lambda_{\text{max}, E}$)
448	9
470	9
505	10
530	10
567	12
591	14
627	4
655	1

^a λ_{max} refers to the manufacturers specified average value for dominant wavelength.

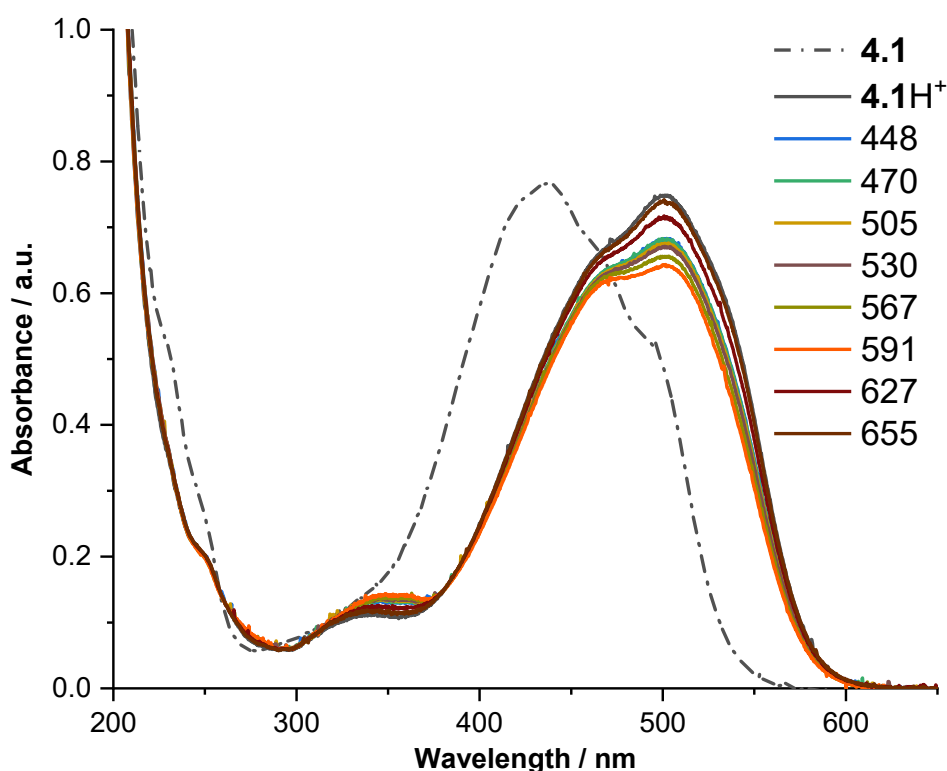


Figure 4.18 Effect of different LED light sources on the photoswitching of 4.1H^+ (34 μM , CH_3CN , 298 K). Spectra were collected after light irradiation with the appropriate wavelength for 15 seconds.

4.10 Computed geometries and proton affinities

4.10.1 Computed geometries

To improve the understanding of these phenomena, DFT, DLPNO-CCSD(T)/CBS¹³³ and the SMD implicit solvent model¹³⁴ calculations were used to determine the optimised geometries and energies of the isomers of **4.1–3**, and their various protonated forms. Calculated geometries (see 8.13 for computational details and Tables 8.10-12 for structures) show for each of **4.1–3** that the *Z* isomer has a twisted (non-planar) conformation in the ground state. Fuchter and co-workers have previously shown that substituents (or atoms with lone pairs) in the *ortho* position to an azo group can lead to such twisted configurations^{23b} which do not benefit from stabilising dispersive interactions in the *Z* isomer. This is consistent with the observation that these complexes have half-lives on the time scale of minutes to seconds, rather than years as observed for the unsymmetric pyrazole switches.^{23a, 23b}

The lowest energy conformations were calculated for the protonated molecules where either the ring or azo nitrogen is protonated for both the *E* and *Z* isomers. In all cases the protonated azo species (referred to as HAzo) were significantly higher in energy ($\geq 34 \text{ kJ}\cdot\text{mol}^{-1}$) than the alternative species protonated on the ring nitrogen (referred to as HIm, HOx and HTh respectively). Therefore, protonation preferentially occurs on the ring nitrogen.

Protonated compounds *E-4.2H*⁺ and *E-4.3H*⁺ are sufficiently acidic in all conformations (calculated $\text{p}K_{\text{a}}$ values in acetonitrile ≤ 2 , see Table 4.8) that they should not be protonated at the TFA concentrations used, reflected in the lack of changes in the UV-vis and ¹H NMR spectra. However, compound *E-4.1H*⁺ has a calculated $\text{p}K_{\text{a}}$ in acetonitrile of 11.7, in good agreement with the measured value (11) and consistent with the observed spectral changes upon addition of TFA.

Table 4.8 Summary of calculated pK_a values for **4.1-3H⁺**.

Compound	Calculated pK_a in acetonitrile
<i>E</i> -[4.1HIm] ⁺	11.7
<i>E</i> -[4.1HAzo] ⁺	0.5
<i>Z</i> -[4.1HIm] ⁺	12.8
<i>Z</i> -[4.1HAzo] ⁺	1.0
<i>E</i> -[4.2HOx] ⁺	0.2
<i>E</i> -[4.2HAzo] ⁺	-8.4
<i>Z</i> -[4.2HOx] ⁺	2.6
<i>Z</i> -[4.2HAzo] ⁺	-5.6
<i>E</i> -[4.3HTh] ⁺	1.7
<i>E</i> -[4.3HAzo] ⁺	-7.2
<i>Z</i> -[4.3HTh] ⁺	3.1
<i>Z</i> -[4.3HAzo] ⁺	-2.6

In all cases, the *Z* isomers of **4.1–3** were calculated to be more basic than the thermally stable *E* isomers (calculated pK_a difference of 1.1 to 2.4 units) due to the formation of an intramolecular hydrogen bond (Figure 4.19), as observed for related systems.^{22, 135} The validity of this interaction was confirmed by atoms-in-molecule analysis, see Section 8.14. The calculated pK_a values for *Z*-**4.2H⁺** and *Z*-**4.3H⁺** are sufficiently low that these species are not observed upon addition of TFA. However, compound *Z*-**4.1H⁺** has a calculated pK_a in acetonitrile of 12.8 which indicates that at low TFA concentrations *Z*-**4.1H⁺** will be formed preferentially over *E*-**4.1H⁺**, explaining the observed sensitivity of the PSS spectrum to low concentrations of acid.

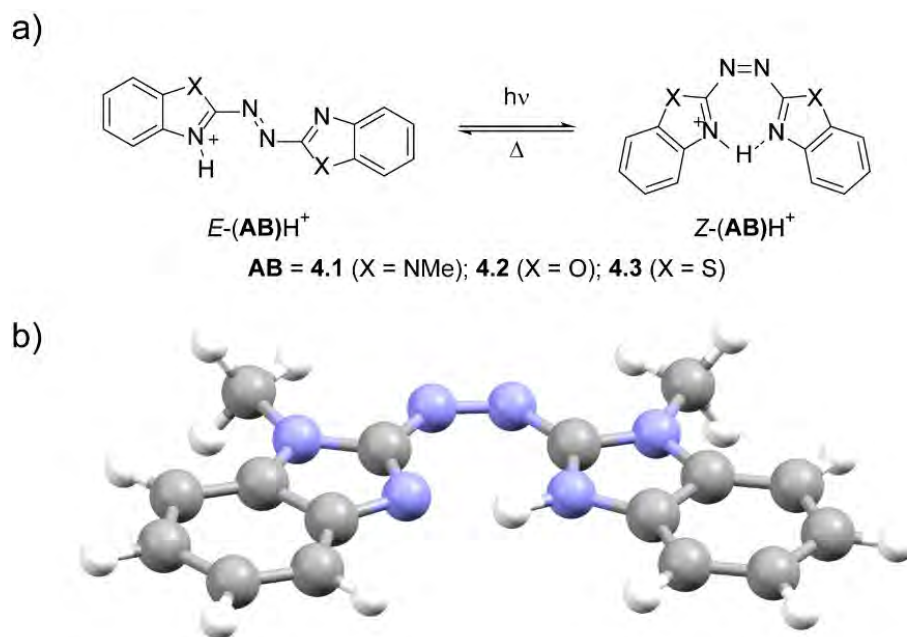


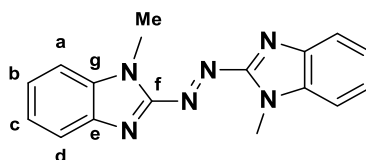
Figure 4.19 Photoswitching of **4.1-3H⁺** showing the proposed intramolecular hydrogen bond in the *Z* isomer. b) Optimised geometry for *Z*-**4.1H⁺** in acetonitrile (M06-2X/6-31+G(d,p)) showing the proposed hydrogen bonding interaction and the resulting planarity of the molecule.

4.11 Conclusion

We introduce azobenzazoles as visible light responsive photoswitches, with sufficiently long thermal half-lives (0.4 to 520 s) for many applications. Their absorption properties, thermal half-lives and fatigue resistance were thoroughly characterised in a range of organic solvents. Compound **4.1** can be readily protonated with TFA and the *Z* isomer is more basic than the *E* isomer due to an intramolecular hydrogen-bond. *E*-**4.1H⁺** has absorption extending past 600 nm and can be photoswitched with 591 nm light. Conversely, compound **4.2** is unaffected by acid addition. Compound **4.3** shows no change in absorption upon acid addition, and yet significant changes in the rates of thermal equilibration consistent with a protonated intermediate that significantly increases the thermal half-life. This latter discovery could offer a new mechanism for altering the thermal stability of azobenzene-type photoswitches. Overall, the reported compounds demonstrate photoswitching that can be extended well into the visible, modulated with acid and amongst the longest thermal half-lives of azoheteroarenes switchable with visible light.

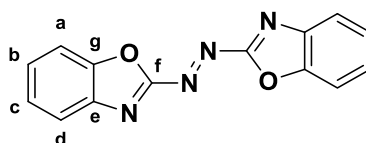
4.12 Experimental

4.12.1 Synthesis of 1,2-bis(1-methyl-benzo[d]imidazol-2-yl)diazene (4.1)



FeSO₄·7H₂O (1.13 g, 4.1 mmol) and KMnO₄ (0.97 mg, 6.0 mmol) were ground together using a mortar and pestle until homogenous. The powder was added to a solution of 2-amino-1-methylbenzimidazole (0.30 g, 2.0 mmol) dissolved in DCM (25 mL) and the resulting suspension stirred at room temperature for 24 h. The suspension was filtered through a short column of silica and the solvent removed under reduced pressure to give a bright red solid (135 mg, 0.47 mmol, 46%). Spectral data matches that previously reported.¹²¹ ¹H NMR (600 MHz, CDCl₃) δ 8.00 (d, *J* = 8.1 Hz, 2H, H^d), 7.57 (d, *J* = 8.1 Hz, 2H, H^a), 7.49 (t, *J* = 7.5 Hz, 2H, H^b), 7.44 (t, *J* = 7.5 Hz, 2H, H^c), 4.38 (s, 6H, H^{Me}). ¹³C {¹H} NMR (151 MHz, CDCl₃) δ 155.3 (C^f), 141.5 (C^e), 136.6 (C^g), 126.3 (C^b), 125.8 (C^c), 122.2 (C^d), 110.9 (C^a), 30.8 (C^{Me}). HR-ESI-MS *m/z* 291.1355 [M+H]⁺ requires 291.1358. UV-Vis (CHCl₃): λ_{max}/nm (ε/10² dm³ mol⁻¹ cm⁻¹) 446 (187). Melting point 285 °C (decomp.).

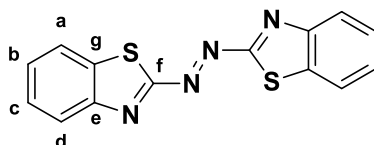
4.12.2 Synthesis of 1,2-bis(benzo[d]oxazol-2-yl)diazene (4.2)



FeSO₄·7H₂O (10.3 g, 44.7 mmol) and KMnO₄ (8.8 g, 67.1 mmol) were ground together using a mortar and pestle until homogenous. The powder was added to a solution of 2-aminobenzoxazole (2.5 g, 22.4 mmol) dissolved in DCM (100 mL) and the resulting suspension refluxed for 72 h. The suspension was filtered through a short column of silica and the solvent removed under reduced pressure to give **4.2** as a bright orange solid (29 mg, 0.11 mmol, 1%). ¹H NMR (600 MHz, CDCl₃) δ 8.04 (d, *J* = 8.3 Hz, 2H, H^d), 7.70 (d, *J* = 8.3 Hz, 2H, H^a), 7.60 (ddd, *J* = 8.3, 7.4, 1.2 Hz, 2H, H^b), 7.52 (ddd, *J* = 8.3, 7.4, 1.0 Hz, 2H, H^c). ¹³C {¹H} NMR (151 MHz, CDCl₃) δ 164.1 (C^f), 150.1 (C^g), 143.4 (C^e), 130.1 (C^b), 126.4 (C^c), 123.1 (C^d), 112.2 (C^a). HR-ESI-MS *m/z* 265.0720 [M+H]⁺ requires

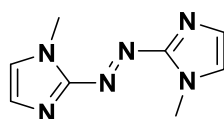
265.0725; m/z 287.0538 $[M+Na]^+$ requires 287.0545. UV-Vis ($CHCl_3$): λ_{max}/nm ($\epsilon / 10^2 dm^3 mol^{-1} cm^{-1}$) 438 (296). Melting point 295 °C (decomp.).

4.12.3 Synthesis of 1,2-bis(benzo[d]thiazol-2-yl)diazene (4.3)



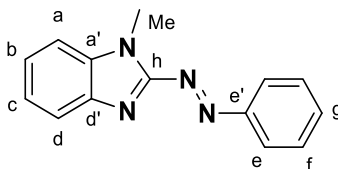
$FeSO_4 \cdot 7H_2O$ (1.10 g, 4.0 mmol) and $KMnO_4$ (0.94 mg, 6.0 mmol) were ground together using a mortar and pestle until homogenous. The powder was added to 2-aminobenzothiazole (0.30 g, 2.0 mmol) dissolved in DCM (25 mL) and the resulting suspension stirred at room temperature for 24 h. The suspension was filtered through a short column of silica and the solvent removed under reduced pressure to give a bright orange solid (68 mg, 0.23 mmol, 23%). Spectral data matches that previously reported.¹²² 1H NMR (600 MHz, $CDCl_3$) δ 8.26 (ddd, $J = 8.1, 1.4, 0.7$ Hz, 1H, H^d), 7.96 (ddd, $J = 7.8, 1.4, 0.7$ Hz, 2H, H^a), 7.60 (ddd, $J = 8.1, 7.2, 1.4$ Hz, 2H, H^c), 7.56 (ddd, $J = 7.8, 7.2, 1.4$ Hz, 2H, H^b). $^{13}C\{^1H\}$ NMR (151 MHz, $CDCl_3$) δ 173.6 (C^f), 153.4 (C^e), 135.6 (C^g), 129.1 (C^b), 127.5 (C^c), 125.9 (C^d), 122.7 (C^a). HR-ESI-MS m/z 297.0235 $[M+H]^+$ requires 297.0269; m/z 319.0054 $[M+Na]^+$ requires 319.0088. UV-Vis ($CHCl_3$): λ_{max}/nm ($\epsilon / 10^2 dm^3 mol^{-1} cm^{-1}$) 430 (276). Melting point 310 °C (decomp.).

4.12.4 Synthesis of 1,2-bis(1-methyl-1H-imidazol-2-yl)diazene (4.4)



The title compound was synthesised by a literature procedure.²² However in our hands separation from the related azoxy compound was difficult, and only trace amounts of the pure compound could be obtained. Spectral data matches that previously reported.²² UV-Vis (Acetonitrile): λ_{max}/nm 396

4.12.5 Synthesis of 1-methyl-2-(phenyldiazenyl)-1H-benzo[d]imidazole (4.6)



To a solution of 2-aminobenzimidazole (250 mg, 1.70 mmol) in pyridine/40% aq. NaOH (1:1, 6 mL) was added nitrosobenzene (200 mg, 1.87 mmol) and the resulting mixture was stirred at 80 °C under nitrogen for 16 h. The mixture was allowed to cool to room temperature, quenched with water (20 mL) and extracted with EtOAc (3 x 25 mL). The organic fraction was washed with brine (100 mL) and dried over MgSO₄. The solution was concentrated under reduced pressure to give **4.6** as a yellow solid (380 mg, 94%). ¹H NMR (600 MHz, CDCl₃) δ 8.14 – 8.10 (m, 2H, H^e), 7.92 (br d, *J* = 7.7 Hz, 1H, H^d), 7.57 – 7.54 (m, 3H, H^{f+g}), 7.48 (br d, *J* = 7.9 Hz, 1H, H^a) 7.39 (ddd, *J* = 7.9, 7.3, 1.2 Hz, 1H, H^b), 7.36 (ddd, *J* = 7.7, 7.3, 1.2 Hz, 1H, H^c), 4.24 (s, 3H, H^{Me}). ¹³C{¹H} NMR (151 MHz, CDCl₃) δ 155.1 (C^h), 153.4 (C^{e'}), 142.2 (C^{d'}), 136.3 (C^{a'}), 132.9 (C^g), 129.4 (C^f), 124.7 (C^{b/c}), 124.2 (C^{b/c}), 123.9 (C^e), 122.2 (C^d), 110.1 (C^a), 30.00 (C^{Me}). UV-Vis (CHCl₃): λ_{max}/nm (ε / 10² dm³ mol⁻¹ cm⁻¹) 378.

4.12.6 General information for photoswitching

Fatigue measurements for compounds **4.1-3** were collected. Solutions of the compounds were equilibrated in the dark and once the absorbance reached a constant value the samples were subjected to 20 photoswitching cycles of 10 s irradiation (with 448 nm light) followed by 500 s of darkness with the absorbance measured at the λ_{max} every 0.25 s. After 20 cycles the absorbance was allowed to reach a constant value to allow calculation of recovery/cycle.

Exponential regression analysis (performed in OriginPro 2018b) was used to determine the thermal half-lives of the $Z \rightarrow E$ reversion over several cycles. 10 cycles were sampled and subjected to a global fit routine, where the curves were fitted to equation (1) where y = absorbance, y_0 = y offset, A = amplitude, R_0 = rate constant and x = time in seconds. From these fits, the thermal half-life time (in seconds) was derived using equation (2).

$$y = y_0 + Ae^{(R_0x)} \quad (1)$$

$$t_{1/2} = \frac{\ln(2)}{-R_0} \quad (2)$$

Recovery/cycle was calculated using equation (3) where I = Absorbance after photoswitching cycles, I_0 = Initial absorbance and n = number of cycles

$$\text{Recovery} = \left(\frac{I}{I_0}\right)^n \quad (3)$$

4.13 X-ray crystallography

	<i>E-4.1</i>	<i>E-4.2</i>
Empirical formula	C ₈ H ₇ N ₃	C ₁₄ H ₈ N ₄ O ₂
Formula weight	145.17	264.24
Temperature/K	100	99.75
Crystal system	monoclinic	monoclinic
Space group	C2/c	P2 ₁ /n
a/Å	29.863(6)	5.5283(13)
b/Å	5.7410(11)	5.4362(13)
c/Å	7.9890(16)	18.772(4)
α/°	90	90
β/°	92.91(3)	96.392(9)
γ/°	90	90
Volume/Å ³	1367.9(5)	560.6(2)
Z	8	2
ρ _{calc} /cm ³	1.410	1.565
μ/mm ⁻¹	0.091	0.110
F(000)	608.0	272.0
Crystal size/mm ³	0.2 × 0.05 × 0.01	0.3 × 0.1 × 0.1
Radiation	Synchrotron (λ = 0.71073)	MoKα (λ = 0.71073)
2θ range for data collection/°	8.198 to 63.172	7.496 to 65.516
Index ranges	-43 ≤ h ≤ 43, -8 ≤ k ≤ 8, - 11 ≤ l ≤ 11	-8 ≤ h ≤ 8, -8 ≤ k ≤ 8, -28 ≤ l ≤ 28
Reflections collected	9123	26471
Independent reflections	1831 [R _{int} = 0.0275, R _{sigma} = 0.0191]	2072 [R _{int} = 0.1378, R _{sigma} = 0.0607]
Data/restraints/parameters	1831/0/105	2072/0/108
Goodness-of-fit on F ²	1.039	1.044
Final R indexes [I ≥ 2σ(I)]	R ₁ = 0.0450, wR ₂ = 0.1174	R ₁ = 0.0513, wR ₂ = 0.1135
Final R indexes [all data]	R ₁ = 0.0472, wR ₂ = 0.1188	R ₁ = 0.0989, wR ₂ = 0.1440
Largest diff. peak/hole / e Å ⁻³	0.47/-0.27	0.37/-0.31

	<i>E-4.3</i>	<i>E-4.4</i>
Empirical formula	C ₁₄ H ₈ N ₄ S ₂	C ₈ H ₁₀ N ₆
Formula weight	296.36	190.22
Temperature/K	100	150
Crystal system	monoclinic	monoclinic
Space group	P2 ₁ /c	P2 ₁ /n
a/Å	11.086(2)	7.657(2)
b/Å	4.7500(9)	7.409(2)
c/Å	11.824(2)	8.058(2)
α/°	90	90
β/°	93.60(3)	92.609(4)
γ/°	90	90
Volume/Å ³	621.4(2)	456.6(2)
Z	2	2
ρ _{calc} /cm ³	1.584	1.384
μ/mm ⁻¹	0.421	0.095
F(000)	304	200
Crystal size/mm ³	0.1 × 0.05 × 0.01	0.36 × 0.21 × 0.1
Radiation	Synchrotron (λ = 0.71073)	MoKα (λ = 0.71073)
2θ range for data collection/°	6.906 to 63.504	7.18 to 60.678
Index ranges	-14 ≤ h ≤ 14, -5 ≤ k ≤ 5, -15 ≤ l ≤ 15	-10 ≤ h ≤ 10, -10 ≤ k ≤ 10, -11 ≤ l ≤ 11
Reflections collected	10791	12107
Independent reflections	1652 [R _{int} = 0.0727, R _{sigma} = 0.0413]	1371 [R _{int} = 0.0538, R _{sigma} = 0.0248]
Data/restraints/parameters	1652/0/92	1371/0/65
Goodness-of-fit on F ²	1.068	1.095
Final R indexes [I ≥ 2σ (I)]	R ₁ = 0.0705, wR ₂ = 0.1781	R ₁ = 0.0458, wR ₂ = 0.1322
Final R indexes [all data]	R ₁ = 0.0910, wR ₂ = 0.1913	R ₁ = 0.0510, wR ₂ = 0.1378
Largest diff. peak/hole / e Å ⁻³	0.84/-0.77	0.43/-0.37

	<i>E-4.5</i>	<i>E-4.6</i>
Empirical formula	C ₈ H ₁₈ N ₆ O ₅	C ₁₄ H ₁₅ ClN ₄ O
Formula weight	278.28	291.76
Temperature/K	150.01	293.15
Crystal system	triclinic	orthorhombic
Space group	P-1	P2 ₁ 2 ₁ 2 ₁
a/Å	6.9291(11)	5.2070(10)
b/Å	10.6366(17)	16.577(3)
c/Å	10.744(2)	16.828(3)
α/°	60.416(4)	90
β/°	74.428(6)	90
γ/°	79.027(4)	90
Volume/Å ³	661.8(2)	1452.5(5)
Z	2	4
ρ _{calc} /g/cm ³	1.397	1.334
μ/mm ⁻¹	0.116	0.264
F(000)	296	612.0
Crystal size/mm ³	0.3 × 0.18 × 0.1	0.4 × 0.2 × 0.1
Radiation	MoKα (λ = 0.71073)	MoKα (λ = 0.71073)
2θ range for data collection/°	4.414 to 49.994	4.842 to 52.214
Index ranges	-8 ≤ h ≤ 8, -12 ≤ k ≤ 12, -12 ≤ l ≤ 12	-6 ≤ h ≤ 6, -20 ≤ k ≤ 20, -20 ≤ l ≤ 20
Reflections collected	27236	28490
Independent reflections	2331 [R _{int} = 0.0897, R _{sigma} = 0.0509]	2838 [R _{int} = 0.1551, R _{sigma} = 0.0748]
Data/restraints/parameters	2331/0/202	2838/0/183
Goodness-of-fit on F ²	1.075	1.127
Final R indexes [I ≥ 2σ (I)]	R ₁ = 0.0559, wR ₂ = 0.1187	R ₁ = 0.0637, wR ₂ = 0.1024
Final R indexes [all data]	R ₁ = 0.0983, wR ₂ = 0.1434	R ₁ = 0.0893, wR ₂ = 0.1095
Largest diff. peak/hole / e Å ⁻³	0.36/-0.35	0.28/-0.25

4.13.1 Structure of *E*-4.1

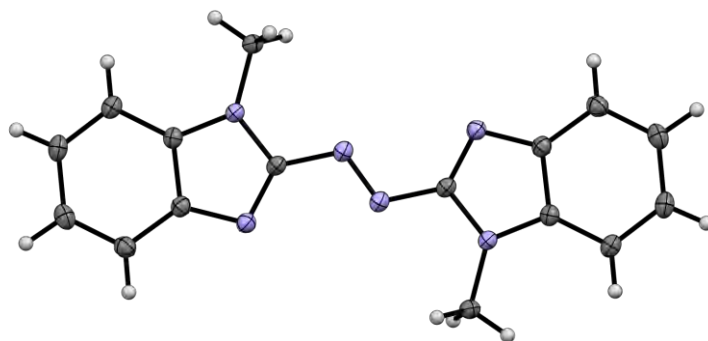


Figure 4.20 An ORTEP representation of the X-ray crystal structure of *E*-4.1. Thermal ellipsoids are drawn at 50% probability.

Red needles of *E*-4.1 were grown by slow evaporation of a solution of the compound in dichloromethane. The crystal of *E*-4.1 with dimensions 0.1 x 0.05 x 0.01 mm was coated in Paratone and transferred to the goniometer under a cold stream at 100 K. Diffraction measurements were carried out using Si<111> monochromated synchrotron X-ray radiation ($\lambda = 0.71073 \text{ \AA}$) on the MX1 Beamline at the Australian Synchrotron.¹³⁶ Data collection was carried out using Australian Synchrotron QEGUI software and unit cell refinement, data reduction and processing were carried out with XDS.¹¹¹ The structure was solved using dual space methods with SHELXT.¹³⁷ The least-squares refinement was carried out with SHELXL-2016¹³⁷ through the Olex2¹¹⁴ suite of software. The non-hydrogen atoms were refined anisotropically.

4.13.2 Structure of *E*-4.2

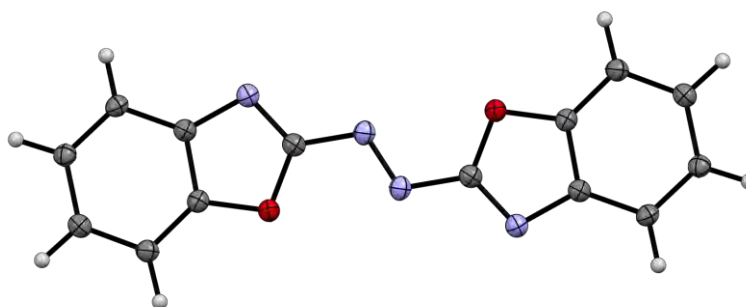


Figure 4.21 An ORTEP representation of the X-ray crystal structure of *E*-4.2. Thermal ellipsoids are drawn at 50% probability.

Orange blocks of *E*-4.2 were grown by slow evaporation of a solution of the compound in chloroform. The crystal of *E*-4.2 with dimensions of 0.27 x 0.19 x 0.11 mm, selected under the polarising microscope (Leica M165Z), mounted on a MicroMount (MiTeGen, USA) consisting of a thin polymer tip with a wicking aperture. The single crystal was mounted on the goniometer using cryo loops for intensity measurements, was coated with paraffin oil and then quickly transferred to the cold stream using an Oxford Cryo stream 800 attachment. The X-ray diffraction measurements were carried out on a Bruker D8 Quest Single Crystal diffractometer with a Photon II detector at 100 K by using a I μ S 3.0 Microfocus Source with Mo-K α radiation ($\lambda = 0.710723 \text{ \AA}$). Symmetry related absorption corrections using the program SADABS¹¹² were applied and the data were corrected for Lorentz and polarisation effects using Bruker APEX3 software.¹³⁸ The structure was solved using SHELXT (intrinsic phasing)¹³⁷ and the full-matrix least-square refinement was carried out using SHELXL-2016¹³⁷ through the Olex2¹¹⁴ suite of software. The non-hydrogen atoms were refined anisotropically.

4.13.3 Structure of *E*-4.3

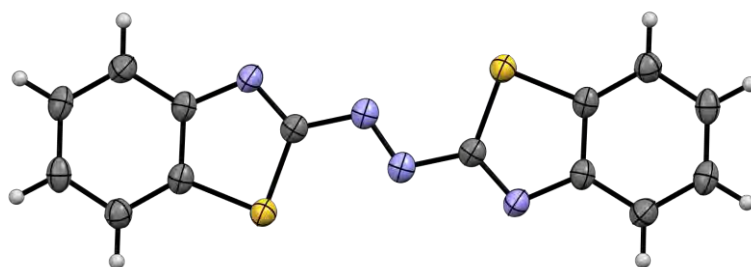


Figure 4.22 An ORTEP representation of the X-ray crystal structure of *E*-4.3. Thermal ellipsoids are drawn at 50% probability.

Red needles of *E*-4.3 were grown by slow evaporation of a solution of the compound in 2-methyltetrahydrofuran. The crystal of *E*-4.3 with dimensions 0.1 x 0.05 x 0.01 mm was coated in Paratone and transferred to the goniometer under a cold stream of 100 K. Diffraction measurements were carried out using Si<111> monochromated synchrotron X-ray radiation ($\lambda = 0.71073 \text{ \AA}$) on the MX1 Beamline at the Australian Synchrotron.¹³⁶ Data collection was carried out using Australian Synchrotron QEGUI software and unit cell refinement, data reduction and processing were carried out with XDS.¹¹¹ The structure was solved using dual space methods with SHELXT.¹³⁷ The least-squares refinement was carried out with SHELXL-2016¹³⁷ through Olex2¹¹⁴ suite of software. The non-hydrogen atoms were refined anisotropically.

4.13.4 Structure of *E*-4.4

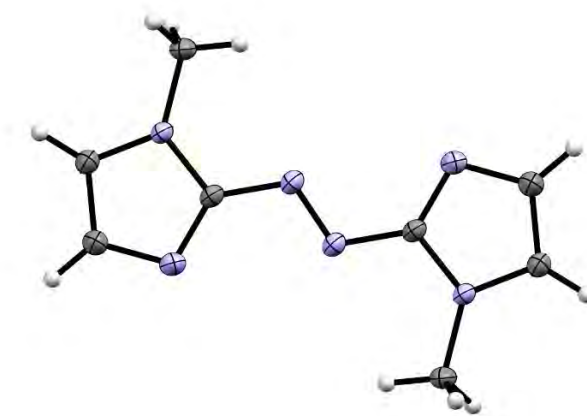


Figure 4.23 An ORTEP representation of the X-ray crystal structure of *E*-4.4. Thermal ellipsoids are drawn at 50% probability.

Orange plates of **4.4** were grown by vapour diffusion of pentane into a mixture of *E*-4.4 and *E*-4.5 in acetone. The crystal of **4.4** with dimensions 0.36 x 0.21 x 0.1 mm was selected under the polarising microscope (Leica M165Z) and mounted on a MicroMount (MiTeGen, USA) consisting of a thin polymer tip with a wicking aperture. The single crystal was mounted on the goniometer using cryo loops for intensity measurements, coated with paraffin oil and then quickly transferred to the cold stream using an Oxford Cryo stream 700 attachment. The X-ray diffraction measurements were carried out on a Bruker Kappa-II CCD diffractometer at 150 K using a I μ S Incoatec Microfocus Source with Mo-K α radiation ($\lambda = 0.710723$ Å). Symmetry related absorption corrections using the program SADABS¹¹² were applied and the data were corrected for Lorentz and polarisation effects using Bruker APEX3 software.¹³⁸ The structure was solved using SHELXT (intrinsic phasing)¹³⁷ and the full-matrix least-square refinement was carried out using SHELXL-2016¹³⁷ through the Olex2¹¹⁴ suite of software. The non-hydrogen atoms were refined anisotropically.

4.13.5 Structure of *E*-4.5

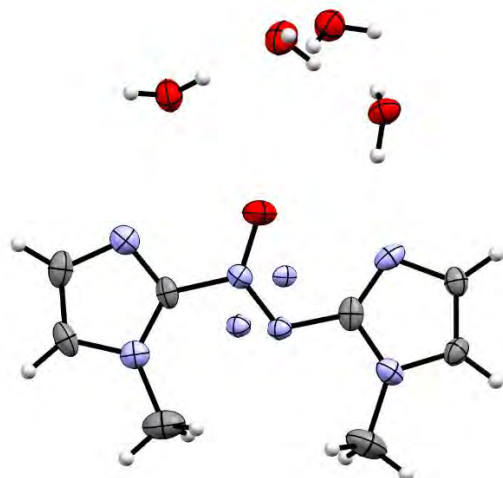


Figure 4.24 An ORTEP representation of the X-ray crystal structure of *E*-4.5. Thermal ellipsoids are drawn at 50% probability.

Yellow plates of **4.5** were grown by vapour diffusion of pentane into a mixture of *E*-4.4 and *E*-4.5 in acetone. The crystal of **4.5** with dimensions 0.30 x 0.18 x 0.10 mm was selected under the polarising microscope (Leica M165Z) and mounted on a MicroMount (MiTeGen, USA) consisting of a thin polymer tip with a wicking aperture. The single crystal was mounted on the goniometer using cryo loops for intensity measurements, coated with paraffin oil and then quickly transferred to the cold stream using an Oxford Cryo stream 700 attachment. The X-ray diffraction measurements were carried out on a Bruker Kappa-II CCD diffractometer at 150 K using a I μ S Incoatec Microfocus Source with Mo-K α radiation ($\lambda = 0.710723$ Å). Symmetry related absorption corrections using the program SADABS¹¹² were applied and the data were corrected for Lorentz and polarisation effects using Bruker APEX3 software.¹³⁸ The structure was solved using SHELXT (intrinsic phasing)¹³⁷ and the full-matrix least-square refinement was carried out using SHELXL-2016¹³⁷ through the Olex2¹¹⁴ suite of software. The non-hydrogen atoms were refined anisotropically.

4.13.6 Structure of [E-4.6D]Cl·H₂O

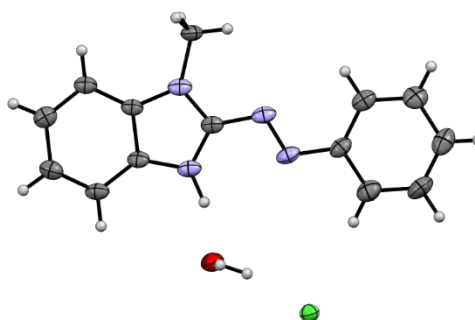


Figure 4.25 An ORTEP representation of the X-ray crystal structure of [E-4.6D]Cl. Thermal ellipsoids are drawn at 50% probability.

Yellow needles of [E-4.6D]Cl·H₂O were grown by slow evaporation of a solution of the compound in CDCl₃. The crystal of [E-4.6D]Cl with dimensions 0.4 x 0.2 x 0.1 mm was selected under the polarising microscope (Leica M165Z), mounted on a MicroMount (MiTeGen, USA) consisting of a thin polymer tip with a wicking aperture. The single crystal was mounted on the goniometer using cryo loops for intensity measurements, was coated with paraffin oil and then quickly transferred to the cold stream using an Oxford Cryo stream 800 attachment. The X-ray diffraction measurements were carried out on a Bruker D8 Quest Single Crystal diffractometer with a Photon II detector at 100 K by using a I μ S 3.0 Microfocus Source with Mo-K α radiation ($\lambda = 0.710723$ Å). Symmetry related absorption corrections using the program SADABS¹¹² were applied and the data were corrected for Lorentz and polarisation effects using Bruker APEX3 software.¹³⁸ The structure was solved using SHELXT (intrinsic phasing)¹³⁷ and the full-matrix least-square refinement was carried out using SHELXL-2016¹³⁷ through the Olex2¹¹⁴ suite of software. The non-hydrogen atoms were refined anisotropically.

4.14 References

12. Bandara, H. M. D.; Burdette, S. C., *Chem. Soc. Rev.* **2012**, *41* (5), 1809-1825.
17. (a) Coelho, P. J.; Carvalho, L. M.; Fonseca, A. M. C.; Raposo, M. M. M., *Tetrahedron Lett.* **2006**, *47* (22), 3711-3714; (b) Klapötke, T. M.; Piercey, D. G., *Inorg. Chem.* **2011**, *50* (7), 2732-2734; (c) Wendler, T.; Schütt, C.; Näther, C.; Herges, R., *J. Org. Chem.* **2012**, *77* (7), 3284-3287; (d) He, J.; Kimani, F. W.; Jewett, J. C., *J. Am. Chem. Soc.* **2015**, *137* (31), 9764-9767; (e) Garcia-Amoros, J.; Cuadrado, A.; Reig, M.; De Waele, V.; Poizat, O.; Velasco, D., *Chem.-Eur. J.* **2015**, *21* (41), 14292-14296; (f) Kolarski, D.; Szymanski, W.; Feringa, B. L., *Org. Lett.* **2017**, *19* (19), 5090-5093; (g) Travieso-Puente, R.; Budzak, S.; Chen, J.; Stacko, P.; Jastrzebski, J. T. B. H.; Jacquemin, D.; Otten, E., *J. Am. Chem. Soc.* **2017**, *139* (9), 3328-3331; (h) Bartova, K.; Cechova, L.; Prochazkova, E.; Socha, O.; Janeba, Z.; Dracinsky, M., *J. Org. Chem.* **2017**, *82* (19), 10350-10359; (i) Devi, S.; Saraswat, M.; Grewal, S.; Venkataramani, S., *J. Org. Chem.* **2018**, *83* (8), 4307-4322; (j) Stricker, L.; Boeckmann, M.; Kirse, T. M.; Doltsinis, N. L.; Ravoo, B. J., *Chem.-Eur. J.* **2018**, *24* (34), 8639-8647; (k) Harris, J. D.; Moran, M. J.; Aprahamian, I., *Proc. Natl Acad. Sci. U. S. A.* **2018**, *115* (38), 9414-9422; (l) Simeth, N. A.; Crespi, S.; Fagnoni, M.; König, B., *J. Am. Chem. Soc.* **2018**, *140* (8), 2940-2946; (m) Crespi, S.; Simeth, N. A.; Bellisario, A.; Fagnoni, M.; König, B., *J. Phys. Chem. A* **2019**, *123* (9), 1814-1823; (n) Kumar, P.; Srivastava, A.; Sah, C.; Devi, S.; Venkataramani, S., *Chem.-Eur. J.* **2019**, *25*, 11924-11932
22. Weston, C. E.; Richardson, R. D.; Fuchter, M. J., *Chem. Commun.* **2016**, *52* (24), 4521-4524.
23. (a) Weston, C. E.; Richardson, R. D.; Haycock, P. R.; White, A. J. P.; Fuchter, M. J., *J. Am. Chem. Soc.* **2014**, *136* (34), 11878-11881; (b) Calbo, J.; Weston, C. E.; White, A. J. P.; Rzepa, H. S.; Contreras-García, J.; Fuchter, M. J., *J. Am. Chem. Soc.* **2017**, *139* (3), 1261-1274; (c) Gibson, R. S. L.; Calbo, J.; Fuchter, M. J., *ChemPhotoChem* **2019**, *3* (6), 372-377; (d) Stricker, L.; Fritz, E.-C.; Peterlechner, M.; Doltsinis, N. L.; Ravoo, B. J., *J. Am. Chem. Soc.* **2016**, *138* (13), 4547-4554; (e) Wang, Y.-T.; Liu, X.-Y.; Cui, G.; Fang, W.-H.; Thiel, W., *Angew. Chem., Int. Ed.* **2016**, *55* (45), 14009-14013; (f) Zhang, Z.-Y.; He, Y.; Zhou, Y.; Yu, C.; Han, L.; Li, T., *Chem.-Eur. J.* **2019**, *25* (58), 13402-13410.
25. (a) Beharry, A. A.; Woolley, G. A., *Chem. Soc. Rev.* **2011**, *40* (8), 4422-4437; (b) Samanta, S.; Babalhavaeji, A.; Dong, M. X.; Woolley, G. A., *Angew. Chem. Int. Ed.* **2013**, *52* (52), 14127-30; (c) Samanta, S.; Beharry, A. A.; Sadovski, O.; McCormick, T. M.; Babalhavaeji, A.; Tropepe, V.; Woolley, G. A., *J. Am. Chem. Soc.* **2013**, *135* (26), 9777-9784; (d) Dong, M.; Babalhavaeji, A.; Samanta, S.; Beharry, A. A.; Woolley, G. A., *Acc. Chem. Res.* **2015**, *48* (10), 2662-2670; (e) Szymański, W.; Beierle, J. M.; Kistemaker, H. A. V.; Velema, W. A.; Feringa, B. L., *Chem. Rev.* **2013**, *113* (8), 6114-6178; (f) Ferreira, R.; Nilsson, J. R.; Solano, C.; Andreasson, J.; Grotli, M., *Sci. Rep.* **2015**, *5*.
28. (a) Garcia-Amoros, J.; Nonell, S.; Velasco, D., *Chem. Commun.* **2011**, *47* (13), 4022-4024; (b) Garcia-Amorós, J.; Díaz-Lobo, M.; Nonell, S.; Velasco, D., *Angew. Chem. Int. Ed.* **2012**, *51* (51), 12820-12823; (c) García-Amorós, J.; Velasco, D., *Beilstein J. Org. Chem.* **2012**, *8*, 1003-1017; (d) Garcia-Amorós, J.; Maerz, B.; Reig, M.; Cuadrado, A.; Blancafort, L.; Samoylova, E.; Velasco, D., *Chem.-Eur. J.* **2019**, *25* (32), 7726-7732.
30. (a) Sanchez, A. M.; Barra, M.; de Rossi, R. H., *J. Org. Chem.* **1999**, *64* (5), 1604-1609; (b) Sokalski, W. A.; Góra, R. W.; Bartkowiak, W.; Kobyliński, P.;

- Sworakowski, J.; Chyla, A.; Leszczyński, J., *J. Chem. Phys.* **2001**, *114* (13), 5504-5508.
111. Kabsch, W., *Acta Crystallograph. Sect. D* **2010**, *66* (2), 125-132.
112. Bruker *SADABS*, Bruker: 2001.
114. Dolomanov, O. V.; Bourhis, L. J.; Gildea, R. J.; Howard, J. A. K.; Puschmann, H., *J. Appl. Crystallogr.* **2009**, *42* (2), 339-341.
119. Bull, J. N.; Scholz, M. S.; Coughlan, N. J. A.; Bieske, E. J., *PCCP* **2017**, *19* (20), 12776-12783.
120. Cusati, T.; Granucci, G.; Persico, M.; Spighi, G., *J. Chem. Phys.* **2008**, *128* (19), 194312.
121. Okumura, S.; Lin, C.-H.; Takeda, Y.; Minakata, S., *J. Org. Chem.* **2013**, *78* (23), 12090-12105.
122. Takeda, Y.; Okumura, S.; Minakata, S., *Angew. Chem. Int. Ed.* **2012**, *51* (31), 7804-7808.
123. (a) Noureldin, N. A.; Bellegarde, J. W., *Synthesis* **1999**, *1999* (06), 939-942; (b) Merino, E., *Chem. Soc. Rev.* **2011**, *40* (7), 3835.
124. (a) Otsuki, J.; Suwa, K.; Narutaki, K.; Sinha, C.; Yoshikawa, I.; Araki, K., *J. Phys. Chem. A* **2005**, *109* (35), 8064-8069; (b) Otsuki, J.; Suwa, K.; Sarker, K. K.; Sinha, C., *J. Phys. Chem. A* **2007**, *111* (8), 1403-1409.
125. Harada, J.; Ogawa, K., *J. Am. Chem. Soc.* **2001**, *123* (44), 10884-10888.
126. Antoine John, A.; Lin, Q., *J. Org. Chem.* **2017**, *82* (18), 9873-9876.
127. Priewisch, B.; Rück-Braun, K., *J. Org. Chem.* **2005**, *70* (6), 2350-2352.
128. There are relatively few visible-light responsive azoheteroarenes. The longest half-lives reported to date are for 6-azopurine (530 nm, $t_{1/2}$ = 46 min, DMSO), 5-phenylazopyrimidine (405 nm, $t_{1/2}$ = 8 min, MeCN), phenylazoindole (400 nm, $t_{1/2}$ = 2.6 days, dry DMSO), azobis(2-imidazole) (415 nm, $t_{1/2}$ = 16 s, H₂O, 448 nm, $t_{1/2}$ = 3 min, MeCN - this work).
129. Hill, D. G., *J. Am. Chem. Soc.* **1932**, *54* (1), 32-40.
130. (a) Feldmeier, C.; Bartling, H.; Riedle, E.; Gschwind, R. M., *J. Magn. Reson.* **2013**, *232*, 39-44; (b) Mallo, N.; Brown, P. T.; Iranmanesh, H.; MacDonald, T. S. C.; Teusner, M. J.; Harper, J. B.; Ball, G. E.; Beves, J. E., *Chem. Commun.* **2016**, *52* (93), 13576-13579; (c) Procházková, E.; Čechová, L.; Kind, J.; Janeba, Z.; Thiele, C. M.; Dračinský, M., *Chem.-Eur. J.* **2018**, *24* (2), 492-498; (d) Čechová, L.; Kind, J.; Dračinský, M.; Filo, J.; Janeba, Z.; Thiele, C. M.; Cigáň, M.; Procházková, E., *J. Org. Chem.* **2018**, *83* (11), 5986-5998; (e) Mallo, N.; Foley, E. D.; Iranmanesh, H.; Kennedy, A. D. W.; Luis, E. T.; Ho, J.; Harper, J. B.; Beves, J. E., *Chem. Sci.* **2018**, *9* (43), 8242-8252; (f) Nitschke, P.; Lokesh, N.; Gschwind, R. M., *Prog. Nucl. Magn. Reson. Spectrosc.* **2019**, *114-115*, 86-134.
131. CDCl₃ was used due to the limited solubility of 1-3 in CD₃CN at low temperatures.
132. More complex behavior was observed in chloroform. The observed changes (see Figures 8.53 and 8.56) appear to be consistent with partial protonation and a degree of decomposition. However, anion binding effects may be important as some changes were observed in the UV-vis spectra upon addition of chloride anions (Figures 8.59 and 8.60).
133. Riplinger, C.; Neese, F., *J. Chem. Phys.* **2013**, *138* (3), 034106.
134. Marenich, A. V.; Cramer, C. J.; Truhlar, D. G., *J. Phys. Chem. B* **2009**, *113* (18), 6378-6396.
135. Koeppe, B.; Rühl, S.; Römpf, F., *ChemPhotoChem* **2019**, *3* (2), 71-74.

136. Cowieson, N. P.; Aragao, D.; Clift, M.; Ericsson, D. J.; Gee, C.; Harrop, S. J.; Mudie, N.; Panjikar, S.; Price, J. R.; Riboldi-Tunnicliffe, A.; Williamson, R.; Caradoc-Davies, T., *J. Synchrotron Rad.* **2015**, *22* (1), 187-190.
137. Sheldrick, G., *Acta Crystallograph. Sect. A* **2015**, *71* (1), 3-8.
138. Bruker-AXS *APEX3*, Bruker AXS: Madison, Wisconsin, USA, 2012.

5 PHOTOSWITCHABLE SELF- ASSEMBLED STRUCTURES

5.1 Summary

This chapter discusses *o*-fluoroazobenzene visible light photoswitches derivatives for incorporation into larger self-assembled structures. Two pathways were investigated for the incorporation of visible light switches into larger structures: imine formation and metal-ligand bonding via Pd(0) cross-couplings. Reaction of the aldehyde functionalised molecule with aliphatic diamines gave some evidence of formation of a [2+2] macrocycle. Self-assembly of a pyridyl functionalised photoswitch with palladium(II) gave a mixture of two self-assembled cages, assigned as a [Pd₃L₆]⁶⁺ double-walled triangle and a [Pd₄L₈]⁸⁺ distorted tetrahedron. These species could be interconverted using blue light or heating and selectively disassembled using green light. The kinetics of formation and light-induced re-equilibration were studied in detail.

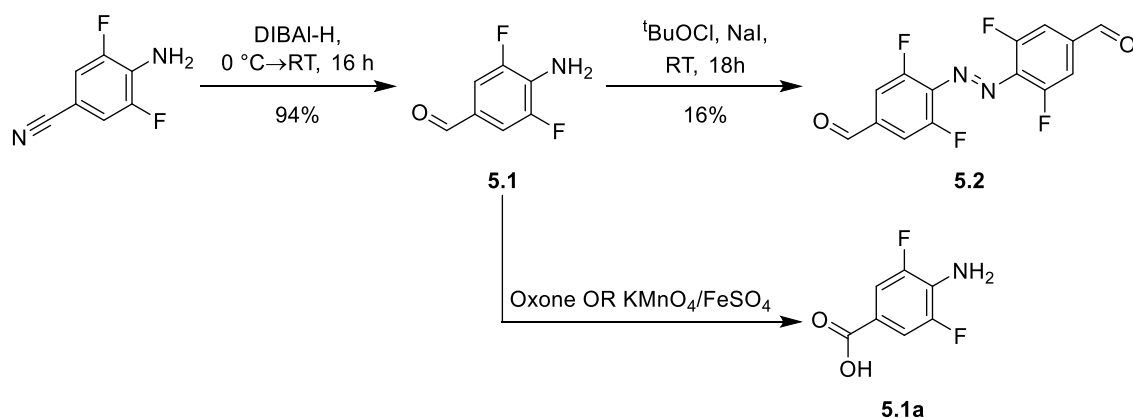
5.2 Strategies for derivatising *o*-fluoroazobenzenes

Conceptually, there are two approaches to derivatise *o*-fluoroazobenzenes for incorporation into larger structures: peripheral functionalisation after azo-bond formation or azo-coupling of functionalised subunits. Functionalisation of azo-coupled derivatives is more practically accessible, as the azo-coupling strategies commonly used are low-yielding and lack functional group tolerance.^{123b} Dynamic imine exchange was explored for construction of larger assemblies from *o*-fluoroazobenzenes. This strategy allows the construction of complex 3D architectures, due to the reversible nature of the imine bond.^{65c, 83c, 93b, 139}

5.3 Synthesis of aldehyde appended *o*-fluoroazobenzene

Dialdehyde **5.2** was synthesised in two steps from commercially available 4-amino-2,6-difluorobenzonitrile (Scheme 5.1). DIBAL-H reduction of the benzonitrile gave access to 4-amino-2,6-difluorobenzaldehyde (**5.1**) in excellent yield with an indicative ¹H NMR peak at 9.73 ppm for the aldehyde proton (Figure 5.1). Oxidative dimerisation using *tert*-butyl hypoiodite¹²² (generated *in situ* from ^tBuOCl and NaI) gave **5.2** in 16% yield. Azo-couplings to form *o*-fluoroazobenzenes are commonly low yielding^{24b} as the aniline moiety is electron poor due to the fluorine substituents, but sufficient compound was generated for a preliminary study. Disappearance of the amine signal at 4.33 ppm was indicative of the formation of the azo bond, and the signal

associated with the aldehyde proton moved slightly downfield to 10.00 ppm. Confirmation of the retention of the aldehyde functionality is important due to the possibility for over-oxidation to the carboxylic acid. The use of alternative reagents for azo-coupling such as Oxone¹²⁷ or KMnO₄ supported on FeSO₄·7H₂O^{123a} did not lead to the desired product due to competing formation of the 4-amino,2,6-difluorobenzoic acid **5.1a** (Scheme 5.1)



Scheme 5.1 Synthesis of aldehyde appended *o*-fluoroazobenzene **5.2**.

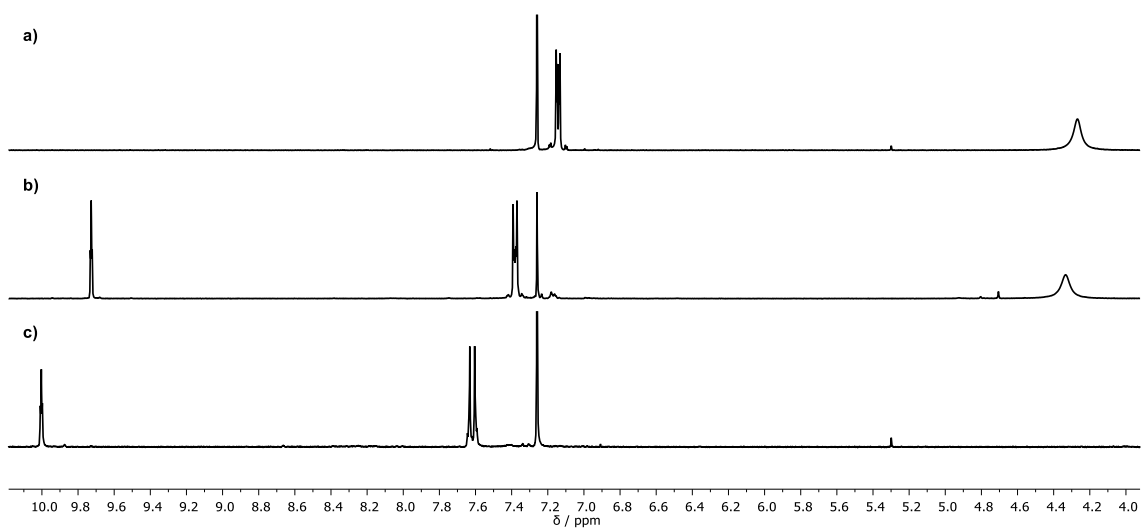


Figure 5.1 Partial ¹H NMR spectra (400 MHz, CDCl₃, 298 K) of a) 4-amino-2,6-difluorobenzonitrile; b) 4-amino-2,6-difluorobenzaldehyde (**5.1**) and c) *o*-fluoroazobenzene **5.2**

5.4 Photoswitching of dialdehyde functionalised *o*-fluoroazobenzene

5.4.1 Absorption spectra and visible-light photoswitching

Compound *E*-5.2 has an intense absorbance in the visible region (Figure 5.2), with an absorption λ_{max} (CHCl₃) at 473 nm assigned as an n- π^* transition. This absorbance maximum is comparable to the ethyl ester derivative (λ_{max} (MeCN) = 469 nm) previously synthesised by Hecht and co-workers.^{24a} Although measured in different solvents, the absorbance bands of these switches are known to be insensitive to solvent polarity.^{24a} Irradiation with a visible light LED (λ_{max} = 567 nm) generated a new species, assigned as *Z*-5.2. The ¹H and ¹⁹F NMR spectrum of this irradiated sample (Figure 5.3) shows this PSS is comprised of 75% *Z*-5.2, which is slightly lower than expected for this class of molecules.^{24a, 24b} The 567 nm LED has a broad spectral distribution (476-714 nm) and a shoulder band with λ_{max} = 425 nm, which is near the λ_{max} for *Z*-5.2, which may explain the lack of selective switching. The UV-vis spectrum of *Z*-5.2 was calculated based on the ¹H NMR integrations using identical light sources in the same solvent, and the assumption that the spectrum at the PSS is a linear combination of the *E*-5.2 and *Z*-5.2 spectra (See Chapter 3, Section 3.5 for further discussion). The calculated spectrum of *Z*-5.2 has a λ_{max} = 420 nm, identical to the ethyl ester derivative.^{24a}

The molecule shows reversible visible light switching, with almost complete recovery of *E*-5.2 upon irradiation with 405 nm light (PSD = 97% *E*-5.2). The half-life of *Z*-5.2 remains long with no observable change in absorbance after 16 h at 298 K. Overall, this result shows that a useful synthetic handle can be appended onto an *o*-fluoroazobenzene without substantial detriment to its switching properties.

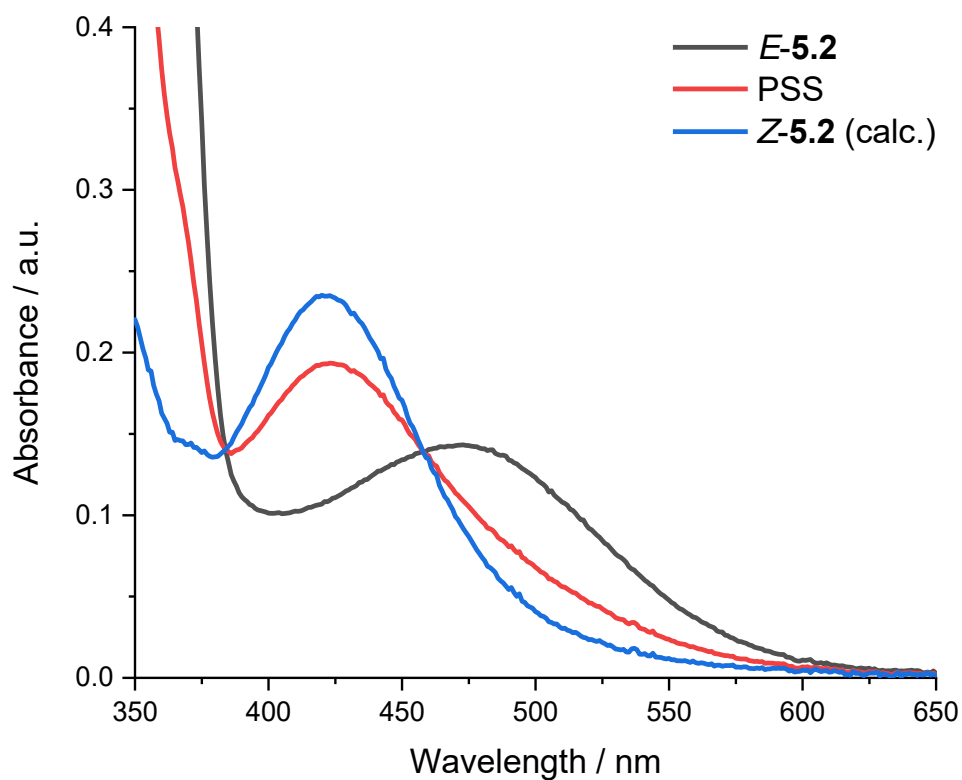


Figure 5.2 Photoswitching of **5.2** in CHCl_3 ($30 \mu\text{M}$, 298 K). The PSS was generated by irradiation with a 567 nm LED for 30 min. The spectrum of Z-5.2 was calculated based on ^1H NMR integrations using the same light source.

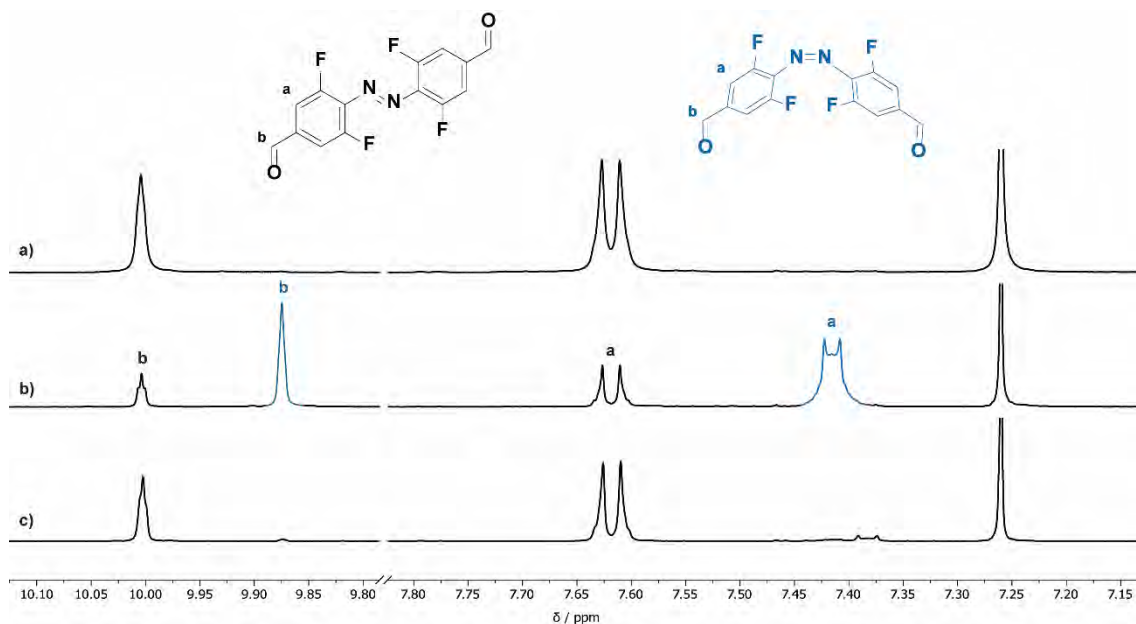


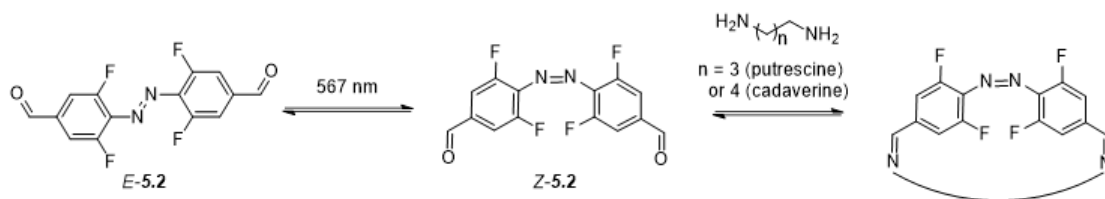
Figure 5.3 *In situ* ^1H NMR switching of **5.2** (CDCl_3 , 500 MHz, 298 K). a) Initial sample; b) after irradiation with 567 nm light for 45 min and c) subsequent irradiation with 405 nm light.

5.5 Reaction with aliphatic diamines

Having synthesised compound **5.2**, incorporation into larger structures was investigated. Particularly interesting was the potential to use the photoswitchable nature of the azo sub-unit to generate a 3D conformation which would otherwise be unfavourable. Macrocyclisation was initially targeted using dynamic covalent chemistry (DCC).¹⁴⁰ There are several reports of covalent macrocycles containing azobenzene subunits,¹⁴¹ but none contain bidirectional visible light switchable sub-units.¹⁴² Schmidt and co-workers have reported a related [2+2] macrocycle assembled using halogen bonding incorporating *tetra*- and *ortho*-fluoroazobenzenes.¹⁴³ Their study focused primarily on solid-phase characterisation of the *tetra*-fluoroazobenzenes, owing to difficulties with solution-state studies. They did not show any switching of the self-assembled species and suggested that photoswitching leads to disassembly of the macrocycle. They also suggested that the *ortho*-fluoroazobenzenes based macrocycle does not persist in solution, presumably due to weaker halogen bonding interactions. The formation of covalent species should allow the construction of a more robust assembly.

The possibility to “trap” the *Z*-isomer using imine exchange is appealing. Formation of a [1+1] macrocycle with an appropriate diamine would lock the molecule in the metastable conformer, giving a structure resembling the diazocene switches explored by Herges and Trauner.^{24c, 26b, 31} Imine formation at both ends of the molecule would restrict the ability to relax to the *E*-isomer, potentially leading to novel switching properties.

To prepare a sample enriched in the *Z*-isomer, **5.2** was dissolved in CDCl₃ and irradiated with 567 nm light (Scheme 5.2). The appropriate diamine (putrescine or cadaverine) was then added and the mixture heated at 40 °C and monitored by NMR over four days (Figure 5.4). Substantial precipitation was observed, presumably due to formation of extended polymer species.¹⁴⁴ The ¹H NMR spectrum revealed a complex mixture of signals which was not resolved by heating. After four days signals were still present in the range 10.03-9.88 ppm, indicating unreacted aldehyde groups. Proton signals for both *E* and *Z* isomers were present, as expected due to the long thermal half-life. New signals were observed between 8.30-8.11 ppm, indicating the formation of imine bonds.



Scheme 5.2 Attempted formation of macrocycles from aldehyde appended **5.2** and selected aliphatic diamines.

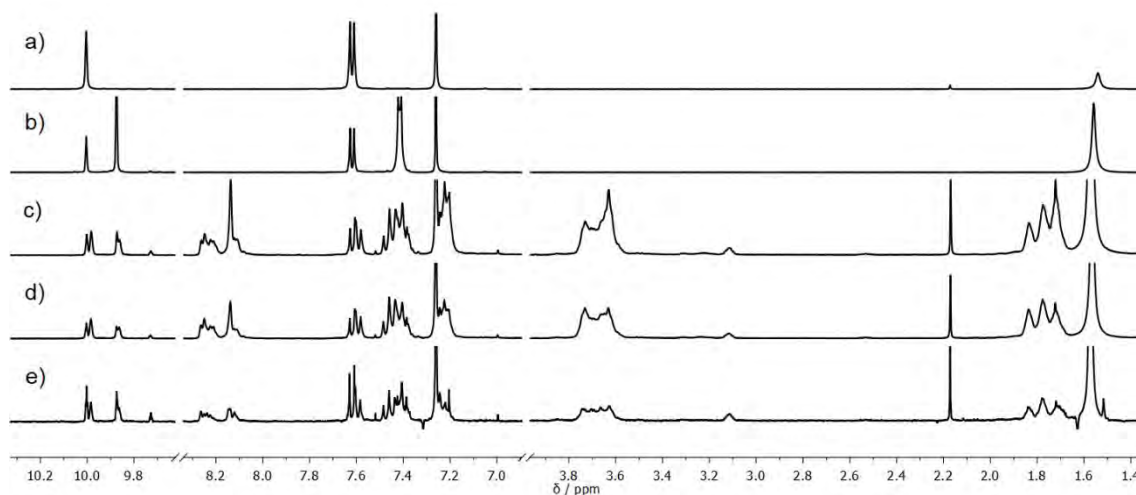


Figure 5.4 Reaction between **5.2** (*Z* isomer enriched) and putrescine in CDCl₃ (500 MHz, 298 K). a) *E*-**5.2** (17 mM in 600 μL CDCl₃); b) after 30 minutes irradiation by a 567 nm LED; c) addition of putrescine (23 μL of a 45 mM solution in CDCl₃) and heating (40 °C, 16 h); d) further heating (40 °C, 22 h) and e) 5 days at 40 °C. Note the artefacts at 7.31 and 1.63 ppm are due to vibrations of the NMR magnet.

ESI-MS allowed elucidation of the products of self-assembly. Peaks were observed corresponding to successive oxidation of the [2+1] adduct between two molecules of **5.2** and one of cadaverine (Figure 5.5). There was no evidence for the [1+1] adduct, however a peak was detected for the [2+2] adduct. Although the structures in Figure 5.5 are all depicted as the *Z*-isomer, this was difficult to confirm given the complexity of the ¹H and ¹⁹F NMR spectra.

A complex mixture of signals might be expected due to both the lack of symmetry in the [2+1] (and possibly [2+2]) derivatives and the presence of *E* and *Z* isomers. This precluded further NMR investigation of the photoswitching properties. However, this is the first example of a macrocycle incorporating *o*-fluoroazobenzene subunits in solution. The complex ¹H NMR spectrum and the presence of unreacted aldehyde units prompted investigation into the reactivity of **5.2** in imine formation reactions. The lack of imine formation could be ascribed to the electron poor nature of the aromatic ring. If the imine

coupling can be promoted, perhaps the formation of the [2+2] macrocycle can be favoured.

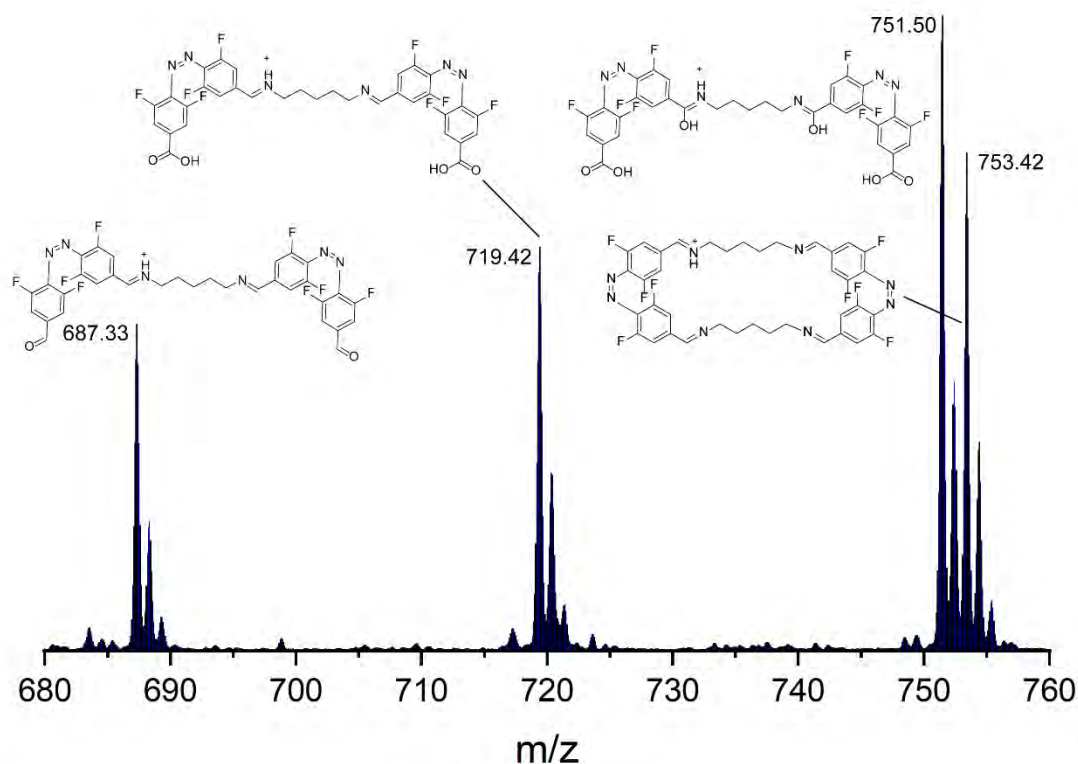
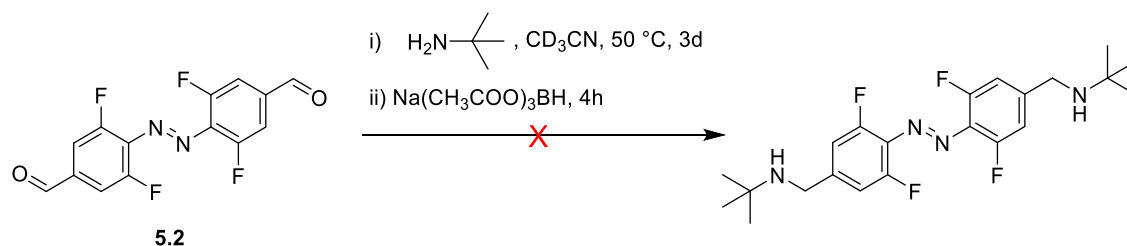


Figure 5.5 ESI-MS of reaction product of **5.2** and cadaverine with proposed structures. Note that all *o*-fluoroazobenzene units have been drawn as the *Z*-isomer, however this was not confirmed.

5.6 Limited reactivity of **5.2** in imine formation

The reactivity of **5.2** was investigated by reaction with ${}^t\text{BuNH}_2$ in CD_3CN (Figure 5.6). This choice of amine was to reflect the possible steric congestion during macrocycle formation. Prolonged heating (72 h) of the sample led to almost complete consumption of the aldehyde, as monitored by ${}^1\text{H}$ NMR. Two sets of signals were observed in the ${}^1\text{H}$ and ${}^{19}\text{F}$ NMR spectra, which would not be expected for the symmetric species shown in Scheme 5.3.



Scheme 5.3 Attempted reaction of **5.2** and tertbutylamine in CD₃CN

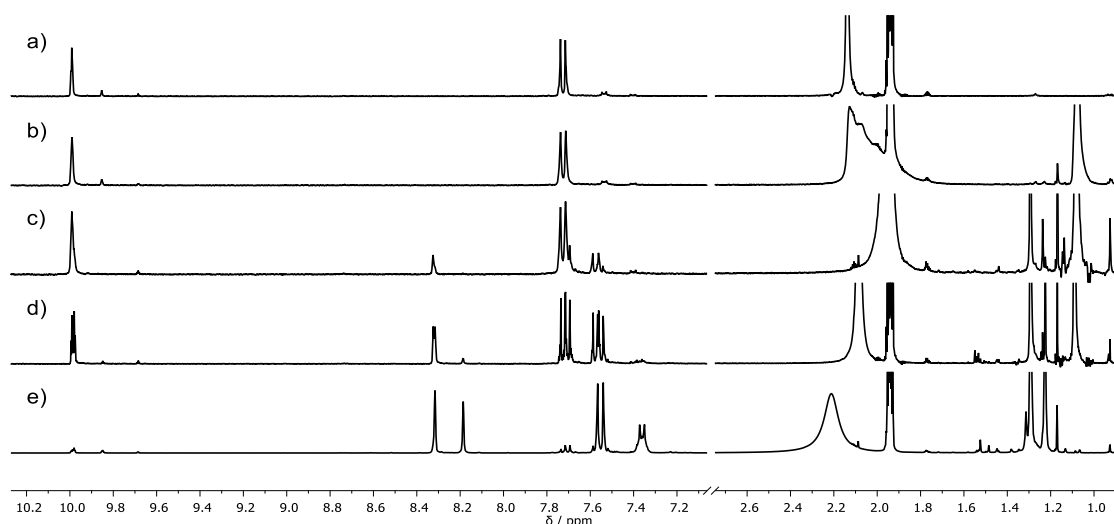


Figure 5.6 Reaction of **5.2** and tertbutylamine in CD₃CN monitored by ¹H NMR (26 mM, 400 MHz, 298 K). a) **5.2** in CD₃CN; b) addition of tertbutylamine (40 μL of a 0.6 M solution in CD₃CN); c) heated 323 K for 2h; d) heated 323 K for 3.5 h and e) heated 323 K for 3 days.

The addition of a reducing agent such a sodium triacetoxyborohydride (STAB) perturbs the imine formation equilibrium, as imines are more readily reduced than ketones and aldehydes, leading to irreversible formation of the secondary amine product.¹⁴⁵ Addition of STAB led to a decrease in the signals associated with the imine proton as expected, along with the growth of signals between 4.6 and 3.7 ppm, assigned to the new benzylic proton environments (Figure 5.7). However, the ¹H and ¹⁹F spectra were not consistent with the symmetric derivative proposed in Scheme 5.3. It suggests unwanted reduction of the aldehyde group to the alcohol, despite the use of STAB as a selective reagent. This suggests that the aldehyde functionality of **5.2** has limited reactivity towards amines, possibly requiring Lewis acid catalysis or dehydrative conditions to promote imine formation.

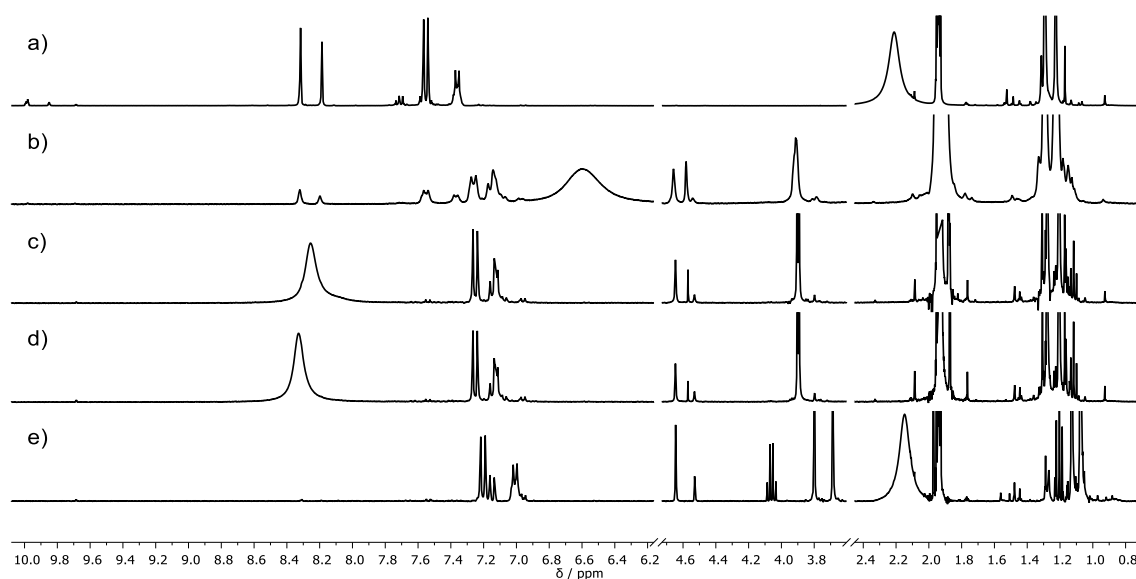


Figure 5.7 Attempted reduction of the reaction product between **5.2** and tertbutylamine in CD₃CN monitored by ¹H NMR (26 mM, 400 MHz, 298 K). a) **5.2** + tertbutylamine after 3 days at 323 K; b) addition of sodium triacetoxyborohydride (7.6 mg, 45 μmol); c) 2h at 298 K; d) 4h at 298 K and e) after work up (extraction into diethyl ether).

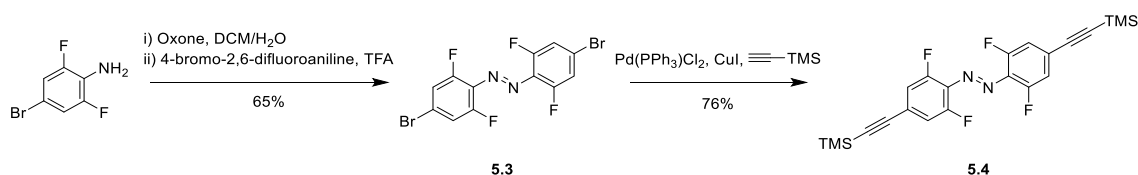
DCC relies on the lability of imine formation,^{140b} however for supramolecular applications it is often desirable¹⁴⁶ to “lock” the imines by reduction to secondary amines to prevent further unwanted reactivity or structural disassembly. In the first case of attempted macrocycle formation, the presence of unreacted aldehyde is undesirable. For the test case reaction with tertbutylamine the formation of significant side products is also undesirable, as it would affect the interpretation of the self-assembly process. Dialdehyde **5.2** retains interesting potential as it possesses good switching properties and considerable synthetic diversity may be introduced through the aldehyde motif. However, given the limitations identified this compound was not investigated further.

5.7 Palladium catalysed couplings of *o*-fluoroazobenzenes

There are a small number of examples of Suzuki¹⁴⁷ and Sonogashira¹⁴⁸ couplings using *o*-fluoroazobenzenes in the literature. The reactivity of such compounds in palladium cross-coupling reactions was investigated.

It is generally more favourable to derivatise after the azo-bond formation step. The reported synthesis of **5.3** used oxidation of 4-bromo-2,6-difluoroaniline with KMnO₄ supported on FeSO₄, to give the compound in low yield.^{24a} The use of a two-step procedure involving formation of the nitroso intermediate then a modified Mills coupling allowed preparation of **5.3** in good yield on a gram scale.

Sonogashira coupling is a versatile technique for combining functional units into supramolecular assemblies and to this end the reactivity of **5.3** towards Sonogashira coupling was explored. The reaction between **5.3** and trimethylsilylacetylene using Pd(PPh₃)₂Cl₂ and CuI gave **5.4** in 76% yield as the pure *E*-isomer (Scheme 5.4). The compound was stable to air and easily purified. A single crystal of *E*-**5.4** was obtained by slow evaporation of a solution in DCM (Figure 5.8). As the diffraction was relatively poor, the structure serves only to confirm atom connectivity.



Scheme 5.4 Sonogashira coupling of *o*-fluoroazobenzene **5.3**.

Deprotection of the TMS-acetylene groups using K₂CO₃ in methanol led to degradation of the molecule as observed by ¹H NMR spectroscopy. Due to time constraints alternate deprotection methodologies were not explored, such as tetrabutylammonium fluoride. However the functionalised *o*-fluoroazobenzene could also be exploited for incorporation into covalent organic cages¹⁴⁹ using Eglington coupling, or macrocyclic structures using Glaser coupling.¹⁵⁰

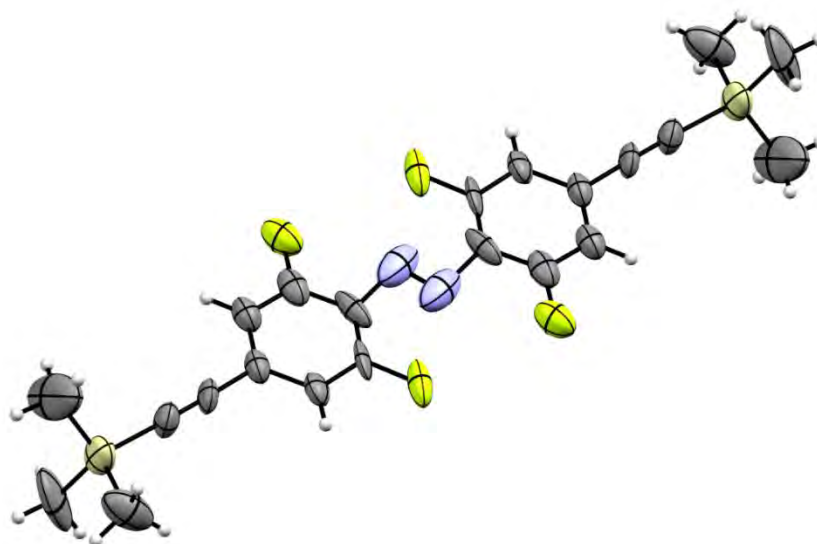
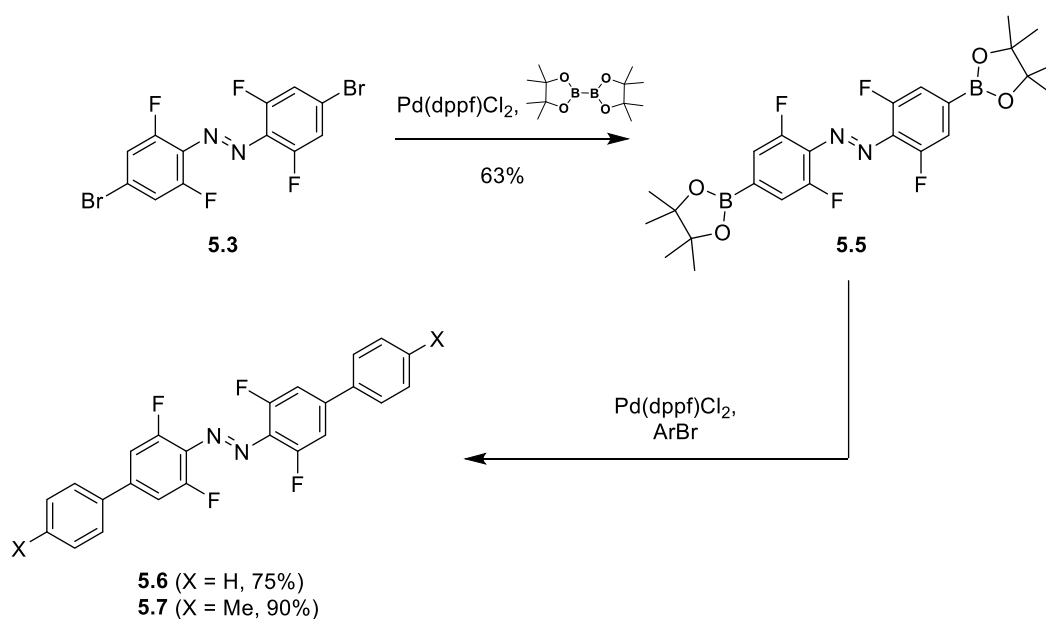


Figure 5.8 An ORTEP representation of one of the molecules in the asymmetric unit in the X-ray crystal structure of **5.4**. Thermal ellipsoids are drawn at 50% probability.

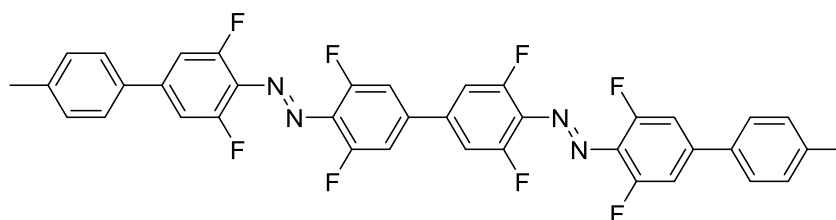
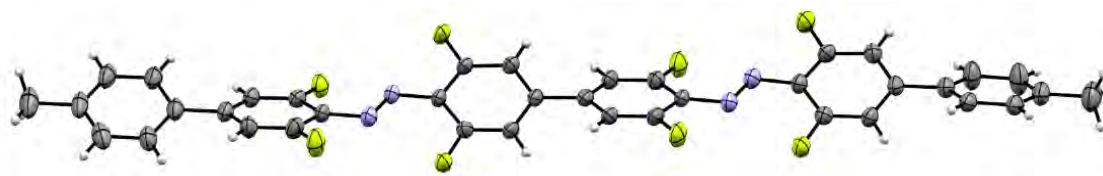
5.8 Suzuki coupling of *o*-fluoroazobenzenes

In all cases of Suzuki couplings using *o*-fluoroazobenzenes in the literature, the bromo-substituted derivative **5.3** or the unsymmetric mono-bromo substituted compound were employed. Previous work in the group¹⁵¹ has used Suzuki coupling to append pentacene derivatives to the boronic acid substituted **5.5**. Compound **5.5** was prepared on a gram scale in 75% yield and ¹H and ¹⁹F spectra match that reported.¹⁵² Reaction of **5.3** with phenylbromide or tolylbromide in THF/water gave the novel compounds **5.6** (75%) and **5.7** (90%) (Scheme 5.5).



Scheme 5.5 Suzuki coupling of boronic ester substituted **5.5** and some simple aromatic systems.

Interestingly, upon attempting to grow single crystals of **5.7** for X-ray diffraction, the structure shown in Figure 5.9 was obtained. This structure can be rationalised as a homocoupling between two mono-substituted species, which is known to occur for boronic esters.¹⁵³ Re-examining the ¹⁹F and ¹H NMR spectra finds the presence of other ¹⁹F and ¹H environments, however at low concentrations. While this result is surprising, it suggests the mono-substituted species has significantly different reactivity to compound **5.5**. In order to form compound **5.8**, the rate of coupling to the halide substituted compound must be slowed relative to the background oxidative homocoupling.



5.8

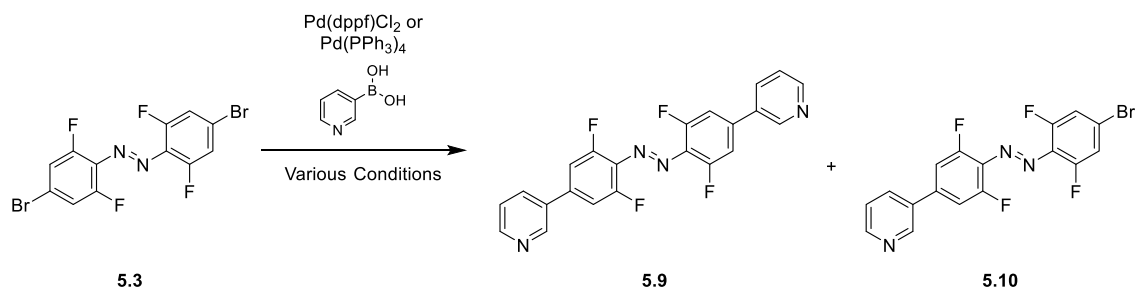
Figure 5.9 Structure of extended *o*-fluoroazobenzene, collected from attempted crystallisation of **5.7**. Top: an ORTEP representation of the asymmetric unit in the X-ray crystal structure. Thermal ellipsoids are drawn at 50% probability.

The above results show that *o*-fluoroazobenzenes are amenable to derivatisation for use in larger structures. However, their reactivity must be considered due to the electron-withdrawing nature of the azo-bond and fluoro substituents. Sonogashira coupling is a promising methodology for incorporating useful functionalities, however optimisation is required. Finally, it was shown that Suzuki coupling allows incorporation of aromatic functionalities at the periphery of the switching unit. However, this does not easily allow for the generation of electronically disconnected subunits. This could be achieved through installation of *o*-methyl units, which are known to interrupt conjugation.¹⁵⁴

5.9 Synthesis of pyridyl substituted *o*-fluoroazobenzenes.

The most widely exploited functionality for metal-ligand template self-assembly is the combination of a (bi)pyridyl ligand and a labile metal ion. The 3-pyridyl derivative was targeted as it should give a convergent “banana-shaped” ligand, which has been used with great success by a number of groups to generate discrete self-assembled structures.^{68c} Furthermore, minimising electronic communication between the photoswitching unit and the metal centre should allow retention of the advantageous photoswitching properties of *o*-fluoroazobenzenes. Initial efforts to synthesise pyridyl-appended ligand **5.9** used bromo-substituted **5.3** and 3-pyridylboronic acid (Scheme 5.6). Crude ¹H NMR suggested some product formation, however significant formation of other products was observed. A small range of conditions were investigated, including varying the catalyst (Pd(PPh₃)₄ or Pd(dppf)Cl₂), solvent (THF:water, dioxane:water or DMF) or reaction temperature (60

°C, 80 °C or 120 °C (microwave heating). Reaction in THF/water (10:1) allowed isolation of the non-symmetric product **5.10** in 31% yield, suggesting the second coupling was unfavourable. X-Ray quality crystals of **5.10** were obtained by slow evaporation of ethyl acetate, showing the reaction at only one site (Figure 5.10). This is a potentially useful intermediate for incorporating visible-light photoswitching into larger systems but was not explored further in this work.



Scheme 5.6 Synthesis of pyridine-appended o-fluoroazobenzene **5.9** and the non-symmetric by-product **5.10**.

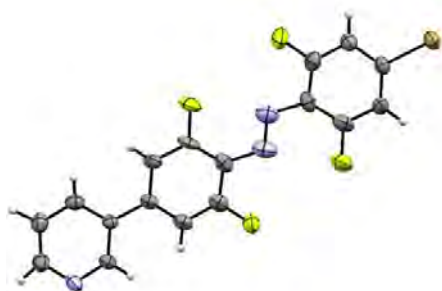


Figure 5.10 Structure of unsymmetric pyridine substituted derivative **5.10**. An ORTEP representation of the asymmetric unit in the X-ray crystal structure of **5.10**. Thermal ellipsoids are drawn at 50% probability.

5.10 An aside: the green impurity

In several cases a major impurity was noted during attempted Suzuki coupling the identity of which remains unknown. Couplings attempted in mixed aqueous organic systems (for example THF/H₂O or dioxane/H₂O) at elevated temperatures led to the formation of a forest green solution. This solution changed colour to red upon addition of acid, and the ¹H and ¹⁹F NMR signals were not consistent with the desired symmetric product. During column chromatography, in all cases a green band was observed at the top of the silica, which did not elute during the separation. This species is tentatively assigned to a hydroxyl substituted fluoroazobenzene (Figure 5.11), formed by nucleophilic aromatic attack at the fluorine, which is known to occur for aromatic

fluorines.¹⁵⁵ This impurity may be of future importance when incorporating *o*-fluoroazobenzenes into larger structures.

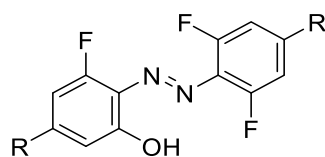
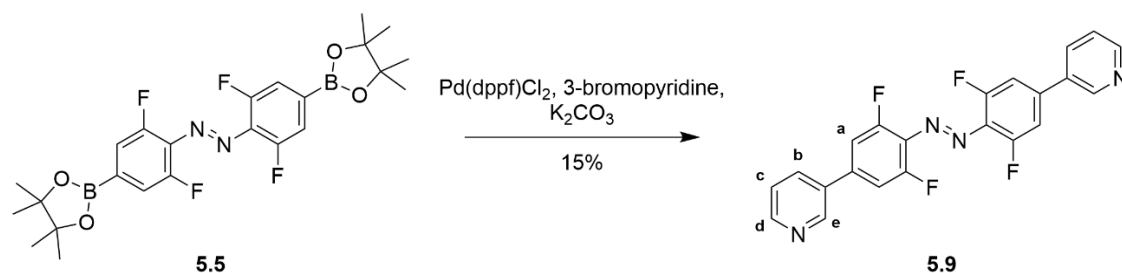


Figure 5.11 Proposed impurity formed during Suzuki coupling with compounds **5.3** and **5.5**.

5.11 Characterisation of pyridyl ligand **5.9**

The desired compound **5.9** was obtained in 15% yield by using microwave assisted coupling between boronic ester **5.5** and 3-bromopyridine (Scheme 5.7). The compound was isolated as a mixture of *E* and *Z* isomers as no care was taken to exclude light from the preparation.



Scheme 5.7 Synthesis of pyridyl substituted *o*-fluoroazobenzene **5.9**.

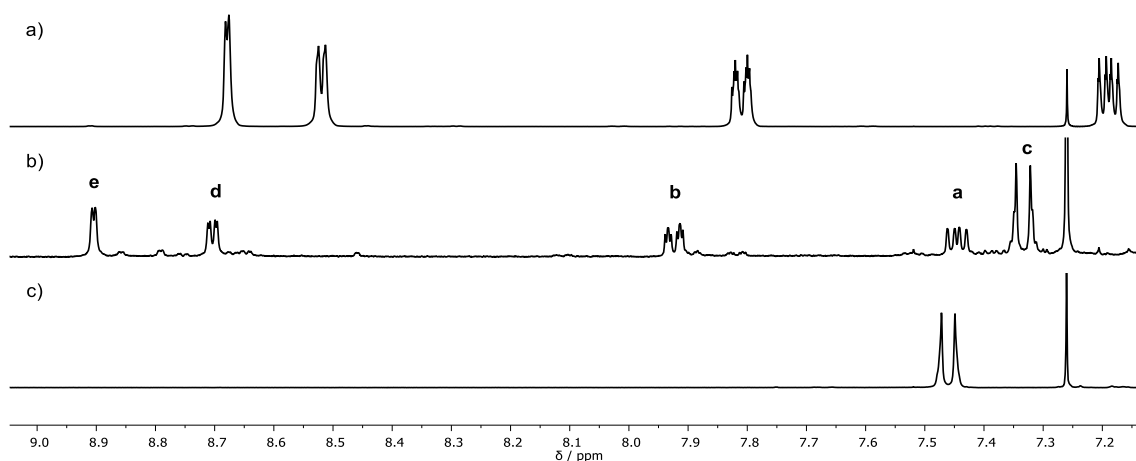


Figure 5.12 Partial stacked ¹H NMR spectra (CDCl₃, 400 MHz, 298 K) of a) 3-bromopyridine; b) *o*-fluoroazobenzene **5.9** and c) boronic acid substituted compound **5.5**.

The absorption spectrum of *E*-**5.9** extends into the visible, with an absorption λ_{max} at 459 nm in DMSO, assigned as the $n\text{-}\pi^*$ band (Figure 5.13). This is very similar to the unsubstituted *o*-tetrafluoroazobenzene (λ_{max} (DMSO) = 460 nm),^{24a} suggesting little

impact by the peripheral pyridyl rings on this electronic transition. The π - π^* band has a λ_{max} at 350 nm, which is significantly red-shifted relative to previously reported *o*-fluoroazobenzenes, which typically have π - π^* absorption λ_{max} values of 305-320 nm.^{24b} This is consistent with an increase in conjugation length upon appending the pyridyl rings.

Compound **5.9** shows reversible visible-light photoswitching. Irradiation at 530 nm generates a photostationary state comprising 78% *Z*-**5.9** based on ¹H and ¹⁹F NMR data (Figure 5.14). Subsequent irradiation at 410 nm generates a new photostationary state, comprising 83% *E*-**5.9**. Calculated spectra of the pure *E* and *Z* isomers were generated from two different PSS spectra, as discussed in Chapter 3. The calculated *Z*-**5.9** spectrum shows a n - π^* peak with a $\lambda_{\text{max}} = 430$ nm, slightly red-shifted compared to unsubstituted or amide substituted *o*-fluoroazobenzenes ($\lambda_{\text{max}} = 415$ -420 nm). A commonly discussed parameter for these systems is $\Delta\lambda_{n-\pi^*}$, which is the separation between the n - π^* bands for the respective isomers.^{24b} For this system $\Delta\lambda_{n-\pi^*} = 29$ nm, which is lower than previous examples (for instance the di-ester substituted *o*-fluoroazobenzene has a $\Delta\lambda_{n-\pi^*} = 50$ nm, which allows selective generation ($\geq 90\%$) of either isomer.

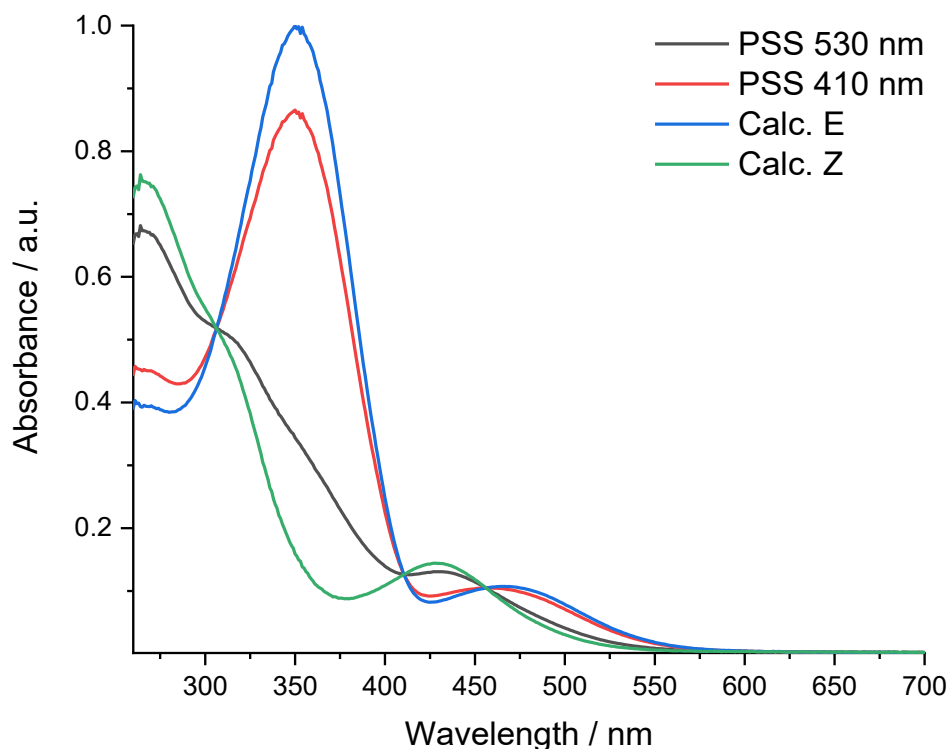


Figure 5.13 Switching between *E*-**5.9** and *Z*-**5.9** monitored by UV-vis spectroscopy at 298 K in DMSO. Pure *E* and pure *Z* spectra calculated as discussed in Chapter 3.

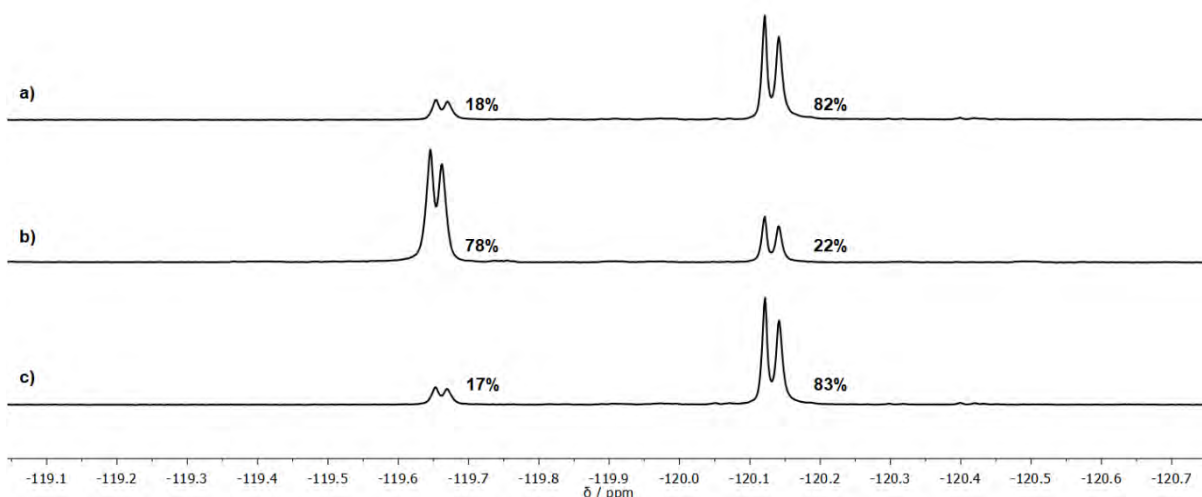


Figure 5.14 Photoswitching of **5.9** in DMSO- d_6 monitored with ^{19}F NMR (564.6 MHz, 298 K). a) Initial spectrum; b) after 30 minutes *ex situ* irradiation with a 530 nm LED; c) subsequent *ex situ* irradiation for 30 minutes with a 410 nm LED.

5.12 Synthesis of self-assembled structures with palladium

In order to self-assemble larger structures with the pyridyl functionalised ligand, the “naked metal-ion” strategy was employed. This relies on the well-defined square-planar geometry of palladium(II) in combination with pyridyl ligands, and has been exploited most often to form M_2L_4 architectures (although others are known).^{68c} Combination of **5.9** and $[\text{Pd}(\text{CH}_3\text{CN})_4](\text{BF}_4)_2$ in DMSO- d_6 led to immediate formation of a new species as observed by ^1H NMR, with identical symmetry to the parent azobenzene (Figure 5.15). Characteristic downfield shifts of the pyridyl ring protons indicated coordination to the metal ion.^{68d, 107e} The proton NMR signal for H^a shifts upfield by ≈ 0.2 ppm, consistent with shielding effects commonly seen for self-assembled structures.^{68c, 68e, 107e, 156} Despite the ligand being present as a mixture of *E* and *Z* isomers, one major product was initially formed with no evidence of species formed from a mixture of isomers. The reduced symmetry of these mixed-isomer species would lead to significantly reduced intensity in the ^1H NMR spectrum due to the increased number of non-equivalent protons. There is also precedent for a “self-sorting” effect in palladium-pyridine self-assemblies, where the homoleptic structures are substantially favoured.^{68e,}

Equilibration of this sample in the dark at room temperature slowly formed another species, with twice as many signals as the ligand. These new signals are in a 1:1 ratio, suggesting they all correspond to the same species. An equilibrium was reached after 24 hours comprising 65% of the less symmetric assembly (Figure 5.15). A ^1H DOSY NMR spectrum showed the signals could be separated into two groups based on diffusion constant (Figure 5.16 and 5.17). The symmetrical assembly diffused at a slightly faster rate (average diffusion constant: $6.89 \times 10^{-11} \text{ m}^2 \text{ s}^{-1}$) compared to the non-symmetric (average diffusion constant $6.17 \times 10^{-11} \text{ m}^2 \text{ s}^{-1}$). These species can roughly be approximated as spheres with hydrodynamic radii of 1.58 and 1.75 nm respectively.

The self-assembly was also followed by ^{19}F NMR (Section 9.1). Addition of $[\text{Pd}(\text{CH}_3\text{CN})_4](\text{BF}_4)_2$ to **5.9** led to a downfield shift by 1.5 ppm of the fluorine signal associated with ligand **5.9**, followed by the slow growth of two new signals in a 1:1 ratio, mirroring the observations in the ^1H NMR spectra.

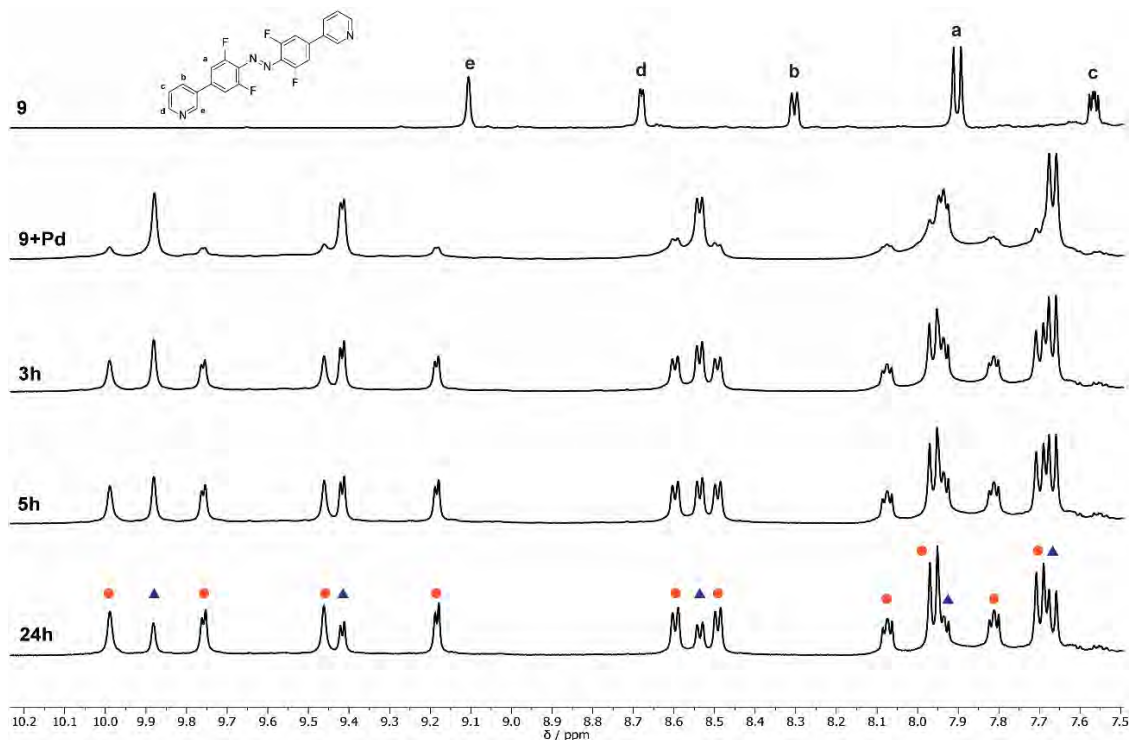


Figure 5.15 Reaction between **5.9** and $[\text{Pd}(\text{CH}_3\text{CN})_4](\text{BF}_4)_2$ monitored by ^1H NMR ($\text{DMSO}-d_6$, 600 MHz, 298 K). Signals have been grouped based on diffusion data (see Figure 5.16).

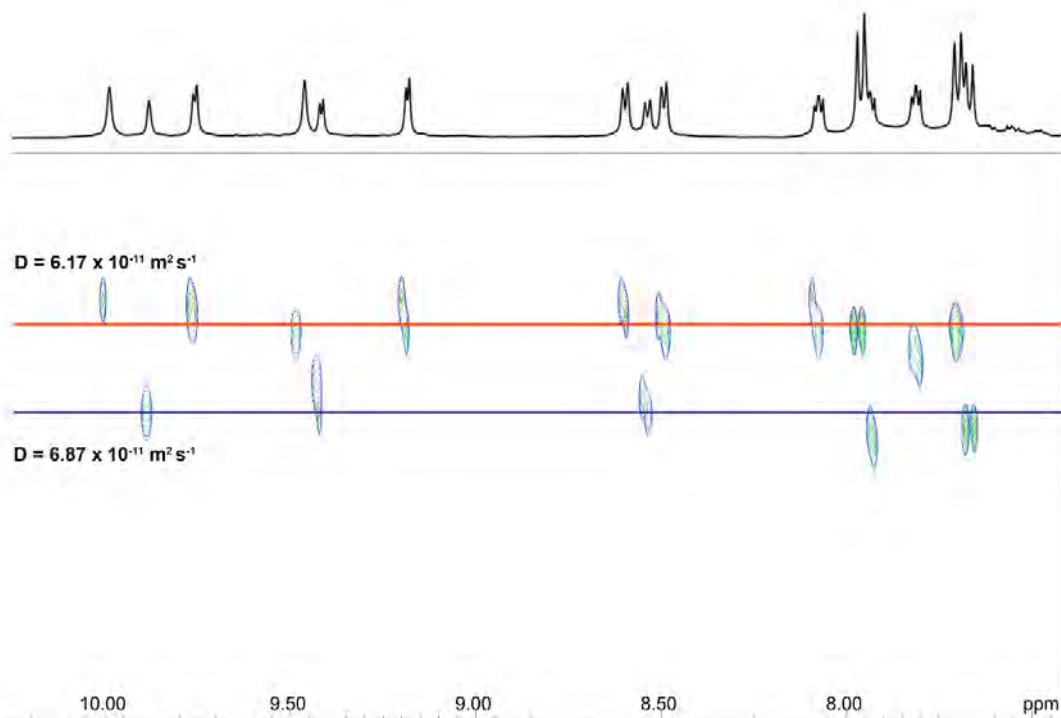


Figure 5.16 ^1H DOSY NMR spectrum of a mixture of $[\text{Pd}_3(\mathbf{5.9})_6]^{6+}$ and $[\text{Pd}_4(\mathbf{5.9})_8]^{8+}$ in $\text{DMSO-}d_6$ (600 MHz, 298 K).

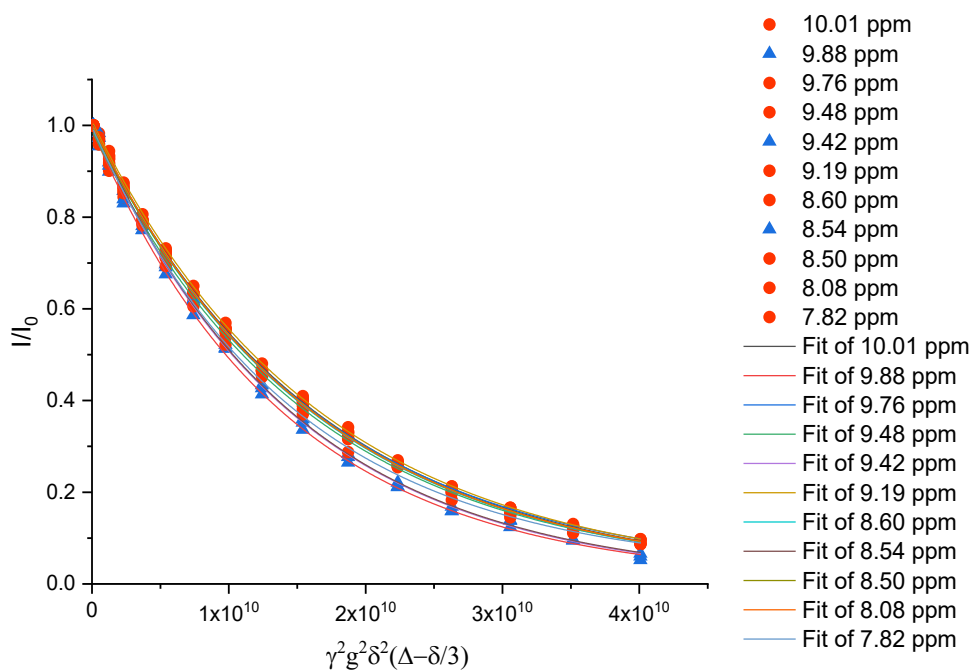


Figure 5.17 Fitting of integrals from the ^1H NMR diffusion data of the self-assembly product ($\text{DMSO-}d_6$, 600 MHz, 298K). Data were fit to a mono-exponential function.

5.13 High resolution ESI-MS of the Pd(II) assemblies

High resolution ESI-MS of the NMR sample in DMSO- d_6 showed a series of peaks corresponding to the structural formulae $[\text{Pd}_3(\mathbf{5.9})_6]^{n+}$ (where $n = 2-5$) and $[\text{Pd}_4(\mathbf{5.9})_8]^{n+}$ (where $n = 2-7$), corresponding to sequential BF_4^- anion loss (Figure 5.18). Isotope patterns match those predicted (Figure 5.19 and Section 9.2). There was no evidence for other structural configurations (e.g. barrel-shaped M_2L_4 or tetrahedral M_4L_6).

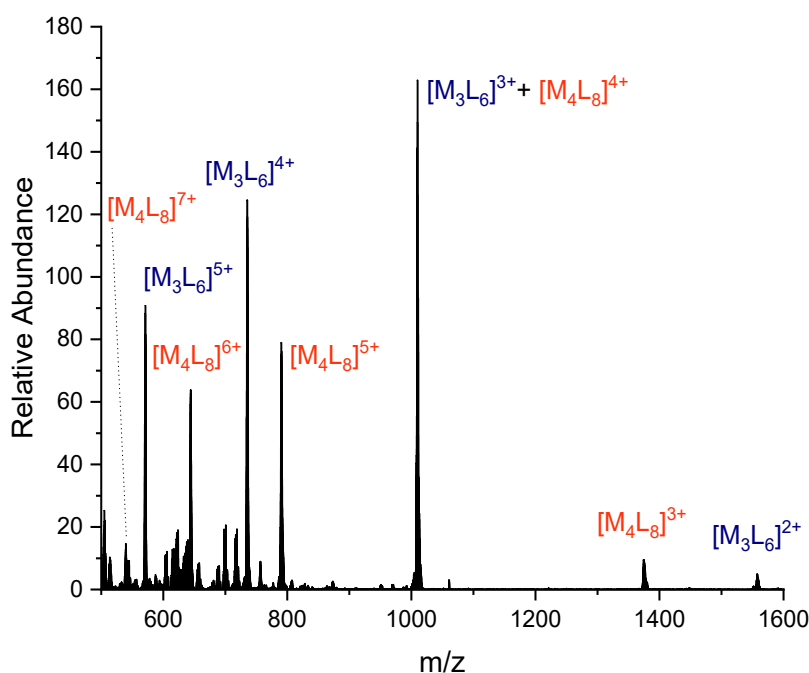


Figure 5.18 HR ESI mass spectrum of $[(\text{Pd}_3(\mathbf{5.9})_6) + n\text{BF}_4]^{m+}$ (for $1 \leq n \leq 4$, $m = 6 - n$) and $[(\text{Pd}_4(\mathbf{5.9})_8) + n\text{BF}_4]^{m+}$ (for $1 \leq n \leq 5$, $m = 8 - n$) in DMSO- d_6 .

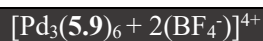
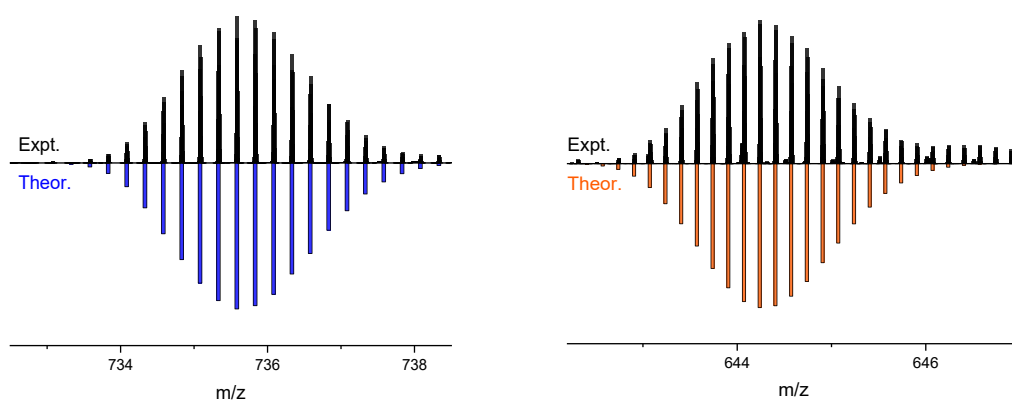


Figure 5.19 Selected isotope patterns for the $[\text{Pd}_3(\mathbf{5.9})_6]^{6+}$ and $[\text{Pd}_4(\mathbf{5.9})_8]^{8+}$ species. The full range of peaks is given in Section 9.2

5.14 Elucidation of structure

Having determined the structural composition by ESI-MS, it remained to determine the self-assembled structures. ^1H - ^1H COSY and ROESY NMR spectra (Figure 5.20 and 3.21), combined with the ^1H DOSY measurements above, allowed grouping of the signals, denoted by the blue triangles and orange circles in Figure 5.15. Key to this was the identification of a ROESY cross-peak between the signal for H^{d} and $\text{H}^{\text{e}'}$. These signals have no COSY cross-peaks, so they likely correspond to two different ligands as a part of the same self-assembled structure.

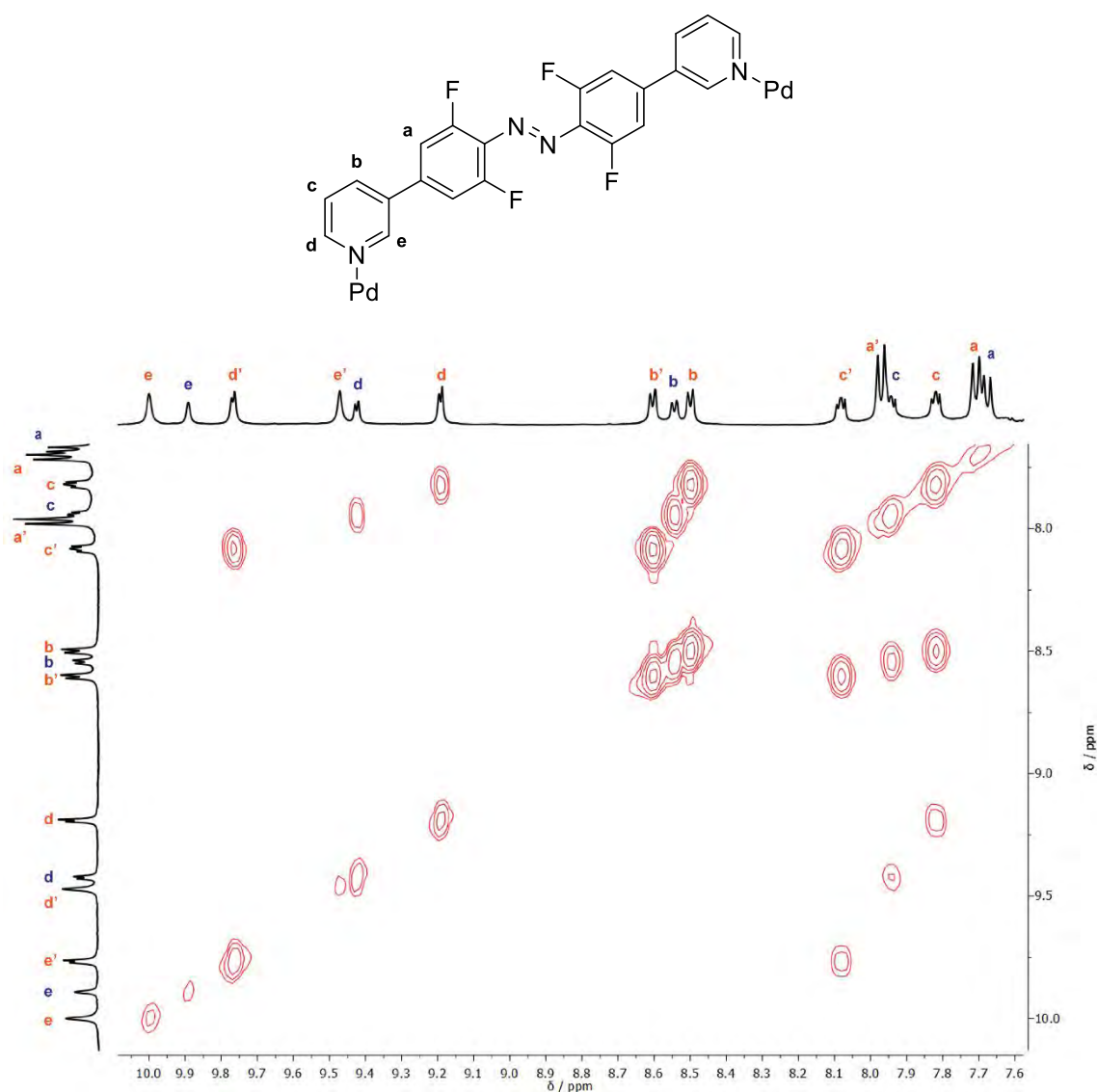


Figure 5.20 ^1H - ^1H COSY spectrum (DMSO- d_6 600 MHz, 298 K) of a mixture of $[\text{Pd}_3(\mathbf{5.9})_6]^{6+}$ and $[\text{Pd}_4(\mathbf{5.9})_8]^{8+}$.

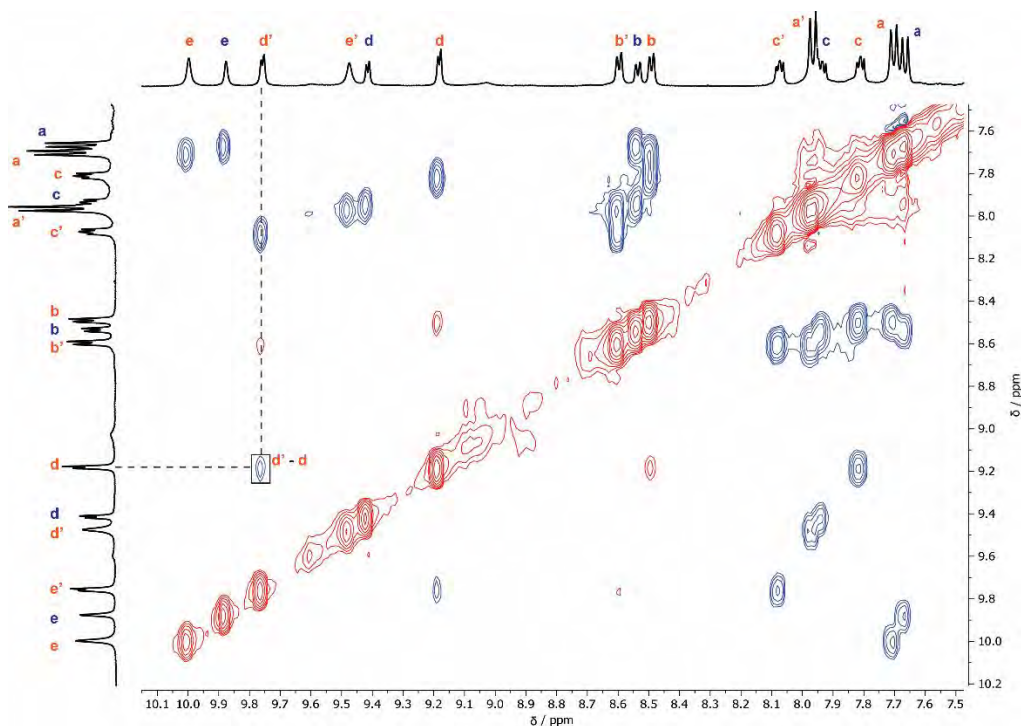


Figure 5.21 ^1H - ^1H ROESY spectrum (DMSO- d_6 600 MHz, 298 K) of a mixture of $[\text{Pd}_3(\mathbf{5.9})_6]^{6+}$ and $[\text{Pd}_4(\mathbf{5.9})_8]^{8+}$.

This discussion will be divided between the two species differentiated in terms of hydrodynamic radii. For those signals denoted as blue triangles, the species has the same symmetry as the free ligand. As diffusion NMR shows this corresponds to the species with the smaller hydrodynamic radii, these signals are assigned to a symmetric double-walled triangle denoted as $[\text{Pd}_3(\mathbf{5.9})_6]^{6+}$ (Figure 5.22). As this structure has (on average) D_{3h} symmetry all the ligands are identical, leading to the same number of proton signals observed in the NMR spectrum as the free ligand.

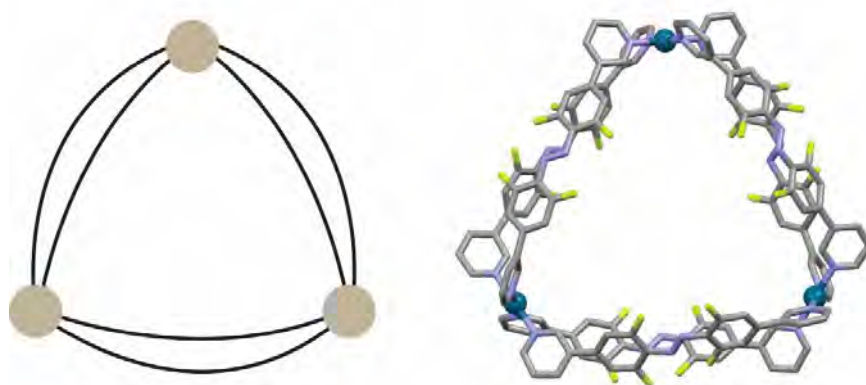


Figure 5.22 Proposed self-assembled structure for the $[\text{Pd}_3(\mathbf{5.9})_6]^{6+}$ species. In the $[\text{Pd}_3(\mathbf{5.9})_6]^{6+}$ species, all ligands are identical by symmetry and each palladium(II) centre is bridged by two ligands.

Secondly, there are several possible geometries available with an $M_4L_8^{8+}$ structural composition (Figure 5.23). These include a regular square,¹⁵⁸ which can be considered a single vertex expansion of the $M_3L_6^{6+}$ geometry; an interpenetrated double cage,¹⁵⁹ driven by the interaction between two $M_2L_4^{4+}$ species; or more unusually, a distorted tetrahedron¹⁶⁰ where two of the tetrahedron edges are joined by two ligands and the remaining four are bridged by one ligand. The square connectivity can be dismissed on symmetry grounds, as this structure has D_{4h} symmetry and all the ligands are identical. This symmetry has been previously been observed in the 1H NMR spectrum of an double-walled square assembly and is inconsistent with the 1H spectrum observed.^{158d} The catenated $[M_4L_8]^{8+}$ assemblies, as thoroughly explored by Clever and co-workers^{159a, 159b, 159e, 159f} would lead to a non-symmetrical ligand, due to shielding of the ligand protons by the inside of the cavity. However, during the formation of the interpenetrated cages they observed a transient $[M_2L_4]^{4+}$ species by 1H NMR, which subsequently re-arranged to the interpenetrated structure. For the present example, the lack of observation of this smaller species by 1H NMR or ESI-MS, as well as rudimentary molecular modelling, suggests this structure does not accurately describe the assembly.

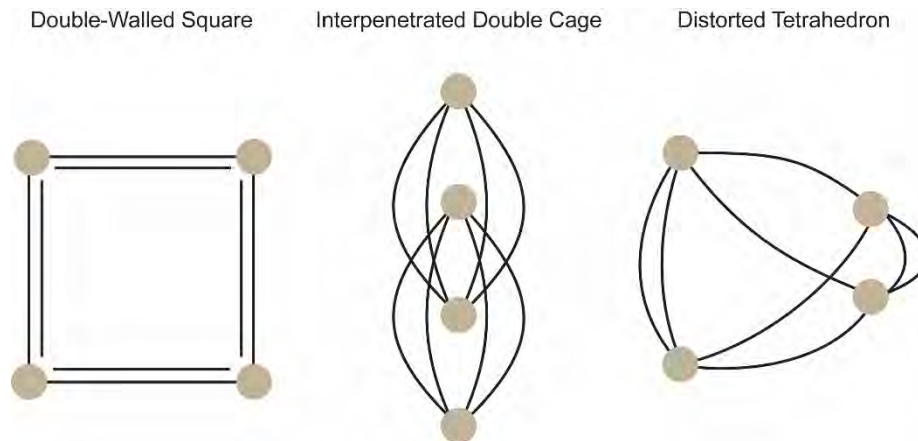


Figure 5.23 Possible geometries with the $[Pd_4(\mathbf{5.9})_8]^{8+}$ structural formula.

Therefore, the structure of the $[Pd_4(\mathbf{5.9})_8]^{8+}$ assembly is proposed as a distorted tetrahedron (Figure 5.24). This structure has only been described on three previous occasions, resulting from the use of rigid, divergent 3-pyridyl ligands (Figure 5.25).¹⁶⁰⁻¹⁶¹ The reduced symmetry of the 1H and ^{19}F NMR spectra are ascribed to the presence of two different types of ligand in the distorted tetrahedron; namely whether the two metal centres are bridged by one or two ligands. This gives a structure (on average) with overall C_{2v} symmetry. The predicted hydrodynamic radius is only slightly larger than the double-walled triangle, consistent with the 1H DOSY results above. The analogous distorted

tetrahedron structure formed from an iron(II)-clathrochelate ligand¹⁶¹ has a similar separation between pyridyl groups (py-N to py-N: 16.5 Å for ligand (**5.9**) vs. 13.5 Å for the clathrochelate). The diffusion constant for the self-assembled species is also similar, with a measured value for the $[\text{Pd}_4(\mathbf{5.9})_8]^{8+}$ species of $6.12 \times 10^{-11} \text{ m}^2 \text{ s}^{-1}$ (cf. $7.64 \times 10^{-11} \text{ m}^2 \text{ s}^{-1}$ in DMSO-*d*₆ for the clathrochelate species), with the difference ascribed to the difference in bridging ligand lengths. Overall, and in the absence of a single crystal structure to unequivocally prove the geometry, these results are consistent with the proposed distorted tetrahedron structure.

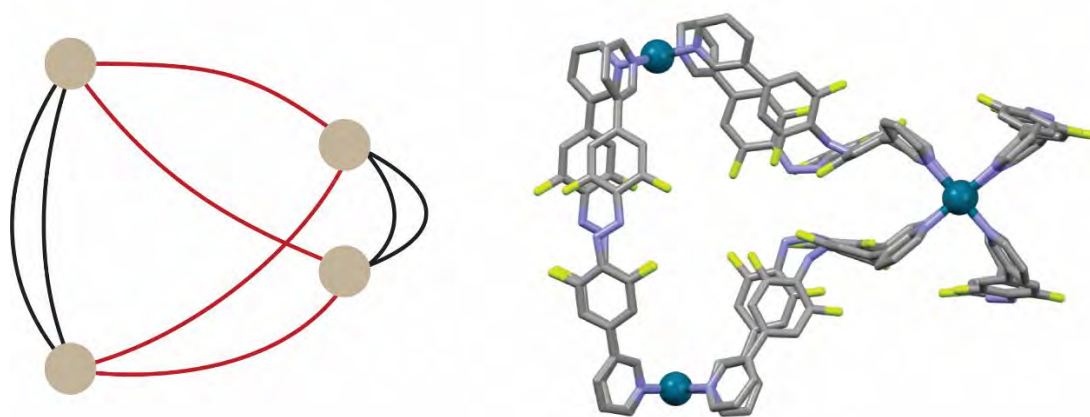


Figure 5.24 Proposed structure of the $[\text{Pd}_4(\mathbf{5.9})_8]^{8+}$ distorted tetrahedron (MMFF). Black edges denote *E*-**5.9** and red edges denote *Z*-**5.9**.

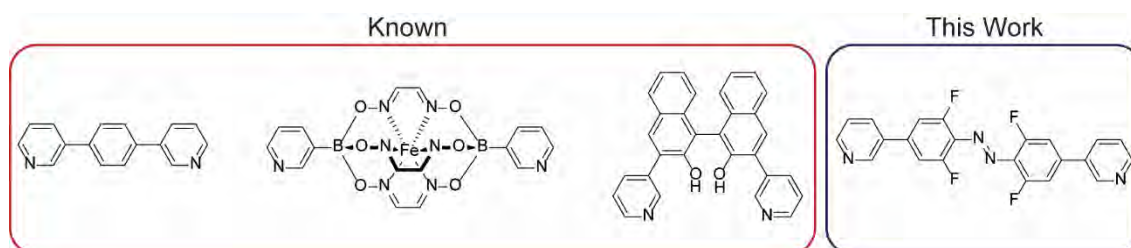


Figure 5.25 Comparison of ligands known to form distorted tetrahedral M_4L_8^+ architectures with the structure of ligand **5.9**

5.15 Kinetics of formation

As the equilibration of the sample is relatively slow in solution, the formation of the $[\text{Pd}_4(\mathbf{5.9})_8]^{8+}$ species was monitored by ¹H NMR spectroscopy (Figure 5.26). As shown in Figure 5.15, there is initial rapid formation of the $[\text{Pd}_3(\mathbf{5.9})_6]^{6+}$ species, followed by a decrease in the observed concentration of this species over time. No increase in the concentration of $[\text{Pd}_3(\mathbf{5.9})_6]^{6+}$ species was observed at any time, suggesting it is formed

rapidly and reaches maximum concentration before the first ^1H NMR measurement. Over the same time period the formation of the $[\text{Pd}_4(\mathbf{5.9})_8]^{8+}$ species is observed. The rate of consumption of the $[\text{Pd}_3(\mathbf{5.9})_6]^{6+}$ species was modelled as pseudo first order and was observed to be much faster ($t_{1/2} \approx 100$ minutes) than the formation of the $[\text{Pd}_4(\mathbf{5.9})_8]^{8+}$ species ($t_{1/2} \approx 240$ minutes) see Table 5.1. This assumption of first-order kinetics is obviously incorrect, given that interconversion between the $[\text{Pd}_3(\mathbf{5.9})_6]^{6+}$ and $[\text{Pd}_4(\mathbf{5.9})_8]^{8+}$ species requires several bond-forming and breaking steps. However, the approximation is sufficient to allow some comments on the kinetics of the reaction. The difference in rates suggest that the formation of the larger species is not simply governed by the disassembly of the smaller unit, and NMR “silent” species must be involved, for example polymers or less-symmetric species. Such species have been observed by Hiraoka and co-workers using Dynamic Light Scattering techniques during assembly of large palladium(II) architectures.^{158a, 158d} They also suggested that the $[\text{Pd}_3\text{L}_6]^{6+}$ species is an intermediate to the self-assembly process of the $[\text{Pd}_4\text{L}_8]^{8+}$ species, which is consistent with the observations here. However, as the final assembly adopts a distorted tetrahedral configuration, rather than the double-walled square, care must be taken when comparing mechanisms of formation.

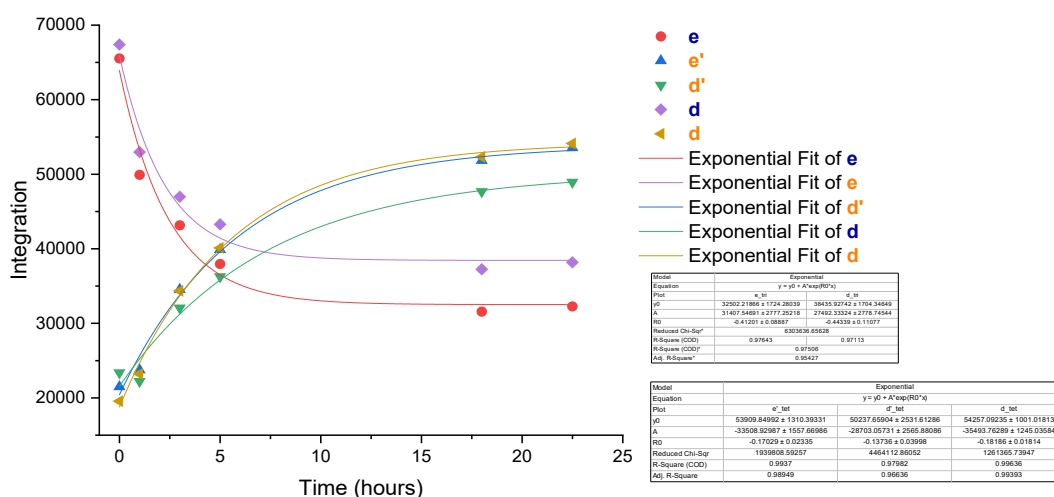


Figure 5.26 Kinetics of formation for $[\text{Pd}_3(\mathbf{5.9})_6]^{6+}$ and $[\text{Pd}_4(\mathbf{5.9})_8]^{8+}$ monitored in $\text{DMSO-}d_6$ (600 MHz, 298 K)

Table 5.1 Tabulated $t_{1/2}$ values for the formation of $[\text{Pd}_3(\mathbf{5.9})_6]^{6+}$ and $[\text{Pd}_4(\mathbf{5.9})_8]^{8+}$. Half-life values calculated by fitting the integration data in Figure 5.26 to a mono-exponential function.

Proton Signal	Calculated $t_{1/2}$ / minutes
H ^e	100
H ^{e'}	245
H ^{d'}	304
H ^d	95
H ^d	230

5.16 Variable temperature measurements

To further explore the equilibrium between self-assemblies, variable temperature ¹H NMR measurements were performed. Heating the mixture in DMSO-*d*₆ led to a significant change in the distribution of species (Figure 5.27 and Figure 5.28). At 333 K the mixture comprises approximately 65% of the $[\text{Pd}_3(\mathbf{5.9})_6]^{6+}$ species, and this is not affected upon further heating up to 353 K (Figure 5.28). The signals corresponding to protons H^{tet,e'} and H^{tet,d'} move significantly, suggesting a change in the coordination environment around the palladium centre. Other peak shifts are seen but they are much smaller than for H^{tet,e'} and H^{tet,d'}. There are also additional, broad peaks present upon heating. This may be attributed to increase ligand exchange forming polymeric species, or a larger self-assembly. Upon initially returning to 298 K the mixture comprised 40% of the $[\text{Pd}_4\mathbf{9}_8]^{8+}$ species, suggesting the system was not equilibrated. Equilibration in the dark overnight (18 h) restored the original product mixture containing 65% of the $[\text{Pd}_4\mathbf{9}_8]^{8+}$ species. These observations confirm the two species are in thermodynamic equilibrium with each other.

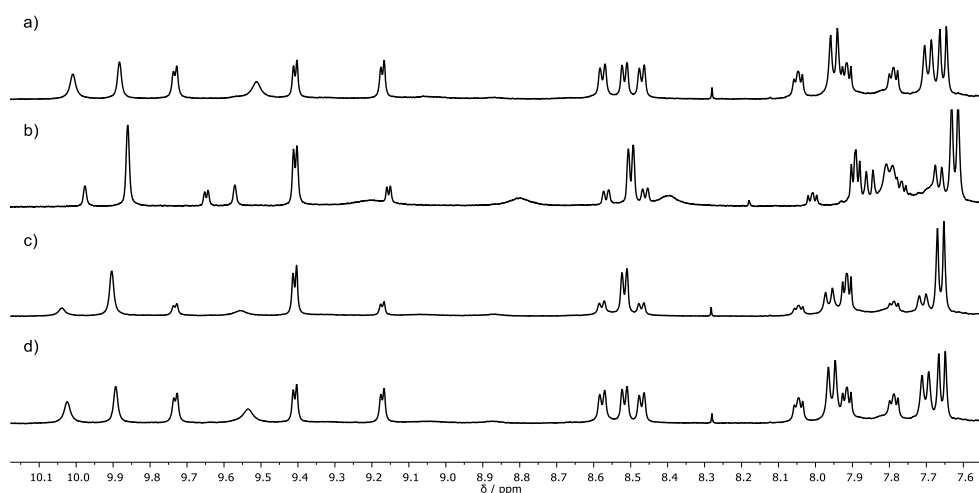


Figure 5.27 Variable temperature ^1H NMR measurement of $[\text{Pd}_3(\mathbf{5.9})_6]^{6+}$ and $[\text{Pd}_4(\mathbf{5.9})_8]^{8+}$ in $\text{DMSO-}d_6$ (600 MHz). a) Initial sample measured at 298 K; b) subsequently heated to 353 K; c) return to 298 K and d) after equilibration in the dark (18 h), measured at 298 K. At each temperature point the sample was allowed to equilibrate for 30 minutes. Full temperature range shown in Section 9.3.

The difference in distribution of the species before and after heating suggests that the $[\text{Pd}_3(\mathbf{5.9})_6]^{6+}$ species is a kinetic trap, which is consistent with the behaviour observed upon initial complex formation (Figure 5.15). The smaller assembly is rapidly formed at room temperature and is favoured at higher temperature due to entropic considerations,¹⁶² however at room temperature in the dark there is a slow equilibration to form the more thermodynamically stable $[\text{Pd}_4(\mathbf{5.9})_8]^{8+}$ species.

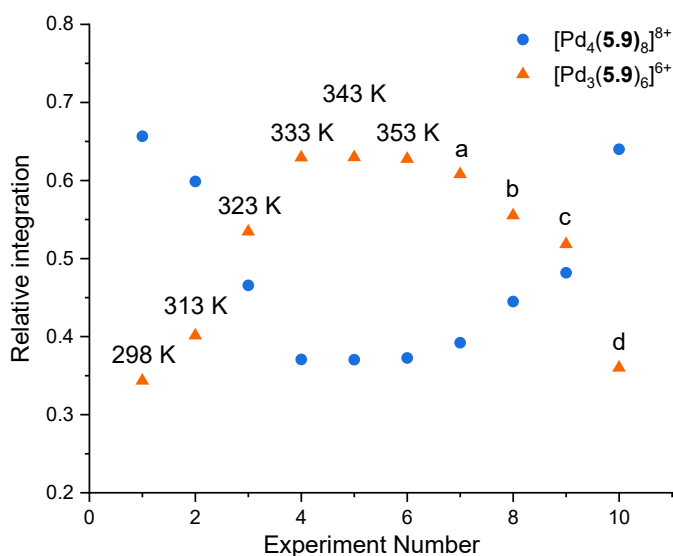


Figure 5.28 Variable temperature ^1H NMR measurement of a mixture of $[\text{Pd}_3(\mathbf{5.9})_6]^{6+}$ and $[\text{Pd}_4(\mathbf{5.9})_8]^{8+}$ in $\text{DMSO-}d_6$ (600 MHz). Integrals for the H^e protons on both species have been

normalised relative to the overall sum and the integrations for protons $H^{\text{tet},e}$ and $H^{\text{tet},e'}$ combined. Data plotted from Fig 9.2. Points a-d are all measured at 298 K, at different time points. a) $t = 0$ h; b) 80 min; c) 120 min and d) 18 h.

5.17 Perturbing equilibrium with light irradiation

Having established the structures of the self-assembled species, the effect of irradiation on the mixture was examined. Retention of initial composition upon irradiation for self-assembled structure is generally unfavourable due to the different geometric constraints on the ligand and metal.^{58c, 163} Irradiation of the mixture of self-assembled species in DMSO- d_6 with 567 nm light led to a poorly defined mixture of species as seen by ^1H and ^{19}F NMR (Figure 5.29). This is evidence for formation of *Z*-**5.9** containing polymeric species, as well as less-symmetric species containing a mixture of isomers. The rate of consumption of the $[\text{Pd}_3(\mathbf{5.9})_6]^{6+}$ species under constant irradiation is slower than for the $[\text{Pd}_4(\mathbf{5.9})_8]^{8+}$ species. This is consistent with a slower rate of ligand exchange for the $[\text{Pd}_3(\mathbf{5.9})_6]^{6+}$ complex compared to the $[\text{Pd}_4(\mathbf{5.9})_8]^{8+}$ species, as isomerisation occurs for the small percentage of free ligand in solution. This observation is further evidence for $[\text{Pd}_3(\mathbf{5.9})_6]^{6+}$ acting as a kinetic trap.

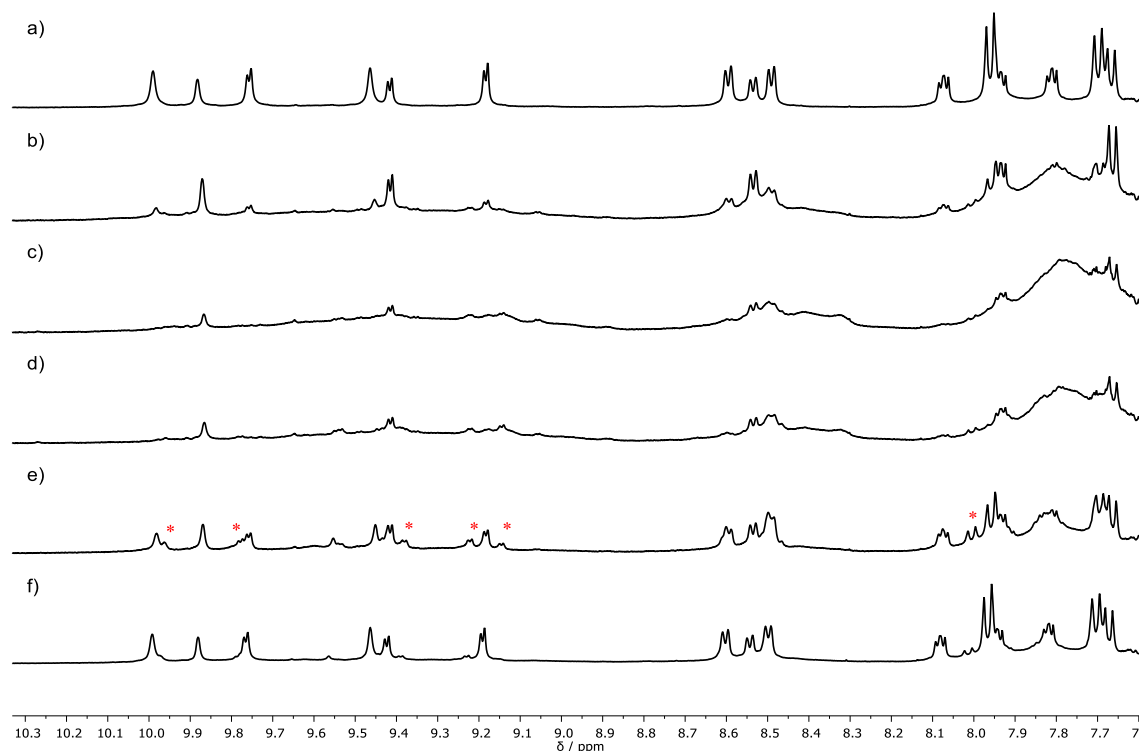


Figure 5.29 Irradiation (567 nm) of a mixture of $[\text{Pd}_3(\mathbf{5.9})_6]^{6+}$ and $[\text{Pd}_4(\mathbf{5.9})_8]^{8+}$ in DMSO- d_6 (600 MHz, 298 K). a) Equilibrated mixture of $[\text{Pd}_3(\mathbf{5.9})_6]^{6+}$ and $[\text{Pd}_4(\mathbf{5.9})_8]^{8+}$; b) after 20 minutes irradiation with a 567 nm LED; c) after 50 minutes irradiation with a 567 nm LED; d) after no

irradiation for 30 min; e) kept in the dark for 24 h and f) kept in the dark for 8 days. Signals associated with a *Z*-**5.9** containing species are marked *.

Equilibration of the irradiated sample in the dark at room temperature led to the reformation of sharp signals in the NMR spectra, however a new mixture of products was formed. This included the $[\text{Pd}_3(\mathbf{5.9})_6]^{6+}$ and $[\text{Pd}_4(\mathbf{5.9})_8]^{8+}$ assemblies, however new signals were present at similar chemical shifts to the previous assemblies. These are ascribed to the formation of *Z*-**5.9** containing structures, the constitutions of which are unknown. The similarity in chemical shift is consistent with only minor structural variation e.g. structures containing one *Z*-**5.9** ligand. Continued equilibration over a week led to a mixture with similar composition to the original mixture but containing a small amount of new signals. Importantly, there was a decrease in the peaks assigned as *Z*-**5.9** containing species over the course of the week suggesting the ligands are isomerising to the thermally more stable *E*-**5.9**.

Irradiation of the sample containing a mixture of self-assembled species in DMSO-*d*₆ with 410 nm light led to rapid redistribution of the species in solution, generating a new mixture comprising 66% of the $[\text{Pd}_3(\mathbf{5.9})_6]^{6+}$ species (Figure 5.30). This was also observed by ¹⁹F NMR, with an increase in intensity for the signal corresponding to the symmetric assembly. No new peaks were observed in the ¹H or ¹⁹F NMR spectrum. Leaving the sample in the dark restored the original equilibrium of $[\text{Pd}_3(\mathbf{5.9})_6]^{6+}$ and $[\text{Pd}_4(\mathbf{5.9})_8]^{8+}$ self-assembled species, giving 36% of the $[\text{Pd}_3(\mathbf{5.9})_6]^{6+}$ distorted tetrahedron.

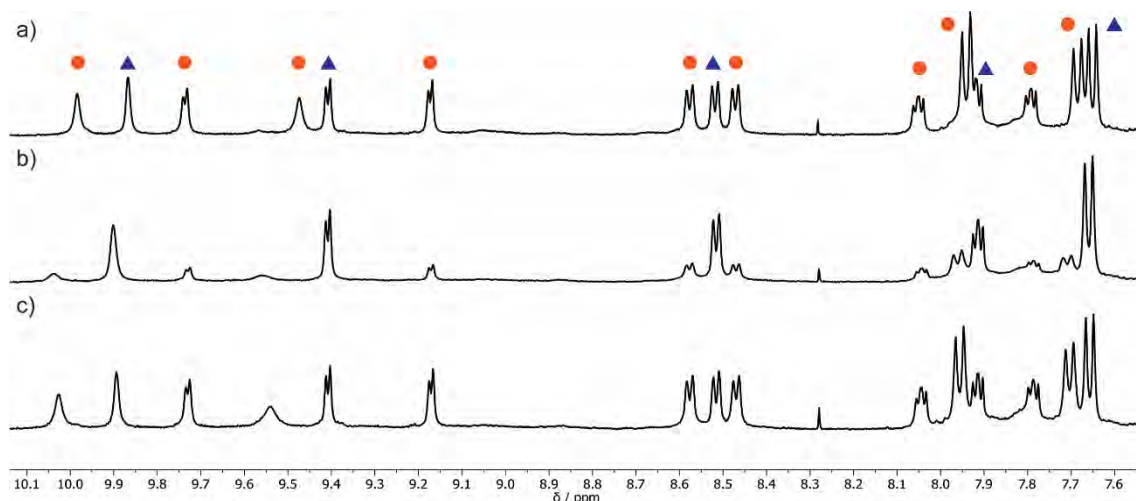


Figure 5.30 Perturbing the equilibrium of $[\text{Pd}_3(\mathbf{5.9})_6]^{6+}$ and $[\text{Pd}_4(\mathbf{5.9})_8]^{8+}$ in $\text{DMSO-}d_6$ (600 MHz, 298 K). a) Mixture of $[\text{Pd}_3(\mathbf{5.9})_6]^{6+}$ and $[\text{Pd}_4(\mathbf{5.9})_8]^{8+}$; b) after 30 minutes irradiation with a 410 nm LED and c) left in the dark at 293 K for 26 h.

The reaction kinetics gave some insight into the equilibration after irradiation (Figure 5.31 and Table 5.2). When compared to the rates observed upon initial addition of palladium to ligand **5.9** (Figure 5.26), the rate of consumption of the $[\text{Pd}_3(\mathbf{5.9})_6]^{6+}$ species after irradiation at 410 nm is slower ($t_{1/2} \approx 280$ minutes vs ≈ 100 minutes upon addition of palladium). Conversely, the rate of formation of the $[\text{Pd}_4(\mathbf{5.9})_8]^{8+}$ species is faster ($t_{1/2} \approx 165$ minutes vs. ≈ 250 minutes upon addition of palladium). In both cases the major species is the $[\text{Pd}_3(\mathbf{5.9})_6]^{6+}$, however fragments of the $[\text{Pd}_4(\mathbf{5.9})_8]^{8+}$ cage may remain after irradiation which are not observed in the ^1H NMR spectrum due to their low symmetry. This presence of these “pre-formed” components may template the reformation of the $[\text{Pd}_4(\mathbf{5.9})_8]^{8+}$ species, causing the enhancement in the rate this species is formed.

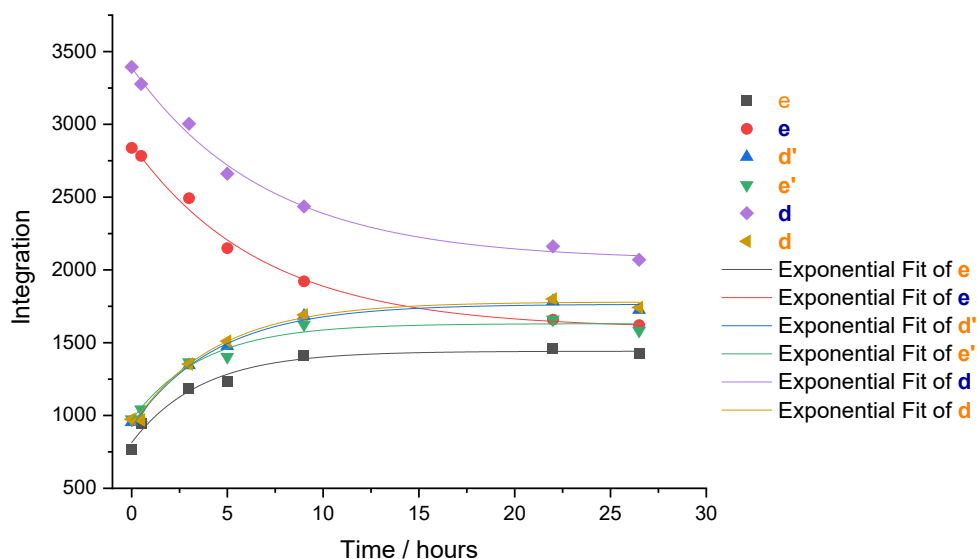


Figure 5.31 Monitoring the thermal equilibration in the dark for a mixture of $[\text{Pd}_3(\mathbf{5.9})_6]^{6+}$ and $[\text{Pd}_4(\mathbf{5.9})_8]^{8+}$ from ^1H NMR data (DMSO- d_6 , 600 MHz, 298 K). Sample labels as Figure 5.20.

Table 5.2 Tabulated $t_{1/2}$ values for the equilibration of $[\text{Pd}_3(\mathbf{5.9})_6]^{6+}$ and $[\text{Pd}_4(\mathbf{5.9})_8]^{8+}$ after 410 nm LED irradiation. $t_{1/2}$ values were calculated by fitting the integration data in Figure 5.31 to a mono-exponential function.

Proton signal	Calculated $t_{1/2}$ / minutes
H^e	150
H^e	280
$\text{H}^{d'}$	180
$\text{H}^{e'}$	150
H^d	290
H^d	180

The photo-responsive behaviour was also observed by high resolution ESI-MS measurements (Figure 5.32). ESI-MS spectra were collected before and after irradiation with 410 nm LED light. Comparison of the same sample before and after irradiation with a 410 nm LED caused a change in relative isotope distribution, favouring the $[\text{Pd}_3\text{L}_6]^{6+}$ species, consistent with the NMR observations. This allowed me to confidently assign the favoured product after 410 nm light irradiation as the $[\text{Pd}_3(\mathbf{5.9})_6]^{6+}$ assembly, which is also consistent with the ^1H DOSY spectrum which shows the symmetric product has a smaller hydrodynamic radius.

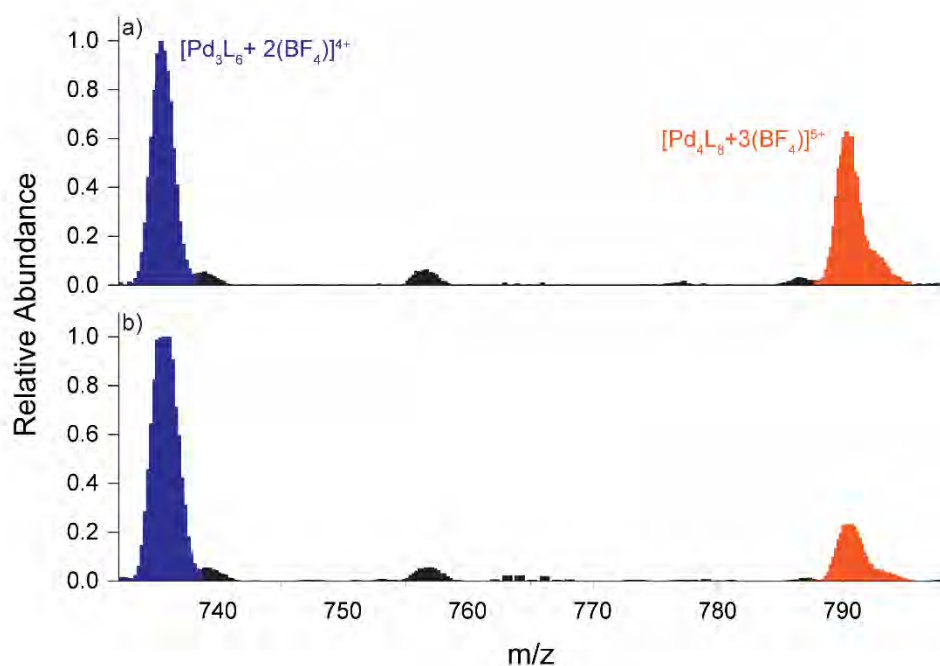


Figure 5.32 Perturbing the equilibrium of $[\text{Pd}_3(\mathbf{5.9})_6]^{6+}$ and $[\text{Pd}_4(\mathbf{5.9})_8]^{8+}$ in $\text{DMSO-}d_6$ monitored by HR ESI-MS. a) Isotope patterns of a mixture of $[\text{Pd}_3(\mathbf{5.9})_6 + 2(\text{BF}_4)]^{4+}$ and $[\text{Pd}_4(\mathbf{5.9})_8 + 3(\text{BF}_4)]^{5+}$; b) after 5 minutes irradiation with a 410 nm LED.

The UV-vis spectra of the self-assembled mixture and the response to isomerisation suggests a possible explanation for the behaviour. The UV-vis spectrum of the self-assembled mixture in the dark poorly resembles the spectrum of either *E*-**5.9** or the calculated spectrum of *Z*-**5.9**, however as shown in Figure 5.33a is well modelled by a linear combination of those spectra. Upon irradiation with 410 nm light, the spectrum is well modelled as 90% *E*-**5.9**, suggesting palladium co-ordination has little effect of the spectrum of the ligand. After irradiation with 530 nm light, the spectrum is well modelled as 80% *Z*-**5.9**, similar to the PSS reached by the free ligand.

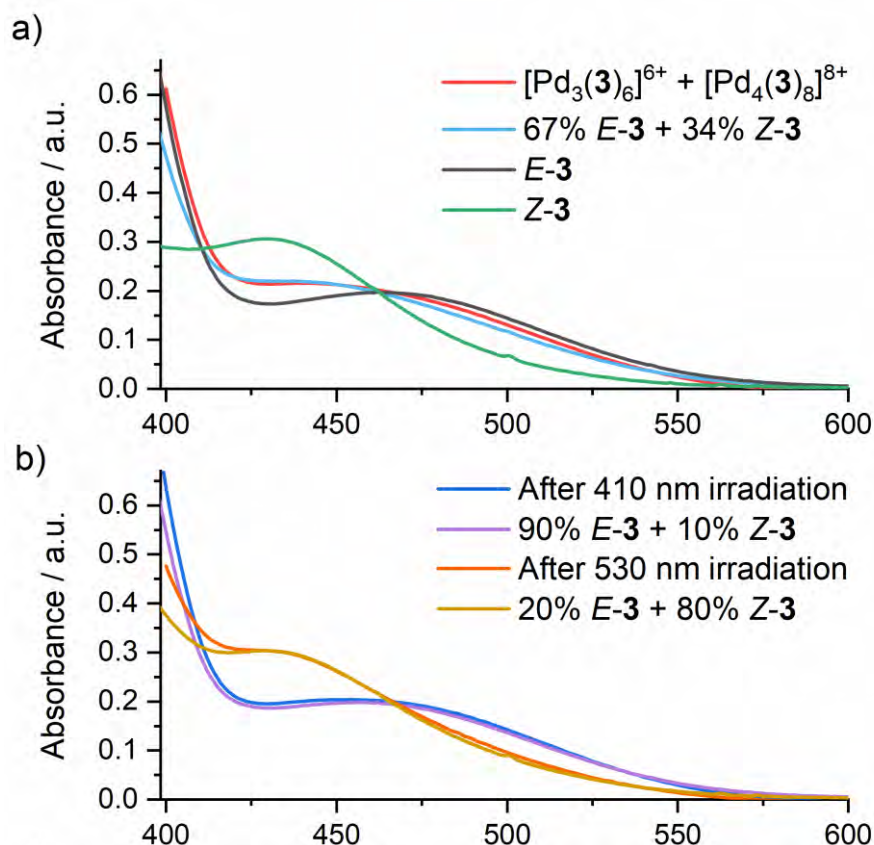


Figure 5.33 Effect of irradiation on the UV-vis spectrum of a mixture of $[\text{Pd}_3(\mathbf{5.9})_6]^{6+}$ and $[\text{Pd}_4(\mathbf{5.9})_8]^{8+}$ in DMSO. a) Comparison of a UV-vis spectrum of a thermally equilibrated mixture with a linear combination of *E*- and *Z*-**5.9**; b) Comparison of the UV-vis spectra after irradiation with 410 or 530 nm light with linear combinations of the *E*-**5.9** and *Z*-**5.9** spectra.

Overall, the above observations suggest that the less symmetric $[\text{Pd}_4(\mathbf{5.9})_8]^{8+}$ species contains a mixture of *E* and *Z* isomers. The proposed structure which preserves the overall symmetry is shown in Figure 5.24. Two pairs of palladium centres are bridged by two *E*-**5.9** ligands and four *Z*-**5.9** ligands complete the distorted tetrahedron structure. Irradiation with 410 nm light causes *Z* to *E* isomerisation, favouring the $[\text{Pd}_3(\mathbf{5.9})_6]^{6+}$ species which is comprised of entirely *E*-**5.9**. The unprecedented *E* to *Z* isomerisation in the dark is surprising, however entirely consistent with the data presented above regarding the isomerisation of the ligand and the self-assembled structures.

There are reports in the literature of solvent or anion induced constitutional change, however to our knowledge this is the first example of reversible constitutional change triggered by visible light. In addition, the previous examples of constitutional change have relied on geometric change induced by isomerisation to drive the structural change, i.e. by incorporating the metastable isomer into the new transient structure. In this case the metastable isomer is incorporated into both stable structures, via a currently

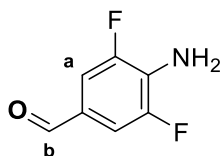
unknown isomerisation mechanism. In both the self-assembled species discussed here the *E*-isomer of **5.9** is incorporated, showing that a stimuli responsive nature can be incorporated into larger structures, and the designed geometry of the ligand can be retained.

5.18 Conclusion

This chapter has discussed the inclusion of visible light switchable *o*-fluoroazobenzenes into larger self-assembled species. A small variety of derivatives were prepared, and three examples of self-assembled structure were formed. A 3-pyridyl substituted azobenzene was prepared which, upon combination with palladium, led to an equilibrium between a double-walled triangle $[\text{Pd}_3\text{L}_6]^{6+}$ species and a distorted tetrahedron $[\text{Pd}_4\text{L}_8]^{8+}$ species. This equilibrium could be perturbed thermally, or through visible light irradiation, and the kinetics of formation and equilibration were studied. Overall this work represents the first example of reversible constitutional change using visible light for metal-based self-assembly. Further work will investigate the guest-binding properties of the systems, the potential for light-stimulated release of guests and potential methodologies to exploit this out-of-equilibrium behaviour.

5.19 Experimental

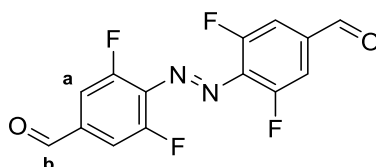
5.19.1 Synthesis of 4-amino-3,5-difluorobenzaldehyde (5.1)



Synthesised by a modified literature procedure.¹⁶⁷ To a stirred solution of 4-cyano-2,6-difluoroaniline (1.0 g, 6.5 mmol) in toluene (9 mL) at 0 °C under N₂ was added dropwise DIBAL-H (1 M in hexanes, 6.5 mL) resulting in the formation of a yellow solution. The mixture was warmed to RT and stirred for 2 h. The mixture was returned to 0 °C and a second equivalent of DIBAL-H (1 M in hexanes, 6.5 mL) was added. The solution was stirred for 14 h, forming an orange gel. This was slowly added to aq. citric acid (10%, 40 mL) forming a yellow precipitate. The precipitate was redissolved in EtOAc (30 mL) and washed with saturated aq. potassium sodium tartrate (25 mL), H₂O

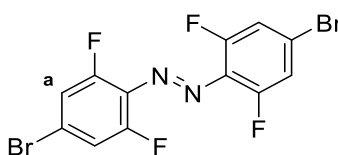
(2 x 25 mL), brine (2 x 25 mL) and dried over MgSO₄. The solvent was removed under reduced pressure to give **5.1** as an off-white solid (957 mg, 94%). ¹H NMR (400 MHz, CDCl₃) δ 9.73 (t, *J* = 1.9 Hz, 1H, H^b), 7.45 – 7.30 (m, 2H, H^a), 4.33 (s, 2H, -NH₂). ¹⁹F NMR (376.50 MHz, CDCl₃) δ -132.17.

5.19.2 Synthesis of 4,4'-(diazene-1,2-diyl)bis(3,5-difluorobenzaldehyde) (5.2)



To a mixture of **5.1** (250 mg, 1.60 mmol) and NaI (477 mg, 3.18 mmol) in Et₂O (10 mL) under N₂ was added ^tBuOCl (346 mg, 3.18 mmol) dropwise leading to the immediate formation of a red solution. The solution was stirred at RT for 2 h and then quenched with aq. Na₂S₂O₃ (1 M, 25 mL). The aqueous layer was extracted with EtOAc (3 x 25 mL), then the combined organic extracts were washed with brine (30 mL) and dried over MgSO₄. The crude product was purified by column chromatography (SiO₂, DCM) to give **5.2** as a red solid (40 mg, 16 %). ¹H NMR (500 MHz, CDCl₃) δ 10.00 (t, *J* = 1.7 Hz, 2H, H^b), 7.62 (d, *J* = 8.5 Hz, 4H, H^a). ¹⁹F NMR (376.50 MHz, CDCl₃) δ -117.8. UV-Vis (CHCl₃): λ_{max}/nm 473

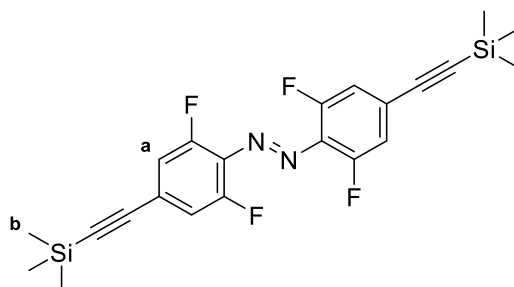
5.19.3 Synthesis of 1,2-bis(4-bromo-2,6-difluorophenyl)diazene (5.3)



The title compound was synthesised by a modified literature procedure.^{24b} 4-bromo-2,6-difluoroaniline (7.12 g, 34.2 mmol) dissolved in DCM (100 mL) was added to Oxone (42.3 g, 68.8 mmol) dissolved in H₂O (400 mL) and stirred vigorously for 16 h, over which time the organic layer turned dark green. The layers were separated and the organic layer washed with aq. HCl (1 M, 100 mL), saturated aq. NaHCO₃ (2 x 100 mL), H₂O (100 mL), brine (100 mL) and dried over MgSO₄. The solvent was removed under reduced pressure to give a greenish solid. This was re-dissolved in toluene (60 mL) and 4-bromo-2,6-difluoroaniline (7.12 g, 34.2 mmol) added. A mixture of acetic acid (60 mL)

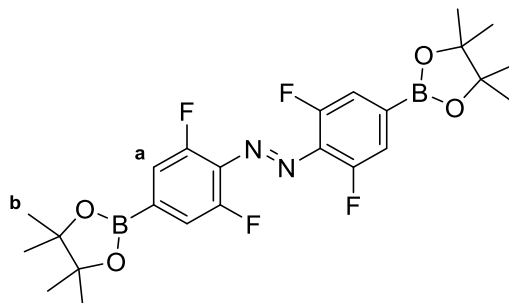
and trifluoroacetic acid (10 mL) was added and the mixture stirred for 3 days, giving a deep red solution, The solvent was removed under reduced pressure and the crude solid purified by recrystallisation from EtOAc:hexanes to give **5.3** as red needles (9.26 g, 65%). ^1H NMR (400 MHz, CDCl_3) δ 7.24 (m, 4H, H^a). ^{19}F NMR (376.5 MHz, CDCl_3) δ -118.6. Spectral data was identical to that previously reported.^{24a}

5.19.4 Synthesis of 1,2-bis(2,6-difluoro-4-((trimethylsilyl)ethynyl)phenyl)diazene (**5.4**)



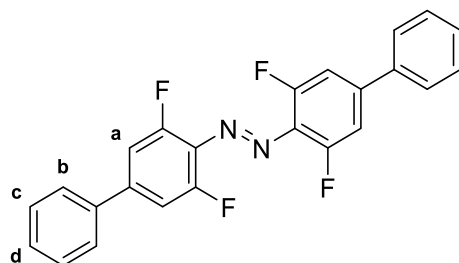
Compound **5.3** (200 mg, 0.49 mmol) was dissolved in a mixture of toluene (8 mL) and TEA (2 mL) and degassed with N_2 for 20 minutes. Trimethylsilylacetylene (483 mg, 700 μL , 4.90 mmol) was added and the solution further degassed for 5 minutes. Finally, CuI (14 mg, 0.07 mmol) and $\text{Pd}(\text{PPh}_3)_2\text{Cl}_2$ (34 mg, 0.049 mmol) were added and the resulting suspension heated at 60 $^\circ\text{C}$ for 24 h. The mixture was filtered through celite and extracted with diethyl ether (2 x 50 mL). The organic layer was washed with H_2O (2 x 50 mL), brine (2 x 50 mL) and dried over MgSO_4 . The solution was concentrated to approximately 1 mL under reduced pressure and the remaining solvent removed under a stream of N_2 . The crude product was purified by column chromatography (SiO_2 , hexanes to hexanes/EtOAc (95:5)) to give **5.4** as a red solid (206 mg, 76 %). Single crystals suitable for X-ray diffraction were obtained by slow evaporation of a solution of **5.4** in DCM. ^1H NMR (600 MHz, CDCl_3) δ 7.14 (d, $J = 9.3$ Hz, 4H, H^a), 0.27 (s, 18H, H^b) ^{19}F NMR (564.60 MHz, CDCl_3) δ -120.4.

5.19.5 Synthesis of 1,2-bis(2,6-difluoro-4-(4,4,5,5-tetramethyl-1,3,2-dioxaborolan-2-yl)phenyl)diazene (5.5)



The title compound was synthesised by a modified literature procedure.¹⁵² Compound **5.3** (500 mg, 1.21 mmol), bis(pinacolato)diboron (678 mg, 2.67 mmol) and potassium acetate (724 mg, 7.40 mmol) were combined in toluene (8 mL) and degassed with Ar for 30 minutes. Pd(dppf)Cl₂ (35 mg, 0.05 mmol) was added and the red suspension further degassed for 5 minutes. The mixture was heated in a microwave reactor at 150 °C for 15 minutes. EtOAc (50 mL) was added and the suspension filtered through Celite to remove reaction insolubles. The organic layer was washed with water (75 mL), brine (75 mL) and dried over MgSO₄. Solvent was removed under reduced pressure to give a red solid. The residue was triturated with cold MeCN to give **5.5** as a deep red solid (385 mg, 63%). ¹H NMR (400 MHz, CDCl₃) δ 7.46 (d, *J* = 9.0 Hz, 4H, H^a), 1.36 (s, 24H, H^b). ¹⁹F NMR (376.5 MHz, CDCl₃) δ -122.3. Spectral data was identical to that previously reported.¹⁵²

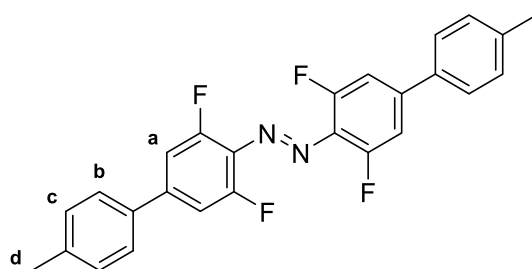
5.19.6 Synthesis of 1,2-bis(3,5-difluoro-[1,1'-biphenyl]-4-yl)diazene (5.6)



5.5 (100 mg, 0.2 mmol), bromobenzene (63 mg, 72 μL) and K₂CO₃ (111 mg, 0.8 mmol) were combined in dioxane and subject to three freeze-pump-thaw cycles. Pd(dppf)Cl₂ (10 mg, 0.012 mmol) was then added and the red suspension heated at 80 °C for 22 h. The suspension was extracted with DCM (25 mL) and the organic layer washed with H₂O (2 x 30 mL), brine (30 mL) and dried over MgSO₄. The crude product was

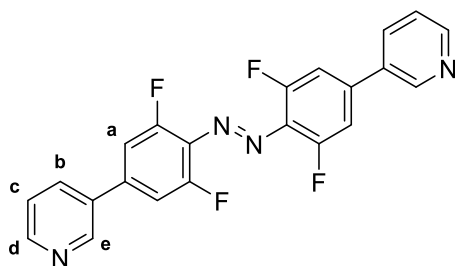
purified by column chromatography (SiO₂, hexanes/EtOAc (9:1)) to give **5.6** as an orange-green solid (60 mg, 75 %). ¹H NMR (400 MHz, CDCl₃) δ 7.66 – 7.60 (m, 4H, H^b), 7.54 – 7.40 (m, 6H, H^{c+d}), 7.35 – 7.29 (m, 4H, H^a). ¹⁹F NMR (376.5 MHz, CDCl₃) δ -120.0.

5.19.7 Synthesis of 1,2-bis(3,5-difluoro-4'-methyl-[1,1'-biphenyl]-4-yl)diazene (5.7)



Synthesised as for **5.6** but using 4-bromotoluene (68 mg, 0.4 mmol). Isolated as an orange solid (79 mg, 90 %). ¹H NMR (400 MHz, CDCl₃) δ 7.53 (d, *J* = 8.1 Hz, 4H, H^b), 7.33-7.27 (m, 8H, H^c + H^a), 2.42 (s, 6H, H^d). ¹⁹F NMR (376.50 MHz, CDCl₃) δ -120.16.

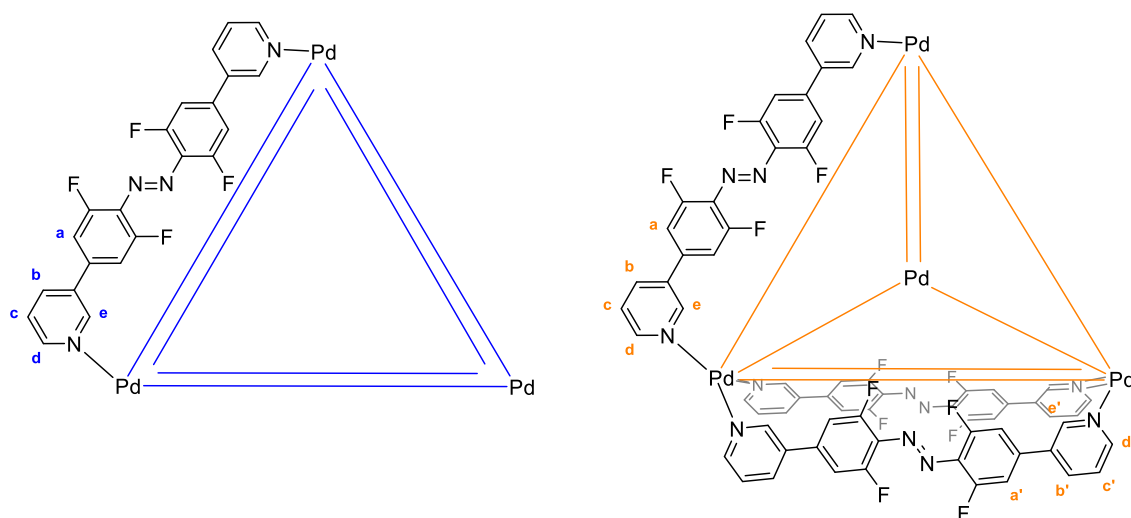
5.19.8 Synthesis of 1,2-bis(2,6-difluoro-4-(pyridin-3-yl)phenyl)diazene (5.9)



5.5 (150 mg, 0.30 mmol) and 3-bromopyridine (281 mg, 171 μL, 1.78 mmol) were combined in dioxane (7 mL) in a microwave tube. K₂CO₃ (82 mg, 0.60 mmol) dissolved in H₂O (1 mL) was added, and the suspension was degassed with Ar for 20 minutes. Pd(dppf)Cl₂ (13 mg, 0.018 mmol) was added and the suspension was further degassed for 5 minutes. The mixture was heated in a microwave reactor at 130 °C for 5 minutes giving a deep red solution. The solution was filtered through celite and extracted with DCM (40 mL). The organic layer was washed with H₂O (2 x 50 mL), brine (50 mL) and dried over MgSO₄. The solvent was removed under reduced pressure and the crude product purified

by column chromatography (SiO₂, EtOAc/TEA (97:3)) to give **5.9** as a red solid (18 mg, 15%). ¹H NMR (600 MHz, DMSO-*d*₆) δ 9.11 (s, 1H, H^c), 8.68 (d, *J* = 4.9 Hz, 1H, H^d), 8.33 – 8.27 (m, 1H, H^b), 7.90 (d, *J* = 10.9 Hz, 2H, H^a), 7.57 (dd, *J* = 7.9, 4.9 Hz, 1H, H^c). ¹⁹F NMR (564.60 MHz, DMSO-*d*₆) δ -120.1 δ HR-ESI-MS *m/z* 409.1020 [M+H]⁺ requires 409.1070. UV-Vis (DMSO): λ_{max}/nm 459.

5.19.9 Synthesis of [Pd₃(**5.9**)₆](BF₄)₆ and [Pd₄(**5.9**)₈](BF₄)₈



To **5.9** (6.2 mg, 15 μmol) dissolved in DMSO-*d*₆ (500 μL) in an NMR tube was added [Pd(CH₃CN)₄](BF₄)₂ (3.4 mg, 8 μmol) dissolved in DMSO-*d*₆ (25 μL) leading to an immediate colour change to deep red. The sample was equilibrated in the dark at room temperature and monitored by ¹H and ¹⁹F NMR over 3 days. ¹H NMR (600 MHz, DMSO, 298 K) δ 9.99 (s, 8H, H^{tet,e}), 9.88 (s, 12H, H^{tri,e}), 9.76 (d, *J* = 5.7 Hz, 8H, H^{tet,d'}), 9.46 (s, 8H, H^{tet,e'}), 9.42 (d, *J* = 5.8 Hz, 12H, H^{tri,d}), 9.18 (d, *J* = 5.6 Hz, 8H, H^{tet,d}), 8.60 (d, *J* = 8.3 Hz, 8H, H^{tet,b'}), 8.54 (d, *J* = 8.1 Hz, 12H, H^{tri,b}), 8.49 (d, *J* = 8.1 Hz, 8H, H^{tet,b}), 8.07 (dd, *J* = 8.2, 5.6 Hz, H^{tet,c'}), 7.98 – 7.91 (m, 28H, H^{tet,a'+tri,c}), 7.81 (dd, *J* = 8.1, 5.7 Hz, 12H, H^{tri,c}), 7.72-7.64 (m, 40H, H^{tet,a+tri,a}). ¹⁹F NMR (564.6 MHz, DMSO-*d*₆) δ -118.7 (F^{tri}), -118.9 (F^{tet}), -119.4 (F^{tet'}), -148.1 (BF₄). HR-ESI-MS *m/z* 1558.1789 [Pd₃(**5.9**)₆ + 4BF₄]²⁺ requires 1558.1709, 1375.4916 [Pd₄(**5.9**)₈ + 5BF₄]³⁺ requires 1375.4845, 1010.1201 [Pd₃(**5.9**)₆ + 3BF₄]³⁺ requires 1009.77842 and [Pd₄(**5.9**)₈ + 4BF₄]⁴⁺ requires 1009.86176, 790.4952 [Pd₄(**5.9**)₈ + 3BF₄]⁵⁺ requires 790.4881, 735.5887 [Pd₃(**5.9**)₆ + 2BF₄]⁴⁺ requires 735.58219, 644.4114 [Pd₄(**5.9**)₈ + 2BF₄]⁶⁺ requires 644.2390, 571.2690 [Pd₃(**5.9**)₆ + BF₄]⁵⁺ requires 571.26445, 539.7804 [Pd₄(**5.9**)₈ + BF₄]⁷⁺ requires 539.7753.

5.20 X-Ray crystallography

	5.4	5.8
Empirical formula	C _{16.5} H _{16.5} F ₃ N _{1.5} Si _{1.5}	C ₁₉ H ₁₁ F ₄ N ₂
Formula weight	334.95	343.3
Temperature/K	150	100(2)
Crystal system	monoclinic	triclinic
Space group	P2 ₁ /c	P-1
a/Å	8.966(4)	7.4460(15)
b/Å	17.134(7)	11.303(2)
c/Å	23.045(10)	18.207(4)
α/°	90	94.38(3)
β/°	80.788(13)	96.07(3)
γ/°	90	101.85(3)
Volume/Å ³	3495(3)	1483.7(5)
Z	8	4
ρ _{calc} /cm ³	1.273	1.537
μ/mm ⁻¹	0.194	0.127
F(000)	1392	700
Crystal size/mm ³	0.5 × 0.2 × 0.1	0.1 × 0.05 × 0.04
Radiation	MoKα (λ = 0.71073)	Synchrotron (λ = 0.71073)
2θ range for data collection/°	2.976 to 41.626	3.7 to 49.426
Index ranges	-8 ≤ h ≤ 8, -17 ≤ k ≤ 17, -23 ≤ l ≤ 23	-8 ≤ h ≤ 8, -12 ≤ k ≤ 12, -21 ≤ l ≤ 21
Reflections collected	46470	17061
Independent reflections	3644 [R _{int} = 0.2925, R _{sigma} = 0.1319]	4497 [R _{int} = 0.0492, R _{sigma} = 0.0436]
Data/restraints/parameters	3644/6/415	4497/0/453
Goodness-of-fit on F ²	1.007	1.025
Final R indexes [I ≥ 2σ (I)]	R ₁ = 0.0694, wR ₂ = 0.1629	R ₁ = 0.0559, wR ₂ = 0.1471
Final R indexes [all data]	R ₁ = 0.1651, wR ₂ = 0.2167	R ₁ = 0.0828, wR ₂ = 0.1680
Largest diff. peak/hole / e Å ⁻³	0.48/-0.40	0.24/-0.30

	5.10
Empirical formula	C ₁₇ H ₈ BrF ₄ N ₃
Formula weight	410.17
Temperature/K	150
Crystal system	triclinic
Space group	P-1
a/Å	7.3829(11)
b/Å	8.2163(12)
c/Å	13.213(2)
α/°	93.791(5)
β/°	105.633(5)
γ/°	99.683(5)
Volume/Å ³	755.6(2)
Z	2
ρ _{calc} /cm ³	1.803
μ/mm ⁻¹	2.77
F(000)	404
Crystal size/mm ³	0.254 × 0.045 × 0.013
Radiation	MoKα (λ = 0.71073)
2θ range for data collection/°	5.064 to 55.084
Index ranges	-9 ≤ h ≤ 9, -10 ≤ k ≤ 10, -17 ≤ l ≤ 16
Reflections collected	8889
Independent reflections	3431 [R _{int} = 0.0954, R _{sigma} = 0.1220]
Data/restraints/parameters	3431/0/258
Goodness-of-fit on F ²	1.023
Final R indexes [I ≥ 2σ (I)]	R ₁ = 0.0622, wR ₂ = 0.1209
Final R indexes [all data]	R ₁ = 0.1253, wR ₂ = 0.1495
Largest diff. peak/hole / e Å ⁻³	0.62/-0.79

5.20.1 Structure of 5.4

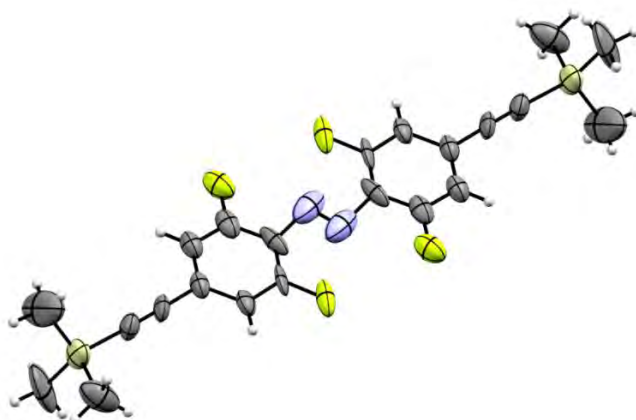


Figure 5.33 An ORTEP representation of the X-ray crystal structure of **5.4**. Thermal ellipsoids are drawn at 50% probability.

Orange needles of **5.4** were grown by slow evaporation of a solution of the compound in dichloromethane. The crystal of **5.4** with dimensions of 0.14 x 0.10 x 0.05 mm, selected under the polarizing microscope (Leica M165Z), was picked up on a MicroMount (MiTeGen, USA) consisting of a thin polymer tip with a wicking aperture. The X-ray diffraction measurements were carried out on a Bruker kappa-II CCD diffractometer at 150 K using I μ S Incoatec Microfocus Source with Mo-K α radiation ($\lambda = 0.710723$ Å). The single crystal, mounted on the goniometer using a cryo loop for intensity measurements, was coated with immersion oil type NVH and then quickly transferred to the cold nitrogen stream generated by an Oxford Cryostream 700 series. Symmetry related absorption corrections using the program SADABS¹⁶⁸ were applied and the data were corrected for Lorentz and polarisation effects using Bruker APEX3 software.¹⁶⁹ The structure was solved by program SHELXT¹³⁷ (with intrinsic phasing) and the full-matrix least-square refinements were carried out using SHELXL-2016¹³⁷ through Olex2¹¹⁴ suite of software. The non-hydrogen atoms were refined anisotropically.

5.20.2 Structure of 5.8

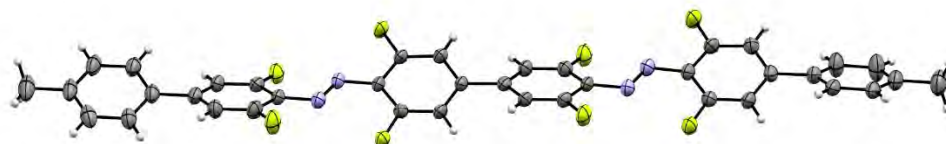


Figure 5.34 An ORTEP representation of the X-ray crystal structure of **5.8**. Thermal ellipsoids are drawn at 50% probability.

Orange needles of **5.8** were grown by slow evaporation of a solution of the compound in CDCl_3 . The crystal of **5.8** with dimensions 0.10 x 0.05 x 0.04 mm was coated in Paratone and transferred to the goniometer under a cold stream at 100 K. Diffraction measurements were carried out using Si<111> monochromated synchrotron X-ray radiation ($\lambda = 0.71073 \text{ \AA}$) on the MX1 Beamline at the Australian Synchrotron.¹³⁶ Data collection was carried out using Australian Synchrotron QEGUI software and unit cell refinement, data reduction and processing were carried out with XDS.¹¹¹ The structure was solved using dual space methods with SHELXT.¹³⁷ The least-squares refinement was carried out with SHELXL-2016¹³⁷ through the Olex2¹¹⁴ suite of software. The non-hydrogen atoms were refined anisotropically.

5.20.3 Structure of 5.10

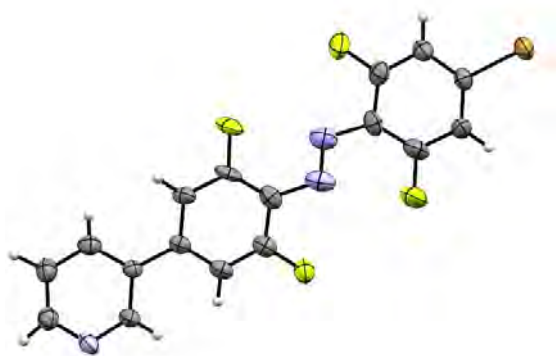


Figure 5.35 An ORTEP representation of the X-ray crystal structure of **5.10**. Thermal ellipsoids are drawn at 50% probability.

Orange-red needles of **5.10** were grown by slow evaporation of CDCl_3 . The crystal of **5.10** with dimensions $0.01 \times 0.05 \times 0.25$ mm was selected under the polarizing microscope (Leica M165Z). A MicroLoop (MiTeGen, USA) consisting of a thin polymer tip with a loop was used to pick up the single crystal, coated with NVH type immersion oil, which was then mounted on the goniometer using a cryo loop for intensity measurements and transferred to the cold nitrogen stream generated by an Oxford Cryostream 800 series. The X-ray diffraction measurements were carried out at 150 K on a Bruker D8 Quest Single Crystal diffractometer using Incoatec $\text{I}\mu\text{S}$ 3.0 Microfocus Source with Mo- $\text{K}\alpha$ radiation ($\lambda = 0.710723$ Å). Symmetry related absorption corrections using the program SADABS¹⁶⁸ were applied and the data were corrected for Lorentz and polarisation effects using Bruker APEX3 software.¹⁶⁹ The structure was solved with SHELXT¹³⁷ (intrinsic phasing) and the full-matrix least-square refinements were carried out using SHELXL-2014¹³⁷ through Olex2¹¹⁴ suite of software. The non-hydrogen atoms were refined anisotropically.

5.21 References

24. (a) Bléger, D.; Schwarz, J.; Brouwer, A. M.; Hecht, S., *J. Am. Chem. Soc.* **2012**, *134* (51), 20597-20600; (b) Knie, C.; Utecht, M.; Zhao, F.; Kulla, H.; Kovalenko, S.; Brouwer, A. M.; Saalfrank, P.; Hecht, S.; Bléger, D., *Chem.-Eur. J.* **2014**, *20* (50), 16492-16501; (c) Siewertsen, R.; Neumann, H.; Buchheim-Stehn, B.; Herges, R.; Naether, C.; Renth, F.; Temps, F., *J. Am. Chem. Soc.* **2009**, *131* (43), 15594-+; (d) Beharry, A. A.; Sadovski, O.; Woolley, G. A., *J. Am. Chem. Soc.* **2011**, *133* (49), 19684-19687; (e) Bléger, D.; Hecht, S., *Angew. Chem. Int. Ed.* **2015**, *54* (39), 11338-11349.
26. (a) Sadovski, O.; Beharry, A. A.; Zhang, F.; Woolley, G. A., *Angew. Chem. Int. Ed.* **2009**, *48* (8), 1484-1486; (b) Lentès, P.; Stadler, E.; Röhricht, F.; Brahm, A.; Gröbner, J.; Sönnichsen, F. D.; Gescheidt, G.; Herges, R., *J. Am. Chem. Soc.* **2019**, *141* (34), 13592-13600.
28. (a) Garcia-Amoros, J.; Nonell, S.; Velasco, D., *Chem. Commun.* **2011**, *47* (13), 4022-4024; (b) Garcia-Amorós, J.; Díaz-Lobo, M.; Nonell, S.; Velasco, D., *Angew. Chem. Int. Ed.* **2012**, *51* (51), 12820-12823; (c) García-Amorós, J.; Velasco, D., *Beilstein J. Org. Chem.* **2012**, *8*, 1003-1017; (d) Garcia-Amorós, J.; Maerz, B.; Reig, M.; Cuadrado, A.; Blancafort, L.; Samoylova, E.; Velasco, D., *Chem.-Eur. J.* **2019**, *25* (32), 7726-7732.
31. Hammerich, M.; Schütt, C.; Stähler, C.; Lentès, P.; Röhricht, F.; Höppner, R.; Herges, R., *J. Am. Chem. Soc.* **2016**, *138* (40), 13111-13114.
58. (a) Han, M.; Luo, Y.; Damaschke, B.; Gómez, L.; Ribas, X.; Jose, A.; Peretzki, P.; Seibt, M.; Clever, G. H., *Angew. Chem. Int. Ed.* **2016**, *55* (1), 445-449; (b) Sun, S.-S.; Anspach, J. A.; Lees, A. J., *Inorg. Chem.* **2002**, *41* (7), 1862-1869; (c) Yan, X.; Xu, J.-F.; Cook, T. R.; Huang, F.; Yang, Q.-Z.; Tung, C.-H.; Stang, P. J., *Proc. Natl Acad. Sci. U. S. A.* **2014**, *111* (24), 8717-8722.
65. (a) Caulder, D. L.; Brückner, C.; Powers, R. E.; König, S.; Parac, T. N.; Leary, J. A.; Raymond, K. N., *J. Am. Chem. Soc.* **2001**, *123* (37), 8923-8938; (b) Fleming, J. S.; Mann, K. L. V.; Carraz, C.-A.; Psillakis, E.; Jeffery, J. C.; McCleverty, J. A.; Ward, M. D., *Angew. Chem. Int. Ed.* **1998**, *37* (9), 1279-1281; (c) Mal, P.; Breiner, B.; Rissanen, K.; Nitschke, J. R., *Science* **2009**, *324* (5935), 1697-1699; (d) Neelakandan, P. P.; Jimenez, A.; Nitschke, J. R., *Chem. Sci.* **2014**, *5* (3), 908-915; (e) Kaphan, D. M.; Levin, M. D.; Bergman, R. G.; Raymond, K. N.; Toste, F. D., *Science* **2015**, *350* (6265), 1235-1238; (f) Caulder, D. L.; Powers, R. E.; Parac, T. N.; Raymond, K. N., *Angew. Chem., Int. Ed.* **1998**, *37* (13-14), 1840-1843.
68. (a) Paul, R. L.; Bell, Z. R.; Jeffery, J. C.; McCleverty, J. A.; Ward, M. D., *Proc. Natl Acad. Sci. U. S. A.* **2002**, *99* (8), 4883-4888; (b) Clever, G. H.; Tashiro, S.; Shionoya, M., *Angew. Chem. Int. Ed.* **2009**, *48* (38), 7010-7012; (c) Han, M.; Engelhard, D. M.; Clever, G. H., *Chem. Soc. Rev.* **2014**, *43* (6), 1848-1860; (d) Lewis, J. E. M.; Gavey, E. L.; Cameron, S. A.; Crowley, J. D., *Chem. Sci.* **2012**, *3* (3), 778-784; (e) Preston, D.; Barnsley, J. E.; Gordon, K. C.; Crowley, J. D., *J. Am. Chem. Soc.* **2016**, *138* (33), 10578-10585; (f) Yang, J.; Bhadbhade, M.; Donald, W. A.; Iranmanesh, H.; Moore, E. G.; Yan, H.; Beves, J. E., *Chem. Commun.* **2015**, *51* (21), 4465-4468.
83. (a) Preston, D.; Fox-Charles, A.; Lo, W. K. C.; Crowley, J. D., *Chem. Commun.* **2015**, *51* (43), 9042-9045; (b) Gan, Q.; Ronson, T. K.; Vosburg, D. A.; Thoburn, J. D.; Nitschke, J. R., *J. Am. Chem. Soc.* **2015**, *137* (5), 1770-1773; (c) Mal, P.; Schultz, D.; Beyeh, K.; Rissanen, K.; Nitschke, J. R., *Angew. Chem. Int. Ed.* **2008**,

- 47 (43), 8297-8301; (d) Zhang, D. W.; Ronson, T. K.; Guryel, S.; Thoburn, J. D.; Wales, D. J.; Nitschke, J. R., *J. Am. Chem. Soc.* **2019**, *141* (37), 14534-14538; (e) Jansze, S. M.; Cecot, G.; Severin, K., *Chem. Sci.* **2018**, *9* (18), 4253-4257; (f) Kim, T. Y.; Vasdev, R. A. S.; Preston, D.; Crowley, J. D., *Chem.-Eur. J.* **2018**, *24* (56), 14878-14890.
93. (a) Carrano, C. J.; Raymond, K. N., *J. Am. Chem. Soc.* **1978**, *100* (17), 5371-5374; (b) Kramer, R.; Lehn, J. M.; Marquis-Rigault, A., *Proc. Natl Acad. Sci. U. S. A.* **1993**, *90* (12), 5394-5398; (c) Hannon, M. J.; Painting, C. L.; Jackson, A.; Hamblin, J.; Errington, W., *Chem. Commun.* **1997**, 1807-1808; (d) Piguet, C.; Bernardinelli, G.; Hopfgartner, G., *Chem. Rev.* **1997**, *97* (6), 2005-2062; (e) Albrecht, M., *Chem. Rev.* **2001**, *101* (11), 3457-3498; (f) Hannon, M. J.; Childs, L. J., *Supramol. Chem.* **2004**, *16* (1), 7-22; (g) Archer, R. J.; Hawes, C. S.; Jameson, G. N. L.; McKee, V.; Moubaraki, B.; Chilton, N. F.; Murray, K. S.; Schmitt, W.; Kruger, P. E., *Dalton Trans.* **2011**, *40* (45), 12368-12373; (h) Kumar, S. V.; Lo, W. K. C.; Brooks, H. J. L.; Crowley, J. D., *Inorg. Chim. Acta* **2015**, *425*, 1-6; (i) Jana, B.; Cera, L.; Akhuli, B.; Naskar, S.; Schalley, C. A.; Ghosh, P., *Inorg. Chem.* **2017**, *56* (20), 12505-12513; (j) Chen, X.; Gerger, T. M.; Räuber, C.; Raabe, G.; Göb, C.; Oppel, I. M.; Albrecht, M., *Angew. Chem. Int. Ed.* **2018**, *57* (36), 11817-11820.
107. (a) Beves, J. E.; Chapman, B. E.; Kuchel, P. W.; Lindoy, L. F.; McMurtrie, J.; McPartlin, M.; Thordarson, P.; Wei, G., *Dalton Trans.* **2006**, *5*, 744-750; (b) Beves, J. E.; Constable, E. C.; Housecroft, C. E.; Neuburger, M.; Schaffner, S.; Shardlow, E. J., *Dalton Trans.* **2007**, 1593-1602; (c) Wang, C.; Hao, X.-Q.; Wang, M.; Guo, C.; Xu, B.; Tan, E. N.; Zhang, Y.-Y.; Yu, Y.; Li, Z.-Y.; Yang, H.-B.; Song, M.-P.; Li, X., *Chem. Sci.* **2014**, *5* (3), 1221-1226; (d) Avram, L.; Cohen, Y., *Chem. Soc. Rev.* **2015**, *44*, 586; (e) Shen, C.; Kennedy, A. D. W.; Donald, W. A.; Torres, A. M.; Price, W. S.; Beves, J. E., *Inorg. Chim. Acta* **2017**, *458*, 122-128; (f) Bloch, W. M.; Holstein, J. J.; Hiller, W.; Clever, G. H., *Angew. Chem. Int. Ed.* **2017**, *56* (28), 8285-8289; (g) Turunen, L.; Warzok, U.; Schalley, C. A.; Rissanen, K., *Chem* **2017**, *3* (5), 861-869; (h) Jiang, Z.; Li, Y.; Wang, M.; Liu, D.; Yuan, J.; Chen, M.; Wang, J.; Newkome, G. R.; Sun, W.; Li, X.; Wang, P., *Angew. Chem. Int. Ed.* **2017**, *56* (38), 11450-11455; (i) Song, B.; Zhang, Z.; Wang, K.; Hsu, C.-H.; Bolarinwa, O.; Wang, J.; Li, Y.; Yin, G.-Q.; Rivera, E.; Yang, H.-B.; Liu, C.; Xu, B.; Li, X., *Angew. Chem. Int. Ed.* **2017**, *56* (19), 5258-5262; (j) Chen, Z.; Sahli, B. J.; MacLachlan, M. J., *Inorg. Chem.* **2017**, *56* (9), 5383-5391; (k) Luis, E. T.; Iranmanesh, H.; Arachchige, K. S. A.; Donald, W. A.; Quach, G.; Moore, E. G.; Beves, J. E., *Inorg. Chem.* **2018**, *57* (14), 8476-8486; (l) Findlay, J. A.; McAdam, C. J.; Sutton, J. J.; Preston, D.; Gordon, K. C.; Crowley, J. D., *Inorg. Chem.* **2018**, *57* (7), 3602-3614.
111. Kabsch, W., *Acta Crystallograph. Sect. D* **2010**, *66* (2), 125-132.
114. Dolomanov, O. V.; Bourhis, L. J.; Gildea, R. J.; Howard, J. A. K.; Puschmann, H., *J. Appl. Crystallogr.* **2009**, *42* (2), 339-341.
122. Takeda, Y.; Okumura, S.; Minakata, S., *Angew. Chem. Int. Ed.* **2012**, *51* (31), 7804-7808.
123. (a) Noureldin, N. A.; Bellegarde, J. W., *Synthesis* **1999**, *1999* (06), 939-942; (b) Merino, E., *Chem. Soc. Rev.* **2011**, *40* (7), 3835.
127. Priewisch, B.; Rück-Braun, K., *J. Org. Chem.* **2005**, *70* (6), 2350-2352.
136. Cowieson, N. P.; Aragao, D.; Clift, M.; Ericsson, D. J.; Gee, C.; Harrop, S. J.; Mudie, N.; Panjkar, S.; Price, J. R.; Riboldi-Tunncliffe, A.; Williamson, R.; Caradoc-Davies, T., *J. Synchrotron Rad.* **2015**, *22* (1), 187-190.

137. Sheldrick, G., *Acta Crystallograph. Sect. A* **2015**, *71* (1), 3-8.
139. (a) Lehn, J., *Science* **1993**, *260* (5115), 1762-1763; (b) Hasenknopf, B.; Lehn, J.-M.; Boumediene, N.; Leize, E.; Van Dorsselaer, A., *Angew. Chem. Int. Ed.* **1998**, *37* (23), 3265-3268.
140. (a) Lehn, J.-M., *Chem.-Eur. J.* **1999**, *5* (9), 2455-2463; (b) Rowan, S. J.; Cantrill, S. J.; Cousins, G. R. L.; Sanders, J. K. M.; Stoddart, J. F., *Angew. Chem. Int. Ed.* **2002**, *41* (6), 898-952.
141. (a) Chi, X.; Cen, W.; Queenan, J. A.; Long, L.; Lynch, V. M.; Khashab, N. M.; Sessler, J. L., *J. Am. Chem. Soc.* **2019**, *141* (16), 6468-6472; (b) Reuter, R.; Wegner, H. A., *Chem. Commun.* **2011**, *47* (45), 12267-12276; (c) Haberhauer, G.; Kallweit, C.; Wölper, C.; Bläser, D., *Angew. Chem. Int. Ed.* **2013**, *52* (30), 7879-7882; (d) Haberhauer, G.; Kallweit, C., *Angew. Chem. Int. Ed.* **2010**, *49* (13), 2418-2421; (e) Mathews, M.; Tamaoki, N., *J. Am. Chem. Soc.* **2008**, *130* (34), 11409-11416; (f) Maciejewski, J.; Sobczuk, A.; Claveau, A.; Nicolai, A.; Petraglia, R.; Cervini, L.; Baudat, E.; Miéville, P.; Fazzi, D.; Corminboeuf, C.; Sforazzini, G., *Chem. Sci.* **2017**, *8* (1), 361-365; (g) Basheer, M. C.; Oka, Y.; Mathews, M.; Tamaoki, N., *Chem.-Eur. J.* **2010**, *16* (11), 3489-3496; (h) Kawamoto, M.; Aoki, T.; Wada, T., *Chem. Commun.* **2007**, *9*, 930-932; (i) Li, Z.; Liang, J.; Xue, W.; Liu, G.; Liu, S. H.; Yin, J., *Supramol. Chem.* **2014**, *26* (1), 54-65.
143. (a) Nieland, E.; Topornicki, T.; Kunde, T.; Schmidt, B. M., *Chem. Commun.* **2019**, *55* (60), 8768-8771; (b) Nieland, E.; Weingart, O.; Schmidt, B. M., *Beilstein J. Org. Chem.* **2019**, *15*, 2013-2019.
144. Ayme, J.-F.; Beves, J. E.; Leigh, D. A.; McBurney, R. T.; Rissanen, K.; Schultz, D., *Nat. Chem.* **2012**, *4* (1), 15-20.
145. Abdel-Magid, A. F.; Mehrman, S. J., *Org. Process Rev. Dev.* **2006**, *10* (5), 971-1031.
146. (a) Price, J. R.; Clegg, J. K.; Fenton, R. R.; Lindoy, L. F.; McMurtrie, J. C.; Meehan, G. V.; Parkin, A.; Perkins, D.; Turner, P., *Aust. J. Chem.* **2009**, *62* (9), 1014-1019; (b) Lindoy, L. F., *Quarterly Reviews, Chemical Society* **1971**, *25* (3), 379-391.
147. (a) Moreno, J.; Grubert, L.; Schwarz, J.; Bléger, D.; Hecht, S., *Chem.-Eur. J.* **2017**, *23* (56), 14090-14095; (b) Liu, Q.; Dong, H.; Li, Y.; Li, H.; Chen, D.; Wang, L.; Xu, Q.; Lu, J., *Chem.-Asian J.* **2016**, *11* (4), 512-519.
148. Opie, C. R.; Kumagai, N.; Shibasaki, M., *Angew. Chem.* **2017**, *129* (12), 3397-3401.
149. Avellaneda, A.; Valente, P.; Burgun, A.; Evans, J. D.; Markwell-Heys, A. W.; Rankine, D.; Nielsen, D. J.; Hill, M. R.; Sumbly, C. J.; Doonan, C. J., *Angew. Chem.* **2013**, *125* (13), 3834-3837.
150. Peeks, M. D.; Claridge, T. D. W.; Anderson, H. L., *Nature* **2017**, *541* (7636), 200-203.
151. Mallo, N. Visible light-responsive photoswitches. PhD Thesis, UNSW Sydney, Sydney, Australia, 2019.
152. Iamsaard, S.; Anger, E.; Abhoff, S. J.; Depauw, A.; Fletcher, S. P.; Katsonis, N., *Angew. Chem. Int. Ed.* **2016**, *55* (34), 9908-9912.
153. Adamo, C.; Amatore, C.; Ciofini, I.; Jutand, A.; Lakmini, H., *J. Am. Chem. Soc.* **2006**, *128* (21), 6829-6836.
154. (a) Pasco, S. T.; Baker, G. L., *Synth. Met.* **1997**, *84* (1), 275-276; (b) Deng, H.; Grunder, S.; Cordova, K. E.; Valente, C.; Furukawa, H.; Hmadeh, M.; Gándara,

- F.; Whalley, A. C.; Liu, Z.; Asahina, S.; Kazumori, H.; O’Keeffe, M.; Terasaki, O.; Stoddart, J. F.; Yaghi, O. M., *Science* **2012**, *336* (6084), 1018-1023.
155. Vlasov, V. M., *J. Fluorine Chem.* **1993**, *61* (3), 193-216.
156. Kennedy, A. D. W.; de Haas, N.; Iranmanesh, H.; Luis, E. T.; Shen, C.; Wang, P.; Price, J. R.; Donald, W. A.; Andréasson, J.; Huang, F.; Beves, J. E., *Chem.- Eur. J.* **2019**, *25* (22), 5708-5718.
157. Lewis, J. E. M.; Tarzia, A.; White, A. J. P.; Jelfs, K. E., *Chem. Sci.* **2020**, *11* (3), 677-683.
158. (a) Kai, S.; Tateishi, T.; Kojima, T.; Takahashi, S.; Hiraoka, S., *Inorg. Chem.* **2018**, *57* (21), 13083-13086; (b) Kumar Chand, D.; Fujita, M.; Biradha, K.; Sakamoto, S.; Yamaguchi, K., *Dalton Trans.* **2003**, *13*, 2750-2756; (c) Suzuki, K.; Kawano, M.; Fujita, M., *Angew. Chem. Int. Ed.* **2007**, *46* (16), 2819-2822; (d) Tateishi, T.; Zhu, W.; Foianesi-Takeshige, L. H.; Kojima, T.; Ogata, K.; Hiraoka, S., *Eur. J. Inorg. Chem.* **2018**, *2018* (10), 1192-1197.
159. (a) Freye, S.; Michel, R.; Stalke, D.; Pawliczek, M.; Frauendorf, H.; Clever, G. H., *J. Am. Chem. Soc.* **2013**, *135* (23), 8476-8479; (b) Frank, M.; Johnstone, M. D.; Clever, G. H., *Chem.- Eur. J.* **2016**, *22* (40), 14104-14125; (c) Fukuda, M.; Sekiya, R.; Kuroda, R., *Angew. Chem. Int. Ed.* **2008**, *47* (4), 706-710; (d) Löffler, S.; Lübben, J.; Krause, L.; Stalke, D.; Dittrich, B.; Clever, G. H., *J. Am. Chem. Soc.* **2015**, *137* (3), 1060-1063; (e) Freye, S.; Hey, J.; Torras-Galán, A.; Stalke, D.; Herbst-Irmer, R.; John, M.; Clever, G. H., *Angew. Chem. Int. Ed.* **2012**, *51* (9), 2191-2194; (f) Dieterich, J. M.; Clever, G. H.; Mata, R. A., *PCCP* **2012**, *14* (37), 12746-12749.
160. (a) Chand, D. K.; Biradha, K.; Kawano, M.; Sakamoto, S.; Yamaguchi, K.; Fujita, M., *Chem.- Asian J.* **2006**, *1* (1-2), 82-90; (b) Klein, C.; Gütz, C.; Bogner, M.; Topić, F.; Rissanen, K.; Lützen, A., *Angew. Chem. Int. Ed.* **2014**, *53* (14), 3739-3742.
161. Jansze, S. M.; Cecot, G.; Wise, M. D.; Zhurov, K. O.; Ronson, T. K.; Castilla, A. M.; Finelli, A.; Pattison, P.; Solari, E.; Scopelliti, R.; Zelinskii, G. E.; Vologzhanina, A. V.; Voloshin, Y. Z.; Nitschke, J. R.; Severin, K., *J. Am. Chem. Soc.* **2016**, *138* (6), 2046-2054.
162. (a) Baxter, P. N. W.; Lehn, J. M.; Baum, G.; Fenske, D., *Chem.- Eur. J.* **2000**, *6* (24), 4510-4517; (b) Piguet, C., *Chem. Commun.* **2010**, *46* (34), 6209-6231.
163. Fu, S.; Luo, Q.; Zang, M.; Tian, J.; Zhang, Z.; Zeng, M.; Ji, Y.; Xu, J.; Liu, J., *Mater. Chem. Front.* **2019**, *3* (6), 1238-1243.
164. Luis, E. T.; Iranmanesh, H.; Beves, J. E., *Polyhedron* **2019**, *160*, 1-9.
165. Yamashita, K.-i.; Sato, K.-i.; Kawano, M.; Fujita, M., *New J. Chem.* **2009**, *33* (2), 264-270.
166. Garcia-Amorós, J.; Massad, W. A.; Nonell, S.; Velasco, D., *Org. Lett.* **2010**, *12* (15), 3514-3517.
167. Moffat, D. C. F.; Pintat, S.; Davies, S. Preparation of amino(aroyle or heteroaroyle)pyridinones, particularly amino acid derivatives of pyridin-2-ones, as inhibitors of p38 MAP kinase useful for treating inflammatory and autoimmune diseases. WO2007129040, 2007.
168. Sheldrick, G. *SADABS*, University of Göttingen, Germany, 1996.
169. Bruker *APEX3*, Bruker AXS Inc.: Madison, Wisconsin, USA, 2016.

6 CONCLUSIONS AND FUTURE OUTLOOK

The work in this thesis has explored the intersection of photoactive units and self-assembly. The work presented encompasses multiple approaches and functionalities but is unified by the interaction between discrete species and light irradiation.

The “supramolecular protecting group” strategy developed in Chapter 2 explored the formation of a M_2L_3 helicate from a photoactive TPE unit. Diastereoselective reaction of the amino-functionalised TPE unit led to a self-assembled structure containing pendant amine units, rare for this system of pyridyl-imine templation. These were also compatible with derivatisation with acid chlorides, unusual for iron(II) self-assemblies. This work presents the possibility of using the helicate as a “super-amine”, for incorporation into even larger structures. Assembly of larger structures from the individual sub-components provides better control over the resulting assembly and gives a better understanding of the larger structure, based on the insight into these subunits. This structure could also allow access to unique topologies, if post-assembly modification was used to link either the ligand arms or to construct discrete macrocycles. The possibilities would also incorporate the AIE behaviour of TPE, potentially giving multi-stimuli responsive behaviour.

Chapters 4 and 5 presented novel photoswitches and in both cases discussion of the degree of switching was important. Where photoswitches are linked to a change in function, a large change in the distribution of isomers is required to generate a large observable change in properties. There is no universal methodology for calculating the degree of isomerisation and therefore consideration of the specific switch and its properties are required. To fully exploit photoswitches for applications, it is important to have methodologies and tools to quantify the behaviour of the discrete photoswitching units. These methods were discussed and employed in chapters 4 and 5.

The development of visible-light photoswitches, mostly guided by biological considerations, has been a major area of interest to the photoswitching community. Chapter 4 contributed to this growing class of compounds, exploiting benzazoles as the heteroaromatic unit.¹⁸ Exploration of symmetric azoheteroarene systems has been relatively limited, but it is nevertheless important to fully understand the design of new switches and in informing future development. The use of the heteroaromatic rings in azoheteroarenes as metal-binding ligands has only been partially probed, but conceptually this could provide another methodology for tuning the properties of photoswitches, building on the rich chemistry of inorganic systems.

Strategies to incorporate and derivatise *o*-fluoroazobenzenes for use in larger structures were discussed in Chapter 5. Although this discussion centres on one specific example of a photoswitch the methodology is applicable for generally incorporating photoswitches into larger architectures. A good understanding of the discrete ligand allows insightful interpretation upon self-assembly, which is complicated by the dynamic behaviour and numerous interactions between sub-components. Techniques honed and developed through investigation of static and well-defined self-assembly systems (see Chapter 2) can be applied to dynamic systems and aid in the analysis of “out-of-equilibrium” behaviour.

Recently, efforts have been made towards developing dynamic self-assembly, that is, self-assembly away from equilibrium.¹⁷⁰ An argument has been made that photoswitchable molecules are key to this, due to their ability to populate a metastable states, avoiding the issue of microscopic reversibility.^{55a} The development of a conceptual framework with which to analyse and view such dynamic systems is important. This requires collaboration between not only chemists, but mathematicians and physicists as well. The systems discussed in this work and related systems are of importance in providing a well-defined but non-trivial basis for discussion, which allows the rules and relationships to be probed thoroughly.

The phrase “molecular Lego” has never been more apt than when considering the molecular photoswitching and self-assembly fields, both individually and at their intersection. Both areas have a diverse array of functionalities, which can be tuned for the desired application. In photoswitching, we are beginning to move away from simple azobenzene and develop more complex molecules with increasingly tailored properties. Relatively simple photoswitching systems allow changes in molecular properties and the elucidation of the guiding principles which inform future development. Azoheteroarenes are underexplored compared to azobenzenes, and yet focused research efforts are showing that they are equal to, and for some applications better than, the parent systems.

Self-assembly allows the formation of some of the most elegant and complex systems in nature. In the supramolecular community, self-assembly is used as a tool to generate beautiful and functional structures. The workhorses of supramolecular chemistry are the non-covalent interactions we can access. Of these, metal-template self-assembly provides an excellent framework for developing and designing architectures. A handful of tools (such as the predictable geometry of pyridine and palladium(II) or iron(II)

pyridyl-imine templation) and insights (the importance of ligand bend angle and shape complementarity) allow not only formation of unique architectures, but rationalisation of the structures formed.

This thesis has shown two surprising examples of metal-template self-assembly, in Chapters 2 and 5. An *ad hoc* prediction of structure from the individual sub-components might have suggested a M_8L_6 cube for the TPE-imine ligand and perhaps an M_2L_4 architecture for the *o*-fluoroazobenzene pyridyl ligand. Yet, both examples led to properties that were solely due to their self-assembled nature. The design principles of metal-template self-assembly are yet to be fully elucidated, despite many excellent efforts. However, by careful inspection of the behaviour, novel functions have emerged.

Maybe there is still room for serendipity.

6.1 References

18. Crespi, S.; Simeth, N. A.; König, B., *Nat. Rev. Chem* **2019**, 3 (3), 133-146.
55. (a) Kathan, M.; Hecht, S., *Chem. Soc. Rev.* **2017**, 46 (18), 5536-5550; (b) Ragazzon, G.; Baroncini, M.; Silvi, S.; Venturi, M.; Credi, A., *Nat. Nanotechnol.* **2015**, 10 (1), 70-75.
170. (a) Grzybowski, B. A.; Fitzner, K.; Paczesny, J.; Granick, S., *Chem. Soc. Rev.* **2017**, 46 (18), 5647-5678; (b) Grzybowski, B. A.; Stone, H. A.; Whitesides, G. M., *Nature* **2000**, 405 (6790), 1033-1036.

7 APPENDIX- CHAPTER 2

7.1 General methods

NMR spectroscopy was performed using a Bruker Avance III 400 with a Prodigy CryoProbe, a Bruker Avance III 500, a Bruker Avance III 600 or a Bruker Avance III HD 600 with a TCI CryoProbe. The chemical shifts for the ^1H and $^{13}\text{C}\{^1\text{H}\}$ NMR spectra conducted in CDCl_3 and CD_3CN are referenced to residual solvent resonances, with the signal at 2.75 ppm used for DMF- d_7 . CDCl_3 was stored over K_2CO_3 prior to use to ensure the solution was not acidic. Coupling constants (J) are reported in hertz (Hz). Signals in the NMR spectra are reported as broad (br), singlet (s), doublets (d), triplets (t), quartets (q), quintets (qu), sextets (sx), septets (sept), or unclear multiplets (m). NMR spectra were processed with MestReNova 12.0.0 software. All NMR data are assigned unambiguously, except where specified.

High-resolution mass spectrometry experiments were performed on a hybrid linear quadrupole ion trap mass spectrometer (Thermo LTQ Orbitrap XL) equipped with an external electrospray ionisation (ESI) source. Low resolution ESI-MS measurements were performed using a Thermo LCQ Fleet Ion Trap mass spectrometer. UV-Visible absorption spectra were recorded on a Varian Cary 60 or Cary 50 spectrophotometer. Fluorescence measurements were performed using a Varian Cary Eclipse spectrophotometer. Dynamic Light Scattering measurements were performed on a Malvern Zetasizer Particle Sizer. Reagents and solvents were purchased from Sigma-Aldrich, Merck, Chem Supply, Combi-Blocks or Alfa Aesar, and were used without purification unless stated otherwise. $\text{Fe}(\text{NTf}_2)_2 \cdot 4\text{H}_2\text{O}$ was prepared according to the literature.¹

UV-Vis absorbance spectroscopy experiments were performed on an Agilent Cary 60 Bio UV-visible spectrophotometer equipped with a customized Cary Single Cell Peltier Accessory, maintaining the samples at 298 K. The cell holder was modified to allow for irradiation perpendicular to the direction of measurement. A Luxeon Rebel LED was mounted on a heat sink positioned 4 cm away from the cell and driven using a 1000 mA LuxDrive PowerPuck. The beam was focused on the cuvette using a Carclo 20.0 mm Fibre Coupling Lens. All samples were stirred to ensure homogeneity. A timer relay module (FRM01) was used to control the irradiation cycles.

Table 7.1 Specifications of the LEDs used in this work

LED Part Number (Descriptor)	Dominant Wavelength		
	Minimum	Maximum	Typical
LXML-PR02-A900 (Royal Blue)	440	460	448
LXML-PB01-0040 (Blue)	460	485	470
LXML-PE01-0070 (Cyan)	490	515	505
LXML-PM01-0100 (Green)	520	540	530
LXML-PX02-0000 (Lime)	566	569	567
LXM2-PL01-0000 (PC Amber)	588	592	591
LXM2-PD01-0050 (Red)	620	645	627
LXM3-PD01 (Deep Red)	650	670	655

7.2 Additional spectroscopic data for 2.1, 2.3 and $[\text{Fe}_2(\mathbf{2.2})_3](\text{PF}_6)_4$

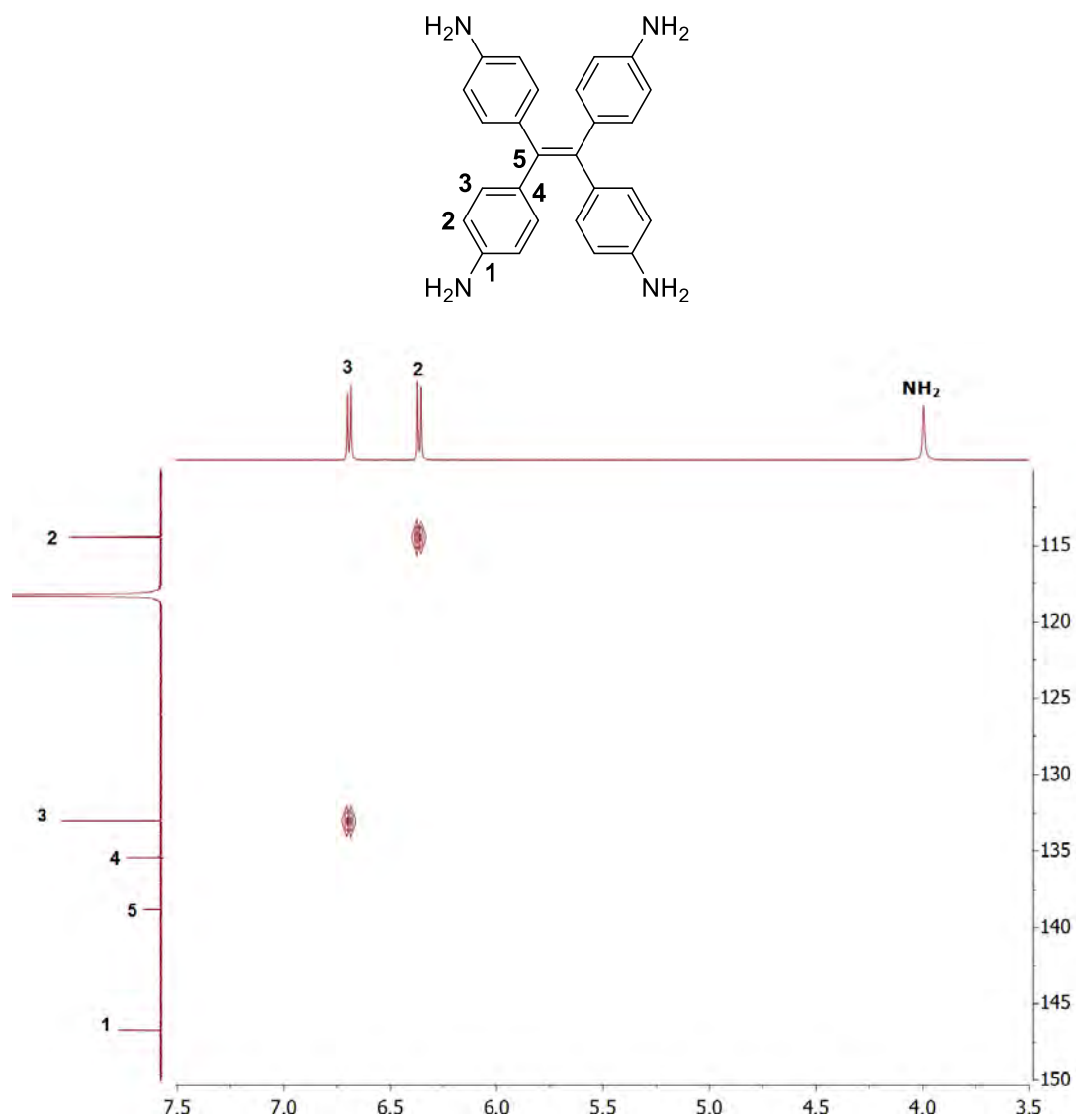


Figure 7.1 ^1H - ^{13}C HSQC spectrum (500 MHz, CD_3CN) of tetraamine **2.1**.

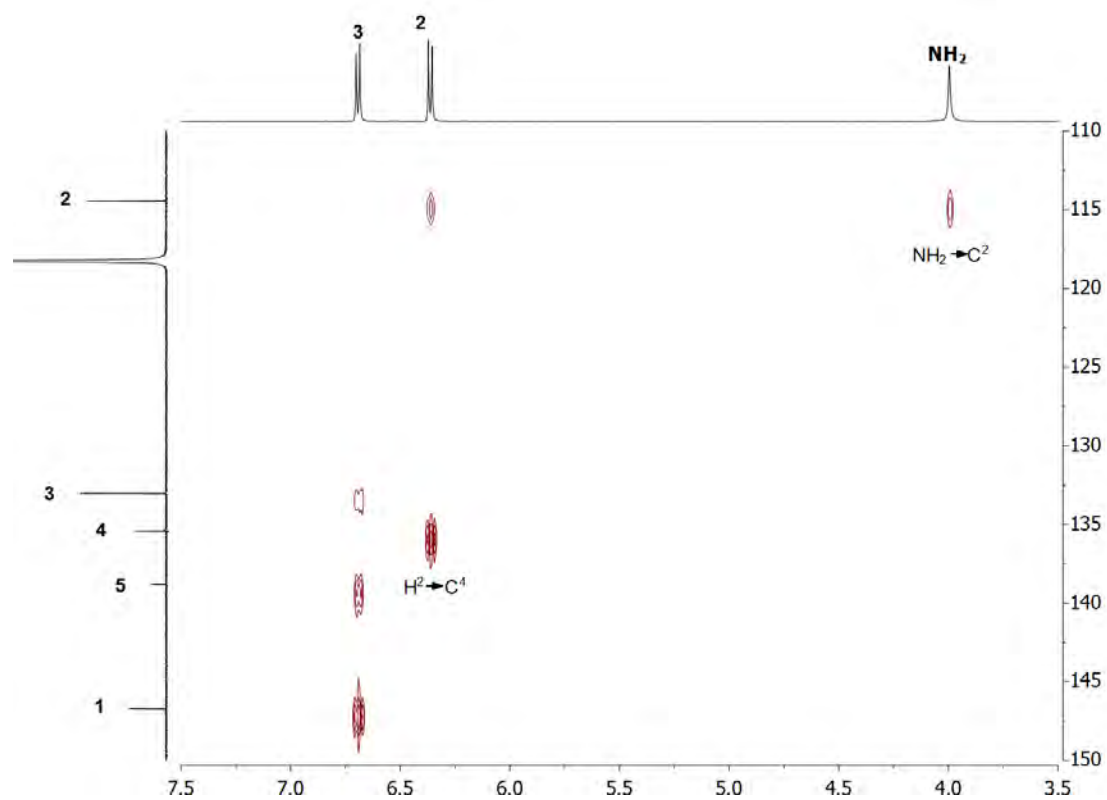


Figure 7.2 ^1H - ^{13}C HMBC spectrum (500 MHz, CD_3CN) of tetraamine **2.1** showing correlations between H^{NH} and C^2 , and H^2 and C^4 .

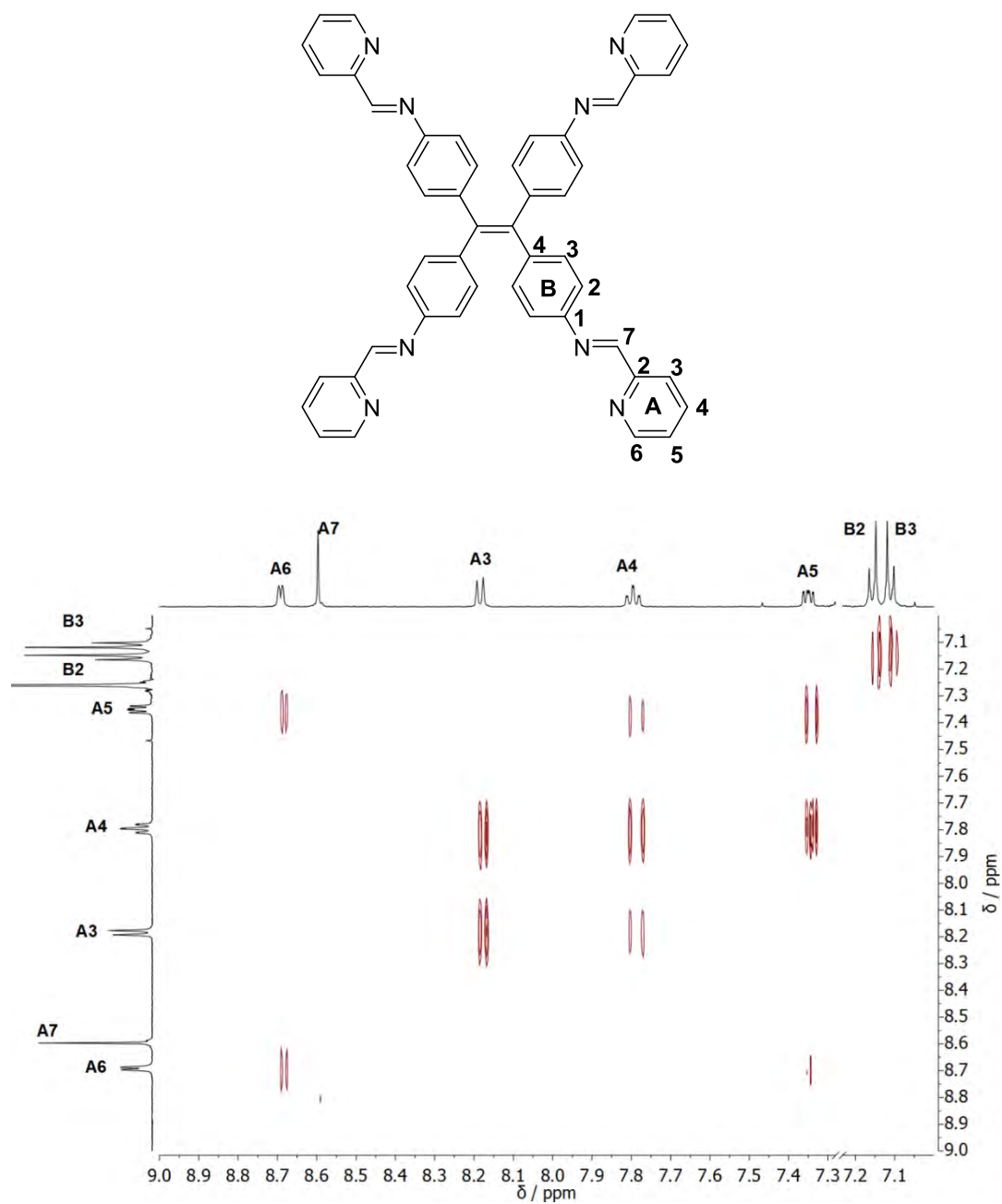


Figure 7.3 ^1H - ^1H COSY spectrum (500 MHz, CDCl_3) of tetraimine **2.3**.

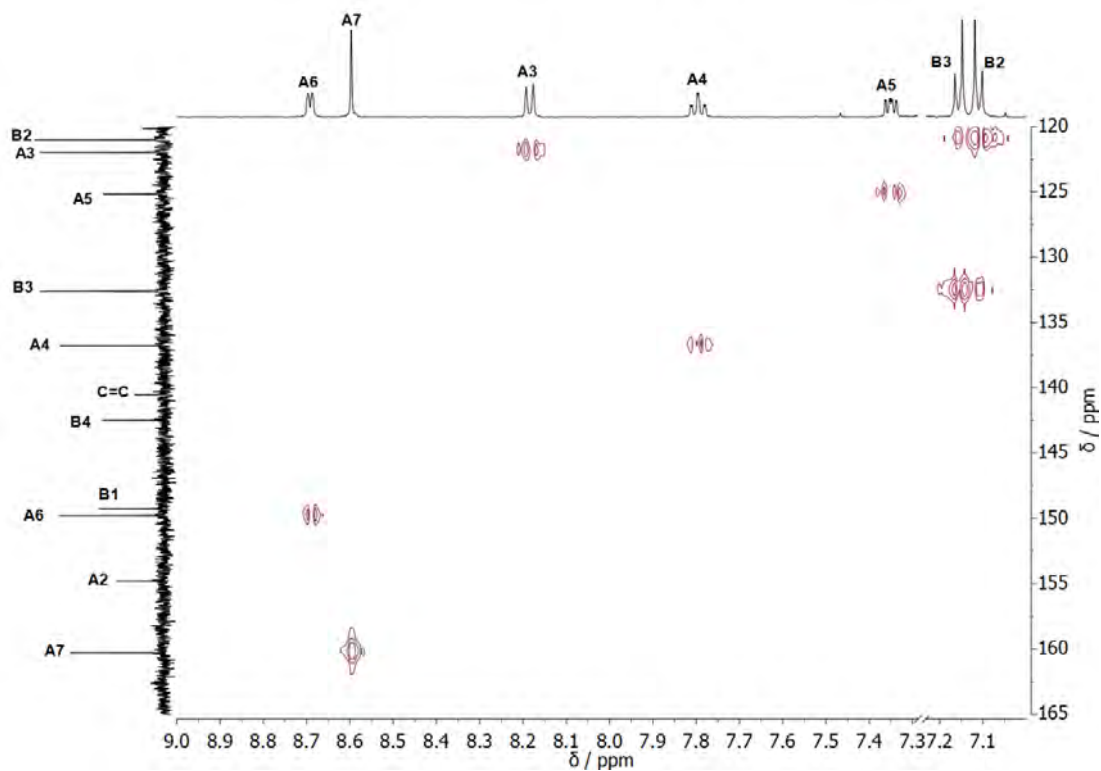


Figure 7.4 ^1H - ^{13}C HSQC spectrum (500 MHz, CD_3CN) of tetraamine **2.3**.

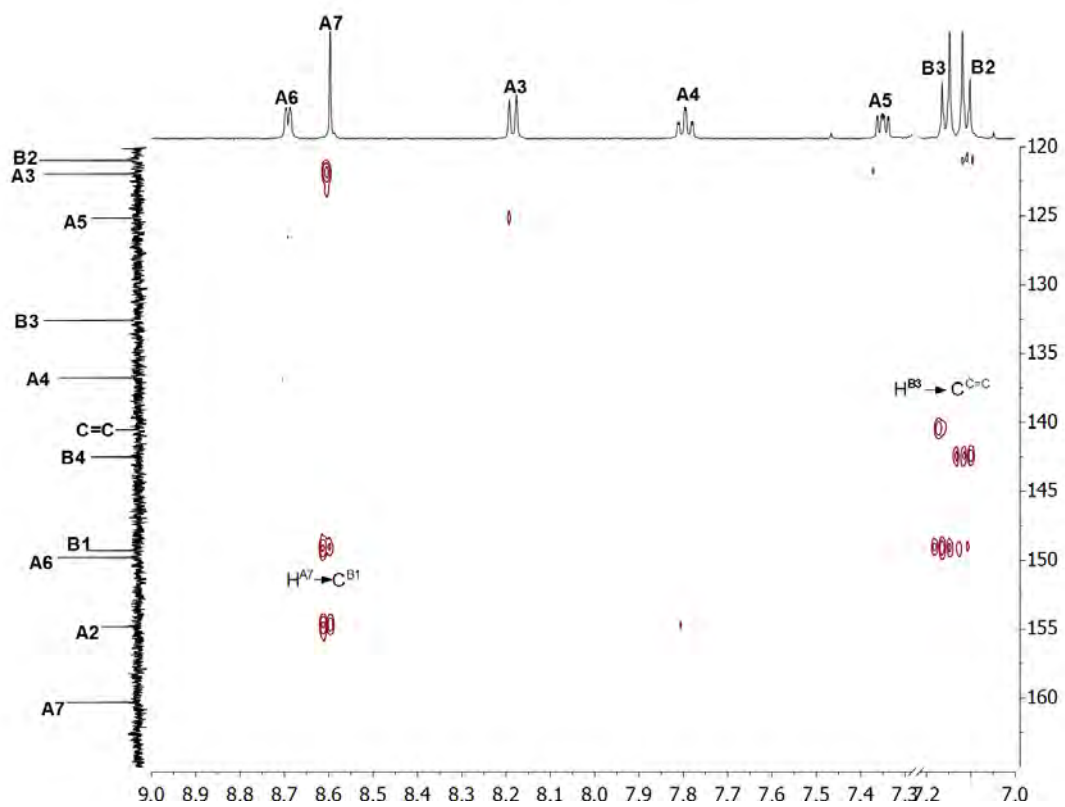


Figure 7.5 ^1H - ^{13}C HMBC spectrum (500 MHz, CDCl_3) of tetramine **2.3** showing correlations between $\text{H}^{\text{A}7}$ and $\text{C}^{\text{B}1}$ and $\text{H}^{\text{B}3}$ and $\text{C}^{\text{C}=\text{C}}$.

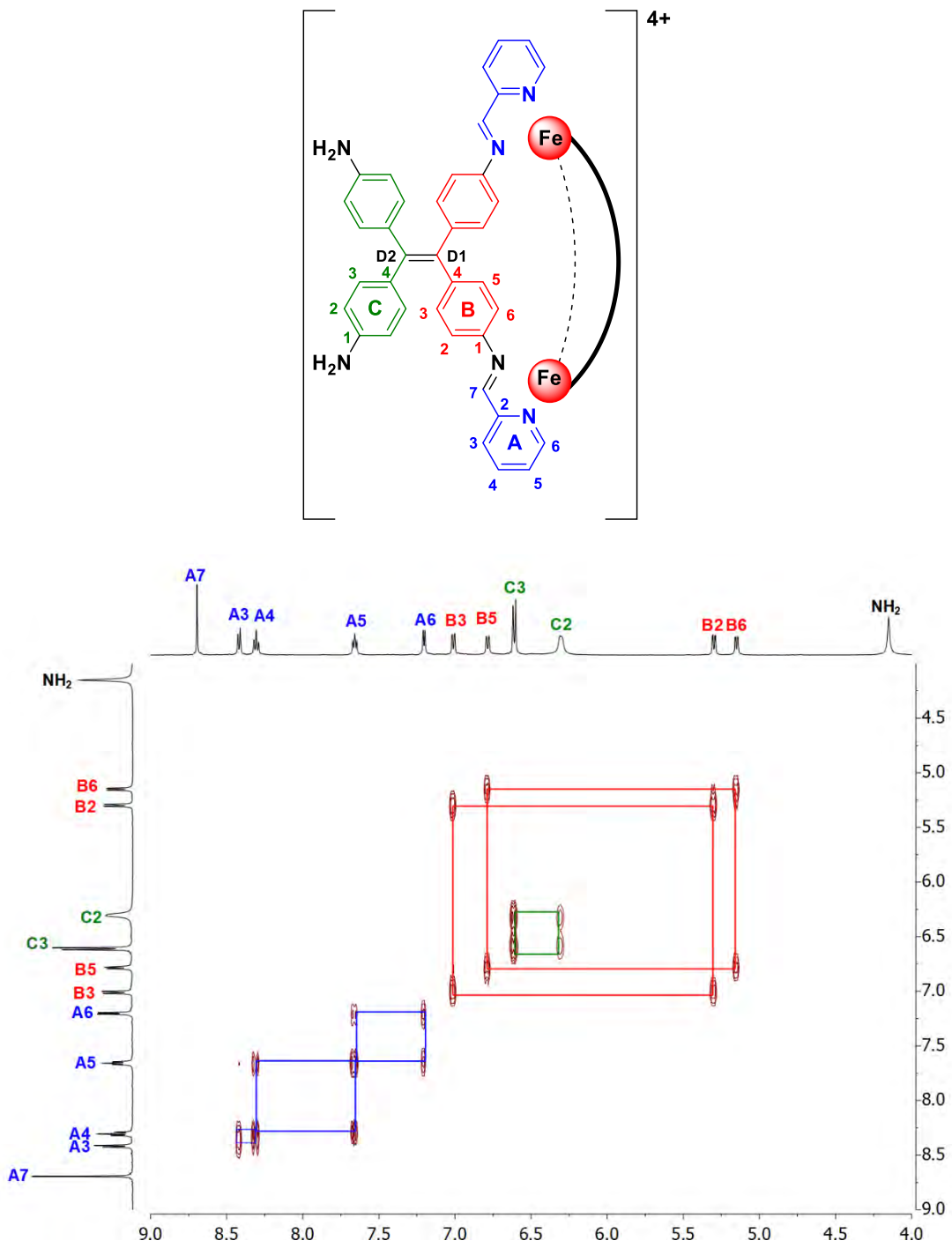


Figure 7.6 ^1H - ^1H COSY spectrum (500 MHz, CD_3CN) of $[\text{Fe}_2(\mathbf{2.2})_3]^{4+}$ showing coupling between protons on individual phenyl rings and no coupling for the amine proton.

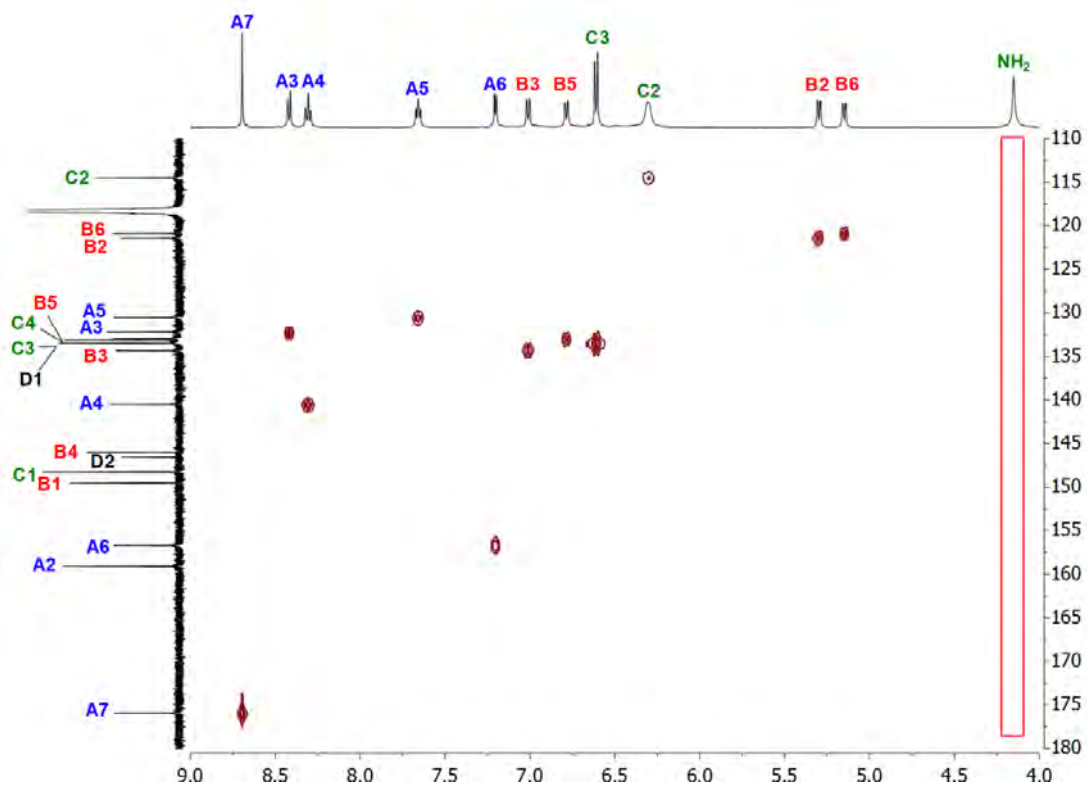


Figure 7.7 ^1H - ^{13}C HSQC spectrum (500 MHz, CD_3CN) of $[\text{Fe}_2(\mathbf{2.2})_3]^{4+}$ showing no coupling for the amine proton.

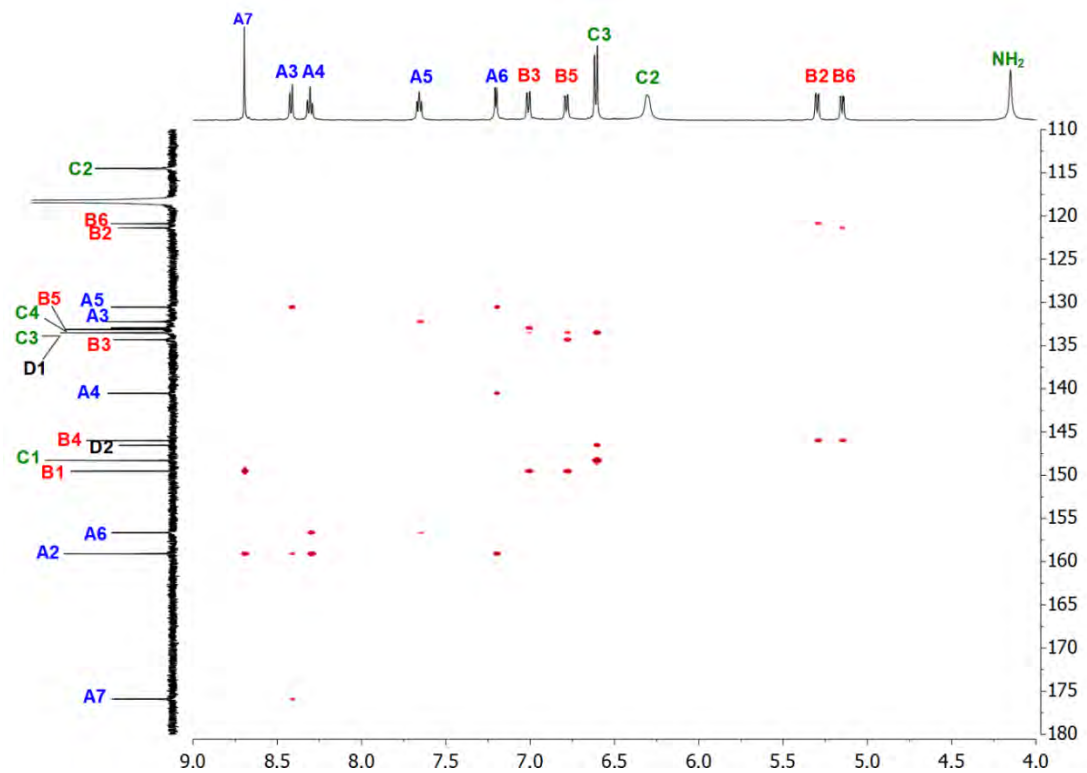


Figure 7.8 ^1H - ^{13}C HMBC spectrum (600 MHz, CD_3CN) of $[\text{Fe}_2(\mathbf{2.2})_3]^{4+}$.

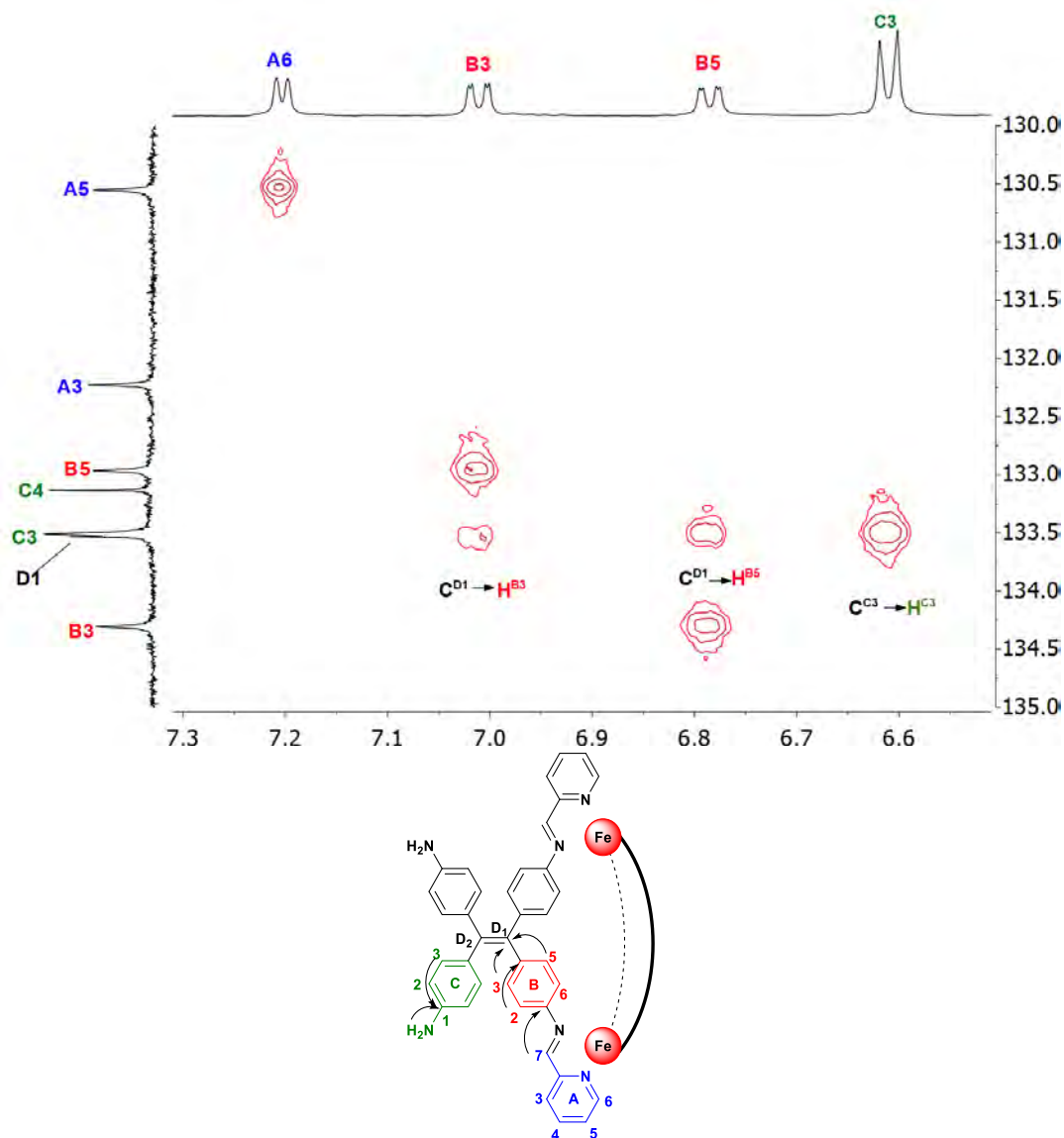


Figure 7.9 Expansion of the ^1H - ^{13}C HMBC spectrum (600 MHz, CD_3CN) of $[\text{Fe}_2(\mathbf{2.2})_3]^{4+}$ showing correlations between C^{D1} and H^{B3} , C^{D1} and H^{B5} , and C^{C3} and H^{C3} . Bottom: Key HMBC couplings for $[\text{Fe}_2(\mathbf{2})_3]^{4+}$.

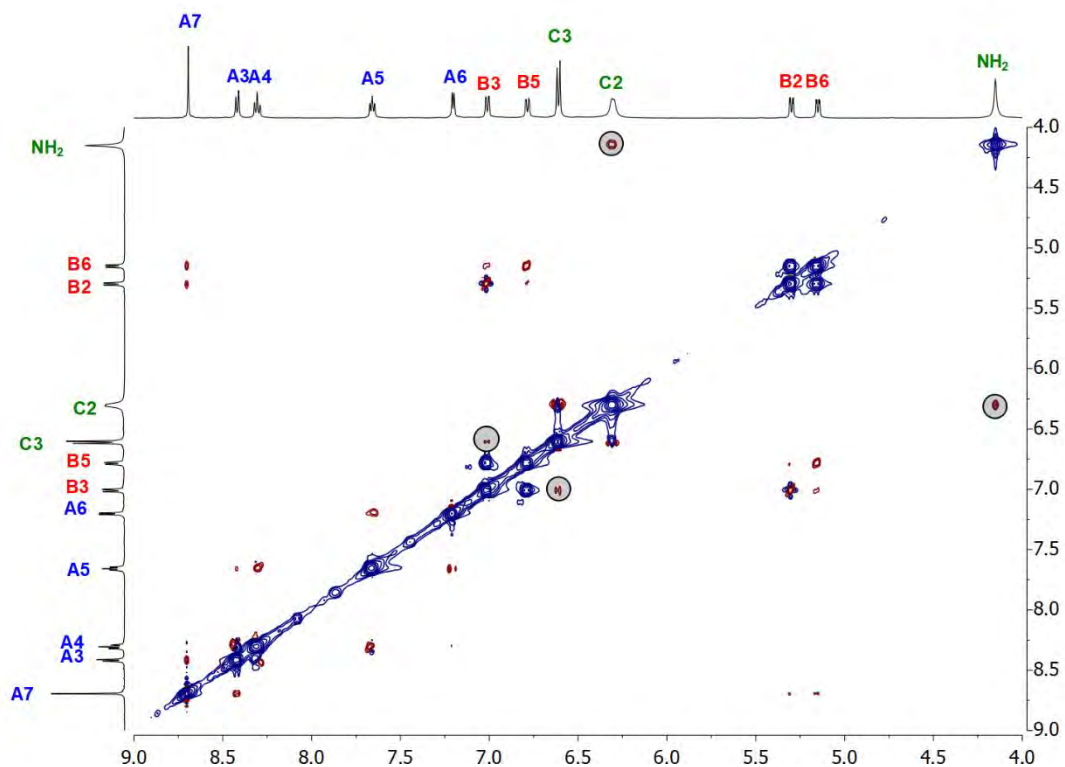


Figure 7.10 ^1H - ^1H NOESY spectrum (500 MHz, CD_3CN) of $[\text{Fe}_2(\mathbf{2.2})_3]^{4+}$ showing the interaction between $\text{H}^{\text{B}3}$ and $\text{H}^{\text{C}3}$, and $\text{H}^{\text{C}2}$ and the amine protons.

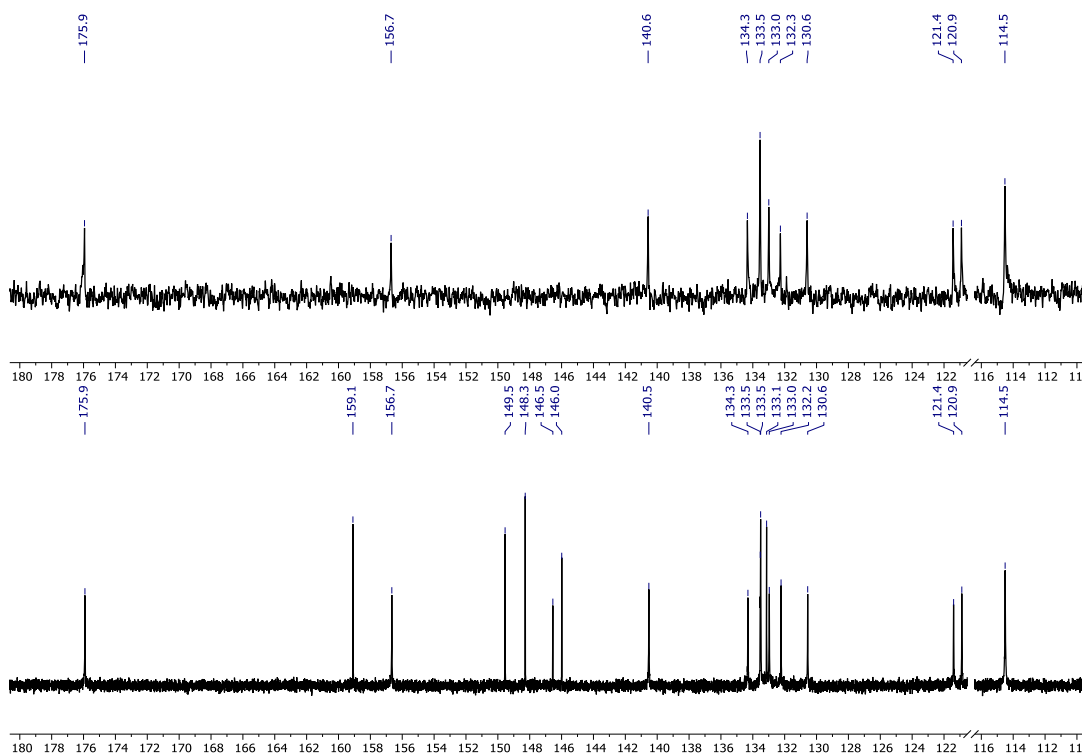


Figure 7.11 ^{13}C -DEPT (top, CD_3CN , 101 MHz) and $^{13}\text{C}\{^1\text{H}\}$ (bottom) NMR (CD_3CN , 151 MHz) spectra of the $[\text{Fe}_2(\mathbf{2.2})_3](\text{PF}_6)_4$ helicate.

7.4 Full ESI-MS of $[\text{Fe}_2(\mathbf{2.2})_3](\text{PF}_6)_4$ helicate

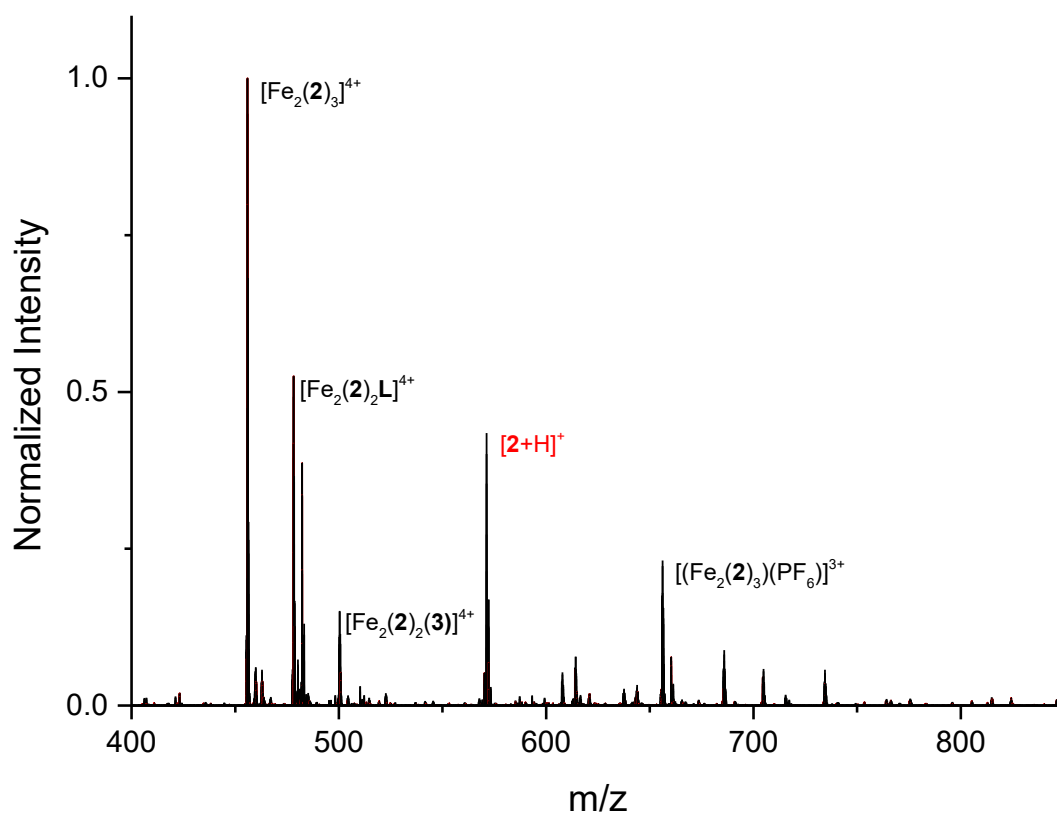


Figure 7.12 ESI-MS of the $[\text{Fe}_2(\mathbf{2.2})_3](\text{PF}_6)_4$ helicate

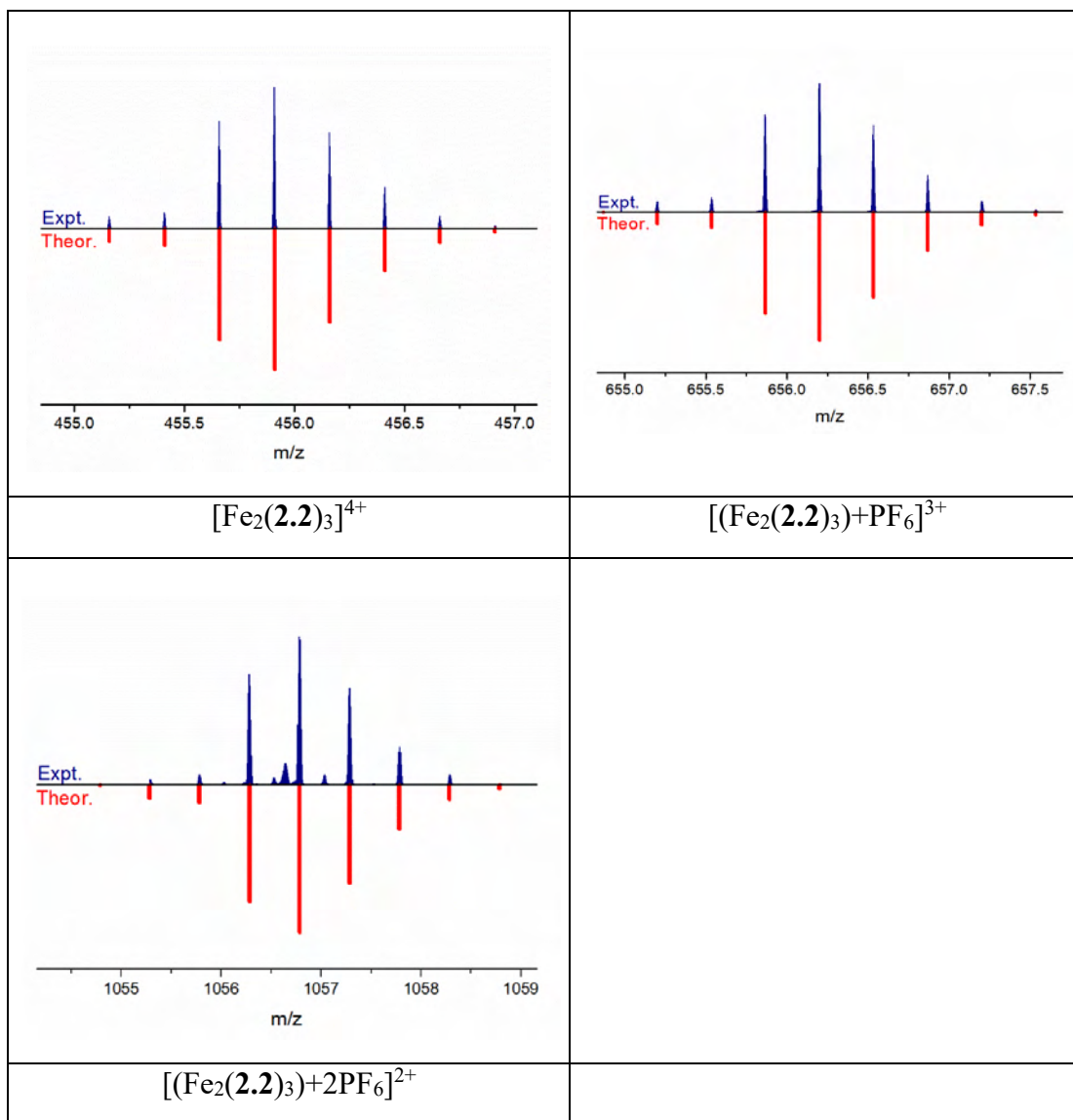


Figure 7.13 Zoom scans of select ESI-MS peaks, with simulated isotope patterns of the $[\text{Fe}_2(\mathbf{2.2})_3](\text{PF}_6)_4$ helicate

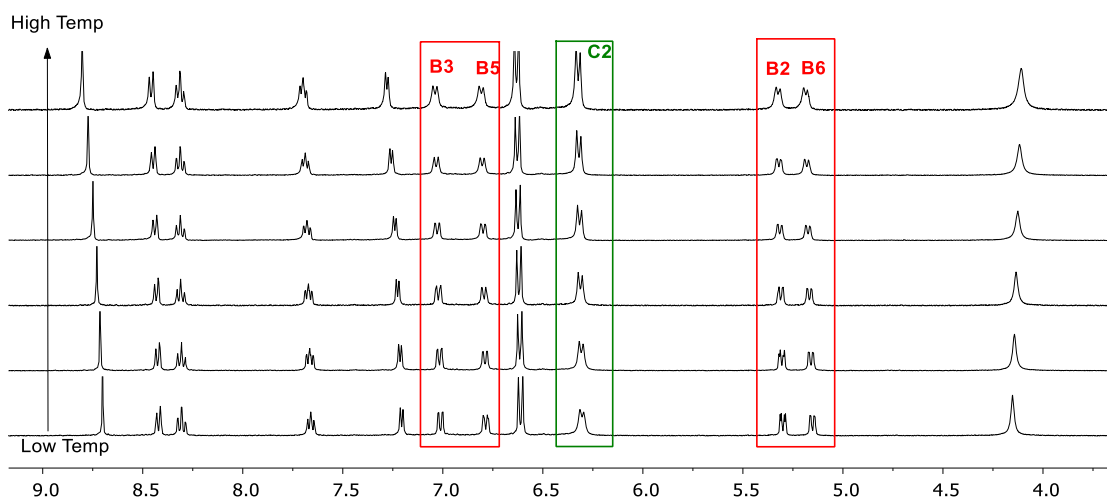


Figure 7.14 ^1H NMR of $[\text{Fe}_2(\mathbf{2.2})_3]^{4+}$ (400 MHz, CD_3CN) at 25 °C, 30 °C, 35 °C, 40 °C, 45 °C and 50 °C (bottom to top) showing broadening of the signals of B phenyl ring protons and sharpening of the signal of $\text{H}^{\text{C}2}$.

7.5 Influence of reaction stoichiometry on product formation

All reactions below were conducted in DMF solution at room temperature for 48 h, followed by the standard aqueous workup as described in the main text. In all cases the same major species is obtained.

Table 7.2 Reaction stoichiometry used to form helicate $[\text{Fe}_2(\mathbf{2.2})_3](\text{PF}_6)_4$ in DMF.

Entry	Tetraaniline 2.1	2-pyridinecarboxaldehyde	$\text{Fe}(\text{BF}_4)_2 \cdot 4\text{H}_2\text{O}$
1	3	6	1.5
2	3	6	3
3	3	6	6
4	3	12	1.5
5	3	12	3
6	3	12	6

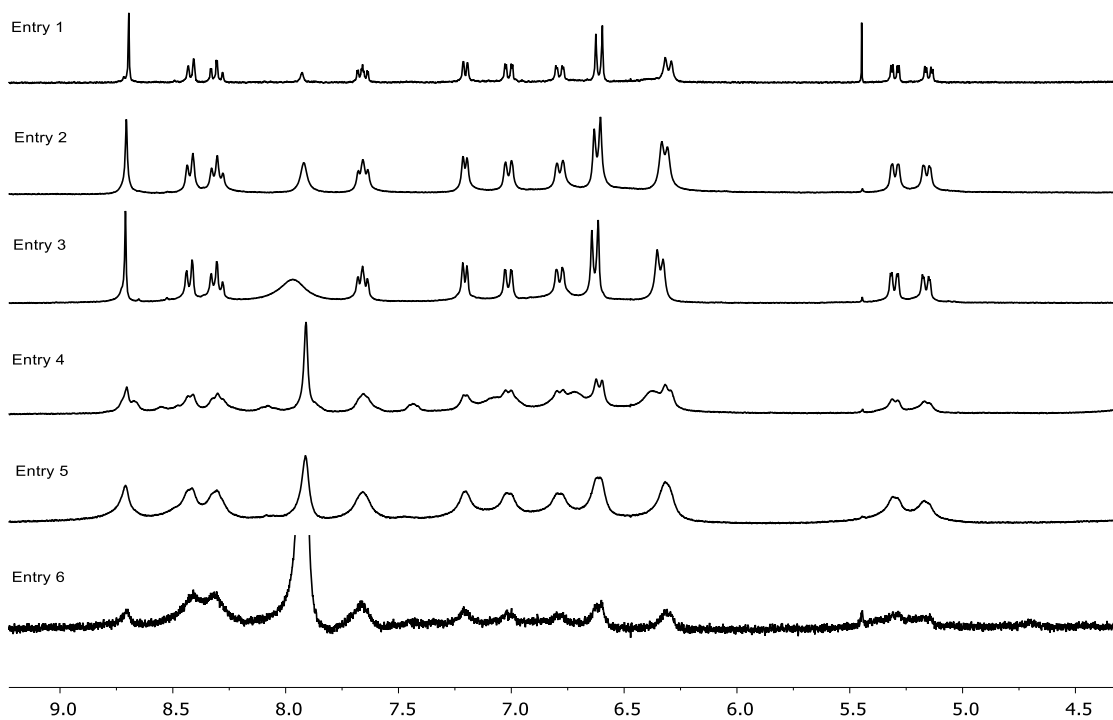


Figure 7.15 ¹H NMR (300 MHz, CD₃CN) spectra of the reaction mixtures (in DMF) from different ratios (See Table 7.2) of **2.1**, 2-pyridinecarboxaldehyde and Fe(BF₄)·4H₂O, after aqueous workup. In all cases the same major species is obtained.

7.6 Additional spectroscopic data for derivatised helicates

7.6.1 Additional ^1H NMR and HR ESI-MS data for $[\text{Fe}_2(\mathbf{2.4})_3]^{4+}$

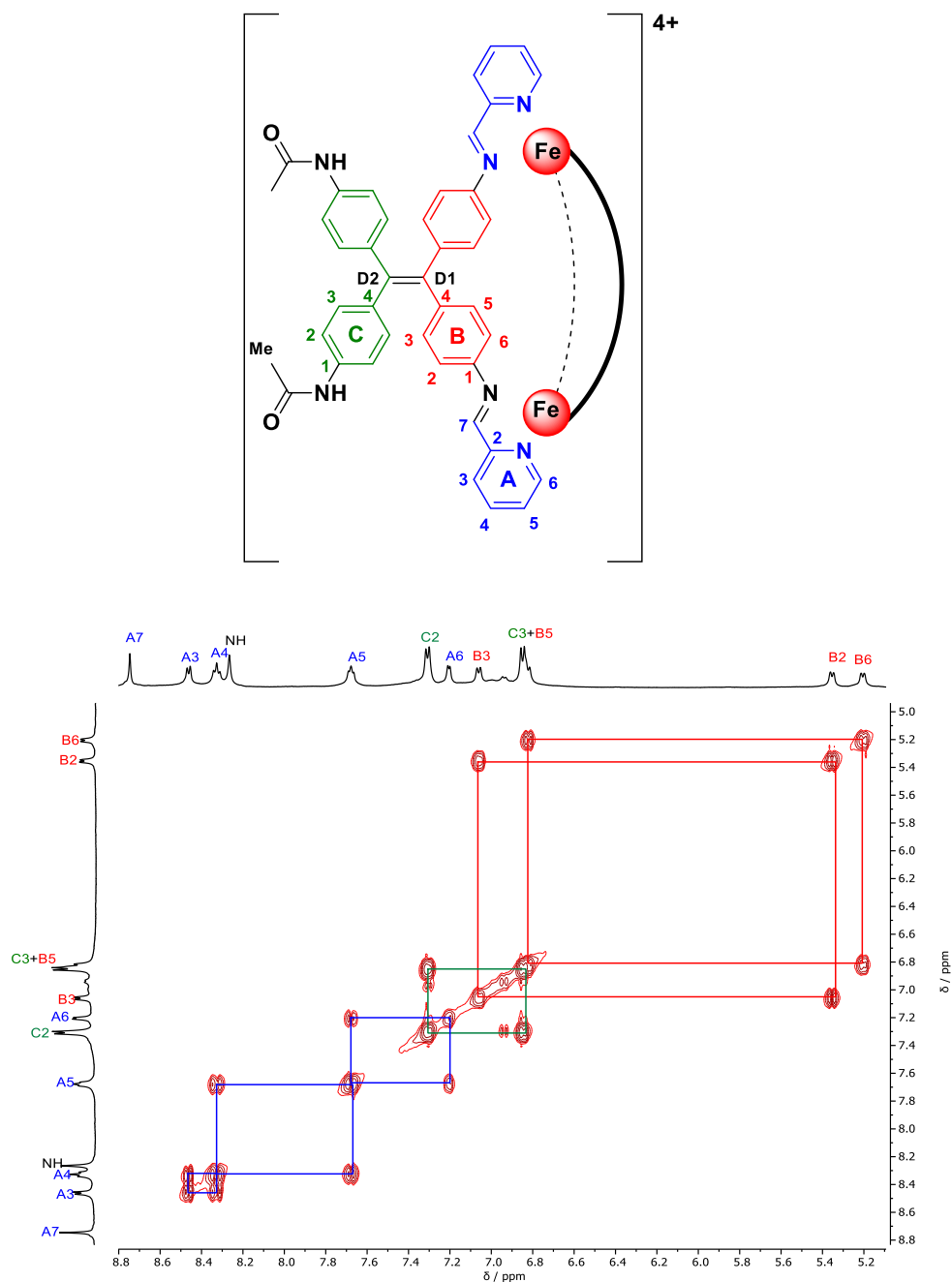


Figure 7.16 ^1H - ^1H COSY spectrum (500 MHz, CD_3CN) of $[\text{Fe}_2(\mathbf{2.4})_3]^{4+}$ showing coupling between protons on individual ring systems.

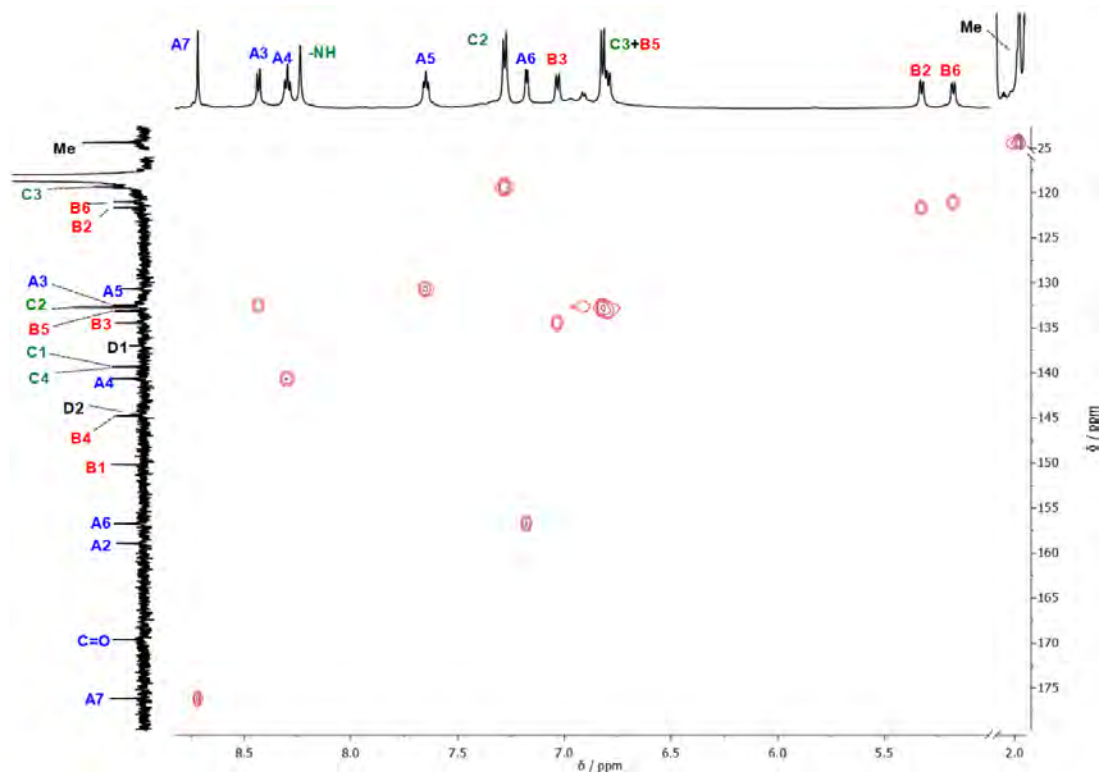


Figure 7.17 ^1H - ^{13}C HSQC spectrum (500 MHz, CD_3CN) of $[\text{Fe}_2(\mathbf{2.4})_3]^{4+}$.

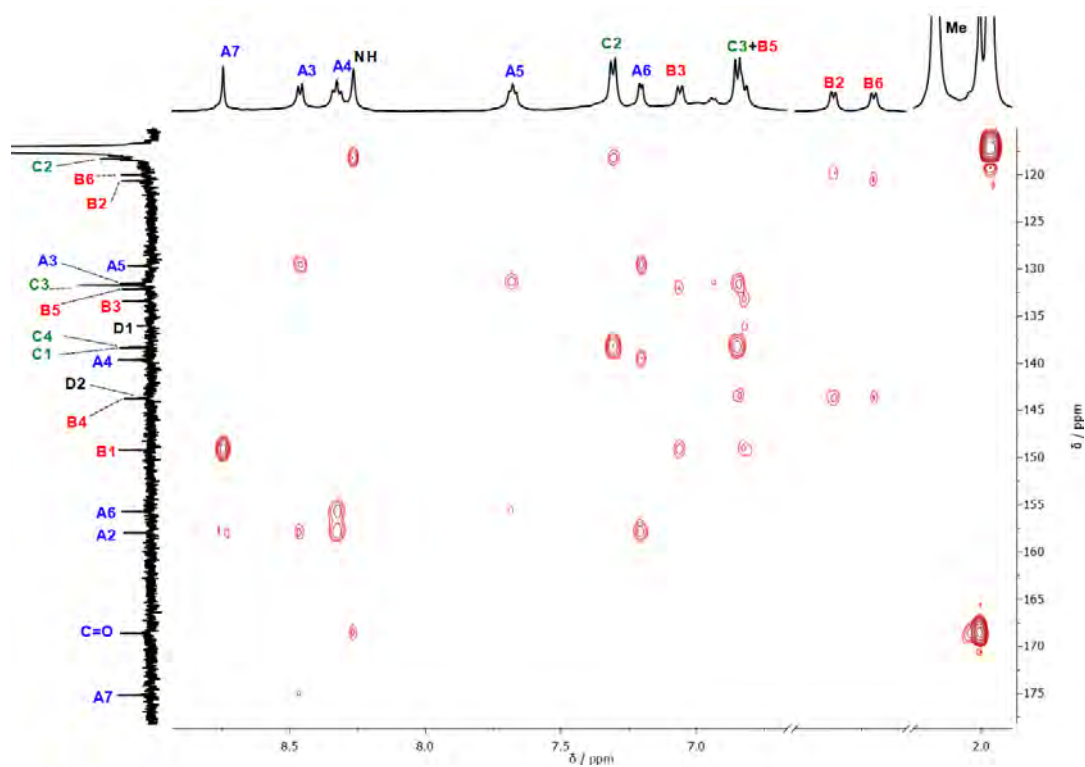


Figure 7.18 ^1H - ^{13}C HMBC spectrum (500 MHz, CD_3CN) of $[\text{Fe}_2(\mathbf{2.4})_3]^{4+}$.

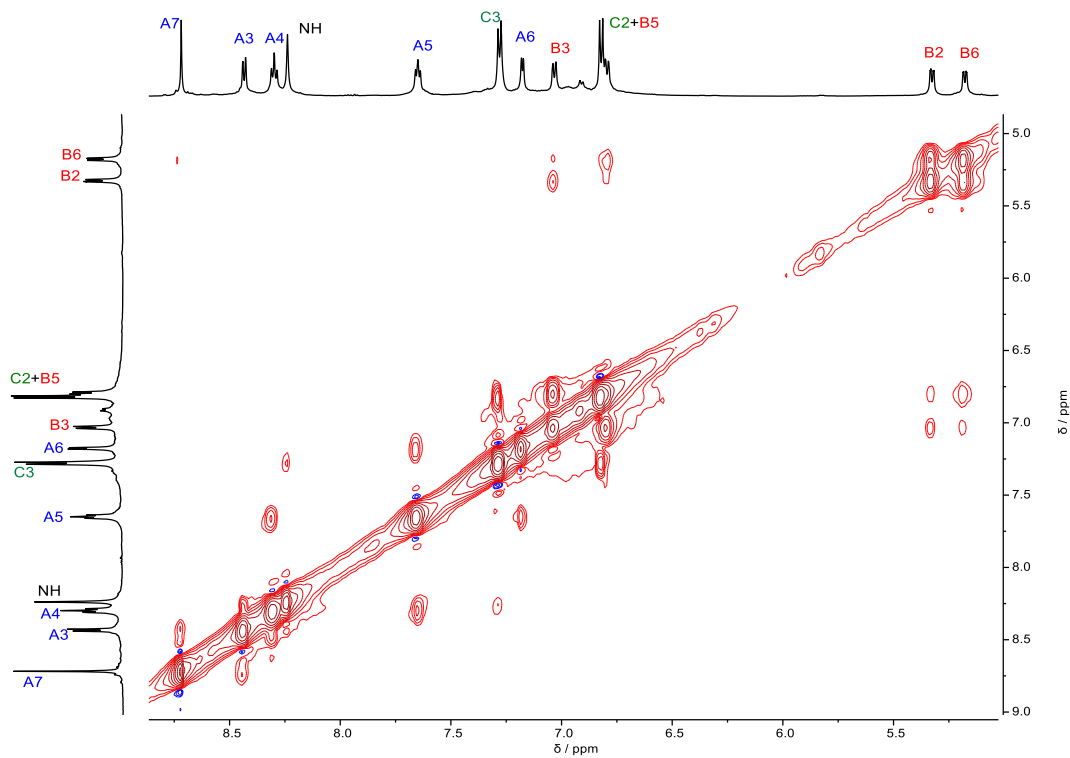


Figure 7.19 ^1H - ^1H NOESY spectrum (500 MHz, CD_3CN) of $[\text{Fe}_2(\mathbf{2.4})_3]^{4+}$.

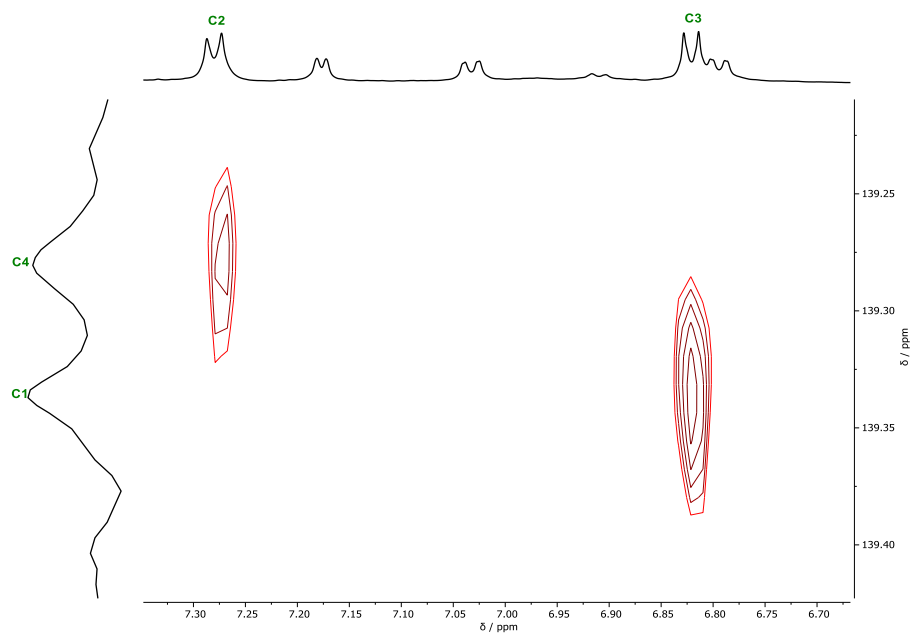


Figure 7.20 Band selective ^1H - ^{13}C HMBC (500 MHz, CD_3CN) of $[\text{Fe}_2(\mathbf{2.4})_3](\text{PF}_6)_4$ helicate.

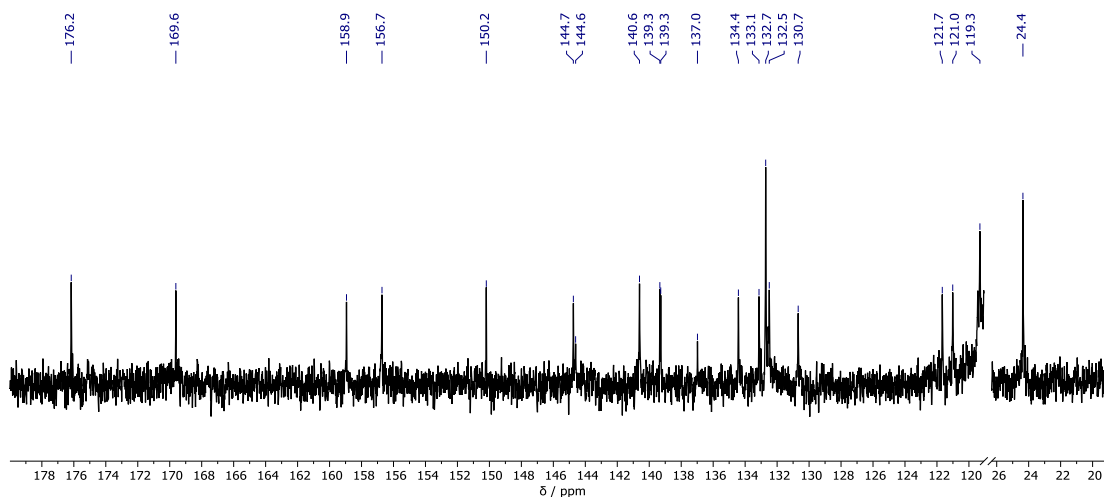


Figure 7.21 $^{13}\text{C}\{^1\text{H}\}$ NMR spectra (151 MHz, CD_3CN) of $[\text{Fe}_2(\mathbf{2.4})_3](\text{PF}_6)_4$ helicite.

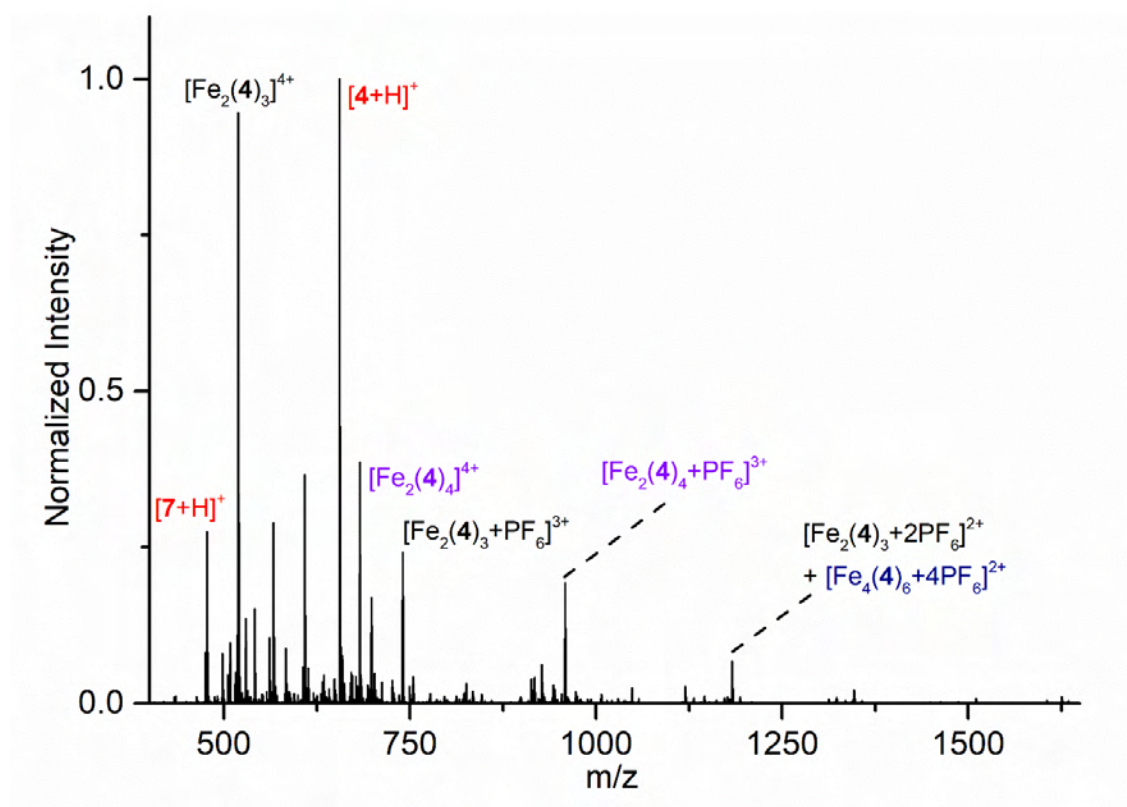


Figure 7.22 HR-ESI-MS of the $[\text{Fe}_2(\mathbf{2.4})_3](\text{PF}_6)_4$ helicite.

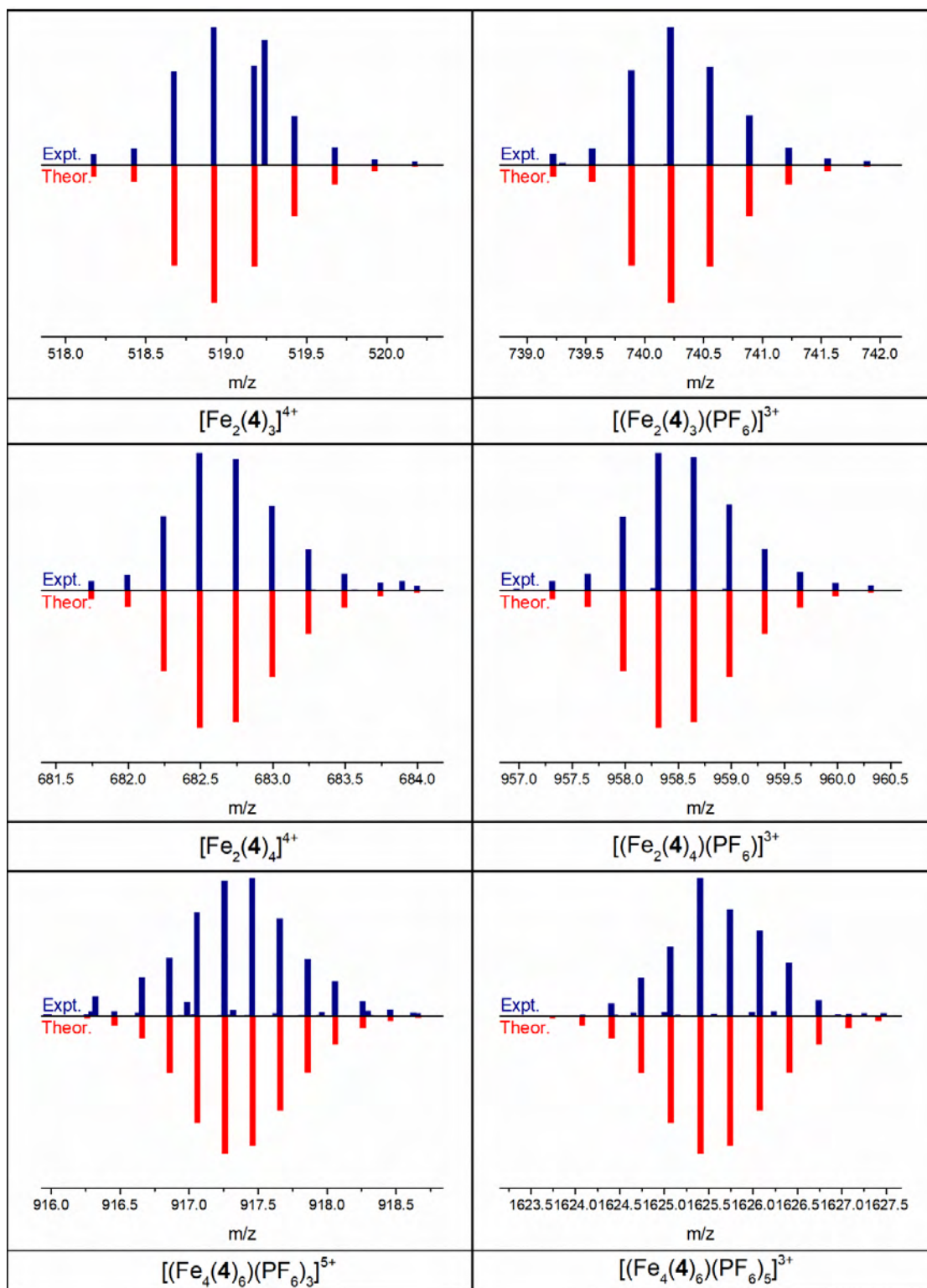


Figure 7.23 Zoom scans of select ESI-MS peaks, with simulated isotope patterns ESI-MS of $[\text{Fe}_2(\mathbf{2.4})_3](\text{PF}_6)_4$ helicate.

7.6.2 Additional ^1H NMR and HR ESI-MS data for $[\text{Fe}_2(\mathbf{2.5})_3]^{4+}$

Similar connectivity for the $[\text{Fe}_2(\mathbf{2.5})_3]^{4+}$ helicate was traced using ^1H - ^{13}C HSQC and HMBC spectroscopy to identify the ^1H NMR signals of the new phenyl ring ($\text{H}^{\text{E}2}$, $\text{H}^{\text{E}3}$, $\text{H}^{\text{E}4}$). The proton signal of $\text{H}^{\text{E}2}$ shows a HMBC coupling to the carbonyl carbon (165.7), which is in turn coupled to the NH proton at 8.69 ppm and indicates the successful amide formation on the helicate.

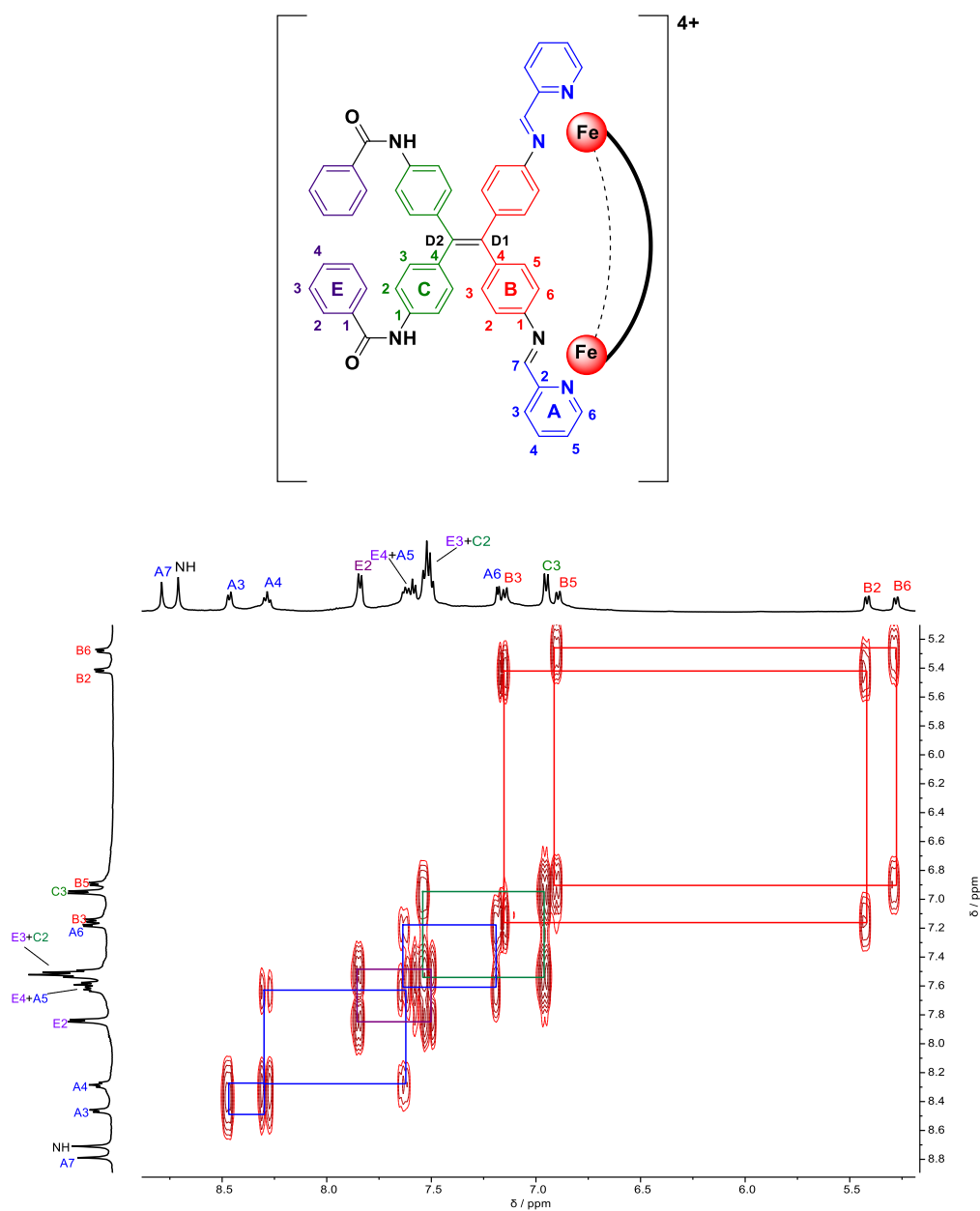


Figure 7.24 ^1H - ^1H COSY spectrum (500 MHz, CD_3CN) of $[\text{Fe}_2(\mathbf{2.5})_3]^{4+}$ showing coupling between protons on individual ring systems.

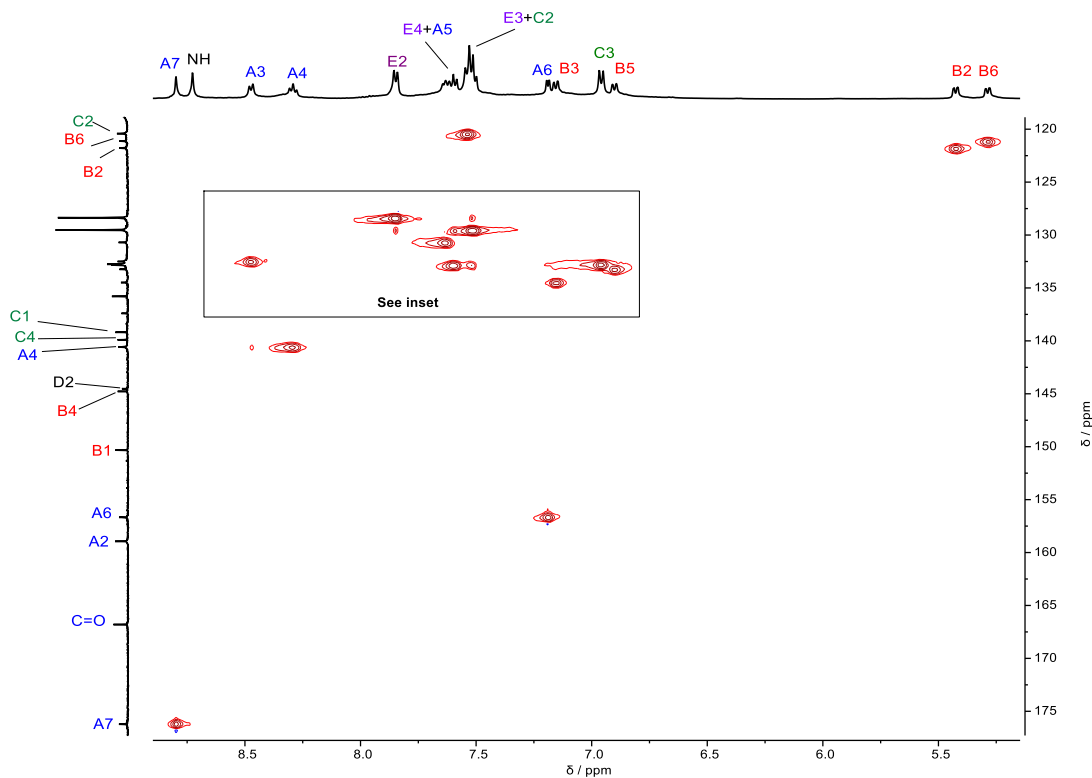


Figure 7.25 ^1H - ^{13}C HSQC spectrum (500 MHz, CD_3CN) of $[\text{Fe}_2(\mathbf{2.5})_3]^{4+}$.

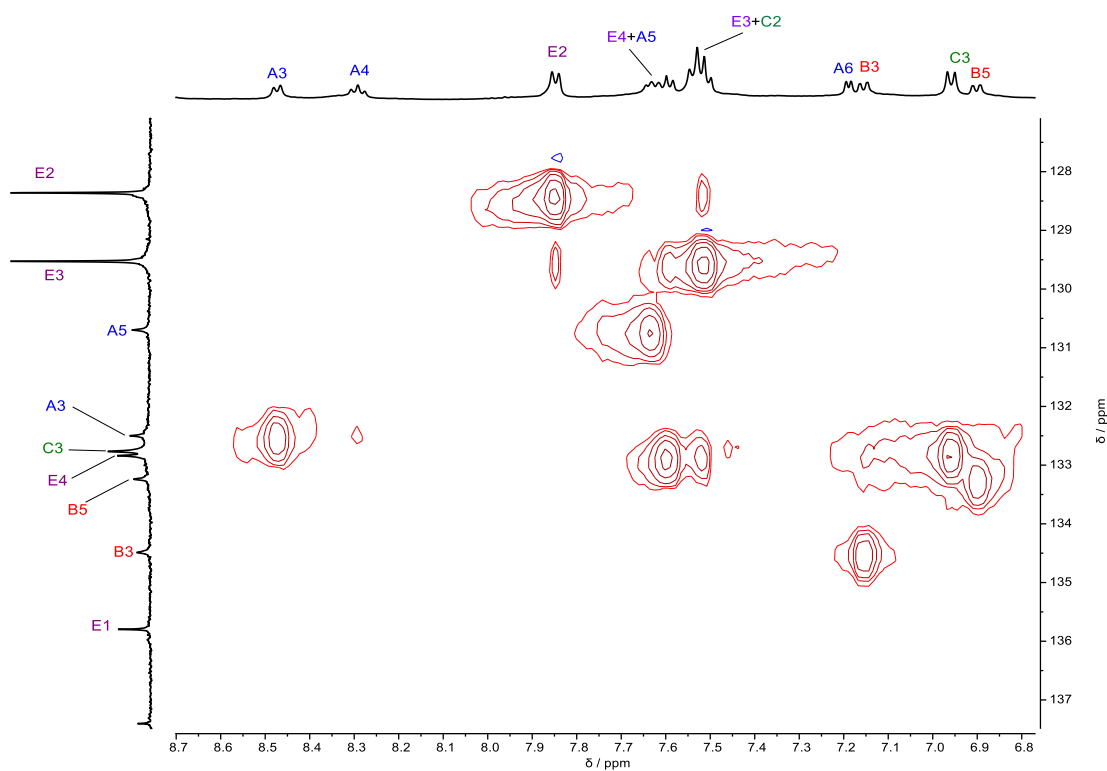


Figure 7.26 Expansion of ^1H - ^{13}C HSQC spectrum (500 MHz, CD_3CN) of $[\text{Fe}_2(\mathbf{2.5})_3]^{4+}$.

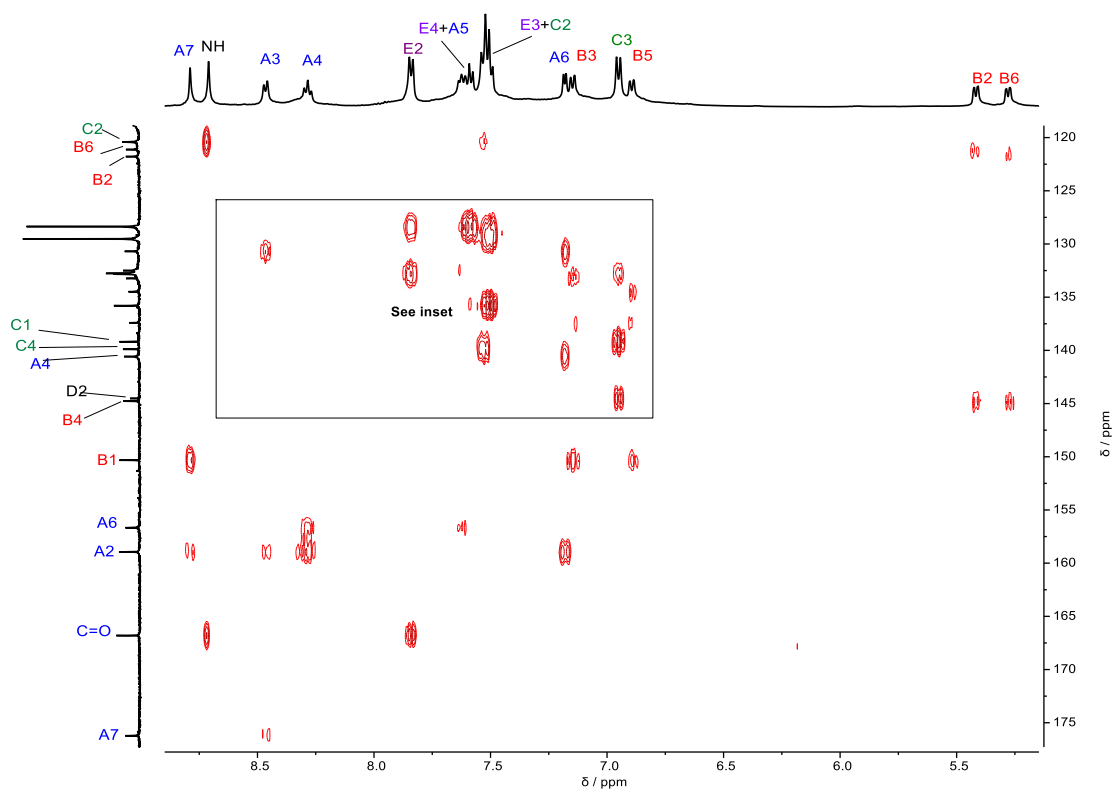


Figure 7.27 ^1H - ^{13}C HMBC spectrum (500 MHz, CD_3CN) of $[\text{Fe}_2(\mathbf{2.5})_3]^{4+}$.

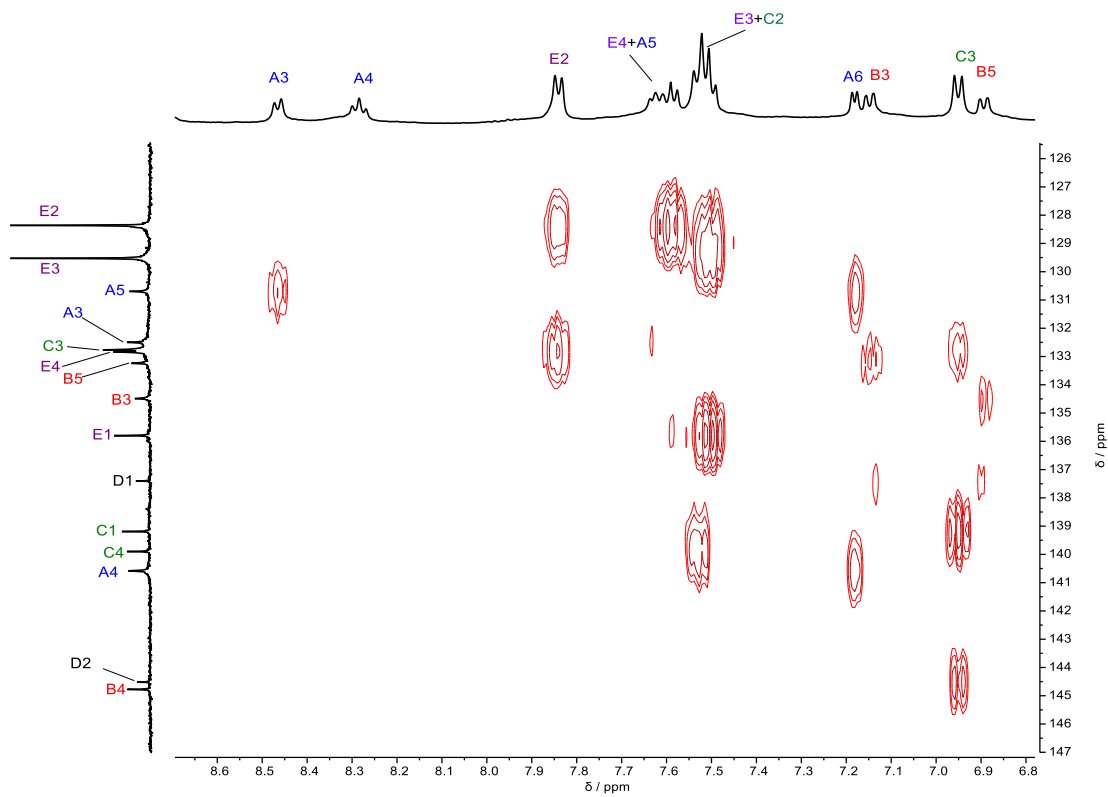


Figure 7.28 Expansion of ^1H - ^{13}C HMBC spectrum (500 MHz, CD_3CN) of $[\text{Fe}_2(\mathbf{2.5})_3]^{4+}$

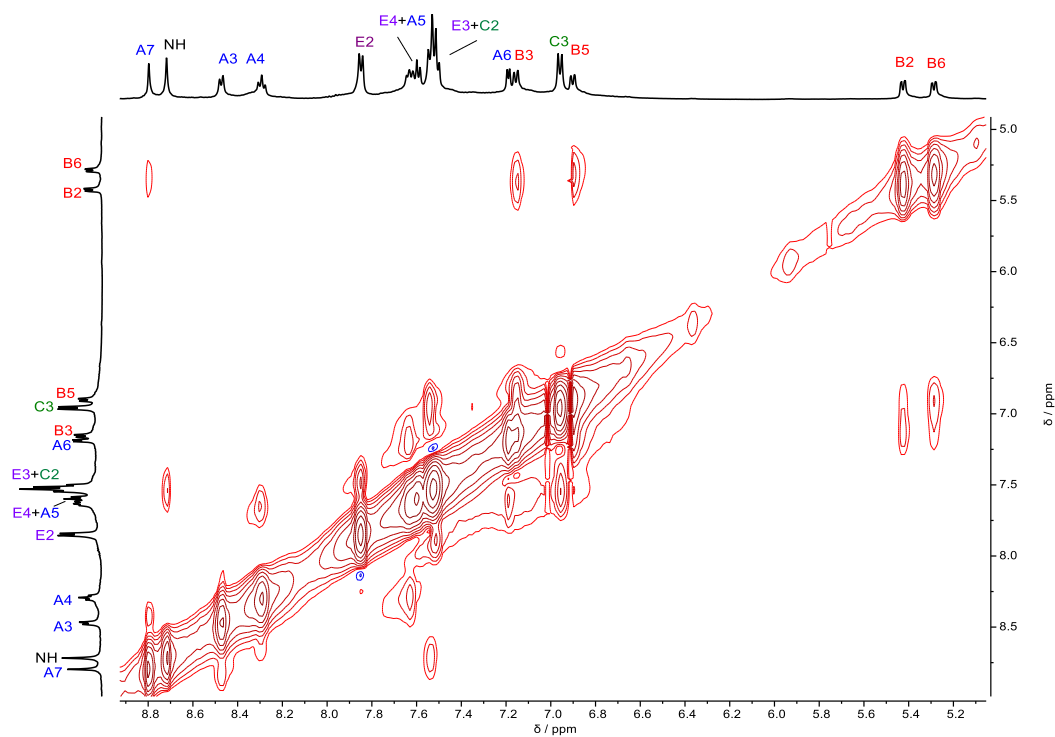


Figure 7.29 ^1H - ^1H NOESY spectrum (500 MHz, CD_3CN) of $[\text{Fe}_2(\mathbf{2.5})_3]^{4+}$.

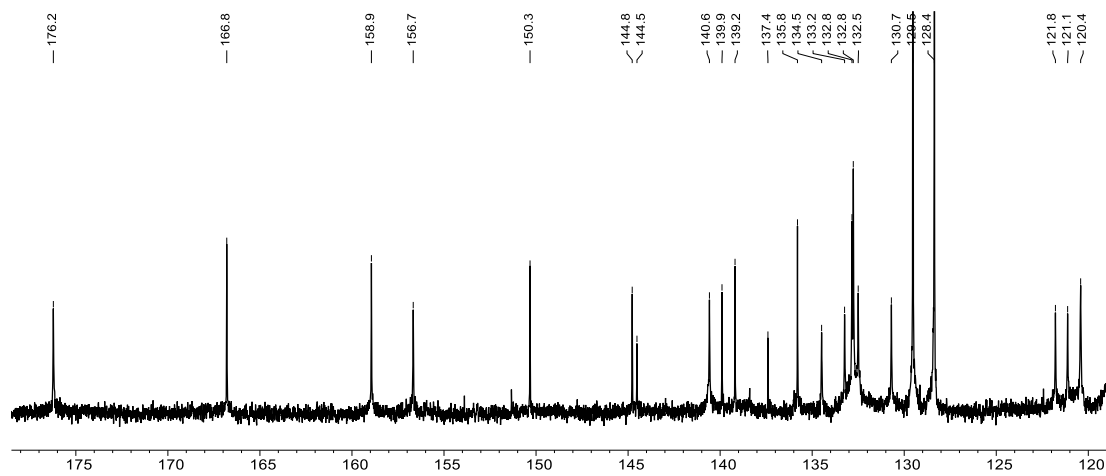


Figure 7.30 $^{13}\text{C}\{^1\text{H}\}$ NMR spectrum of (151 MHz, CD_3CN) of $[\text{Fe}_2(\mathbf{2.5})_3]^{4+}$.

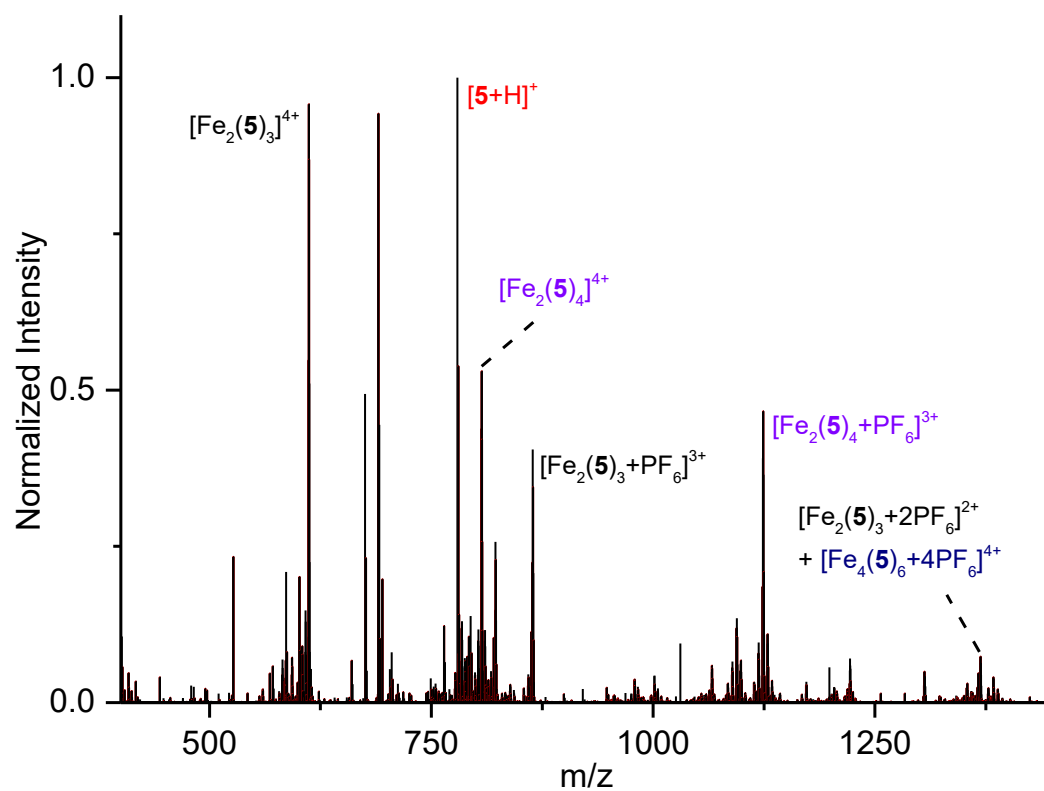


Figure 7.31 ESI-MS of the $[\text{Fe}_2(\mathbf{2.5})_3](\text{PF}_6)_4$ helicite

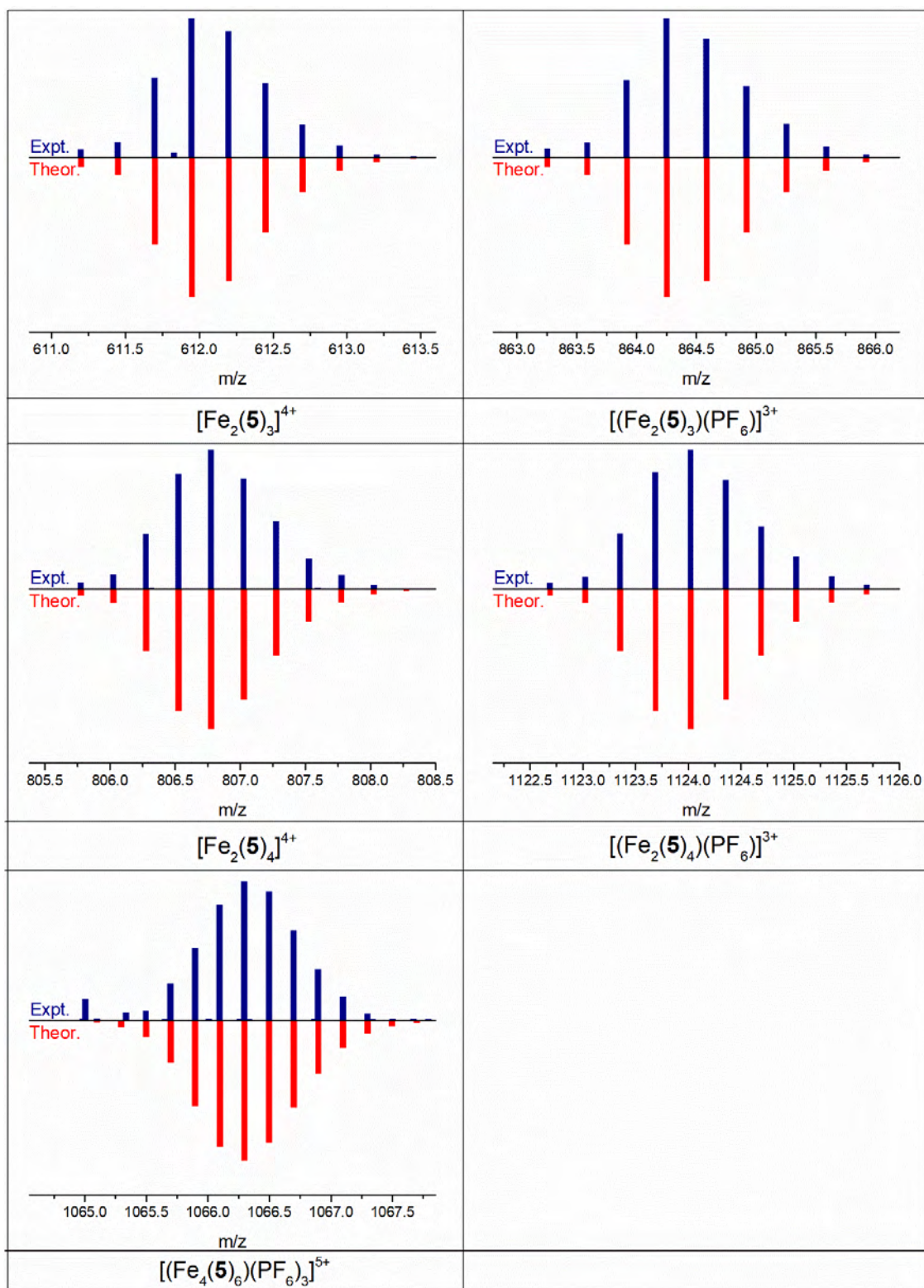


Figure 7.32 Zoom scans of select ESI-MS peaks, with simulated isotope patterns ESI-MS of $[\text{Fe}_2(\mathbf{2.5})_3](\text{PF}_6)_4$ helicate.

7.6.3 Additional ^1H NMR and HR ESI-MS data for $[\text{Fe}_2(\mathbf{2.6})_3]^{4+}$

Assignment of the structure of $[\text{Fe}_2(\mathbf{2.6})_3]^{4+}$ was made by comparison to $[\text{Fe}_2(\mathbf{2.4})_3]^{4+}$ as the ^1H NMR spectra are almost identical, excluding the peaks associated with the aliphatic chain, which can be assigned based on chemical shift.

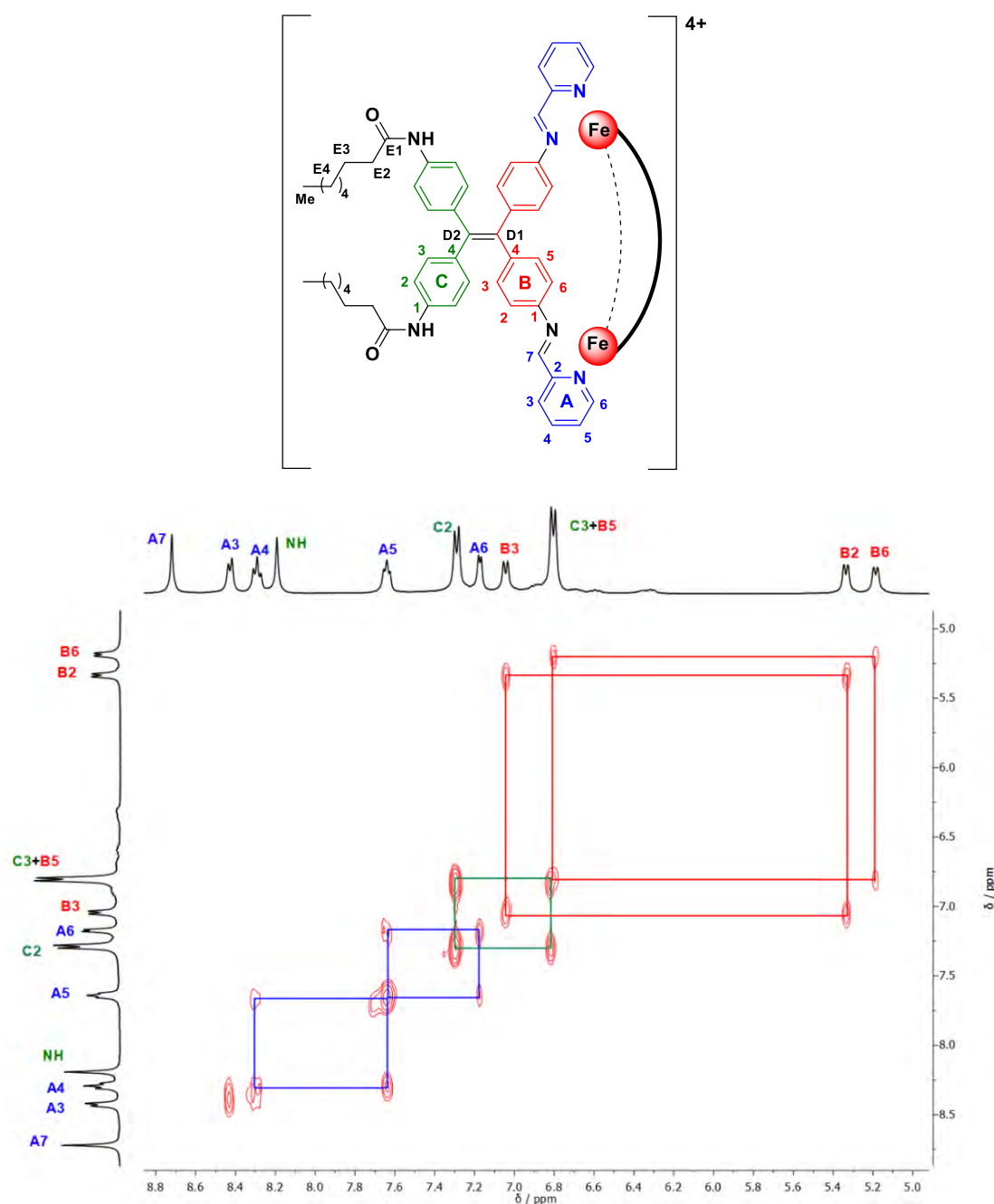


Figure 7.33 Partial ^1H - ^1H COSY Spectrum of $[\text{Fe}_2(\mathbf{2.6})_3]^{4+}$ (500 MHz, CD_3CN , 298 K) showing aromatic proton coupling.

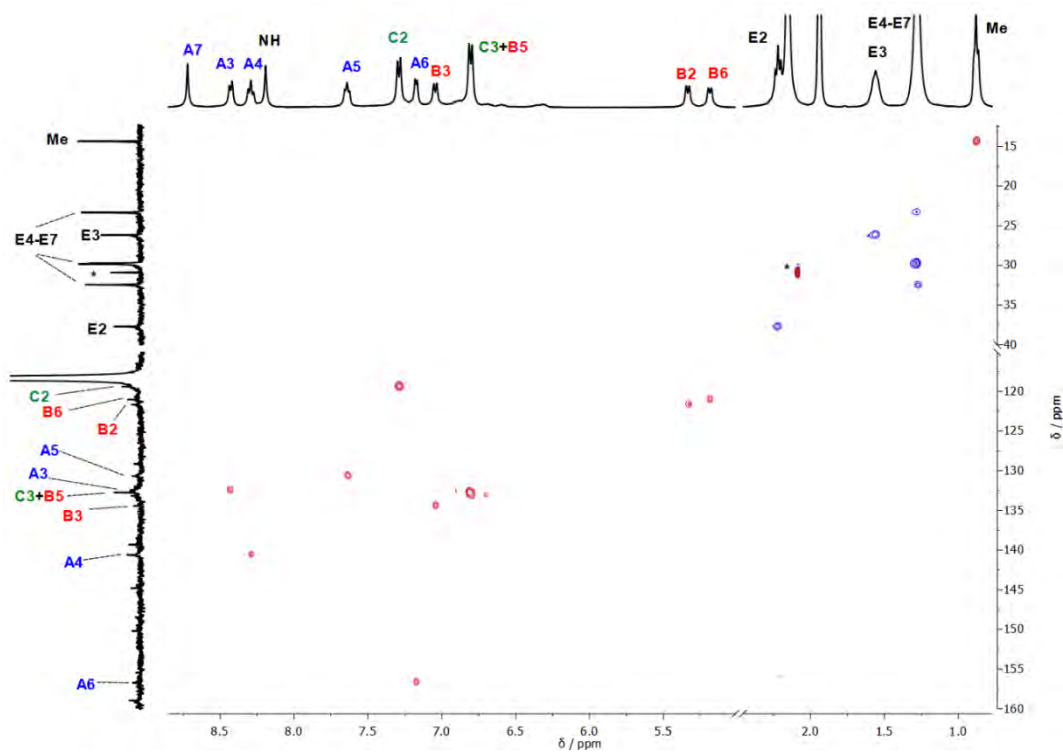


Figure 7.34 ^1H - ^{13}C HSQC spectrum (500 MHz, CD_3CN) of $[\text{Fe}_2(\mathbf{2.6})_3]^{4+}$.

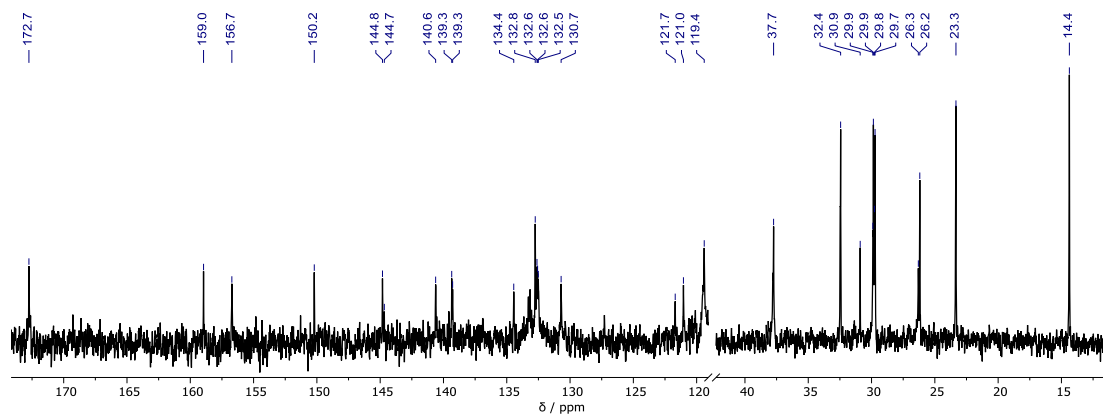


Figure 7.35 $^{13}\text{C}\{^1\text{H}\}$ NMR spectrum (101 MHz, CD_3CN) of $[\text{Fe}_2(\mathbf{2.6})_3]^{4+}$.

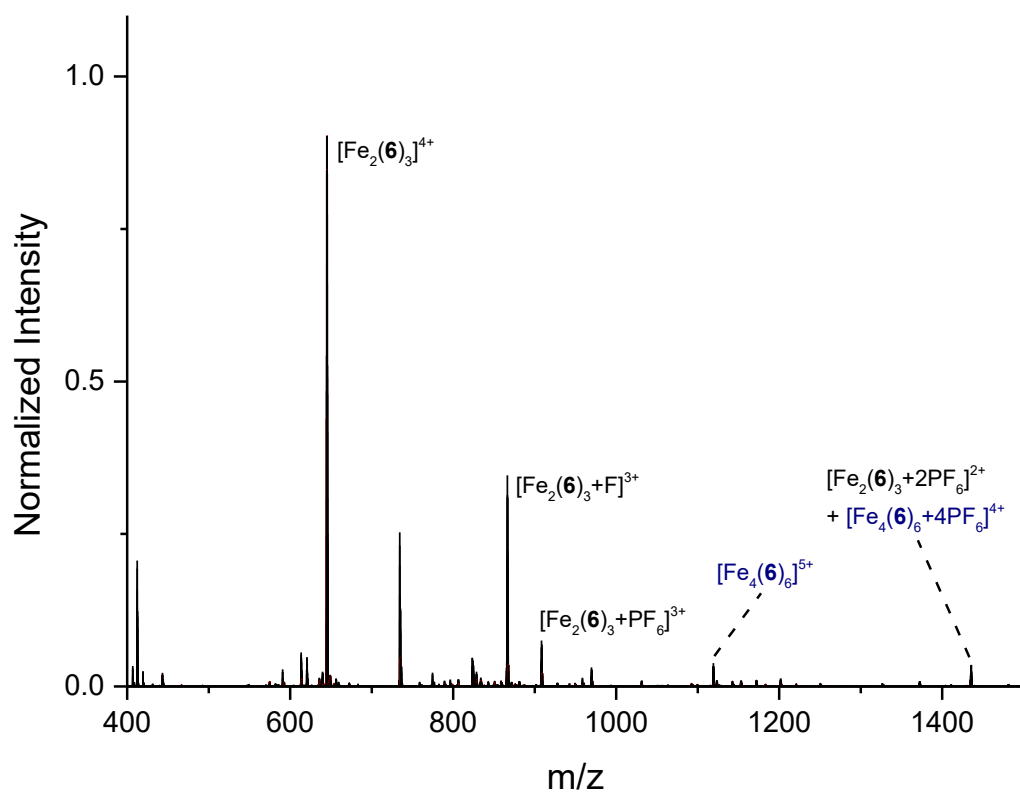


Figure 7.36 HR ESI-MS of the $[\text{Fe}_2(\mathbf{2.6})_3](\text{PF}_6)_4$ helicate.

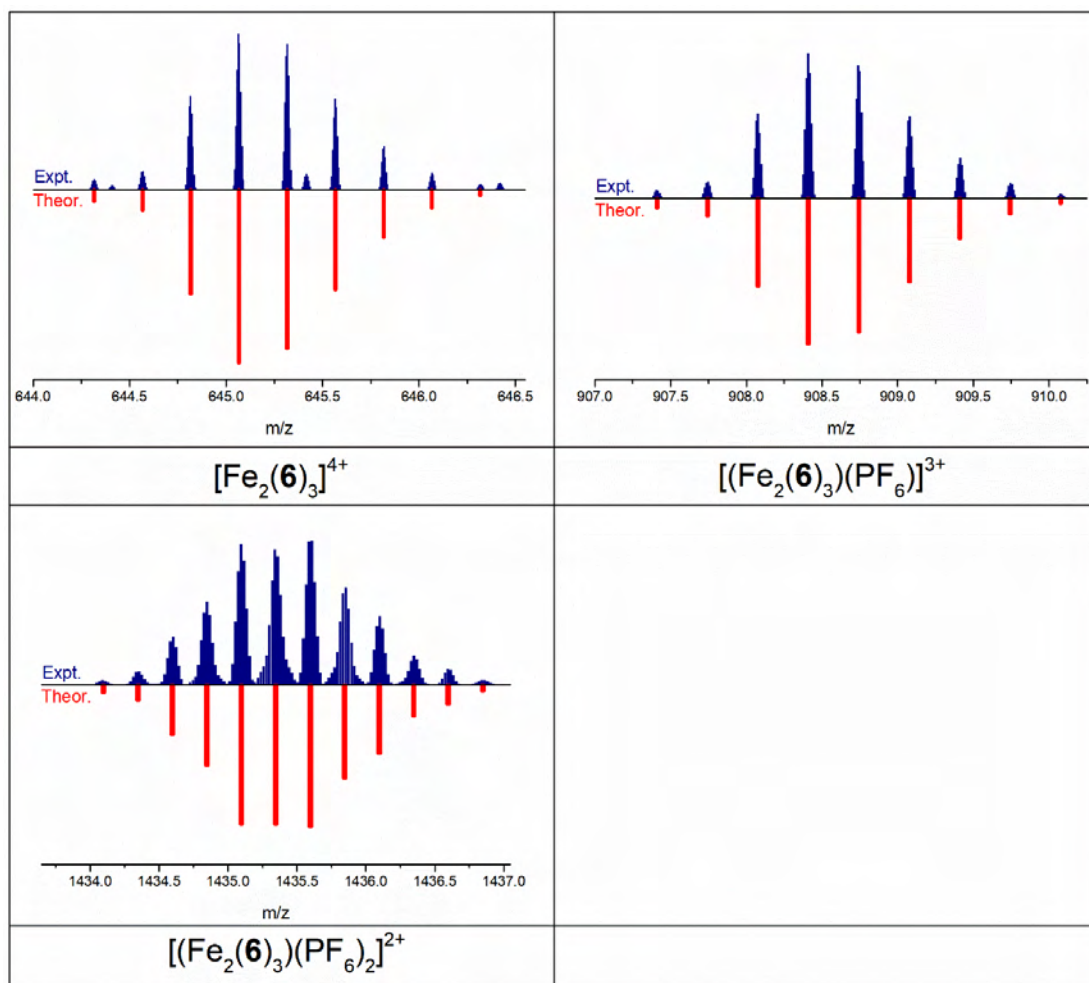
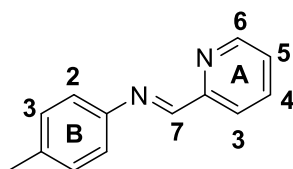


Figure 7.37 HR ESI-MS of the $[\text{Fe}_2(\mathbf{2.6})_3](\text{PF}_6)_4$ helicate.

7.7 Synthesis of 4-methyl-N-(pyridin-2-ylmethylidene)aniline (2.7)



A solution of *p*-toluidine (100 mg, 0.93 mmol) and 2-pyridinecarboxaldehyde (89 μL , 100 mg, 0.94 mmol) in methanol (40 mL) was heated at reflux for 16 hours. Filtration of reaction insolubles and removal of solvent afforded a pale yellow solid which was recrystallized from diethyl ether and pentane to give the title compound as pale brown block crystals (164 mg, 0.84 mmol, 90%) ^1H NMR (400 MHz, CD_3CN) δ 8.69 (ddd, $J = 4.8, 1.8, 1.0$ Hz, 1H, $\text{H}^{\text{A}6}$), 8.60 (s, 1H, $\text{H}^{\text{A}7}$), 8.16 (dt, $J = 7.9, 1.1$ Hz, 1H, $\text{H}^{\text{A}3}$), 7.90-

7.85 (m, 1H, H^{A4}), 7.44 (ddd, $J = 7.5, 4.8, 1.2$ Hz, 1H, H^{A5}), 7.30 – 7.19 (m, 4H, H^{B2+B3}), 2.37 (s, 3H, H^{CH3}).

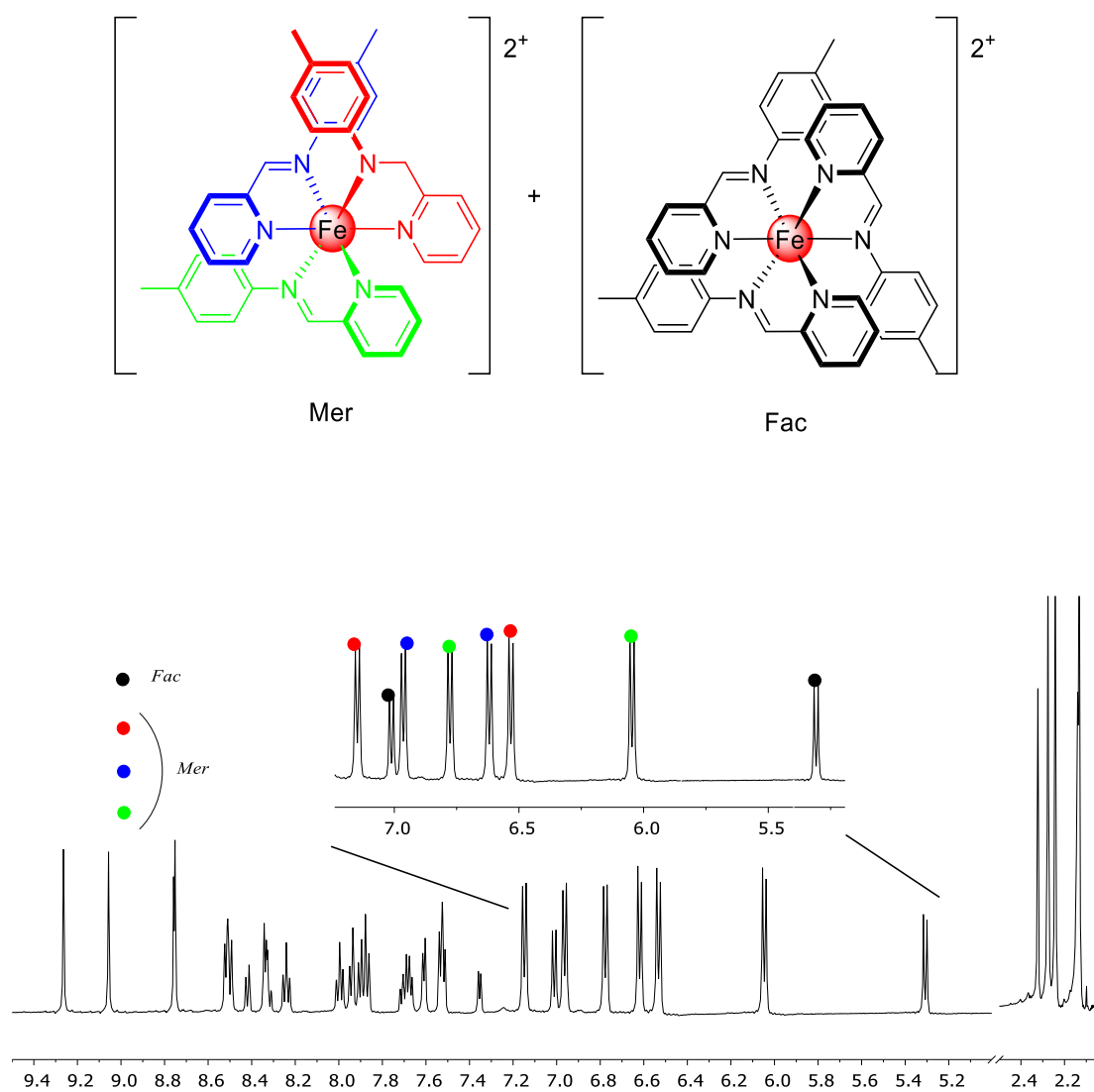


Figure 7.38 ^1H NMR spectrum (400 MHz, CD_3CN) of model complex $[\text{Fe}(\mathbf{2.7})_3]^{2+}$ with expansion of the tolyl ring signals.

7.8 UV-Vis spectra of helicates $[\text{Fe}_2(\text{L})_3]^{4+}$ and model complex $[\text{Fe}(\mathbf{2.7})_3]^{2+}$

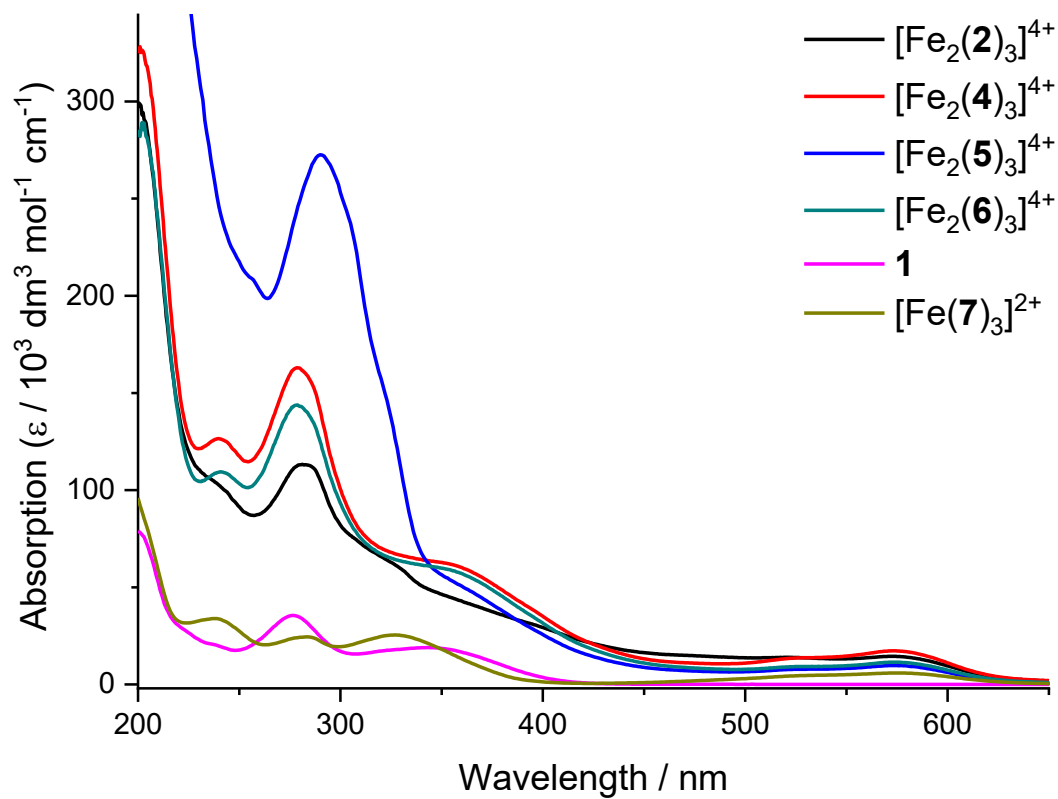


Figure 7.39 UV-Vis spectra (MeCN, 298K) of helicates $[\text{Fe}_2(\text{L})_3]^{4+}$ ($\text{L} = \mathbf{2.2}, \mathbf{2.4-6}$) and model complex $[\text{Fe}(\mathbf{2.7})_3]^{2+}$ measured at $8.3, 7.8, 5.3, 1.0$ and $16.0 \times 10^{-6} \text{ mol L}^{-1}$ respectively.

7.9 ^1H NMR monitoring self-assembly

7.9.1 *In situ* monitoring of $[\text{Fe}_2(\mathbf{2.2})_3]^{4+}$ formation in $\text{DMF-}d_7$ (cube stoichiometry)

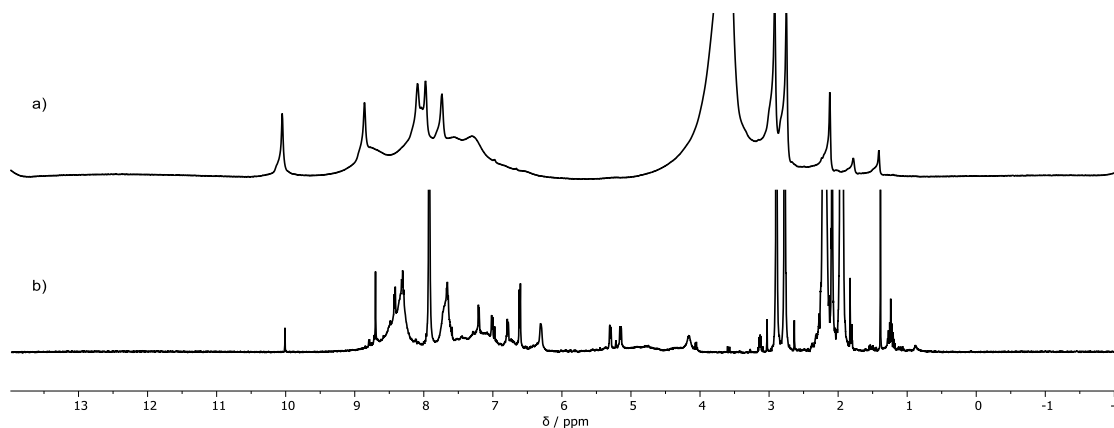


Figure 7.40 ^1H NMR spectra (500 MHz, 298 K) of 15 μmol tetraamine **2.1**, 61 μmol 2-pyridinecarboxaldehyde and 20 μmol $\text{FeCl}_2 \cdot 4\text{H}_2\text{O}$ combined in $\text{DMF-}d_7$. a) immediately after combination and (b) after 24 at room temperature, then aqueous workup.

7.9.2 *In situ* monitoring of $[\text{Fe}_2(\mathbf{2.2})_3]^{4+}$ formation in $\text{DMF-}d_7$ (helicate stoichiometry)

Tetraamine **2.1** (8 mg, 20 μmol), 2-pyridylcarboxaldehyde (4 μL , 4 mg, 41 μmol) and $\text{Fe}(\text{BF}_4)_2 \cdot 6\text{H}_2\text{O}$ (5 mg, 14 μmol) were combined in $\text{DMF-}d_7$ (500 μL) in an NMR tube and thoroughly mixed. After 32 hours the sample was added to a saturated aqueous solution of KPF_6 (5 mL), resulting in the formation of a purple precipitate. The solid was collected on Celite and washed with water (3 x 5 mL), DCM (2 x 5 mL) and Et_2O (2 x 5 mL). The solid was dissolved in acetonitrile and the solvent removed under reduced pressure to give $[\text{Fe}_2(\mathbf{2.2})_3](\text{PF}_6)_4$.

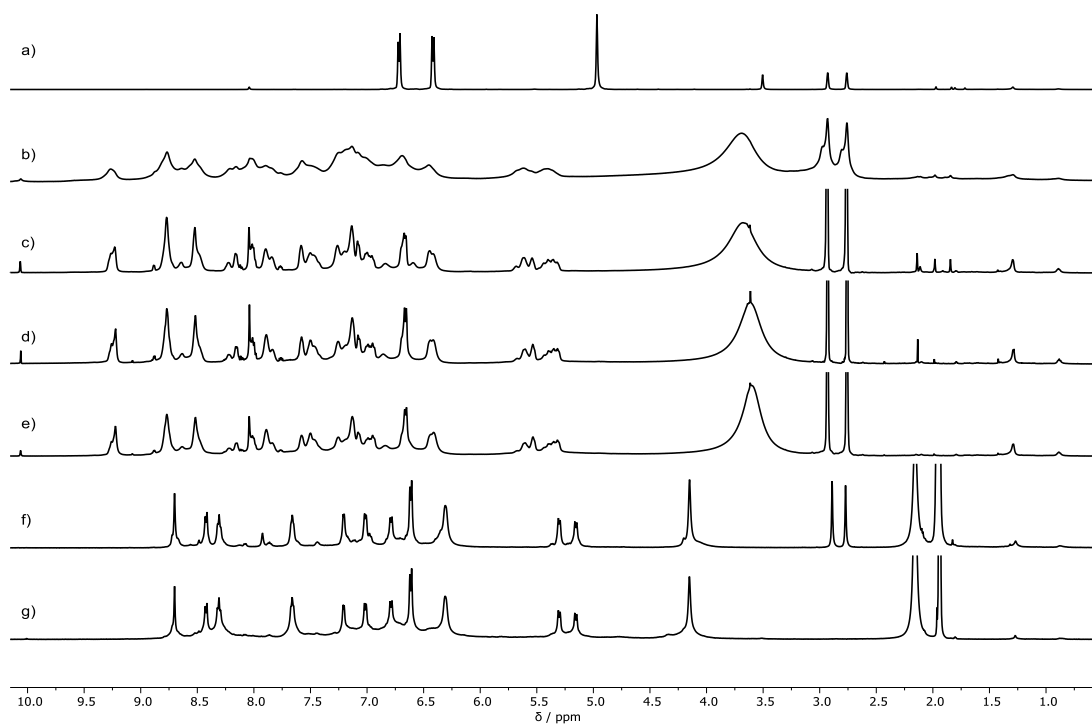


Figure 7.41 ^1H NMR spectra (500 MHz, 298 K) of tetraamine **2.1**, 2-pyridinecarboxaldehyde and $\text{Fe}(\text{BF}_4)_2 \cdot 6\text{H}_2\text{O}$ combined in $\text{DMF-}d_7$. a) **2.1**; b) Combined **2.1**, 2-pyridylcarboxaldehyde and $\text{Fe}(\text{BF}_4)_2 \cdot 6\text{H}_2\text{O}$ as described above. Reaction mixture at 298 K after c) 15 min, d) 24h, e) 32h. f) After aqueous work-up of reaction mixture and redissolving in CD_3CN and g) authentic sample of $[\text{Fe}_2(\mathbf{2.2})_3]^{4+}$ in CD_3CN .

7.9.3 *In situ* monitoring of $[\text{Fe}_2(2.2)_3]^{4+}$ formation in $\text{DMF-}d_7$ (cube stoichiometry)

Tetraamine **2.1** (8 mg, 20 μmol), 2-pyridylcarboxaldehyde (8 μL , 9 mg, 82 μmol) and $\text{Fe}(\text{BF}_4)_2 \cdot 6\text{H}_2\text{O}$ (9 mg, 27 μmol) were combined in $\text{DMF-}d_7$ (500 μL) in an NMR tube and thoroughly mixed. The reaction was monitored by ^1H NMR spectroscopy.

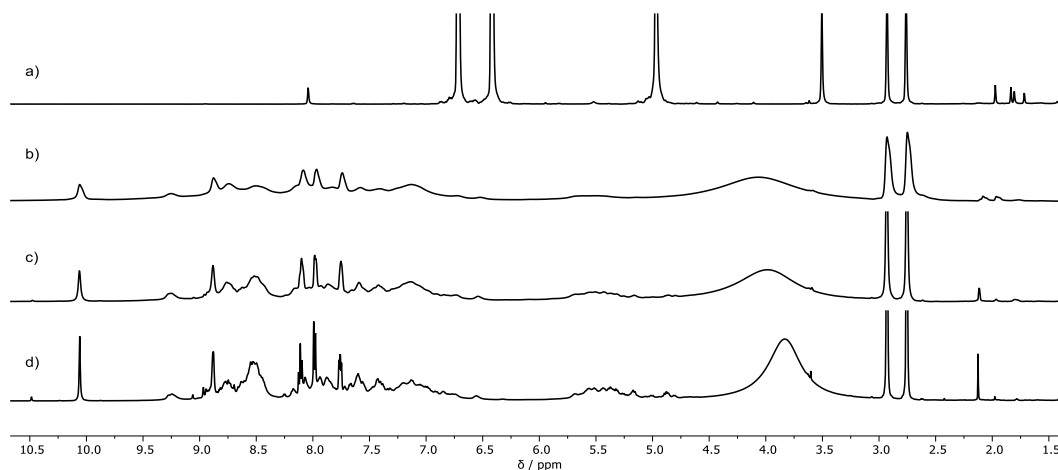


Figure 7.42 ^1H NMR spectra (500 MHz, 298 K) of tetraamine **2.1**, 2-pyridinecarboxaldehyde and $\text{Fe}(\text{BF}_4)_2 \cdot 6\text{H}_2\text{O}$ combined in $\text{DMF-}d_7$. a) **2.1**; b) Combined **2.1**, 2-pyridylcarboxaldehyde and $\text{Fe}(\text{BF}_4)_2 \cdot 6\text{H}_2\text{O}$ as described above. Reaction mixture at 298 K after c) 1h and d) 22h.

7.9.4 *In situ* monitoring of $[\text{Fe}_2(2.2)_3]^{4+}$ formation in CD_3CN (cube stoichiometry)

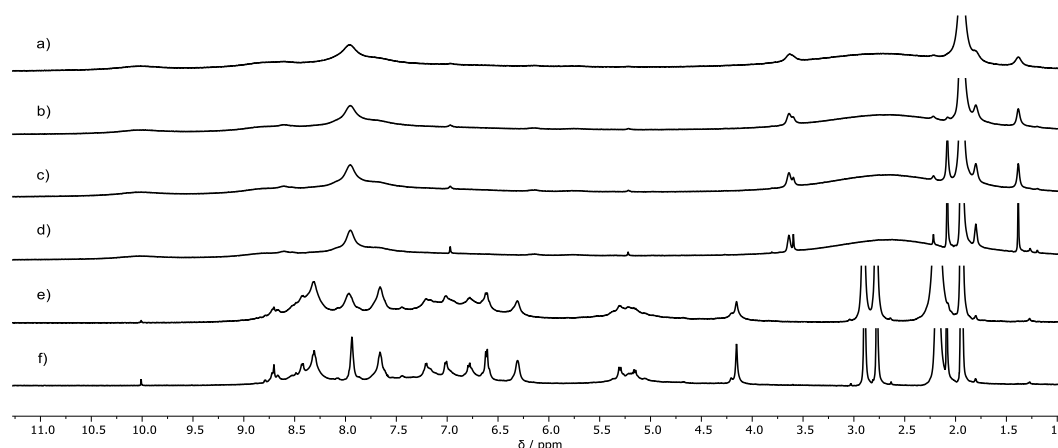


Figure 7.43 ^1H NMR spectrum (CD_3CN , 298 K, 500 MHz) of 20 μmol $\text{Fe}(\text{BF}_4)_2 \cdot 4\text{H}_2\text{O}$ and 15 μmol tetraamine **2.1** and 61 μmol 2-pyridinecarboxaldehyde in 0.7 mL CD_3CN at room

temperature after (a) immediately after addition; (b) 3h, (c) 16h (d) 18h, (e) after aqueous workup, (f) sample (e) after 3 days stored at room temperature.

7.9.5 In situ monitoring of $[\text{Fe}_2(\mathbf{2.2})_3]^{4+}$ formation in CD_3CN (helicate stoichiometry)

Tetraamine **2.1** (8 mg, 20 μmol), 2-pyridylcarboxaldehyde (4 μL , 4 mg, 41 μmol) and $\text{Fe}(\text{NTf}_2)_2 \cdot 4\text{H}_2\text{O}$ (8 mg, 14 μmol) were combined in CD_3CN (500 μL) in an NMR tube, thoroughly mixed and heated at 50 $^\circ\text{C}$ for 40 hours with monitoring by ^1H NMR spectroscopy. After 40 hours the sample was added to a saturated aqueous solution of KPF_6 (10 mL), resulting in the formation of a purple precipitate. The solid was collected on Celite and washed with water (2 x 10 mL), EtOH (2 x 10 mL) and Et_2O (2 x 10 mL). The solid was dissolved in acetonitrile and the solvent removed under reduced pressure to give $[\text{Fe}_2(\mathbf{2.2})_3](\text{PF}_6)_4$.

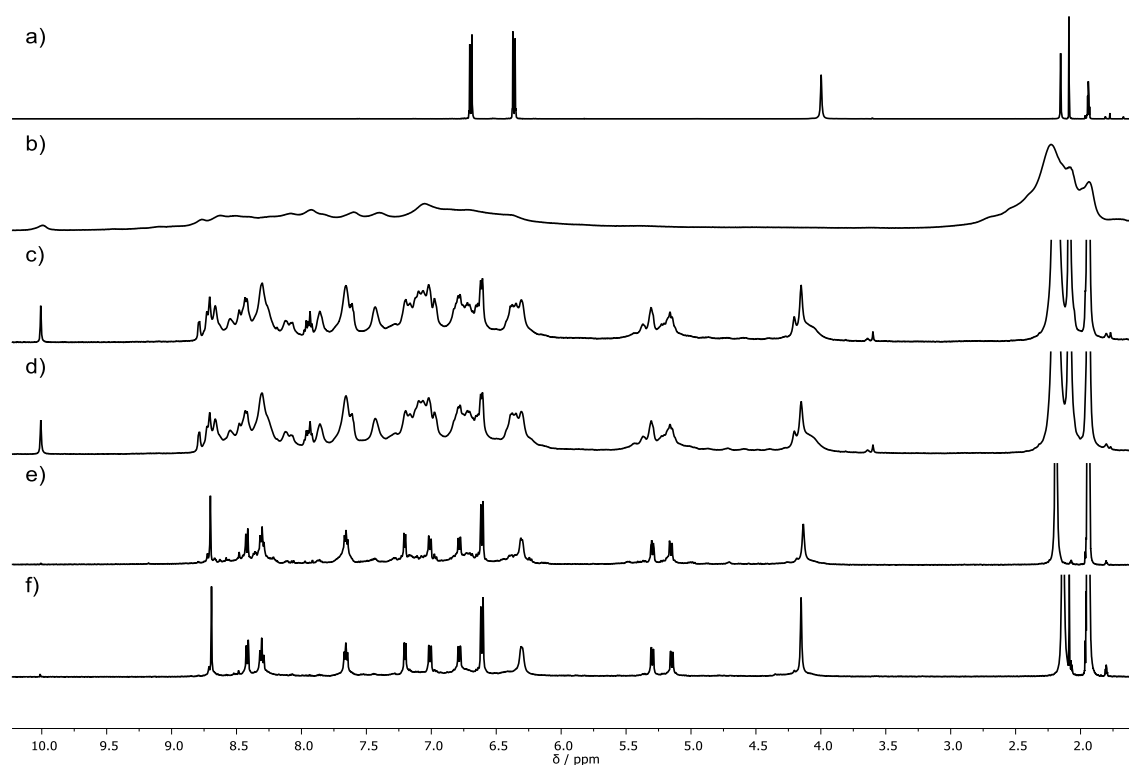


Figure 7.44 ^1H NMR spectra (500 MHz, 298 K) of tetraamine **2.1**, 2-pyridinecarboxaldehyde and $\text{Fe}(\text{NTf}_2)_2 \cdot 4.5\text{H}_2\text{O}$ combined in CD_3CN . a) **2.1**; b) Combined **2.1**, 2-pyridylcarboxaldehyde and $\text{Fe}(\text{NTf}_2)_2 \cdot 4.5\text{H}_2\text{O}$ as described above. Reaction mixture measured at 298 K after heating at 323 K for c) 20h, d) 40h. e) After aqueous work-up of reaction mixture and redissolving in CD_3CN . f) Authentic sample of $[\text{Fe}_2(\mathbf{2.2})_3]^{4+}$ in CD_3CN .

7.9.6 *In situ* monitoring of $[\text{Fe}_8(\mathbf{2.3})_6]^{16+}$ formation in CD_3CN (cube stoichiometry)

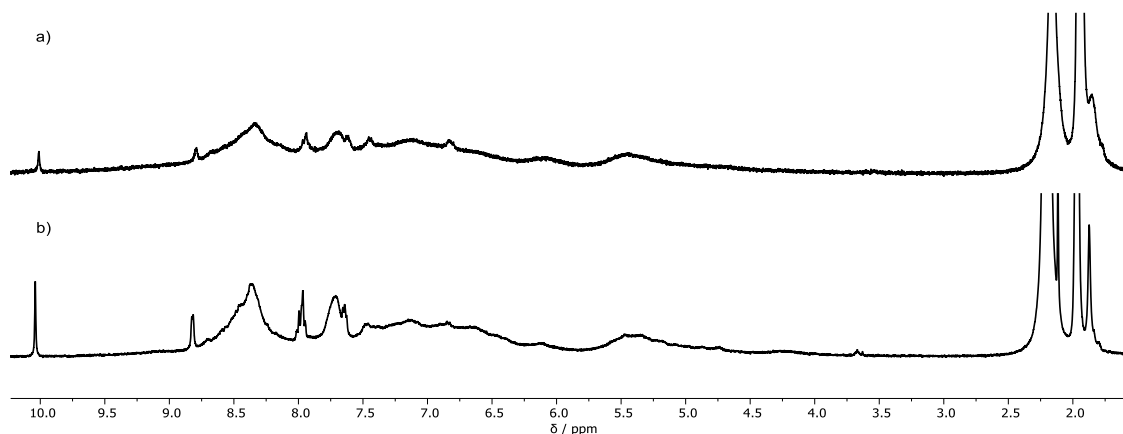


Figure 7.45 ^1H NMR spectrum (CD_3CN , 298 K, 400 MHz) of 9 μmol $\text{Fe}(\text{NTf}_2)_2 \cdot 4\text{H}_2\text{O}$ and 7 μmol tetraimine **2.3** and 0.7 mL CD_3CN at room temperature after (a) immediately after addition; (b) 24h.

7.10 Synthesis of $[\text{Fe}_8(\mathbf{2.3})_6](\text{NTf}_2)_{16}$ cube

$\text{Fe}(\text{NTf}_2)_2$ (22 mg, 36 μmol) was added to a suspension of **2.3** (20 mg, 27 μmol) in dry acetonitrile, leading to the immediate formation of a burnt orange colour. The reaction was then heated at 50 $^\circ\text{C}$ for 7 days, causing a colour change to dark purple. The reaction was monitored by ^1H NMR (the solvent was removed from aliquots under reduced pressure and the solid was re-dissolved in CD_3CN), shown below. After 7 days of heating at 50 $^\circ\text{C}$ the sample was added to a saturated aqueous solution of KPF_6 (10 mL), resulting in the formation of a purple precipitate. The solid was collected on Celite and washed with water (2 x 10 mL), EtOH (2 x 10 mL) and Et_2O (2 x 10 mL). The solid was dissolved in acetonitrile and the solvent removed under reduced pressure to give a purple powder (18 mg, 7.5 μmol , 54%). The ^1H NMR spectrum is consistent with isolation of the $[\text{Fe}_2(\mathbf{2.2})_3](\text{PF}_6)_4$ helicate as the major product.

7.11 Behavior of $[\text{Fe}_2(\mathbf{2.2})_3](\text{PF}_6)_4$, $[\text{Fe}_2(\mathbf{2.4})_3](\text{PF}_6)_4$ and $[\text{Fe}_2(\mathbf{2.5})_3](\text{PF}_6)_4$ in $\text{DMSO-}d_6$

Helicates $[\text{Fe}_2(\mathbf{2.4})_3](\text{PF}_6)_4$ and $[\text{Fe}_2(\mathbf{2.5})_3](\text{PF}_6)_2$ were found to be unstable in $\text{DMSO-}d_6$ solutions, over time re-arranging to form smaller, presumably monomeric, species. Helicate $[\text{Fe}_2(\mathbf{2.2})_3](\text{PF}_6)_4$ also showed the formation of other species, however no rearrangement was seen over time

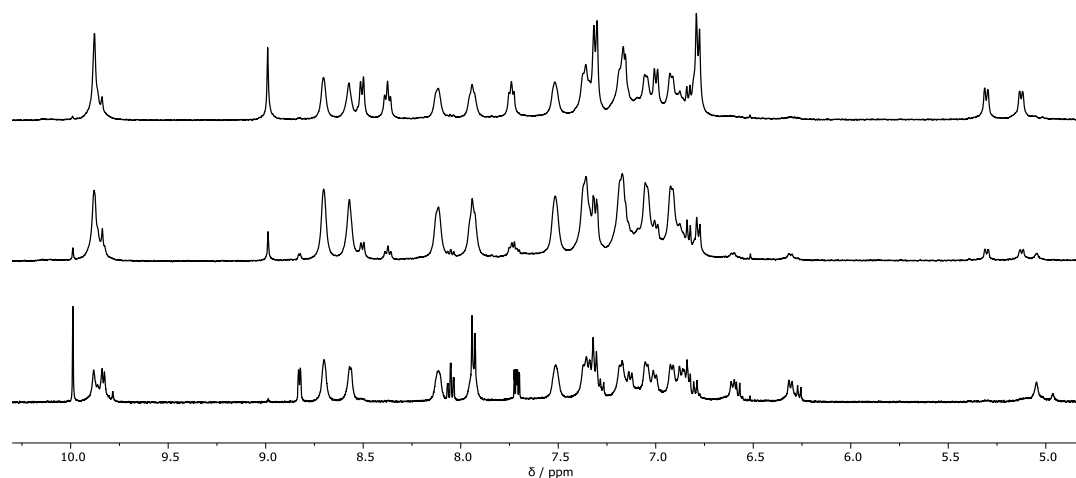


Figure 7.46 ^1H NMR (500 MHz, $\text{DMSO-}d_6$) of $[\text{Fe}_2(\mathbf{2.4})_3](\text{PF}_6)_4$ monitored at room temperature. $[\text{Fe}_2(\mathbf{2.4})_3](\text{PF}_6)_4$ in $\text{DMSO-}d_6$ (top); after 2 h (middle) and after 4 days (bottom).

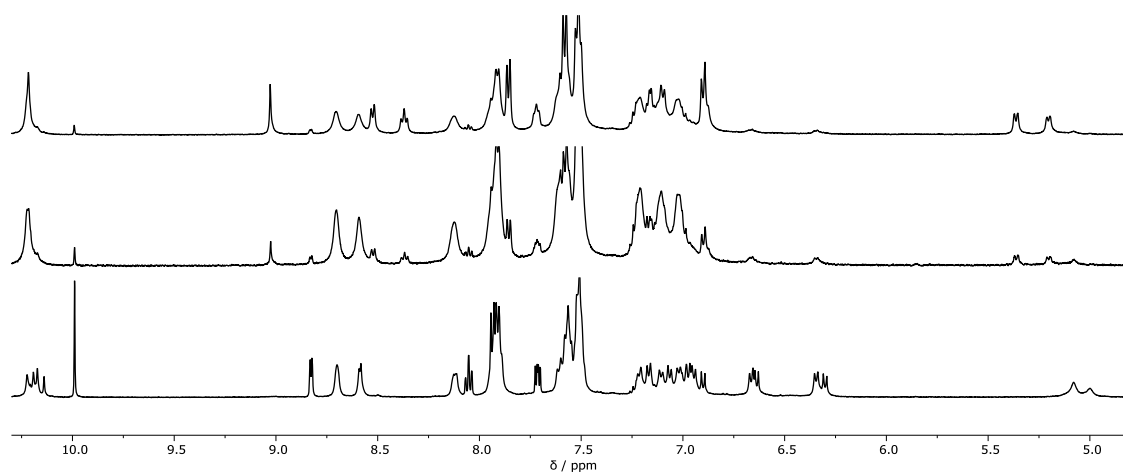
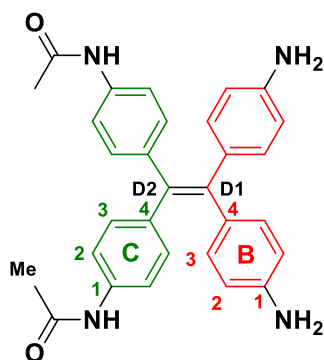


Figure 7.47 ^1H NMR (500 MHz, $\text{DMSO-}d_6$) of $[\text{Fe}_2(\mathbf{2.5})_3](\text{PF}_6)_4$ monitored at room temperature after a) 5 mins, b) 1h, c) 76 days.

7.12 Isolation of selectively functionalized tetraphenylethene units

7.12.1 Isolation of tetraphenylethene unit **2.8**



Tris(2-aminoethyl)amine (19 μL , 19 mg, 125 μmol) was added to a solution of $[\text{Fe}_2(\mathbf{2.5})_3](\text{PF}_6)_4$ (60 mg, 23 μmol) in CH_3CN (10 mL). The solution was then stirred for 20 h before being diluted into 100 mL diethyl ether. The ethereal layer was separated and washed with water (3 x 80 mL) and brine (80 mL) before the solvent was removed under reduced pressure to give crude **2.8**. The crude material was columned on silica that was deactivated with triethylamine using EtOAc/MeCN (1:1) to give a yellow solid (6 mg, 12 μmol , 53%). ^1H NMR (600 MHz, $\text{DMSO-}d_6$) δ 9.79 (s, 2H, -NH), 7.28 (d, $J = 8.6$ Hz, 4H, $\text{H}^{\text{C}2}$), 6.80 (d, $J = 8.6$ Hz, 4H, $\text{H}^{\text{C}3}$), 6.58 (d, $J = 8.5$ Hz, 4H, $\text{H}^{\text{B}3}$), 6.27 (d, $J = 8.5$ Hz, 4H, $\text{H}^{\text{B}2}$), 4.97 (s, 4H, - NH_2), 1.99 (s, 6H, Me). $^{13}\text{C}\{^1\text{H}\}$ NMR (151 MHz, DMSO) δ 168.0 (C=O), 146.9 ($\text{C}^{\text{B}1}$), 140.8 ($\text{C}^{\text{D}1}$), 139.7 ($\text{C}^{\text{C}4}$), 136.7 ($\text{C}^{\text{C}1}$), 134.7 ($\text{C}^{\text{D}2}$), 131.8 ($\text{C}^{\text{B}3}$), 131.4 ($\text{C}^{\text{B}4}$), 131.2 ($\text{C}^{\text{C}3}$), 118.2 ($\text{C}^{\text{C}2}$), 113.1 ($\text{C}^{\text{B}2}$), 23.9 (C^{Me}). UV-Vis: THF, $\lambda_{\text{max}}/\text{nm}$ ($\epsilon / 10^3 \text{ dm}^3 \text{ mol}^{-1} \text{ cm}^{-1}$) 277 (29), 356 (15). ESI-MS 477.25 [**2.8**+H] $^+$ required 477.23 m/z .

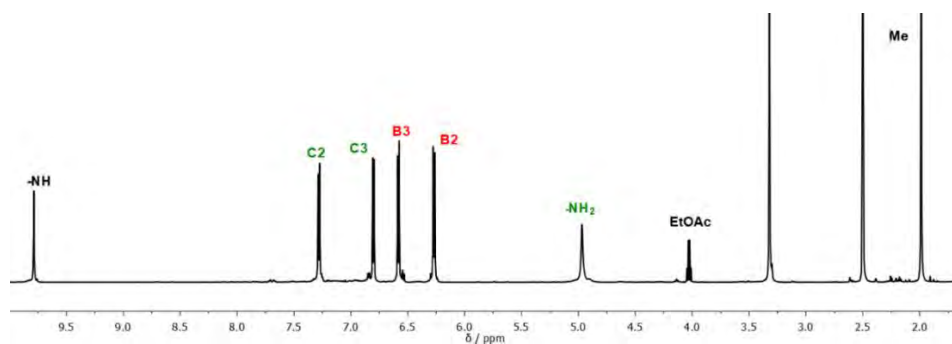


Figure 7.48 ^1H NMR (600 MHz, $\text{DMSO-}d_6$, 298K) of compound **2.8**.

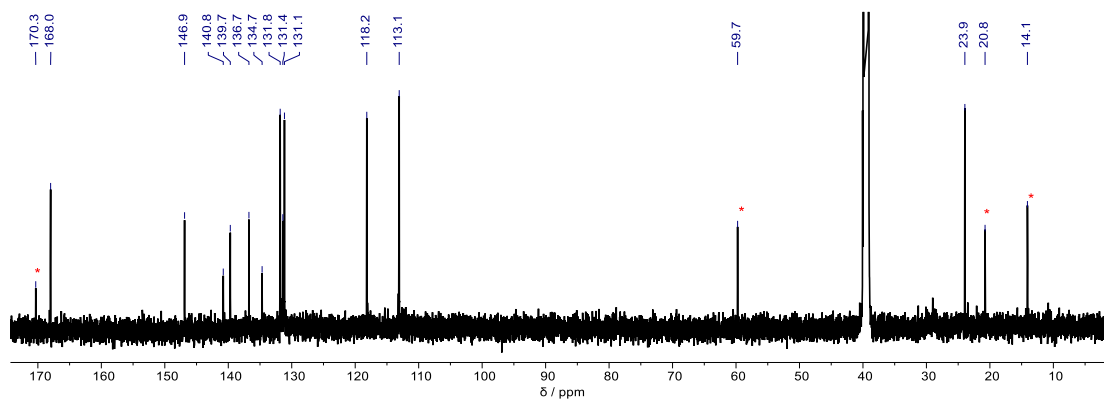


Figure 7.49 $^{13}\text{C}\{^1\text{H}\}$ NMR (151 MHz, $\text{DMSO-}d_6$, 298K) of compound **2.8**. Ethyl acetate impurities are shown with *.

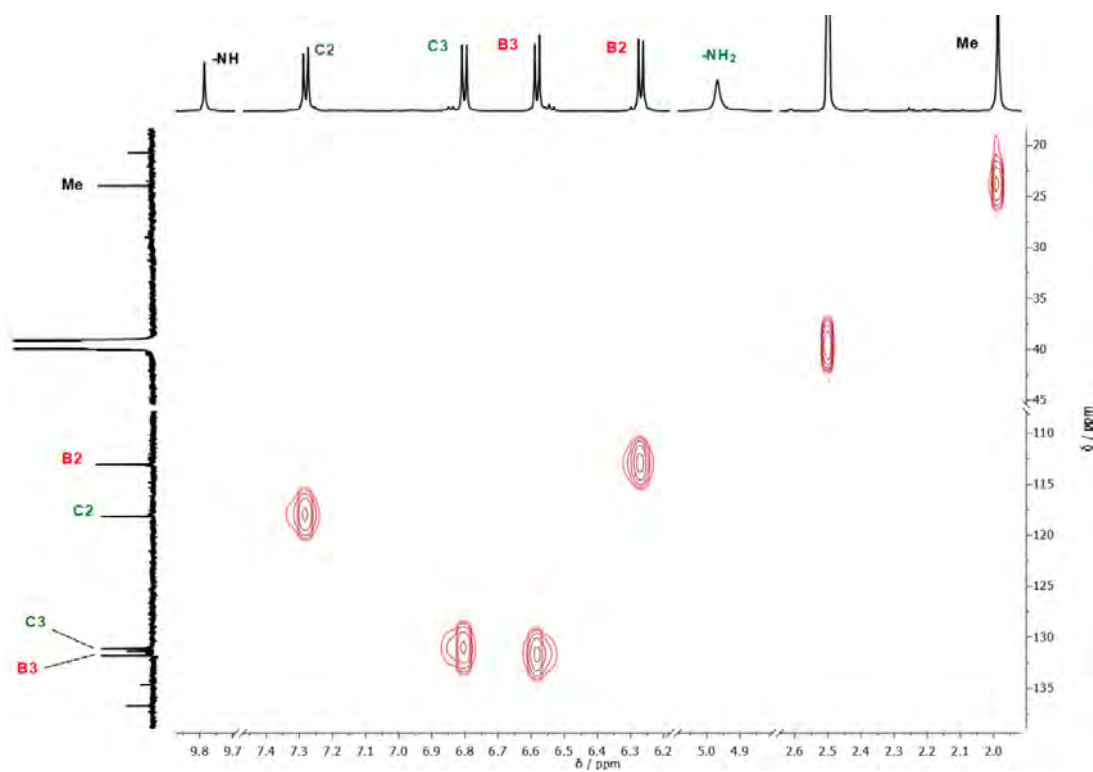


Figure 7.50 $^1\text{H-}^{13}\text{C}$ HSQC NMR (600 MHz, $\text{DMSO-}d_6$, 298K) of compound **2.8**.

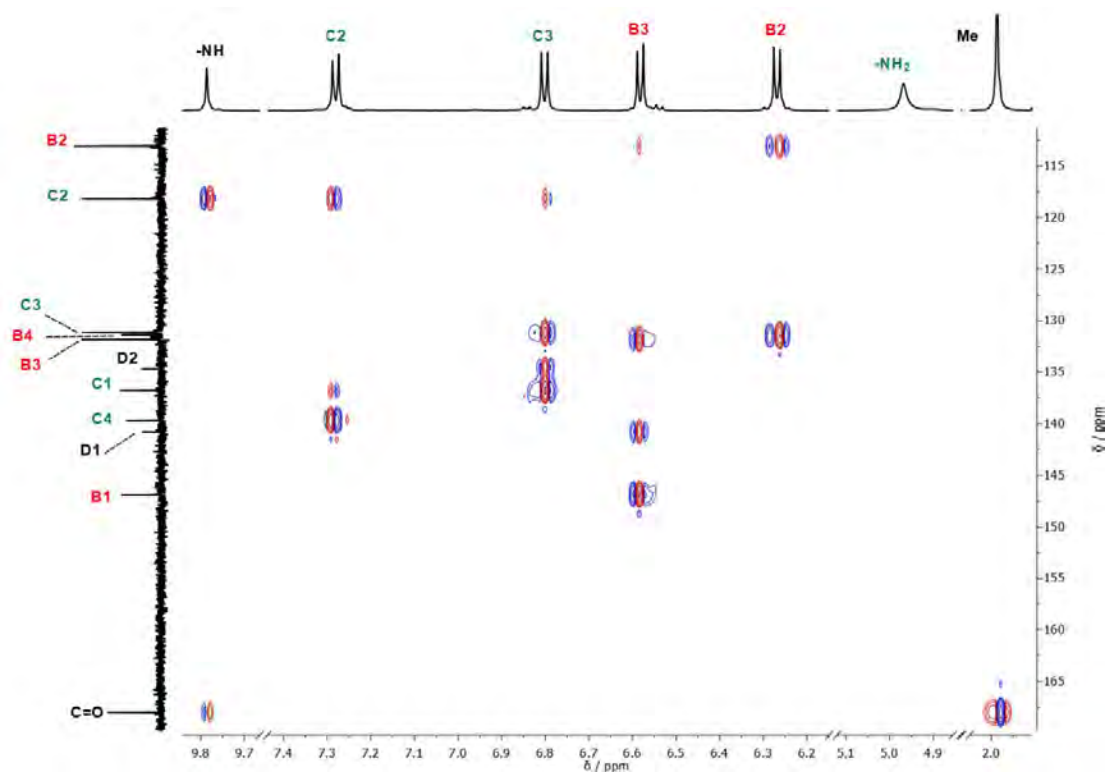
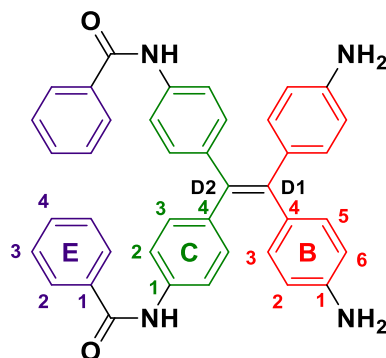


Figure 7.51 ^1H - ^{13}C HMBC NMR (600 MHz, DMSO- d_6 , 298K) of compound 2.8

7.12.2 Isolation of tetraphenylethene unit 2.9



Compound **2.9** was isolated by the same procedure as for compound **2.8**. Crude product was columned on deactivated silica using EtOAc/Hexanes (4:1) to give a pale yellow solid (7 mg, 12 μmol , 50%) ^1H NMR (600 MHz, $\text{DMSO-}d_6$) δ 10.14 (s, 2H, -NH), 7.95-7.86 (m, 4H, $\text{H}^{\text{E}2}$), 7.59 – 7.55 (m, 2H, $\text{H}^{\text{E}4}$), 7.54- 7.49 (m, 8H, $\text{H}^{\text{E}3+\text{C}2}$), 6.91 (d, $J = 8.7$ Hz, 4H, $\text{H}^{\text{C}3}$), 6.64 (d, $J = 8.5$ Hz, 4H, $\text{H}^{\text{B}3}$), 6.30 (d, $J = 8.5$ Hz, 4H, $\text{H}^{\text{B}2}$), 5.00 (s, 4H, - NH_2). $^{13}\text{C}\{^1\text{H}\}$ NMR (151 MHz, DMSO) δ 165.3 (C=O), 147.0 ($\text{C}^{\text{B}1}$), 141.2 ($\text{C}^{\text{D}1}$), 140.4 ($\text{C}^{\text{C}4}$), 136.6 ($\text{C}^{\text{C}1}$), 135.1 ($\text{C}^{\text{E}1}$), 134.6 ($\text{C}^{\text{D}2}$), 131.9 ($\text{C}^{\text{B}3}$), 131.43 ($\text{C}^{\text{B}2}$), 131.39 ($\text{C}^{\text{E}4}$), 131.2 ($\text{C}^{\text{C}3}$), 128.4 ($\text{C}^{\text{E}3}$), 127.6 ($\text{C}^{\text{E}2}$), 119.6 ($\text{C}^{\text{C}2}$), 113.1 ($\text{C}^{\text{B}2}$). ESI-MS 601.33 [**2.9** +H] $^+$ requires 601.26 m/z . UV-vis: THF, λ_{max} /nm ($\epsilon / 10^3 \text{ dm}^3 \text{ mol}^{-1} \text{ cm}^{-1}$) 277 (28), 356 (15).

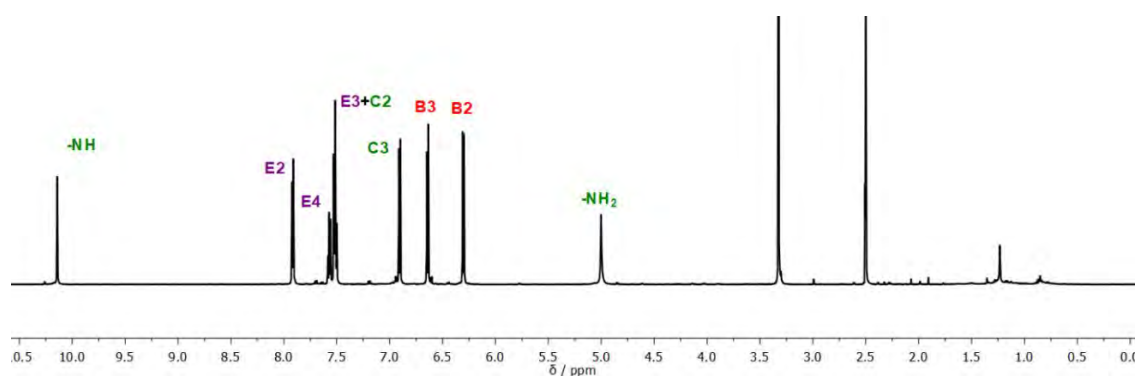


Figure 7.52 ^1H NMR (600 MHz, $\text{DMSO-}d_6$, 298 K) of compound **2.9**.

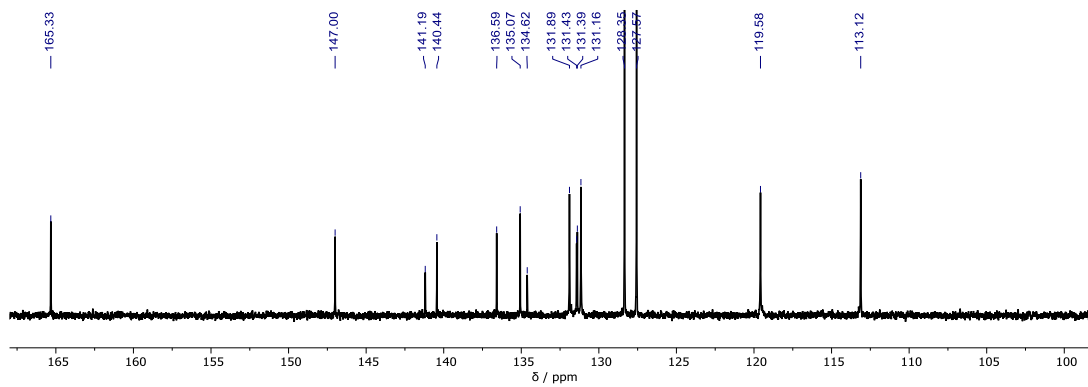


Figure 7.53 $^{13}\text{C}\{^1\text{H}\}$ NMR (101 MHz, $\text{DMSO}-d_6$, 298 K) of compound **2.9**.

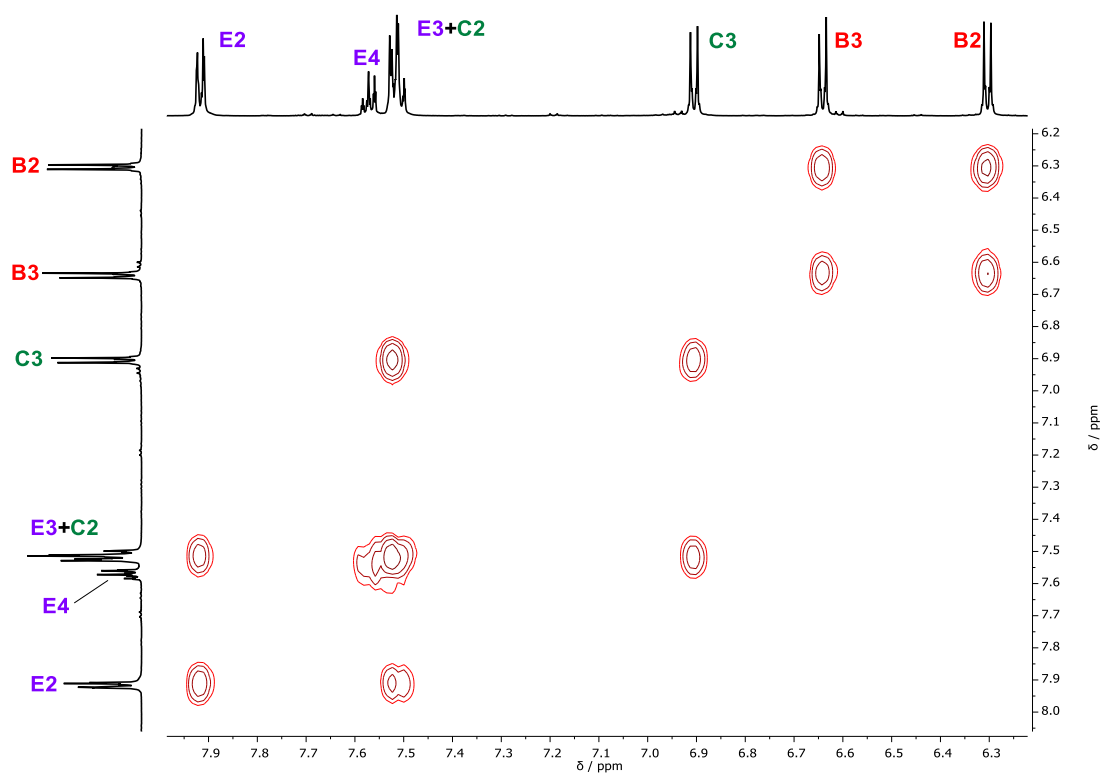


Figure 7.54 $^1\text{H}-^1\text{H}$ COSY NMR (500 MHz, $\text{DMSO}-d_6$, 298 K) of compound **2.9**.

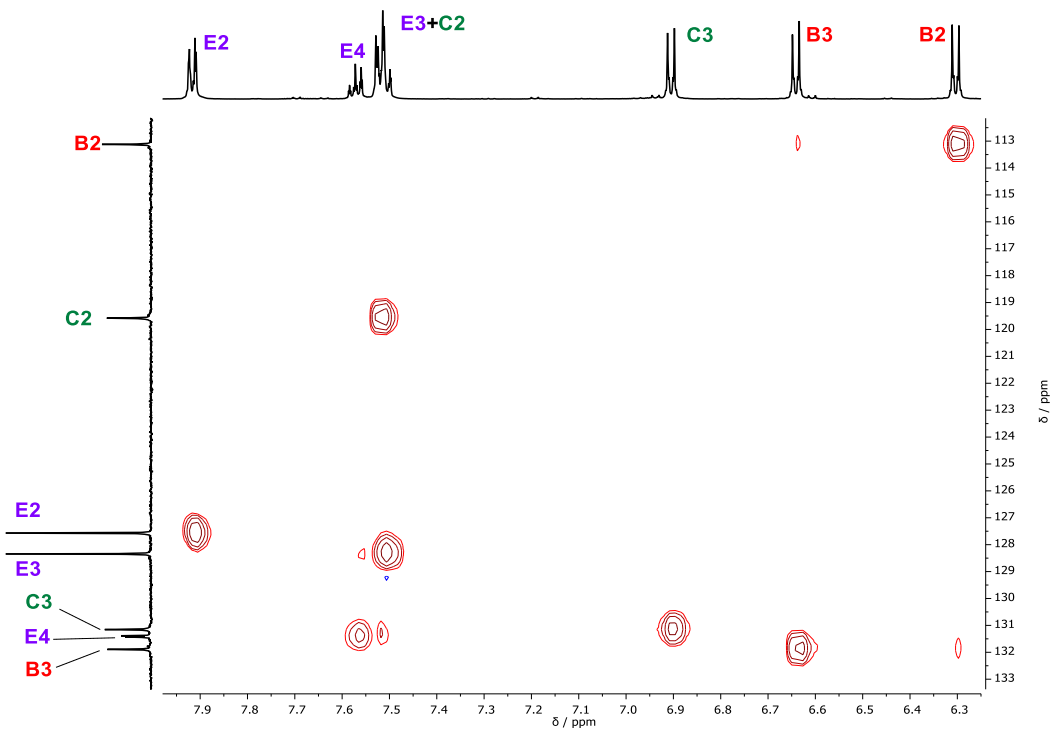


Figure 7.55 ^1H - ^{13}C HSQC NMR (500 MHz, DMSO-d_6 , 298K) of compound **2.9**.

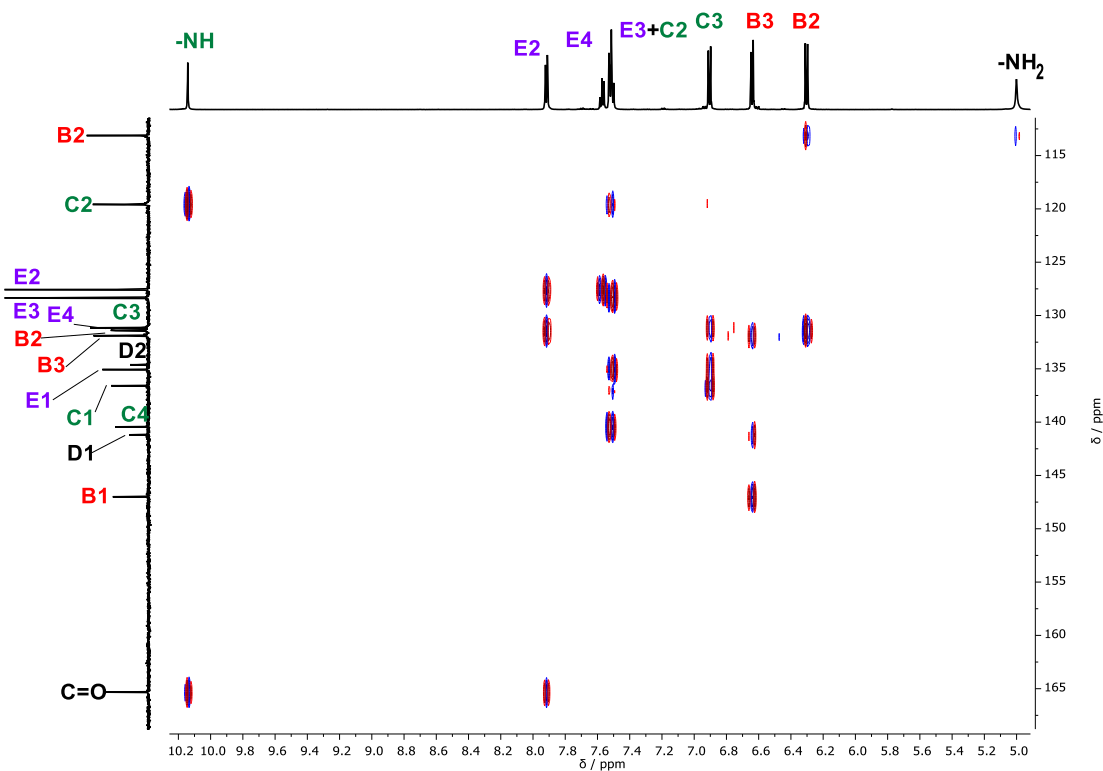


Figure 7.56 ^1H - ^{13}C HMBC NMR (500 MHz, DMSO-d_6 , 298 K) of compound **2.9**.

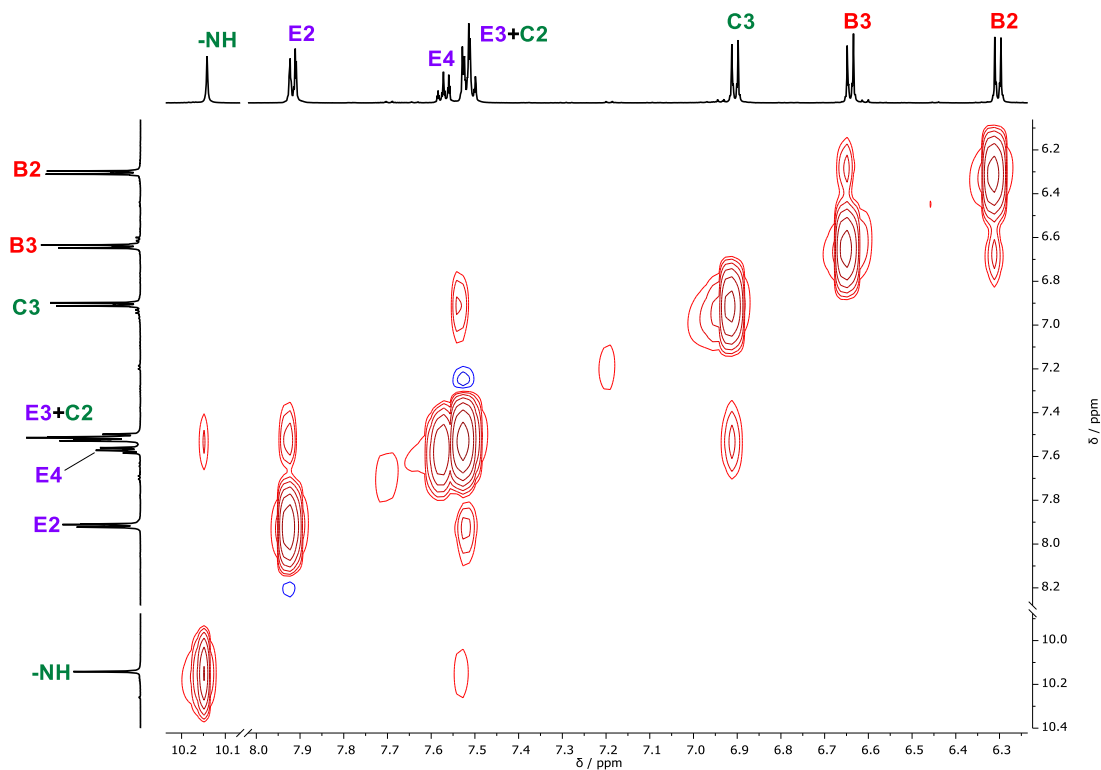
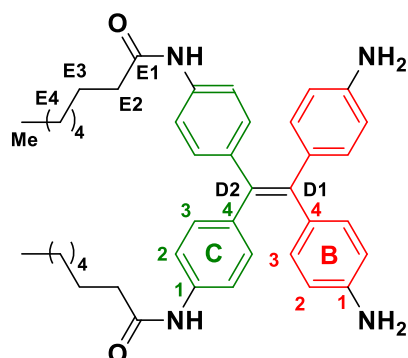


Figure 7.57 ^1H - ^1H NOESY NMR (500 MHz, $\text{DMSO-}d_6$, 298K) of compound **2.9**.

7.12.3 Isolation of tetraphenylethene unit **2.10**



Compound **2.10** was isolated by the same procedure as for compound **2.8**. Crude product was columned on deactivated silica using EtOAc:hexanes (4:1) to give a yellow oil (7 mg, 10 μmol , 86%). ^1H NMR (400 MHz, CDCl_3) δ 7.24 (d, $J = 8.3$ Hz, 4H, $\text{H}^{\text{C}2}$), 7.09 (s, 2H, -NH), 6.94 (d, $J = 8.3$ Hz, 4H, $\text{H}^{\text{C}3}$), 6.80 (d, $J = 8.4$ Hz, 4H, $\text{H}^{\text{B}3}$), 6.40 (d, $J = 8.4$ Hz, 4H, $\text{H}^{\text{B}2}$), 3.56 (s, 2H, - NH_2), 2.30 (t, $J = 7.6$ Hz, 2H, $\text{H}^{\text{E}2}$), 1.75 – 1.64 (m, 2H, $\text{H}^{\text{E}3}$), 1.40 – 1.22 (m, 8H, $\text{H}^{\text{E}4}$), 0.95 – 0.79 (m, 3H, Me). $^{13}\text{C}\{^1\text{H}\}$ NMR (101 MHz, CDCl_3) δ 171.3 (C=O), 144.8 ($\text{C}^{\text{B}1}$), 140.83 ($\text{C}^{\text{D}1}$), 140.78 ($\text{C}^{\text{C}2}$), 136.6 ($\text{C}^{\text{D}2}$), 135.9 ($\text{C}^{\text{C}1}$), 134.7 ($\text{C}^{\text{B}4}$), 132.7 ($\text{C}^{\text{B}3}$), 132.2 ($\text{C}^{\text{C}3}$), 118.9 ($\text{C}^{\text{C}2}$), 114.5 ($\text{C}^{\text{B}2}$), 38.0 ($\text{C}^{\text{E}2}$), 31.8 ($\text{C}^{\text{E}4-7}$), 29.4 ($\text{C}^{\text{E}4-7}$), 29.2 ($\text{C}^{\text{E}4-7}$), 25.8 ($\text{C}^{\text{E}3}$), 22.8 ($\text{C}^{\text{E}4-7}$), 14.2 (C^{Me}). UV-Vis: THF, $\lambda_{\text{max}}/\text{nm}$ ($\epsilon / 10^3 \text{ dm}^3 \text{ mol}^{-1} \text{ cm}^{-1}$) 279 (32), 352 (15). ESI-MS 645.50 [**2.10** + H] $^+$ required 645.42 m/z .

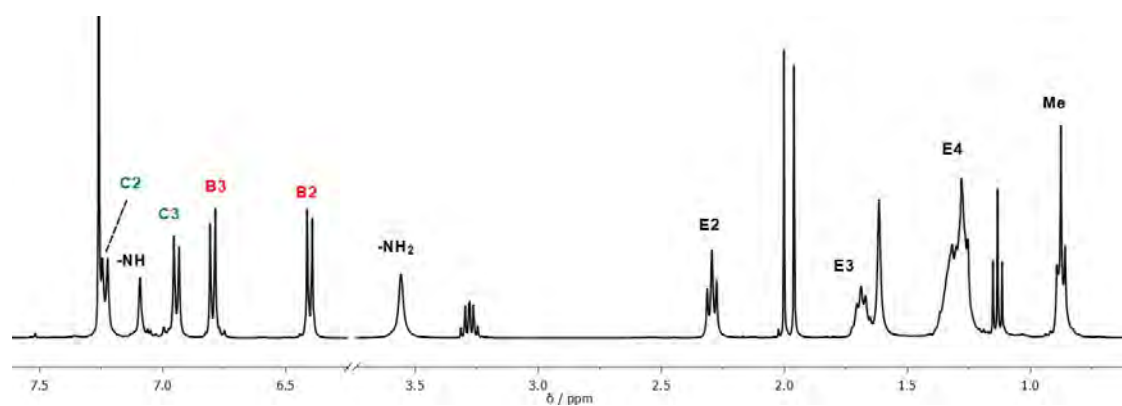


Figure 7.58 ^1H NMR (400 MHz, CDCl_3 , 298K) of compound **2.10**.

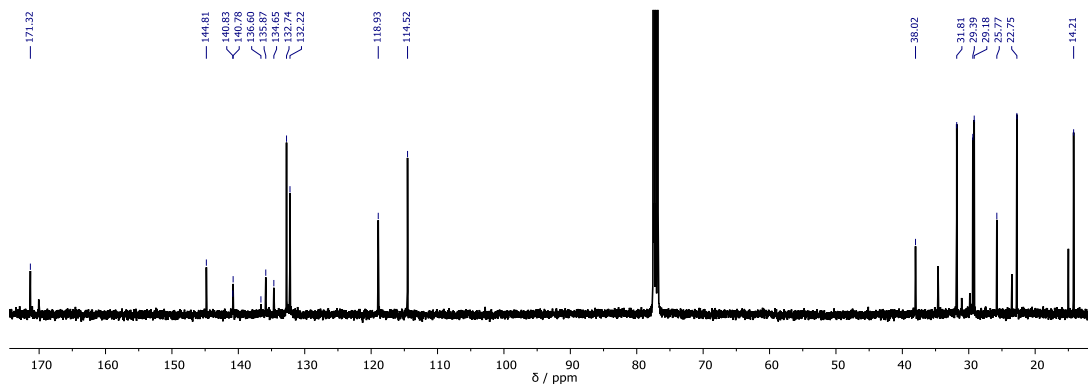


Figure 7.59 $^{13}\text{C}\{^1\text{H}\}$ NMR (101 MHz, CDCl_3 , 298K) of compound **2.10**.

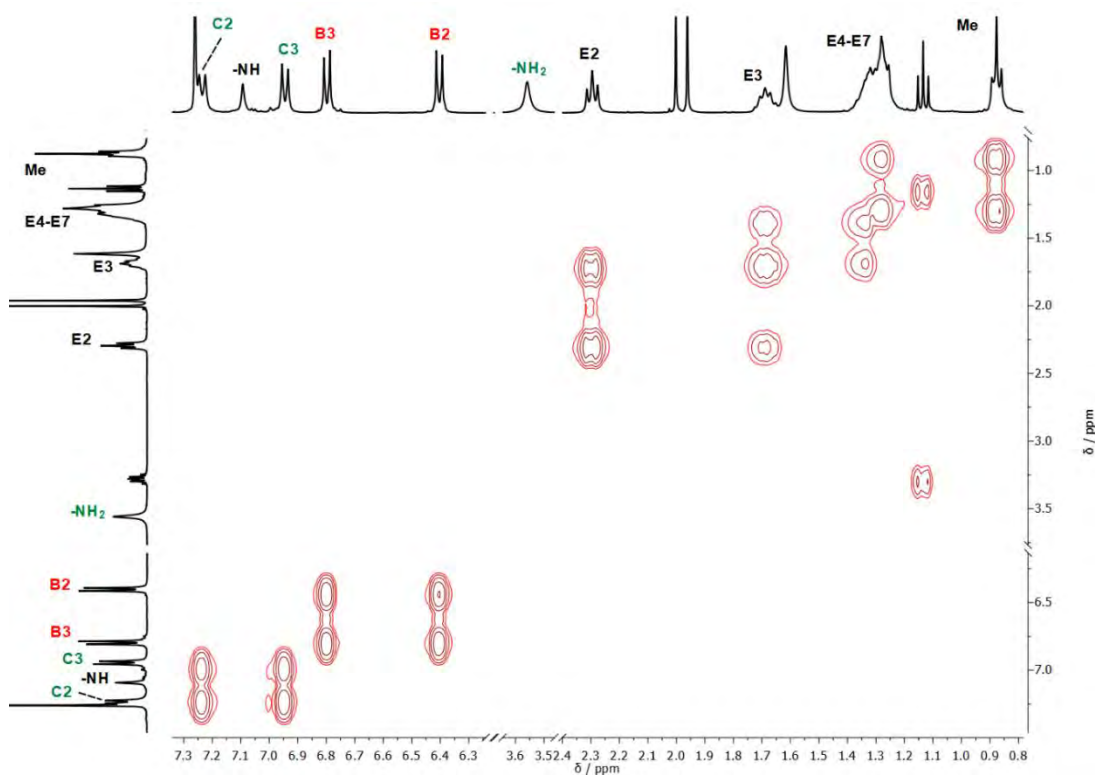


Figure 7.60 $^1\text{H}\text{-}^1\text{H}$ COSY NMR (400 MHz, CDCl_3 , 298K) of compound **2.10**.

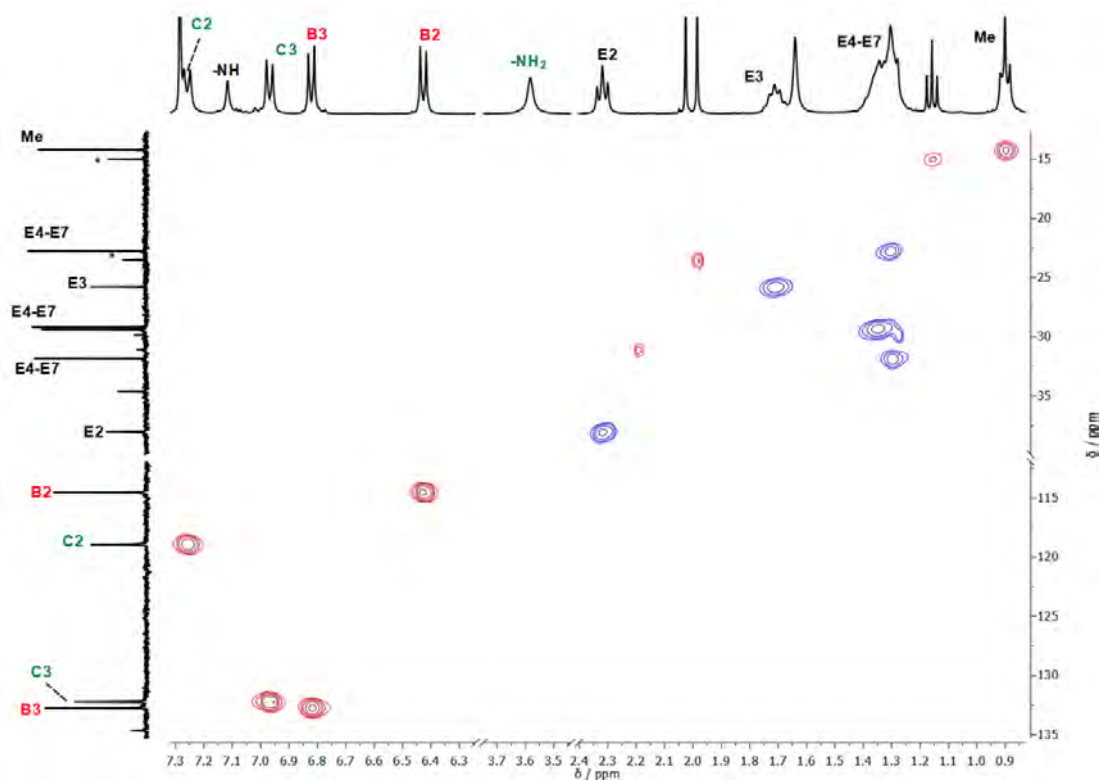


Figure 7.61 ^1H - ^{13}C HSQC NMR (400 MHz, CDCl_3 , 298K) of compound **2.10**.

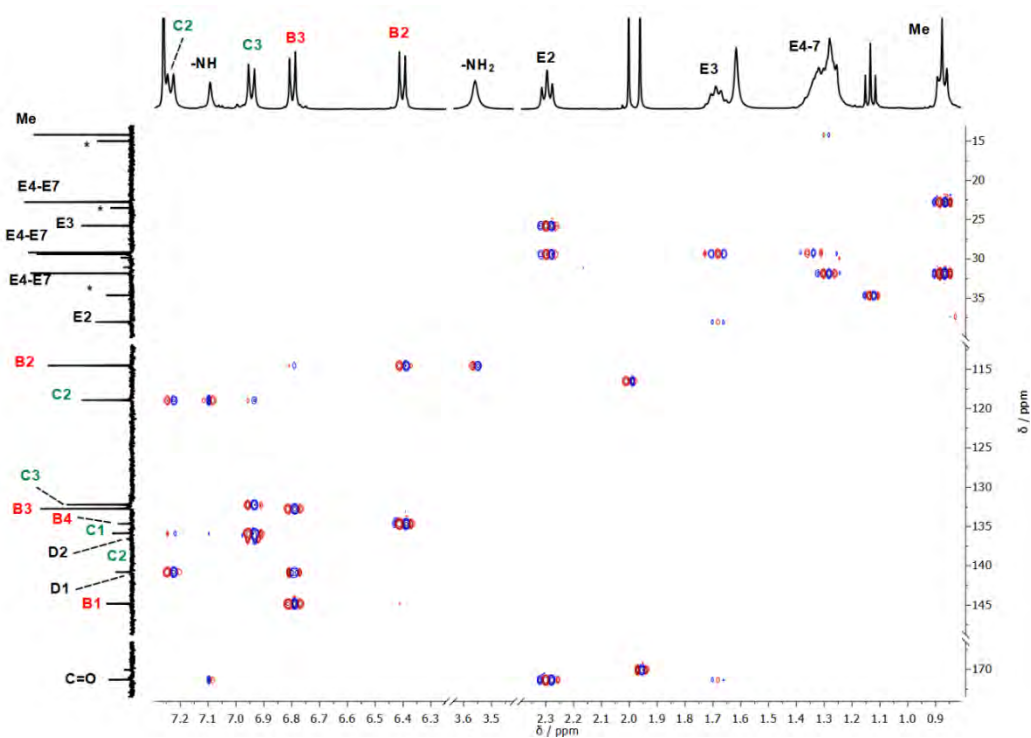
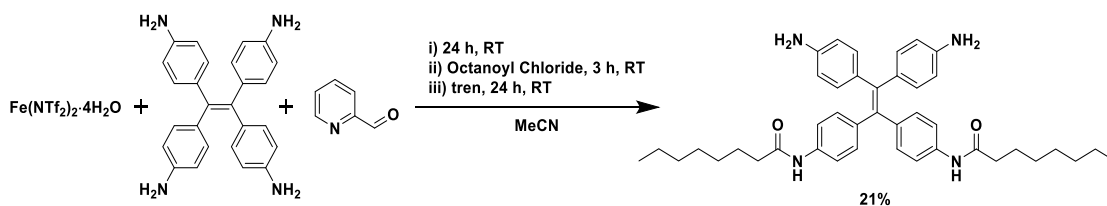


Figure 7.62 ^1H - ^{13}C HMBC NMR (400 MHz, CDCl_3 , 298K) of compound **2.10**.

7.13 One pot synthesis of compound **2.10** from tetraniline **2.1**



Compound **2.1** (40 mg, 102 μmol) and 2-pyridinecarboxaldehyde (21 mg, 19 μL , 200 μmol) were combined in CH_3CN (20 mL) and stirred for 10 minutes. $\text{Fe}(\text{NTf}_2)_2 \cdot 4\text{H}_2\text{O}$ (47 mg, 68 μmol) was then added, leading to the immediate formation of a deep purple-red solution. The reaction mixture was stirred at RT for 24 h, before octanoyl chloride (33 mg, 35 μL , 204 μmol) was added and the resulting mixture stirred at RT for 3h. Tris(2-aminoethyl)amine (24 mg, 25 μL , 170 μmol) was added and the reaction was stirred for a further 24 h, leading to the formation of a purple solution. The solution was diluted with water (50 mL) and extracted with diethyl ether (50 mL). The ethereal layer was washed with saturated aqueous KNO_3 (30 mL), water (2 x 40 mL) and brine (1 x 40 mL). The combined aqueous fraction was washed with diethyl ether (50 mL) and the combined organic fractions were dried over MgSO_4 . The solvent was removed under reduced pressure to give crude **2.10**. The crude product was columned on deactivated silica using EtOAc/Hexanes (50:50 to 100:0 gradient) as an orange solid (14 mg, 21 μmol , 21%). The ^1H NMR spectrum was consistent with that determined above.

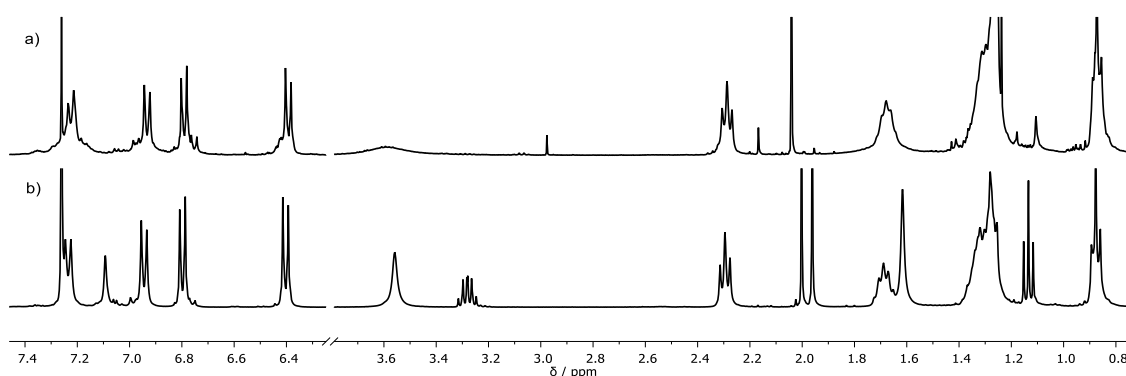


Figure 7.63 Stacked ^1H NMR (400 MHz, CDCl_3 , 298K) of one a) Isolated **2.10** after one-pot reaction; b) Genuine sample of **2.10**.

7.14 Emission behaviour of functionalised TPE units

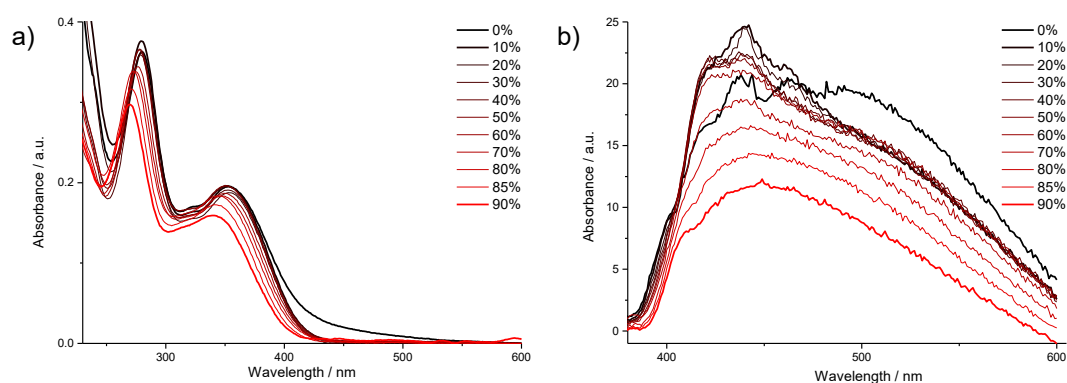


Figure 7.64 Change in emission behavior upon addition of water to a THF solution of TPE **2.1**. Overall concentration was kept constant at 1.7×10^{-5} M. a) UV-Vis absorbance spectra change upon addition of water to **2.1**; b) Emission spectra change ($\lambda_{\text{ex}} = 355$ nm).

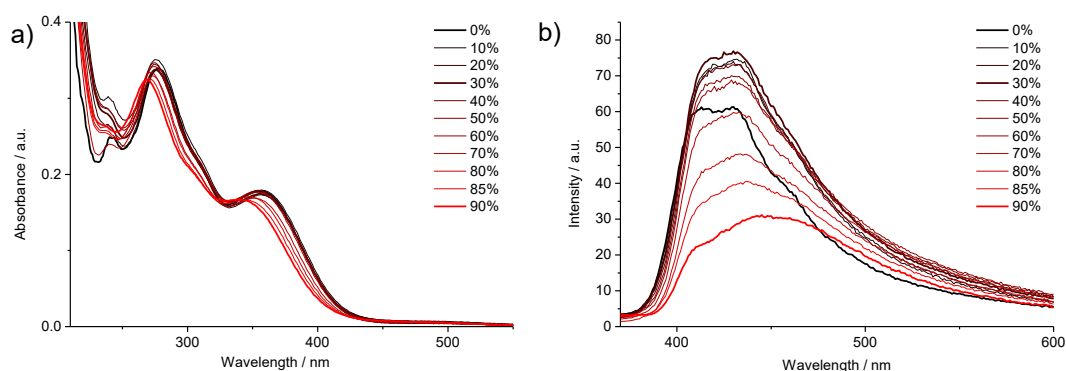


Figure 7.65 Change in emission behavior upon addition of water to a THF solution of TPE **2.8**. Overall concentration was kept constant at 8.4×10^{-6} M. a) UV-Vis absorbance spectra change upon addition of water to **2.8**; b) Emission spectra change ($\lambda_{\text{ex}} = 355$ nm).

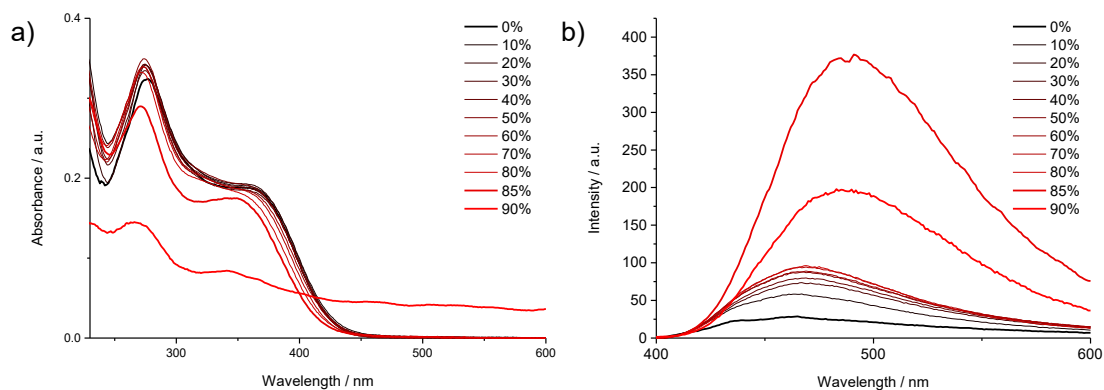


Figure 7.66 Change in emission behavior upon addition of water to a THF solution of TPE **2.9**. Overall concentration was kept constant at 7.7×10^{-6} M. a) UV-Vis absorbance spectra change upon addition of water to **2.9**; b) Emission spectra change ($\lambda_{ex} = 355$ nm).

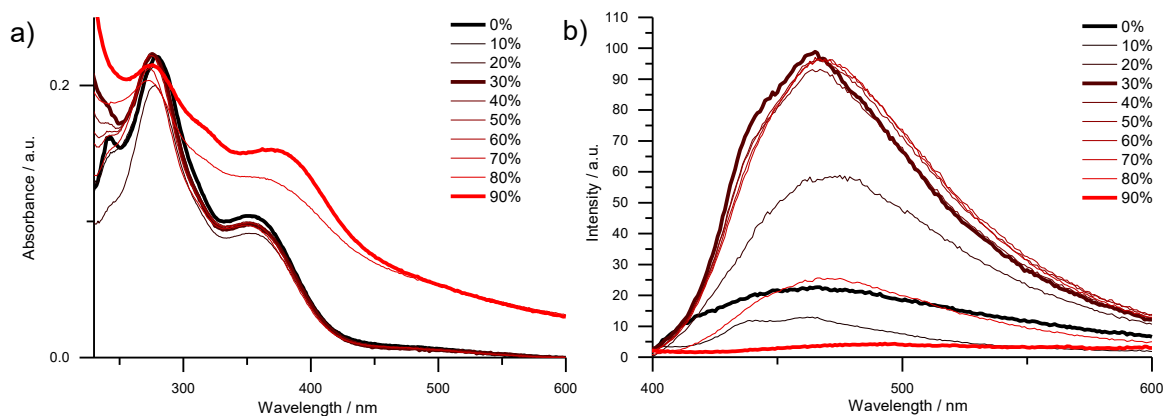


Figure 7.67 Change in emission behavior upon addition of water to a THF solution of TPE **2.10**. Overall concentration was kept constant at 6.8×10^{-6} M. a) UV-Vis absorbance spectra change upon addition of water to **2.10**; b) Emission spectra change ($\lambda_{ex} = 355$ nm).

7.15 Dynamic Light Scattering measurement of compound 2.1.

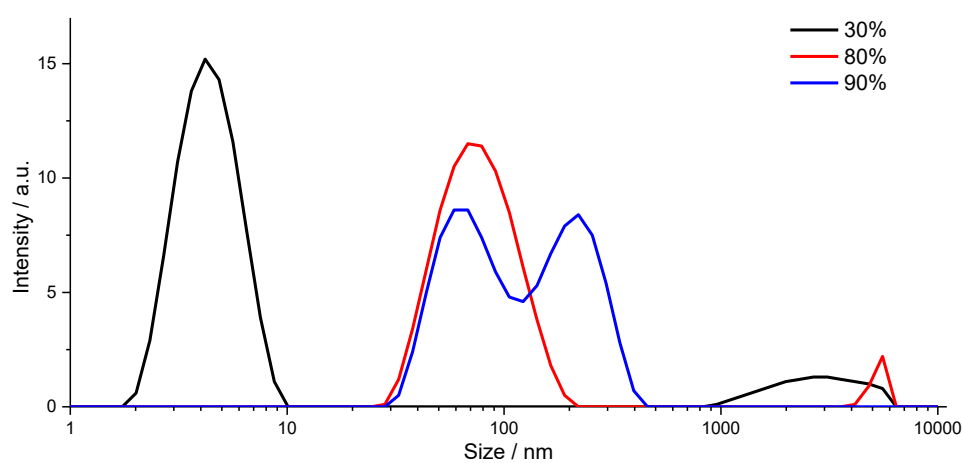


Figure 7.68 DLS Measurement of compound 2.1 with different percentages of water in THF.

7.16 Diffusion NMR data of Fe₂L₃ helicates and Fe₈L₆ cube

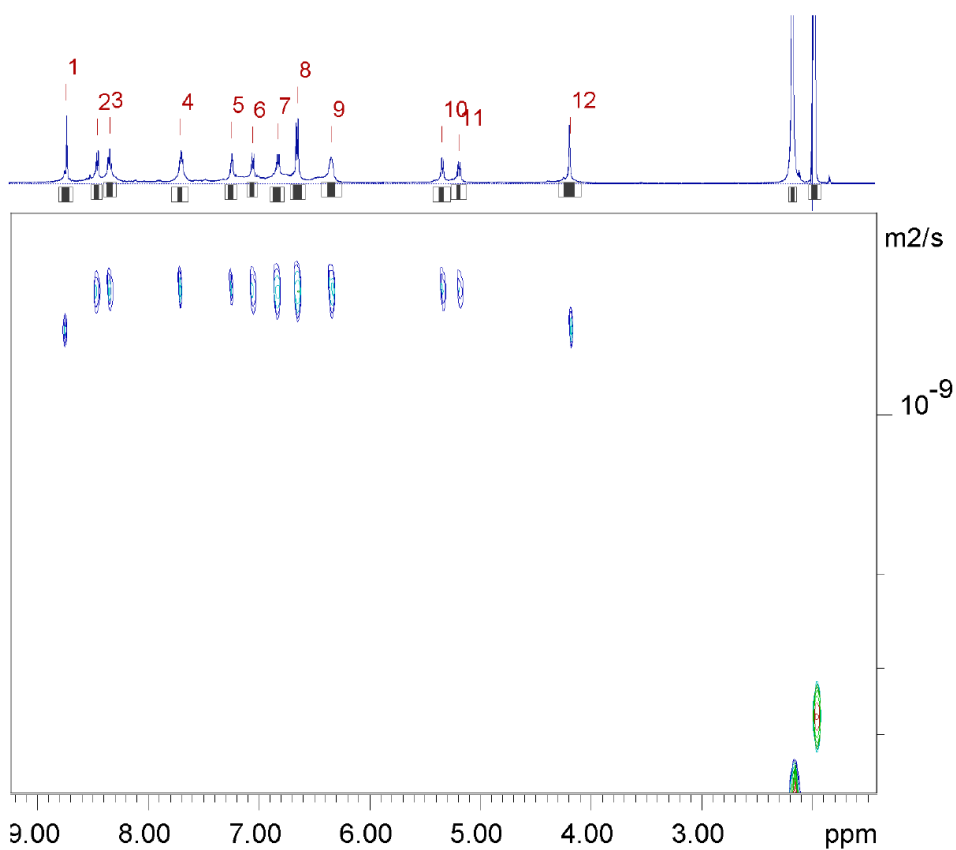
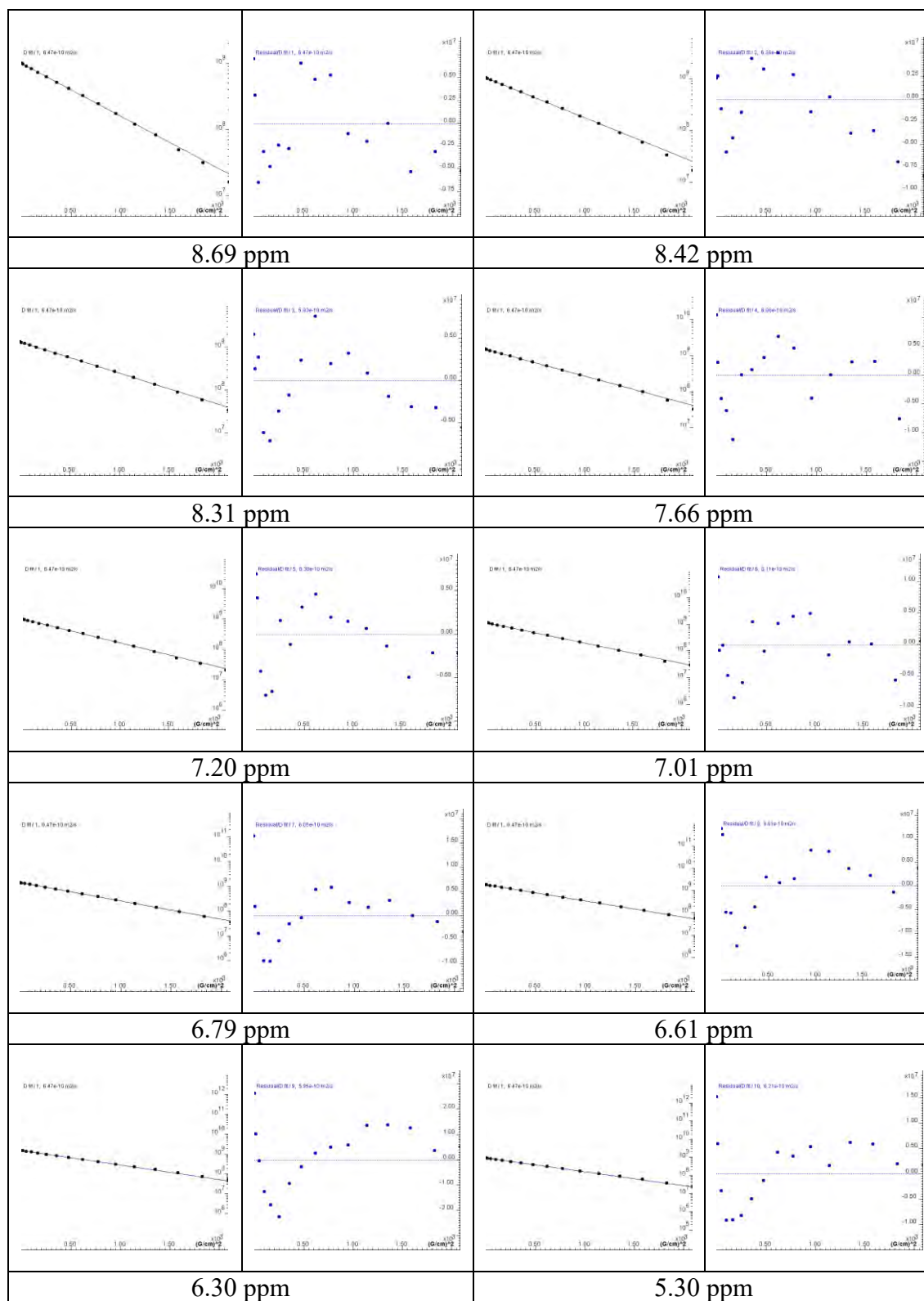


Figure 7.69 ¹H DOSY NMR (500 MHz, CD₃CN, 298K) of compound [Fe₂(2.2)₃]⁴⁺, Δ = 100 ms and δ = 2 ms.

Table 7.3 Fitted diffusion data for $[\text{Fe}_2(2.2)_3]^{4+}$ ^1H NMR peaks.



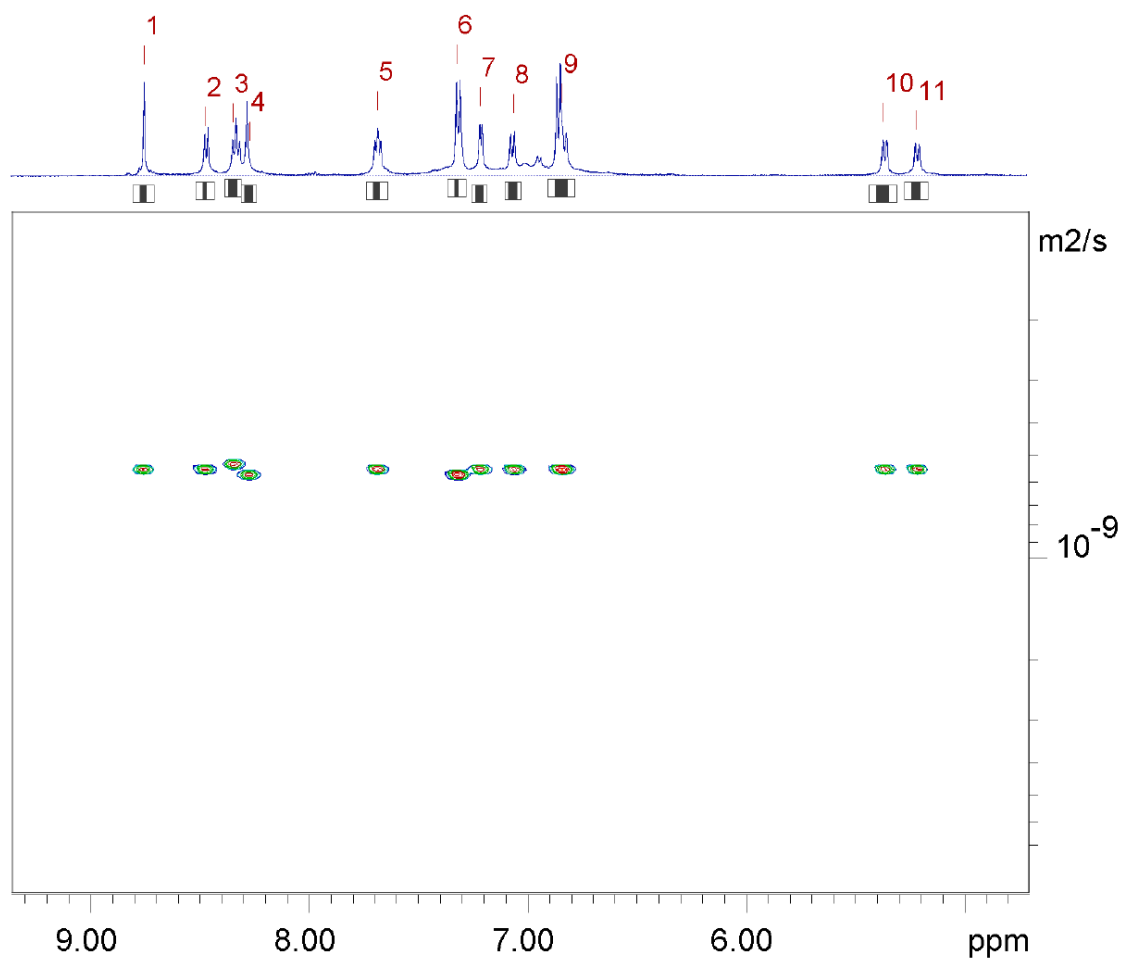
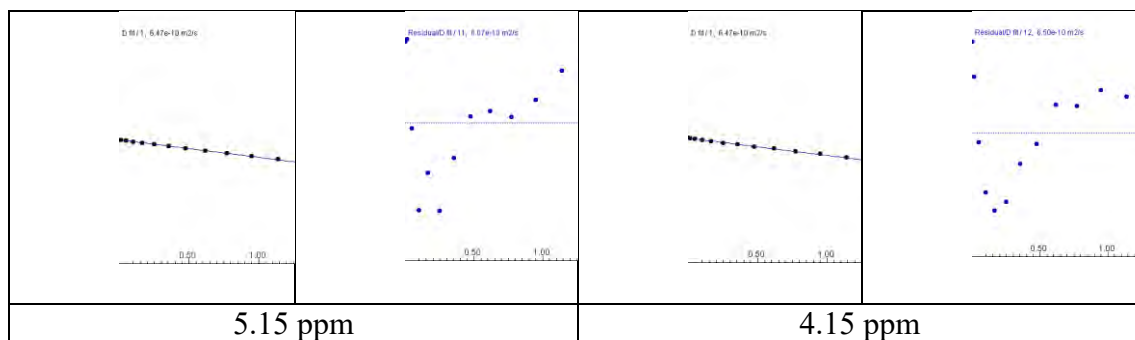
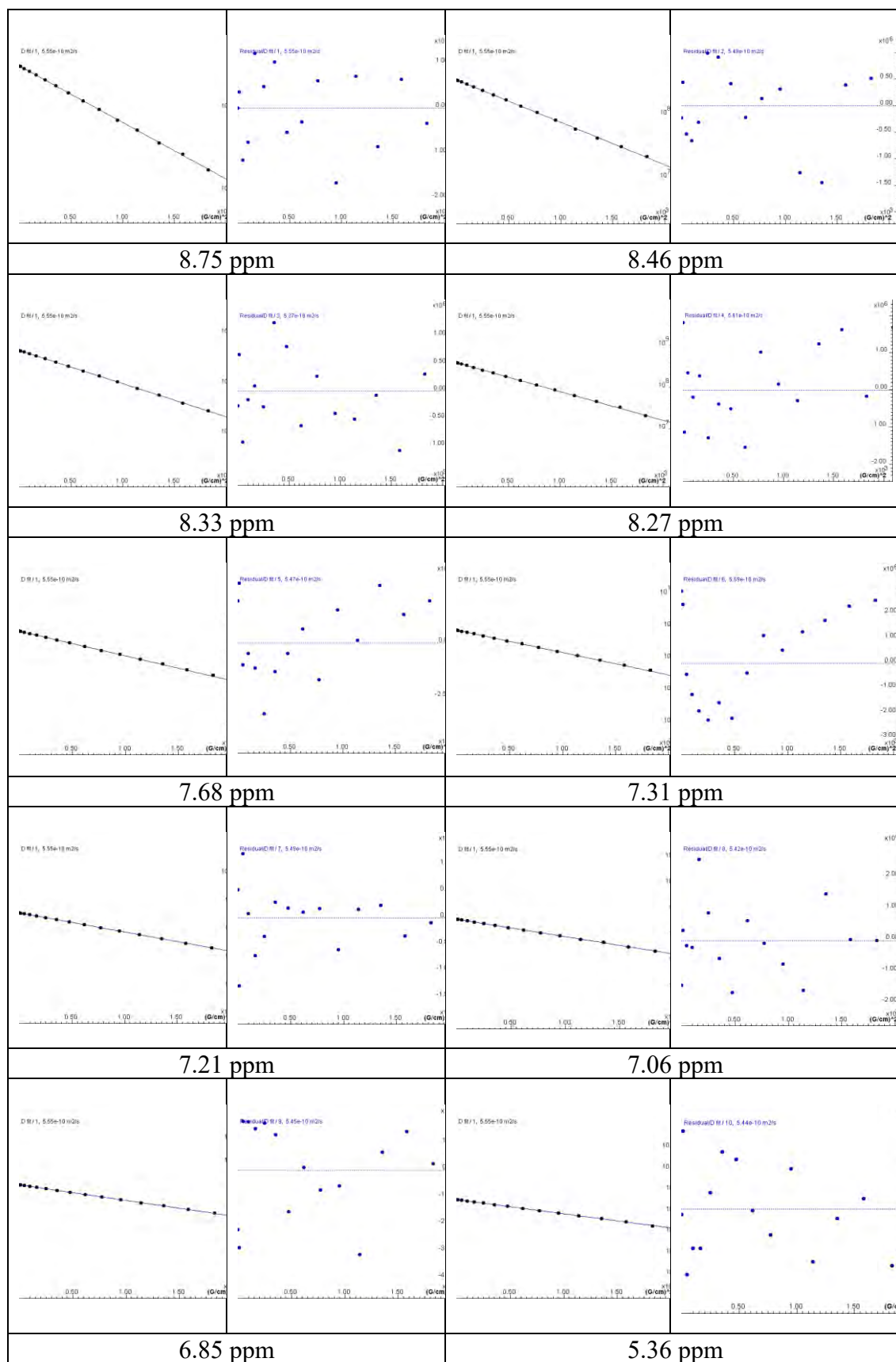


Figure 7.70 ¹H DOSY NMR (500 MHz, CD₃CN, 298K) of compound [Fe₂(**2.4**)₃]⁴⁺, Δ = 100 ms and δ = 2 ms.

Table 7.4 Fitted diffusion data for $[\text{Fe}_2(\mathbf{2.4})_3]^{4+}$ ^1H NMR peaks.



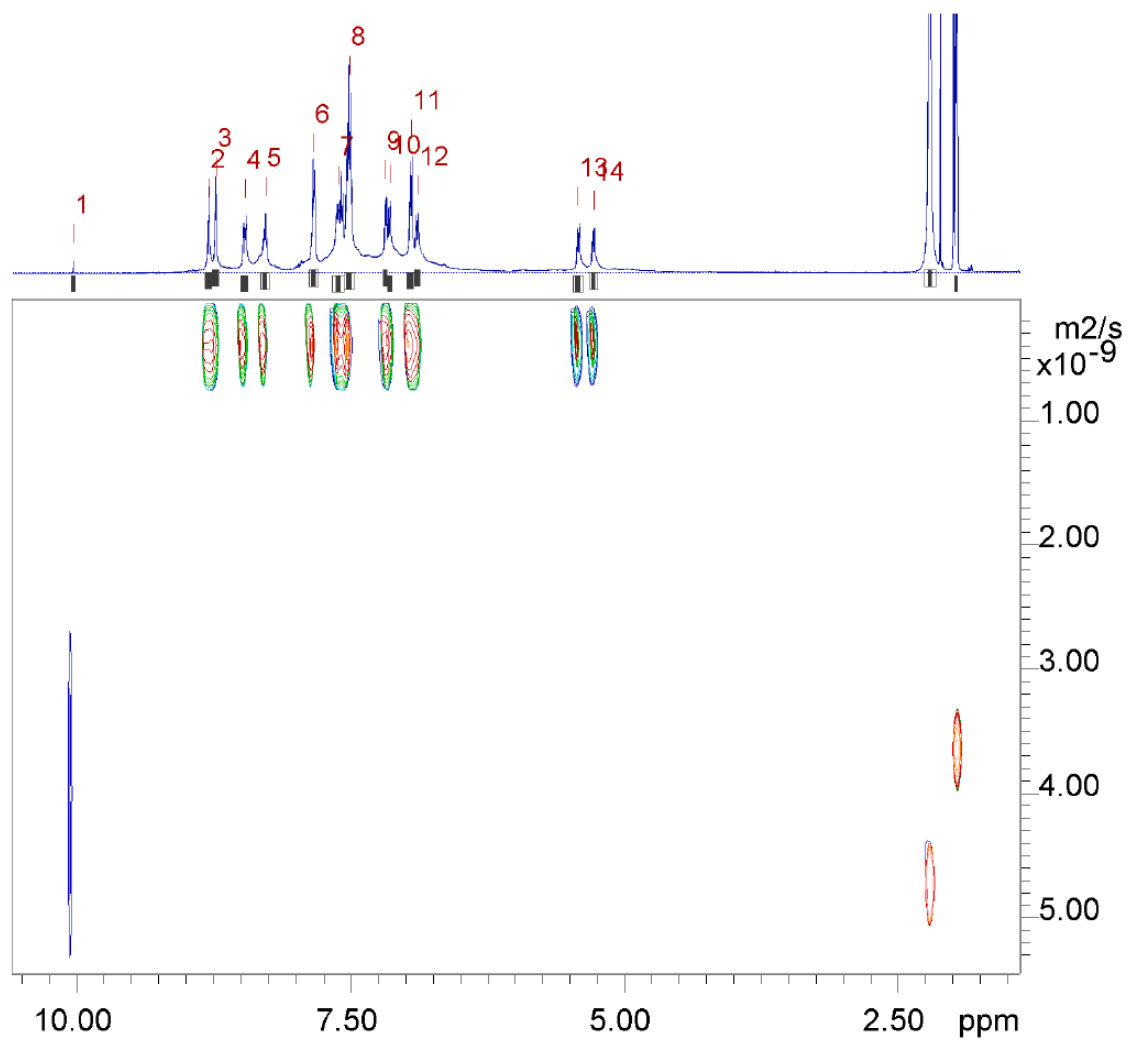
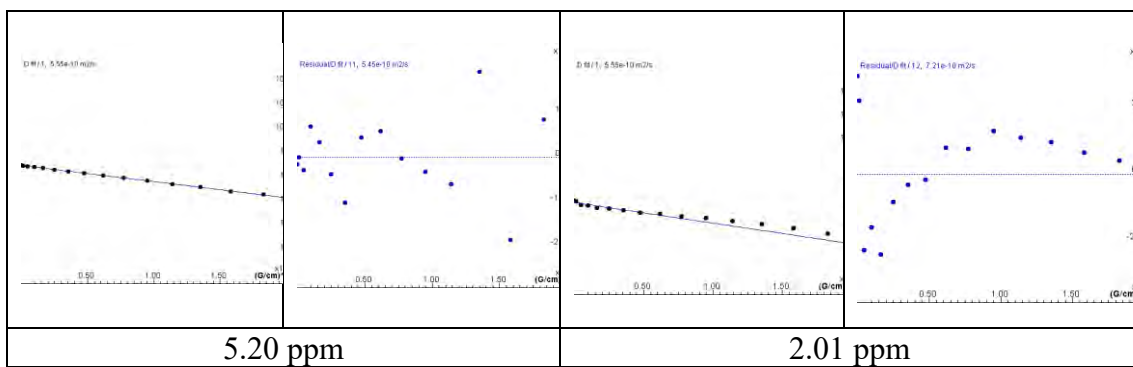
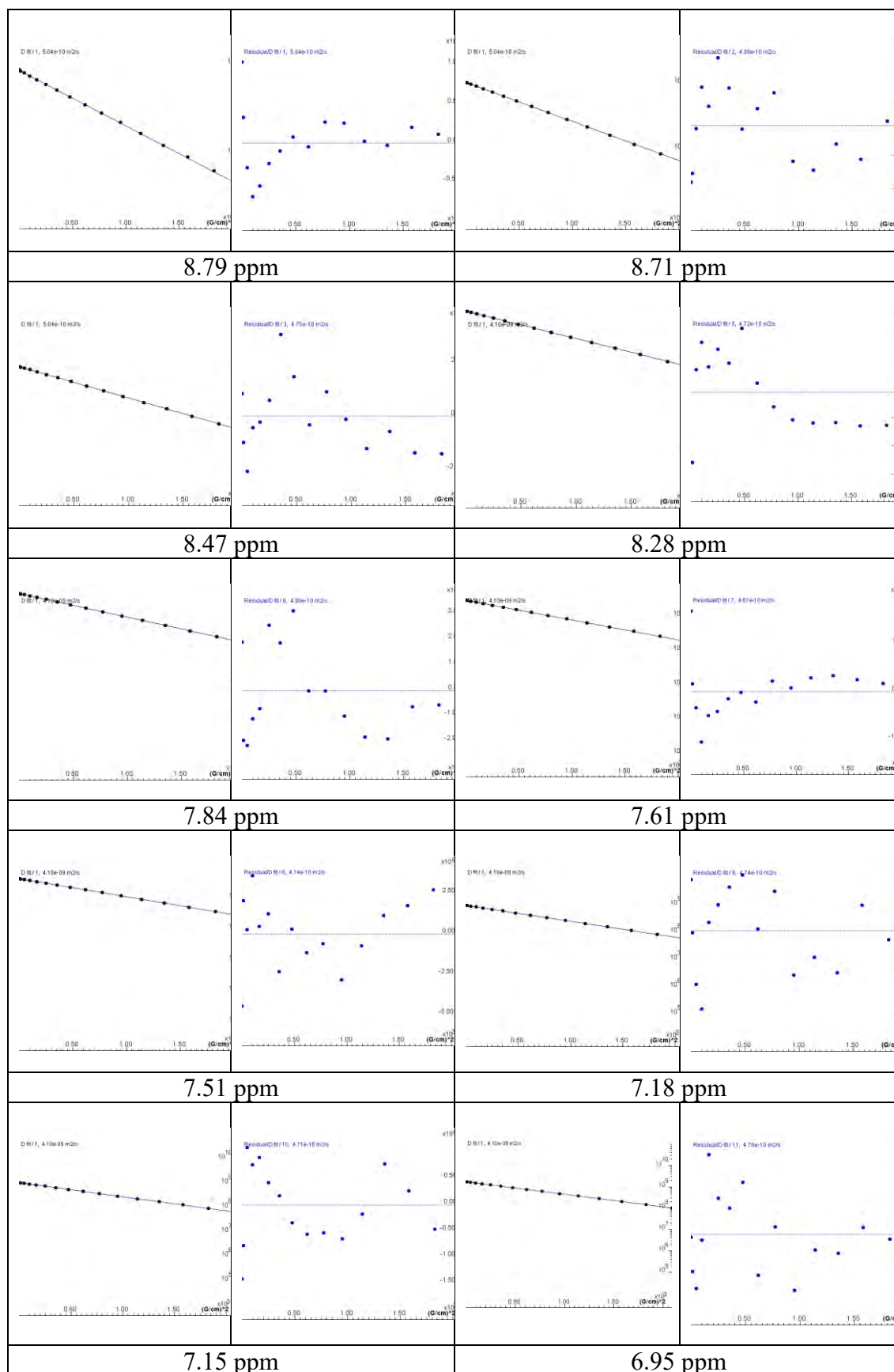


Figure 7.71 ^1H DOSY NMR (500 MHz, CD_3CN , 298K) of compound $[\text{Fe}_2(\mathbf{2.5})_3]^{4+}$, $\Delta = 100$ ms and $\delta = 2$ ms.

Table S7.5 Fitted diffusion data for $[\text{Fe}_2(2.5)_3]^{4+}$ ^1H NMR peaks



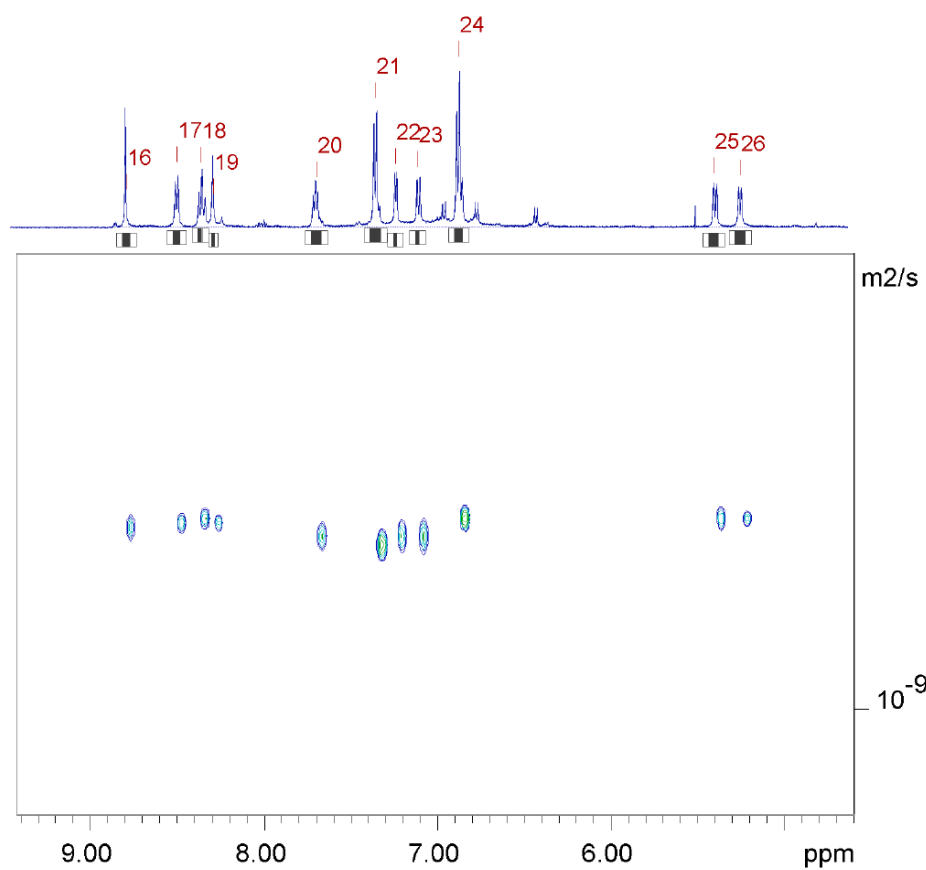
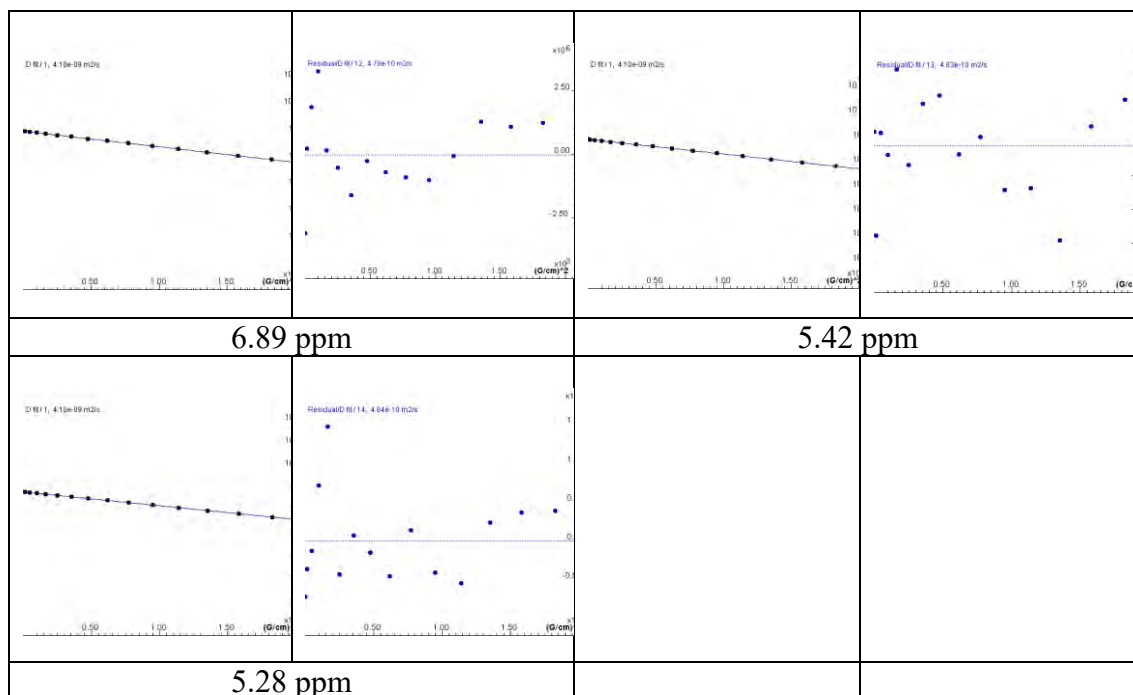
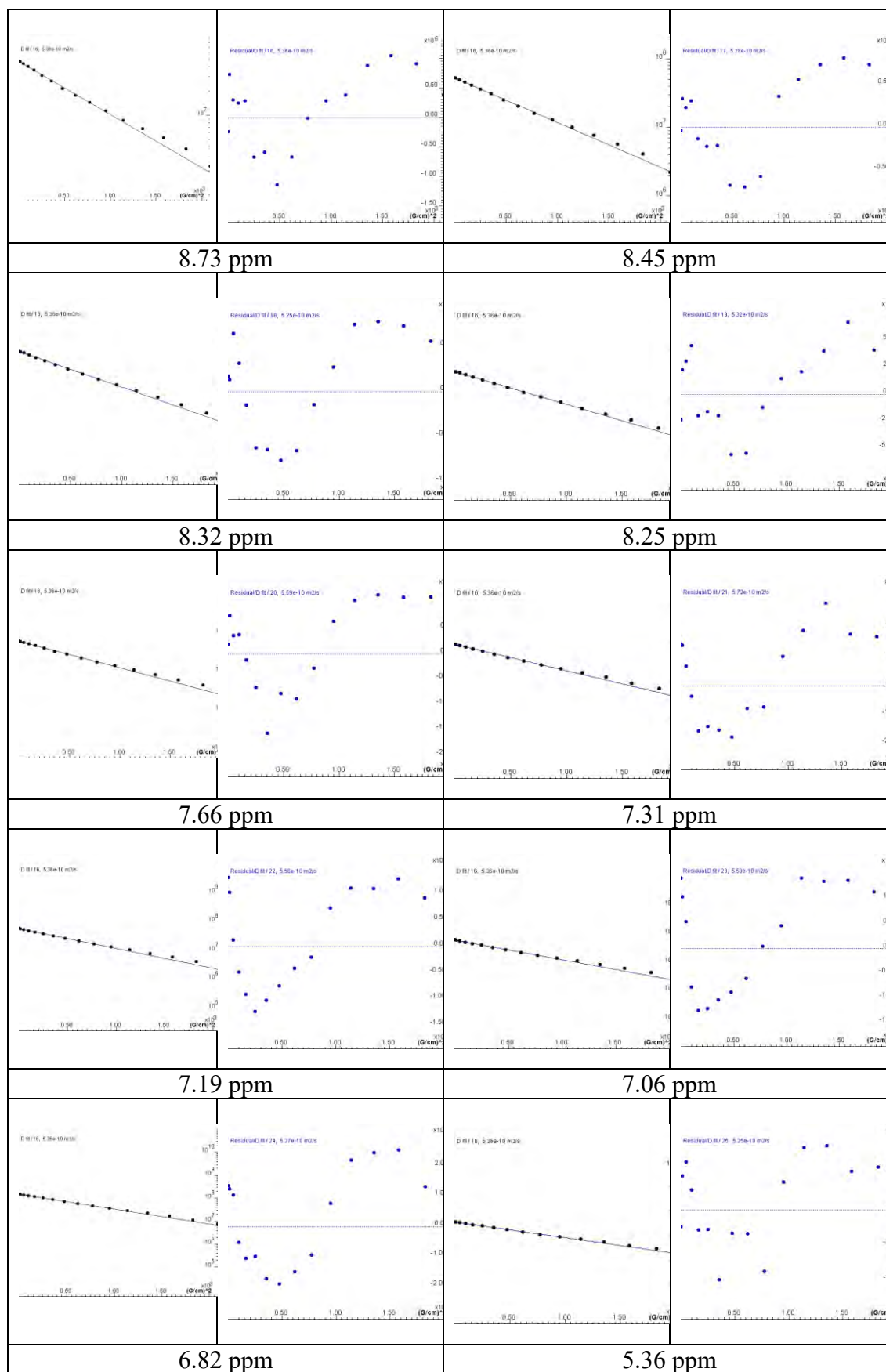


Figure 7.72 ^1H DOSY NMR (500 MHz, CD_3CN , 298K) of compound $[\text{Fe}_2(\mathbf{2.6})_3]^{4+}$, $\Delta = 100$ ms and $\delta = 2$ ms.

Table 7.6 Fitted diffusion data for $[\text{Fe}_2(\mathbf{2.6})_3]^{4+}$ ^1H NMR peaks



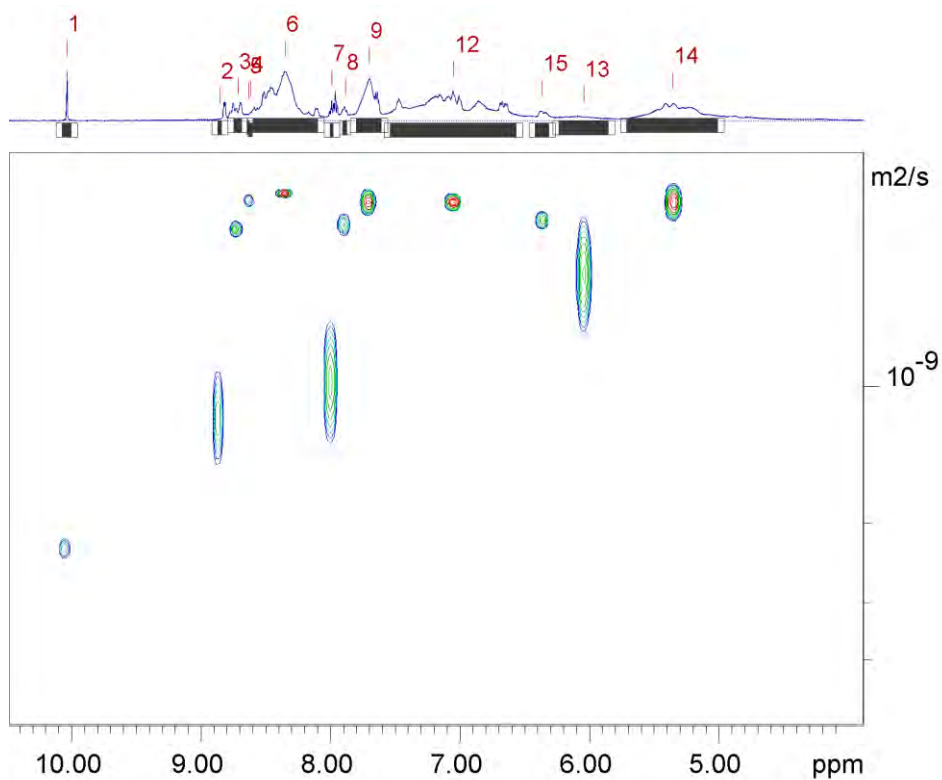
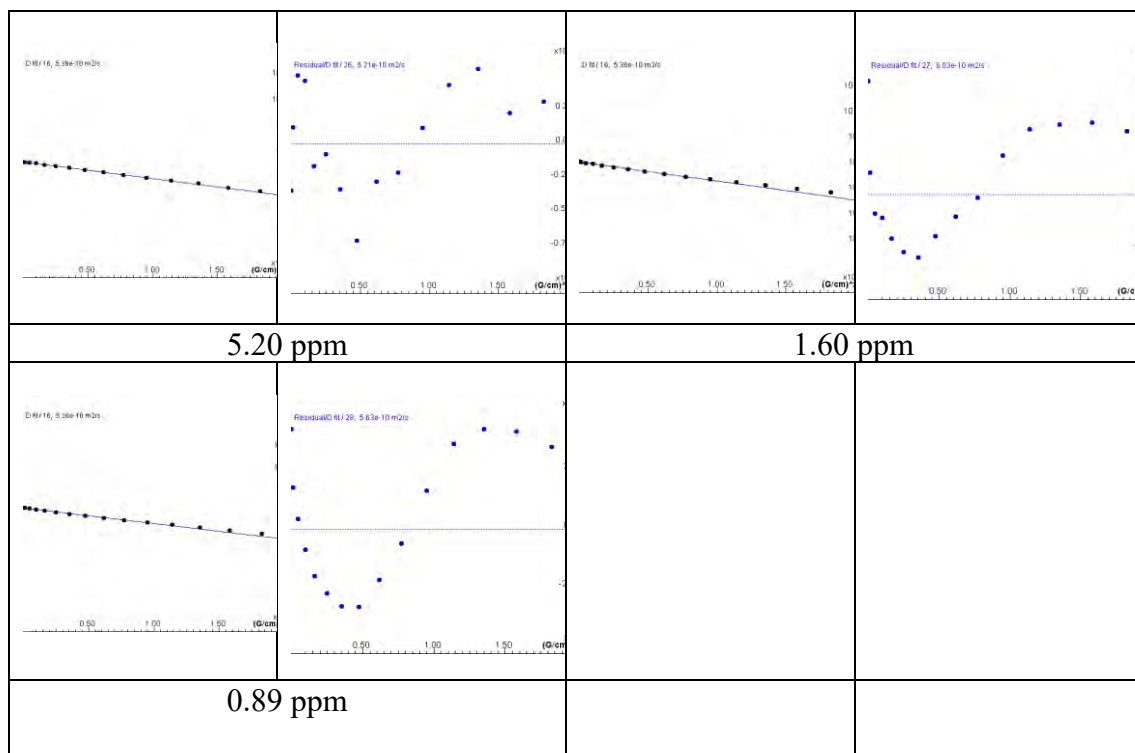
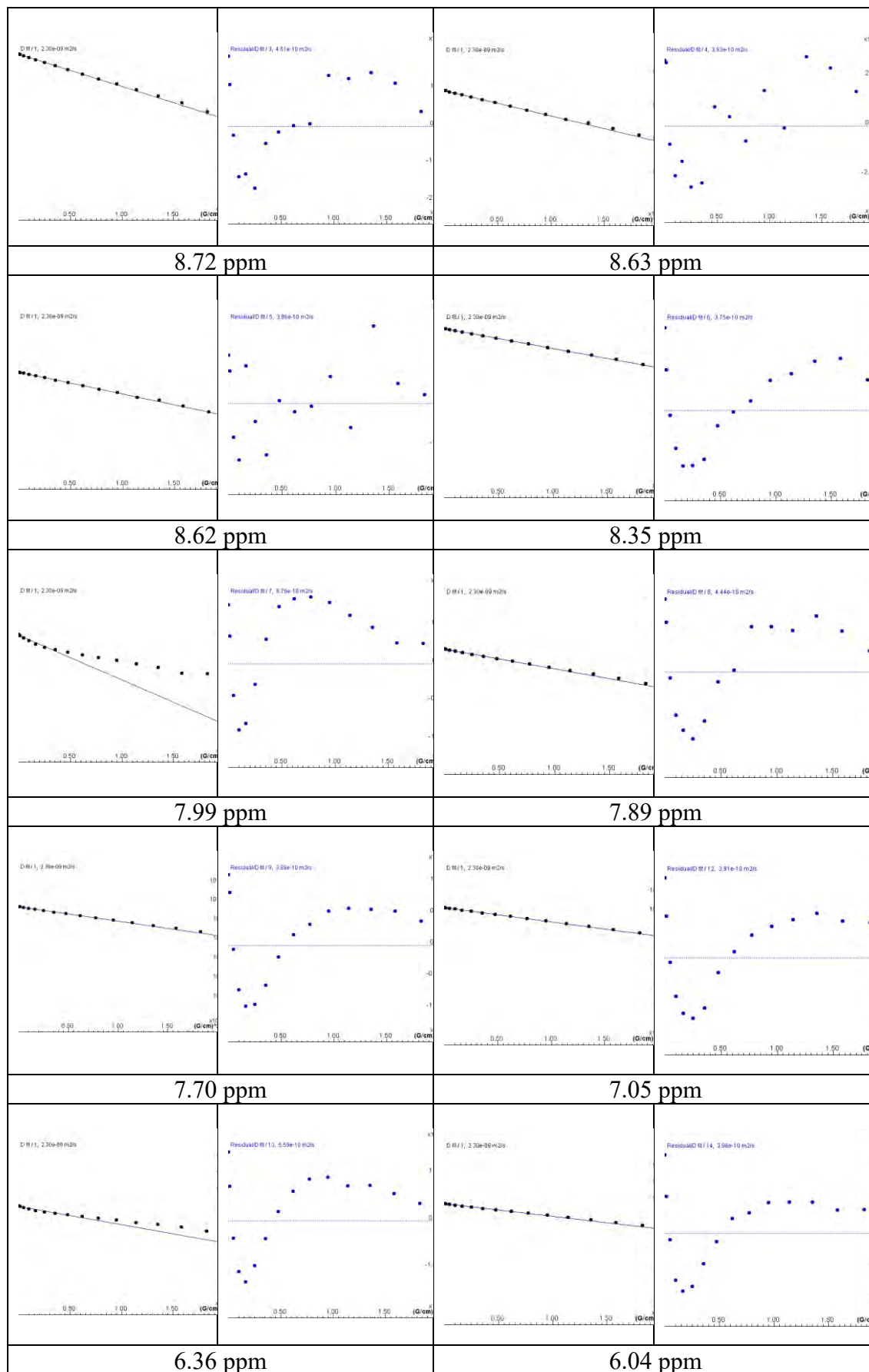
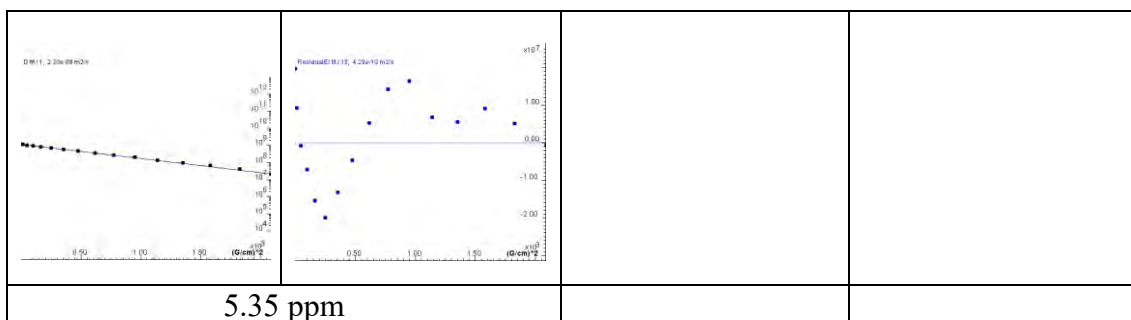


Figure 7.73 ^1H DOSY NMR (500 MHz, CD_3CN , 298K) of compound $[\text{Fe}_8(\mathbf{2.3})_6]^{16+}$, $\Delta = 100$ ms and $\delta = 2.5$ ms.

Table 7.7 Fitted diffusion data for $[\text{Fe}_8(2.3)_6]^{16+}$ ^1H NMR peaks





8 APPENDIX – CHAPTER 4

8.1 NMR spectra for 4.1 in CDCl₃

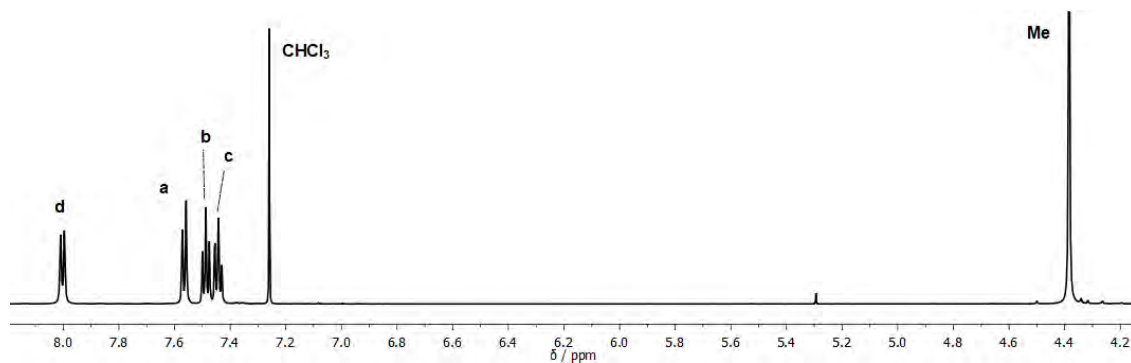


Figure 8.1 Partial ¹H NMR spectrum (600 MHz, CDCl₃, 298 K) of 4.1.

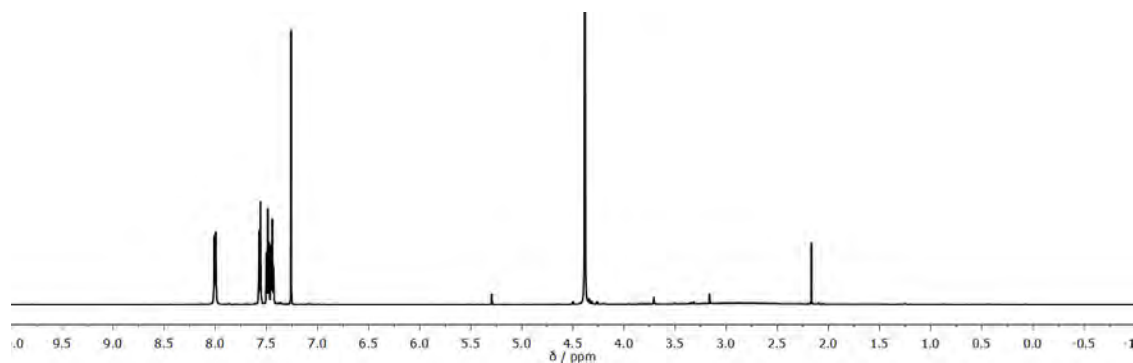


Figure 8.2 ¹H NMR spectrum (600 MHz, CDCl₃, 298 K) of 4.1.

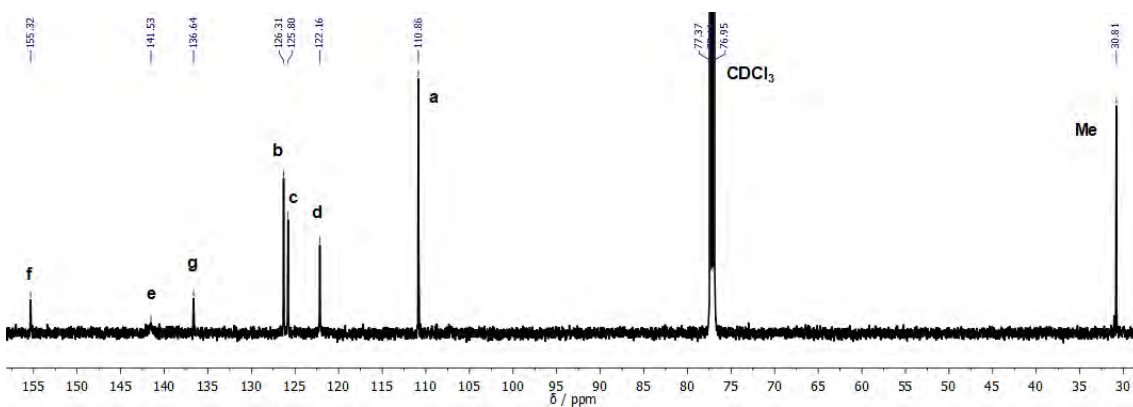


Figure 8.3 Partial ¹³C{¹H} NMR spectrum (151 MHz, CDCl₃, 298 K) of 4.1.

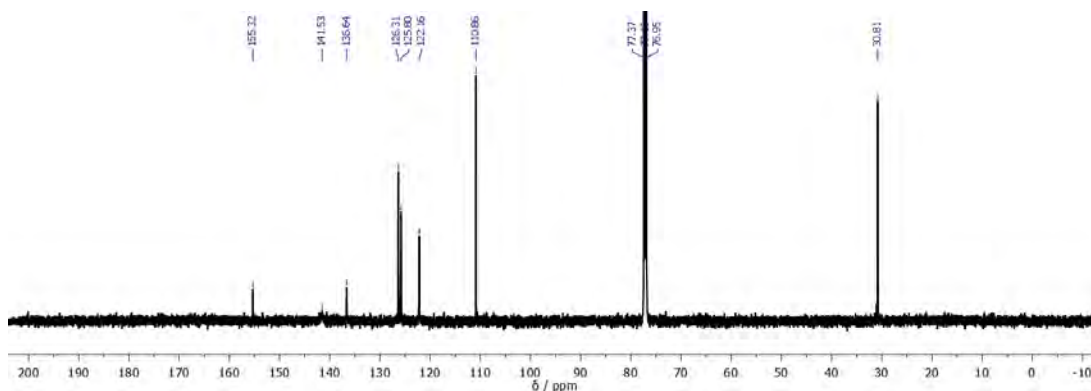


Figure 8.4 $^{13}\text{C}\{^1\text{H}\}$ NMR spectrum (151 MHz, CDCl_3 , 298 K) of **4.1**.

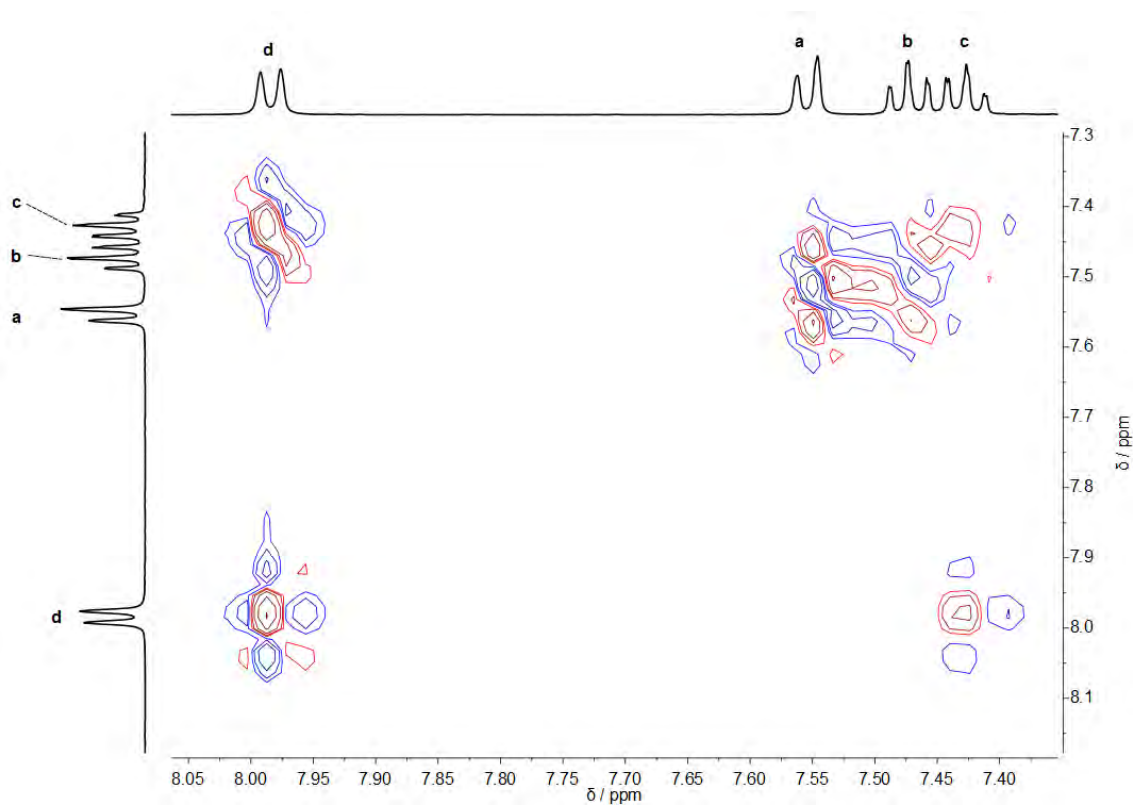


Figure 8.5 ^1H - ^1H COSY NMR spectrum (500 MHz, CDCl_3 , 298 K) of **4.1**.

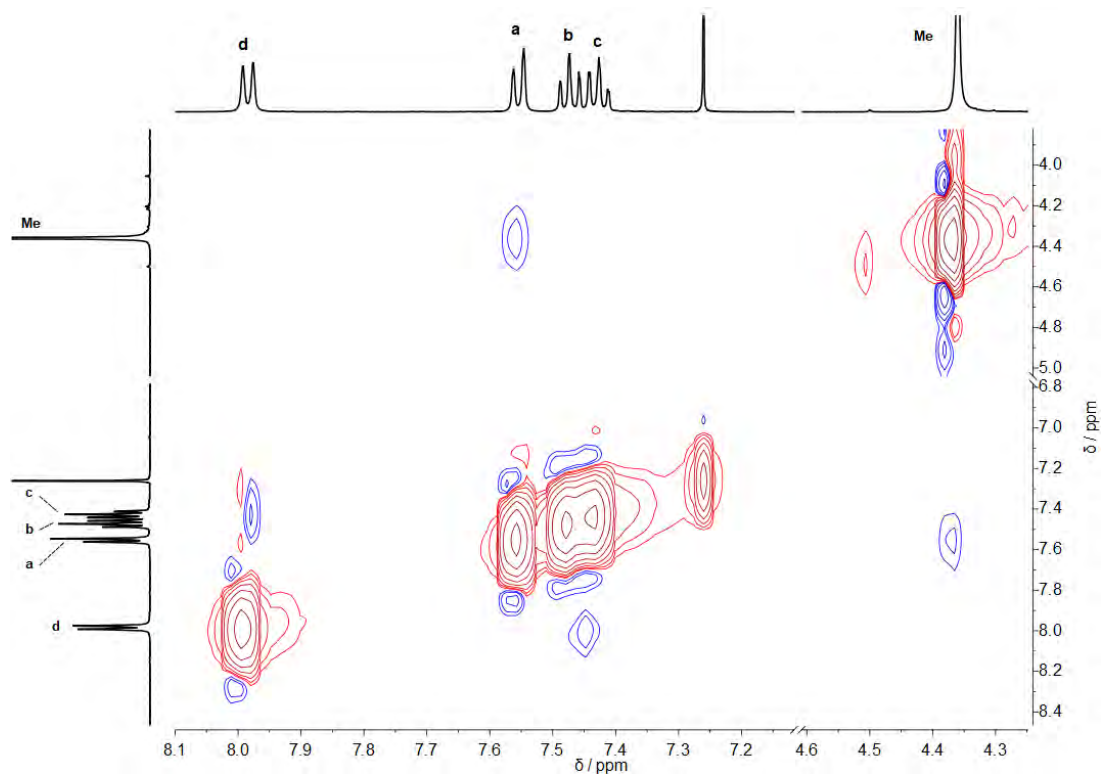


Figure 8.6 ^1H - ^1H NOESY NMR spectrum (500 MHz, CDCl_3 , 298 K) of 4.1.

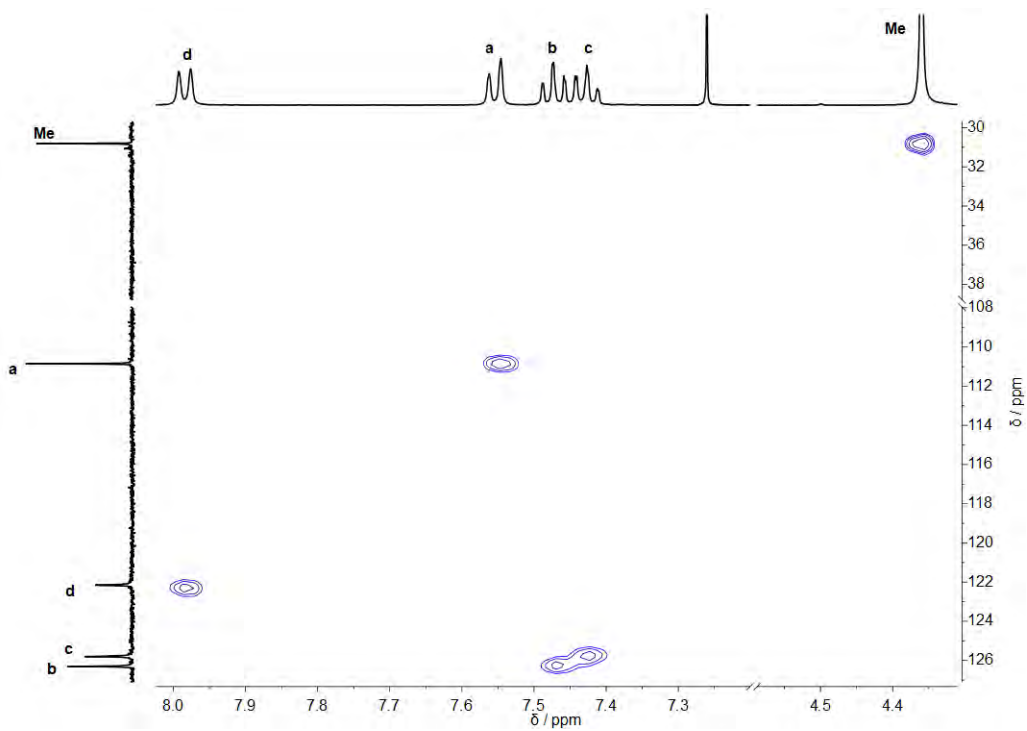


Figure 8.7 ^1H - ^{13}C HSQC NMR spectrum (500 MHz, CDCl_3 , 298 K) of 4.1.

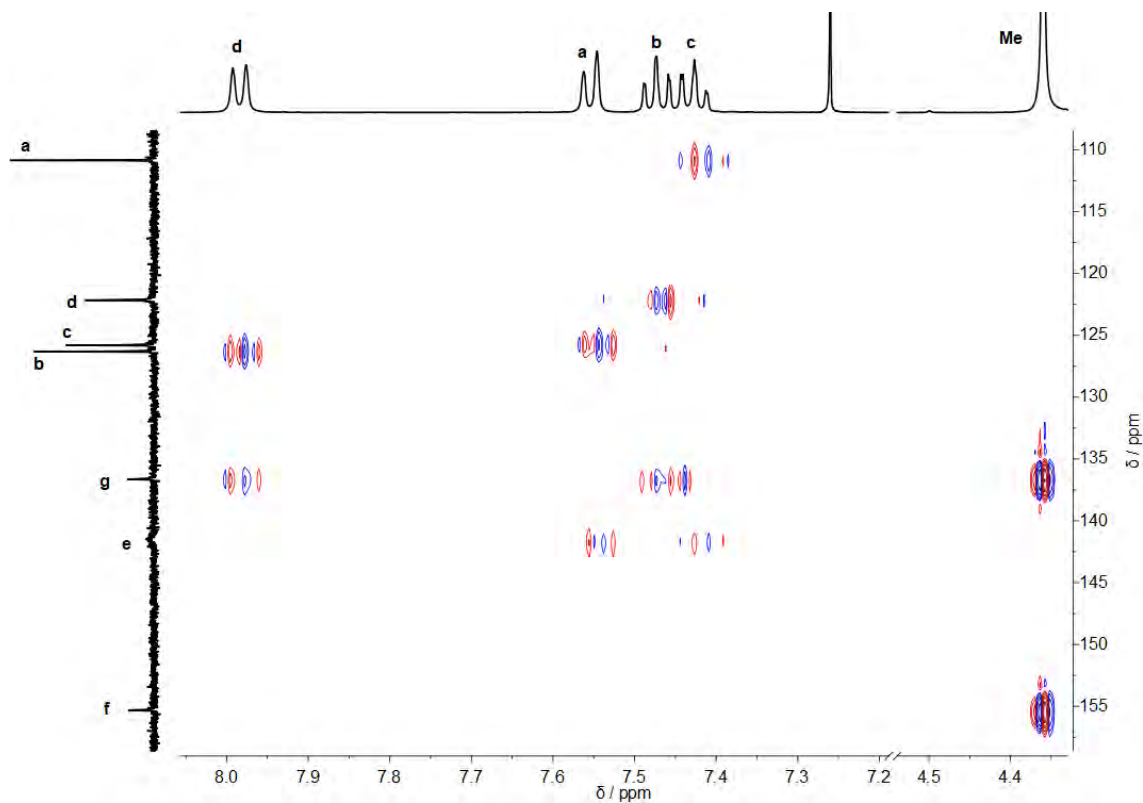


Figure 8.8 ^1H - ^{13}C HMBC NMR spectrum (500 MHz, CDCl_3 , 298 K) of **4.1**.

8.2 NMR spectra for **4.2** in CDCl_3

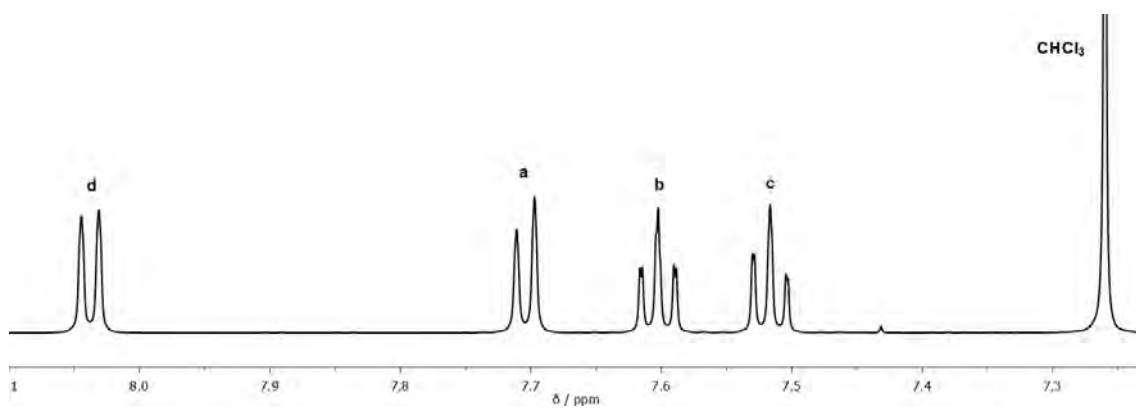


Figure 8.9 Partial ^1H NMR spectrum (600 MHz, CDCl_3 , 298 K) of **4.2**.

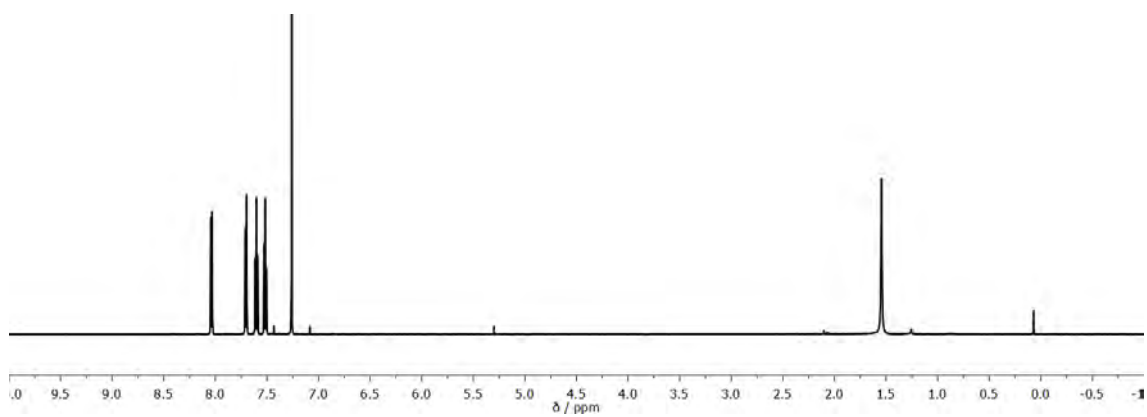


Figure 8.10 ^1H NMR spectrum (600 MHz, CDCl_3 , 298 K) of **4.2**.

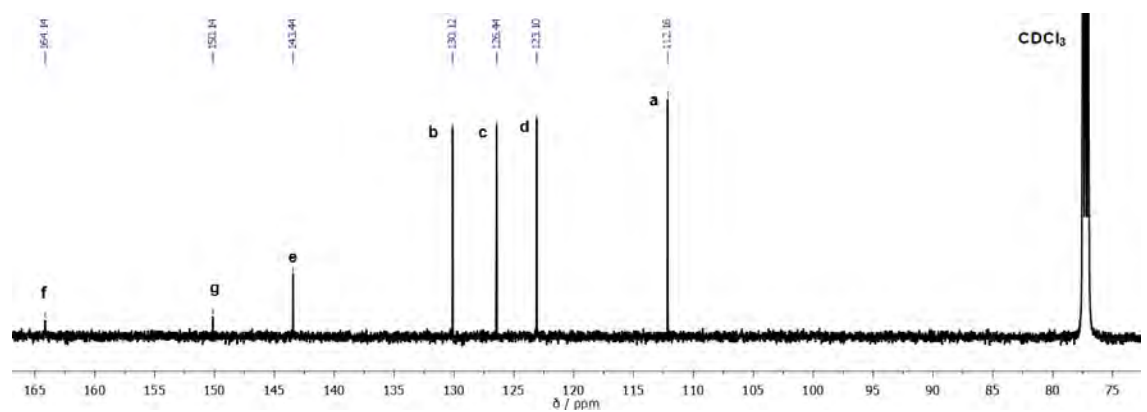


Figure 8.11 Partial $^{13}\text{C}\{^1\text{H}\}$ NMR spectrum (151 MHz, CDCl_3 , 298 K) of **4.2**.

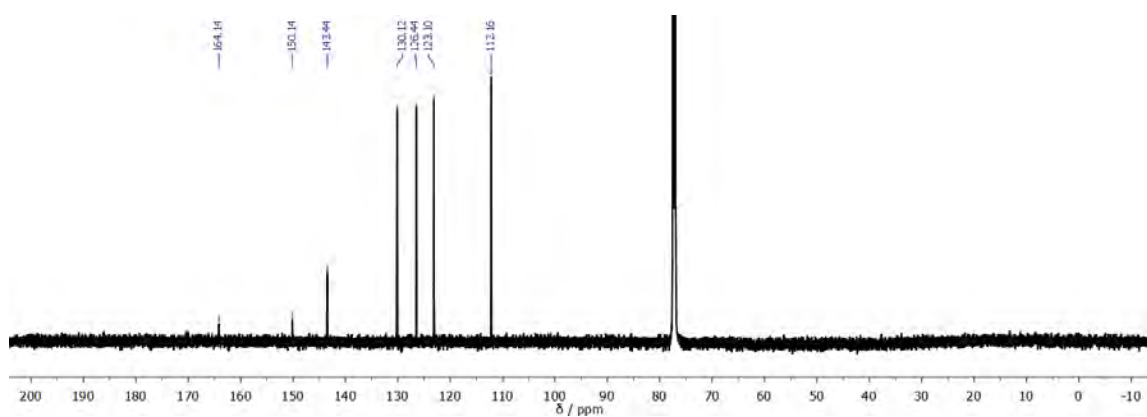


Figure 8.12 $^{13}\text{C}\{^1\text{H}\}$ NMR spectrum (151 MHz, CDCl_3 , 298 K) of **4.2**.

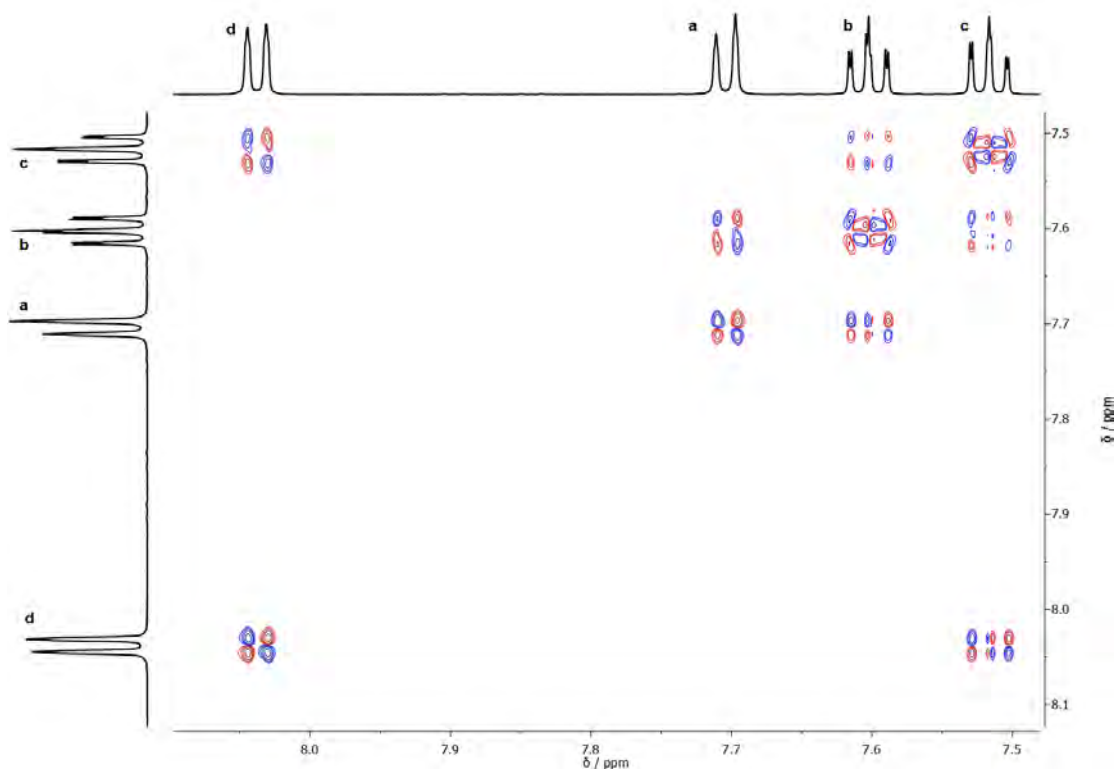


Figure 8.13 ^1H - ^1H COSY NMR spectrum (600 MHz, CDCl_3 , 298 K) of **4.2**.

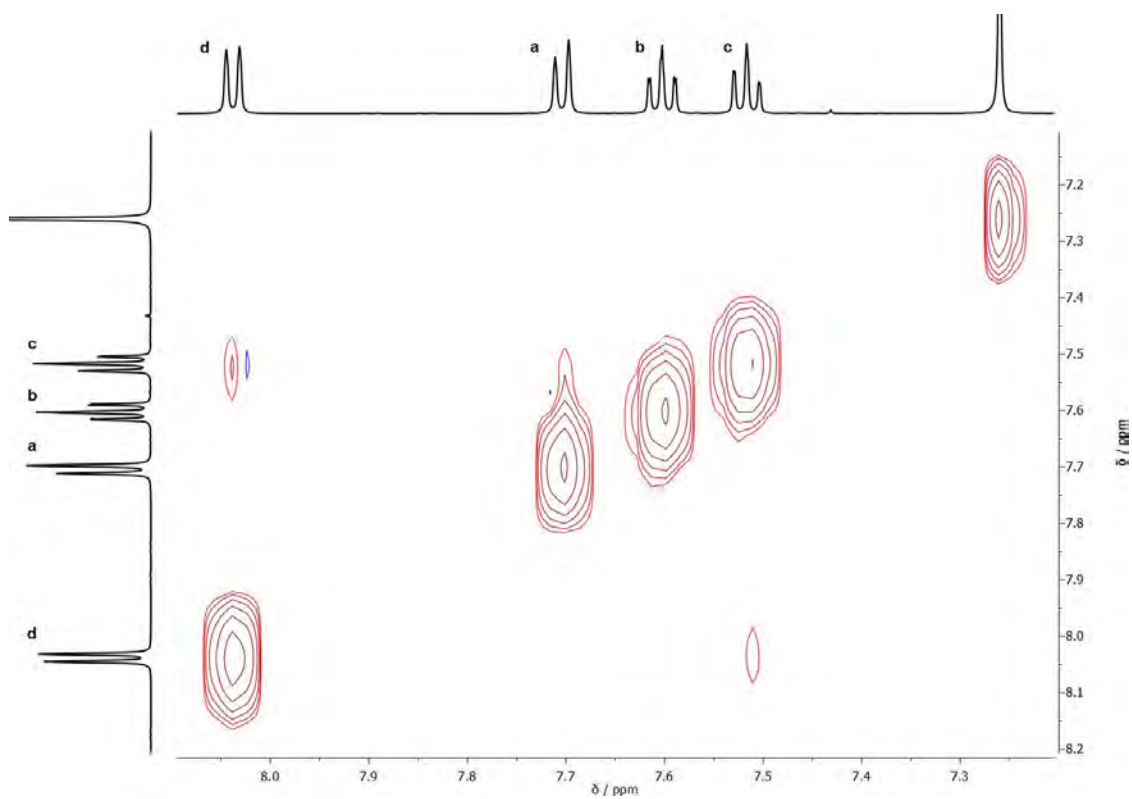


Figure 8.14 ^1H - ^1H NOESY NMR spectrum (600 MHz, CDCl_3 , 298 K) of **4.2**.

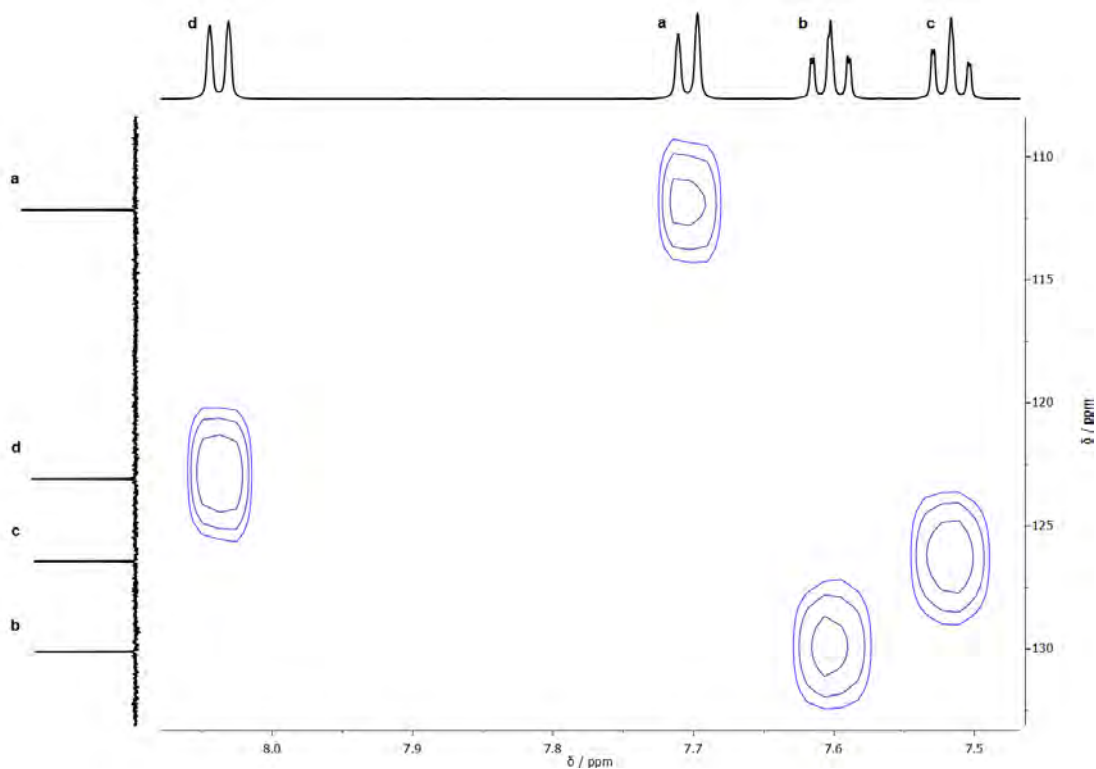


Figure 8.15 ^1H - ^{13}C HSQC NMR spectrum (600 MHz, CDCl_3 , 298 K) of **4.2**.

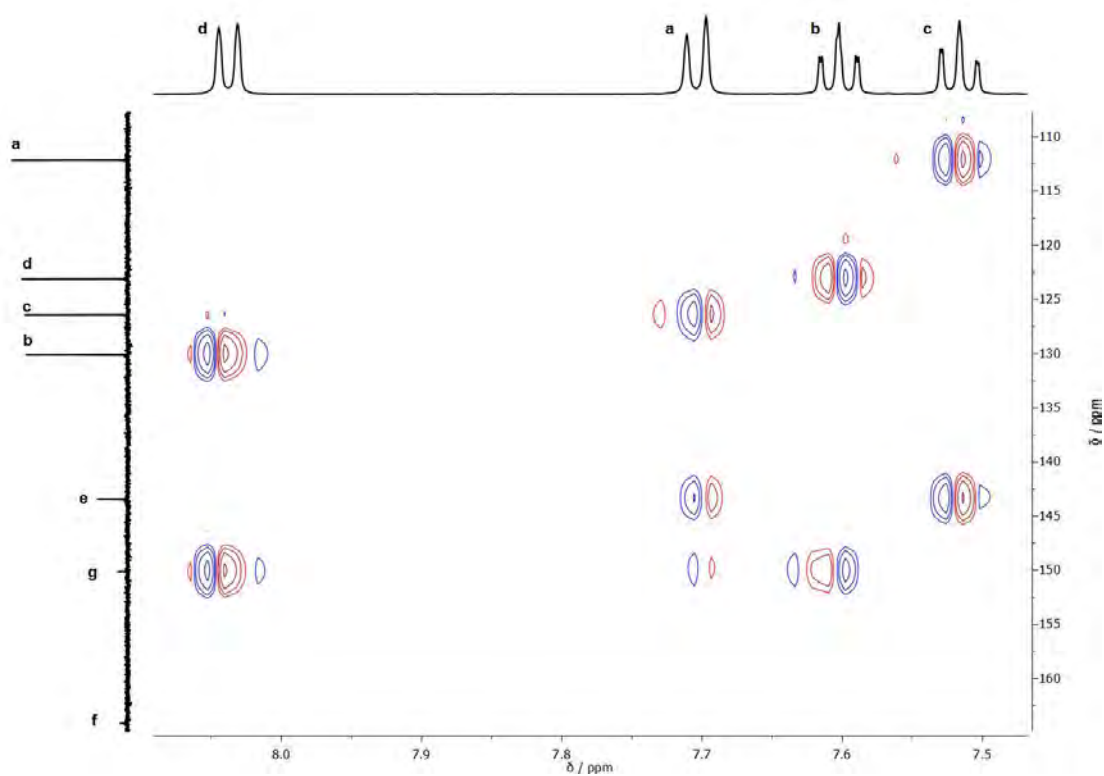


Figure 8.16 ^1H - ^{13}C HMBC NMR spectrum (600 MHz, CDCl_3 , 298 K) of **4.2**.

8.3 NMR spectra for 4.3 in CDCl₃

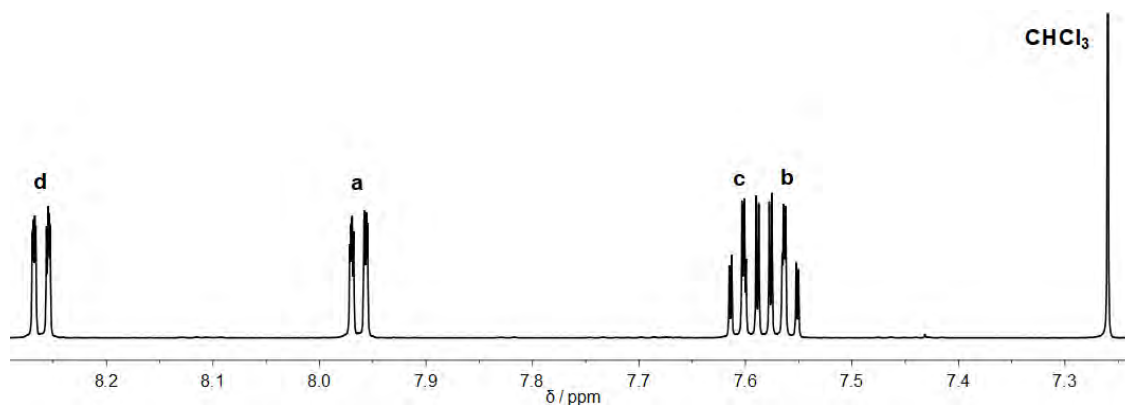


Figure 8.17 Partial ¹H NMR spectrum (600 MHz, CDCl₃, 298 K) of 4.3.

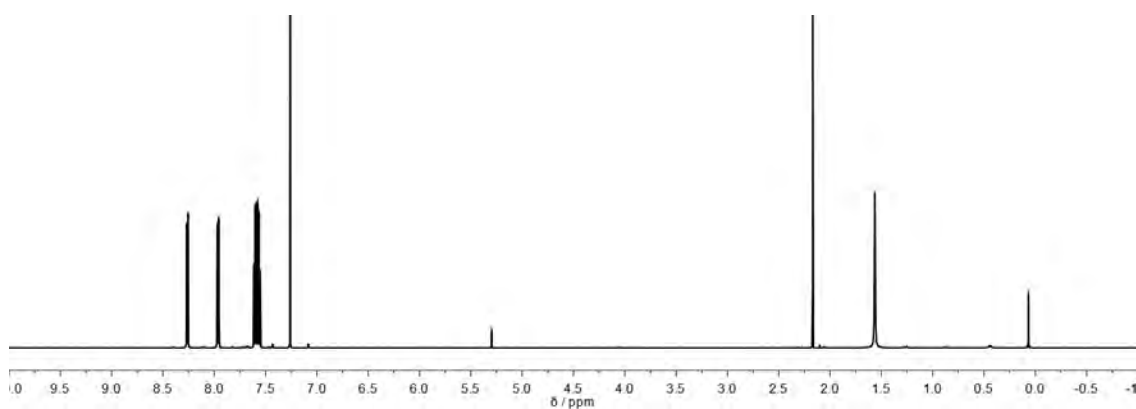


Figure 8.18 ¹H NMR spectrum (600 MHz, CDCl₃, 298 K) of 4.3.

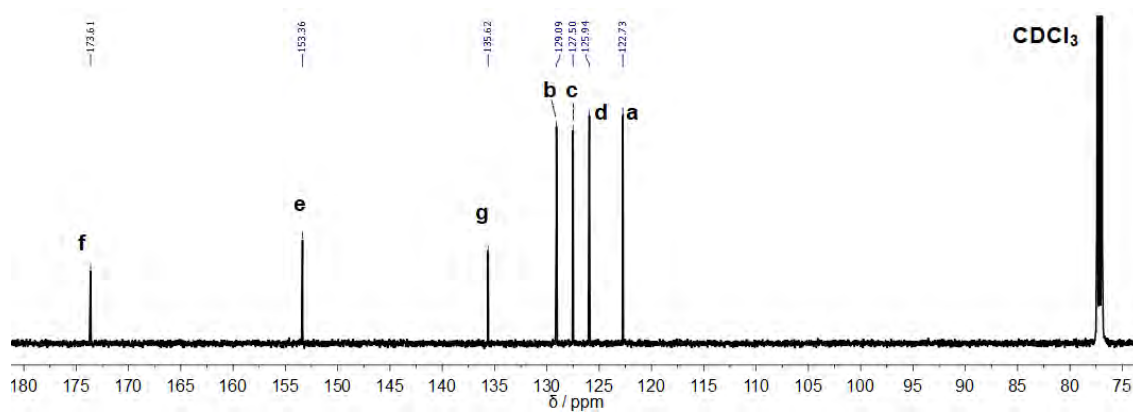


Figure 8.19 Partial ¹³C {¹H} NMR spectrum (151 MHz, CDCl₃, 298 K) of 4.3.

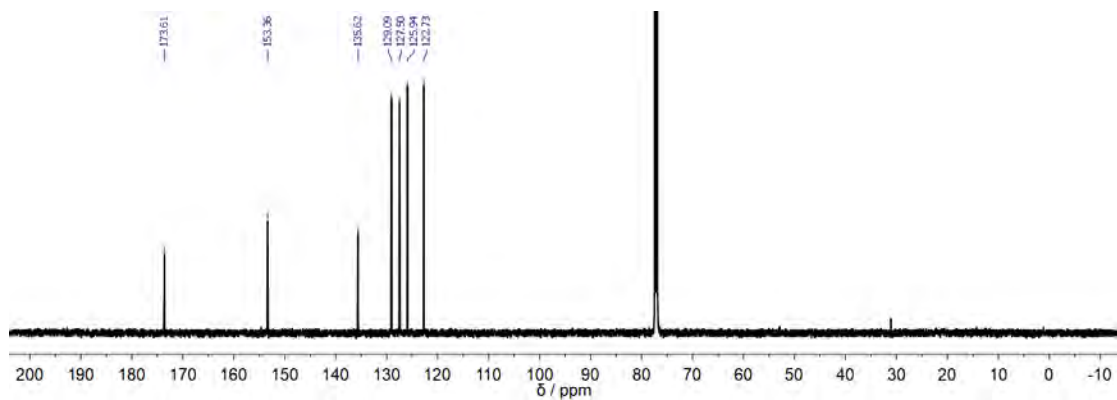


Figure 8.20 $^{13}\text{C}\{^1\text{H}\}$ NMR spectrum (151 MHz, CDCl_3 , 298 K) of **4.3**.

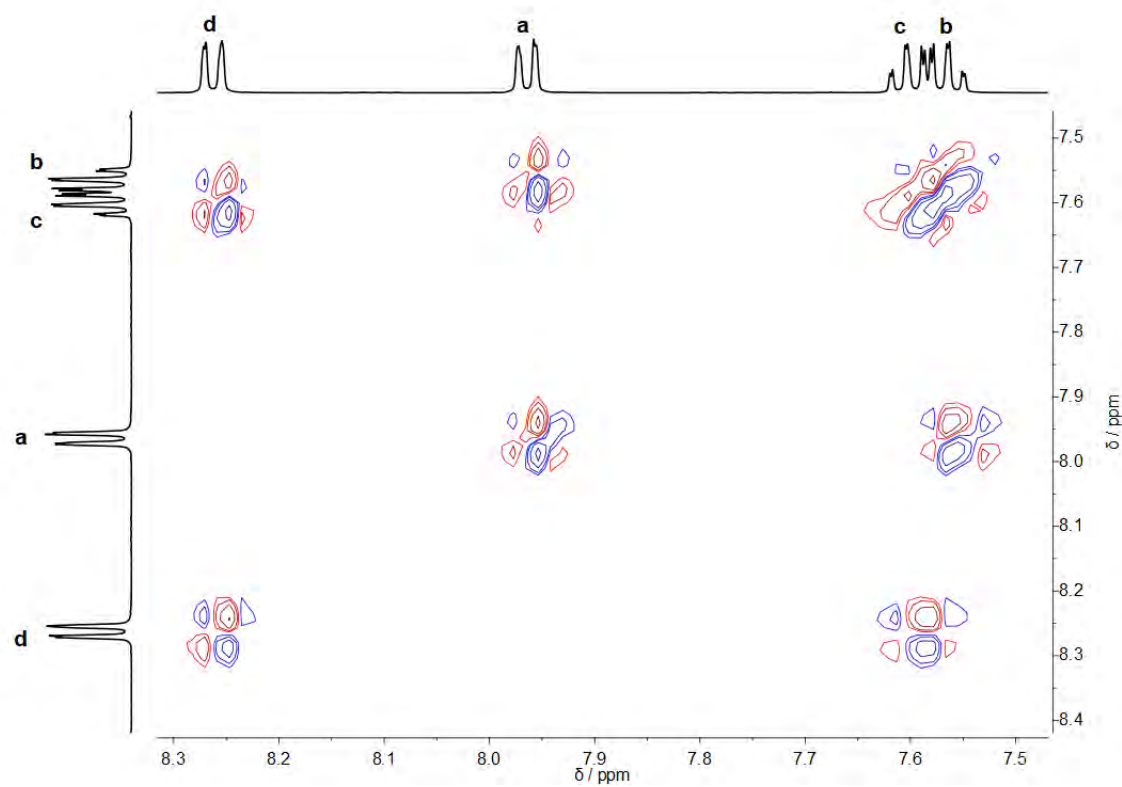


Figure 8.21 $^1\text{H}\text{-}^1\text{H}$ COSY NMR spectrum (500 MHz, CDCl_3 , 298 K) of **4.3**.

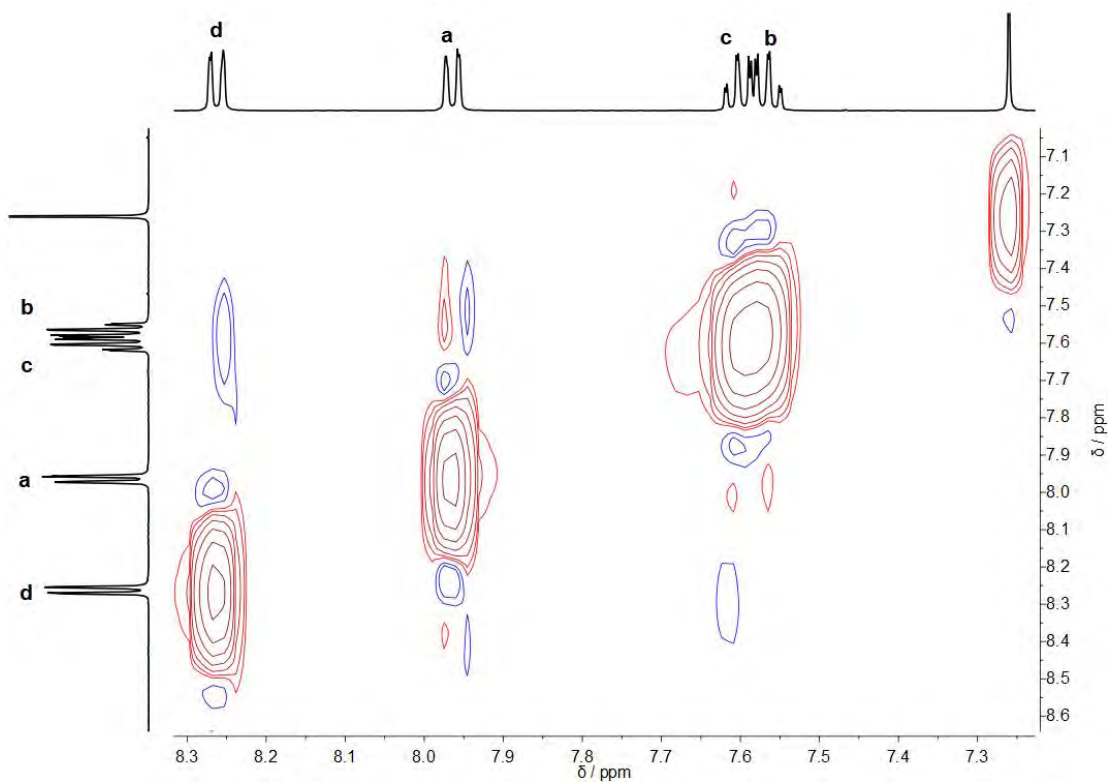


Figure 8.22 ^1H - ^1H NOESY NMR spectrum (500 MHz, CDCl_3 , 298 K) of **4.3**.

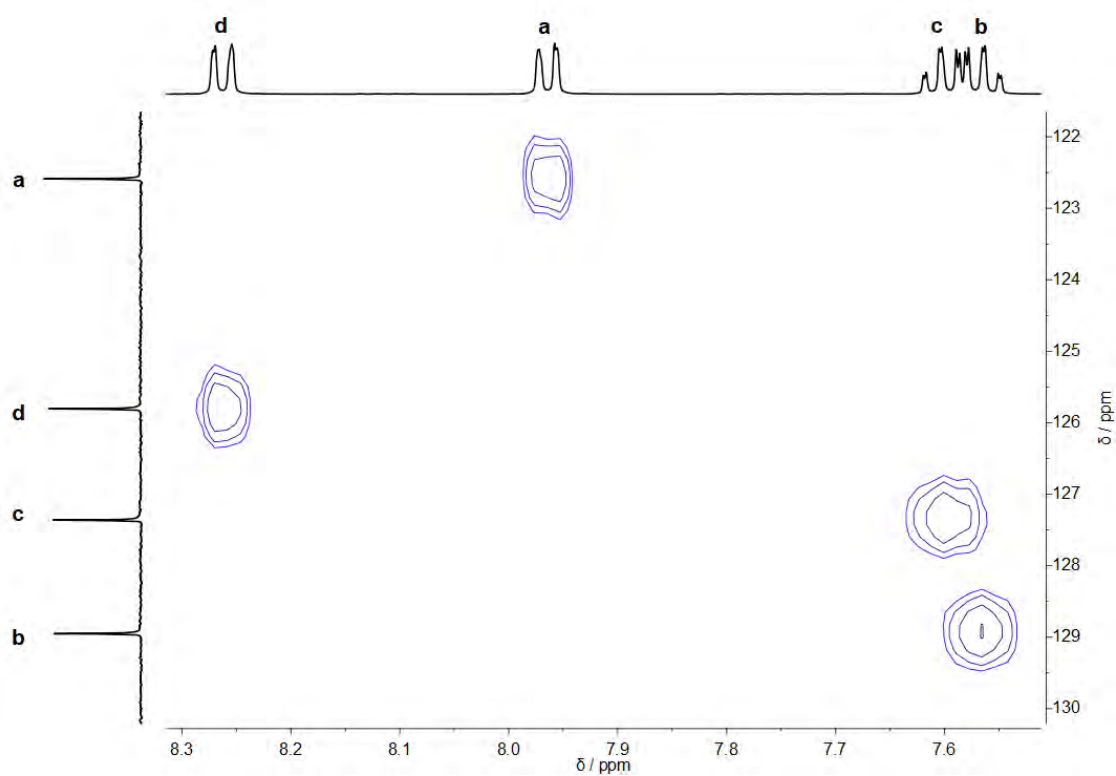


Figure 8.23 ^1H - ^{13}C HSQC NMR spectrum (500 MHz, CDCl_3 , 298 K) of **4.3**.

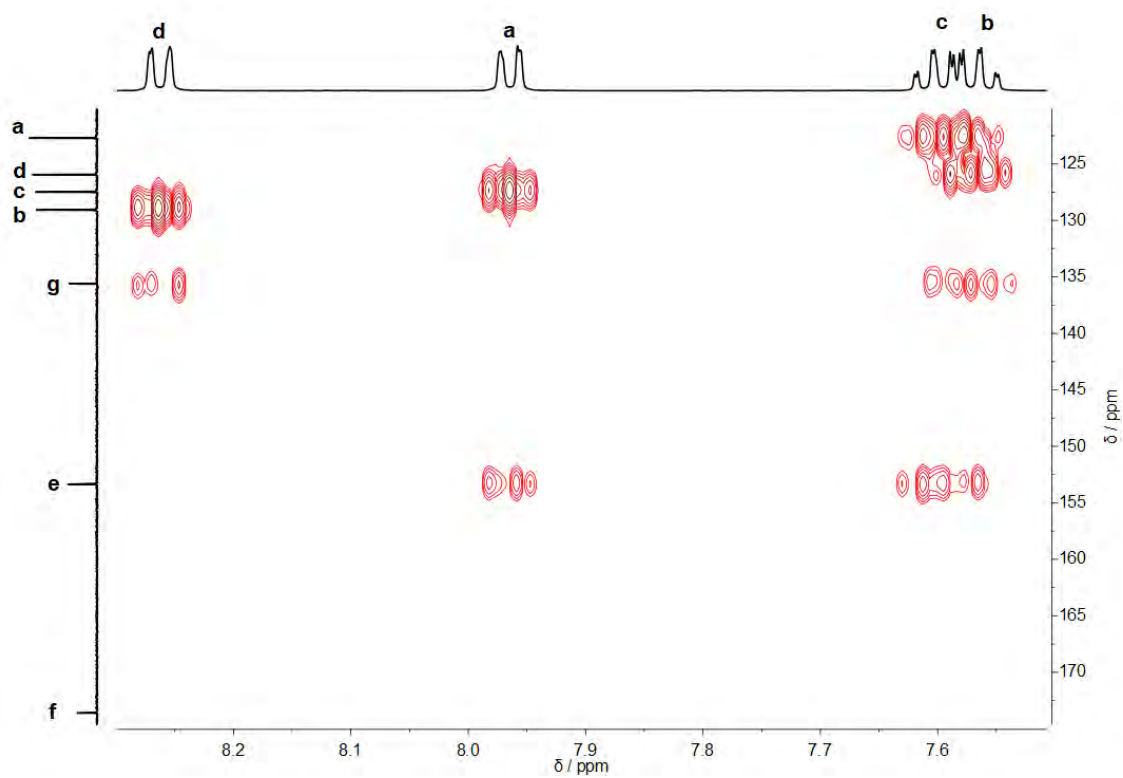


Figure 8.24 ^1H - ^{13}C HMBC NMR spectrum (500 MHz, CDCl_3 , 298 K) of **4.3**.

8.4 Photoswitching and calculated spectra for Azobis(2-imidazole) (4.4)

For comparison of λ_{max} and switching parameters the spectrum of azobis(2-imidazole) was recorded in acetonitrile and a PSS was generated using 448 nm light. Note this is not the wavelength of maximum switching for azobis(2-imidazole), however this wavelength was used for comparisons sake.

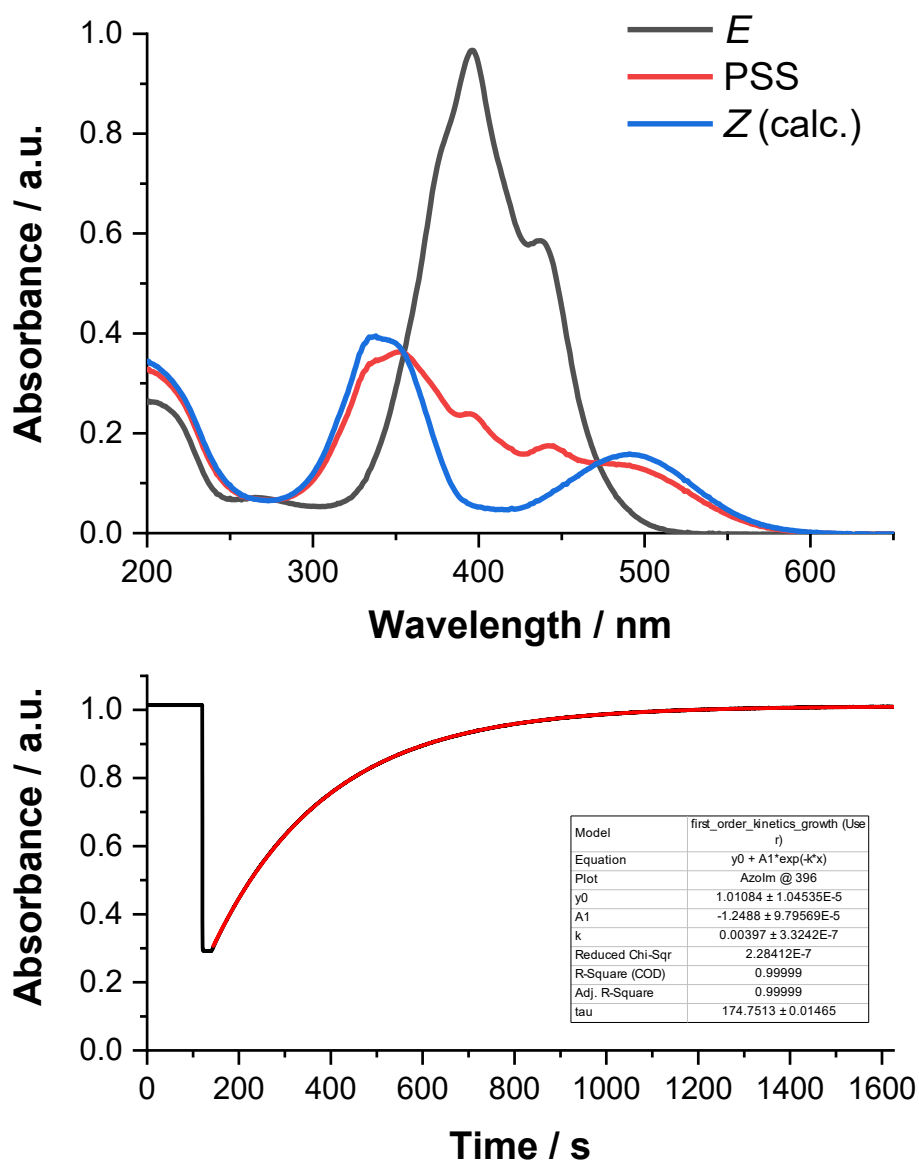


Figure 8.25 Photophysical properties of azobis(2-imidazole) in acetonitrile (298 K) a) A comparison of *E*, PSS and *Z* isomer spectra (calculated as discussed in Chapter 3). b) A photoswitching cycle showing the calculation of *Z*→*E* thermal half-life.

8.5 Photoswitching of 4.1

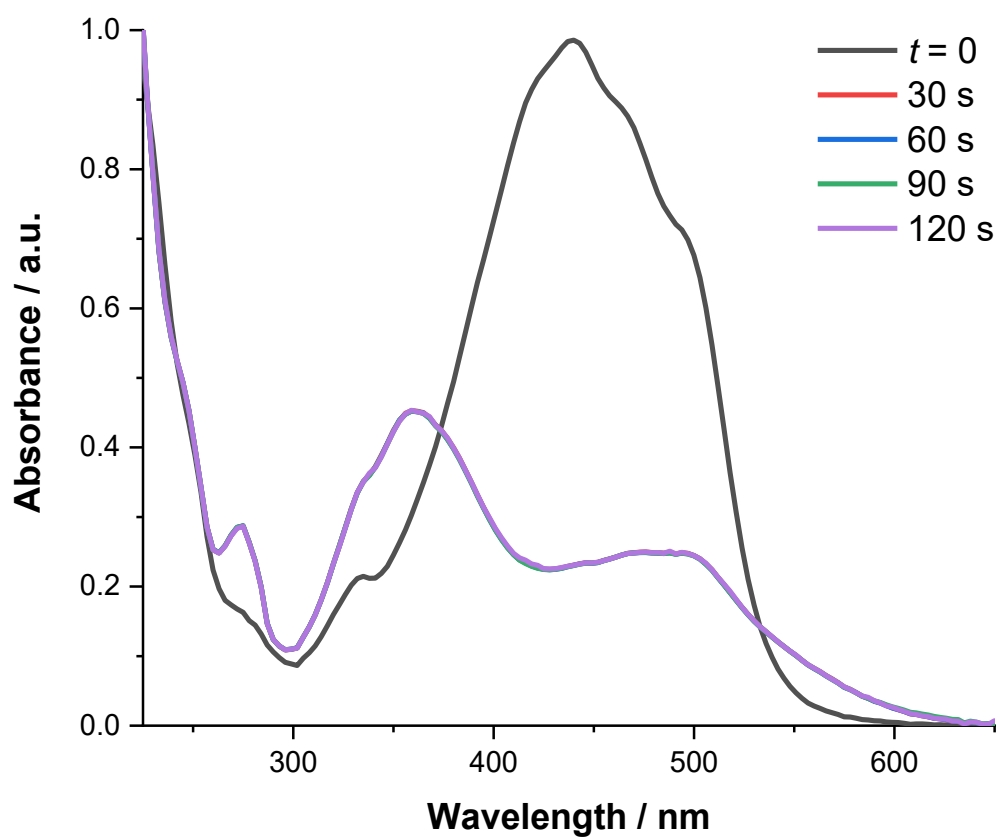


Figure 8.26 UV-Vis spectra of 4.1 in acetonitrile measured at 30 second intervals under constant irradiation at 448 nm. Equilibrium is reached by 30 seconds, and further irradiation does not affect the spectrum. This was observed for all solvents investigated.

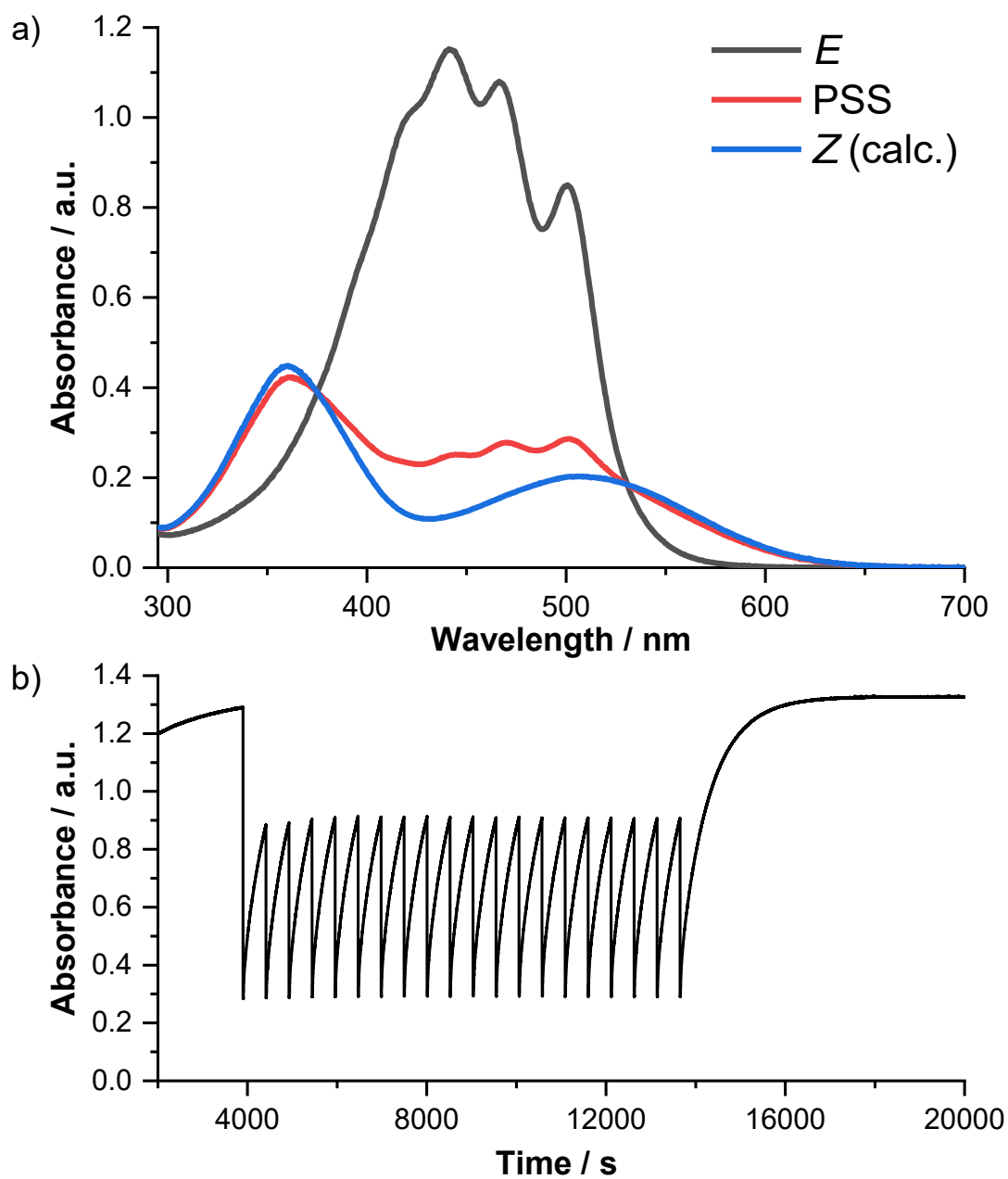


Figure 8.27 The fatigue resistance of **4.1** (toluene, 298 K) during 20 switching cycles of 448 nm light irradiation (10 s light on; 500 s light off). a) A comparison of *E*, PSS and *Z* isomer spectra (calculated as discussed in Chapter 3Error! Reference source not found.). b) 20 photoswitching cycles showing the fatigue resistance.

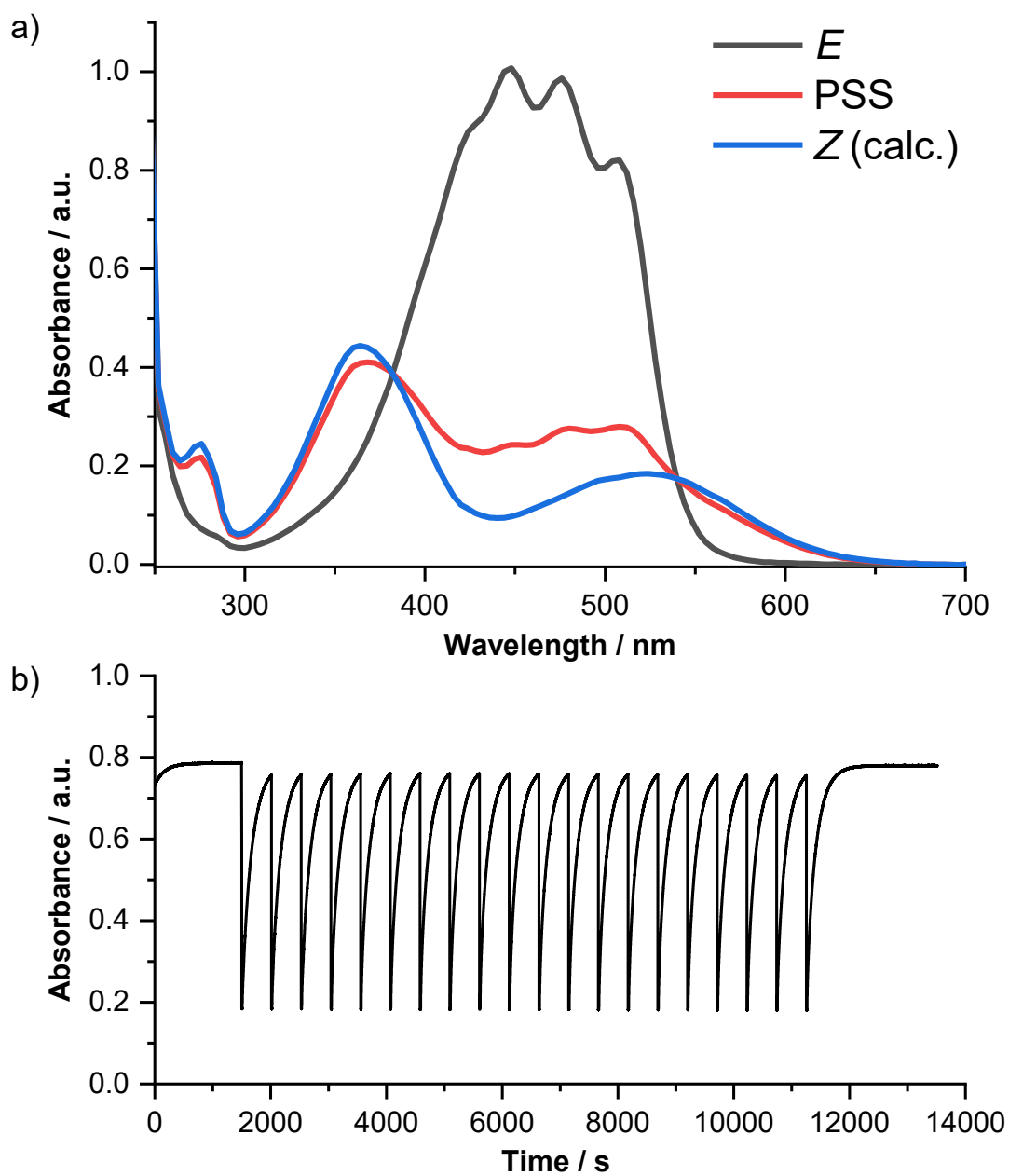


Figure 8.28 The fatigue resistance of **4.1** (chloroform, 298 K) during 20 switching cycles of 448 nm light irradiation (10 s light on; 500 s light off). a) A comparison of E, PSS and Z isomer spectra (calculated as discussed in Chapter 3) b) 20 photoswitching cycles showing the fatigue resistance.

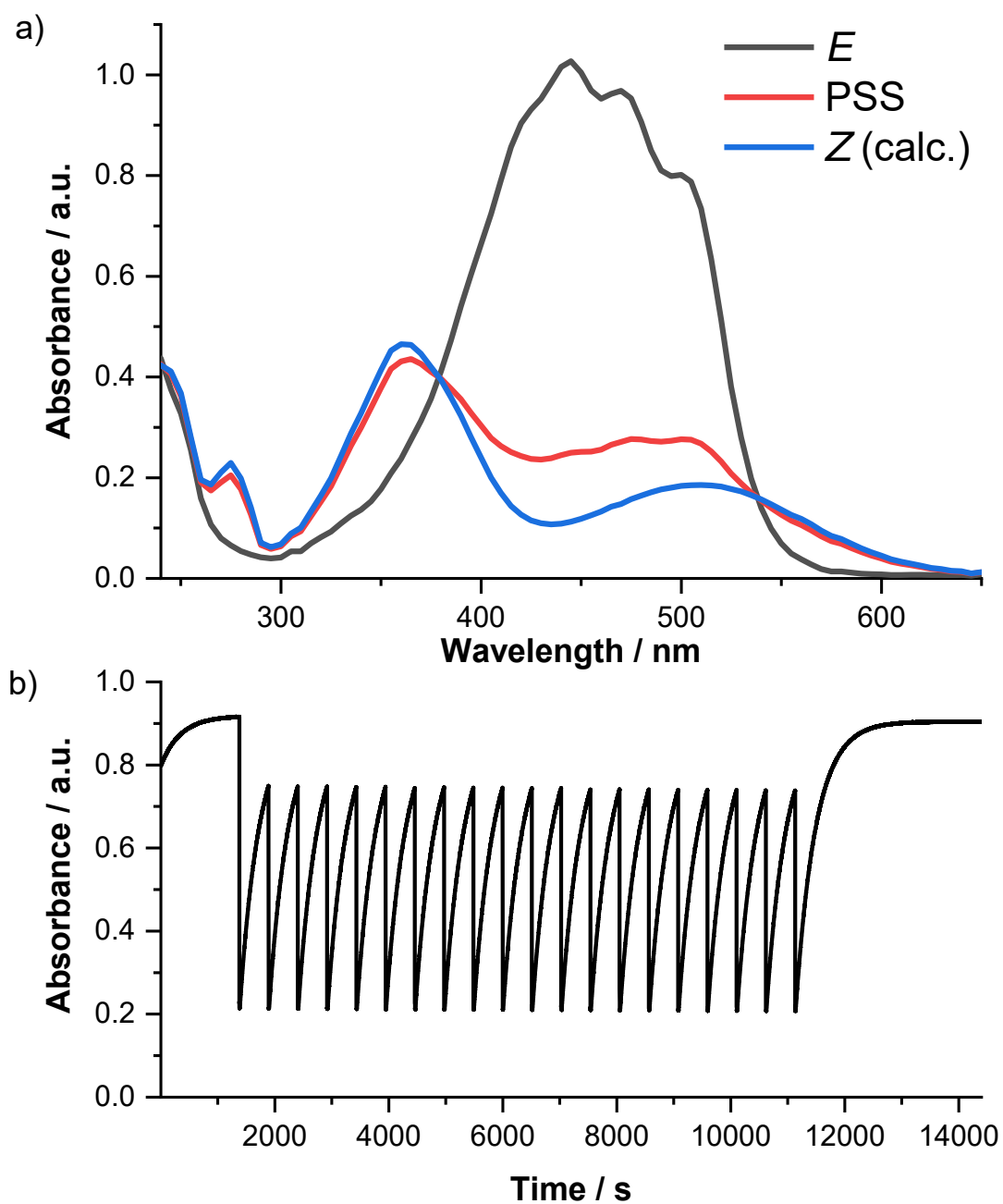


Figure 8.29 The fatigue resistance of **4.1** (DCM, 298 K) during 20 switching cycles of 448 nm light irradiation (10 s light on; 500 s light off). a) A comparison of *E*, PSS and *Z* isomer spectra (calculated as discussed in Chapter 3). b) 20 photoswitching cycles showing the fatigue resistance.

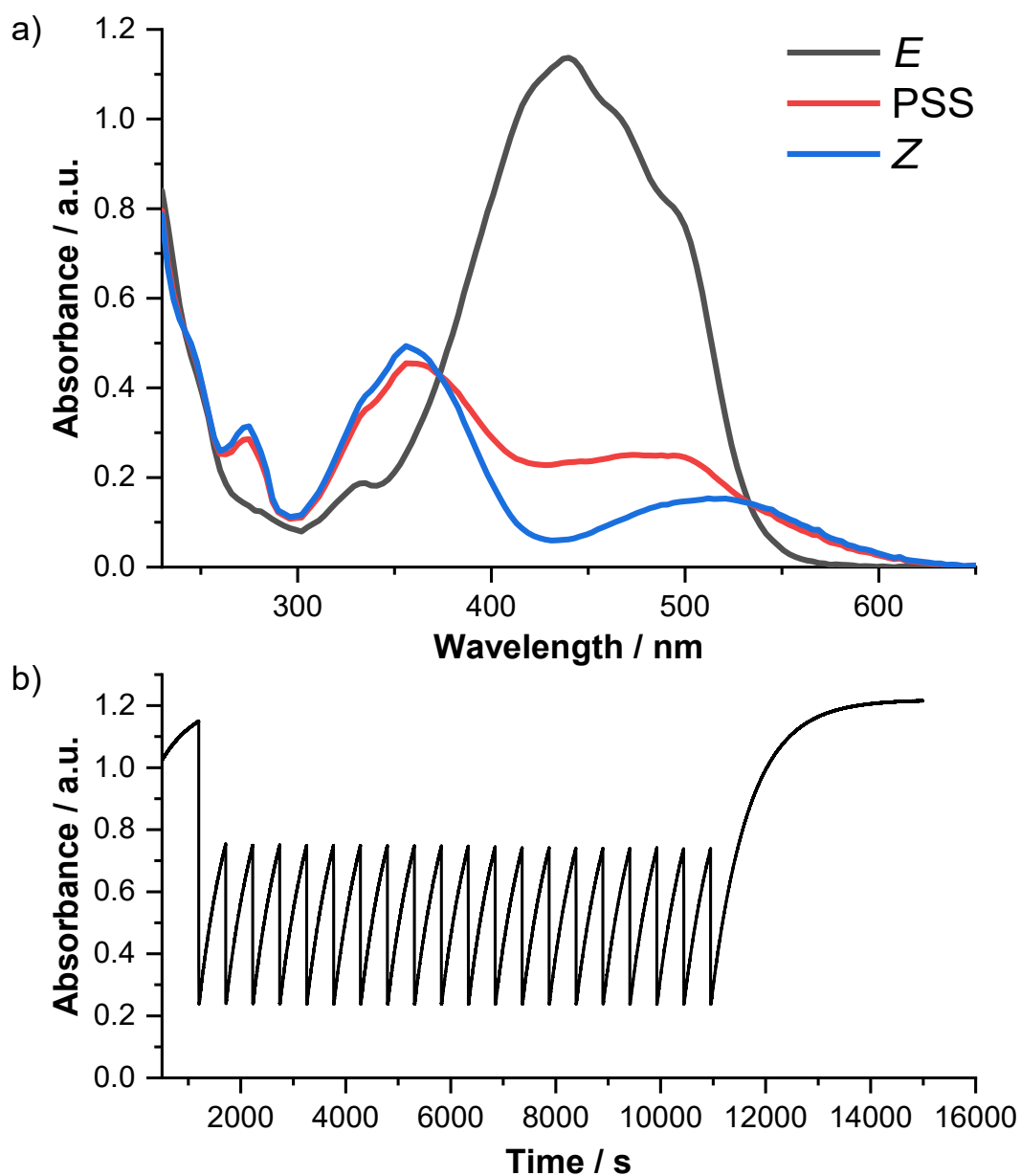


Figure 8.30 The fatigue resistance of **4.1** (acetonitrile, 298 K) during 20 switching cycles of 448 nm light irradiation (10 s light on; 500 s light off). a) A comparison of *E*, PSS and *Z* isomer spectra (calculated as discussed in Chapter 3). b) 20 photoswitching cycles showing the fatigue resistance.

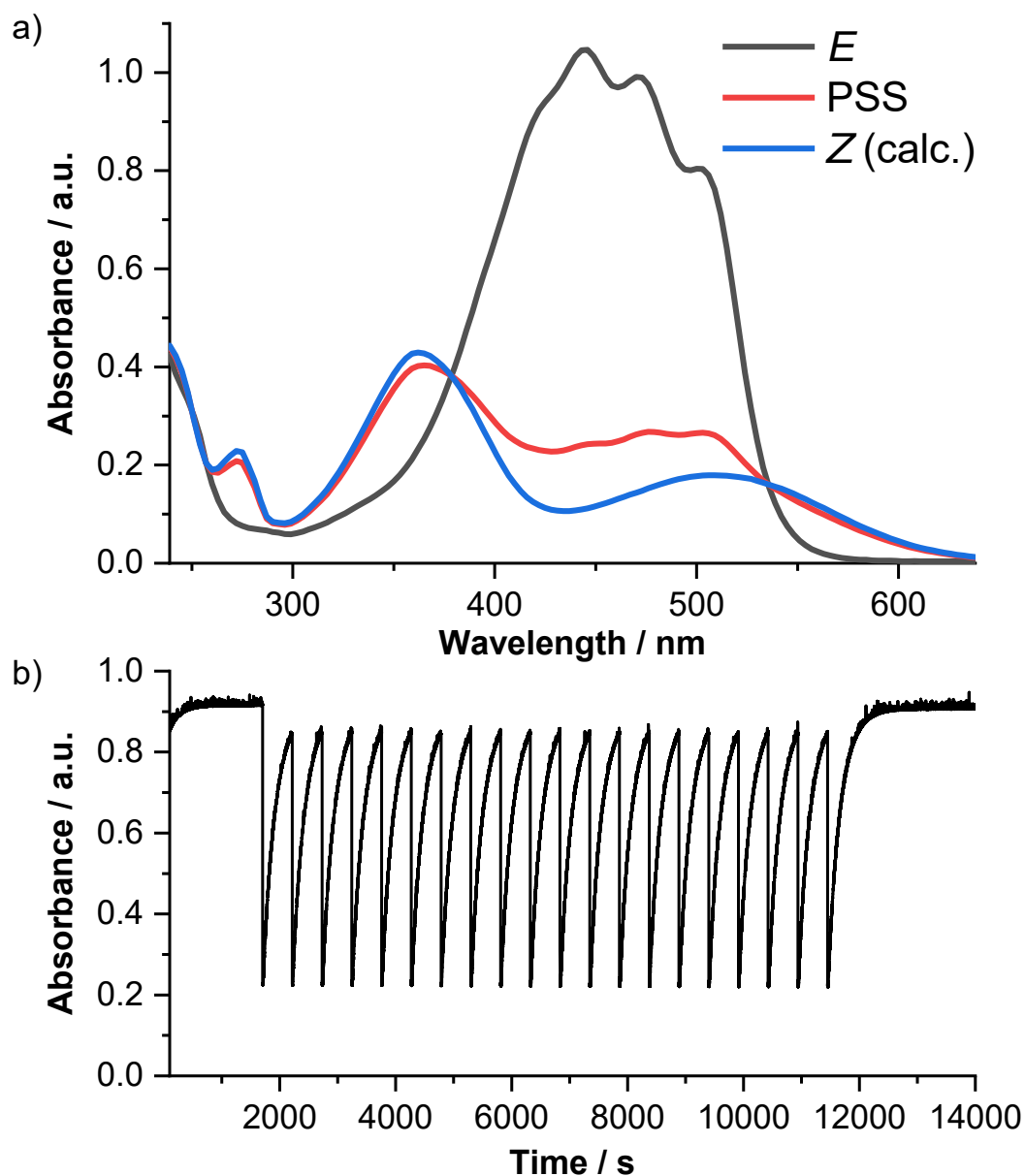


Figure 8.31 The fatigue resistance of **4.1** (methanol, 298 K) during 20 switching cycles of 448 nm light irradiation (10 s light on; 500 s light off). a) A comparison of *E*, PSS and *Z* isomer spectra (calculated as discussed in Chapter 3). b) 20 photoswitching cycles showing the fatigue resistance.

8.6 Photoswitching of 4.2

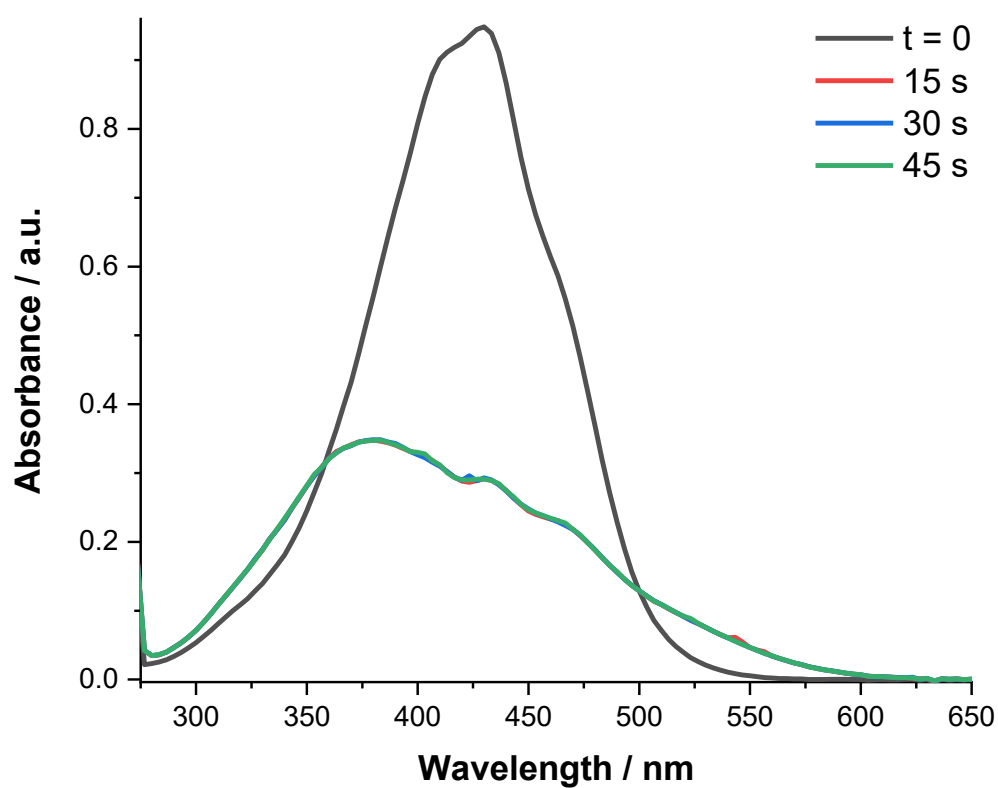


Figure 8.32 UV-Vis spectra of 4.2 in acetonitrile measured at 15 second intervals under constant irradiation at 448 nm. Equilibrium is reached by 15 seconds, and further irradiation does not affect the spectrum. This was observed for all solvents investigated.

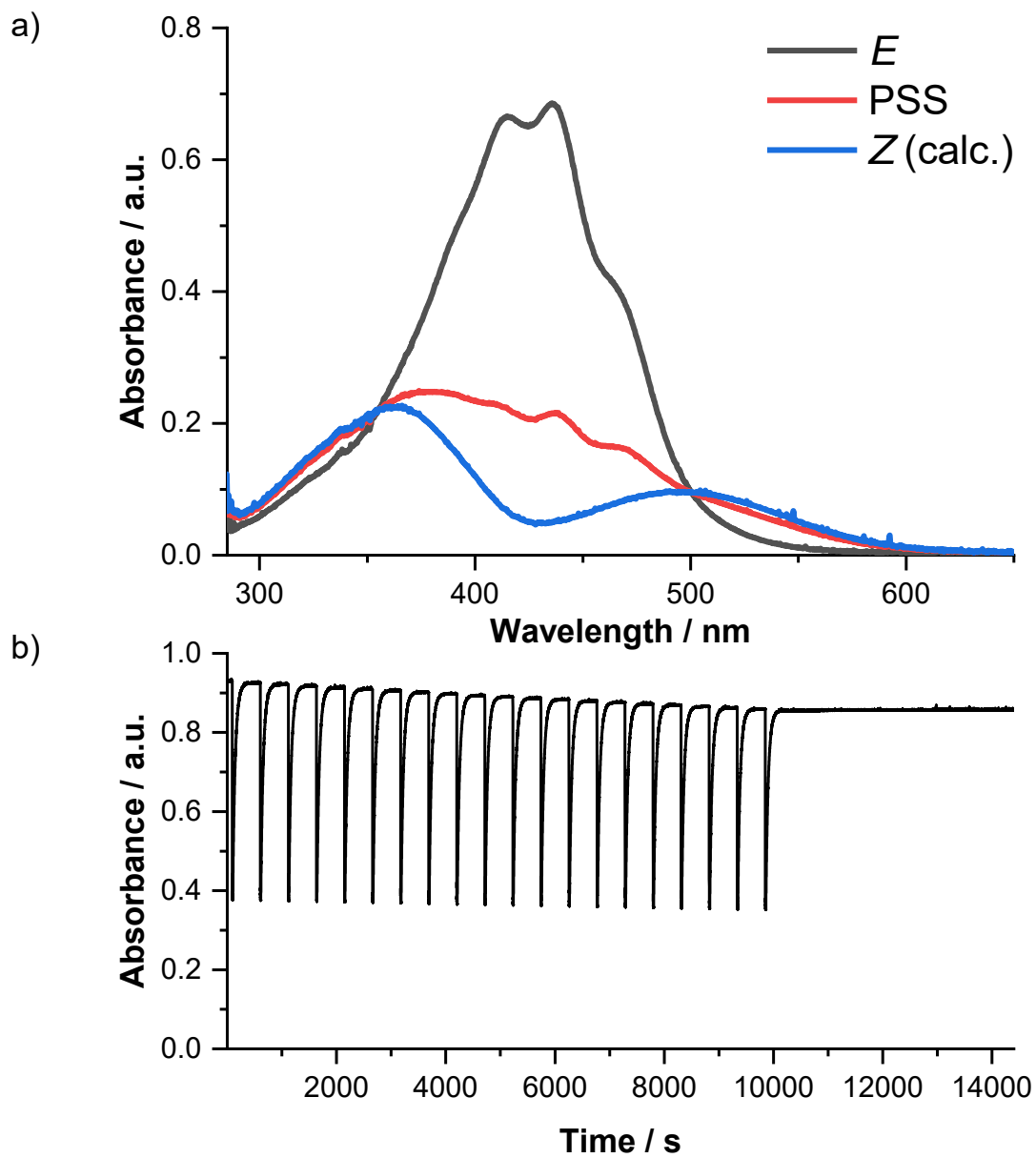


Figure 8.33 The fatigue resistance of **4.2** (toluene, 298 K) during 20 switching cycles of 448 nm light irradiation (10 s light on; 500 s light off). a) A comparison of *E*, PSS and *Z* isomer spectra (calculated as discussed in Chapter 3). b) 20 photoswitching cycles showing the fatigue resistance

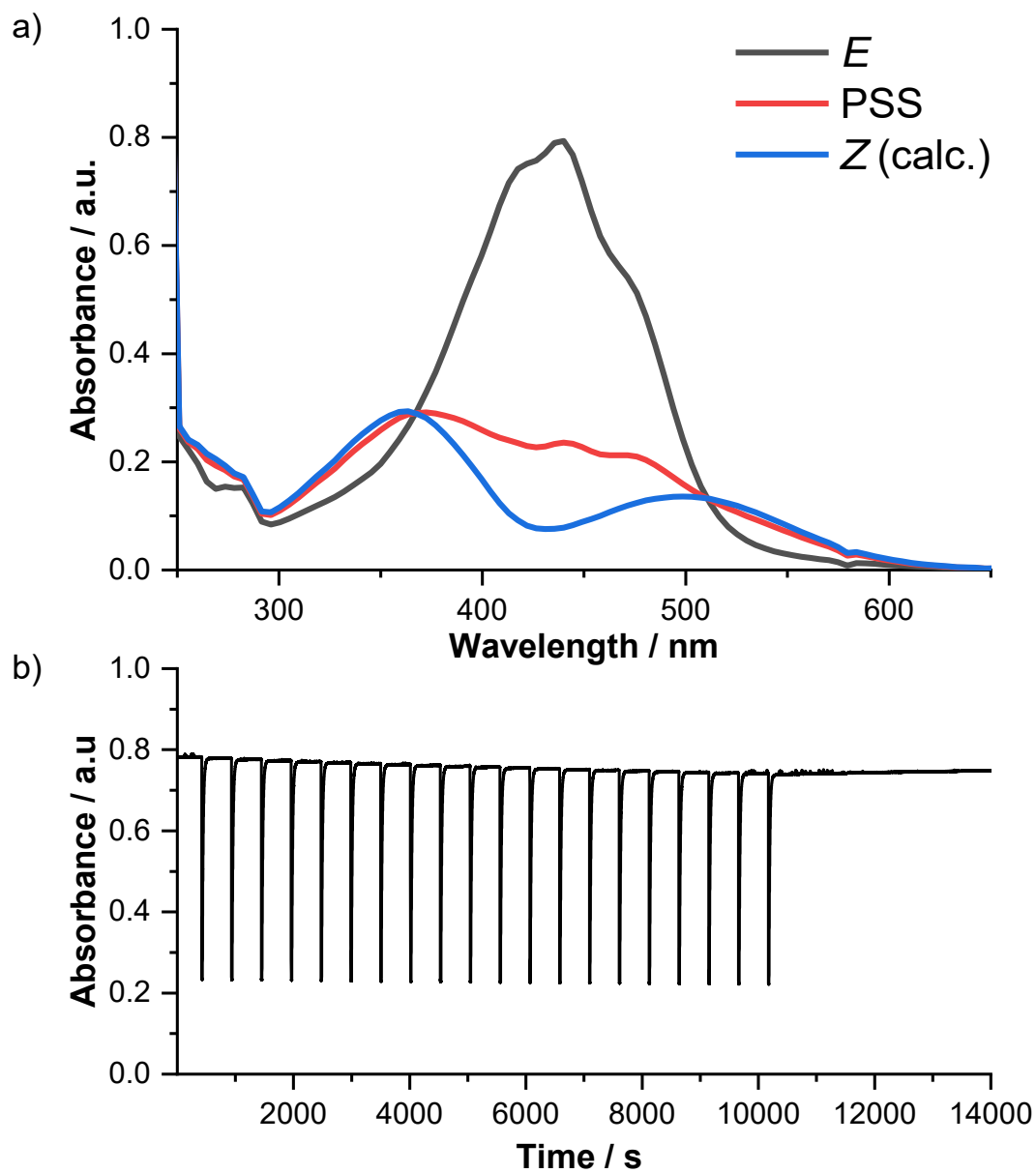


Figure 8.34 The fatigue resistance of **4.2** (chloroform, 298 K) during 20 switching cycles of 448 nm light irradiation (10 s light on; 500 s light off). a) A comparison of *E*, PSS and *Z* isomer spectra (calculated as discussed in Chapter 3). b) 20 photoswitching cycles showing the fatigue resistance.

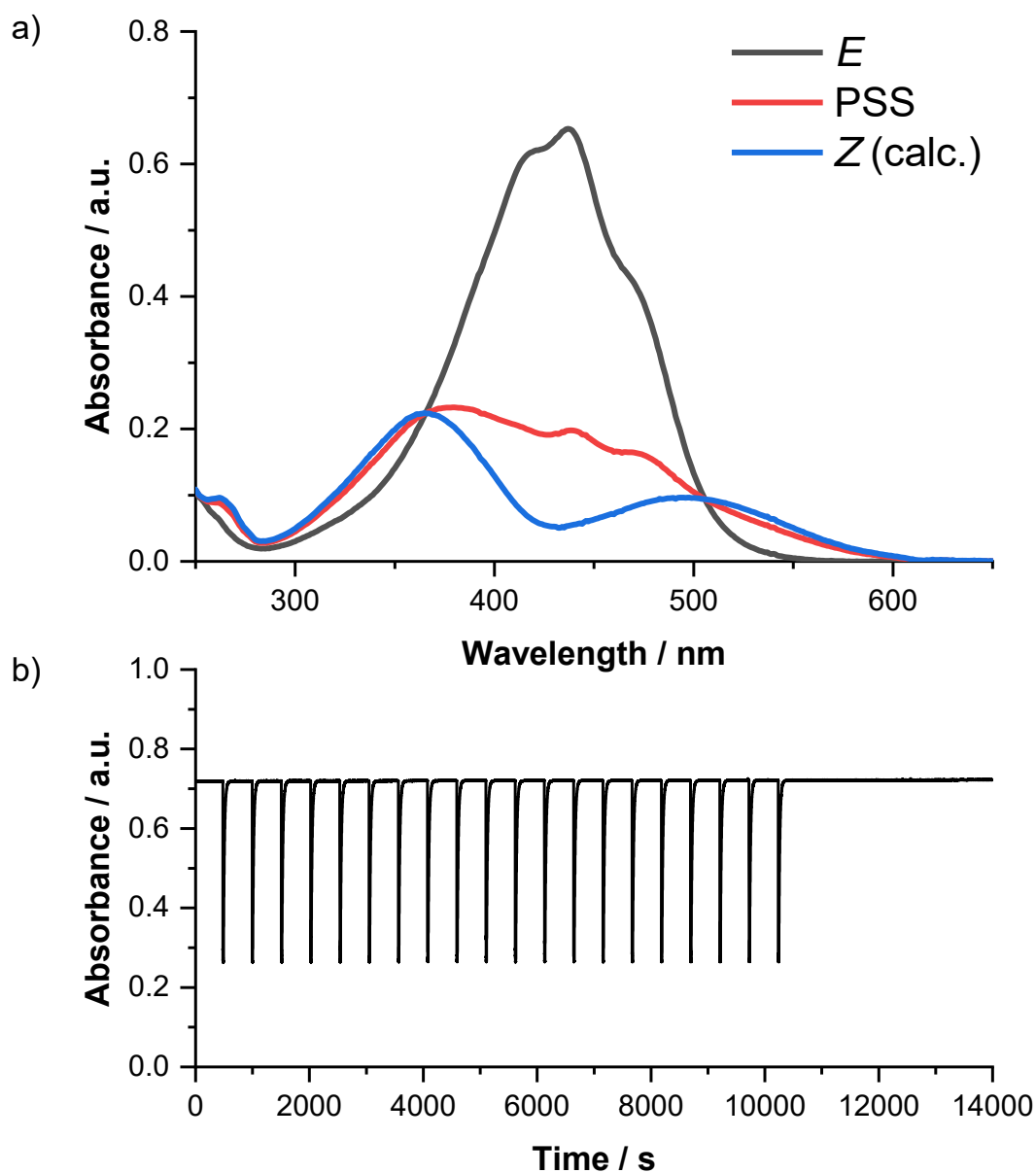


Figure 8.35 The fatigue resistance of **4.2** (DCM, 298 K) during 20 switching cycles of 448 nm light irradiation (10 s light on; 500 s light off). a) A comparison of *E*, PSS and *Z* isomer spectra (calculated as discussed in Chapter 3). b) 20 photoswitching cycles showing the fatigue resistance.

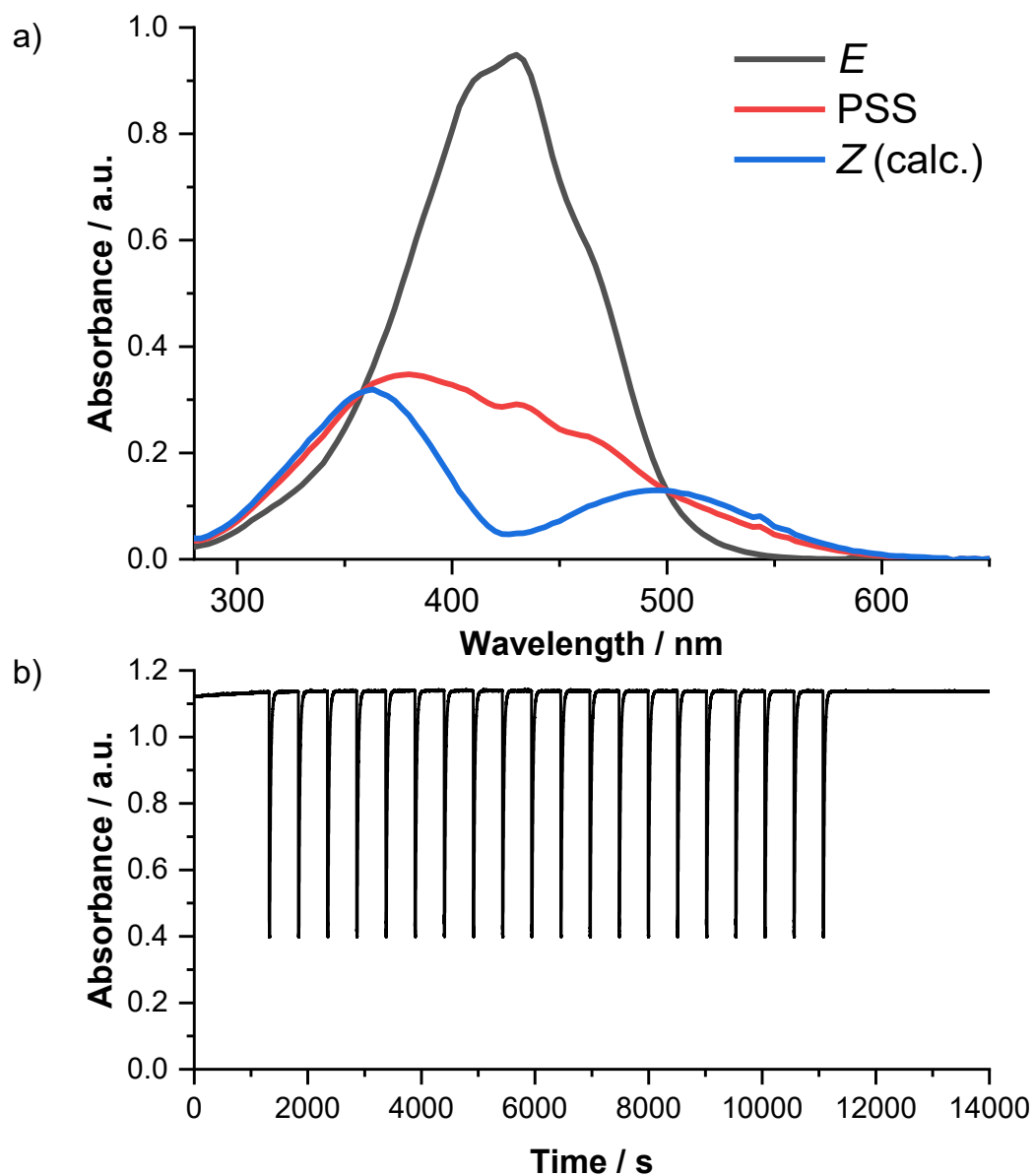


Figure 8.36 The fatigue resistance of **4.2** (acetonitrile, 298 K) during 20 switching cycles of 448 nm light irradiation (10 s light on; 500 s light off). a) A comparison of *E*, PSS and *Z* isomer spectra (calculated as discussed in Chapter 3). b) 20 photoswitching cycles showing the fatigue resistance.

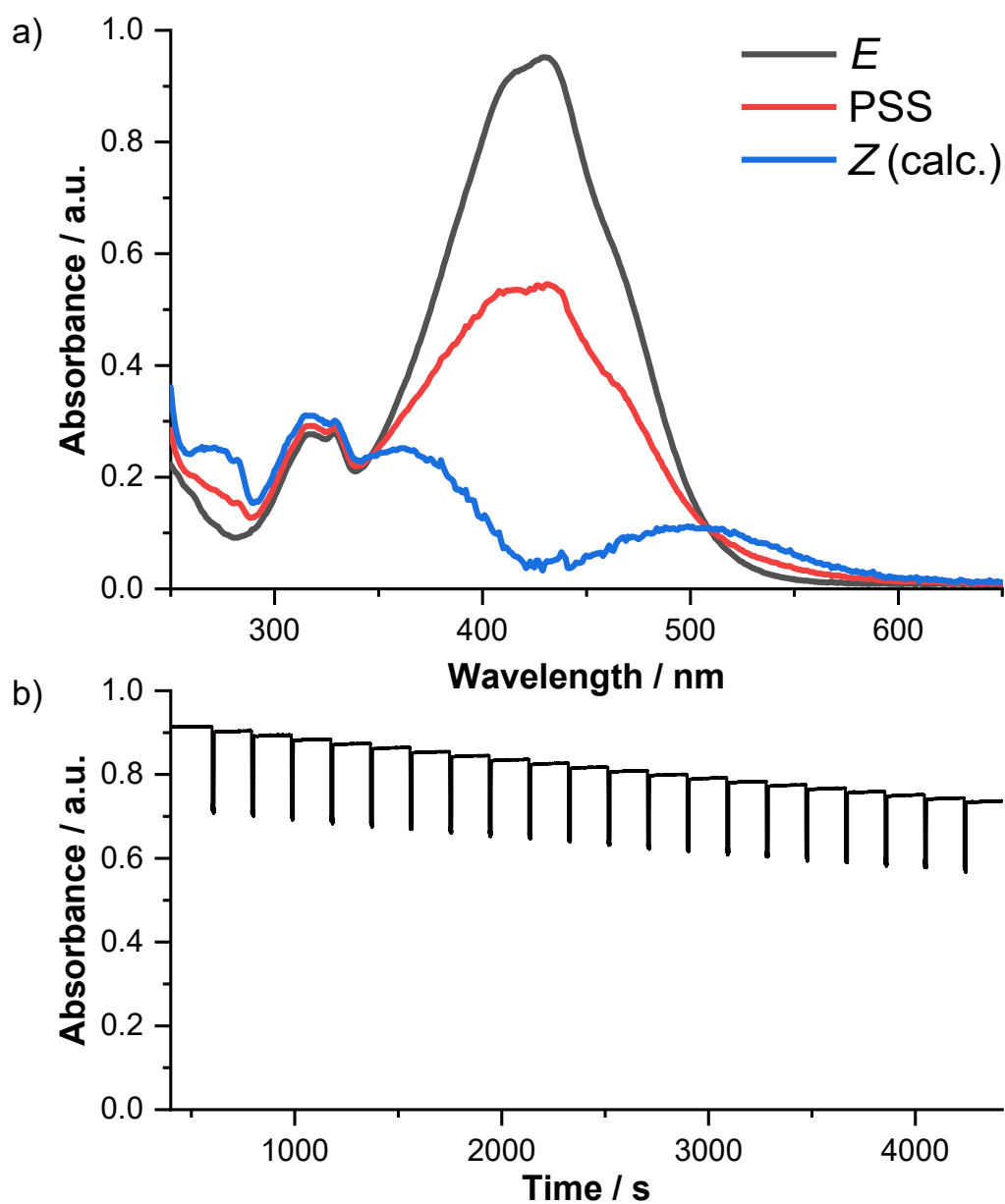


Figure 8.37 The fatigue resistance of **4.2** (methanol, 298 K) during 20 switching cycles of 448 nm light irradiation (10 s light on; 180 s light off). a) A comparison of *E*, PSS and *Z* isomer spectra (calculated as discussed in Chapter 3). b) 20 photoswitching cycles showing the fatigue resistance. Note that the time between switching cycles has been decreased to 180 s due to the very short thermal half-life. The observed decrease in absorption over time suggests this compound photodegrades in methanol.

8.7 Photoswitching of 4.3

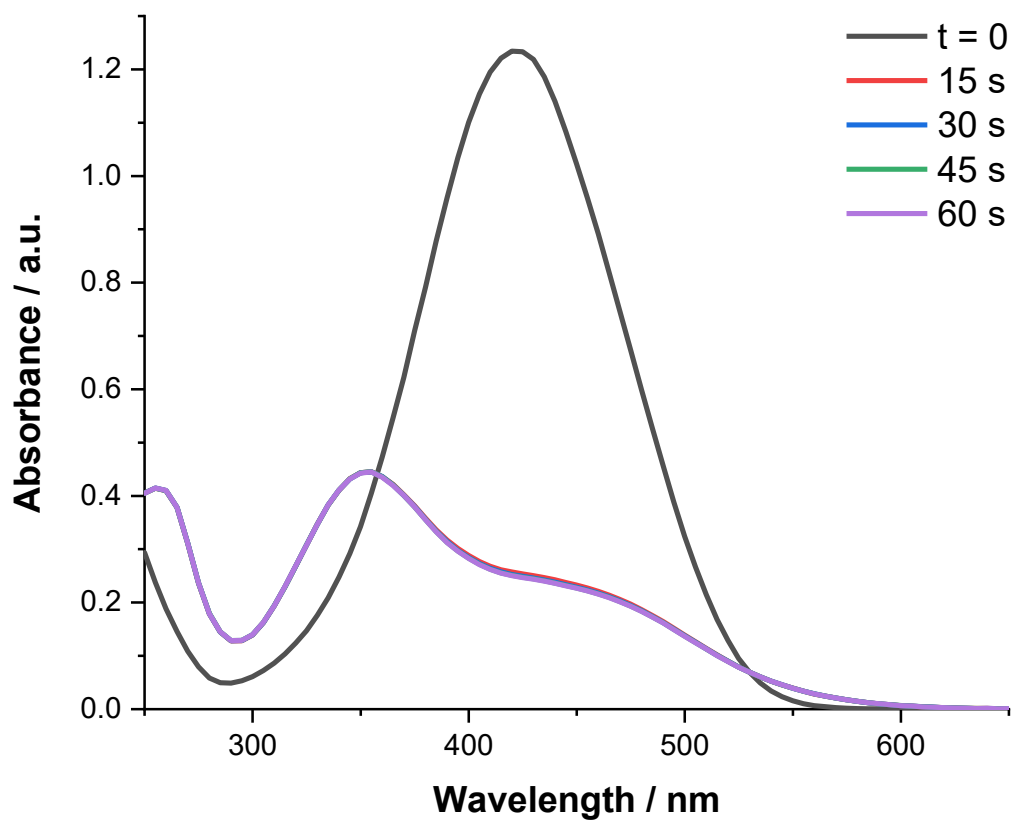


Figure 8.38 UV-Vis spectra of **4.3** in acetonitrile measured at 15 second intervals under constant irradiation at 448 nm. Equilibrium is reached by 15 seconds, and further irradiation does not affect the spectrum. This was observed for all solvents investigated.

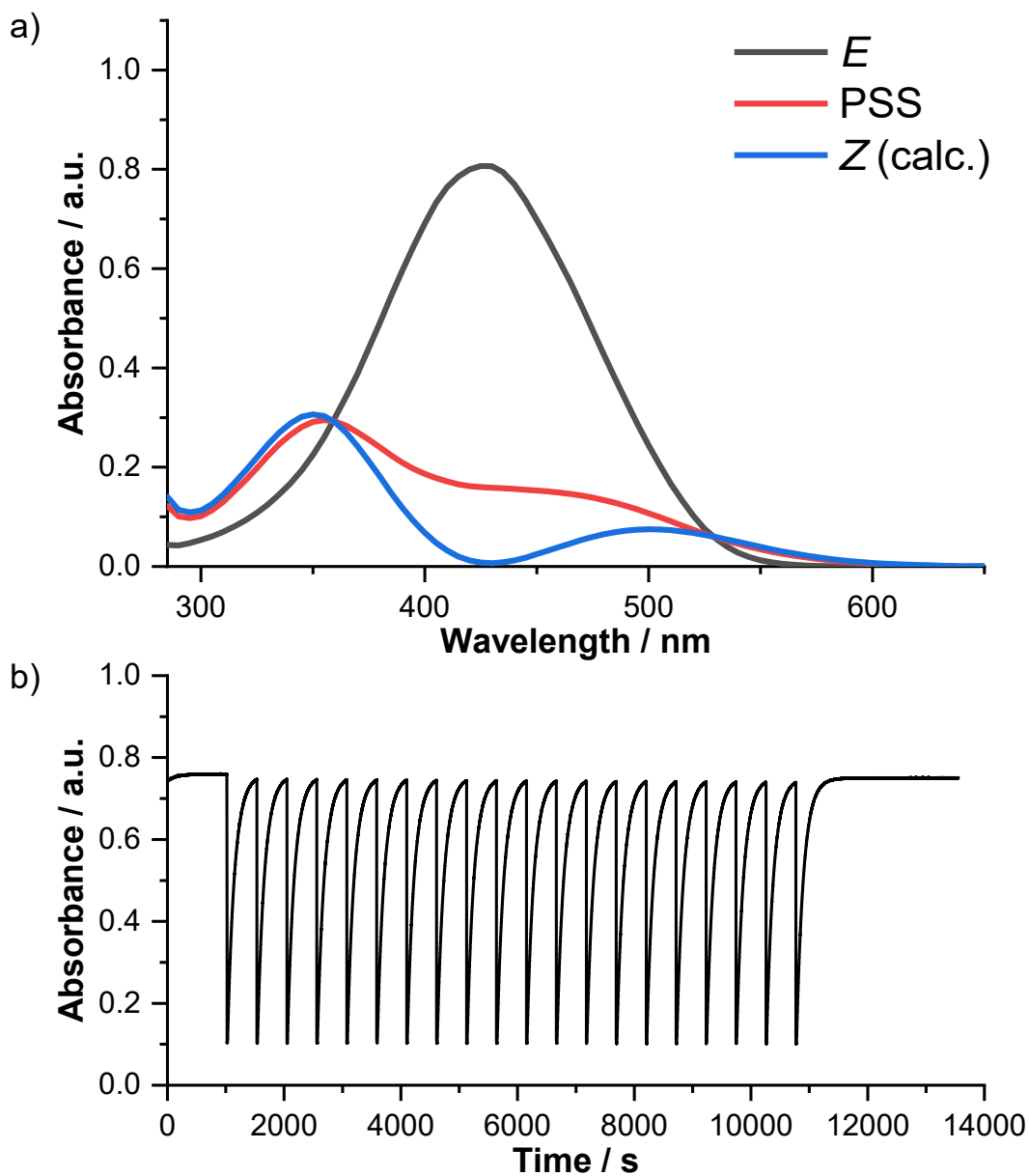


Figure 8.39 The fatigue resistance of **4.3** (toluene, 298 K) during 20 switching cycles of 448 nm light irradiation (10 s light on; 500 s light off). a) A comparison of E, PSS and Z isomer spectra (calculated as discussed in Chapter 3). b) 20 photoswitching cycles showing the fatigue resistance.

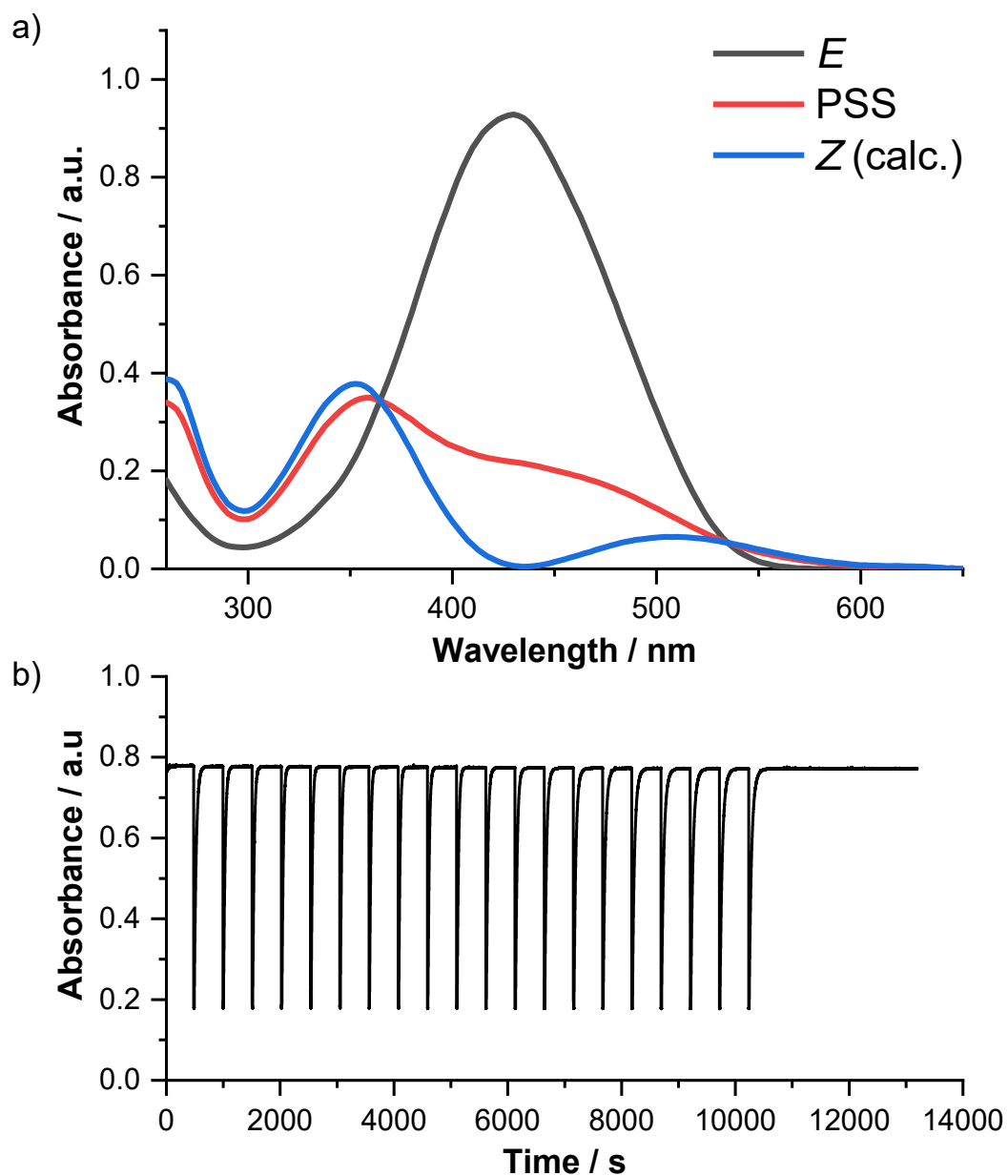


Figure 8.40 The fatigue resistance of **4.3** (chloroform, 298 K) during 20 switching cycles of 448 nm light irradiation (10 s light on; 500 s light off). a) A comparison of *E*, PSS and *Z* isomer spectra (calculated as discussed in Chapter 3). b) 20 photoswitching cycles showing the fatigue resistance.

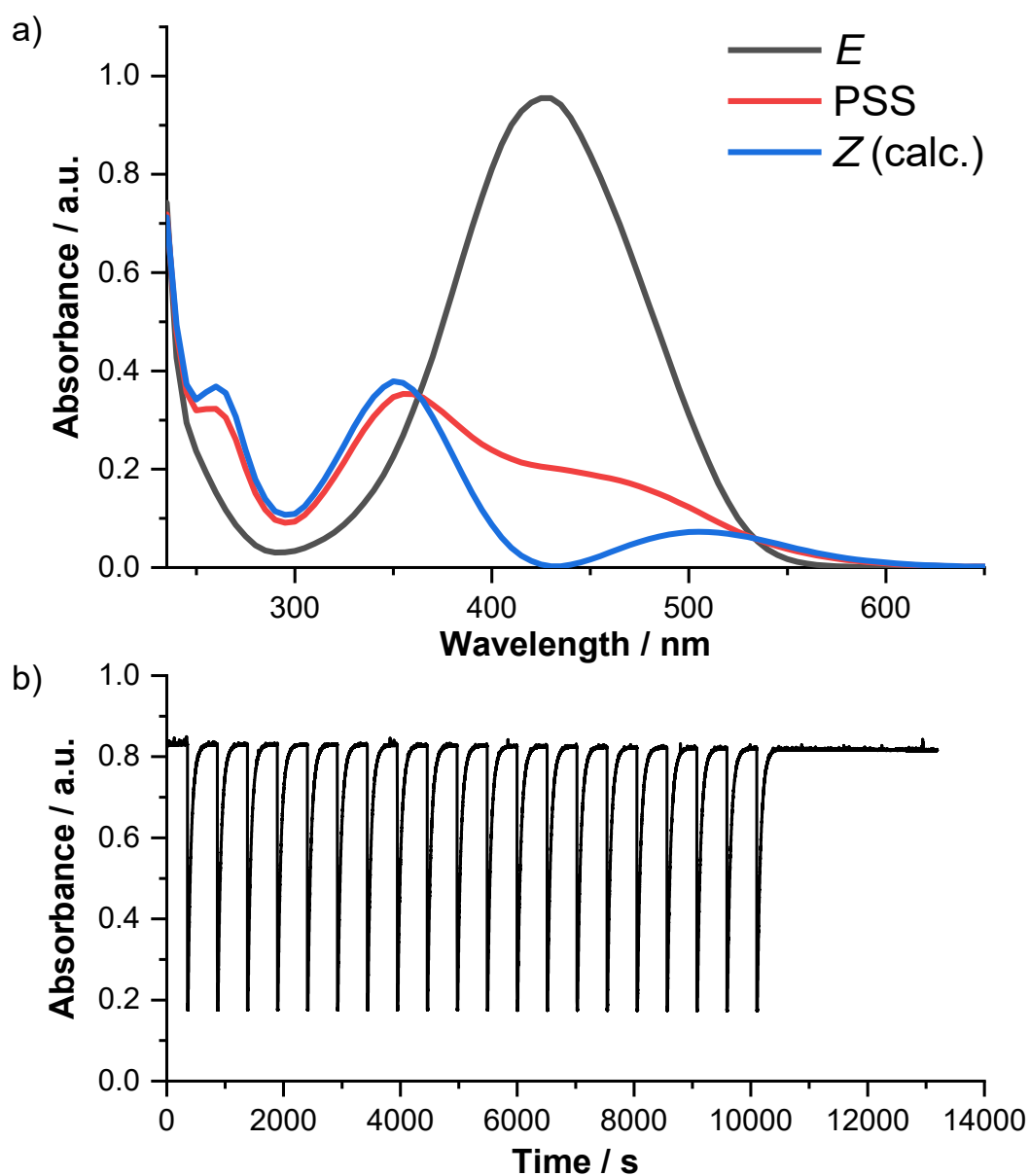


Figure 8.41 The fatigue resistance of **4.3** (DCM, 298 K) during 20 switching cycles of 448 nm light irradiation (10 s light on; 500 s light off). a) A comparison of *E*, PSS and *Z* isomer spectra (calculated as discussed in Chapter 3). b) 20 photoswitching cycles showing the fatigue

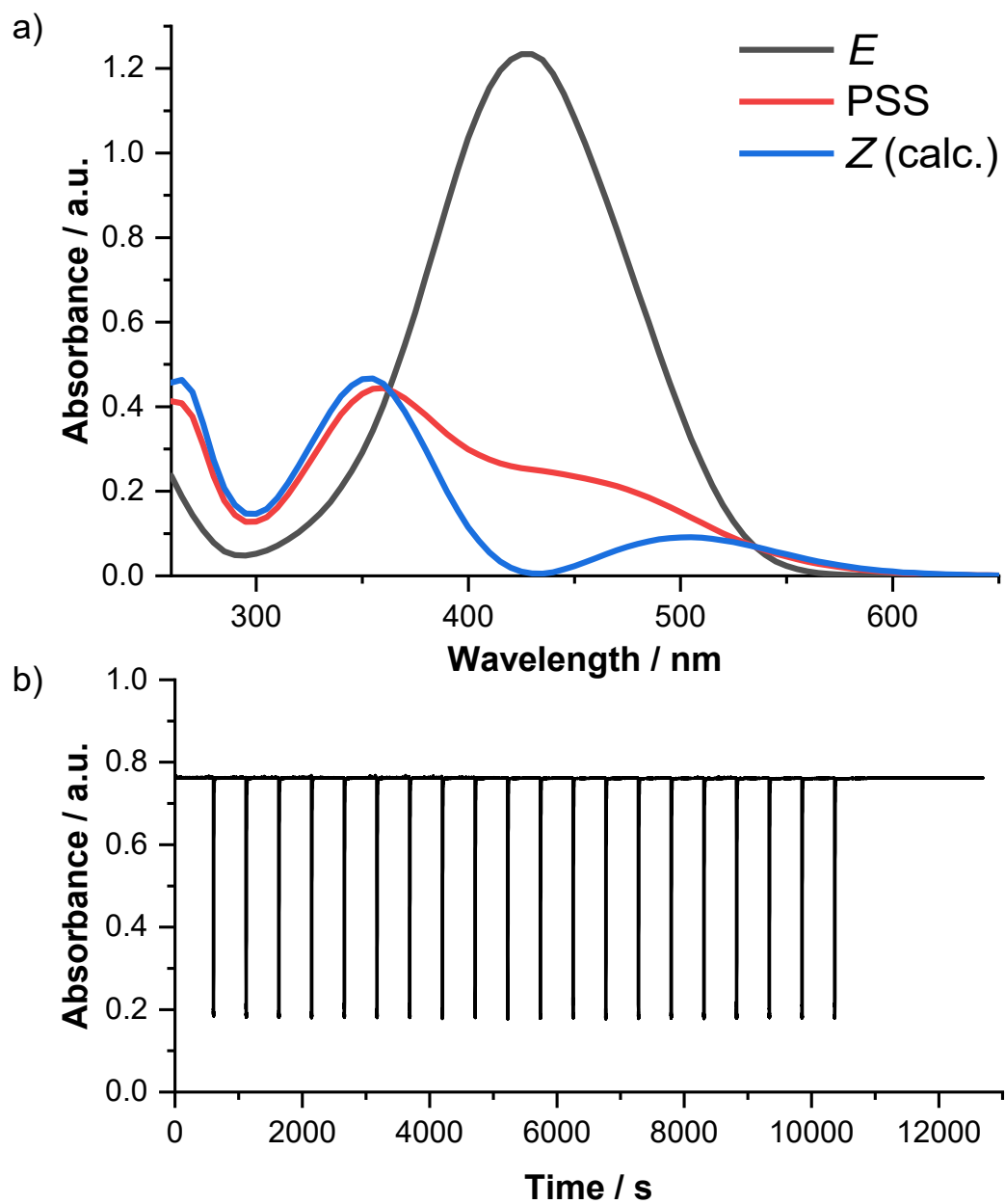


Figure 8.42 The fatigue resistance of **4.3** (acetonitrile, 298 K) during 20 switching cycles of 448 nm light irradiation (10 s light on; 500 s light off). a) A comparison of *E*, PSS and *Z* isomer spectra (calculated as discussed in Chapter 3). b) 20 photoswitching cycles showing the fatigue resistance.

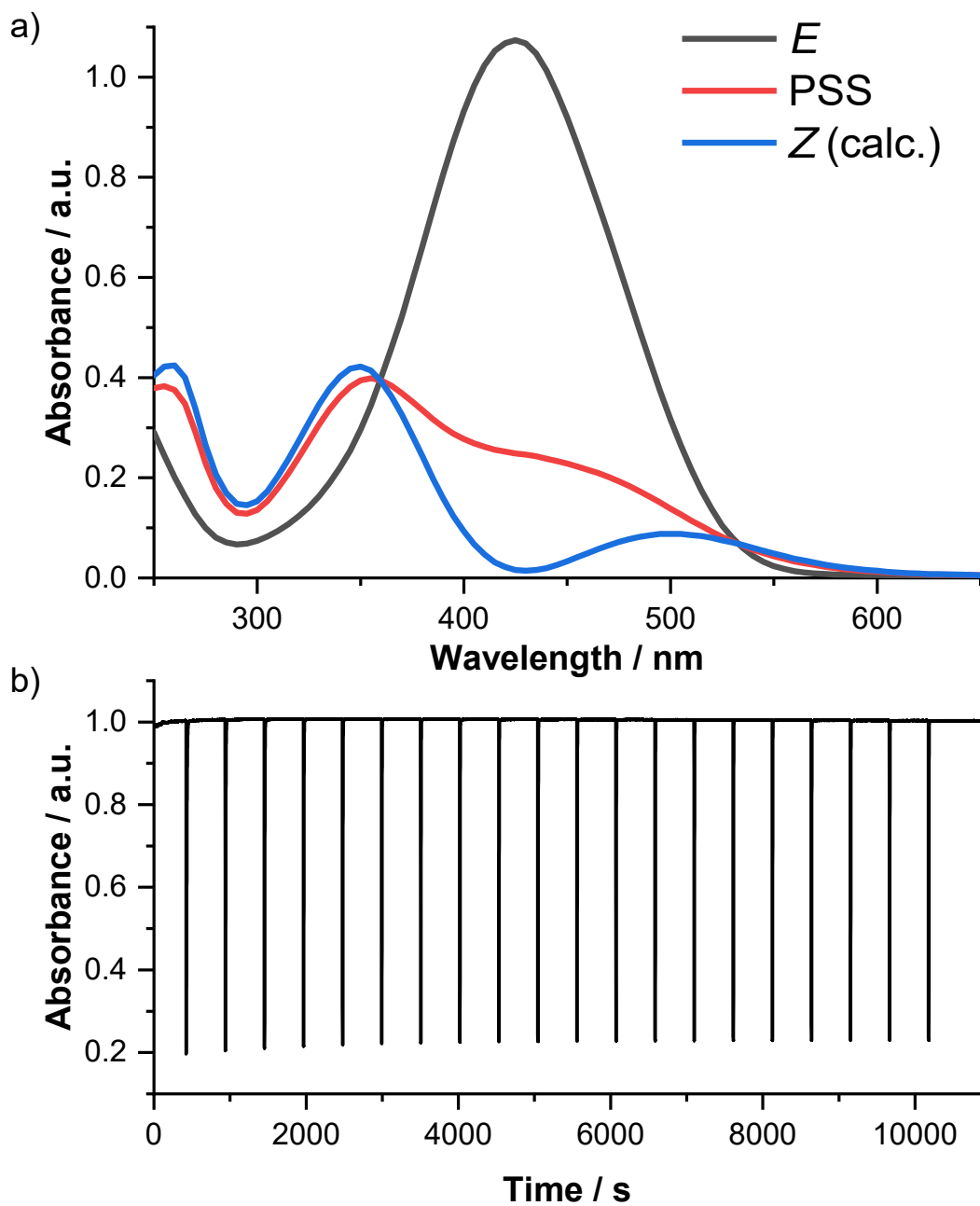


Figure 8.43 The fatigue resistance of **4.3** (methanol, 298 K) during 20 switching cycles of 448 nm light irradiation (10 s light on; 500 s light off). a) A comparison of *E*, PSS and *Z* isomer spectra (calculated as discussed in Chapter 3). b) 20 photoswitching cycles showing the fatigue resistance.

8.8 *In situ* ^1H NMR switching of compounds 4.1-3 in CDCl_3

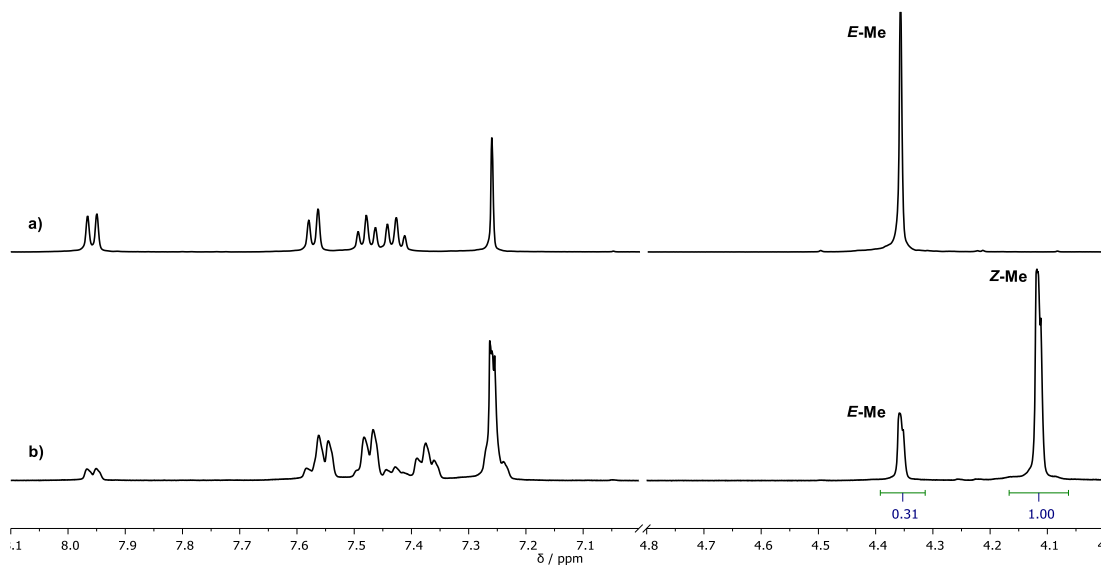


Figure 8.44 Comparison of *E* and PSD ^1H NMR spectra of **4.1** (500 MHz, CDCl_3 , 243 K). a) Initial spectrum. b) After irradiation with 448 nm light for 80 minutes.

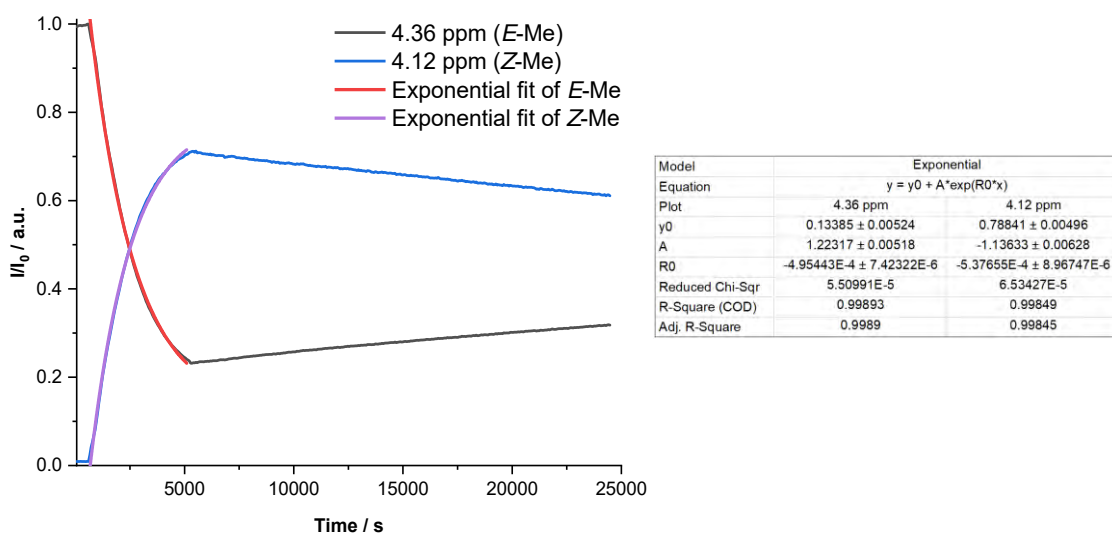


Figure 8.45 *In situ* photoswitching of **4.1** monitored by ^1H NMR (500 MHz, CDCl_3 , 243 K). The red and purple lines denote mono-exponential fits for the intensity of *E*-Me and *Z*-Me respectively while under constant irradiation.

Table 8.1 Comparison of the photoswitching parameters of **4.1** as measured by ^1H NMR and UV-vis spectroscopy.

Method	PSD (Z:E)	$t_{1/2}$ / s	Calculated Z→E barrier / kJ mol^{-1}
^1H NMR (CDCl_3 , 243 K) ^a	85:15	73500	82.5
UV-Vis (CHCl_3 , 298 K) ^b	84:16	114	85.4

^a Thermal lifetime was calculated for a single cycle using the equation discussed in **Error! Reference source not found.**. The proton signals for *E*-Me and *Z*-Me were fitted to a mono-exponential function, allowing calculation of the equilibrated PSD. ^b Thermal lifetime and PSD were calculated using UV-vis spectroscopy as discussed in **Error! Reference source not found.** and Chapter 3.

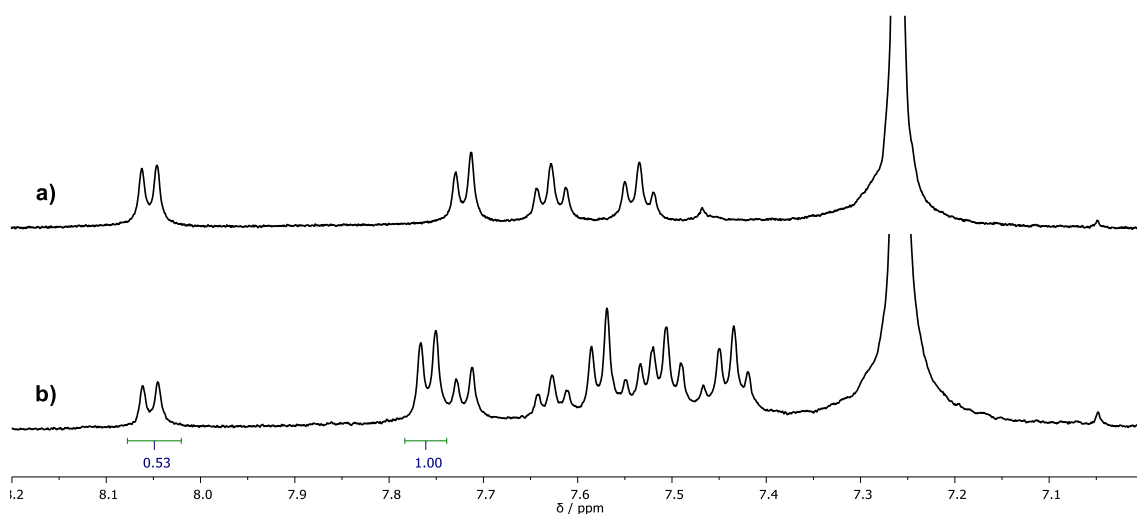


Figure 8.46 Comparison of *E* and PSD ^1H NMR spectra of **4.2** (500 MHz, CDCl_3 , 243 K). a) Initial spectrum. b) After irradiation with 448 nm light for 45 minutes.

Table 8.2 Comparison of the photoswitching parameters of **4.2** as measured by ^1H NMR and UV-vis spectroscopy

Method	PSD (Z:E)	$t_{1/2}$ / s	Calculated Z→E barrier / kJ mol^{-1}
^1H NMR (CDCl_3 , 243 K) ^a	66:34	7200	77.8
UV-Vis (CHCl_3 , 298 K) ^b	78:22	10	79.8

^a Thermal lifetime was calculated for a single cycle using the equation discussed in **Error! Reference source not found.**. PSD was calculated using the relative integrals of protons of *E*-H^d and *Z*-H^d due to overlap of the *E* and *Z* isomers signals which prevent adequate data fitting. ^b Thermal lifetime, PSD were calculated using UV-vis spectroscopy as discussed in **Error! Reference source not found.** and Chapter 3.

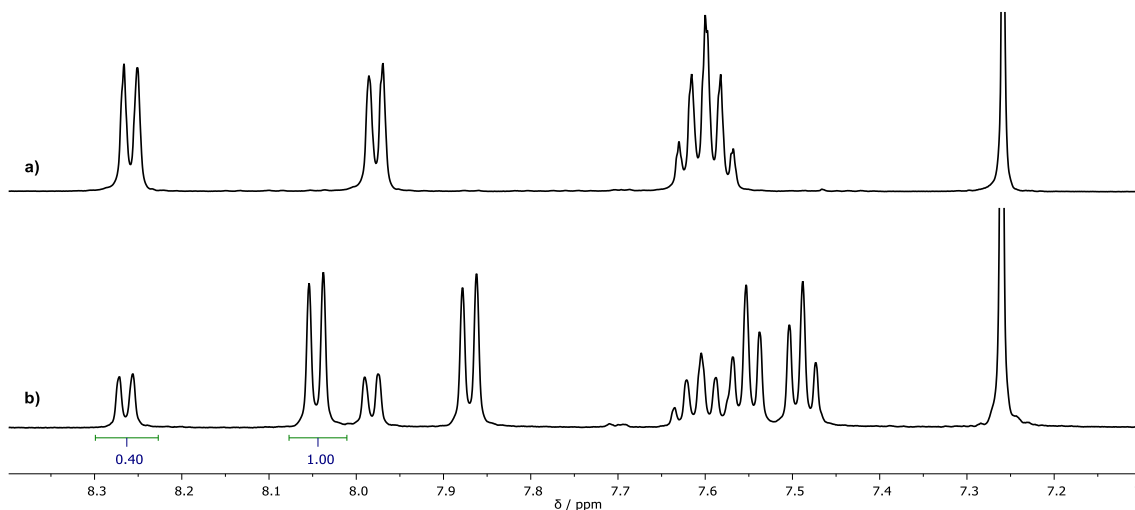


Figure 8.47 Comparison of *E* and PSD ^1H NMR spectra of **4.3** (500 MHz, CDCl_3 , 243 K). a) Initial spectrum. b) After irradiation with 448 nm light for 70 minutes.

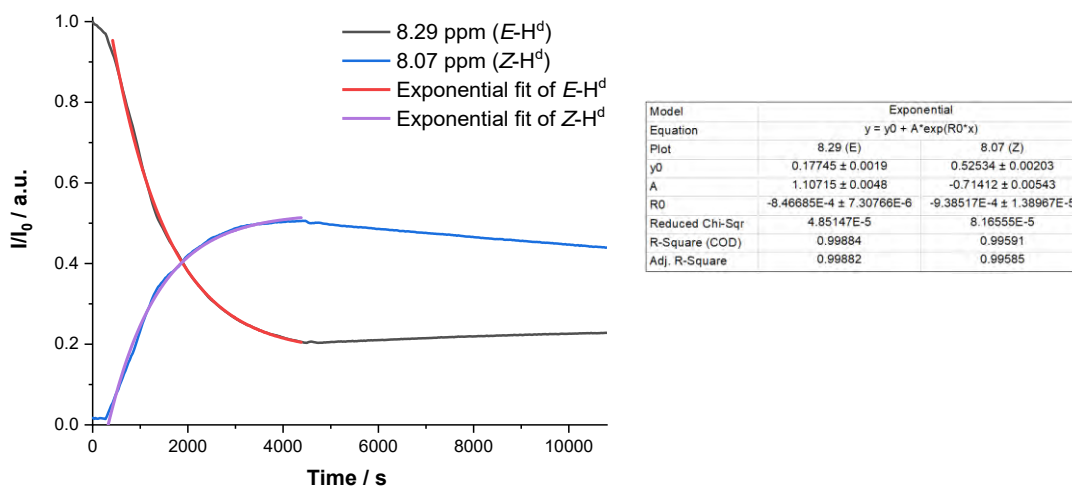


Figure 8.48 *In situ* photoswitching of **4.3** monitored by ^1H NMR (500 MHz, CDCl_3 , 243 K). The red and purple lines denote mono-exponential fits for the intensity of *E*- H^d and *Z*- H^d respectively while under constant irradiation

Table 8.3 Comparison of the photoswitching parameters of **4.3** as measured by ^1H NMR and UV-vis spectroscopy.

Method	PSD (Z:E)	$t_{1/2}$ / s	Calculated Z→E barrier / kJ mol^{-1}
^1H NMR (CDCl_3 , 243 K) ^a	75:25	16400	79.5
UV-Vis (CHCl_3 , 298 K) ^b	77:23	32	79.5

^a Thermal lifetime was calculated for a single cycle using the equation discussed in Error! Reference source not found.. The proton signals for *E*- H^d and *Z*- H^d were fitted to a mono-exponential function, allowing calculation of the equilibrated PSD. ^b Thermal lifetime, PSD were calculated using UV-vis spectroscopy as discussed in Error! Reference source not found. and Chapter 3.

8.9 The effect of protonation on photophysical properties in chloroform

The effect of protonation of the UV-visible spectra of **4.1-3** was studied by sequential addition of TFA to a solution of compound in CHCl_3 (3.5 mL). At low concentrations (0.001 to 0.01 mol L^{-1}), aliquots of a TFA stock solution in CHCl_3 (1:20 TFA/ CHCl_3) were added. For higher concentrations neat TFA was added directly to the solution. The sample was initially equilibrated in the dark for 20 minutes, then after each acid addition for 5 minutes (at least three half-lives) before the spectrum was measured. Three photoswitching cycles were then measured (448 nm LED irradiation; **4.1** = 10 s irradiation, 400 s dark; **4.2** and **4.3** = 10 s irradiation, 200 s dark) and the thermal half-life calculated as discussed in **Error! Reference source not found.**

8.9.1 UV-Vis spectra and photoswitching of **4.1** with TFA in chloroform

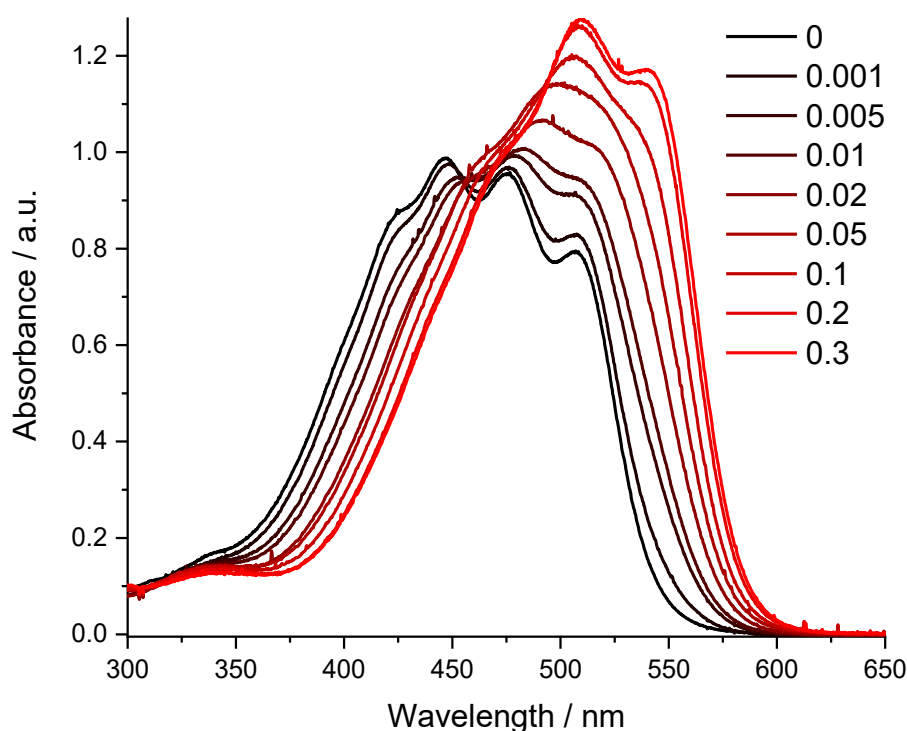


Figure 8.49 Change in the UV-visible spectra of **4.1** (chloroform, 35 μM) as TFA is added. The overall concentration of TFA (mol L^{-1}) is given on the right.

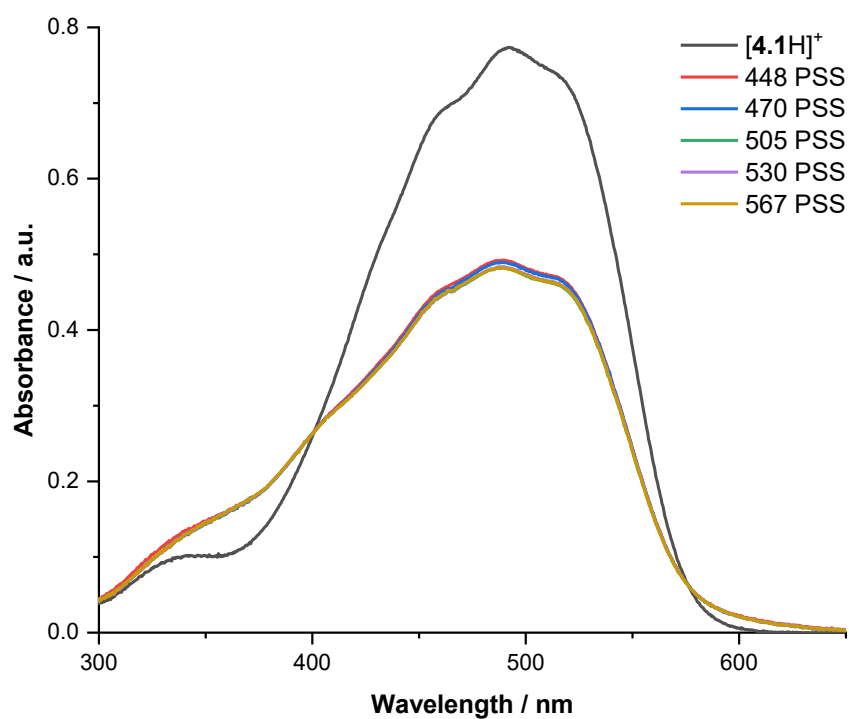


Figure 8.50 Photoswitching of **4.1** (27 μM , CHCl_3) + TFA with different LEDs. [TFA] = 0.02 mol L^{-1} . In all cases absorbance (measured at 492 nm) decreases by 37%.

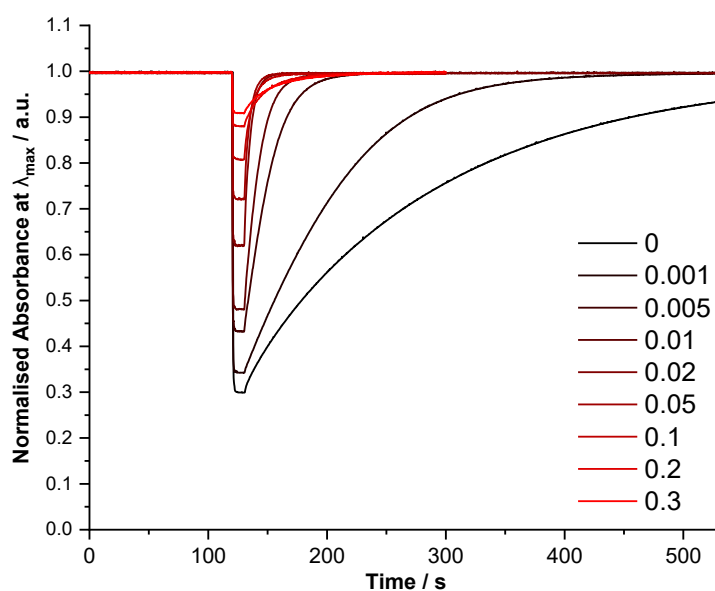


Figure 8.51 Change in the rate of *Z* to *E* thermal reversion of **4.1** (chloroform, 35 μM) as TFA is added, measured by UV-vis. The overall concentration of TFA (mol L^{-1}) is given on the right. Calculated $t_{1/2}$ values and change in absorbance are tabulated in Table 8.4

Table 8.4 Change in the photoswitching parameters of **4.1** as TFA is added in chloroform.

[TFA] / mol L ⁻¹	<i>t</i> _{1/2} / s ^a	Change in absorbance at PSS (% of max, measured at λ _{max, E})
0	114	70
0.001	61	66
0.005	15	57
0.01	8	52
0.02	4	38
0.05	3	28
0.1	5	19
0.2	13	12
0.3	18	9

^a Thermal lifetime was determined as discussed in **Error! Reference source not found.** using three switching cycles.

8.9.2 ¹H NMR spectra of **4.1** with TFA in CDCl₃

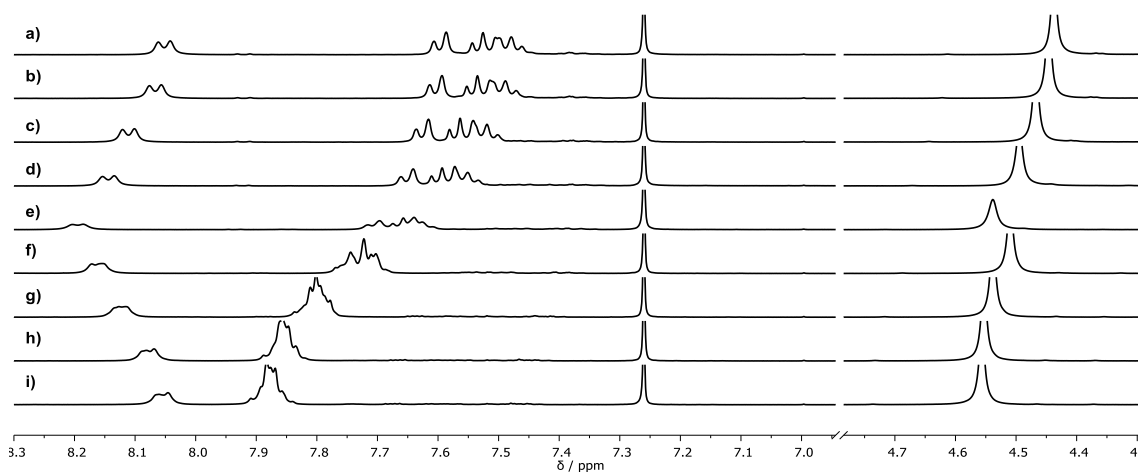


Figure 8.52 Partial ¹H NMR spectrum (400 MHz, CDCl₃, 298 K) of **4.1** (17 mM) with added TFA. [TFA]: a) 0 M; b) 0.001 M; c) 0.005 M; d) 0.01 M; e) 0.02 M; f) 0.05 M; g) 0.1 M; h) 0.2 M and i) 0.3 M.

8.9.3 UV-Vis spectra and photoswitching of 4.2 with TFA in chloroform

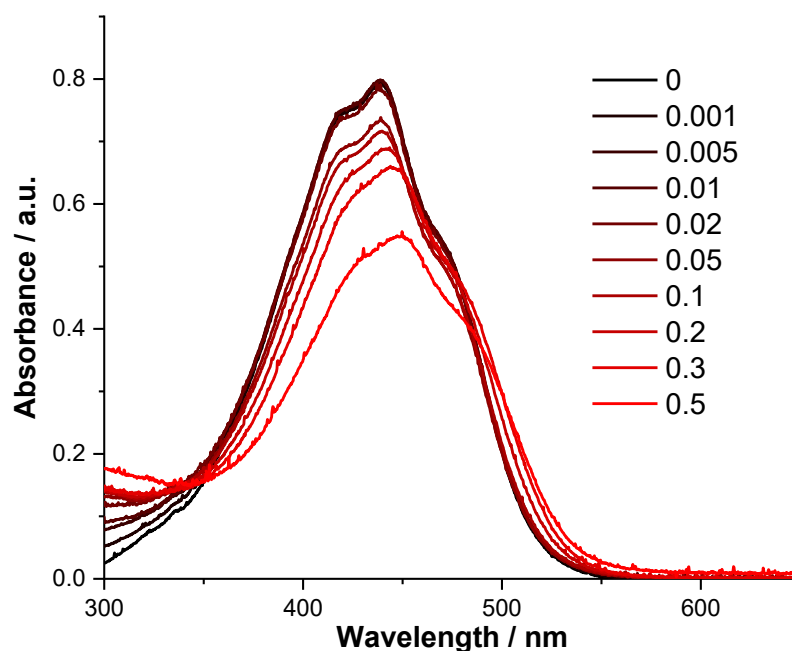


Figure 8.53 Change in the UV-visible spectra of **4.2** (CHCl_3 , $27 \mu\text{M}$, 298 K) as TFA is added. The overall concentration of TFA (mol L^{-1}) is given on the right. Spectra have been corrected to account for the change in volume as TFA is added.

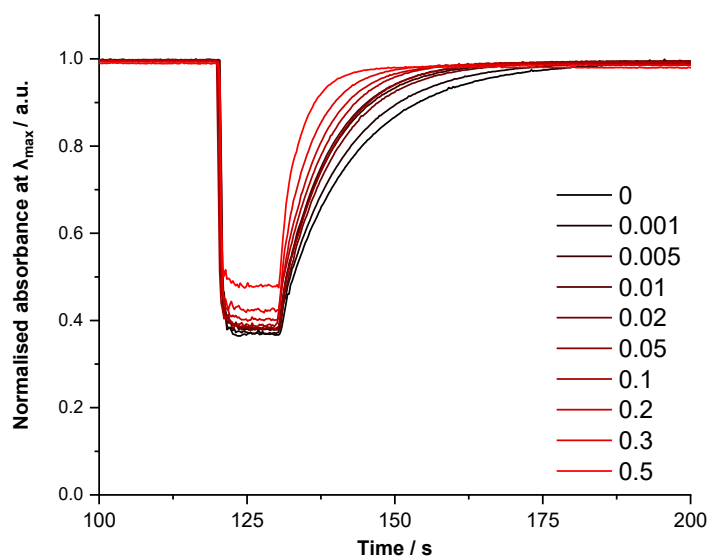


Figure 8.54 Change in the rate of *Z* to *E* thermal reversion for **4.2** (CHCl_3 , $27 \mu\text{M}$, 298 K) as TFA is added. The overall concentration of TFA (mol L^{-1}) is given on the right. Calculated $t_{1/2}$ values and change in absorbance are tabulated in Table 8.5

Table 8.5 Change in the photoswitching parameters of **4.2** as TFA is added in chloroform

[TFA] / mol L ⁻¹	t _{1/2} / s ^a	Change in absorbance at PSD (% of max, measured at λ _{max, E})
0	8	63
0.001	7	63
0.005	6	62
0.01	6	62
0.02	6	62
0.05	6	62
0.1	5	61
0.2	5	60
0.3	4	58
0.5	3	52

^a Thermal lifetime was determined as discussed in Error! Reference source not found. using three switching cycles.

8.9.4 ¹H NMR spectra of **4.2** with TFA in CDCl₃

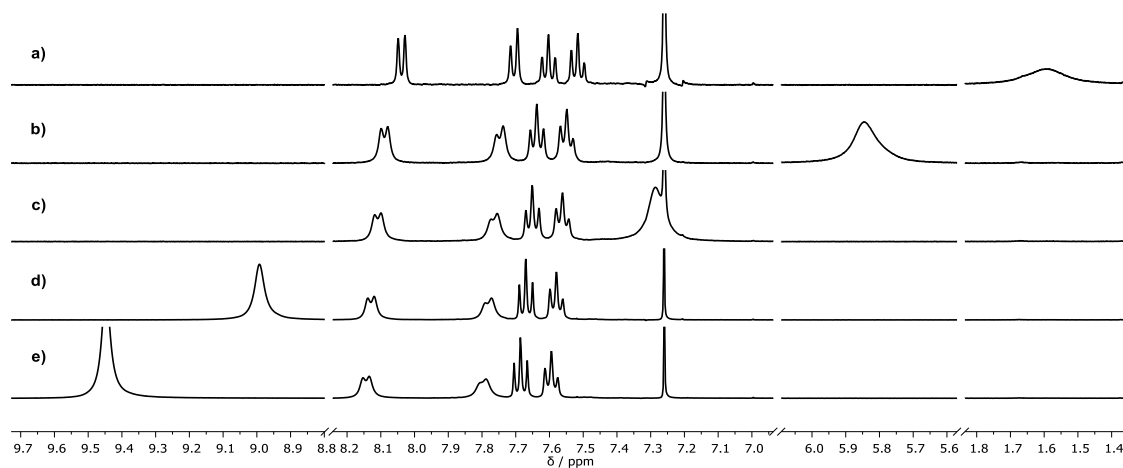


Figure 8.55 Partial ¹H NMR spectrum (400 MHz, CDCl₃, 298 K) of **4.2** (26 mM) with added TFA. [TFA]: a) 0 M; b) 0.02 M; c) 0.04 M; d) 0.1 M and e) 0.2 M.

8.9.5 UV-Vis spectra and photoswitching of 4.3 with TFA in chloroform

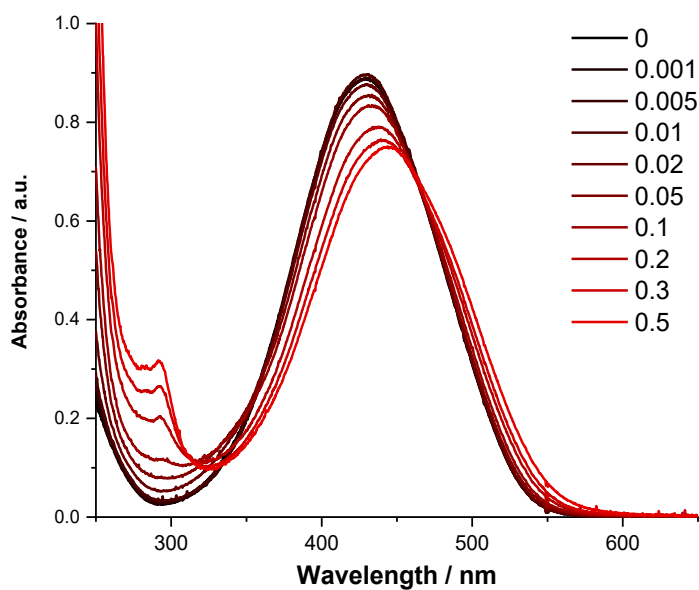


Figure 8.56 Change in the UV-vis spectrum of **4.3** (CHCl_3 , $30 \mu\text{M}$, 298 K) as TFA is added. The overall concentration of TFA (mol L^{-1}) is given on the right. Spectra have been corrected to account for the change in volume as TFA is added.

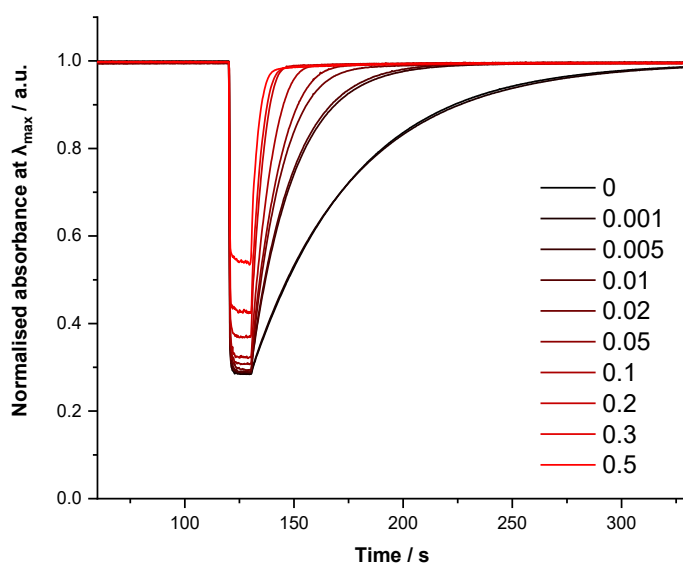


Figure 8.57 Change in the rate of *Z* to *E* thermal reversion for **4.3** (CHCl_3 , $30 \mu\text{M}$, 298 K) as TFA is added. The overall concentration of TFA (mol L^{-1}) is given on the right. Calculated $t_{1/2}$ values and change in absorbance is tabulated in Table 8.6

Table 8.6 Change in the photoswitching parameters of **4.3** as TFA is added in chloroform

[TFA] / mol L ⁻¹	t _{1/2} / s ^a	Change in absorbance at PSD (% of max, measured at λ _{max} , E)
0	31	72
0.001	33	72
0.005	15	71
0.01	14	71
0.02	9	71
0.05	9	69
0.1	6	68
0.2	4	63
0.3	3	58
0.5	2	46

^a Thermal lifetime was determined as discussed in Error! Reference source not found. using three switching cycles.

8.9.6 ¹H NMR spectra of **4.3** with TFA in CDCl₃

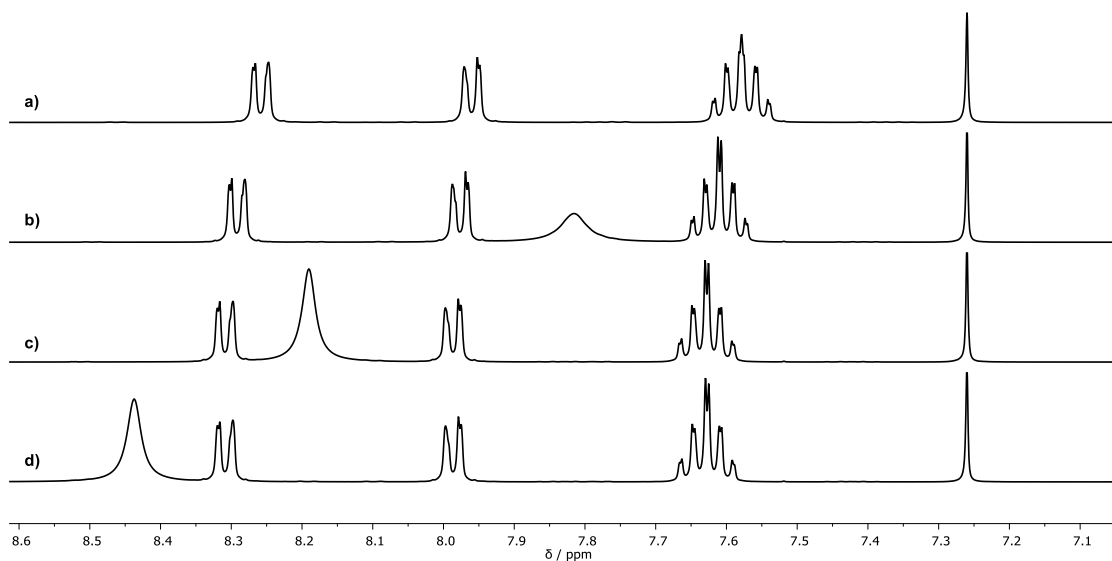


Figure 8.58 Partial ¹H NMR spectrum (400 MHz, CDCl₃, 298 K) of **4.3** (23 mM) with added TFA. [TFA]: a) 0 M; b) 0.02 M; c) 0.04 M and d) 0.2 M.

8.9.7 UV-Vis spectra of compounds 4.2 and 4.3 with added Cl⁻

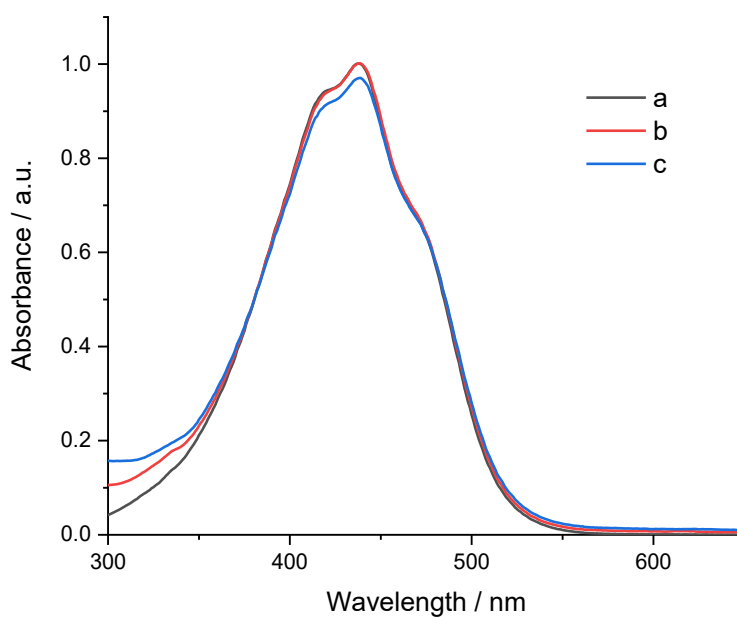


Figure 8.59 Response of **4.2** (chloroform, 34 μ M) to chloride addition and acid. a) **4.2** in chloroform; b) upon addition of tetrabutylammonium chloride (83 mg, total conc. = 0.1 M) and c) upon addition of TFA (34 μ L, total conc. = 0.1 M).

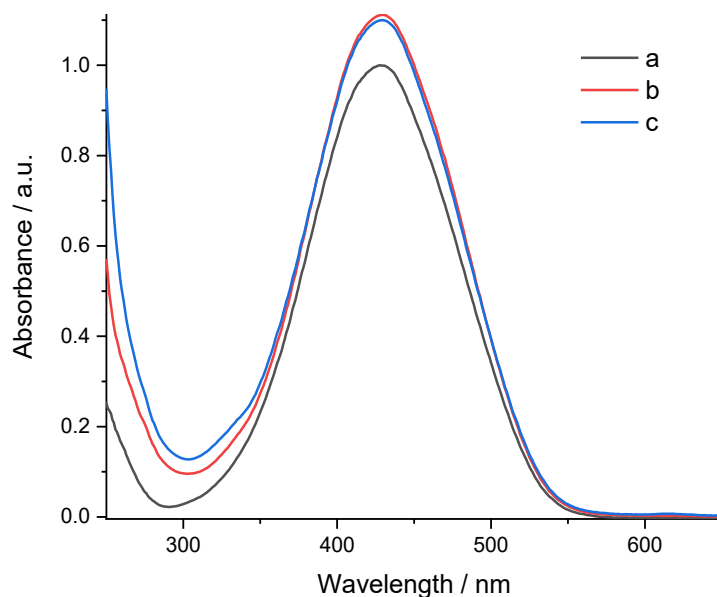


Figure 8.60 Response of **4.3** (chloroform, 33 μ M) to chloride addition and acid. a) **4.3** in chloroform; b) upon addition of tetrabutylammonium chloride (83 mg, total conc. = 0.1 M) and c) upon addition of TFA (34 μ L, total conc. = 0.1 M).

8.10 The effect of protonation on photophysical properties in acetonitrile

8.10.1 UV-Vis spectra and photoswitching of 4.1 with TFA in acetonitrile

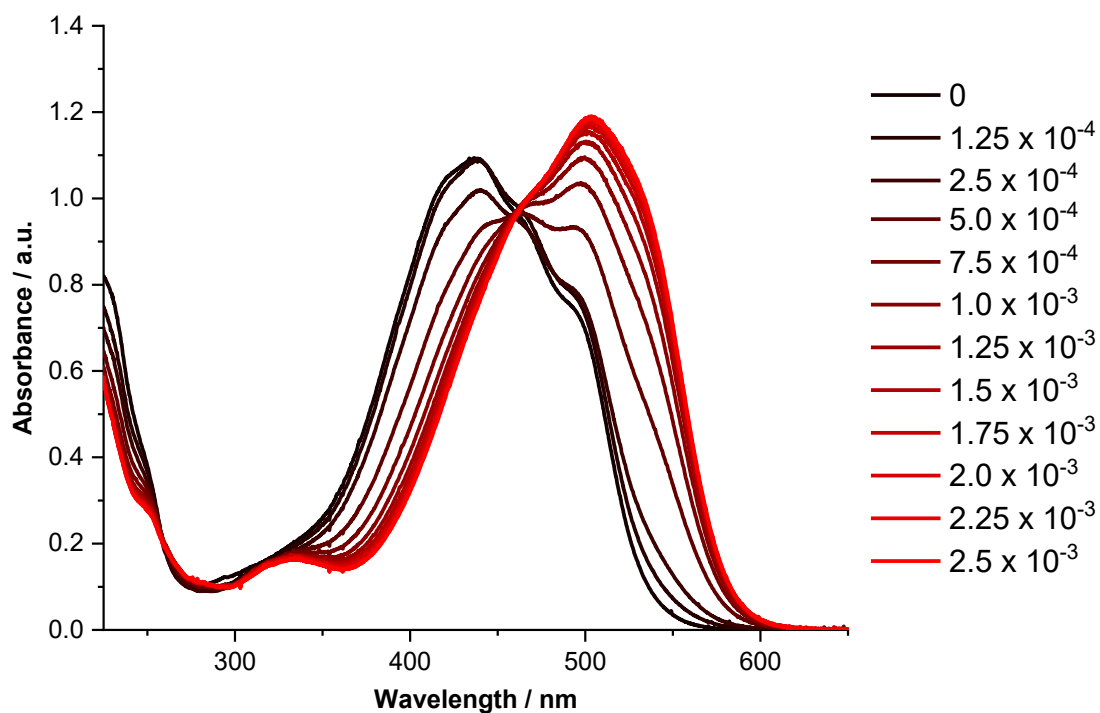


Figure 8.61 Change in the UV-visible spectra of **4.1** (acetonitrile, 50 μ M) as TFA is added. The overall concentration of TFA (mol L^{-1}) is given on the right.

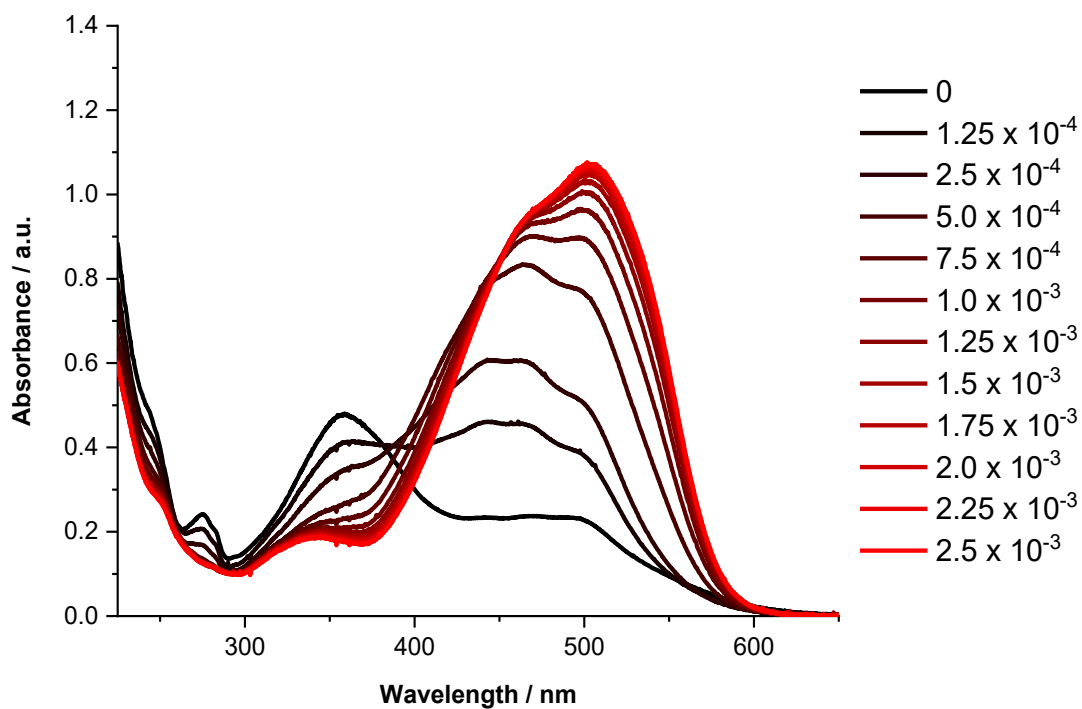


Figure 8.62 Change in the PSD spectra of **4.1** (acetonitrile, 50 μM) as TFA is added. PSD was generated by irradiation with 448 nm light. The overall concentration of TFA (mol L^{-1}) is given on the right.

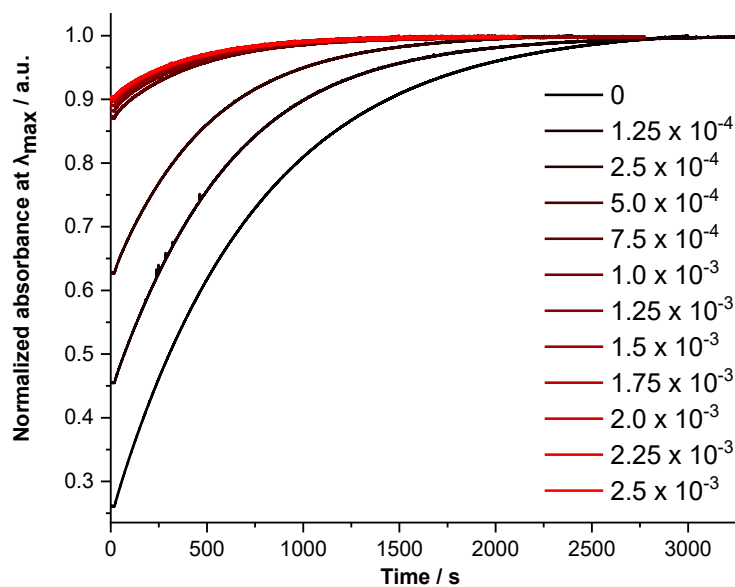


Figure 8.63 Change in the rate of *Z* to *E* thermal reversion for **4.1** (acetonitrile, 50 μM , 298 K) as TFA is added. The overall concentration of TFA (mol L^{-1}) is given on the right. Calculated $t_{1/2}$ values and change in absorbance are tabulated in Table 8.7.

Table 8.7 Change in the photoswitching parameters of **4.1** as TFA is added in acetonitrile

[TFA] / mol L ⁻¹	t _{1/2} / s ^a	Change in absorbance at PSS (% of max, measured at λ _{max, E})
0	523	74
1.25 x 10 ⁻⁴	407	54
2.5 x 10 ⁻⁴	347	27
5.0 x 10 ⁻⁴	311	13
7.5 x 10 ⁻³	295	13
1.0 x 10 ⁻³	287	12
1.25 x 10 ⁻³	282	11
1.5 x 10 ⁻³	281	10
1.75 x 10 ⁻³	280	10
2.0 x 10 ⁻³	279	10
2.25 x 10 ⁻³	281	10
2.5 x 10 ⁻³	280	10

^a Thermal lifetime was determined as discussed in Error! Reference source not found. using three switching cycles.

8.10.2 ¹H NMR spectra of **4.1** with TFA in CD₃CN

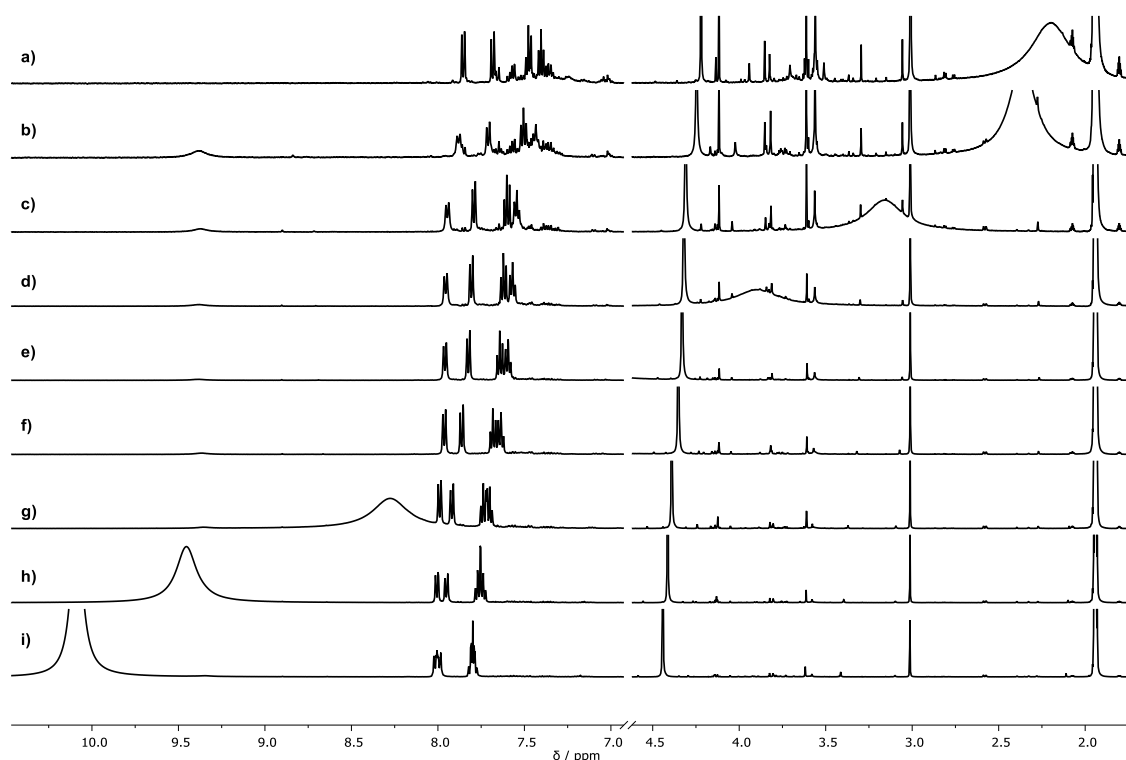


Figure 8.64 Partial ¹H NMR spectrum (400 MHz, CD₃CN, 298 K) of **4.1** with added TFA. [TFA]: a) 0 M; b) 0.001 M; c) 0.005 M; d) 0.01 M; e) 0.02 M; f) 0.05 M; g) 0.1 M; h) 0.2 M and i) 0.4 M. Note that neutral **4.1** has limited solubility in CD₃CN, leading to an enhancement of the small impurity signals which are more soluble in CD₃CN.

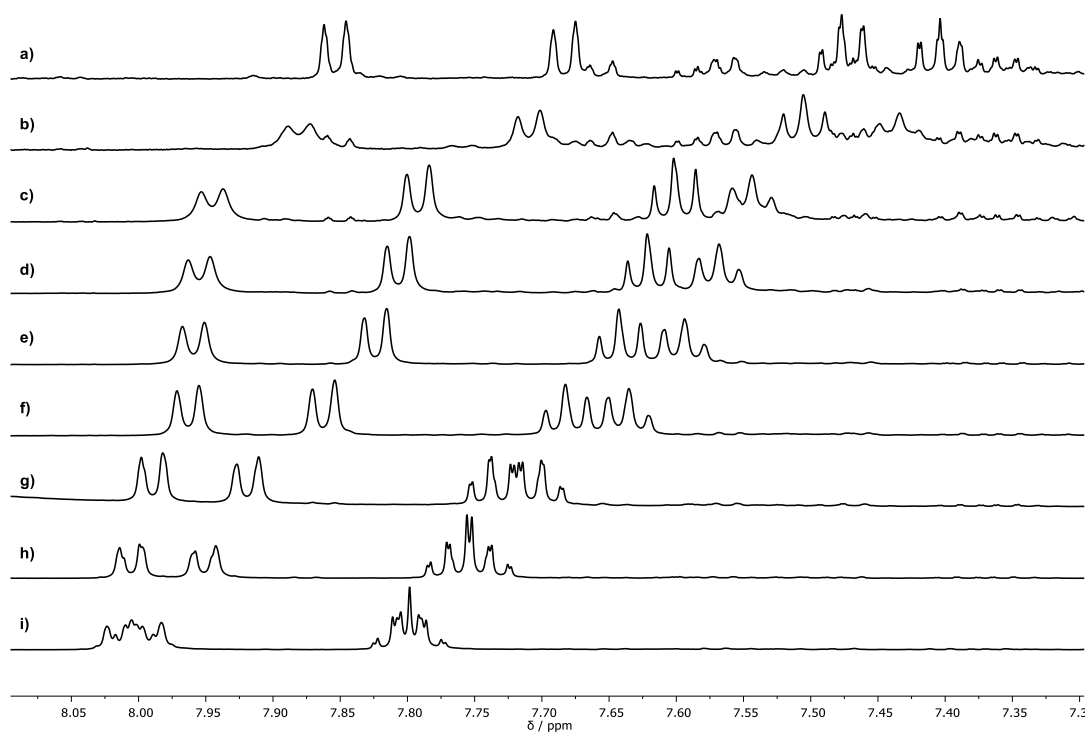


Figure 8.65 Expansion of the aromatic region of Figure 8.64. [TFA]: a) 0 M; b) 0.001 M; c) 0.005 M; d) 0.01 M; e) 0.02 M; f) 0.05 M; g) 0.1 M; h) 0.2 M and i) 0.4 M.

8.10.3 UV-Vis spectra and photoswitching of 4.2 with TFA in acetonitrile

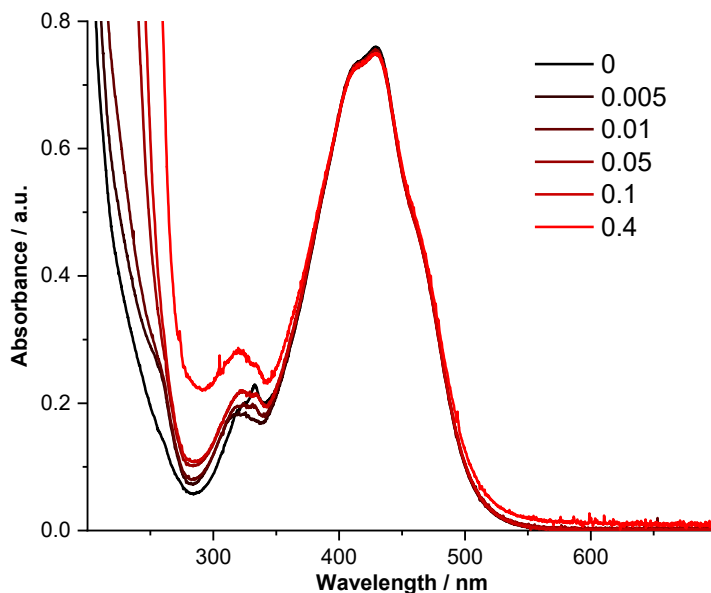


Figure 8.66 Change in the UV-visible spectrum of **4.2** (acetonitrile, 25 μM , 298 K) as TFA is added. The overall concentration of TFA (mol L^{-1}) is given on the right. Spectra have been corrected to account for the change in volume as TFA is added.

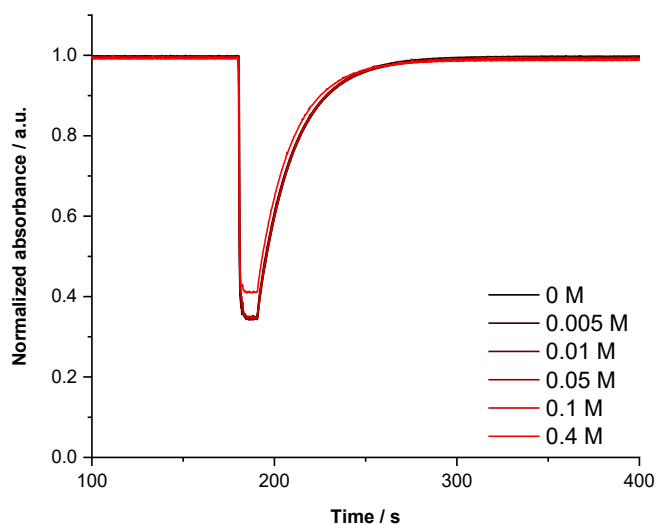


Figure 8.67 Change in the rate of *Z* to *E* thermal reversion for **4.2** (acetonitrile, 25 μM , 298 K) as TFA is added. The overall concentration of TFA (mol L^{-1}) is given on the right. The calculated $t_{1/2}$ value for all concentrations is 14 s.

8.10.4 ^1H NMR spectra of **4.2** with TFA in CD_3CN

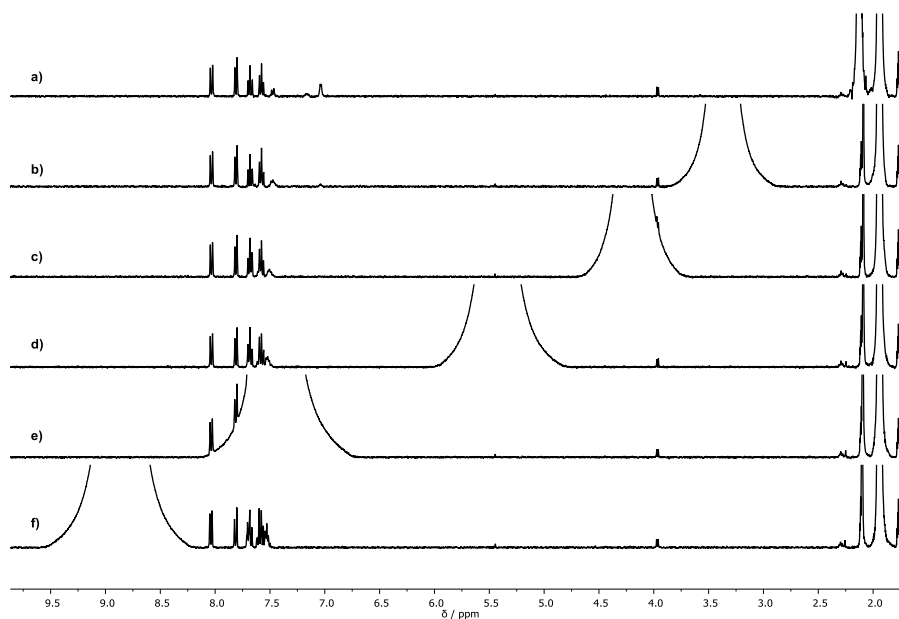


Figure 8.68 Partial ^1H NMR spectrum (400 MHz, CD_3CN , 298 K) of **4.2** with added TFA. [TFA]: a) 0 M; b) 0.01 M; c) 0.02 M; d) 0.04 M; e) 0.1 M and f) 0.2 M. Note that neutral **4.2** has limited solubility in CD_3CN , leading to an enhancement of the small impurity signals which are more soluble in CD_3CN .

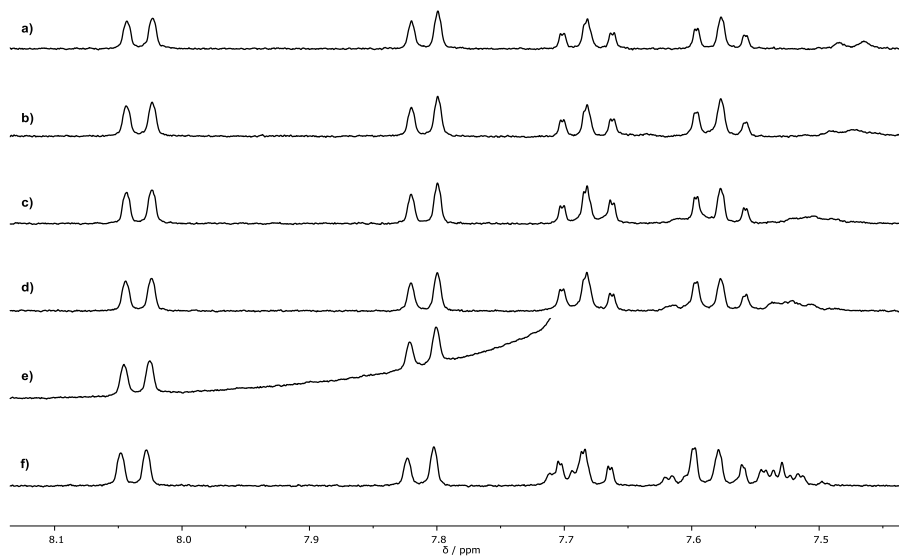


Figure 8.69 Expansion of the aromatic region of Figure 8.68. [TFA]: a) 0 M; b) 0.01 M; c) 0.02 M; d) 0.04 M; e) 0.1 M and f) 0.2 M.

8.10.5 UV-Vis spectra and photoswitching of 4.3 with a small excess of TFA in acetonitrile

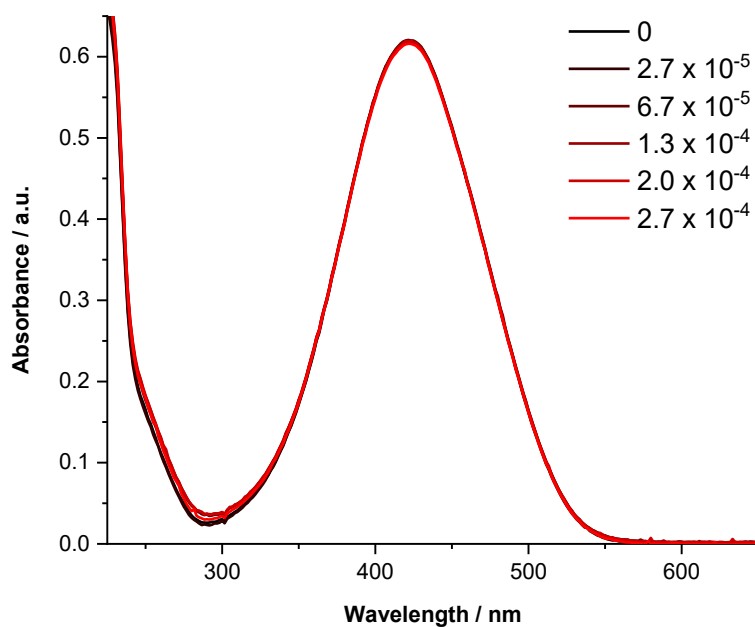


Figure 8.70 Change in the UV-visible spectrum of **4.3** (acetonitrile, 27 μM , 298 K) as TFA is added. The overall concentration of TFA (mol L^{-1}) is given on the right. Spectra have been corrected to account for the change in volume as TFA is added.

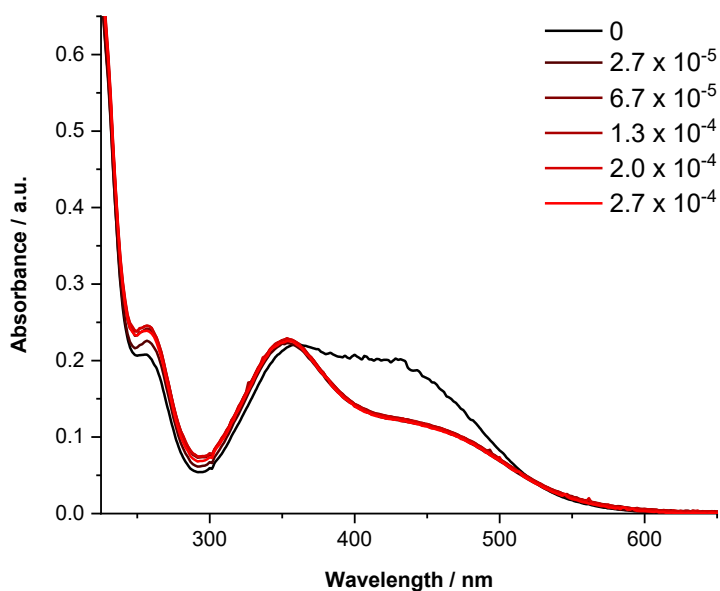


Figure 8.71 Change in the PSD spectrum of **4.3** (acetonitrile, 27 μM , 298 K) as TFA is added. PSD was generated through irradiation with 448 nm light. The overall concentration of TFA (mol L^{-1}) is given on the right. Spectra have been corrected to account for the change in volume as TFA is added.

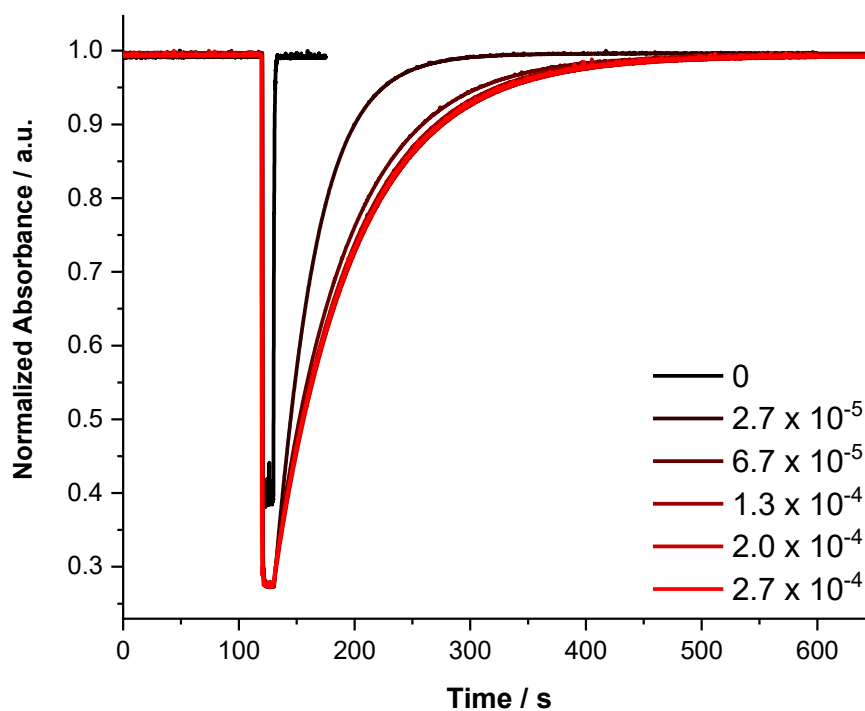


Figure 8.72 Change in the rate of *Z* to *E* thermal reversion of **4.3** (acetonitrile, 27 μM) as TFA is added. The overall concentration of TFA (mol L^{-1}) is given on the right.

Table 8.8 Change in the photoswitching parameters of **4.3** as TFA is added in acetonitrile.

[TFA] / mol L^{-1}	$t_{1/2}$ / s^{a}	Change in absorbance at PSS (% of max, measured at $\lambda_{\text{max,E}}$)
0	0.4	60
2.7×10^{-5}	24	73
6.7×10^{-5}	43	73
1.3×10^{-4}	48	73
2.0×10^{-4}	49	73
2.7×10^{-4}	49	73

^a Thermal lifetime was determined as discussed in Error! Reference source not found. using three switching cycles.

8.10.6 UV-Vis spectra and photoswitching of 4.3 with a large excess of TFA in acetonitrile

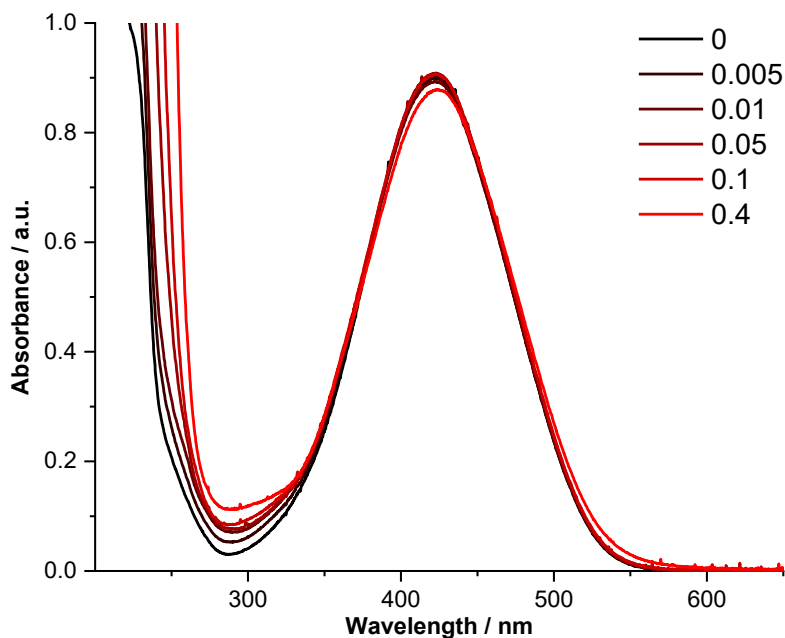


Figure 8.73 Change in the UV-vis spectrum of **4.3** (acetonitrile, 40 μ M, 298 K) as TFA is added. The overall concentration of TFA (mol L^{-1}) is given on the right. Spectra have been corrected to account for the change in volume as TFA is added.

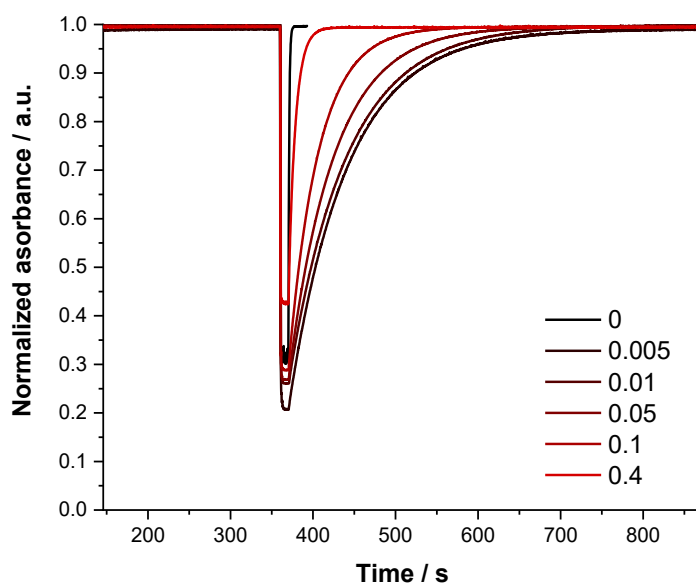


Figure 8.74 Change in the rate of Z to E thermal reversion of **4.3** (acetonitrile, 40 μ M, 298K) as TFA is added. The overall concentration of TFA (mol L^{-1}) is given on the right.

Table 8.9 Change in the photoswitching parameters of **4.3** as TFA is added in acetonitrile.

[TFA] / mol L ⁻¹	t _{1/2} / s ^a	Change in absorbance at PSS (% of max, measured at λ _{max, E})
0	0.4	68
0.005	49	80
0.01	49	74
0.05	38	73
0.1	25	71
0.4	6	57

^a Thermal lifetime was determined as discussed in Error! Reference source not found. using three switching cycles.

8.10.7 ¹H NMR spectra of **4.3** with TFA in CD₃CN

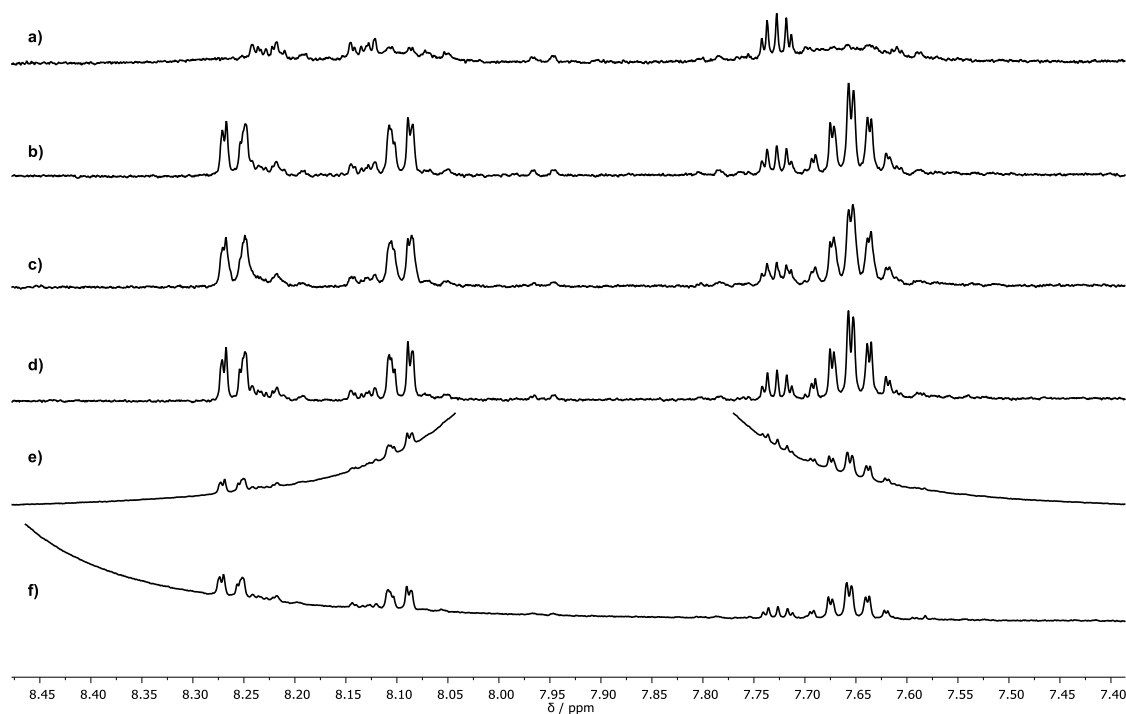


Figure 8.75 Partial ¹H NMR spectrum (400 MHz, CD₃CN, 298 K) of **4.3** (14 mM) with added TFA. [TFA]: a) 0 M; b) 0.01 M; c) 0.02 M; d) 0.04 M; e) 0.14 M; f) 0.2 M. Note that **4.3** has limited solubility in CD₃CN, leading to an enhancement of the small impurity signals which are more soluble in CD₃CN.

8.11 Approximation of pK_a for compound **4.1**

The pK_a for **4.1** was approximated using two methodologies based on UV-vis titration data (Figure 8.61). This was done using the data in CH_3CN because the data in CHCl_3 appears to show multiple processes. Addition of TFA to a solution of **4.1** in CH_3CN lead to the formation of a new species which absorbs at longer wavelength which we assign as $\mathbf{4.1H}^+$.

The reaction between **4.1** and TFA can be described in terms of the equilibrium constant K .

$$K = \frac{[\text{CF}_3\text{COO}]^- [\mathbf{4.1H}^+]}{[\text{CF}_3\text{COOH}] [\mathbf{4.1}]}$$

The pK_a of $[\mathbf{4.1H}^+]$ is then calculated from the known pK_a of TFA²:

$$pK_{a,1H^+} = \log_{10}(K) + pK_{a,TFA}$$

The first methodology estimates K using equation 1, which is written in terms of equivalents of acid (E) relative to the total moles of **4.1**. At the point where $A = \frac{1}{2} A_{\text{max}}$ then the following are true:

$$[\mathbf{4.1}] = [\mathbf{4.1H}^+] = [\text{CF}_3\text{COO}]^- = x$$

$$[\text{CF}_3\text{COOH}]_{\text{total}} = [\text{CF}_3\text{COOH}] + [\text{CF}_3\text{COO}]^-$$

$$[\text{CF}_3\text{COOH}]_{\text{total}} = [\text{CF}_3\text{COOH}] + x$$

$$E = \frac{[\text{CF}_3\text{COOH}]_{\text{total}}}{[\mathbf{4.1}]_{\text{total}}} = \frac{[\text{CF}_3\text{COOH}]_{\text{total}}}{2x} = \frac{[\text{CF}_3\text{COOH}] + x}{2x}$$

$$[\text{CF}_3\text{COOH}] = x(2E - 1)$$

$$\therefore K = \frac{x^2}{x(2E-1)x} = \frac{1}{2E-1} \quad (4)$$

This assumes that only $\mathbf{4.1H}^+$ absorbs at the chosen wavelength, so only $\lambda > 564$ nm were used where $A_1 < 0.01$ (see Figure 8.61). This gives an approximate pK_a value of ≈ 11.3 , which is more acidic than TFA in acetonitrile ($pK_a = 12.65$).

The second methodology is based on the observation that the absorbance (A) at every point can be described as a linear combination of the **4.1** and $[\mathbf{4.1H}]^+$ spectra such that:

$$A_1 = \varepsilon_{1,1}[\mathbf{4.1}] + \varepsilon_{1,[1H]^+}[\mathbf{4.1H}]^+$$

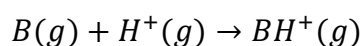
$$A_2 = \varepsilon_{2,1}[\mathbf{4.1}] + \varepsilon_{2,[1H]^+}[\mathbf{4.1H}]^+$$

Where $\varepsilon_{x,y}$ is the extinction coefficient at x nm for the respective protonation state. These can be calculated assuming that the initial and final species are **4.1** and $[\mathbf{4.1H}]^+$ respectively, i.e. the compound has been fully mono-protonated. This assumption is valid as further addition of TFA does not appear to affect the spectrum. Solving the simultaneous equations with the condition that $[\mathbf{4.1}] + [\mathbf{4.1H}]^+ = [\mathbf{4.1}]_{\text{initial}}$ gives both $[\mathbf{4.1}]$ and $[\mathbf{4.1H}]^+$ for a range of acid concentrations. This allows calculation of K given that $[\text{CF}_3\text{COO}]^- = [\mathbf{4.1H}]^+$ assuming that CF_3COOH can only protonate **4.1**. This gives an $\text{p}K_a$ of ≈ 11.9 , where $\text{p}K_a$ was calculated from K as above.

8.12 Computational Details

Geometry optimization and corresponding frequency calculations were carried out at the M06-2X/6-31+G(d,p) level of theory³ using Gaussian16 revision A03.⁴ Thermal corrections to the Gibbs free energies were computed using the quasiharmonic oscillator (QHO) approximation⁵ where vibrational frequencies below 20 cm^{-1} were raised to this value. Systematic conformer searches were carried out to locate the lowest energy conformer of each species in acetonitrile. Solvent effects were taken into account by using the SMD implicit solvent model.⁶

Single point calculations were performed at the DLPNO-CCSD(T)/CBS level⁷ with ORCA 4.1.0⁸ in the gas phase to obtain an improved estimate of the gas phase Gibbs free energies for the calculation of proton affinity, gas phase basicity and $\text{p}K_a$ values. The proton affinity and gas-phase basicity⁹ are the negative of the enthalpy and the negative of the Gibbs free energy, respectively, corresponding to the following reaction in the gas phase:



Relative energies between the conformers were calculated following a thermodynamic cycle as depicted in Figure 8.76. For the calculation of pK_a values a proton exchange scheme¹⁰ as shown in Figure 8.77 was used, which is in general more accurate than a direct calculation due to the cancellation of errors in the calculation of free energies of solvation. The superscript * indicates a standard state of 1 mol L⁻¹. As a reference acid protonated benzimidazole was used, which has an experimentally determined pK_a value of 13.52 in acetonitrile.¹¹ For the enthalpy and the free energy of the proton in the gas phase, values¹² of 6.197 kJ mol⁻¹ and -26.550 kJ mol⁻¹, respectively, were used.

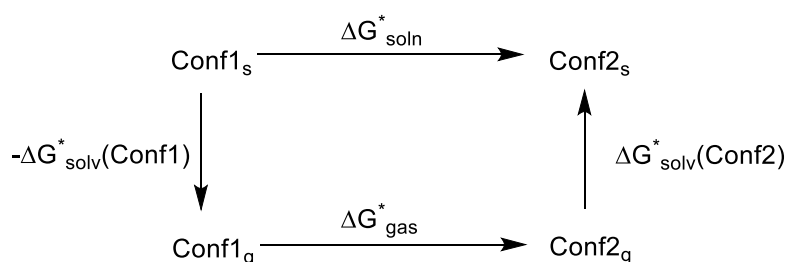


Figure 8.76 Thermodynamic cycle used for the calculation of the relative Gibbs free energies of the conformers.

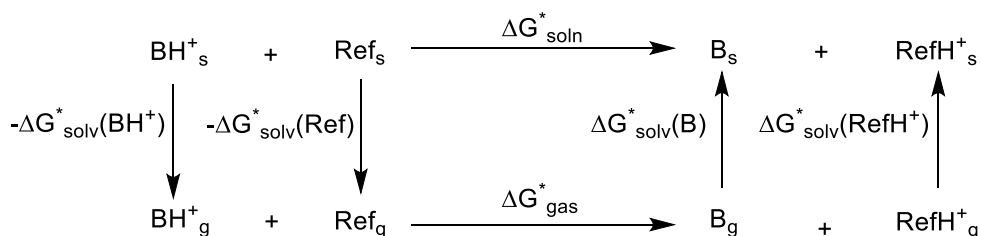


Figure 8.77. Thermodynamic cycle used for the calculation of Gibbs free energies of dissociation, from which pK_a values were calculated.

The free energies of solvation $\Delta G_{solv}^*(BH^+)$ and $\Delta G_{solv}^*(B)$ were calculated as

$$\Delta G_{solv}^* = E_s(R_s) - E_g(R_g)$$

where E_s and E_g are the solvent-phase and gas-phase energies calculated on geometries optimized in the respective phases. In the above equation, E_s contains the non-

electrostatic contributions to the free energy of solvation. The free energy and pK_a were calculated according to

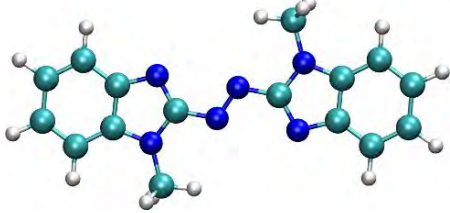
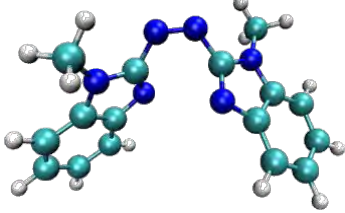
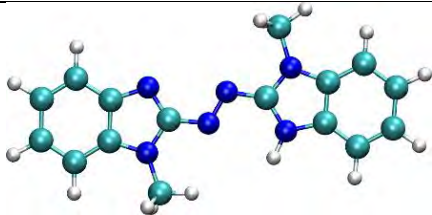
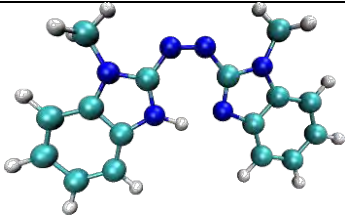
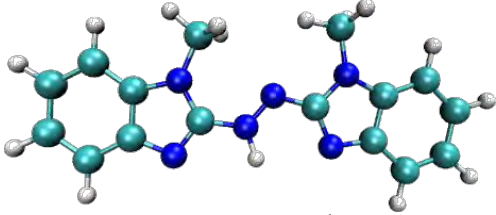
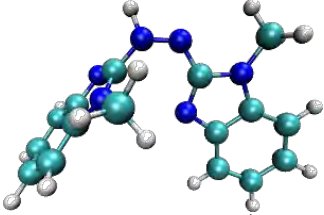
$$\Delta G_{soln}^* = \Delta G_{gas}^* + \Delta G_{solv}^*(B) + \Delta G_{solv}^*(RefH^+) - \Delta G_{solv}^*(BH^+) - \Delta G_{solv}^*(Ref)$$

$$pK_a(BH^+) = \frac{\Delta G_{soln}^*}{RT \ln(10)} + pK_a^{Exp}(RefH^+)$$

Compounds **4.1-3** each have multiple possible protonation sites. Energy minimizations were carried out on structures where the proton was localized on theazole ring (denoted [4.1HIm]⁺, [4.2HOx]⁺ or [4.3HTh]⁺) and where the proton was localized on the azo double bond (denoted [4.1HAzo]⁺, [4.2HAzo]⁺ or [4.3HAzo]⁺). Electrostatic potential (ESP) plots were generated using IQMOL using Mulliken charges¹³ derived at the M06-2X/6-31+G(d,p) level of theory using the SMD solvation model for acetonitrile in Q-Chem, version 5.2.0.¹⁴

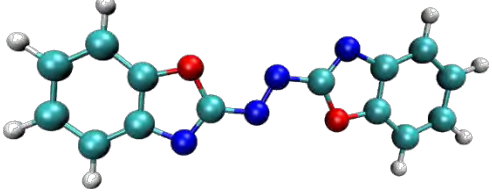
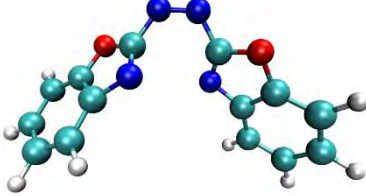
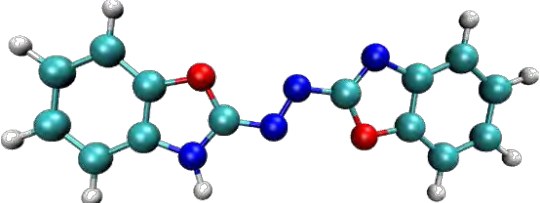
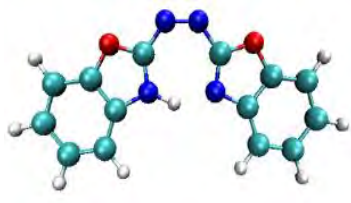
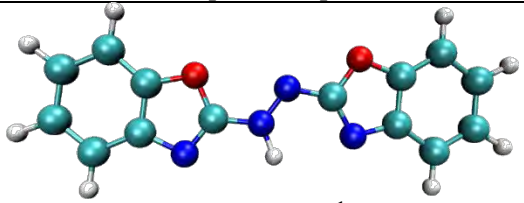
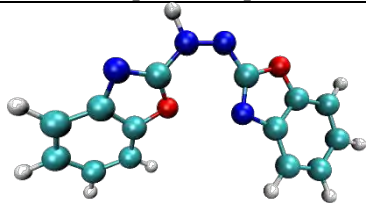
8.12.1 Energy minimized structures of 4.1 and [4.1H]⁺

Table 8.10 Lowest energy conformer for each species of 4.1 in acetonitrile. Relative solution phase Gibbs free energies are calculated using the thermodynamic cycle shown in Figure 8.76.

 0.0 kJ mol ⁻¹ <i>E</i> -4.1	 41.9 kJ mol ⁻¹ <i>Z</i> -4.1
 0.0 kJ mol ⁻¹ <i>E</i> -[4.1HIm] ⁺	 36.0 kJ mol ⁻¹ <i>Z</i> -[4.1HIm] ⁺
 64.0 kJ mol ⁻¹ <i>E</i> -[4.1HAzo] ⁺	 103.1 kJ mol ⁻¹ <i>Z</i> -[4.1HAzo] ⁺

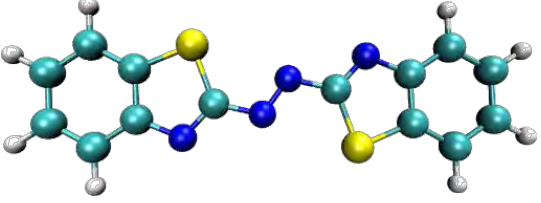
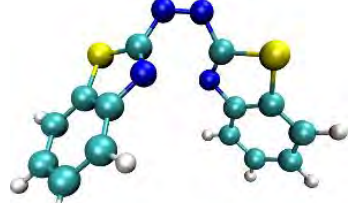
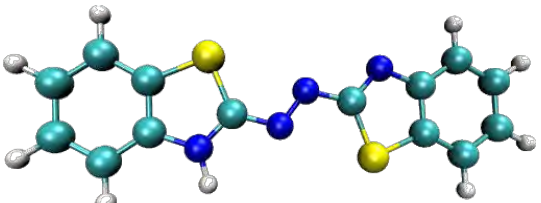
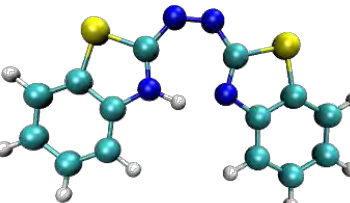
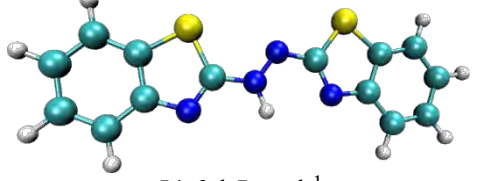
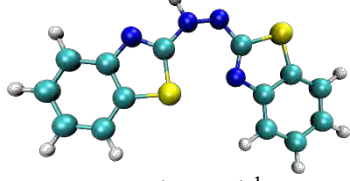
8.12.2 Energy minimized structures of 4.2 and [4.2H]⁺

Table 8.11 Lowest energy conformer for each species of 4.2 in acetonitrile. Relative solution phase Gibbs free energies are calculated using the thermodynamic cycle shown in Figure 8.76.

 0.0 kJ mol ⁻¹ <i>E</i> -4.2	 47.6 kJ mol ⁻¹ <i>Z</i> -4.2
 0.0 kJ mol ⁻¹ <i>E</i> -[4.2HOx] ⁺	 33.9 kJ mol ⁻¹ <i>Z</i> -[4.2HOx] ⁺
 49.2 kJ mol ⁻¹ <i>E</i> -[4.2HAzo] ⁺	 81.0 kJ mol ⁻¹ <i>Z</i> -[4.2HAzo] ⁺

8.12.3 Energy minimized structures of 4.3 and [4.3H]⁺

Table 8.12 Lowest energy conformer for each species of 4.3 in acetonitrile. Relative solution phase Gibbs free energies are calculated using the thermodynamic cycle shown in Figure 8.76.

 <p>0.0 kJ mol⁻¹ <i>E</i>-4.3</p>	 <p>57.4 kJ mol⁻¹ <i>Z</i>-4.3</p>
 <p>0.0 kJ mol⁻¹ <i>E</i>-[4.3HTh]⁺</p>	 <p>49.4 kJ mol⁻¹ <i>Z</i>-[4.3HTh]⁺</p>
 <p>51.0 kJ mol⁻¹ <i>E</i>-[4.3HAzo]⁺</p>	 <p>81.9 kJ mol⁻¹ <i>Z</i>-[4.3HAzo]⁺</p>

8.12.4 Calculated proton affinities, gas-phase basicity and pK_a values for 4.1-3H⁺

Table 8.13 Summary of calculated proton affinities, gas-phase basicity and pK_a values for 4.1-3H⁺.

Compound	Proton affinity / kJ mol ⁻¹	Gas-phase basicity / kJ mol ⁻¹	pK_a in acetonitrile
<i>E</i> -[4.1HIm] ⁺	995.9	968.9	11.7
<i>E</i> -[4.1HAzo] ⁺	944.5	912.0	0.5
<i>Z</i> -[4.1HIm] ⁺	1025.8	989.3	12.8
<i>Z</i> -[4.1HAzo] ⁺	933.3	897.3	1.0
<i>E</i> -[4.2HOx] ⁺	919.5	887.2	0.2
<i>E</i> -[4.2HAzo] ⁺	886.6	853.7	-8.4
<i>Z</i> -[4.2HOx] ⁺	933.2	897.8	2.6
<i>Z</i> -[4.2HAzo] ⁺	888.1	854.9	-5.6
<i>E</i> -[4.3HTh] ⁺	933.3	901.3	1.7
<i>E</i> -[4.3HAzo] ⁺	901.5	868.7	-7.2
<i>Z</i> -[4.3HTh] ⁺	950.8	915.2	3.1
<i>Z</i> -[4.3HAzo] ⁺	920.2	885.4	-2.6

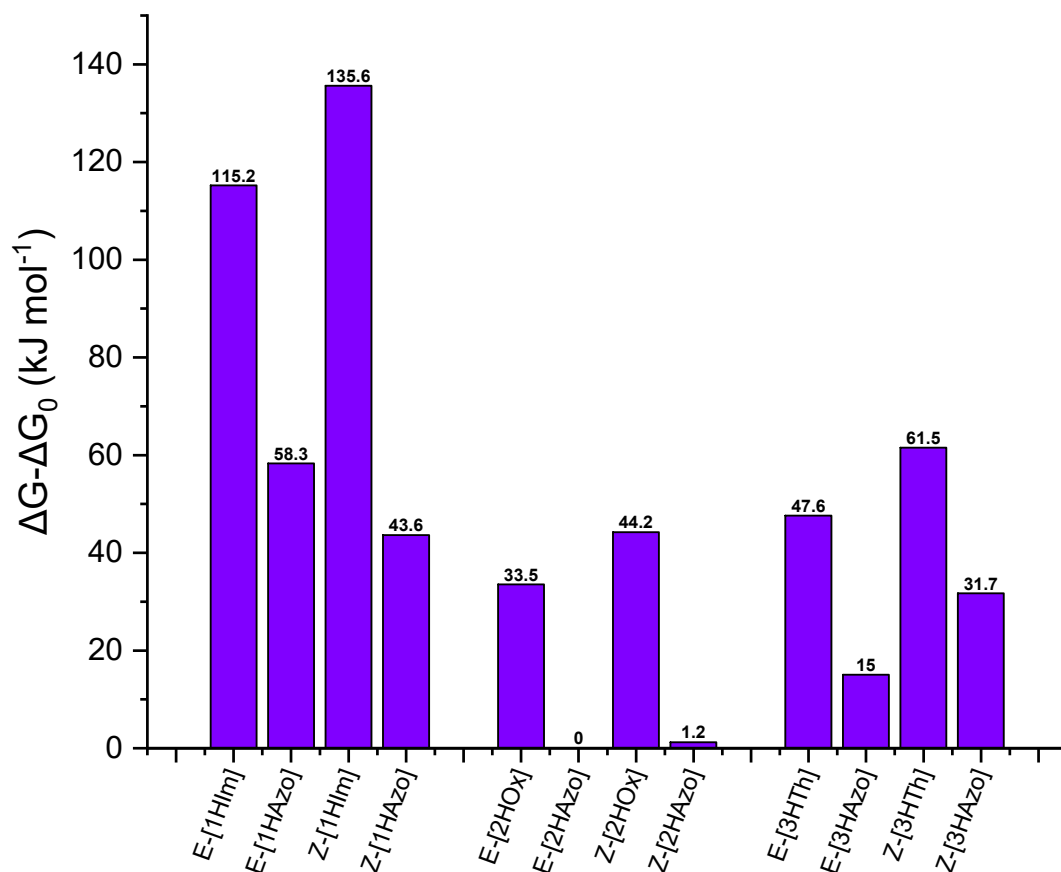


Figure 8.78 Calculated gas-phase basicities for compounds **4.1-3** at different protonation sites and different isomers. Data have been plotted as $\Delta\Delta G$ (relative to E -[**4.2HAzo**]⁺) to allow for ease of comparison.

Table 8.14 Summary of computed proton affinities and gas-phase basicity for the first deprotonation of doubly protonated **4.1-3**.

Compound	Proton affinity / kJ mol ⁻¹	Gas-phase basicity / kJ mol ⁻¹
E -[4.1-2H] ²⁺	695.1	675.6
Z -[4.1-2H] ²⁺	596.5	566.3

8.12.5 Comparison of calculated geometric parameters for 4.1-3

Table 8.15 Comparison of measured angles and bond lengths in the calculated *Z* isomer conformations of 4.1-3.

Compound	C-N=N-C torsion (°)	Angle between planes (°)	N=N bond length (Å)
4.1	14.8	65.7	1.243
[4.1-HIm] ⁺	0.0	0	1.257
[4.1-HAzo] ⁺	2.5	69.0	1.272
4.2	14.1	65.8	1.240
[4.2-HIm] ⁺	0.0	0	1.255
[4.2-HAzo] ⁺	12.5	39.4	1.266
4.3	11.0	64.1	1.240
[4.3-HIm] ⁺	0.0	0	1.256
[4.3-HAzo] ⁺	0.0	0.0	1.258

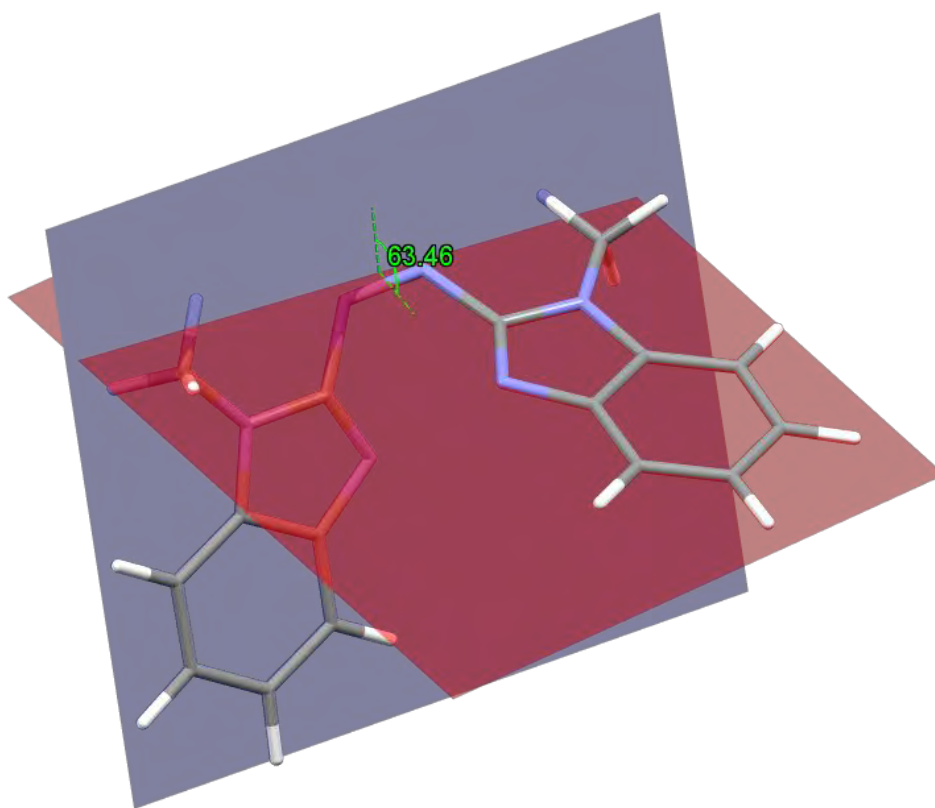


Figure 8.79 Representation of the angle between planes for compound *Z*-4.1.

Table 8.16 Comparison of bond lengths between calculated and X-ray structures of the *E* isomer conformation of **4.1-3**.

Compound	N=N bond length
<i>E</i> - 4.1 (experimental) ^a	1.270
<i>E</i> - 4.1 (calc.)	1.249
<i>E</i> - 4.2 (experimental) ^a	1.276
<i>E</i> - 4.2 (calc.)	1.251
<i>E</i> - 4.3 (experimental) ^a	1.266
<i>E</i> - 4.3 (calc.)	1.247

^a Single crystal X-ray data

8.13 Atoms-in-Molecules analysis

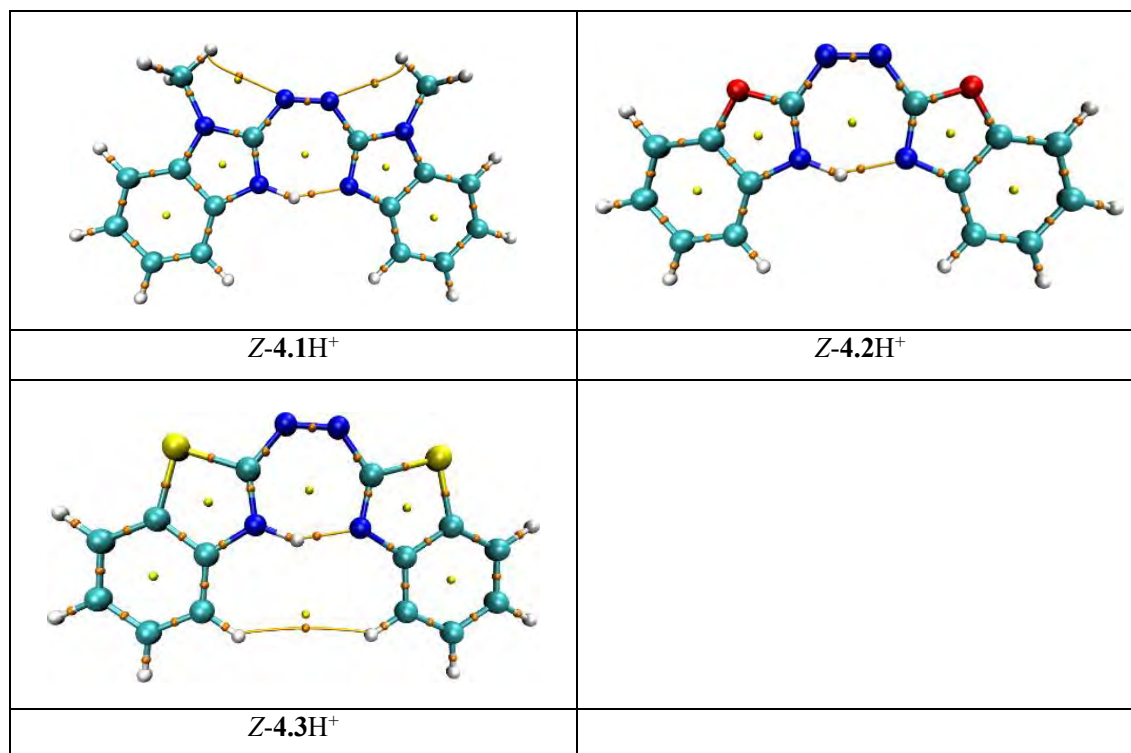
In order to provide supporting evidence for the presence of an intramolecular hydrogen bond in *Z*-(**1-3H**⁺), atoms-in-molecules (AIM)¹⁵ analyses were carried out using the Multiwfn program package¹⁶ and plotted with VMD.¹⁷

The geometrical parameters of the hydrogen bond as well as values obtained from the AIM analysis are listed in Table 8.17, and the bond critical points and bond paths are depicted in Table 8.18.

Table 8.17 Geometrical parameters and results of the AIM analysis for compounds *Z*-(**4.1-4.3H**⁺)

	<i>Z</i> - 4.1H ⁺	<i>Z</i> - 4.2H ⁺	<i>Z</i> - 4.3H ⁺
Hydrogen bond length [Å]	1.615	1.649	1.600
N--N distance [Å]	2.573	2.584	2.580
N-H--N angle [degrees]	146.81	144.43	149.36
electron density at BCP [a.u.]	0.06498	0.06013	0.06852
Laplacian at BCP [a.u.]	0.12506	0.12557	0.11937

Table 8.18 Atoms-in-molecules analysis of Z-4.1H⁺, Z-4.2H⁺ and Z-4.3H⁺. The orange spheres represent bond critical points and the orange lines bond paths.



Within the AIM framework the necessary criteria¹⁸ for the presence of a hydrogen bond is the existence of a bond critical point (BCP) as well as a bond path connecting these two atoms. A BCP is where the gradient of the electron density vanishes between the hydrogen atom and the acceptor atom. For all Z conformers a BCP and a bond path can be found (Figure S89). The electron density at the BCP for Z-4.1H⁺, Z-4.2H⁺ and Z-4.3H⁺ is in a similar range as that of the NH₃--H-Br dimer^{18a} (0.0642 a.u.) and the NH₃--NH₄⁺ dimer¹⁹ (0.0667 a.u.). The electron density at the BCP has been shown to correlate with the strength of the hydrogen bond.¹⁹ All three molecules show a positive sign of the Laplacian of the electron density at the BCP, which indicates shared-shell (covalent) interactions, and the values are within the expected range of 0.024 to 0.139 a.u.^{18b}

Table 8.19 Calculated bonded radii and nonbonded radii for compounds Z-(4.1-4.3H⁺). Nonbonded radii were calculated using the corresponding *E*-(1-3H⁺) conformer.

	Z-4.1H ⁺	Z-4.2H ⁺	Z-4.3H ⁺
Bonded radii: [Å]			
H	0.532	0.533	0.522
N	1.111	1.132	1.103
Sum of bonded radii [Å]	1.642	1.665	1.625
Nonbonded radii: [Å]			
H	1.159	1.136	1.150
N	1.916	1.885	1.894
Sum of nonbonded radii [Å]	3.074	3.021	3.044
Difference in radii	1.432	1.356	1.419

Mutual penetration of hydrogen atom and acceptor atom radii is considered a sufficient condition to predict the presence of a hydrogen bond.^{18a, 18b} Accordingly, the sum of the bonded radii (distance between the nucleus and the BCP) has to be smaller than the sum of the nonbonded radii (distance between the nucleus and the charge density contour corresponding to a value of 0.001 a.u.). The nonbonded radii were obtained from the corresponding *E* conformers, which have a similar electronic but without the presence of a hydrogen bond. The nonbonded radius was obtained from the Multiwfn program where it is defined as the shortest distance between the nucleus and the 0.001 a.u. contour line. For all three molecules the mutual penetration is more than 1.3 Å, which provides further supporting evidence for the presence of the intramolecular hydrogen bond in Z-4.1-3H⁺

8.14 M06-2X/6-31+G(d,p) optimised geometries

1_E_gasphase

```
1\1\GINC-R522\FOpt\RM062X\6-31+G(d,p)\C16H14N6\ROOT\30-Jul-2019\0\#\#P
M062X/6-31+G(d,p) INT(grid=ultrafine) Opt Freq\Optimisation in gaspha
se\0,1\N,-3.5025280447,-1.2668257581,-0.4239705668\N,-2.7323896182,-1
.5331878947,0.5208776701\C,-1.4024592026,-1.7137248326,0.1342694431\N,
-0.8641489306,-1.6430588097,-1.0601948532\C,0.4660410017,-1.9065337101
,-0.847758774\C,0.7111791196,-2.1399957534,0.5267995017\N,-0.507615797
4,-2.0102695854,1.1387727296\C,1.5285903523,-1.9666589714,-1.763810748
3\C,2.7895063379,-2.2564174329,-1.273566138\C,3.0144361871,-2.48672916
78,0.103939711\C,1.9844553911,-2.4335332818,1.0287024276\C,-4.83257626
63,-1.0869589958,-0.0374552459\N,-5.7274164396,-0.7903958537,-1.041955
9826\C,-6.9463183984,-0.6612786274,-0.430067172\C,-6.7012425089,-0.895
0946804,0.9444420268\N,-5.3709861399,-1.1581916371,1.1569304998\C,-8.2
196402802,-0.368000564,-0.9320060669\C,-9.2497357468,-0.3154570198,-0.
0073337844\C,-9.0248703976,-0.5461356874,1.3701211961\C,-7.7639054557,
-0.8356156488,1.8604044143\H,1.3491149924,-1.7890154743,-2.8186917618\
H,3.630673696,-2.3098134569,-1.9569328007\H,4.0207040486,-2.7107304576
,0.4429027047\H,2.1582881181,-2.6104161947,2.0852725486\H,-8.393423513
3,-0.1908360859,-1.988537154\H,-10.2560452685,-0.0916927244,-0.3463296
322\H,-9.8661274942,-0.4932501699,2.0534170874\H,-7.5844785717,-1.0135
34919,2.9152471969\C,-5.4594307389,-0.6405321864,-2.4605867093\C,-0.77
54997855,-2.1595546221,2.5574836727\H,-4.3964579553,-0.8036490045,-2.6
30237635\H,-5.733813869,0.3670260628,-2.7841130962\H,-6.0396656719,-1.
37463208,-3.0258777042\H,-0.5014271829,-3.16709958268,2.8813264231\I,-0
.1949522134,-1.4254597451,3.1224599744\H,-1.8383977536,-1.9960122038,2
.7271935971\Version=ES64L-G16RevA.03\State=1-A\HF=-946.2836766\RMSD=8
.091e-09\RMSF=9.410e-06\Dipole=0.0000424,0.000241,0.0000334\Quadrupole
=8.140396,-10.6248932,2.4844972,-4.9484785,10.1313712,-3.7917695\PG=C0
1 [X(C16H14N6)]\@
```

1_E_hazo_gasphase

```
1\1\GINC-R298\FOpt\RM062X\6-31+G(d,p)\C16H15N6(1+)\ROOT\05-Apr-2019\0\
#\#P M062X/6-31+G(d,p) INT(grid=ultrafine) Opt Freq\Optimisation\1,1\
H,3.638338272,-1.1669094214,0.5292851749\C,2.8457802441,-0.8408908603,
-0.1345319774\C,1.5834689934,-0.5306482087,0.3180034401\H,1.3554742678
,-0.6096398799,1.3749978345\C,0.5604097442,-0.1053851256,-0.5706924708
\H,-0.418275744,0.1275278468,-0.1648044631\C,0.766363466,0.0223020193,
-1.9322404033\H,-0.0305107842,0.348862907,-2.5905242871\C,2.0494699298
,-0.292861384,-2.3938054596\C,3.0839207347,-0.7196793699,-1.5183719669
\N,2.6038077484,-0.2813441162,-3.658085261\N,4.2261316537,-0.959773107
,-2.22011706\C,3.895270686,-0.6898322764,-3.465183974\C,1.9232334273,
0.0893074856,-4.8944550868\H,0.8995380732,0.3578403828,-0.639660717\H
```

```
,1.9107278039,-0.7512921858,-5.5896571245\H,2.4137672059,0.9466201787,
-5.3574646541\N,4.8514773017,-0.8369030655,-4.4438488343\N,4.679703676
1,-0.6147875528,-5.6824644119\C,5.7726780833,-0.8317312078,-6.44909639
42\N,5.726416836,-0.6296918817,-7.8113611768\N,6.9557614777,-1.2425102
22,-6.0063366891\C,6.9701342919,-0.9341633625,-8.2658925279\C,7.726653
6978,-1.3172422264,-7.1122656101\C,7.522072364,-0.9185953126,-9.558297
9011\C,9.0824367865,-1.6990173007,-7.2485021976\C,8.8430692082,-1.2958
613391,-9.6526771519\H,6.9457575428,-0.6278806943,-10.429511448\C,9.61
471155,-1.6814317846,-8.5129616826\H,9.6590143641,-1.9898058385,-6.378
0052291\H,10.6499438884,-1.9663359493,-8.6642886863\H,9.3215608921,-1.
3026547203,-10.6262838204\H,5.7741486962,-1.1567213633,-4.1039184403\C
,4.5935760879,-0.1842311474,-8.6111998885\H,4.3443194843,-0.9489503657
,-9.3494245716\H,4.8466648018,0.7509599386,-9.1145066236\H,3.742693247
,-0.0240394893,-7.9510235579\Version=ES64L-G16RevA.03\State=1-A\HF=-9
46.6484507\RMSD=3.533e-09\RMSF=1.174e-05\Dipole=-0.7162201,0.4705393,-
1.8761881\Quadrupole=10.8275271,-31.0038563,20.1763292,-9.2283336,-28.
1622626,0.8777596\PG=C01 [X(C16H15N6)]\@
```

1_E_hazo_mecn

```
1\1\GINC-R3351\FOpt\RM062X\6-31+G(d,p)\C16H15N6(1+)\ROOT\23-Jun-2019\0\
#\#P M062X/6-31+G(d,p) INT(grid=ultrafine) Opt Freq SCRF=(SMD,Solvent=
Acetonitrile)\Optimisation in solution\1,1\H,3.476039426,-1.12993858
03,0.608666819\C,2.7293510206,-0.8097753942,-0.1109086409\C,1.44202159
86,-0.4814119414,0.2648082551\H,1.1554007296,-0.5413047662,1.309753055
9\C,0.4757554034,-0.0642998425,-0.686484363\H,-0.5237242695,0.18352136
39,-0.3433277116\C,0.7656956817,0.0367561773,-2.0360469511\H,0.0185057
676,0.3568355955,-2.7539470114\C,2.0726132161,-0.2968199209,-2.4160390
562\C,3.0485948765,-0.7149270426,-1.478167511\N,2.6960763428,-0.310950
2736,-3.6454960735\N,4.231027416,-0.9756719704,-2.1183484284\C,3.96716
59807,-0.7230746095,-3.3807484612\C,2.0774636519,0.0482498324,-4.92153
0928\H,1.0451312616,0.3249266816,-4.7152307636\H,2.0984111081,-0.80420
5926,-5.6013825635\H,2.6008151357,0.8952317205,-5.3665436966\N,4.96255
15785,-0.8859951598,-4.3286157101\N,4.793711371,-0.6657947367,-5.56066
35942\C,5.8579361236,-0.8692665522,-6.3619153764\N,5.7366160108,-0.646
3784109,-7.7143805882\N,7.0705214075,-1.278645113,-5.9908343048\C,6.94
84484659,-0.9314124152,-8.2410915991\C,7.7741657693,-1.3275013317,-7.1
402120121\C,7.4233747454,-0.8883426502,-9.5666415073\C,9.124051859,-1.
6950767973,-7.3648114997\C,8.7375319062,-1.2515896554,-9.7462098031\H,
6.7852627206,-0.5860415705,-10.38992526\C,9.5790229323,-1.6505057133,-
8.6585986174\H,9.7568459129,-1.9964563234,-6.5367997048\H,10.606355851
8,-1.9237461398,-8.8765172312\H,9.1593350534,-1.2378659249,-10.7460806
952\H,5.8763382182,-1.2060819176,-3.9652897657\C,4.5554618675,-0.19672
22323,-8.4435540838\H,4.2814123098,-0.9551454679,-9.178683201\H,4.7837
941744,0.745986164,-8.9434441681\H,3.7406273747,-0.0539491557,-7.73582
7248\Version=ES64L-G16RevA.03\State=1-A\HF=-946.7470645\RMSD=6.591e-0
9\RMSF=4.498e-05\Dipole=-0.8513116,0.7042725,-3.2736819\Quadrupole=10.
```

0028332,-25.8368791,15.8340458,-8.5058201,-20.4286627,-0.0779026\PG=C0
1 [X(C16H15N6)]\@

::::::::::

1_E_him_gasphase.ar

::::::::::

1\1\GINC-R2401\FOpt\RM062X\6-31+G(d,p)\C16H15N6(1+)\ROOT\09-Aug-2019\0
\#M062X/6-31+G(d,p) OPT Freq=noraman INT(grid=ultrafine)\a4 b1\1,1\
H,3.1199983206,-0.6463937801,0.9043334302\C,2.4647823166,-0.4894911908
,0.0551535085\C,1.1118577621,-0.2335343783,0.2142469739\H,0.696381545,
-0.1887767375,1.2146822418\C,0.2599991739,-0.0295149547,-0.890559507\H
, -0.7914796839,0.1675617914,-0.7148972077\C,0.7290969521,-0.0738727817
, -2.1937596807\H,0.0656019097,0.0843799355,-3.0358960346\C,2.091644288
2,-0.3315008298,-2.3581817435\C,2.9377608354,-0.5343289677,-1.25565489
58\N,2.8817659485,-0.4437474468,-3.4979683788\N,4.2025089376,-0.760293
6824,-1.7786037546\C,4.1395178449,-0.7004220088,-3.119463678\C,2.45305
97802,-0.3112304602,-4.8930134584\H,1.385171565,-0.1045408001,-4.89805
64535\H,2.6552854261,-1.2395643321,-5.4266015115\H,2.993470937,0.50923
20786,-5.3644071873\N,5.1389474217,-0.8607339831,-4.0458047635\N,6.258
6653418,-1.0967555065,-3.4974852995\C,7.2982325487,-1.267081927,-4.360
7664076\N,8.5571089593,-1.5289482972,-3.8425223326\N,7.2733479684,-1.2
151291521,-5.6863115346\C,9.3789298482,-1.6497008701,-4.9157564081\C,8
.5499165853,-1.4486800924,-6.0604497461\C,10.7564322885,-1.9124815238,
-5.0168676795\C,9.111432222,-1.5111078054,-7.3582643137\C,11.267942345
3,-1.9659435182,-6.2948906058\H,11.3819390885,-2.0644803779,-4.1440948
769\C,10.4566277267,-1.7678706881,-7.45290179\H,8.4855936465,-1.359074
6001,-8.2302426244\H,10.926892032,-1.8241152359,-8.4284187225\H,12.325
5330691,-2.1655780906,-6.432074235\H,5.0631096153,-0.9444760436,-1.279
0642177\C,8.9561707109,-1.6556466691,-2.4500185397\H,9.36817568,-2.651
9028519,-2.2749350353\H,8.0815589802,-1.5088627567,-1.8204004589\H,9.7
072200636,-0.8990144593,-2.2126140714\Version=ES64L-G16RevA.03\State=
1-A\HF=-946.6693655\RMSD=6.484e-09\RMSF=3.353e-05\Dipole=-1.063849,0.1
444075,1.7237192\Quadrupole=35.891026,-33.4342098,-2.4568162,-13.27426
83,-17.2357113,2.1426034\PG=C01 [X(C16H15N6)]\@

1_E_him_mecn

1\1\GINC-R3207\FOpt\RM062X\6-31+G(d,p)\C16H15N6(1+)\ROOT\09-Aug-2019\0
\#M062X/6-31+G(d,p) OPT Freq=noraman INT(grid=ultrafine) SCRF=(SMD,Solvent=Acetonitrile)\a4 b1\1,1\
H,3.1478843725,-0.6514604553,0.8959860
71\C,2.47912074,-0.4923283963,0.057616083\C,1.1285396261,-0.2370181353
,0.2223436607\H,0.7163607837,-0.1929674045,1.2250579494\C,0.2682328071
, -0.0314300479,-0.8808563786\H,-0.7827106487,0.1652750042,-0.697484825
9\C,0.7270595697,-0.073734468,-2.1863723572\H,0.0646081351,0.084356655
5,-3.0298025242\C,2.0915548226,-0.3315074108,-2.3575019107\C,2.9443385
984,-0.5354747569,-1.2589723985\N,2.8742764814,-0.4423780257,-3.496141
5257\N,4.201501479,-0.7600480762,-1.7800938558\C,4.1290071867,-0.69857
2782,-3.1147471046\C,2.4328869511,-0.3075689087,-4.8870067028\H,1.3651
315041,-0.1012820089,-4.8815326355\H,2.6276307848,-1.2386910227,-5.418

8096393\H,2.96736369,0.5181338507,-5.356343913\N,5.137618048,-0.860386
3274,-4.0492316555\N,6.247205138,-1.0941343519,-3.5097993938\C,7.29826
76446,-1.2661437061,-4.3878095859\N,8.5390158417,-1.5247850529,-3.8616
481938\N,7.2750748628,-1.214671441,-5.7085886848\C,9.3771288853,-1.648
8551839,-4.9297866579\C,8.5666025274,-1.4512537678,-6.0785839167\C,10.
7545668455,-1.9123196518,-5.0111647041\C,9.1409972942,-1.5165540771,-7
.3652040252\C,11.2893620372,-1.9704798024,-6.283242583\H,11.3604835159
, -2.0610704868,-4.1233936914\C,10.4933370672,-1.775187343,-7.445929943
3\H,8.5303694788,-1.3669981059,-8.2500183951\H,10.9709479947,-1.832929
8038,-8.4189145378\H,12.3492641567,-2.1711280422,-6.4043326578\H,5.054
8342111,-0.9436724798,-1.2566867529\C,8.9226368823,-1.6487987616,-2.46
10733162\H,9.3340472228,-2.6451288896,-2.287874438\H,8.0424733246,-1.5
006817668,-1.8390713489\H,9.6731801376,-0.8917475694,-2.2255145103\Ver
sion=ES64L-G16RevA.03\State=1-A\HF=-946.7706931\RMSD=5.414e-09\RMSF=2
.862e-05\Dipole=-2.0799246,0.2924477,3.0854852\Quadrupole=34.0512931,-
30.26993,-3.7813631,-12.5889889,-8.8588196,0.6852974\PG=C01 [X(C16H15N
6)]\@

1_E_mecn

1\1\GINC-R2699\FOpt\RM062X\6-31+G(d,p)\C16H14N6\ROOT\30-Jul-2019\0\#P
M062X/6-31+G(d,p) INT(grid=ultrafine) Opt Freq SCRF=(SMD,Solvent=Acet
onitrile)\Optimisation in solution\0,1\N,-3.4989146489,-1.2676915703
, -0.4282016639\N,-2.7362765419,-1.533878064,0.5248929725\C,-1.40351928
29,-1.716531527,0.153026202\N,-0.8674690623,-1.6441118596,-1.048715106
2\C,0.4646883719,-1.9065710064,-0.844349242\C,0.7090681061,-2.14007080
12,0.5299362591\N,-0.5075403314,-2.011672749,1.1459828357\C,1.52677046
42,-1.9656732547,-1.7643039195\C,2.7871812027,-2.2554728252,-1.2718021
527\C,3.0122415405,-2.486389334,0.1083380413\C,1.9832459689,-2.4338886
277,1.0339549691\C,-4.8316477914,-1.0849009852,-0.0563158513\N,-5.7276
227853,-0.789737117,-1.049269324\C,-6.9442112829,-0.6612257353,-0.4332
070014\C,-6.6998237895,-0.8946815975,0.9410845843\N,-5.3676812202,-1.1
57225335,1.145438687\C,-8.218377309,-0.3673404951,-0.9372163305\C,-9.2
473523835,-0.3147233288,-0.0115832292\C,-9.02228399,-0.5455942195,1.36
85632829\C,-7.7618855711,-0.8354639492,1.8610552889\H,1.3531493529,-1.
7885989216,-2.8213247286\H,3.6292570432,-2.308746208,-1.9549186171\H,4
.0193506467,-2.7102159773,0.4460964333\H,2.1517884793,-2.610153949,2.0
915836824\H,-8.386925782,-0.1911089202,-1.9948497173\H,-10.2544510555,
-0.0908372784,-0.3493333597\H,-9.8643433959,-0.4922274494,2.0516927164
\H,-7.5882582434,-1.0125030934,2.9180809713\C,-5.482599286,-0.63502770
78,-2.4762359734\C,-0.7525781635,-2.1664635113,2.572938202\H,-4.424111
2216,-0.79413023,-2.6712220751\H,-5.767119114,0.3730114028,-2.78557089
78\H,-6.0735958586,-1.3699709096,-3.0271540952\H,-0.4679676888,-3.1744
881191,2.8822367983\H,-0.1616637503,-1.4315864316,3.1238993725\H,-1.81
10856267,-2.0074713154,2.7679089856\Version=ES64L-G16RevA.03\State=1-
A\HF=-946.3248641\RMSD=7.624e-09\RMSF=7.046e-06\Dipole=-0.000027,-0.0
00154,-0.0000021\Quadrupole=14.5445483,-15.2808902,0.7363418,-7.88479
73,16.3523515,-5.3907183\PG=C01 [X(C16H14N6)]\@

1_Z_gasphase

1\1\GINC-R655\FOpt\RM062X\6-31+G(d,p)\C16H14N6\ROOT\05-Apr-2019\0\#\#P M062X/6-31+G(d,p) INT(grid=ultrafine) Opt Freq\Optimisation\0,1\H,5.8155615784,0.9309528503,-1.9935766828\C,4.771787078,0.7839152213,-2.2492834917\C,3.7656092433,1.5607056777,-1.6961150608\H,4.0213621616,2.3387577185,-0.98432121\C,2.4106869591,1.3690535532,-2.0398328353\H,1.6553738834,2.0013432416,-1.5846116864\C,2.0216154762,0.3929765455,-2.9464724565\H,0.9795667743,0.248638608,-3.2132129268\C,3.040187875,-0.3900980805,-3.4934129155\C,4.4034789309,-0.2050859381,-3.1703820858\N,3.0174647175,-1.4380473537,-4.3883613718\N,5.1870357558,-1.0957770739,-3.8760117885\C,4.3263016844,-1.7744283916,-4.5879492109\C,1.8598050064,-1.9750750451,-5.0743532218\H,1.5245670557,-1.2913302498,-5.8589805241\H,1.0547717765,-2.1304007463,-4.3525936086\H,2.1333193609,-2.932286966,-5.5187864694\N,4.6310279116,-2.9299158757,-5.3493395714\N,5.6019234779,-2.9249345462,-6.1234992767\C,6.2105332825,-1.6985665133,-6.4884639722\N,7.5688974743,-1.6468734235,-6.6236511908\N,5.5714923425,-0.6396564339,-6.9111145496\C,7.8394205117,-0.3963131774,-7.1360330305\C,6.5770182993,0.2093922551,-7.3273423924\C,9.0398521319,0.2462193199,-7.4458019513\C,6.4993517212,1.4987850713,-7.8692127196\C,8.9383349153,1.5242566994,-7.9772365329\H,10.0033015808,-0.225695838,-7.2817646515\C,7.6864955607,2.1405715384,-8.1863701452\H,5.5344349624,1.9700586507,-8.0218820258\H,7.6578401182,3.1425488255,-8.6018735514\H,9.8431625678,2.0637724156,-8.2374782403\C,8.5312270543,-2.6401825809,-6.1918951683\H,8.9910412913,-2.3458351105,-5.2445459077\H,9.3027029439,-2.7493206223,-6.9574379095\H,8.0141865351,-3.5915642254,-6.0648996662\Version=ES64L-G16RevA.03\State=1-A\HF=-946.2681738\RMSD=7.944e-09\RMSF=5.659e-06\Dipole=-0.0028859,-0.0225227,-0.0037317\Quadrupole=14.8472513,-4.7937739,-10.0534773,-1.9430393,-3.4027045,1.3036008\PG=C01 [X(C16H14N6)]\@\

1_Z_hazo_gasphase

1\1\GINC-R303\FOpt\RM062X\6-31+G(d,p)\C16H15N6(1+)\ROOT\05-Apr-2019\0\#\#P M062X/6-31+G(d,p) INT(grid=ultrafine) Opt Freq\Optimisation\1,1\H,4.7313175725,2.1210389728,-1.9927270478\C,3.8507595342,1.5997336209,-2.352255206\C,2.5742509172,2.0635322341,-2.0883072841\H,2.4529287294,2.9700685457,-1.5049473335\C,1.415787847,1.3940333125,-2.5583613246\H,0.4422731448,1.806421595,-2.3174440752\C,1.500619727,0.2378281006,-3.3063065854\H,0.621798281,-0.2843197903,-3.6672749406\C,2.7869037419,-0.2562257311,-3.5853374783\C,3.9328909564,0.4308597906,-3.1178180562\N,3.1627988744,-1.3863044262,-4.2679135129\N,5.0154236633,-0.3052081758,-3.5458438751\C,4.4688038842,-1.344616307,-4.2431560629\N,5.1923587503,-2.4207615709,-4.7921871396\N,6.1986818871,-2.4820840544,-5.5728986365\C,6.7491766824,-1.4112145059,-6.143864351\N,7.8113922596,-1.6302338681,-7.0211199548\N,6.361961699,-0.1270731486,-6.1112900619\C,8.0880385626,-0.4341704292,-7.5725565997\C,7.1580878989,0.4946057739,-6.9899342528\C,9.0489505829,-0.0399651177,-8.5259919956\C,7.1857776235,1.8632380456,-7.3725102104\C,9.0424129354,1.2903621358,-8.8672646946\H,9.747972

054,-0.742684508,-8.9651160285\C,8.1215684061,2.2338938105,-8.2984875628\H,6.4805010591,2.5644832768,-6.9413016676\H,8.1797211068,3.2666937674,-8.6236615989\H,9.7590900026,1.6505296087,-9.5980213714\H,4.7685680396,-3.3296320408,-4.6069434893\C,8.472004209,-2.8957240007,-7.3235636823\H,9.5257962331,-2.8302580924,-7.0461001694\H,8.3786113195,-3.105205285,-8.3907701799\H,7.989634943,-3.6854042506,-6.751807298\C,6.3972567624,-0.0749465281,-3.1647002899\H,6.9841990124,-0.9749774823,-3.3542271238\H,6.4344292504,0.1417133258,-2.0952214507\H,6.815051847,0.7564233962,-3.7359174079\Version=ES64L-G16RevA.03\State=1-A\HF=-946.6328339\RMSD=9.881e-09\RMSF=1.133e-05\Dipole=2.3661806,-0.7266631,-0.7197564\Quadrupole=1.63181,-1.1031953,-0.5286147,-6.8280658,-23.1649878,3.4131037\PG=C01 [X(C16H15N6)]\@\

1_Z_hazo_mecn

1\1\GINC-R125\FOpt\RM062X\6-31+G(d,p)\C16H15N6(1+)\ROOT\23-Jun-2019\0\#\#P M062X/6-31+G(d,p) INT(grid=ultrafine) Opt Freq SCRF=(SMD,Solvent=A cetonitrile)\Optimisation in solution\1,1\H,4.2526016093,0.6749393108,-0.2919410898\C,3.6664928192,0.6927790468,-1.2054745491\C,2.6135995602,1.5759213303,-1.3810012686\H,2.3628287308,2.2727771431,-0.5875201679\C,1.8514553639,1.5942993095,-2.5729069205\H,1.0367394517,2.3056662592,-2.6654277144\C,2.1175321211,0.731136425,-3.6246828634\H,1.5354723446,0.744141631,-4.5405057604\C,3.1846127649,-0.1557282816,-3.4413592554\C,3.9537949413,-0.1884184203,-2.258680645\N,3.7076675975,-1.1354761831,-4.2558918525\N,4.9286633696,-1.1645983316,-2.3589994804\C,4.7413108466,-1.6631364218,-3.5510295438\C,3.2370735688,-1.4868695929,-5.5855925969\H,3.5545173003,-0.7293427872,-6.3061704907\H,2.1478354334,-1.5512875309,-5.5651185235\H,3.6398970712,-2.4610005058,-5.865974782\N,5.5277759276,-2.7336242618,-4.0541292915\N,6.3237693721,-2.7514745073,-5.0467489864\C,6.5977967506,-1.6908689654,-5.793036524\N,7.5094432463,-1.8546929572,-6.8348156287\N,6.162032857,-0.4187774565,-5.6858695409\C,7.6579024288,-0.6481938766,-7.3913019589\C,6.8017112537,0.2432557931,-6.6490003825\C,8.4502957178,-0.207119296,-8.4766251792\C,6.7337588862,1.6221070462,-7.0015176522\C,8.3546598996,1.1254274336,-8.7794403164\H,9.0911955204,-0.8875180391,-9.0260836775\C,7.5051335759,2.0330188928,-8.0507561138\H,6.0913882767,2.2976756824,-6.4470793851\H,7.4890009908,3.0733654854,-8.3581200688\H,8.9394985236,1.5247818252,-9.6019248853\H,5.5034005649,-3.6110996264,-3.5301356562\C,8.1829502684,-3.0835852783,-7.2447104831\H,9.2615098044,-2.9313515984,-7.1821624468\H,7.8944320794,-3.3184323146,-8.2704855006\H,7.8795391614,-3.8873263812,-6.5779088174\Version=ES64L-G16RevA.03\State=1-A\HF=-946.7327024\RMSD=7.674e-09\RMSF=9.923e-06\Dipole=1.4777351,-2.338952,-3.6605411\Quadrupole=2.0460718,3.2788224,-5.3248942,-6.549544,-19.1669154,0.4650434\PG=C01 [X(C16H15N6)]\@\

1_Z_him_gasphase

1\1\GINC-R276\FOpt\RM062X\6-31+G(d,p)\C16H15N6(1+)\ROOT\05-Apr-2019\0\

```
\#P M062X/6-31+G(d,p) INT(grid=ultrafine) Opt Freq\Optimisation\1,1\
H,4.1519275263,2.6459845952,-3.4458145984\C,3.4480317116,1.878484484,-
3.1459153372\C,2.3977511287,2.1443479501,-2.2880012583\H,2.2707086571,
3.1493030954,-1.9012395244\C,1.478238183,1.1413860569,-1.8963795972\H,
0.6724414228,1.4055873352,-1.2206491822\C,1.5791189164,-0.1604774485,-
2.3500753077\H,0.8740911004,-0.9272108705,-2.0491582042\C,2.6424439272
,-0.4323516252,-3.2194346845\C,3.5563209123,0.5617453914,-3.609437205\
N,3.0290928844,-1.5979998729,-3.8458492167\N,4.4576614734,-0.042761896
8,-4.4551210824\C,4.129911106,-1.3364404196,-4.5878110526\C,2.34521889
6,-2.8831019638,-3.7113187103\H,1.3166838978,-2.7740864158,-4.05954084
28\H,2.3564415944,-3.1810721429,-2.6615009312\H,2.8700225965,-3.618450
058,-4.3157128244\N,4.6772290734,-2.3900108809,-5.3011032612\N,5.68930
36473,-2.3722930267,-6.0480579777\C,6.518540285,-1.3180293811,-6.35735
94093\N,7.5545266371,-1.6098572959,-7.2121025044\N,6.5228147188,-0.036
4048175,-5.9874996741\C,8.2519431695,-0.4531666197,-7.3936127447\C,7.5
907448677,0.5295077333,-6.6163144896\C,9.3945332858,-0.1639973859,-8.1
584195335\C,8.0693985415,1.8551588551,-6.5861537198\C,9.8423751748,1.1
387431436,-8.1120452184\H,9.8960006658,-0.9208650395,-8.7512713636\C,9
.1885033761,2.1366280984,-7.3357766023\H,7.5702418661,2.6141403774,-5.
9943378724\H,9.5900905593,3.1439010424,-7.3410161988\H,10.7209605626,1
.417416827,-8.6837631815\C,7.8766711327,-2.8941379526,-7.8254089764\H,
8.8778178421,-3.1988653752,-7.5143852543\H,7.8399520309,-2.7918502437,
-8.9117206957\H,7.1461850166,-3.6290322737,-7.4968968657\H,5.308241612
6,0.3156580208,-4.9827948968\Version=ES64L-G16RevA.03\State=1-A\HF=-9
46.6658137\RMSD=7.851e-09\RMSF=8.406e-06\Dipole=-0.5920173,-0.2498679,
0.3672776\Quadrupole=13.1879468,-6.6982716,-6.4896752,3.1564347,-33.9.10
80984,5.1914375\PG=C01 [X(C16H15N6)]\@\
```

1_Z_him_mecn

```
1\1\GINC-R2388\FOpt\RM062X\6-31+G(d,p)\C16H15N6(1+)\ROOT\02-May-2019\0
\#P M062X/6-31+G(d,p) INT(grid=ultrafine) Opt=(MaxStep=4) Freq SCRF=(
SMD,Solvent=Acetonitrile)\Optimisation in solution\1,1\H,4.144396637
4,2.6467428009,-3.4409919768\C,3.4426490329,1.8791331419,-3.1345205584
\C,2.3908312964,2.1369165853,-2.2755628353\H,2.255911323,3.1418811527,
-1.8896173581\C,1.4784478591,1.1259074317,-1.8808813376\H,0.6711171848
,1.385671883,-1.2041740471\C,1.5876808202,-0.1763469865,-2.3319811203\
H,0.8923192274,-0.9533360712,-2.0332469387\C,2.65338357,-0.4403248164,
-3.2028786438\C,3.5583027158,0.5611668217,-3.5950101392\N,3.0477828622
,-1.6015910853,-3.8264126781\N,4.4601944264,-0.0361067839,-4.438484515
7\C,4.1434429267,-1.3321829577,-4.5694550369\C,2.3653145152,-2.8859937
494,-3.6823816081\H,1.3409336098,-2.778239184,-4.0424426914\H,2.365688
1587,-3.1626829924,-2.6269634949\H,2.8946927303,-3.6323336073,-4.26823
8204\N,4.6991230657,-2.3825369701,-5.2822775106\N,5.7052264024,-2.3693
134708,-6.0352894701\C,6.5322954347,-1.3128297414,-6.3601347417\N,7.55
92724786,-1.60713959,-7.2220570941\N,6.5328184928,-0.0338972871,-5.993
8210771\C,8.2503157998,-0.4483416073,-7.4150137568\C,7.5932543852,0.53
3617235,-6.6350928123\C,9.3841321703,-0.1572799908,-8.1926133323\C,8.0
654283571,1.8613924295,-6.6123086261\C,9.8280113471,1.1491675628,-8.15
48053932\H,9.8785139344,-0.9185798117,-8.7869377844\C,9.1779845749,2.1
```

```
462823446,-7.3750859246\H,7.5657172492,2.6178772467,-6.0159258492\H,9.
5749746244,3.1561822401,-7.386687862\H,10.700204927,1.4294730729,-8.73
68097318\C,7.8850466986,-2.8876563688,-7.8399689083\H,7.1833008809,-3.
638200587,-7.485481188\H,8.9029229442,-3.1668631671,-7.5612422693\H,7.
8106731593,-2.7892735078,-8.9247572984\H,5.293404177,0.3508483852,-4.9
522561858\Version=ES64L-G16RevA.03\State=1-A\HF=-946.7561687\RMSD=1.9
74e-09\RMSF=4.022e-06\Dipole=-1.0304176,-0.6179766,0.5851428\Quadrupol
e=12.2363274,-6.3613406,-5.8749868,2.7907654,-32.1457305,5.1149292\PG=
C01 [X(C16H15N6)]\@\
```

1_Z_mecn

```
1\1\GINC-R3292\FOpt\RM062X\6-31+G(d,p)\C16H14N6\ROOT\23-Jun-2019\0\#P
M062X/6-31+G(d,p) INT(grid=ultrafine) Opt Freq SCRF=(SMD,Solvent=Acet
onitrile)\Optimisation in solution\0,1\H,5.5801560294,1.2325173241,-
2.0102965464\C,4.5494145403,0.9661672719,-2.2234984706\C,3.4876982786,
1.6220070948,-1.6206151066\H,3.6858323404,2.4226820278,-0.9147428986\C
,2.1451536697,1.2775311192,-1.9042135008\H,1.3461306058,1.8203359364,-
1.4087013949\C,1.8247938996,0.2662277053,-2.7980576169\H,0.7961051115,
-0.002081271,-3.0191037657\C,2.9013317977,-0.3964219475,-3.3977634176
\C,4.2487860058,-0.0584034085,-3.1353384456\N,2.9516521077,-1.43545797
75,-4.2967834143\N,5.0890579419,-0.8535464956,-3.8839758962\C,4.276016
8955,-1.6321081018,-4.5607475736\C,1.8110305296,-2.1151052699,-4.89106
05914\H,1.3418409587,-1.4775283715,-5.6440253695\H,1.0913277453,-2.348
8809181,-4.104613063\H,2.155468289,-3.0382221262,-5.3564215846\N,4.64
327695,-2.7557134107,-5.3319663316\N,5.6333377697,-2.7569256619,-6.083
7473496\C,6.2951288788,-1.5718671613,-6.4708063249\N,7.6369950711,-1.6
313221048,-6.7119519351\N,5.7252506525,-0.4444207448,-6.8304137287\C,7
.9762583658,-0.4055047337,-7.234098496\C,6.7641074242,0.3170332693,-7.
3200374559\C,9.2055743744,0.1293932993,-7.6345384527\C,6.7603498815,1.
6194660386,-7.8446608997\C,9.1787263427,1.4187617751,-8.145547374\H,10
.1280784267,-0.4364893808,-7.551997183\C,7.973771027,2.1527627688,-8.2
496781624\H,5.8355173167,2.183271512,-7.9197177643\H,8.006213794,3.159
4473743,-8.6548035643\H,10.105652504,1.8785204558,-8.4742372406\C,8.55
17673713,-2.7219528628,-6.4122526296\H,9.1314988075,-2.4928141891,-5.5
150313162\H,9.2239092411,-2.8611953281,-7.2607568162\H,7.9734505147,-3
.631476651,-6.2518983189\Version=ES64L-G16RevA.03\State=1-A\HF=-946.3
039072\RMSD=8.149e-09\RMSF=1.289e-05\Dipole=-0.0498174,-0.3905206,-0.0
650035\Quadrupole=20.6437935,-7.357415,-13.2863785,-1.9698184,-9.53965
83,2.2234269\PG=C01 [X(C16H14N6)]\@\
```

2_E_gasphase

```
1\1\GINC-R2319\FOpt\RM062X\6-31+G(d,p)\C14H8N4O2\ROOT\05-Apr-2019\0\#
P M062X/6-31+G(d,p) INT(grid=ultrafine) Opt Freq\Optimisation\0,1\H,
3.4089948972,-0.7784763894,0.6487980822\C,2.7101717923,-0.5892913335,-
0.1582075404\C,1.3674060454,-0.3252187159,0.0716326741\H,0.9938799087,
-0.3050581336,1.0898752647\C,0.4690073263,-0.0808110227,-0.9872206638\
H,-0.5719276337,0.1210043386,-0.7571544529\C,0.8765438682,-0.090560157
```

8, -2.3174648894\H, 0.1956498536, 0.0957534066, -3.1392608769\C, 2.222736863, -0.3566053079, -2.5229379144\C, 3.135268725, -0.6025537708, -1.4903913793\O, 2.9022444099, -0.4310841044, -3.7001459808\N, 4.3842811332, -0.8289854474, -2.048056559\C, 4.1779822624, -0.7154215548, -3.3196472616\N, 5.1856800717, -0.8701875329, -4.2693398931\N, 4.784759118, -0.721897332, -5.4440816726\C, 5.79200382, -0.8766025711, -6.394067626\N, 5.585427894, -0.76299154, -7.6656295323\O, 7.0678262158, -1.1609866693, -6.0138010613\C, 6.8343123827, -0.9894201626, -8.2235971894\C, 7.7473027137, -1.235391812, -7.1909973748\C, 7.2590398361, -1.0026233524, -9.5558742437\C, 9.0930034061, -1.5014500133, -7.3968899491\C, 8.6017449967, -1.2667147285, -9.7859309904\H, 6.5601328439, -0.813410496, -10.3627920381\C, 9.5002598307, -1.5111600092, -8.7271964863\H, 9.7740291926, -1.6877998966, -6.5752149677\H, 10.5411405623, -1.7129850087, -8.957508983\H, 8.9751208403, -1.2868606839, -10.8042264946\Version=ES64L-G16RevA.03\State=1-A\HF=-907.3896712\RMSD=7.735e-09\RMSF=8.937e-05\Dipole=0.0000145, -0.0000002, -0.0006936\Quadrupole=8.511922, -12.239735, 3.727813, -3.4938485, -16.2346402, 2.4238059\PG=C01 [X(C14H8N4O2)]\@\

2_E_hazo_gasphase

1\1\GINC-R3179\FOpt\RM062X\6-31+G(d,p)\C14H9N4O2(1+)\ROOT\05-Apr-2019\0\#\#P M062X/6-31+G(d,p) INT(grid=ultrafine) Opt Freq\Optimisation\1, 1\H, 3.3960920614, -0.9078564022, 0.6472646673\C, 2.6963153326, -0.672932937, -0.1461649928\C, 1.3691687101, -0.369052791, 0.0980539449\H, 1.0023865914, -0.3622410506, 1.1182793186\C, 0.4676541171, -0.0643954455, -0.9486819506\H, -0.5622415173, 0.1665120448, -0.6984296635\C, 0.8510778344, -0.0495035317, -2.2867175105\H, 0.1647587191, 0.1830789382, -3.0915122142\C, 2.1809734232, -0.3559355842, -2.5074696241\C, 3.1024260257, -0.6631975057, -1.4886983178\O, 2.8542581641, -0.4231095724, -3.7050340011\N, 4.3312310972, -0.9161187168, -2.0645065601\C, 4.0931876973, -0.7560058864, -3.3262128841\N, 5.0646506778, -0.915045834, -4.288668372\N, 4.8370331846, -0.7592191767, -5.5266533093\C, 5.9005968277, -0.9532363703, -6.329259358\O, 5.6902575736, -0.7943407133, -7.656776389\N, 7.1241515506, -1.2791743595, -5.9790256688\C, 6.8958023923, -1.0434853228, -8.2092871499\C, 7.7985522412, -1.3485832428, -7.1563940503\C, 7.2535387779, -1.022304378, -9.5512608951\C, 9.1469541021, -1.6544372523, -7.438641995\C, 8.5822171987, -1.32617635, -9.7994620854\H, 6.5460846722, -0.7863683932, -10.336501529\C, 9.5119508931, -1.6363631438, -8.7648380586\H, 9.8434592624, -1.8883457244, -6.6421600142\H, 10.5350707073, -1.8633014171, -9.042706796\H, 8.9343190532, -1.3291147443, -10.8257098589\H, 6.003702629, -1.1717151369, -3.9449346825\Version=ES64L-G16RevA.03\State=1-A\HF=-907.7353331\RMSD=9.401e-09\RMSF=6.798e-05\Dipole=0.6513949, -0.1100807, -0.6056324\Quadrupole=12.1622671, -33.5670417, 21.4047747, -8.2571259, -40.4845085, 5.2903104\PG=C01 [X(C14H9N4O2)]\@\

2_E_hazo_mecn

1\1\GINC-R617\FOpt\RM062X\6-31+G(d,p)\C14H9N4O2(1+)\ROOT\23-Jun-2019\0\#\#P M062X/6-31+G(d,p) INT(grid=ultrafine) Opt Freq SCRF=(SMD,Solvent=

Acetonitrile)\Optimisation in solution\1,1\H, 3.2927056643, -0.8865740118, 0.6970557215\C, 2.6300720204, -0.6579718457, -0.130518004\C, 1.2922369097, -0.3468359643, 0.0547537843\H, 0.8836646884, -0.3286398699, 1.0595127822\C, 0.4374732153, -0.0505112458, -1.030732473\H, -0.6020729216, 0.186555133, -0.8287476742\C, 0.8813042345, -0.0518020872, -2.3503858323\H, 0.2323028691, 0.1743090525, -3.188319416\C, 2.2193661359, -0.3651595828, -2.5090458368\C, 3.0931572688, -0.6637882602, -1.4523338345\O, 2.941957584, -0.4469044613, -3.6742238367\N, 4.3479317745, -0.9273297011, -1.9757914067\C, 4.1659088521, -0.7800074954, -3.2455363685\N, 5.1621056732, -0.946649522, -4.1857866362\N, 4.9339571081, -0.7912828083, -5.4174225346\C, 5.9756887848, -0.9780833009, -6.2472352896\O, 5.707655196, -0.8062782733, -7.5654381644\N, 7.2129261237, -1.3033116794, -5.957213594\C, 6.8877473482, -1.0447143795, -8.172384678\C, 7.8341728647, -1.3570349535, -7.1628280014\C, 7.1862637331, -1.0077227246, -9.5285094411\C, 9.1706172212, -1.6550076406, -7.5050285568\C, 8.504006387, -1.3039310143, -9.836276378\H, 6.4449885433, -0.7662228527, -10.2808737082\C, 9.4781620206, -1.6214740615, -8.8456935906\H, 9.9014896404, -1.8949738816, -6.7410132209\H, 10.4893750643, -1.8416713613, -9.1701256873\H, 8.812260153, -1.2948797186, -10.8767834278\H, 6.0982058433, -1.2040714875, -3.8251846958\Version=ES64L-G16RevA.03\State=1-A\HF=-907.8211186\RMSD=9.799e-09\RMSF=1.215e-04\Dipole=1.1331764, -0.1885614, -1.0807898\Quadrupole=11.8322591, -31.1037612, 19.2715021, -7.9142717, -36.1945272, 4.6187229\PG=C01 [X(C14H9N4O2)]\@\

2_E_hox_gasphase

1\1\GINC-R3340\FOpt\RM062X\6-31+G(d,p)\C14H9N4O2(1+)\ROOT\05-Apr-2019\0\#\#P M062X/6-31+G(d,p) INT(grid=ultrafine) Opt Freq\Optimisation\1, 1\H, 3.3439942856, -0.7688503817, 0.7161606407\C, 2.6719484035, -0.5839140991, -0.1134997355\C, 1.3215739671, -0.3160875043, 0.0775446481\H, 0.9298044167, -0.2917313119, 1.0881351092\C, 0.4455224226, -0.0753435794, -0.9980261398\H, -0.5985744627, 0.128295238, -0.7886833859\C, 0.8770578095, -0.0904357916, -2.321329373\H, 0.2166552924, 0.09260725, -3.1600766368\C, 2.2226389478, -0.3584018665, -2.4921758904\C, 3.100479443, -0.5983622532, -1.4372464356\O, 2.9298636993, -0.4380573504, -3.6775136448\N, 4.3342131453, -0.8183974308, -2.0533013139\C, 4.1793772835, -0.7131080286, -3.3667803539\N, 5.2186412441, -0.8789598046, -4.2348662343\N, 4.8508517679, -0.73557921, -5.4439915818\C, 5.8327345957, -0.8868389032, -6.3616716575\N, 5.6180576908, -0.7705740401, -7.6506314064\O, 7.1178262768, -1.1718886538, -6.0034046113\C, 6.837129168, -0.9906317635, -8.2124230126\C, 7.7748081644, -1.2414704257, -7.1837786152\C, 7.2401268363, -0.9982795425, -9.5637858673\C, 9.1177289839, -1.505576161, -7.4141564172\C, 8.5706360403, -1.2590887284, -9.807358436\H, 6.5257089694, -0.8066916751, -10.3559900367\C, 9.4887715956, -1.5074114459, -8.7515873861\H, 9.8189036227, -1.6950448894, -6.6109835413\H, 10.5247948934, -1.7069282879, -9.0051045539\H, 8.9374589718, -1.2777793982, -10.827378912\H, 5.2273565251, -1.0268599612, -1.618885219\Version=ES64L-G16RevA.03\State=1-A\HF=-907.7481854\RMSD=5.899e-09\RMSF=8.519e-05\Dipole=-0.1398161, -0.0965808, 2.2454836\Quadrupole=10.4130034, -36.0411843, 25.628181

,-7.6940314,-38.7216936,4.4672405\PG=C01 [X(C14H9N4O2)]\@

2_E_hox_mecn

1\1\GINC-R646\FOpt\RM062X\6-31+G(d,p)\C14H9N4O2(1+)\ROOT\23-Jun-2019\0
\\#P M062X/6-31+G(d,p) INT(grid=ultrafine) Opt Freq SCRF=(SMD,Solvent=Acetonitrile)\Optimisation in solution\1,1\H,3.3730193,-0.7739460295,0.699710766\C,2.6851713912,-0.5864811088,-0.1162369235\C,1.3381453791,-0.3197499497,0.083989708\H,0.9515295274,-0.2965430719,1.0970380489\C,0.4523111463,-0.0771809187,-0.9873090365\H,-0.5906422089,0.1257928698,-0.7687542304\C,0.8697947721,-0.0892524574,-2.3138936388\H,0.2006937937,0.0952398378,-3.1459018791\C,2.2152980043,-0.3567896505,-2.4939754266\C,3.101787778,-0.5982081554,-1.4456850241\O,2.9158838178,-0.4351670436,-3.6791174888\N,4.327181824,-0.8165777074,-2.0625728103\C,4.1650483203,-0.7105581023,-3.3625495744\N,5.1986935941,-0.8737777103,-4.2592147751\N,4.8218916865,-0.7295883672,-5.4497289237\C,5.8189414198,-0.8830517536,-6.381743105\N,5.6057686183,-0.767729765,-7.6596143529\O,7.0926571634,-1.1661774506,-6.0139721691\C,6.8407244419,-0.9907662007,-8.2246000608\H,7.7643300738,-1.2386933768,-7.1947586506\C,7.253738757,-1.0009674113,-9.5664113347\C,9.1093065769,-1.5040811868,-7.4076102228\C,8.591714351,-1.2637524215,-9.799971335\H,6.5506446347,-0.8111252096,-10.3702203302\C,9.4993845077,-1.5099971532,-8.7414328619\H,9.8000468904,-1.6919327209,-6.5938658612\H,10.5385090698,-1.7107790855,-8.9820197542\H,8.9632610778,-1.2834307432,-10.8190165054\H,5.2212542912,-1.026117956,-1.6133522479\Version=ES64L-G16RevA.03\State=1-A\HF=-907.8399298\RMSD=8.159e-09\RMSF=3.211e-05\Dipole=-0.5768013,-0.1072423,4.0521952\Quadrupole=8.8261245,-34.2556893,25.4295648,-7.2158998,-34.6197425,3.7343428\PG=C01 [X(C14H9N4O2)]\@

2_E_mecn

1\1\GINC-R785\FOpt\RM062X\6-31+G(d,p)\C14H8N4O2\ROOT\23-Jun-2019\0\\#P M062X/6-31+G(d,p) INT(grid=ultrafine) Opt Freq SCRF=(SMD,Solvent=Acetonitrile)\Optimisation in solution\1,1\H,3.4064097359,-0.7784856567,0.657611015\C,2.7100021684,-0.5895840886,-0.1525487058\C,1.366737979,-0.325227573,0.0759201855\H,0.9929034443,-0.3049719771,1.0944051076\C,0.4668864514,-0.0804260781,-0.9837234271\H,-0.5741732959,0.1214325789,-0.7524916408\C,0.8711273453,-0.0894571139,-2.3155894206\H,0.1867066401,0.097503178,-3.1352689859\C,2.2168486101,-0.3557263364,-2.5188353186\C,3.1310152582,-0.6019190358,-1.4871728604\O,2.8987384793,-0.4305090379,-3.6989257835\N,4.3781589305,-0.8277166634,-2.0510421112\C,4.1702802079,-0.7137808303,-3.3235893393\N,5.177977359,-0.8690230431,-4.2667377102\N,4.791520641,-0.7233885478,-5.4473394326\C,5.7992363072,-0.8784606563,-6.3904945814\N,5.5913499659,-0.7645151277,-7.663038831\O,7.0708211274,-1.1616031067,-6.01515111\C,6.8385079901,-0.9901607967,-8.2269110973\C,7.7526983816,-1.2362754182,-7.1952480249\C,7.2595110133,-1.0024153502,-9.5615415681\C,9.0984479352,-1.5023904779,-7.3985208137\C,8.6027996885,-1.2666121545,-9.7900280508\H,6.5630689409,-0.8135690938,-10.3716854038\C,9.5026807154,-1.5113395624,-8.7303882646\H,9.7828992006,-1.6892961887,-6.5788539885\H,10.5437631108,-1.7130731126,-8.9616261066\H,8.9766356677,-1.2867987304,-10.8085137312\Version=ES64L-G16RevA.03

\State=1-A\HF=-907.4151844\RMSD=2.629e-09\RMSF=8.178e-05\Dipole=0.0000195,0.0002014,-0.0000724\Quadrupole=12.4660904,-17.3126063,4.8465159,-5.0033372,-23.4586923,3.5540607\PG=C01 [X(C14H8N4O2)]\@

2_Z_gasphase

1\1\GINC-R507\FOpt\RM062X\6-31+G(d,p)\C14H8N4O2\ROOT\09-Aug-2019\0\\#M 062X/6-31+G(d,p) INT(grid=ultrafine) OPT Freq=noraman\al b1\1\N,-3.598606706,-1.5480657183,-0.4092041247\N,-2.726005325,-1.8161996839,0.4290062607\C,-2.3279974753,-3.1571222767,0.6386398231\N,-2.0114699032,-4.024660487,-0.2589683815\C,-1.4937035709,-5.0802396125,0.4876197144\C,-1.5413768662,-4.7351215738,1.8420546355\O,-2.062004091,-3.4723711443,1.9247322729\C,-0.9879872213,-6.322542932,0.0997853583\C,-0.5549602724,-7.1709863952,1.1113865372\C,-0.6185453047,-6.7997543613,2.4679151386\C,-1.1190645724,-5.5639271291,2.8687432395\C,-4.4102861133,-2.5746850759,-0.9455432406\O,-4.7066703804,-2.4334182064,-2.2556454494\C,-5.6212403615,-3.4252863227,-2.48409056\C,-5.8432828853,-4.078077063,-1.2673594754\N,-5.0384899487,-3.4909116572,-0.2940822707\C,-6.2477577386,-3.7652285614,-3.6720597661\C,-7.1490440607,-4.8230686167,-3.5877427461\C,-7.3948635659,-5.4947592937,-2.3751297961\C,-6.7510230388,-5.1366342425,-1.1970289416\H,-0.9453182668,-6.6032675258,-0.9464328252\H,-0.1575862965,-8.1469817449,0.8536675852\H,-0.2661440798,-7.4952566706,3.222219076\H,-1.1725594223,-5.2646044846,3.9086045245\H,-6.0499344402,-3.2385621059,-4.5979407621\H,-7.6778502637,-5.1371985827,-4.4813730531\H,-8.1059186396,-6.3140230476,-2.3651448807\H,-6.9327501896,-5.6517354844,-0.2606287241\Version=ES64L-G16RevA.03\State=1-A\HF=-907.3726517\RMSD=4.520e-09\RMSF=2.809e-05\Dipole=-0.2663515,-1.524431,-0.2103604\Quadrupole=0.8570419,-5.8455918,4.9885499,-2.3867048,7.7628712,-2.9654204\PG=C01 [X(C14H8N4O2)]\@

2_Z_hazo_gasphase

1\1\GINC-R799\FOpt\RM062X\6-31+G(d,p)\C14H9N4O2(1+)\ROOT\05-Apr-2019\0\\#P M062X/6-31+G(d,p) INT(grid=ultrafine) Opt Freq\Optimisation\1,1\H,4.8218116155,2.1570028661,-2.5751635773\C,3.9265789914,1.5477340645,-2.570180094\C,2.7751707951,1.9079699409,-1.8778181472\H,2.7702879273,2.8387240511,-1.3207813201\C,1.60916503,1.1063688134,-1.8717143533\H,0.7472676031,1.4475066966,-1.309405878\C,1.5438643352,-0.0929511029,-2.5573579973\H,0.6578452821,-0.7169859378,-2.5577704642\C,2.6957650924,-0.4734913315,-3.261435621\C,3.8377370151,0.3464034603,-3.2515561103\N,2.9647289576,-1.593274545,-4.0203192623\O,4.7951146069,-0.2735281824,-4.0161809045\C,4.1765252584,-1.3867441761,-4.4279897285\N,4.8501042218,-2.3735284937,-5.1386036986\N,5.9305073133,-2.4151275095,-5.8080071251\C,6.6077871274,-1.3339876508,-6.2002838671\O,7.8002960574,-1.639067391,-6.7987379347\N,6.2760934,-0.0565000538,-6.2513081066\C,8.2594217516,-0.4625074863,-7.2459506685\C,7.2942068334,0.5293837332,-6.9186539707\C,9.4446569448,-0.1916485747,-7.9209834058\C,7.4991487903,1.8782430854,-7.2935036817\C,9.6189484869,1.1363710409,-8.2703065867\H,10.1658231047,-0.9637107949,-8.1587015782\C,8.6656149766,2.154463172,-7.9636644493\H,6.7656026686,2.6389049867,-7.0537831874\H,8.8805148931,3.170514249,-8.2748697815\H,10.5188274245,1.4210616332,-8.8057642313\H,4.381803

4955,-3.2788885629,-5.0610542686\\Version=ES64L-G16RevA.03\\State=1-A\\HF=-907.720727\\RMSD=5.530e-09\\RMSF=5.680e-05\\Dipole=0.6618795,0.3488081,-0.3124554\\Quadrupole=9.4514838,-6.1965186,-3.2549653,4.418307,-28.8660723,0.6674213\\PG=C01 [X(C14H9N4O2)]\\@

2_Z_hazo_mecn

1\\1\\GINC-R357\\FOpt\\RM062X\\6-31+G(d,p)\\C14H9N4O2(1+)\\ROOT\\23-Jun-2019\\0\\#P M062X/6-31+G(d,p) INT(grid=ultrafine) Opt Freq SCRF=(SMD,Solvent=Acetonitrile)\\Optimisation in solution\\1,1\\H,4.8891714842,2.1046834411,-2.5869300079\\C,3.9766204326,1.5200394861,-2.58569406\\C,2.8265283067,1.9188215345,-1.911961938\\H,2.839593239,2.8550564304,-1.3634434944\\C,1.6413757384,1.1479801329,-1.9168789423\\H,0.7796486557,1.514720007,-1.3691953767\\C,1.5535972716,-0.0560631333,-2.5969187391\\H,0.6489903238,-0.6542755064,-2.60382717\\C,2.7031462766,-0.4726566938,-3.2808675677\\C,3.8637132882,0.3143627092,-3.2576574443\\N,2.9551605995,-1.6065666664,-4.0323934307\\O,4.8139475871,-0.336584888,-4.0010233528\\C,4.1774395223,-1.4374966291,-4.4187898473\\N,4.8594961327,-2.4276239564,-5.1210309506\\N,5.9292208456,-2.4337887614,-5.7983795919\\C,6.5835162586,-1.3410215801,-6.2002935979\\O,7.7802697007,-1.6344056408,-6.7983233206\\N,6.2435956266,-0.0683919236,-6.2522298654\\C,8.2330530327,-0.4524185179,-7.2385447894\\C,7.2596707458,0.5292651689,-6.9120114598\\C,9.4214010141,-0.1696578572,-7.9028842126\\C,7.4568972927,1.8825164054,-7.272877346\\C,9.5893504295,1.1624480606,-8.2394875932\\H,10.1511357175,-0.9345009929,-8.1402932756\\C,8.627487987,2.171514269,-7.9313390511\\H,6.717417052,2.6369105704,-7.0286280088\\H,8.840114032,3.1921698836,-8.2302361414\\H,10.4919761923,1.4579050489,-8.7648775054\\H,4.4276852142,-3.3542304008,-5.0248319189\\Version=ES64L-G16RevA.03\\State=1-A\\HF=-907.8075123\\RMSD=8.466e-09\\RMSF=6.678e-06\\Dipole=1.0553901,-0.0444868,-0.5511696\\Quadrupole=7.0413414,-2.4690773,-4.572264,5.3307362,-25.9062285,0.0566177\\PG=C01 [X(C14H9N4O2)]\\@

2_Z_hox_gasphase

1\\1\\GINC-R1053\\FOpt\\RM062X\\6-31+G(d,p)\\C14H9N4O2(1+)\\ROOT\\05-Apr-2019\\0\\#P M062X/6-31+G(d,p) INT(grid=ultrafine) Opt Freq\\Optimisation\\1,1\\H,4.0300690066,2.6966275214,-3.325454009\\C,3.4219135161,1.8642933655,-2.9922074942\\C,2.3861932401,2.0240239335,-2.0859393267\\H,2.1752772221,3.0134540644,-1.6959784643\\C,1.5921049099,0.9386850639,-1.6503747304\\H,0.7956301169,1.1275932118,-0.9392550154\\C,1.797095239,-0.3576042908,-2.1012429348\\H,1.1970733353,-1.1988803515,-1.776633637\\C,2.8372018065,-0.5013614365,-3.0078354293\\C,3.6300085253,0.5604440817,-3.4473278239\\O,3.2722144272,-1.6433785329,-3.6193364944\\N,4.5348095408,-0.0111550209,-4.3318699353\\C,4.2877824558,-1.3103281617,-4.4028621875\\N,4.8270345767,-2.3853193883,-5.0876977464\\N,5.7899484282,-2.3617983389,-5.8934565974\\C,6.5357114176,-1.272231829,-6.2879367466\\O,7.4952423397,-1.6161756293,-7.1698283454\\N,6.5132297095,0.0087783607,-5.9942051257\\C,8.1396072007,-0.4651687351,-7.465825564\\C,7.5312667721,0.5674425366,-6.7319036002\\C,9.2128801733,-0.272819587,-8.3286836263\\H,7.994910984,1.8892

65443,-6.8389720921\\C,9.6566572967,1.0358831316,-8.4218540786\\H,9.661278416,-1.089134102,-8.8814498289\\C,9.0600647856,2.0967661143,-7.6917687511\\H,7.538090984,2.6980512897,-6.2806861264\\H,9.4588475257,3.0977010205,-7.8130388105\\H,10.4913750507,1.2619848901,-9.0765086466\\H,5.326209798,0.3840613753,-4.9136068317\\Version=ES64L-G16RevA.03\\State=1-A\\HF=-907.7332329\\RMSD=3.984e-09\\RMSF=1.216e-05\\Dipole=-0.3483027,1.8785594,0.6963268\\Quadrupole=13.5491146,-15.5094593,1.9603447,1.1783846,-33.5812168,1.3925135\\PG=C01 [X(C14H9N4O2)]\\@

2_Z_hox_mecn

1\\1\\GINC-R108\\FOpt\\RM062X\\6-31+G(d,p)\\C14H9N4O2(1+)\\ROOT\\07-May-2019\\0\\#P M062X/6-31+G(d,p) INT(grid=ultrafine) Opt Freq SCRF=(SMD,Solvent=Acetonitrile)\\Optimisation in solution\\1,1\\H,2.3404149025,2.7909807323,0.0186979567\\C,3.0279124172,1.9533643263,0.0167657782\\C,4.4038758435,2.1110302604,0.0282238373\\H,4.8198507562,3.1126658993,0.0396060037\\C,5.2893311806,1.007651373,0.0258024069\\H,6.3574944718,1.1966072841,0.0354921408\\C,4.8409655695,-0.3059097,0.0118429271\\H,5.5088208453,-1.1592732143,0.0101469974\\C,3.4610951493,-0.4471090607,0.0005899956\\C,2.576408399,0.6319668509,0.0028197976\\O,2.7277798013,-1.5994333546,-0.0128290357\\N,1.3163661491,0.0621698812,-0.009057198\\C,1.4453379702,-1.250578046,-0.0175826271\\N,0.5973017037,-2.3424957839,-0.0314313755\\N,-0.6579804313,-2.3384446763,-0.0403386438\\C,-1.4935901468,-1.2448163529,-0.0322807821\\O,-2.7971151823,-1.6109752356,-0.063959683\\N,-1.297460338,0.0460766593,0.0012548359\\C,-3.4873591475,-0.4460880854,-0.051813871\\C,-2.5540774407,0.6023789328,-0.0098679901\\C,-4.8636545669,-0.2547637637,-0.0761656852\\C,-2.9786730863,1.9404474866,0.0100458316\\C,-5.2670036644,1.0720945436,-0.0561777963\\H,-5.5627897023,-1.0822746521,-0.1088368838\\C,-4.3445570547,2.1485710685,-0.014123347\\H,-2.2654354409,2.7567188016,0.0417353346\\H,-4.7303220108,3.1623802575,-0.0011269042\\H,-6.3283488535,1.297647519,-0.0737412652\\H,0.3686149069,0.5053120491,-0.0040297555\\Version=ES64L-G16RevA.03\\State=1-A\\HF=-907.8215842\\RMSD=2.801e-09\\RMSF=4.975e-06\\Dipole=1.1177963,2.4695688,0.0221087\\Quadrupole=39.0083662,-14.6759941,-24.3323721,0.4631732,0.5320109,0.1472043\\PG=C01 [X(C14H9N4O2)]\\@

2_Z_mecn

1\\1\\GINC-R691\\FOpt\\RM062X\\6-31+G(d,p)\\C14H8N4O2\\ROOT\\09-Aug-2019\\0\\#M062X/6-31+G(d,p) INT(grid=ultrafine) OPT Freq=norman SCRF=(SMD,Solvent=acetonitrile)\\a1 b1\\0,1\\N,-3.6130787942,-1.644916517,-0.4259550493\\N,-2.7453918863,-1.9131250478,0.4190202813\\C,-2.3280690772,-3.2389140365,0.6577814914\\N,-2.0499960554,-4.1554268354,-0.2046290565\\C,-1.4673761029,-5.1597750182,0.5650691539\\C,-1.4422111119,-4.738585404,1.898689296\\O,-1.9811527858,-3.4806385765,1.9397782259\\C,-0.9608046235,-6.4146893206,0.2145664755\\C,-0.4537620904,-7.1948910307,1.2464910864\\C,-0.4463983509,-6.7468339375,2.5834413315\\C,-0.946800817,-5.4990067565,2.94

61658083\C,-4.4365723511,-2.6437418045,-0.9854982145\O,-4.7848749304,-2.4100326114,-2.2686047461\C,-5.7131849895,-3.3805158176,-2.5350255001\C,-5.8910051054,-4.1209659585,-1.361701157\N,-5.0432528263,-3.6078611292,-0.3826012211\C,-6.3848200479,-3.6287317038,-3.7216906122\C,-7.2882442509,-4.6874548687,-3.6772554267\C,-7.4919287645,-5.4471831615,-2.5069688564\C,-6.8020374004,-5.1808390434,-1.3306244484\H,-0.9720577119,-6.7575294243,-0.8146117232\H,-0.0523282866,-8.177749251,1.0218097833\H,-0.0368151043,-7.3931143284,3.3530499745\H,-0.9448639915,-5.1432631111,3.9702206037\H,-6.2211390703,-3.0366776005,-4.6149576347\H,-7.853811498,-4.9339516538,-4.5700640641\H,-8.2075767222,-6.2626205506,-2.5304409418\H,-6.9528832531,-5.7656575009,-0.4294548595\Version=ES64L-G16RevA.03\State=1-A\HF=-907.393558\RMSD=2.154e-09\RMSF=1.002e-05\Dipole=-0.3615694,-2.0694468,-0.2855684\Quadrupole=2.5574369,-8.6655702,6.1081333,-3.9462322,12.7374217,-4.443984\PG=C01 [X(C14H8N4O2)]\@@

3_E_gasphase

1\1\GINC-R598\FOpt\RM062X\6-31+G(d,p)\C14H8N4S2\ROOT\05-Apr-2019\0\#P M062X/6-31+G(d,p) INT(grid=ultrafine) Opt Freq\Optimisation\1\H,3.4097868365,-0.7695440206,0.4882405251\C,2.5914775667,-0.5628175195,-0.1930177906\C,1.304594978,-0.3225433171,0.2542531044\H,1.0918211015,-0.3380946656,1.3178578811\C,0.262755246,-0.0570206761,-0.6547727419\H,-0.7382370212,0.1283077953,-0.2788061932\C,0.4890539589,-0.0272296692,-2.0232271207\H,-0.3183802647,0.1780070289,-2.7179499486\C,1.7881269098,-0.2695742373,-2.4784449115\C,2.839732143,-0.5368743756,-1.5736263263\S,2.3854174987,-0.3015050216,-4.110917579\N,4.0705431385,-0.75812406,-2.1546502069\C,3.9759492549,-0.6669238111,-3.438313734\N,5.1042967682,-0.8542325939,-4.2485945346\N,4.8643791558,-0.7367562581,-5.4663066697\C,5.9928680045,-0.9244033988,-6.2763127948\N,5.8989553111,-0.8333727124,-7.5598868333\S,7.5837617056,-1.2902747765,-5.6026361167\C,7.1300063457,-1.0549699083,-8.1405576105\C,8.1813909902,-1.3224304501,-7.2356426761\C,7.37841175,-1.0291566906,-9.5211085099\C,9.4804412049,-1.5650763058,-7.690624764\C,8.6653245984,-1.2697378412,-9.9682510757\H,6.5601997926,-0.8222921983,-10.2024390264\C,9.7069547415,-1.5354215397,-9.0590905785\H,10.2877424831,-1.7704433248,-6.9957889255\H,10.7079686437,-1.7209926845,-9.4348815174\H,8.878217158,-1.2542927674,-11.01318333247\Version=ES64L-G16RevA.03\State=1-A\HF=-1553.3285467\RMSD=5.013e-09\RMSF=6.438e-05\Dipole=-0.0014722,0.0000463,0.0004346\Quadrupole=10.4897875,-13.7510128,3.2612253,-4.3279866,-14.8889895,2.0772598\PG=C01 [X(C14H8N4S2)]\@@

3_E_hazo_gasphase

1\1\GINC-R624\FOpt\RM062X\6-31+G(d,p)\C14H9N4S2(1+)\ROOT\05-Apr-2019\0\#P M062X/6-31+G(d,p) INT(grid=ultrafine) Opt Freq\Optimisation\1,1\H,3.8364550997,-1.0239235649,0.2466308945\C,2.9317851435,-0.73869000294,-0.2785852562\C,1.7445411221,-0.4897227747,0.3787066684\H,1.6973118452,-0.5778914285,1.458267405\C,0.5834800638,-0.1200917004,-0.333421869\H,-0.3344098207,0.0688386724,0.2131375946\C,0.5815838545,0.0090746794,-1.7154367963\H,-0.3178844493,0.2937787261,-2.2494906249\C,1.77941028

95,-0.2416569358,-2.3835470029\C,2.954468658,-0.6141182637,-1.67986534\S,2.1012434813,-0.1661495031,-4.0967078231\N,4.0536125153,-0.8275455887,-2.469957737\C,3.7327284294,-0.628398613,-3.7088574408\N,4.7173678148,-0.7957194657,-4.673138624\N,4.5078109735,-0.6262080148,-5.9048972979\C,5.5840239651,-0.8314046446,-6.7194345442\S,5.3862836045,-0.6199241919,-8.4376182947\N,6.7722863774,-1.1815428401,-6.2891171973\C,7.047912185,-1.0369493412,-8.6138316877\C,7.6255533238,-1.3069613797,-7.3327468511\C,7.8097619536,-1.1269353226,-9.7856245776\C,8.9887002749,-1.6718479641,-7.2331664018\C,9.1377035477,-1.4855887355,-9.6546637074\H,7.3757581729,-0.9232280557,-10.7578785005\C,9.7239799395,-1.7561628444,-8.3899355422\H,9.415931524,-1.8741889637,-6.2575148315\H,10.7711948214,-2.0335977369,-8.3452245469\H,9.7524426198,-1.5632112902,-10.5452959667\H,5.6545926697,-1.0720028848,-4.3328941007\Version=ES64L-G16RevA.03\State=1-A\HF=-1553.6790324\RMSD=2.532e-09\RMSF=8.406e-05\Dipole=0.5164827,-0.0819025,-0.5681444\Quadrupole=12.7071444,-35.3233055,22.6161612,-9.4737488,-38.6847559,4.5151215\PG=C01 [X(C14H9N4S2)]\@@

3_E_hazo_mecn

1\1\GINC-R3500\FOpt\RM062X\6-31+G(d,p)\C14H9N4S2(1+)\ROOT\23-Jun-2019\0\#P M062X/6-31+G(d,p) INT(grid=ultrafine) Opt Freq SCRF=(SMD,Solvent=Acetonitrile)\Optimisation in solution\1,1\H,3.7417765902,-1.0071212743,0.3358393796\C,2.8618259454,-0.7244711396,-0.2327251343\C,1.6474016183,-0.4638836489,0.3734946821\H,1.5569332445,-0.5406701805,1.4519016198\C,0.5183407466,-0.0981921566,-0.3885242085\H,-0.4214373216,0.1000880255,0.1168500283\C,0.5766694532,0.0153065164,-1.7711505686\H,-0.2974193597,0.2972097532,-2.3481333053\C,1.8022973631,-0.2475482548,-2.3844538287\C,2.9432140927,-0.6154990321,-1.6313921054\S,2.1975327747,-0.1925523222,-4.0833826808\N,4.077872498,-0.8424685528,-2.3751256626\C,3.813564529,-0.6570670974,-3.6253329713\N,4.8198124151,-0.8317780408,-4.5702345622\N,4.6011959931,-0.6606718005,-5.795193316\C,5.6546429991,-0.8571880805,-6.6384024457\S,5.385527049,-0.6279426697,-8.3466325567\N,6.8592190506,-1.2065078735,-6.2640064281\C,7.0397391906,-1.0363737881,-8.59762486\C,7.6680145438,-1.3170639983,-7.3444031455\C,7.7520506932,-1.11024404904,-9.8013945193\C,9.0352443146,-1.6778517449,-7.30275228\C,9.0858401709,-1.4653433076,-9.726994328\H,7.2763684,-0.8975082077,-10.7526393039\C,9.7234832922,-1.7469781384,-8.489913577\H,9.5024208051,-1.8888216354,-6.3466688378\H,10.7731419759,-2.0209270769,-8.4905509821\H,9.6645055186,-1.5311329462,-10.6428198074\H,5.7558514135,-1.1087709274,-4.2197442946\Version=ES64L-G16RevA.03\State=1-A\HF=-1553.760895\RMSD=7.753e-09\RMSF=2.892e-05\Dipole=0.8427722,-0.1268869,-1.0002449\Quadrupole=12.7772022,-33.0414397,20.2642375,-9.1999349,-35.328779,4.0717423\PG=C01 [X(C14H9N4S2)]\@@

3_E_hth_gasphase

1\1\GINC-R575\FOpt\RM062X\6-31+G(d,p)\C14H9N4S2(1+)\ROOT\05-Apr-2019\0\#P M062X/6-31+G(d,p) INT(grid=ultrafine) Opt Freq\Optimisation\1,1\H,3.3528970758,-0.7630588612,0.5794413529\C,2.5660384318,-0.5606271463,-0.1392353352\C,1.2633551243,-0.314248786,0.260579646\H,1.0220132749

, -0.3234811894, 1.3174933424\C, 0.2472486812, -0.052310402, -0.6769580739\
H, -0.7617441202, 0.1363033828, -0.3275603415\C, 0.5073006266, -0.029893981
, -2.0391150031\H, -0.2788421053, 0.1724004468, -2.7579858873\C, 1.81796632
9, -0.2772113962, -2.4515770976\C, 2.8252148177, -0.537478736, -1.511252012
3\S, 2.4463106703, -0.3155564639, -4.0860958862\N, 4.042831783, -0.75321726
98, -2.14557082\C, 4.009135753, -0.6723463382, -3.4694740692\N, 5.165238021
4, -0.8709061196, -4.1842496351\N, 4.9691662949, -0.7608965553, -5.43017585
98\C, 6.0694801042, -0.9438005088, -6.2175906342\N, 5.9442171936, -0.845379
0708, -7.5174791351\S, 7.6782021641, -1.3101669258, -5.5970039447\C, 7.1395
13021, -1.0581742837, -8.1204151552\C, 8.2254273257, -1.3313706419, -7.2378
386349\C, 7.3497080989, -1.0234855915, -9.5176987684\C, 9.5112759833, -1.56
89966389, -7.7304433476\C, 8.6189788894, -1.2586742785, -9.9927312401\H, 6.
5116912646, -0.8140853052, -10.1731863802\C, 9.6878308472, -1.528679126, -9
.1043025814\H, 10.3421312306, -1.7774190478, -7.0660111929\H, 10.677091102
2, -1.7098956921, -9.5119168956\H, 8.8113027187, -1.238756882, -11.05950296
02\H, 4.9151093981, -0.9599765917, -1.6649334494\Version=ES64L-G16RevA.0
3\State=1-A\HF=-1553.6916424\RMSD=6.632e-09\RMSF=7.002e-05\Dipole=-0.7
026731, 0.0230489, 2.1833176\Quadrupole=15.844545, -38.0160086, 22.1714635
, -9.2304921, -39.6751029, 4.7295284\PG=C01 [X(C14H9N4S2)]\@@

3_E_hth_mecn

1\1\GINC-R3390\FOpt\RM062X\6-31+G(d,p)\C14H9N4S2(1+)\ROOT\23-Jun-2019\
0\#\#P M062X/6-31+G(d,p) INT(grid=ultrafine) Opt Freq SCRF=(SMD,Solvent=Ace
=Acetonitrile)\Optimisation in solution\1,1\H,3.4005607614, -0.771007
2921, 0.545193558\C, 2.5913789497, -0.5654228632, -0.1469882281\C, 1.297098
7776, -0.321967727, 0.2750805666\H, 1.0732294519, -0.3350248835, 1.33625092
7\C, 0.2616636064, -0.0570050255, -0.6446668711\H, -0.740913798, 0.12916502
42, -0.2744454539\C, 0.4918456784, -0.0281820675, -2.0115338226\H, -0.30691
19206, 0.1759645438, -2.7164993678\C, 1.7967283679, -0.2731487929, -2.44566
75481\C, 2.8236959543, -0.5363886883, -1.5255711175\S, 2.400050298, -0.3061
189351, -4.0845672654\N, 4.0269648743, -0.7484505022, -2.1738232571\C, 3.97
05308831, -0.6635132888, -3.4868024398\N, 5.1203193678, -0.8590096796, -4.2
345018897\N, 4.9139154598, -0.7477170866, -5.4652937176\C, 6.0360631905, -0
.9348849391, -6.2553288539\N, 5.9289049619, -0.8406855848, -7.5463757134\S
7, 6.29521908, -1.2995746571, -5.606552887\C, 7.1445281913, -1.0581367167, -
8.1399948911\C, 8.2089705118, -1.3276245604, -7.2437183736\C, 7.3774341072
, -1.0286378821, -9.5281063912\C, 9.5053025615, -1.5689644294, -7.707691295
7\C, 8.6590861169, -1.2675001185, -9.9821953812\H, 6.5547349201, -0.8212455
108, -10.2048305556\C, 9.7113604945, -1.5348757287, -9.0788902329\H, 10.320
9205751, -1.7753563494, -7.0226968732\H, 10.7082148188, -1.7187025967, -9.4
670968736\H, 8.866259686, -1.2507482708, -11.0470099017\H, 4.9046312446, -0
.9566253913, -1.6884658486\Version=ES64L-G16RevA.03\State=1-A\HF=-1553
.7805034\RMSD=6.173e-09\RMSF=1.189e-05\Dipole=-1.298439, 0.0482513, 3.93
3091\Quadrupole=14.6492346, -36.4292661, 21.7800315, -8.8556753, -35.96284
97, 4.0760399\PG=C01 [X(C14H9N4S2)]\@@

3_E_mecn

1\1\GINC-R3404\FOpt\RM062X\6-31+G(d,p)\C14H8N4S2\ROOT\23-Jun-2019\0\#\#
P M062X/6-31+G(d,p) INT(grid=ultrafine) Opt Freq SCRF=(SMD,Solvent=Ace
tonitrile)\Optimisation in solution\0,1\H,3.4060843062, -0.7695546666
, 0.497651219\C, 2.5901336788, -0.562927632, -0.1877385569\C, 1.3025325035,
-0.3222110936, 0.2591245512\H, 1.090384738, -0.3378570302, 1.323201554\C, 0
.2586150499, -0.0560973177, -0.6492729997\H, -0.7418038889, 0.129193663, -0
.2709713228\C, 0.4803658642, -0.025334827, -2.0195325588\H, -0.3284682728,
0.180283216, -2.7131546387\C, 1.7801293639, -0.2682355014, -2.4721338807\C
, 2.8341186485, -0.5360714866, -1.5701564066\S, 2.376173538, -0.2998445782,
-4.1083378154\N, 4.0623823304, -0.7566256931, -2.1588929328\C, 3.966217659
1, -0.6649948194, -3.4445767842\N, 5.0964777854, -0.8534957048, -4.24626018
58\N, 4.872921226, -0.7391763481, -5.467868006\C, 6.00325063, -0.9273505165
, -6.2695358143\N, 5.9070810764, -0.8357302936, -7.555220127\S, 7.593361766
2, -1.2921808314, -5.6057593814\C, 7.1353931923, -1.056051817, -8.143947285
6\C, 8.1894234034, -1.323691639, -7.2419550665\C, 7.3793841244, -1.02915590
52, -9.5263612667\C, 9.4892334324, -1.5663611355, -7.6945481453\C, 8.667035
1493, -1.2696347304, -9.9732124242\H, 6.5634036178, -0.8226808381, -10.2117
609952\C, 9.7109913361, -1.535558709, -9.0648059114\H, 10.2981012463, -1.77
18297854, -7.00092081\H, 10.7114487505, -1.7206650931, -9.4430960688\H, 8.8
791877445, -1.2539488859, -11.0372879392\Version=ES64L-G16RevA.03\State
=1-A\HF=-1553.3532749\RMSD=5.441e-09\RMSF=1.075e-05\Dipole=0.0000644, 0
.0003213, 0.0000196\Quadrupole=15.4334365, -19.5475177, 4.1140812, -6.1758
309, -22.6222999, 3.2833006\PG=C01 [X(C14H8N4S2)]\@@

3_Z_gasphase

1\1\GINC-R838\FOpt\RM062X\6-31+G(d,p)\C14H8N4S2\ROOT\09-Aug-2019\0\#\#m
062X/6-31+G(d,p) INT(grid=ultrafine) OPT Freq=noraman\al b1\0,1\N, -3
.5063902642, -1.21537457, -0.4056162994\N, -2.7100158627, -1.4784950484, 0.
50586484\C, -2.3632544681, -2.8291665964, 0.7973613561\N, -1.9622219978, -3
.6763601731, -0.083506636\C, -1.5632809447, -4.8456854528, 0.5415953337\C,
-1.6768623602, -4.8419078481, 1.9483359117\S, -2.2690858003, -3.2922913503
, 2.4815549845\C, -1.0859129158, -5.9866650402, -0.1165242134\C, -0.7419569
353, -7.0956008585, 0.6388412743\C, -0.8650583502, -7.0832222011, 2.0395763
19\C, -1.3337609071, -5.9615741199, 2.7092045417\C, -4.2683364587, -2.24894
30021, -1.0226266402\S, -4.4344787853, -2.1991594944, -2.763252593\C, -5.53
11346094, -3.5462814735, -2.6255169727\C, -5.7031734672, -3.878179362, -1.2
646053619\N, -4.9673975837, -3.1131915983, -0.375417061\C, -6.1916570888, -
4.2494448526, -3.6352513265\C, -7.0360239047, -5.2850712671, -3.2601498005
\C, -7.2196158237, -5.6200431593, -1.9068377196\C, -6.5616014372, -4.925459
6091, -0.9052428655\H, -1.0018688973, -5.9790487838, -1.1978205127\H, -0.37
36573609, -7.9885520717, 0.1448688545\H, -0.5870299058, -7.9641098343, 2.60
88584183\H, -1.4253458989, -5.9541401539, 3.790033016\H, -6.0539030694, -3
.9917658135, -4.6798845635\H, -7.5646417793, -5.8432241923, -4.025900026\H
, -7.8854903088, -6.435934115, -1.6461687135\H, -6.6872748145, -5.172118958
3, 0.1434174554\Version=ES64L-G16RevA.03\State=1-A\HF=-1553.3055955\RM
SD=4.734e-09\RMSF=1.286e-05\Dipole=-0.2732452, -1.5691538, -0.2142314\Qu

adropole=-2.2156286,-4.9385561,7.1541848,-1.3054099,5.3352909,-2.66068
28\PG=C01 [X(C14H8N4S2)]\ \@

3_Z_hazo_gasphase

1\1\GINC-R204\FOpt\RM062X\6-31+G(d,p)\C14H9N4S2(1+)\ROOT\05-Apr-2019\0
\#P M062X/6-31+G(d,p) INT(grid=ultrafine) Opt Freq\Optimisation\1,1
\H,3.7343535947,2.9842087365,-2.8137521375\C,3.1934600416,2.0630667376
, -2.6278863002\C,2.1302706172,2.0249275622,-1.742105612\H,1.8388814347
,2.9353182545,-1.228907149\C,1.4117448289,0.8321820267,-1.4861635297\H
,0.5864561903,0.8546124695,-0.7833286033\C,1.7454788795,-0.3464731503,
-2.1138239699\H,1.2105895171,-1.2723928515,-1.9345214727\C,2.825808752
6,-0.3308918904,-3.0206677421\C,3.5384573898,0.8686950967,-3.269639464
5\N,3.2778882786,-1.4079120129,-3.7183078392\S,4.8069405255,0.59239977
97,-4.4207093102\C,4.2898612223,-1.0779936105,-4.4751065004\N,4.764151
0921,-2.1858991625,-5.2011336261\N,5.6623041025,-2.4699264306,-6.04296
67608\C,6.5548518802,-1.5818775663,-6.5346983406\S,7.7011156541,-2.224
649812,-7.692529042\N,6.6615484073,-0.3061312274,-6.247699088\C,8.3832
571547,-0.6515428621,-7.8037644007\C,7.6803400849,0.2498003216,-6.9436
383116\C,9.461410395,-0.2128894478,-8.5845544055\C,8.0695432624,1.6086
22381,-6.8704775923\C,9.8163034654,1.1185005402,-8.4905023569\H,9.9968
411534,-0.8923973862,-9.2377349998\C,9.1271256042,2.0242229347,-7.6406
546326\H,7.5304233094,2.2838615175,-6.2155824101\H,9.448321762,3.05921
56436,-7.6058010915\H,10.6473397689,1.485456476,-9.083727219\H,4.18615
16307,-2.9954030677,-4.9514660919\Version=ES64L-G16RevA.03\State=1-A\
HF=-1553.6654764\RMSD=9.466e-09\RMSF=3.261e-05\Dipole=0.388796,0.24324
26,-0.256769\Quadrupole=8.5638483,-6.798055,-1.7657933,1.705915,-33.57
05199,5.9319123\PG=C01 [X(C14H9N4S2)]\ \@

3_Z_hazo_mecn

1\1\GINC-R3430\FOpt\RM062X\6-31+G(d,p)\C14H9N4S2(1+)\ROOT\23-Jun-2019\
0\#P M062X/6-31+G(d,p) INT(grid=ultrafine) Opt Freq SCRF=(SMD,Solvent
=Acetonitrile)\Optimisation in solution\1,1\H,3.765570182,2.97102582
65,-2.8415770952\C,3.2139565358,2.0576100174,-2.6452468022\C,2.1524801
666,2.0357788531,-1.7564545437\H,1.8700465276,2.9524157422,-1.24842913
33\C,1.4255428563,0.8503389804,-1.4923294112\H,0.6013147023,0.88297763
04,-0.787589048\C,1.7483751021,-0.3367518537,-2.1140377888\H,1.2038369
578,-1.2561518063,-1.9254293218\C,2.8260715228,-0.3362193257,-3.022780
2904\C,3.5456158954,0.8539723761,-3.2792693192\N,3.2691586943,-1.42376
12942,-3.7166126475\S,4.8090953772,0.5614423464,-4.4309466292\C,4.2804
26529,-1.1087562686,-4.4767991581\N,4.7570345907,-2.2155764314,-5.2046
050353\N,5.6587109931,-2.4771588704,-6.0421017321\C,6.5484689268,-1.57
93158483,-6.528216014\S,7.6981248405,-2.2182934937,-7.6860764715\N,6.6
534535446,-0.3080112463,-6.2424653575\C,8.3788551956,-0.6418293536,-7.
7960801111\C,7.6728479177,0.2541196271,-6.9367831529\C,9.4565869495,-0
.2018213615,-8.5755730696\C,8.0556470945,1.6133888274,-6.8594530559\C,
9.8072602447,1.1316795046,-8.4787299625\H,9.994183236,-0.8803632606,-9
.2288090352\C,9.1144734456,2.032953567,-7.6290148653\H,7.5130411843,2.
2862139826,-6.2036730741\H,9.4323535304,3.0693814926,-7.591984535\H,10
.6382489275,1.50179002,-9.0706802326\H,4.1904383291,-3.0423683797,-4.9

701031069\Version=ES64L-G16RevA.03\State=1-A\HF=-1553.7484773\RMSD=3.
441e-09\RMSF=1.237e-05\Dipole=0.520759,-0.0485881,-0.4535443\Quadrupol
e=6.6270934,-3.4784618,-3.1486317,2.9185854,-30.2530012,5.4229572\PG=C
01 [X(C14H9N4S2)]\ \@

3_Z_hth_gasphase

1\1\GINC-R575\FOpt\RM062X\6-31+G(d,p)\C14H9N4S2(1+)\ROOT\05-Apr-2019\0
\#P M062X/6-31+G(d,p) INT(grid=ultrafine) Opt Freq\Optimisation\1,1
\H,4.4478363466,2.3304576627,-3.7902363023\C,3.6947793619,1.7057113598
, -3.3230198344\C,2.7555782003,2.226845663,-2.4552883322\H,2.7670559325
,3.2877960367,-2.2319548863\C,1.7782965409,1.4064895449,-1.8510378046\
H,1.0575429499,1.8529758182,-1.174916392\C,1.718710786,0.0472946655,-2
.1011628312\H,0.9664121828,-0.5788421372,-1.6348188261\C,2.6663754753,
-0.4916919094,-2.9796020064\C,3.6395578444,0.3290151095,-3.5804879341\
S,2.857311188,-2.1371580165,-3.4936000296\N,4.4745656344,-0.394639653,
-4.4091460731\C,4.1961068248,-1.6885717105,-4.4695201438\N,4.770474152
5,-2.7526319767,-5.1634611311\N,5.7522830415,-2.7298277904,-5.94632824
43\C,6.5342341651,-1.6468025962,-6.3372308649\S,7.7903255444,-2.103821
5525,-7.4459356742\N,6.4886561845,-0.3718758395,-6.0217569382\C,8.3030
241011,-0.4595838646,-7.4980149572\C,7.4757774958,0.3311755544,-6.6607
118007\C,9.3594210008,0.1120049672,-8.2212822457\C,7.7045487699,1.7164
013869,-6.5413774604\C,9.5648618698,1.4715472015,-8.0888275133\H,9.991
974997,-0.4925058456,-8.8614875734\C,8.7441347344,2.2687395916,-7.2553
570453\H,7.0709570513,2.3198426762,-5.9005642941\H,8.9422904232,3.3322
729339,-7.1818128638\H,10.3748628396,1.9410306925,-8.6365478924\H,5.30
17643615,-0.0519479725,-4.9982521049\Version=ES64L-G16RevA.03\State=1
-A\HF=-1553.6716181\RMSD=4.275e-09\RMSF=1.806e-05\Dipole=-0.4524706,1.
5614612,0.7048435\Quadrupole=12.6940605,-10.7046128,-1.9894477,2.10067
03,-33.0216773,2.3235068\PG=C01 [X(C14H9N4S2)]\ \@

3_Z_hth_mecn

1\1\GINC-R3425\FOpt\RM062X\6-31+G(d,p)\C14H9N4S2(1+)\ROOT\23-Jun-2019\
0\#P M062X/6-31+G(d,p) INT(grid=ultrafine) Opt Freq SCRF=(SMD,Solvent
=Acetonitrile)\Optimisation in solution\1,1\H,4.4558216438,2.3239106
82,-3.798748455\C,3.6979352825,1.7093553455,-3.3249615525\C,2.75837068
74,2.2291368014,-2.4570160912\H,2.7691727957,3.2904550883,-2.233354749
5\C,1.780326674,1.4084082285,-1.8516708833\H,1.0597644162,1.8561010117
, -1.1753444252\C,1.7172339552,0.0482047581,-2.0988322572\H,0.964937113
2,-0.5784029403,-1.632264025\C,2.6654335477,-0.4883597004,-2.977456222
7\C,3.6385821414,0.3319283005,-3.5789774948\S,2.8606085666,-2.13154582
23,-3.4944444009\N,4.4721606161,-0.388258314,-4.4060448563\C,4.2018363
238,-1.6788167947,-4.4717466404\N,4.7733691194,-2.7438319509,-5.164296
7837\N,5.7534381123,-2.735050776,-5.9496055424\C,6.5390862815,-1.65656
07663,-6.3440066965\S,7.801730949,-2.1141160373,-7.4574372096\N,6.4940
292368,-0.3896711732,-6.0308161719\C,8.311327242,-0.4644236172,-7.5059
473749\C,7.4791001221,0.3177148776,-6.6669191512\C,9.3651395504,0.1141
259155,-8.2251117395\C,7.6960636091,1.703157126,-6.5379991505\C,9.5611
66145,1.4765857215,-8.084300208\H,10.0026513856,-0.4837020385,-8.86749

30285\C, 8.7352196808, 2.2650112067, -7.2489700555\H, 7.0524184917, 2.29204
90773, -5.8926047187\H, 8.9272878128, 3.3298317402, -7.1701050312\H, 10.369
9113462, 1.9529381258, -8.6290633069\H, 5.2855971517, -0.0164740755, -4.978
2017769\\Version=ES64L-G16RevA.03\State=1-A\HF=-1553.7556149\RMSD=6.44
3e-09\RMSF=2.040e-05\Dipole=-0.7294112, 2.1841547, 1.064459\Quadrupole=1
2.3566688, -10.8140068, -1.542662, 1.9291628, -31.1906928, 1.9970649\PG=C01
[X(C14H9N4S2)]\@

3_Z_mecn

1\1\GINC-R969\FOpt\RM062X\6-31+G(d,p)\C14H8N4S2\ROOT\09-Aug-2019\0\#\#m
062X/6-31+G(d,p) INT(grid=ultrafine) OPT Freq=noraman SCRF=(SMD,Solven
t=acetonitrile)\al bl\0,1\N, -3.5107839892, -1.2259909415, -0.405515685
4\N, -2.7093950951, -1.489552866, 0.502803611\C, -2.3526187991, -2.83432251
5, 0.8024096127\N, -1.9709976383, -3.6946033079, -0.0759189073\C, -1.559395
5128, -4.8588434347, 0.5536244624\C, -1.64744603, -4.8379164992, 1.96204479
89\S, -2.2278313976, -3.2789590293, 2.4882303429\C, -1.0958918453, -6.00855
89945, -0.1015686894\C, -0.7414992687, -7.1080990554, 0.6638689261\C, -0.84
01282843, -7.0773608549, 2.0676772509\C, -1.2944325763, -5.9470630923, 2.73
43340929\C, -4.2798394169, -2.2487723057, -1.0283564068\S, -4.4686200107, -
2.1716361528, -2.7643509232\C, -5.5569042866, -3.5293269288, -2.6363664781
\C, -5.7106567994, -3.8856879201, -1.2794561511\N, -4.9648407171, -3.130670
7812, -0.3878823568\C, -6.2227562672, -4.2166884917, -3.6539275708\C, -7.05
62938019, -5.2641644415, -3.2845956156\C, -7.2230616524, -5.624707958, -1.9
342078465\C, -6.5587892262, -4.9447304312, -0.9258180888\H, -1.0295557374,
-6.0200714723, -1.1848967547\H, -0.3840440374, -8.0088135611, 0.1752930841
\H, -0.5533834869, -7.9520532911, 2.6427262682\H, -1.3666613546, -5.9256330

9 APPENDIX – CHAPTER 5

9.1 Formation of $[\text{Pd}_3(\mathbf{5.9})_6]^{6+}$ and $[\text{Pd}_4(\mathbf{5.9})_8]^{8+}$ by ^{19}F NMR

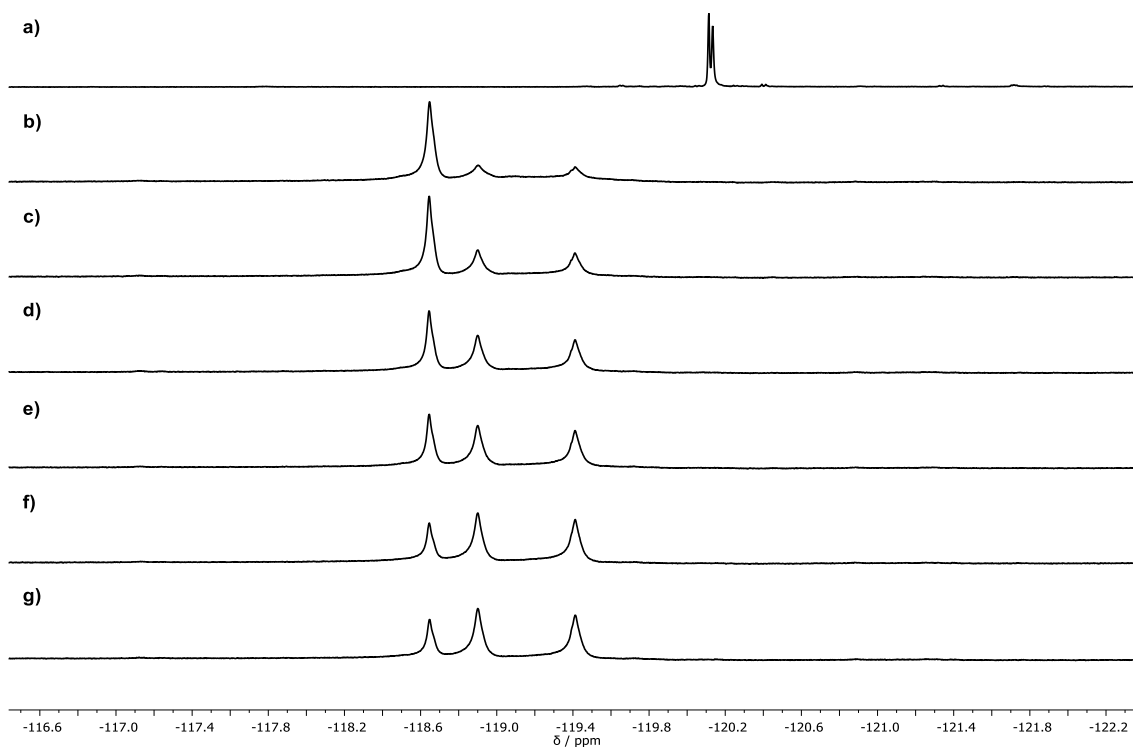


Figure 9.1 Formation of a mixture of $[\text{Pd}_3(\mathbf{5.9})_6]^{6+}$ and $[\text{Pd}_4(\mathbf{5.9})_8]^{8+}$ monitored by ^{19}F NMR in $\text{DMSO-}d_6$ (546.5 MHz, 298 K). a) $\mathbf{5.9}$ in $\text{DMSO-}d_6$; b) addition of $[\text{Pd}(\text{CH}_3\text{CN})_4](\text{BF}_4)_2$; c) 70 minutes; d) 190 minutes e) 5 hours; f) 18 hours and g) 22 hours.

9.2 Isotope patterns of $[\text{Pd}_3(\mathbf{5.9})_6]^{6+}$ and $[\text{Pd}_4(\mathbf{5.9})_8]^{8+}$

Table 9.1 Zoom scans of select ESI-MS peaks, with simulated isotope patterns ESI-MS of $[\text{Pd}_3(\mathbf{5.9})_6]$ double-walled triangle.

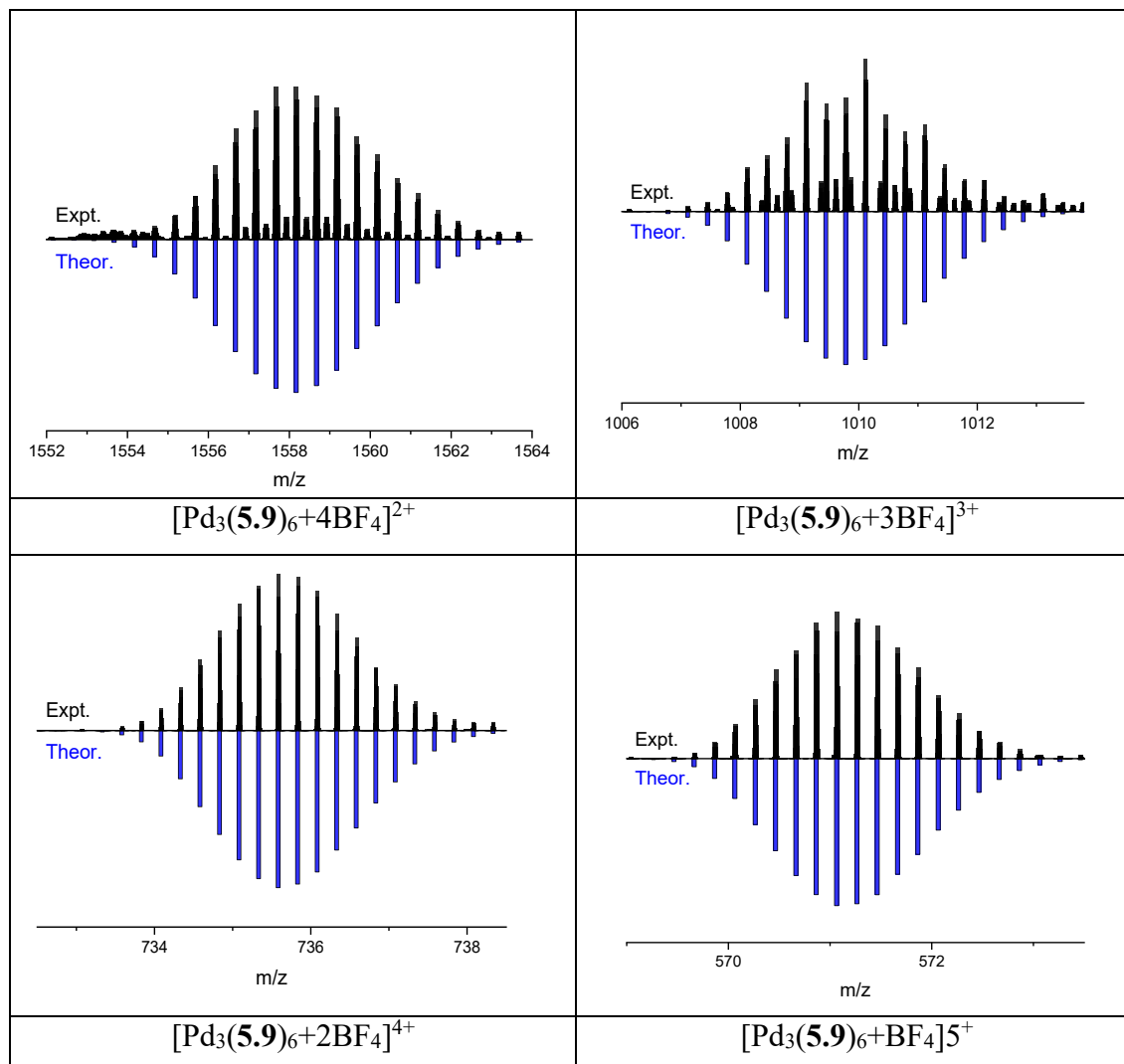
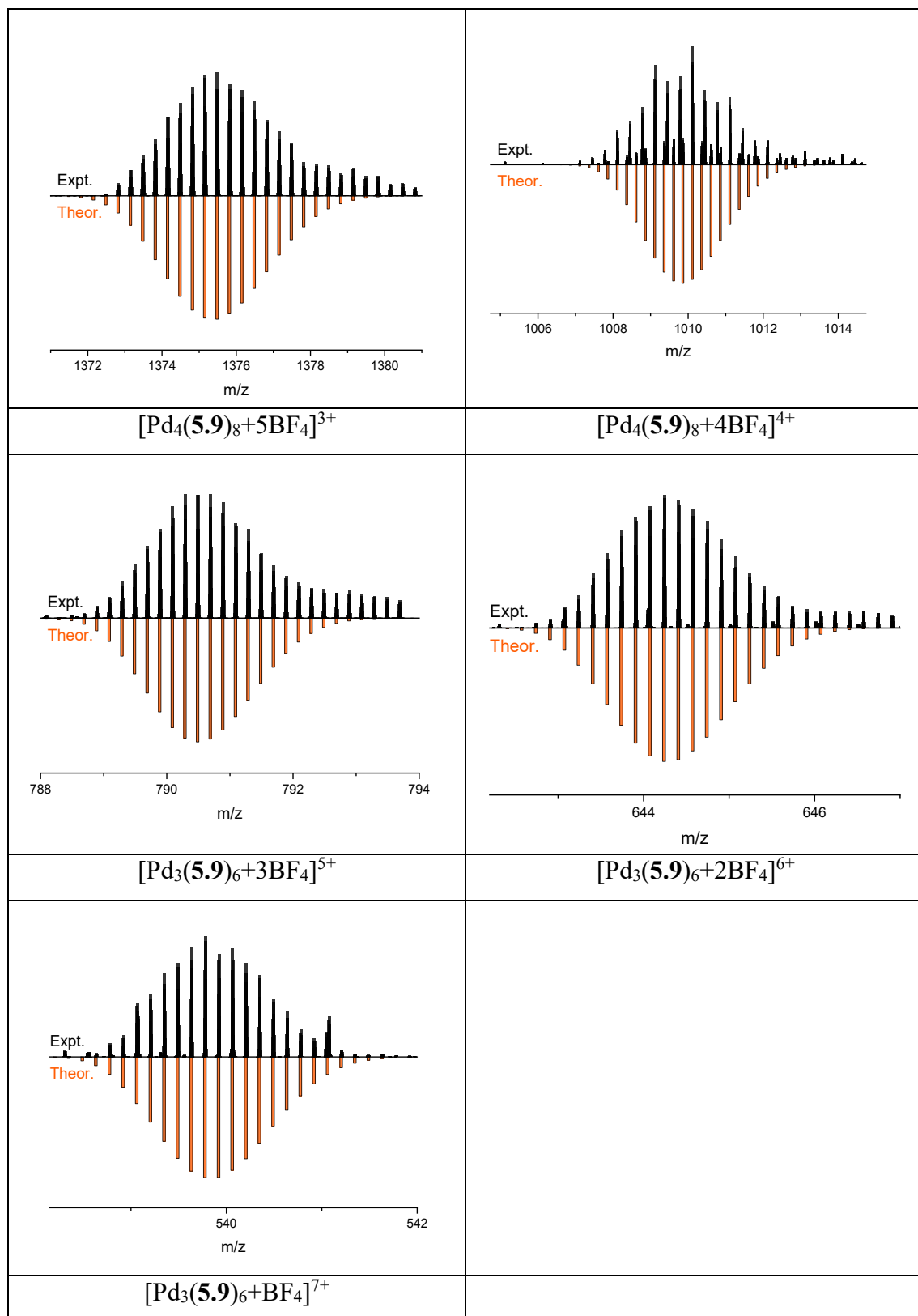


Table 9.2 Zoom scans of select ESI-MS peaks, with simulated isotope patterns ESI-MS of $[\text{Pd}_4(\mathbf{5.9})_8]$ distorted tetrahedron.



9.3 Variable temperature measurement of $[\text{Pd}_3(\mathbf{5.9})_6]^{6+}$ and $[\text{Pd}_4(\mathbf{5.9})_8]^{8+}$ in $\text{DMSO-}d_6$

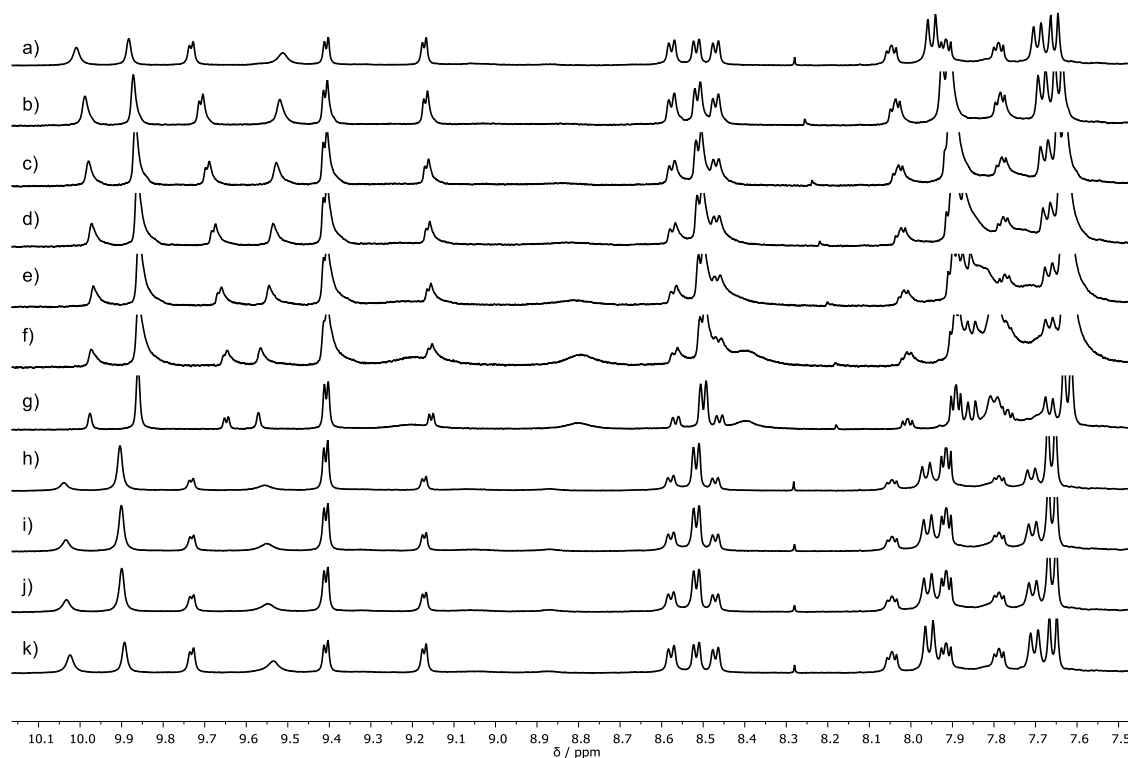


Figure 9.2 Variable temperature measurement of $[\text{Pd}_3(\mathbf{5.9})_6]^{6+}$ and $[\text{Pd}_4(\mathbf{5.9})_8]^{8+}$ in $\text{DMSO-}d_6$. a) Initial sample measured at 298 K; b) 313 K; c) 323 K; d) 333 K; e) 343 K; f) 353 K; g) 353 K after reshimming; h) returned to 298 K; i) 298 K for 1 h; j) 298 K for 1.5 h and k) 298 K after equilibration in the dark (18 h). At each temperature point the sample was allowed to equilibrate for 30 minutes.

9.4 References

1. Pilgrim, B. S.; Roberts, D. A.; Lohr, T. G.; Ronson, T. K.; Nitschke, J. R., *Nat. Chem.* **2017**, *9*, 1276.
2. Eckert, F.; Leito, I.; Kaljurand, I.; Kütt, A.; Klamt, A.; Diedenhofen, M., *J. Comput. Chem.* **2009**, *30* (5), 799-810.
3. Zhao, Y.; Truhlar, D. G., *Theor. Chem. Acc.* **2008**, *120* (1), 215-241.
4. Frisch, M. J.; Trucks, G. W.; Schlegel, H. B.; Scuseria, G. E.; Robb, M. A.; Cheeseman, J. R.; Scalmani, G.; Barone, V.; Petersson, G. A.; Nakatsuji, H.; Li, X.; Caricato, M.; Marenich, A. V.; Bloino, J.; Janesko, B. G.; Gomperts, R.; Mennucci, B.; Hratchian, H. P.; Ortiz, J. V.; Izmaylov, A. F.; Sonnenberg, J. L.; Williams, Ding, F.; Lipparini, F.; Egidi, F.; Goings, J.; Peng, B.; Petrone, A.; Henderson, T.; Ranasinghe, D.; Zakrzewski, V. G.; Gao, J.; Rega, N.; Zheng, G.; Liang, W.; Hada, M.; Ehara, M.; Toyota, K.; Fukuda, R.; Hasegawa, J.; Ishida, M.; Nakajima, T.; Honda, Y.; Kitao, O.; Nakai, H.; Vreven, T.; Throssell, K.; Montgomery Jr., J. A.; Peralta, J. E.; Ogliaro, F.; Bearpark, M. J.; Heyd, J. J.;

- Brothers, E. N.; Kudin, K. N.; Staroverov, V. N.; Keith, T. A.; Kobayashi, R.; Normand, J.; Raghavachari, K.; Rendell, A. P.; Burant, J. C.; Iyengar, S. S.; Tomasi, J.; Cossi, M.; Millam, J. M.; Klene, M.; Adamo, C.; Cammi, R.; Ochterski, J. W.; Martin, R. L.; Morokuma, K.; Farkas, O.; Foresman, J. B.; Fox, D. J. *Gaussian 16 Rev. A.03*, Wallingford, CT, 2016.
5. Ribeiro, R. F.; Marenich, A. V.; Cramer, C. J.; Truhlar, D. G., *J. Phys. Chem. B* **2011**, *115* (49), 14556-14562.
 6. Marenich, A. V.; Cramer, C. J.; Truhlar, D. G., *J. Phys. Chem. B* **2009**, *113* (18), 6378-6396.
 7. (a) Guo, Y.; Riplinger, C.; Becker, U.; Liakos, D. G.; Minenkov, Y.; Cavallo, L.; Neese, F., *J. Chem. Phys.* **2018**, *148* (1), 011101; (b) Neese, F.; Hansen, A.; Liakos, D. G., *J. Chem. Phys.* **2009**, *131* (6), 064103; (c) Paulechka, E.; Kazakov, A., *J. Phys. Chem. A* **2017**, *121* (22), 4379-4387; (d) Riplinger, C.; Neese, F., *J. Chem. Phys.* **2013**, *138* (3), 034106; (e) Riplinger, C.; Pinski, P.; Becker, U.; Valeev, E. F.; Neese, F., *J. Chem. Phys.* **2016**, *144* (2), 024109; (f) Riplinger, C.; Sandhoefer, B.; Hansen, A.; Neese, F., *J. Chem. Phys.* **2013**, *139* (13), 134101.
 8. Neese, F., Wiley Interdisciplinary Reviews: Computational Molecular Science **2012**, *2* (1), 73-78.
 9. Muller, P., Glossary of terms used in physical organic chemistry (IUPAC Recommendations 1994). In *Pure and Applied Chemistry*, 1994; Vol. 66, p 1077.
 10. Ho, J.; Coote, M. L., *Theor. Chem. Acc.* **2009**, *125* (1), 3.
 11. Lõkov, M.; Tshepelevitsh, S.; Heering, A.; Plieger, P. G.; Vianello, R.; Leito, I., *Eur. J. Org. Chem.* **2017**, *2017* (30), 4475-4489.
 12. Marković, Z.; Tošović, J.; Milenković, D.; Marković, S., *Computational and Theoretical Chemistry* **2016**, *1077*, 11-17.
 13. Mulliken, R. S., *J. Chem. Phys.* **1955**, *23* (10), 1833-1840.
 14. Shao, Y.; Gan, Z.; Epifanovsky, E.; Gilbert, A. T. B.; Wormit, M.; Kussmann, J.; Lange, A. W.; Behn, A.; Deng, J.; Feng, X.; Ghosh, D.; Goldey, M.; Horn, P. R.; Jacobson, L. D.; Kaliman, I.; Khaliullin, R. Z.; Kuš, T.; Landau, A.; Liu, J.; Proynov, E. I.; Rhee, Y. M.; Richard, R. M.; Rohrdanz, M. A.; Steele, R. P.; Sundstrom, E. J.; Woodcock, H. L.; Zimmerman, P. M.; Zuev, D.; Albrecht, B.; Alguire, E.; Austin, B.; Beran, G. J. O.; Bernard, Y. A.; Berquist, E.; Brandhorst, K.; Bravaya, K. B.; Brown, S. T.; Casanova, D.; Chang, C.-M.; Chen, Y.; Chien, S. H.; Closser, K. D.; Crittenden, D. L.; Diedenhofen, M.; DiStasio, R. A.; Do, H.; Dutoi, A. D.; Edgar, R. G.; Fatehi, S.; Fusti-Molnar, L.; Ghysels, A.; Golubeva-Zadorozhnaya, A.; Gomes, J.; Hanson-Heine, M. W. D.; Harbach, P. H. P.; Hauser, A. W.; Hohenstein, E. G.; Holden, Z. C.; Jagau, T.-C.; Ji, H.; Kaduk, B.; Khistyayev, K.; Kim, J.; Kim, J.; King, R. A.; Klunzinger, P.; Kosenkov, D.; Kowalczyk, T.; Krauter, C. M.; Lao, K. U.; Laurent, A. D.; Lawler, K. V.; Levchenko, S. V.; Lin, C. Y.; Liu, F.; Livshits, E.; Lochan, R. C.; Luenser, A.; Manohar, P.; Manzer, S. F.; Mao, S.-P.; Mardirossian, N.; Marenich, A. V.; Maurer, S. A.; Mayhall, N. J.; Neuscamman, E.; Oana, C. M.; Olivares-Amaya, R.; O'Neill, D. P.; Parkhill, J. A.; Perrine, T. M.; Peverati, R.; Prociuk, A.; Rehn, D. R.; Rosta, E.; Russ, N. J.; Sharada, S. M.; Sharma, S.; Small, D. W.; Sodt, A.; Stein, T.; Stück, D.; Su, Y.-C.; Thom, A. J. W.; Tsuchimochi, T.; Vanovschi, V.; Vogt, L.; Vydrov, O.; Wang, T.; Watson, M. A.; Wenzel, J.; White, A.; Williams, C. F.; Yang, J.; Yeganeh, S.; Yost, S. R.; You, Z.-Q.; Zhang, I. Y.; Zhang, X.; Zhao, Y.; Brooks, B. R.; Chan, G. K. L.; Chipman, D. M.; Cramer, C. J.; Goddard, W. A.; Gordon, M. S.; Hehre, W. J.; Klamt, A.; Schaefer, H. F.; Schmidt, M. W.;

- Sherrill, C. D.; Truhlar, D. G.; Warshel, A.; Xu, X.; Aspuru-Guzik, A.; Baer, R.; Bell, A. T.; Besley, N. A.; Chai, J.-D.; Dreuw, A.; Dunietz, B. D.; Furlani, T. R.; Gwaltney, S. R.; Hsu, C.-P.; Jung, Y.; Kong, J.; Lambrecht, D. S.; Liang, W.; Ochsenfeld, C.; Rassolov, V. A.; Slipchenko, L. V.; Subotnik, J. E.; Van Voorhis, T.; Herbert, J. M.; Krylov, A. I.; Gill, P. M. W.; Head-Gordon, M., *Mol. Phys.* **2015**, *113* (2), 184-215.
15. Bader, R. F. W., *Atoms in molecules : a quantum theory*. Oxford England : Clarendon Press New York : Oxford University Press: Oxford [England] : New York, 1994.
16. (a) Lu, T.; Chen, F., *J. Comput. Chem.* **2012**, *33* (5), 580-592; (b) Lu, T.; Chen, F., *J. Mol. Graphics Modell.* **2012**, *38*, 314-323.
17. Humphrey, W.; Dalke, A.; Schulten, K., *Journal of Molecular Graphics* **1996**, *14* (1), 33-38.
18. (a) Shahi, A.; Arunan, E., *PCCP* **2014**, *16* (42), 22935-22952; (b) Koch, U.; Popelier, P. L. A., *J. Phys. Chem.* **1995**, *99* (24), 9747-9754; (c) Grabowski, S. J., *Annual Reports Section "C" (Physical Chemistry)* **2006**, *102* (0), 131-165.
19. Parthasarathi, R.; Subramanian, V.; Sathyamurthy, N., *J. Phys. Chem. A* **2006**, *110* (10), 3349-3351.